An Improved Engineering Design Flood Estimation Technique: Removing the Need to Estimate Initial Loss

by

Theresa Michelle Heneker

August 2002

A Thesis Submitted for the Degree of

Doctor of Philosophy

Department of Civil and Environmental Engineering

Adelaide University

Australia

ABSTRACT

The planning, design and construction of engineering infrastructure projects often requires consideration of the potential for flood risk. In Australia, a probabilistic rainfall-based approach recommended by Australian Rainfall and Runoff (ARR, 1987) is commonly used for design flood estimation. This approach involves the conversion of a rainfall event with a given Average Recurrence Interval (ARI) to a flood that is assumed to have the same ARI. However, flood discharges are jointly affected by rainfall and antecedent moisture conditions and large variations in flow can result from the same rainfall event, depending of the initial catchment conditions. The ARR (1987) method essentially incorporates antecedent moisture conditions by assuming a value of initial loss, but little practical guidance is offered on how this value should be selected. In addition, there is no attempt to assign a probability to this parameter, nor provide guidance on how to ensure that the assumption of ARI equality between a rainfall event and its resulting flood remains valid. Recent research has questioned this assumption, emphasising the joint probability relationship that exists between rainfall and antecedent moisture conditions (discussed in terms of initial loss), which affects the magnitude of any resulting flood.

This thesis describes the development of an alternative approach to design flood estimation that aims to address the uncertainties surrounding the selection of initial rainfall loss. The methodology is based on the ARR (1987) design flood estimation method in order to retain a common design approach, and to allow the work of this thesis to be easily integrated into current engineering practice. The key outcome is the use of rainfall excess frequency duration (REFD) proportions, which represent the ratio of the curves from an intensity-frequency-duration (IFD) analysis of rainfall excess and rainfall, to directly convert a design rainfall hyetograph into a rainfall excess hyetograph. The rainfall excess hyetograph is then used as input into a flood estimation model to derive a flood frequency distribution. Because a value of initial loss is not required, one of the factors that creates uncertainty with the assumption that the ARI of the design rainfall will apply to the resulting flood is removed.

The REFD proportions are determined from a continuous simulation of synthetic rainfall at a six-minute time scale, which is transformed to synthetic rainfall excess using a catchment water balance model. Because the effect of initial loss on this transformation is explicitly

accounted for within the structure of the water balance model, the REFD proportions also take the effect of initial loss into account.

A suitable rainfall simulation model was not identified during a review of current literature. As a result, this thesis also develops a stochastic point rainfall model that is capable of adequately generating a synthetic rainfall record at a six-minute time-scale. The model uses an alternating renewal process to produce a series of rectangular pulses that define the gross characteristics of each rainfall event. A conditional random walk on a dimensionless mass curve is then used to model the temporal distribution of intra-event rainfall and to disaggregate these pulses into a six-minute hyetograph. The model is able to replicate various statistical properties of observed data over a range of time scales, including the IFD and aggregated statistics. These properties were not used to calibrate the model, but are used to successfully validate the model for a number of Australian locations within different climatic regions.

An important factor affecting catchment moisture conditions is the level of evaporation that occurs between rainfall events. A stochastic lag-one Markov model, based on the work of Srikanthan and McMahon (1985), is used to generate daily evaporation. Conditional relationships between the amount of daily evaporation and the evaporation of the previous day, the simulated rainfall state on the current and previous days and the time of year, are incorporated based on previous research and an analysis of historical data. The model can be calibrated using both pan evaporation data and potential evaporation data generated using the Priestley-Taylor (Priestley and Taylor, 1972) model. A method developed by Fleming (1972), which uses two daily profile types (clear or cloudy) to define the distribution of evaporation over a day, is used to model the temporal distribution of the daily evaporation. As with the rainfall model, the evaporation model is able to generate synthetic daily evaporation that replicates the observed aggregated statistics at a variety of time scales.

A modified Australian Water Balance Model (Boughton, 1993) is used to transform the synthetic rainfall and evaporation input to synthetic rainfall excess at a six-minute time scale. During calibration, an improved representation of observed streamflow data at a daily time scale is obtained by introducing an alternative surface routing component. The ability to use daily evaporation data is also incorporated to provide a more accurate description of the effect of evaporation. The model shows good results for a number of Australian sites.

An IFD analysis is carried out on the synthetic rainfall and rainfall excess by fitting generalised extreme value (GEV) distributions to the annual maxima data for a range of rainfall burst durations to produce IFD and REFD curves respectively. The ratio of the IFD and REFD curves (the REFD proportions) is determined and used to represent the proportion of rainfall that will become rainfall excess during a rainfall burst of a given duration and ARI. An analysis of the REFD proportions for four Australian sites in different regions shows similar trends with increasing ARIs that are generally independent of duration. For two sites, the REFD proportions are relatively constant with duration and ARI over an ARI range of 5 to 100 years. For the other two sites the curves gradually increase with ARI, but remain constant with duration over the same range of ARIs. This makes it possible to select a value for the REFD proportion for a rainfall burst of a given ARI that is independent of the duration of the event.

The use of the REFD proportions is validated by deriving flood frequency distributions using the KinDog runoff-routing model, based on the work of Field and Williams (1983, 1987). The model is concurrently calibrated using a number of events for each site to determine parameters that are more representative of each catchment, rather than individual events. These parameters provide an adequate representation of each individual event used during calibration. The REFD proportions are then used to convert the ARR (1987) design rainfall intensities to rainfall excess, which is then routed to the catchment outlet and the flood frequency distribution determined. The ARR (1987) temporal patterns were also used. A comparison with a flood frequency analysis of observed floods shows that the approach (the use of REFD proportions) is able to satisfactorily derive flood frequency distributions at all four sites, thus demonstrating the ability to eliminate the need to determine initial loss in the design process.

The alternative design flood estimation methodology developed in this thesis shows considerable promise in terms of providing a more reliable design flood estimation technique. Establishing a relationship between catchment characteristics and the REFD proportions would enable the definition of REFD proportions for generic catchment types, increasing the potential for translation to catchments with limited data but similar hydrologic properties, thereby further improving the design process. The availability of these curves for key catchment areas in Australia will greatly improve the accuracy of the current design methodology.

STATEMENT OF ORIGINALITY

This work contains no material that has been accepted for the award of any other degree or diploma in any university or other tertiary institution and, to the best of my knowledge and belief, contains no material previously published or written by another person, except where due reference has been made in the text.

I give consent to this copy of my thesis, when deposited in the University Library, being available for loan and photocopying.

Signed:. .... Date: .19/8/02.....

Theresa Michelle Heneker

ACKNOWLEDGMENTS

This research was funded by an Australian Postgraduate Award (APA) and a small Australian Research Council (ARC) grant.

I thank the following people and organisations whose assistance was invaluable in completing the work presented in this thesis:

- Dr. Martin Lambert from the Department of Civil and Environmental Engineering at Adelaide University for his supervision of this project and for providing inspiration, ideas and guidance.
- Associate Professor George Kuczera from the Department of Civil, Surveying and Environmental Engineering at the University of Newcastle for many useful and essential ideas and discussions.
- The Department of Water, Land and Biodiversity Conservation, South Australia, for granting study leave to allow me to complete this thesis and for providing access to streamflow data.
- The Department of Natural Resources, Queensland for providing streamflow data.
- Dr. Bryson Bates from CSIRO for providing information and guidance on evaporation modelling in Australia.
- Dr. Brian Williams from the Department of Civil, Surveying and Environmental Engineering at the University of Newcastle for providing essential information and support for the use of the KinDog model.
- My family, in particular my mum and dad, for their support and for the hours spent proof reading this thesis.

Finally, I thank and dedicate this thesis to my husband Derek for his love, understanding, support and encouragement throughout this research. Our discussions, particularly in the final stages of completion, were crucial and without whom the end may not have been reached.

LIST OF PUBLICATIONS

Several papers have been published during this study. They reflect formative ideas for work presented in this thesis. These papers are listed in chronological order:

(1) Heneker, T. M., Lambert, M. F. and Kuczera, G. (1999), *DRIP: A disaggregated rectangular intensity pulse model of point rainfall.* Water '99 Joint Congress, 25th Hydrology and Water Resources Symposium and 2nd International Conference on Water Resources and Environment Research, Volume 1, 539-544. Brisbane, Queensland, 6-8 July.

(2) Heneker, T. M., Lambert, M. F. and Kuczera, G. (2001), A point rainfall model for risk-based design. *Journal of Hydrology*, 247, 54-71.

(3) Heneker, T. M., Lambert, M. F. and Kuczera, G. (2002), Overcoming the Joint Probability Problem Associated with Initial Loss Estimation in Design Flood Estimation. 27th Hydrology and Water Resources Symposium, Melbourne, Victoria, 20-23 May.

TABLE OF CONTENTS

APPENDICES

LIST OF FIGURES

LIST OF TABLES

1. INTRODUCTION AND CURRENT DESIGN FLOOD ESTIMATION METHODS

1.1 INTRODUCTION

1.1.1 Flooding in Australia

The consequences of a flood can be devastating, threatening life, property and the economic well being of communities. Historically, development has occurred near rivers and their floodplains, which are often locations that have usable water sources, timber resources, fertile soils and suitable grazing areas for stock. In the past these areas have also offered transportation potential to other communities and markets. As such, many urbanised and industrialised areas in Australia have been developed on or near significant waterways. Unfortunately, these areas can also present a high flood risk. The result has been enormous costs due to flood damage. Estimates of costs include $90-$100 million for the 1998 flood in Katherine (N.T.), $50 million for the 1990 flood in Nyngan (N.S.W.), $500 million damage during the Hunter Valley (N.S.W.) floods in 1955 and $700 million for the disastrous 1974 flood in Brisbane (Qld.). Aside from loss of life and irreplaceable possessions, it is estimated that the average annual flood damage cost in Australia is between $300-$400 million (Bureau of Transport Economics, 2001). However, damage estimates rarely take into account the costs to improve roads and other infrastructure (in both the public and private sectors), when they are reconstructed post-flood, to establish protection from future floods, that make the actual costs related to flood damage and prevention much greater.

1.1.2 Development, Legislation and Flood Risk

Hundreds of millions of dollars are spent per annum on infrastructure and land developments that require accurate estimates of flood characteristics. However, the rapid and ongoing population growth in many areas of Australia, leading to a huge demand for land, has often resulted in developments occurring in inappropriate areas. History has shown the outcomes from such inappropriate developments through repeated inundation and major flood damage in, for example, Katherine (N.T.) (1957, 1998) and Brisbane (Qld.) (1893, 1931, 1974, 1986).

Appropriate planning and building control measures must be established and maintained in

flood prone areas so that the risk to people and the potential damage to property can be limited to a tolerable level. The converse situation is that development may be unnecessarily prevented in areas where flood levels are conservatively over-predicted. In order to limit the flood risk to new developments and therefore the overall cost of damage due to flood, legislation has been introduced in Australia to limit and/or prohibit construction on or near floodplains. Most local governments have floodplain management strategies to prevent construction on flood pronc land.

Therefore, the planning, design and construction of many engineering projects generally requires consideration of the flood risk. This is usually a probabilistic or statistical estimate and represents the level of risk that has been accepted into the design. The level of risk varies between projects and is often a compromise between the cost of infrastructure and the potential cost of system failure as a result of a flood. One method of quantifying this risk is through the use of an average recurrence interval (ARI) (also referred to as an annual exceedance probability (AEP)) to determine an acceptable flood risk (known as the *design flood*). Hence, accurate estimates of design floods over a range of ARIs are required.

1.1.3 Overall Research Objectives

Flood discharges and flood levels are affected by rainfall and the antecedent moisturc conditions of the catchment at the start of a rainfall event. Large variations in flood discharge are possible from the same rainfall event given different initial moisture conditions on a catchment. Current methods outlined in Australian Rainfall and Runoff (ARR, 1987), which are employed in general engineering practice, generally require a value of rainfall loss to be assumed and incorporated into the determination of the design flood to account for the most likely antecedent conditions. However, little practical guidance is offered on how to estimate the value of initial loss, or determine the influence that the joint probability relationship between a rainfall event and the antecedent conditions (affecting initial loss) has on the assumed relationship between the ARI of a rainfall event and the ARI of the design flood. Walsh *et al.* (1991) attempted to clarify this issue by suggesting values for average initial loss, but these values are quoted with an order of accuracy of between ±50% to ±100%. This was because the derived values of initial loss were found to be sensitive to errors in the design flood input parameters used to obtain them. The combined effect of relatively small errors can lead to a dramatic overestimation or underestimation of the initial loss values. The values in Walsh *et al.* (1991) were often 20-30% higher than the values suggested in ARR (1987).

The objective of the research presented here is to address the considerable uncertainty that currently exists about how to properly address the joint probability effects of different catchment initial conditions on flood frequency distributions, and therefore the level of risk incorporated into development. This issue is not satisfactorily addressed using the currently accepted methods such as those in ARR (1987). The following sections examine in detail the current methods for design flood estimation, the problems in calculating rainfall loss, in particular initial loss, and the rainfall loss models currently in use. Following this, a new approach is outlined that removes the need to evaluate initial loss, provides a logical, consistent approach to the estimation of design floods that enables the risks of failure during the design of new infrastructure or the assessment of environmental systems to be assessed, and that takes into account the stochastic nature of catchment conditions. This will allow a reduction in the likelihood of errors in the determination of design flood events, which in turn will result in economic savings to the community.

1.2 Current Design Flood Estimation in Australia

Current design flood estimation techniques in Australia generally involve one of two alternative approaches. The first is a rainfall-based approach involving an analysis of rainfall data, combined with a *rainfall-runoff* model and an appropriate *loss* model. The second approach involves the frequency analysis of streamflow records observed at a particular catchment of interest. There are advantages and disadvantages to each approach with the choice of method for a particular application constituting one of the most important aspects of the design process (ARR, 1987).

1.2.1 Rainfall-Based Design Event Flood Estimation

The rainfall-based approach to flood estimation recommended for engineering practice in Australia is a probabilistic design event method that is described in ARR (1987). The aim is the conversion of a rainfall event with a given ARI to a flood of the same ARI. Estimation of a design flood by this method involves design event rainfall generation, runoff production and hydrograph formation as shown in Figure 1.1, using the following steps:

(a) choose the required ARI, depending on the project in question. An ARI of 1 in 100 years is usually selected for flood plain applications;

(b) generate the design rainfall by selecting a number of design event durations (D_1, D_2, ... , D_n). Design point rainfall intensities (I_1, I_2, ... , I_n) are then estimated for each of these, from the information contained in ARR (1987). Areal reduction factors (A_1, A_2, ... , A_n) are chosen for each event, which are dependent on the depth, catchment area and duration, and are used to convert point rainfall intensities to average catchment intensities. A design temporal pattern (T_1, T_2, ... , T_n) is then chosen for each event from which design rainfall hyetographs (R_1, R_2, ... , R_n) are calculated;

(c) choose a design loss model and associated parameters to transform the design rainfall hyetographs into rainfall excess hyetographs (RE_1, RE_2, ... , RE_n);

(d) calculate the resulting flow hydrograph using a routing model for which design parameters for catchment response must be selected. This enables the transformation of the rainfall excess hyetographs into surface runoff hydrographs (H_1, H_2, ... , H_n) at the catchment outlet. Design baseflow (B_1, B_2, ... , B_n) is then selected and added to each of the surface runoff hydrographs to produce streamflow hydrographs (F_1, F_2, ... , F_n); and

(e) the rainfall duration producing the hydrograph with the maximum peak discharge is then chosen as the critical duration and the corresponding peak becomes the design flood event for the particular catchment. This design flood is then assumed to have the ARI as the ARI initially selected.

Cordery (1971) was one of the first researchers to consider whether the peak design hydrograph discharges for a given ARI corresponded with the peaks estimated from a flood frequency analysis, following an analysis of observed floods in N.S.W. Since then, the assumption that a design rainfall event of a given ARI can be converted to a design flood of the same ARI in this manner has received much discussion and criticism by researchers, including Beran (1973), Linsley and Crawford (1974), Lumb and James (1976), Ahern and Weinmann (1982), Walsh *et al.* (1991), Consuegra *et al.* (1993) and Rahman *et al.* (1998, 2001). The process assumes that each of the representative design values for the input parameters used at successive stages can be chosen such that they do not influence the ARI of the process. The validity of this approach is crucially dependent on how well this assumption is satisfied. However, there are no definite guidelines on how to select appropriate values of input parameters to ensure that the assumption is satisfied.

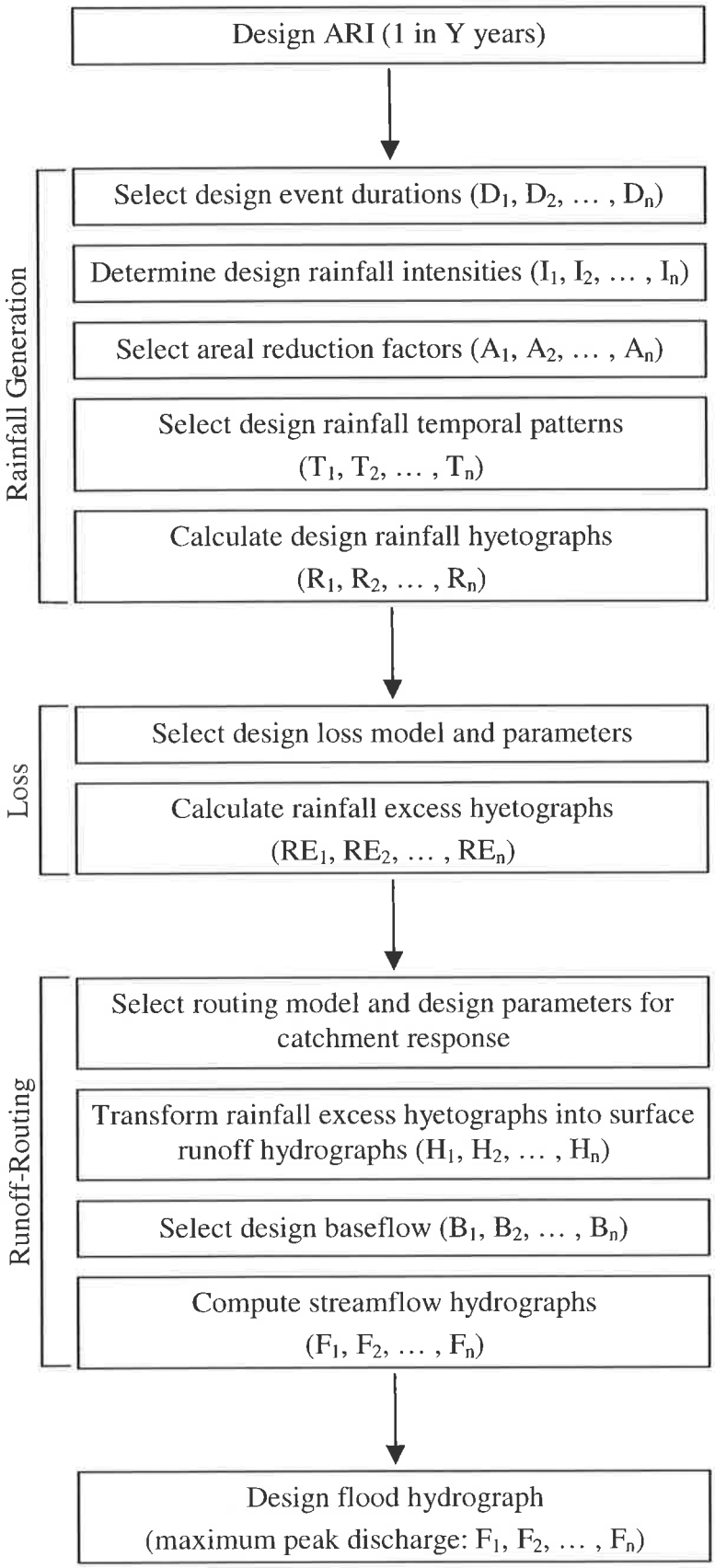

Figure 1.1 Australian Rainfall and Runoff (ARR, 1987) Design Flood Estimation Method.

The current ARR (1987) design approach only considers the probabilistic nature of rainfall intensity and ignores the probabilistic behaviour of other inputs such as rainfall duration, temporal pattern, losses and baseflow. Design flood estimation is sensitive to variations in these input parameters and the criteria surrounding the choice of these values is subjective and often arbitrary, which is likely to lead to inconsistencies, uncertainty and bias in flood estimates for a given ARI. Most importantly, the ARI neutrality of design inputs can not be confirmed and the "real" return periods of the chosen parameters are never truly known (Ahern and Weinmann, 1982; Consuegra *et al.*, 1993). This places doubt on the assumption of equality between the rainfall input and flood peak exceedance probabilities.

While there are many methods available to determine a value for each input parameter, a common method that is location independent is advantageous for design. Median values, based on observed data, are often used and recommended for a particular location. However, the probability of an occurrence of a value that is higher than the median is the same as the probability of a lower value. In addition, the commonly recommended range of values from which to choose the median may be large, particularly for the initial loss parameter. In ARR (1987) the recommended median values either have large variation (for example, a median initial loss value of 15 to 35 mm is suggested as part of a recommended range of 0 to 140 mm for Eastern Queensland) or no direction is provided as is the case for Tasmania. The transformation process between rainfall input and flood output is non-linear, which makes it difficult to know how a representative or median value for initial loss and other inputs to the process should be chosen to preserve the ARI. The supposition that using median values for all variables preserves the ARI of the process has not been widely tested. Some researchers, such as Consuegra *et al.* (1993), have argued against the use of median values and further suggest that the selection of a median initial moisture content has no sound scientific basis.

A design flood is calculated from a combination of various design rainfall and catchment inputs. Because of the uncertainty surrounding the selection of values for these inputs, the use of median or representative values cannot be assumed to ensure that the rainfall input of a given probability is linked to a flood estimate of the same probability (Ahern and Weinmann, 1982). Haan and Schulze (1987) concluded that the use of average values for input parameters is not sufficient to predict events, particularly less frequent ones, and that more input parameters should be treated as random variables. Each part of the design process introduces joint probability such that the true probability of the design flood may be obscured.

Walsh (1991) showed that inappropriate combinations of event factors, losses and catchment characteristics can result in unrealistic outputs, such as an excessively long critical event duration for a small catchment, and consequently non-preservation of the ARI.

Although ARR (1987) has adopted the design event approach as a standard in Australia, it recognises these limitations, the importance of considering the probabilistic nature of flood producing variables and recommends further investigation.

1.2.2 Streamflow-Based Flood Estimation

Flood frequency analysis based on the statistical analysis of observed streamflow data at the design location provides an alternative to rainfall-based design methods for estimating the peak discharge for a given ARI. ARR (1987) describes a methodology for undertaking a valid flood frequency analysis using both graphical and analytical methods.

There are a number of advantages of this method of flood frequency analysis; the most important is that it provides a direct estimate of the discharge for a given ARI without the need to consider the conditional probabilities of other input parameters, as is needed for rainfall-based methods. The factors affecting flood magnitudes are incorporated directly into the observed flood data. Straightforward application of the method makes it a favourable option and computed confidence limits can provide an indication of the accuracy of the results. However, the application of this method for design is limited to situations where a sufficiently long and reliable streamflow record is available. Walsh (1991) showed that streamflow data is often unreliable, particularly for larger events that have required large extrapolations of the associated streamflow gauge rating curve. In addition, it is difficult to use or adjust data if the catchment or recording conditions change during the period of record. Uncertainty can also exist as to the actual or true form of the probability distribution that is applicable to the observed flood events. ARR (1987) recommend the use of the Log Pearson III distribution, although other distributions such as the Generalised Extreme Value (GEV) distribution have also been suggested (NERC, 1975).

1.2.3 Selection of Design Method

The length of rainfall records are typically greater than streamflow records and are more widely available. Therefore, the use of rainfall records in conjunction with a rainfall-runoff model generally allows more accurate flood estimates than those obtained from streamflow

records alone, particularly at sites where data is limited. Streamflow records of a moderate length (10 to 15 years) are desirable if reasonable design flood estimates are to be obtained using flood frequency analysis. However, some streamflow data of a shorter length is suitable for calibrating rainfall-runoff models. Another limitation with the use of streamflow data is that catchment conditions may vary over time due to land clearance, land use change, fire or stream regulation through the establishment of dams. It is difficult, sometimes impossible, to adjust streamflow data to compensate for these or similar changes (ARR, 1987), making the use of a flood frequency approach untenable. As climatic conditions generally remain stable over time, long records of rainfall data are considered more reliable. Therefore, rainfall-based flood estimation techniques are generally recommended and adopted.

1.3 Alternative Methods for Design Flood Estimation

Exploring possible improvements to the current ARR (1987) design approach is an obvious and logical step in developing a better design flood estimation technique because the design framework is already established and widely used. Previous improvements have generally aimed to address the uncertainty in estimating the various input parameters by providing better estimation methods. Irrespective of such research, improving parameter estimation does not overcome the basic limitation of the approach, that is, the assumption of equality between the probabilities of the rainfall input and flood output. While such developments are an easier first step for improvement, rather than the development of an alternative approach, continual research into a method with fundamental weaknesses that appear difficult to overcome, may not produce significantly improved results or a more robust approach. Therefore, alternative approaches have become more popular with research being undertaken into empirical, joint probability and continuous simulation approaches, which are discussed in the following.

1.3.1 Rainfall-Based Empirical Methods

Empirical models for design flood estimation use observed flows to derive coefficients that can then be incorporated into an equation to transform rainfall to runoff (James and Robinson, 1986). Using this approach, the effect of all physical variables on the ARI are incorporated into the coefficients as the flood of a given probability is directly linked with the rainfall of the same probability through a frequency analysis of both observed floods and rainfall (Walsh, 1991).

An example of this type of model is the Probabilistic Rational Method (ARR, 1987) where the runoff coefficient for a given ARI is calculated as follows:

$$C_Y = \frac{Q_Y}{0.278 A I_{t_c,Y}} \tag{1.1}$$

where:

C_Y = peak flow rate (m^3/s) at an ARI of Y years;

A = catchment area (km^2); and

I = average rainfall intensity (mm/hr) for a design duration of t_c and ARI of Y years.

This runoff coefficient is then used in a relationship, along with design rainfall of the same ARI, to estimate a peak discharge. The Probabilistic Rational Method is also an example of a regionalised method, which requires a network of streamflow gauges and a framework for transferring results to ungauged catchments. As the coefficients for the Probabilistic Rational Method in ARR (1987) have been determined for a limited range of catchment sizes and characteristics, extrapolation must be done with caution (ARR, 1987). Sufficient observed streamflow data is the biggest limiting factor in the use of such methods.

Empirical methods overcome the basic limitations of the design event approach through the automatic and lumped consideration of all flood affecting processes. However, since many physical processes are incorporated into a single coefficient (or a small number of coefficients) the design applications must be restricted to areas that fall within the range of conditions that were used to derive and calibrate the coefficient(s).

1.3.2 Joint Probability Approach

The joint probability approach to design flood estimation attempts to overcome limitations in the current ARR (1987) design method through a reduction in the uncertainty and bias surrounding the estimation of input parameters and the consequences of their interaction in calculating design floods. It has been acknowledged that the same peak flood could result from a moderate storm on a saturated catchment or from a large storm on a dry catchment (Weinmann *et al.*, 1998). Because this approach defines the input parameters as random variables, it allows for the consideration of all possible combinations of these parameter values, thereby eliminating the subjectivity in selecting input values and overcoming the need to assume that the correct design flood will be chosen from a single combination of parameters. Consequently, the resulting flood output is defined as a probability distribution

rather than a single value. The theoretical superiority of this approach, which once developed may lead to better and more consistent estimates of design flows, has been recognised by both ARR (1987) and other researchers.

The application of this approach requires the determination of probability distributions for the flood producing input parameters and then combines them with an appropriate rainfall-runoff model to produce the probability distribution of the flood output. The method of combining the input parameters to form the output is generally referred to as a derived distribution approach, which is a combination of deterministic and stochastic hydrologic modelling (Laurenson, 1974). The adopted distributions and any assumed correlation structure for the input parameters define the stochastic elements of the method, while the transformation of these inputs into outputs using a rainfall-runoff model forms the deterministic aspect. A derived probability distribution can be obtained using either analytical or approximate (discrete or simulation) methods as outlined below.

Analytical Methods

Analytical methods involve applying principles of probability to derive a probability distribution of the peak streamflow. The cumulative density function of the peak streamflow is determined by enumeration if the probability distributions of the input parameters are discrete, or by integration if they are continuous (Rahman *et al.*, 1998). The main advantage of this approach is that the effects of the various flood producing input parameters on the resulting ARI can be clearly distinguished in the final set of equations.

Eagleson (1972) produced one of the first analytical methods for obtaining a derived probability distribution of peak streamflow from probability distributions of catchment and climate characteristics, by way of a kinematic runoff model in an idealised V-shaped flow plane. Limited applicability, due to simplified assumptions, has led to modifications and extensions by researchers including Wood (1976) who incorporated random variability in the antecedent catchment moisture conditions, showing the importance of this parameter and the effects of its variability. Hebson and Wood (1982) indicated that the extension of this model to larger catchments may not be possible due to complex flow equations. Poor results were shown in studies conducted by Moughamian *et al.* (1987) and Cadavid *et al.* (1991).

Another analytical method involves the use of a Geomorphologic Unit Hydrograph (GUH), which is an Instantaneous Unit Hydrograph (IUH) and a probabilistic model describing the

movement of a randomly placed water droplet through a catchment (Hebson and Wood, 1982). The model is parameterised in terms of Horton's order laws and Strahler's stream-ordering system, which together provide a systematic description of the topological order exhibited by most natural catchments (Hebson and Wood, 1982). The concept and methodology behind a GUH, relating catchment response to basin geomorphology, has been employed by a number of researchers (Rodriguez-Iturbe and Valdes, 1979; Gupta *et al.*, 1980; Rodriguez-Iturbe *et al.*, 1982a; 1982b) as it is believed to have more promise for modelling large and complex catchments. Hebson and Wood (1982) investigated the possibilities of using a GUH with the effective precipitation model of Eagleson (1972) to study the effect of catchment scale and shape on flood frequency characteristics, achieving reasonable success with the method for two catchments. Diaz-Grandados *et al.* (1984) also utilised the GUH but with the Philip (1957) representation of the infiltration process, again applying the method to two catchments with reasonable results. Extensions to this work have been undertaken by a number of researchers including:

- Wood and Hebson (1986) with a study of flood frequency similarity between catchments;
- Sivapalan *et al.* (1990) in a study on the interrelationships between the processes that underlie the event response in catchments of different scales and physical characteristics as reflected in flood frequency distributions; and
- Troch *et al.* (1994) in an investigation into which processes dominate runoff in a small catchment and the sensitivity of flood frequencies to various model parameters.

While most research has presented the use of the GUH positively, Moughamian *et al.* (1987) found that small errors in the rainfall input parameters and the rainfall-runoff models produced significant errors in the derived flood frequency curves and suggested that the method required fundamental improvements before it can be used in practice with confidence.

Raines and Valdes (1993) were able to improve on the GUH research by using the U.S. Soil Conservation Service (SCS) curve number for the infiltration model but also suggested that improvements were required. The SCS method was also used by Haan and Edwards (1988), who extended work by Haan and Schulze (1987), to provide a methodology for combining rainfall probabilities and the probabilities of various antecedent conditions for estimating the return periods of flows. The SCS method was used to estimate the runoff and maximum rainfall loss with flood frequency curves determined from the joint probability density

function of these variables.

The feasibility of any of the analytical approaches depends on the rainfall-runoff model used and the availability of simple stochastic models for the input parameters so that the derivations are analytically tractable (Rahman *et al.*, 1998). However, this may not be possible when analytical methods are applied to complex catchments.

Approximate Methods

Approximate methods are generally used when an analytical approach becomes too mathematically complex. Approximation is carried out using either:

- discrete methods, where the continuous distributions of input parameters are approximated by discrete distributions and the Theorem of Total Probability is used to obtain a derived frequency distribution; or
- simulation techniques, where random samples are drawn from continuous distributions of input parameters and the resulting outputs are used to determine a derived frequency distribution.

Discrete methods have been used by a number of researchers including Laurenson (1974), Russell *et al.* (1979), Ahern and Weinman (1982) and Fontaine and Potter (1993). Beran (1973) used a combination of the discrete and simulation methods. Simulation techniques have also been utilised by Muzik (1993), Durrans (1995) and Rahman *et al.* (2001).

Laurenson (1974) suggested using a transformation matrix to represent the deterministic components of a system, which would allow the conversion of an input probability distribution to an output probability distribution. This method was applied to calculate frequency distributions of peak outflows from a combination of the frequency distribution of peak inflows and storage contents. A similar application was carried out by Ahern and Weinmann (1982) who used the method to combine the frequency distributions of rainfall and rainfall loss to obtain a frequency distribution of peak flows. This method was found to be more robust than the selection of single representative values for input parameters.

Russell *et al.* (1979) considered the stochastic nature of event rainfall and of the parameters characterising catchment response to produce a methodology for calculating design flows. The Clark runoff model was used to transform rainfall into rainfall excess, and three model parameters, namely, the time of concentration (T), a storage constant for a linear reservoir (R)

and an infiltration function (I), were all assumed to be independent random variables. The continuous distributions for these variables were obtained from observed data and discretised. Seven values of T, nine of R and three of I were used to obtain 120 reasonable parameter combinations. The infiltration rate was assumed to be constant for any particular event. The probabilistic nature of rainfall properties (duration, depth and temporal pattern) were described using the observed variability of the 60 largest complete events contained in 15 years of historic data. Streamflow hydrographs were then generated from all the possible combinations of rainfall and catchment conditions with the peak flows used to determine the conditional probabilities of 50 specified flows.

Fontaine and Potter (1993) defined a method for calculating the exceedance probability of a given flood using joint probability relationships between extreme rainfall and antecedent moisture conditions. Discrete probability distributions of the antecedent moisture conditions were represented by three curve numbers of the SCS method, a simplified assumption for the use of this method. The joint probability relationship with extreme rainfall was then calculated by using a rainfall-runoff model (HEC-1) that simulated floods resulting from all significant combinations of the two variables.

Beran (1973) used a discrete method combined with a simulation component to derive a flood frequency distribution. Continuous distributions of rainfall duration, temporal pattern and catchment wetness index (CWI) were discretised to allow each variable to assume one of a finite number of possible values, each with a probability weight attached. A unit hydrograph method for catchment response was used in conjunction with 12 values of duration, 36 temporal patterns and 12 values of CWI. The simulation technique sampled all possible ways in which an event with an ARI of *Y* years may cause a flood and derived its probability distribution. The procedure followed a rainfall-based design process but instead of an arbitrary choice at each step, the choice was made from a selection of values, each with a frequency proportional to its probability of occurrence (probability weight). It was observed that small changes to the CWI produced large variations in the resulting floods and a CWI chosen close to the median of the distribution yielded peak discharges five percent greater than expected. Overall, the derived curves were much flatter than the observed, indicating that the observed flood frequency distribution was severely underestimated. There is also a question as to the validity of this approach as it determines a probability distribution of event duration from complete events, but then uses published Intensity-Frequency-Duration (IFD)

curves, which are determined from rainfall bursts, to determine rainfall depth.

Muzik (1993) used a modified SCS curve number method to determine rainfall loss and hence runoff. For each simulation the total rainfall amount (P) was chosen randomly from a Gumbel distribution. A Log Pearson III distribution was used to represent the initial rainfall loss (I_a) and the five day antecedent rainfall (P_5), with the maximum potential loss (S) determined from a conditional relationship between S and P_5. These parameters were used to transform P into the rainfall excess depth (P_e), which was then transformed deterministically into streamflow using a dimensionless unit hydrograph. A Monte Carlo simulation was then used to derive a synthetic flood frequency curve, which was capable of reasonably predicting runoff. It was concluded that even if the true distribution of the input variables such as P_5, S and I_a are not exactly known, the effects of their variation within physically realistic limits can be assessed and considered using a Monte Carlo simulation. The use of a Monte Carlo simulation to study flood probabilities was emphasised by Muzik (1993) as a superior approach for statistically fitting probability distributions to observed flows.

Durrans (1995) presented a simulation procedure for determining a flood frequency curve for regulated catchments. The procedure used Monte Carlo techniques to sample the unregulated annual flood peak and volume, the dimensionless initial reservoir depth and the dimensionless gate opening area from defined distributions. The hydrograph was then routed through the reservoir and the process repeated thousands of times to obtain outflow hydrograph peaks, which were used to empirically define the regulated flood frequency distribution. This process was also suggested as a method that could be used to empirically quantify the joint distribution of both regulated flood peaks and volumes.

Rahman *et al.* (2001) developed a Monte Carlo simulation technique for deriving flood frequency curves and applied it to three Victorian catchments. It was based on a joint probability approach and considered the probability-distributed nature of various input parameters and their inter-dependencies to determine design flood probability distributions. The modelling framework used existing loss models and runoff-routing models as deterministic elements to simulate a derived flood frequency curve. Rainfall duration, intensity, temporal pattern and initial loss were treated as random variables of probability distributions. However, in order to use the existing Intensity-Frequency-Duration (IFD) information of intense rainfall bursts, the analysis was undertaken in terms of *storm-cores*, which are defined as "the most intense rainfall burst within a complete storm". A storm-core

duration was assumed to follow an exponential distribution and IFD curves were developed based on a partial series of storm-core events. A storm-core temporal pattern was randomly selected from an observed set of storm-core patterns, with the storm-core initial loss assumed to follow a beta distribution. A simple runoff-routing model, consisting of a single non-linear storage located at the catchment outlet, was calibrated and used in conjunction with an average value for baseflow to generate a streamflow hydrograph. The peaks of all simulated hydrographs were then used to determine a derived flood frequency curve. This curve was shown to be sensitive to the choice of rainfall intensity distribution, temporal pattern representation and initial loss distribution. While the method was reported to give reasonable estimates for flood frequencies up to an ARI of 1 in 100 years, it was stated that further work was needed before the procedure could be adopted by industry for practical use for design.

Rahman *et al.* (1998) carried out a detailed review of joint probability approaches for design flood estimation. This review recognised that a large amount of research has been undertaken into the derivation of flood frequency distributions from the joint consideration of flood producing input parameters. However, most of these applications have not been considered for their practical application to routine design, particularly in light of the model complexities, difficulties in parameter estimation and limited flexibility in the approach.

1.3.3 Continuous Simulation

Continuous simulation provides a promising alternative to the methods so far discussed and has the potential to address the limitations of the current ARR (1987) design approach, which are discussed in Section 1.2. The aim of continuous simulation is to effectively describe the major processes responsible for converting catchment rainfall inputs into flood outputs. Using inputs from rainfall, potential evaporation and other climatological data, the rainfall to runoff process is then simulated for long periods from which outflow hydrographs are generated. One of the important components of the method is a continuous water budget model that eliminates any subjectivity in the selection of initial loss as the conditions antecedent to each storm event are known and the effects of these are included in the continuous time series of flows. Other positive aspects of the method are that it overcomes the problem of critical event duration as the resultant outflows are simulated for all events (Lumb and James, 1976). Frequency analysis of the flow can also be undertaken by statistically analysing the time series of the model, as opposed to assuming an equal probability of floods based on the causative rainfall (Huber *et al.*, 1986).

The application of a continuous simulation method requires adequate modelling of soil moisture balance, long records of rainfall and evaporation as well as a representation of any correlation between input parameters (Lumb and James, 1976; Ahern and Weinmann, 1982; James and Robinson, 1986). The method uses input variables that have a lesser potential to introduce bias and uncertainty but involves a more complex modelling process (Linsley and Crawford, 1974; Rahman *et al.*, 1998). As such, less research has been done in this area.

A recent development by Boughton (2000a) and Boughton *et al.* (1999, 2000) involved the use of a continuous simulation approach of design flood estimation for several Victorian catchments. Newton and Walton (2000) also applied this approach to a Western Australian catchment. The approach involved a transition probability matrix model for the generation of daily rainfall sequences that were disaggregated into hourly values. The Australian Water Balance Model (AWBM) was then used to convert this rainfall into rainfall excess, explicitly accounting for losses. A single, non-linear concentrated storage model was developed to route this rainfall excess to the catchment outlet and determine the resulting outflow hydrograph. A comparison of the average flood frequency distribution from ten simulations with the observed flood frequency distribution demonstrated the potential of this approach to overcome some of the estimation limitations of existing design flood methodology.

1.3.4 Summary of Alternative Design Flood Estimation Methods

The alternatives for estimating design floods and flood frequency curves that have been discussed generally involve rainfall generation, runoff determination and hydrograph formation. Differences exist in how each phase is implemented and how the flood producing input parameters are treated. The rainfall generation phase uses the input parameters of event duration, event intensity/depth, temporal distribution and areal distribution. In most studies, including the current ARR (1987) design event approach, event intensity or depth is considered as a random variable. The stochastic nature of other input variables has been considered in more recent research. All these variables are inputs to the runoff phase, where the transformation of rainfall to rainfall excess is determined. This is a deterministic process. The rainfall excess is the main input into a routing model to obtain a streamflow hydrograph, with some routing models also requiring the addition of baseflow in the routing process. The major factor affecting hydrograph production is the adequacy of the routing model to represent the physical processes that describe catchment response.

1.4 Rainfall Loss Models for Design Flood Estimation

It has been established that the value of rainfall loss assumed during the conversion of rainfall to rainfall excess strongly influences the magnitude and shape of the flood hydrograph (Keifer and Chu, 1957; Cordery, 1970a; Beran, 1973; Walsh, 1991; Nandakumar *et al.*, 1994; Rahman *et al.*, 1998). To achieve significant improvement for design flood estimation, a method for appropriately selecting or calculating rainfall loss needs to be developed.

The *loss* during an event refers to the rainfall that does not appear as direct runoff. This includes all processes associated with interception by vegetation (interception loss), percolation into soil (infiltration), surface storage retention (depression storage), loss through the streambed and banks (transmission losses) and evaporation. This rainfall loss exhibits both temporal and spatial variability. When modelling or describing losses they are usually categorised as occurring either before or after surface runoff commences. Losses may occur after rainfall has ceased but this is extremely difficult to quantify.

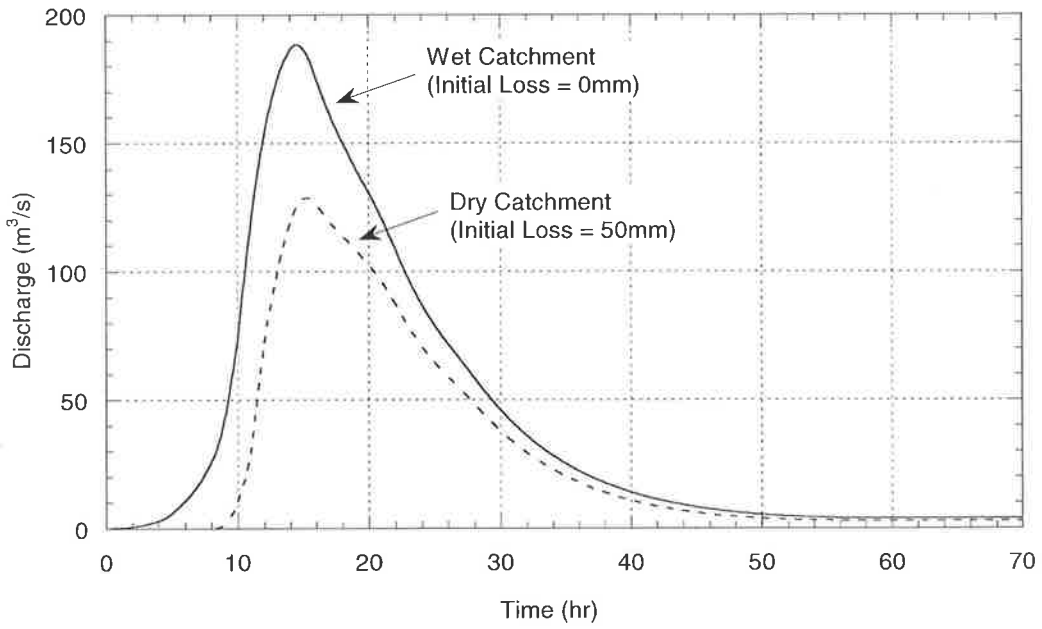

Figure 1.2 The effect of catchment wetness.

Catchment antecedent moisture conditions, and hence the assumed value of *initial loss* (the loss that occurs before the commencement of runoff) produces a stronger influence on runoff than the loss that occurs after runoff commences. Figure 1.2 shows how a given rainfall on a dry catchment can produce significantly less runoff than the same rainfall on a wet catchment.

Aside from rainfall intensity, the appropriate choice of loss and in particular initial loss is considered the most important design flood input parameter (Beran, 1973; Rahman *et al.*, 1998). Some of the different approaches that have been used to model rainfall loss and hence initial loss are presented in the following.

1.4.1 Point Infiltration Loss Models

As discussed above, many processes and mechanisms contribute to rainfall loss. Because of the difficulty in defining equations and obtaining meaningful parameter estimates from limited data, most models do not consider each mechanism separately, but consider the total loss as infiltration into the soil. A number of the previously discussed derived distribution studies have utilised this type of loss representation, the most basic of which assumes a constant infiltration rate for all events. This was used by Eagleson (1972), Russell *et al.* (1979) and Hebson and Wood (1982). Wood (1976) also used a constant infiltration rate for any particular event but allowed it to vary between events.

Other infiltration models attempt to incorporate a reduction of the infiltration rate/capacity with time using empirical equations (Horton, 1933), or analytical solutions to complex equations for the water movement in the soil (Green and Ampt, 1911; Philip, 1957). Figure 1.3 represents this type of model.

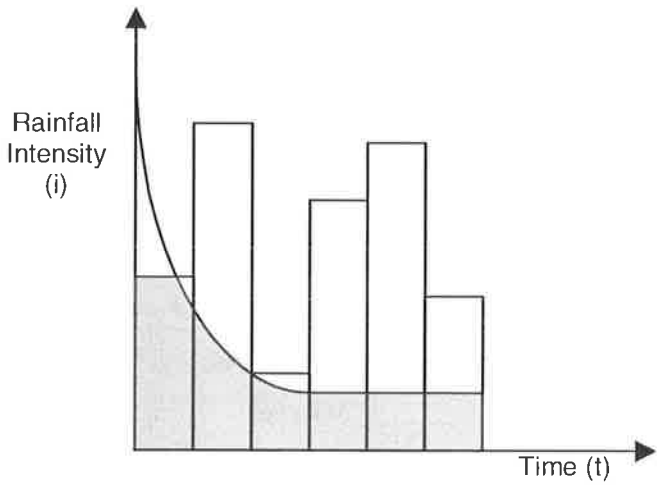

Figure 1.3 Infiltration curve model.

The *Horton* (1933) model for infiltration, as defined by Chow *et al.* (1988) is:

$$f(t) = f_c + (f_0 - f_c)e^{-kt} \tag{1.2}$$

where:

$f(t)$ = infiltration rate at time t (mm/hr);

f_0 = initial infiltration capacity (mm/hr);

f_c = final infiltration capacity (mm/hr);

t = time (hr); and

k = exponential decay constant (hr^{-1}).

This describes the rate of decrease in infiltration capacity to a constant value over time, and is only applicable under shallow ponded conditions. It has been extended to improve the representation of the infiltration process for conditions where the infiltration rate is less than the maximum at the commencement of an event (Bauer, 1974; Akan, 1992; Nandakumar *et al.*, 1994). However, it has still been used in its original form by researchers including Ormsbee (1989) to investigate the effects of rainfall disaggregation procedures on design flood estimation, and by Walsh and Pilgrim (1993) to obtain design flood estimates with reasonable success. In addition, the Horton model is used for the infiltration component of the ILSAX model (O'Loughlin, 1986), which is commonly used in Australia for urban stormwater design.

The *Green and Ampt* (1911) infiltration model, as defined by Nandakumar *et al.* (1994) is:

$$f(t) = K_s \left(1+\frac{M\psi}{F(t)}\right) \tag{1.3}$$

where:

$f(t)$ = infiltration rate at time t (mm/hr);

K_s = saturated hydraulic conductivity (mm/hr);

M = initial soil moisture deficit (vol/vol);

ψ = capillary suction at the wetting front (mm of water); and

$F(t)$ = cumulative infiltrated volume from start of event to time t (mm).

This was developed through the application of Darcy's Law under ponded conditions, constant matric potential and uniform moisture content and conductivity.

Mein and Larson (1973) showed that this could be adapted to predict the volume of infiltration prior to the occurrence of ponded conditions, where the rainfall intensity may be less than the infiltration capacity of the soil, and also to model infiltration under steady

rainfall. Chu (1978) and Mein (1980) both showed the model can be applied with variable intensity rainfall with Chu (1978) obtaining good agreement between predicted rainfall excess and observed runoff for a number of events. James *et al.* (1992) applied the Green-Ampt model and the SCS curve method to 23 events over seven catchments and concluded that the Green-Ampt model is preferable for high rainfall depths. Hill (1998) applied the model to nine catchments and reported that while the results were adequate they were not on average superior to those obtained using simplified conceptual loss models, which are discussed in Section 1.4.2.

The *Philip* (1957) infiltration model is a series solution to the physically based mathematical model of flow in porous media of Richards (1931), and is defined by Chow *et al.* (1988) as:

$$f(t) = \frac{1}{2} S t^{-\frac{1}{2}} + K \tag{1.4}$$

where:

$f(t)$ = infiltration rate at time t (mm/hr);

S = sorptivity (mm/hr);

K = hydraulic conductivity (mm/hr); and

t = time (hr).

The model applies to an homogeneous soil of uniform initial moisture content with ponded conditions at the surface (Nandakumar *et al.*, 1994), and has been combined with various catchment runoff-routing models to derive flood frequency distributions by Diaz-Granados *et al.* (1984), Sivapalan *et al.* (1990) and Cadavid *et al.* (1991).

In many cases it is possible to define the processes that contribute to rainfall loss at a point on the catchment but becomes more difficult when trying to estimate a representative value of loss for an entire catchment. The point infiltration models described above may fail to adequately simulate actual catchment losses because of the spatial variability of the physical runoff generation mechanisms (Nandakumar *et al.*, 1994). Even for small catchments there is often large variations in catchment characteristics associated with topography, vegetation and soils, as well as the distribution of rainfall during any particular event. This makes it difficult to determine the appropriate parameters to use in a point model and hence determine the link between physical catchment characteristics and rainfall loss.

1.4.2 Conceptual Loss Models

To overcome the limitations of point infiltration models, losses can be defined as part of a conceptual loss model. There are two main types of conceptual loss models, lumped and distributed, both of which are applied at a catchment scale.

Lumped Loss Models

Lumped models are based on a spatial averaging over the catchment or sub-catchment and consequently are functions of time only. Model parameters are estimated using the total catchment runoff, which does not consider the separate variations of processes within the catchment on an individual basis. While defined as functions of time, the actual temporal patterns of the losses are not considered and catchments are assumed to have uniform loss and evaporation characteristics. There are a number of lumped loss models used to form the basis of current runoff process models used for flood estimation. The use of these conceptual loss models is often preferred over mathematical equations for infiltration, particularly for design applications, because of their ability to approximate whole of catchment runoff behaviour (Nandakumar *et al.*, 1994).

The *constant loss model* assumes that the rainfall excess is the residual after a constant rate of loss is reached (Figure 1.4).

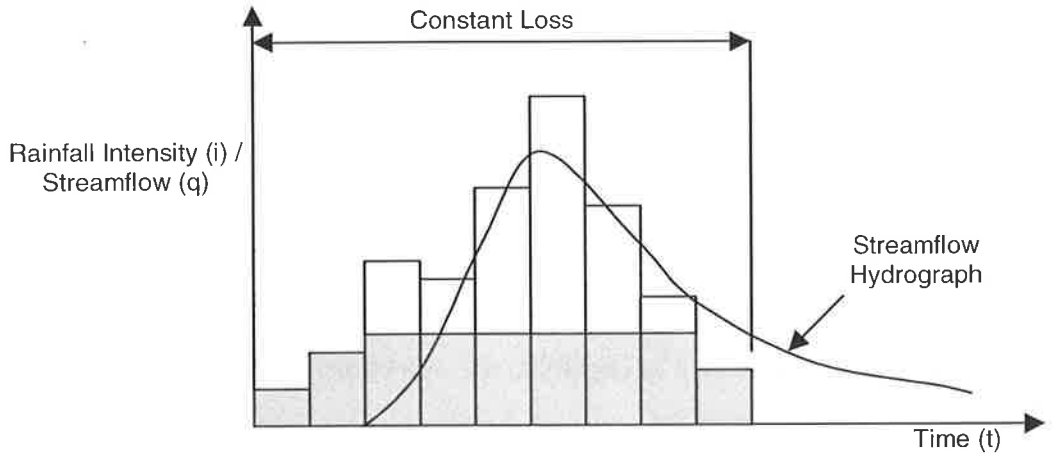

Figure 1.4 Constant Loss Model
(adapted from Hill *et al.*, 1996a).

This model has not been widely used in design applications because it is not considered sufficiently complex to fully describe the actual loss processes (Nandakumar *et al.*, 1994). However, it has been applied in areas having high runoff and low losses, such as the Kimberly

region of Western Australia (Flavell and Belstead, 1986).

The *initial loss-continuing loss model* is one of the most commonly used loss models in Australia (ARR, 1987; Hill *et al.*, 1996a; 1996b; Hill, 1998) and has been used in design flood estimation studies by Flavell and Belstead (1986), Walsh (1991), Hill *et al.* (1996a, 1996b) and Rahman *et al.* (2001). Shown in Figure 1.5, the initial loss is the loss that occurs prior to the commencement of surface runoff and is assumed to be composed of the interception loss, depression storage and infiltration that occurs before the soil surface becomes saturated. The model assumes that no runoff occurs until a given loss volume has been reached, regardless of the rainfall intensity. The continuing loss is assumed to be a constant average rate of loss throughout the remainder of the event.

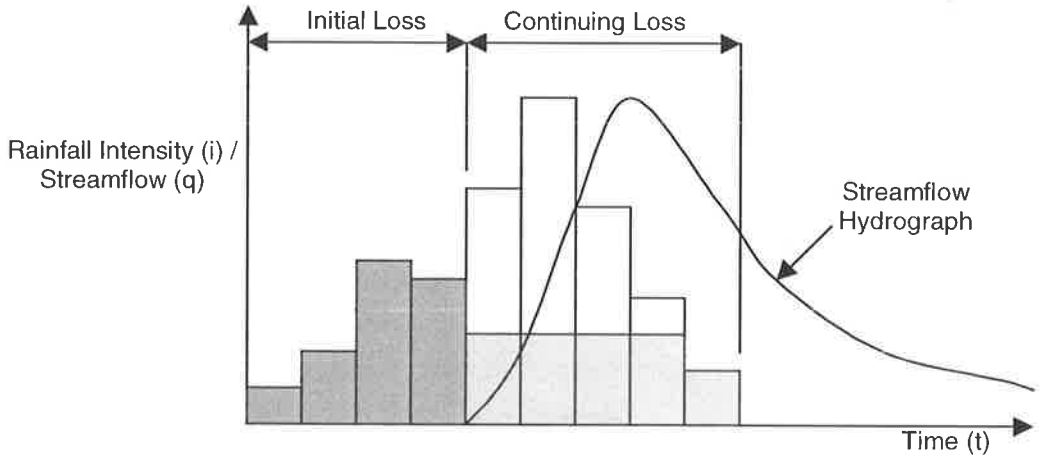

Figure 1.5 Initial Loss-Continuing Loss Model
(adapted from Hill *et al.*, 1996a).

The model is consistent with the concept of runoff being produced by infiltration excess, that is, runoff occurs when the rainfall intensity exceeds the infiltration capacity of the soil. Although the model is physically acceptable, the selection of an appropriate initial loss component is often arbitrary and the constant continuing loss rate is a simplification of the physical infiltration decay process. Loss values have been determined for both initial loss and continuing loss from a limited number of studies and are contained in ARR (1987). ARR (1987) states that the large range of values may only be applicable for about 40% of Australia. For locations where design loss rates have not been obtained, ARR (1987) recommends the use of loss values for regions that have similar characteristics. However, ARR (1987) also cautions on the use of these values for areas where they were not calibrated because of

complex interactions between climate, vegetation and geology. Nandakumar *et al.* (1994) supports this by suggesting that research has demonstrated difficulties in obtaining relationships between catchment characteristics and the median continuing loss rate, which indicates that the transposition of loss values between "similar" catchments may not be appropriate.

The *initial loss-proportional loss model* has been developed in recent years (Harvey, 1982; Flavell and Belstead, 1986; Dyer *et al.*, 1994; Nandakumar *et al.*, 1994), based in part on its consistency to the theory of the saturated overland flow runoff generating mechanism. This model assumes that runoff is generated from the saturated portions of the catchment, with the saturated area dependent on the duration and severity of the event. The initial loss is again the loss that occurs prior to the commencement of surface runoff and the proportional loss is assumed to be a constant fraction of the rainfall after surface runoff has commenced (Figure 1.6). For simplicity, the proportional loss value is usually taken as a constant for a catchment, rather than for an event (Hill *et al.*, 1996a).

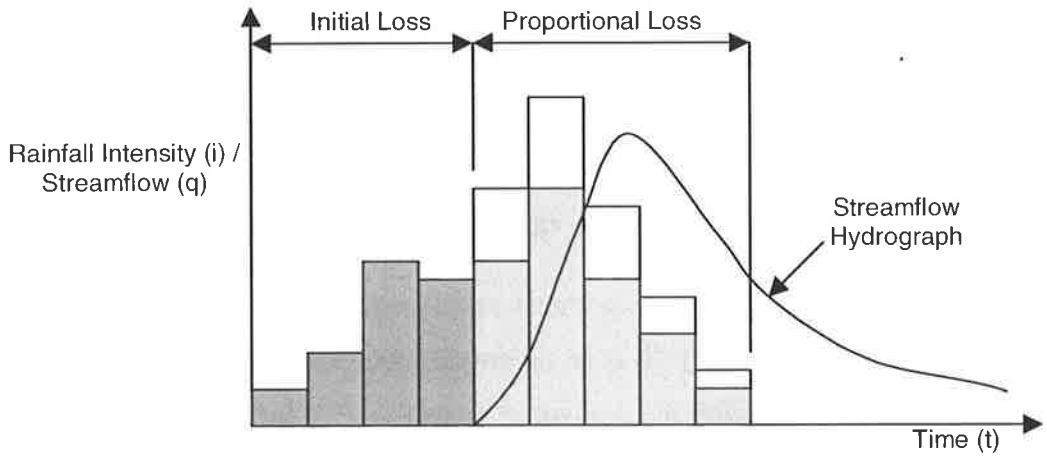

Figure 1.6 Initial Loss-Proportional Loss Model
(adapted from Hill *et al.*, 1996a).

Hill *et al.* (1996a) suggested that while this loss model was theoretically superior for catchments where runoff is predominantly generated by saturated overland flow, the lack of guidance in ARR (1987) for the selection of suitable values for proportional loss reduces its potential for use in design without further investigation. Hill *et al.* (1996a) found the initial loss-proportional loss model to be inferior for estimating design events. However, Harvey (1982) found that this model performed well in south Western Australia while Flavell and

Belstead (1986) used it to derive design losses. Dyer *et al.* (1994) found the model performed better than the initial loss-continuing loss model when fitting the RORB model to observed streamflow hydrographs for 24 catchments.

A limitation of the model is that the loss proportion is assumed to remain constant for the entire length of the event and that this proportion is often used for all events. This has led to the development of a *variable proportional loss model* (Siriwardena and Mein, 1995; Siriwardena *et al.*, 1997; Hill, 1998) to describe the change in runoff producing areas during events, by using pre-event baseflow to indicate the antecedent wetness of a catchment. The separation of initial loss is not required and as rainfall occurs the size of the saturation area of the catchment increases, resulting in an increased proportion of rainfall contributing to runoff. A disadvantage of the method is that the use of baseflow to determine antecedent wetness is only valid when baseflow occurs in measurable quantities, as is the case for the predominantly Victorian catchments that have been tested. Its use for many Australian catchments that are ephemeral is questionable. It is also questionable for use on catchments with high levels of sustained baseflow as the pre-storm baseflow will not necessarily be a good indicator of catchment wetness (Hill, 1998). The method was unable to account for the changes in catchment wetness during dry periods, often leading to overestimation of runoff coefficients towards the end of protracted events (Hill, 1998). Finally, as the model was based on the analysis of complete events rather than intense bursts it is therefore currently incompatible with the properties used in the current ARR (1987) design method.

The *SCS curve number method* rainfall-runoff relationship was developed by the US Soil Conservation Service (1972, 1985). It is an empirical procedure that aims to provide a set of curves (Figure 1.7) for estimating the amount of runoff from rainfall based on the soil type, antecedent moisture condition, land use treatment and hydrological condition of the catchment (Nandakumar *et al.*, 1994).

Achieving appropriate flood estimations using these curves is sensitive to the choice of rainfall curve number, the selection of the appropriate antecedent moisture conditions and the method for estimating the time of concentration (Walsh, 1991; Nandakumar *et al.*, 1994). Haan and Schulze (1987), Haan and Edwards (1988), Raines and Valdes (1992) and Fontaine and Potter (1993) used the method for deriving flood frequency distributions, but ARR (1987) and Nandakumar *et al.* (1994) have reported poor results when applied to Australian catchments.

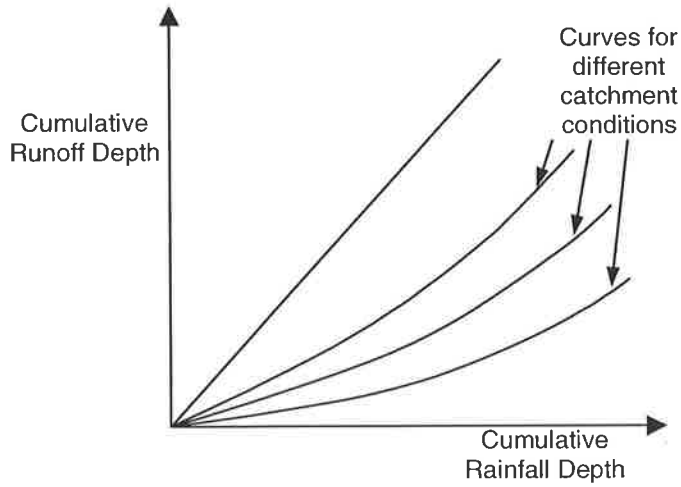

Figure 1.7 SCS curve number method
(adapted from Nandakumar *et al.*, 1994).

Titmarsh *et al.* (1989) carried out extensive testing of a similar method on 140 catchments in Eastern Australia using alternative curves. The alternative probabilistic curve numbers were derived to ensure that peak discharges estimated from design rainfall were equal to peak discharges determined from a frequency analysis of observed floods. Curve numbers derived in this manner were shown to produce reasonable design flood estimation and improved on the estimation made using the standard SCS methods.

The *antecedent precipitation index (API)*, also called the *catchment wetness index (CWI)* is a measure of the antecedent conditions of a catchment that govern infiltration loss and baseflow. Mein *et al.* (1995) defines this index as:

$$API_0 = P_0 + P_1 K + P_2 K^2 + \cdots + P_n K^n \qquad K < 1 \qquad (1.5)$$

where:

K = recession factor; and

P_n = daily rainfall, n days antecedent to the rainfall event.

Fontaine and Potter (1993) and Beran (1973) have used this index as an input for design. Beran (1973) developed a probability distribution for the API, which was calculated from the soil moisture deficit and a five-day antecedent precipitation index determined from observed daily rainfalls. Cordery (1970b, 1971) developed a relationship between initial loss and API for New South Wales catchments, which, when combined with daily rainfall, was used to determine the potential initial loss for every day of the rainfall record. These daily values were then used to calculate the median potential initial loss for the catchments.

Distributed Loss Models

None of the conceptual lumped models can handle the dynamic and spatial nature of rainfall excess of a catchment during a rainfall event or throughout the year, as the effect of catchment variability on runoff generation is not explicitly taken into account. This has led to the development of distributed models. Distributed models are functions of both space and time that consider the location at which loss is occurring. However, for these types of models to be utilised an enormous amount of catchment information data is required. This effectively precludes their application to flood estimation in Australia due to the limited data available.

1.4.3 Probability Distribution of Initial Loss

Some effort has been directed towards determining probability distributions for initial loss. Most probability distributions that have been developed have been based on an analysis of complete events rather than bursts. Haan and Schulze (1987) derived a probability distribution for maximum potential initial loss using observed rainfall data, runoff data and SCS curve number. Fontaine and Potter (1993) derived a probability distribution of antecedent soil moisture from observed daily rainfall data. Rahman *et al.* (2001) used a beta distribution to represent the initial loss from storm cores.

1.4.4 Discussion

Many of the loss models discussed above have difficulties or limitations when applied to design flood estimation. The main difficulty is the need to estimate the level of initial loss. Most estimates have been derived from a study of complete events. However, design rainfall intensities and temporal patterns have been derived from intense rainfall bursts, which leads to incompatibilities between input parameters within the process. This was highlighted by Rigby and Bannigan (1996) and Hill and Mein (1996c). ARR (1987) also suggests that since antecedent rainfall will pre-wet the catchment, losses derived for complete events will tend to be too high for application to bursts. Rahman *et al.* (2001) has been one of the first to consider the relationship between initial loss based on a burst and initial loss based on an event.

Hill and Mein (1996c) stated that "it is unlikely that separate analyses of the component factors which are used to calculate design floods will produce estimates which match observations." For this reason, a new approach has been investigated to eliminate the need to

examine or calculate the initial loss component for engineering design flood estimation.

1.5 PROPOSED DESIGN FLOOD ESTIMATION APPROACH

There have been two main approaches to design flood estimation developed for Australian catchments in recent years, the joint probability approach of Rahman *et al.* (2001) and the continuous simulation approach of Boughton (2000a). While both models show potential to overcome existing design flood estimation difficulties, neither retains the simple procedure of the current design techniques. This study seeks to develop an approach that improves the existing design flood estimation techniques, but at the same time retains the basic design methodology to enable the method to be readily used for routine design applications.

1.5.1 Methodology

The main area that is targeted for improvement is rainfall loss estimation, by eliminating the need to estimate a value or distribution for the initial loss. Figure 1.8 outlines the methodology used to achieve this aim and involves:

(a) use of a continuous simulation model of rainfall to generate synthetic rainfall data at the finest resolution possible. The critical requirements of the rainfall model is to be able to represent:

- the inter-event time (the interval between one event ending and another beginning is the time during which evapotranspiration can occur);
- the event duration (this partially determines the beginning and end of the infiltration process);
- the event intensity (this ultimately limits the maximum level of runoff that may be generated and the water available for infiltration and groundwater recharge); and
- the internal event characteristics (temporal distribution).;

(b) use of a continuous simulation model of evaporation, conditioned on daily rainfall, which generates synthetic evaporation data. A stochastic evaporation model is used because evaporation is an important controller of the antecedent soil moisture conditions that in turn affects the rainfall excess produced during an event;

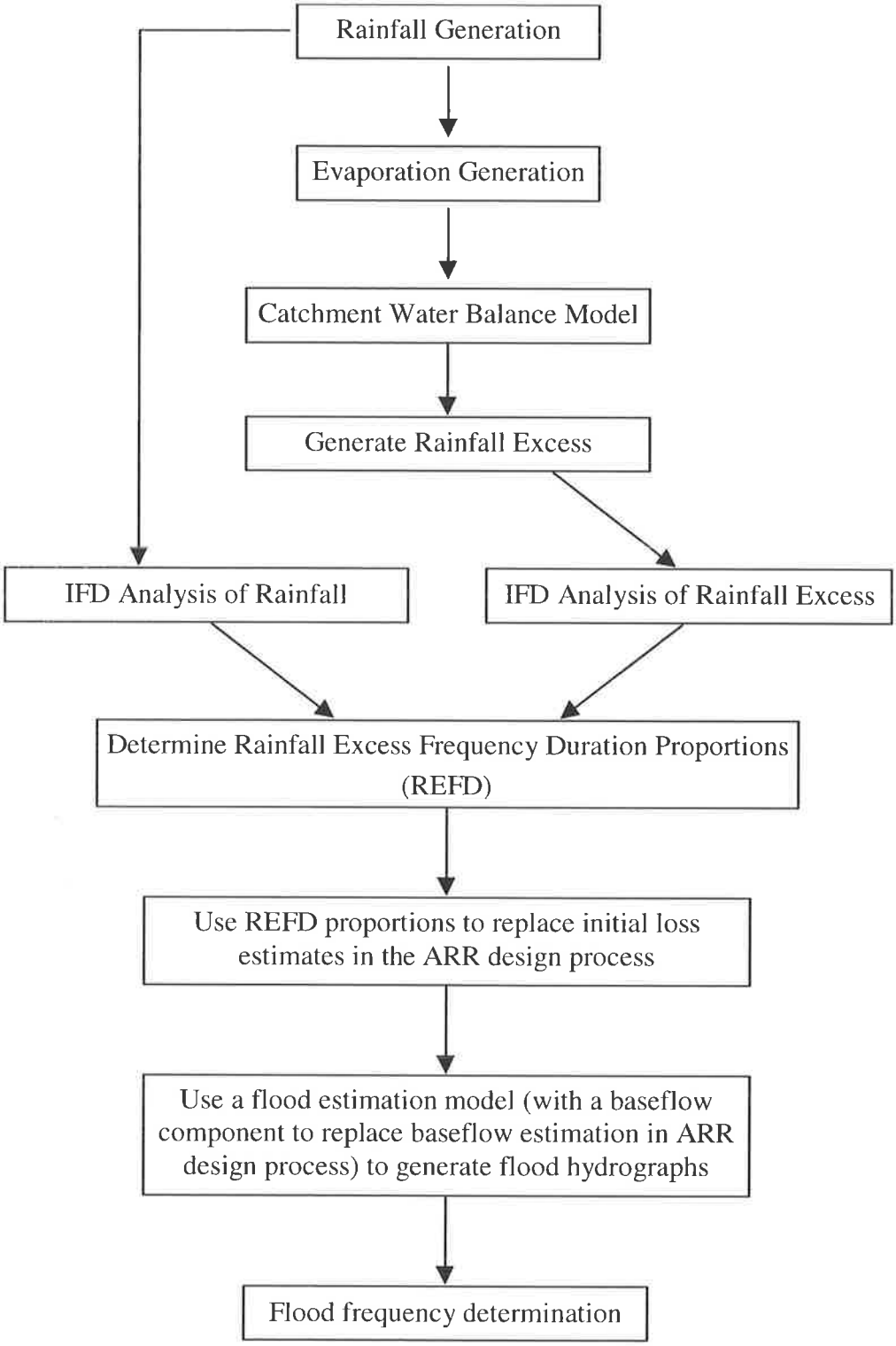

Figure 1.8 Methodology for developing an improved design flood estimation approach.

(c) use of a conceptual catchment water balance model with the rainfall and evaporation models as inputs to continuously simulate rainfall loss and rainfall excess;

(d) an IFD analysis of the rainfall input to produce a series of curves that describe the probabilistic nature of rainfall intensity, dependent upon duration;

(e) an IFD analysis of the rainfall excess output to produce a series of curves describing the probabilistic nature of rainfall excess dependent upon duration;

(f) a probabilistic description of rainfall excess that is dependent upon rainfall intensity and duration obtained by developing a relationship between the rainfall IFD curves and the rainfall excess IFD curves. The factors used to describe these relationships are called the Rainfall-Excess-Frequency-Duration (REFD) proportions and indicate the proportion of rainfall that will become rainfall excess for an event with a particular ARI; and

(g) validation of the approach. It is envisaged that these REFD proportions can be used directly with the current design flood estimation methodology. The REFD proportions are combined with design rainfall and temporal patterns and used as input to a flood estimation model to determine a flood frequency distribution. To remove the requirement of selecting values of design baseflow, a flood estimation model with a baseflow component was used to route the rainfall excess to the catchment outlet. The calibration of the flood estimation model to observed events determines the parameters governing baseflow and as such there is no need to estimate baseflow values for the design ARI.

1.5.2 Routine Design Flood Estimation

While this study uses continuous simulation techniques to develop REFD proportions, eliminating the need to select values of initial loss, continuous simulation is not practical for routine design flood estimation. Figure 1.1 shows the current ARR (1987) design flood estimation method, which requires the estimation of initial loss. Figure 1.9 shows how this procedure can be modified with the incorporation of the REFD proportions.

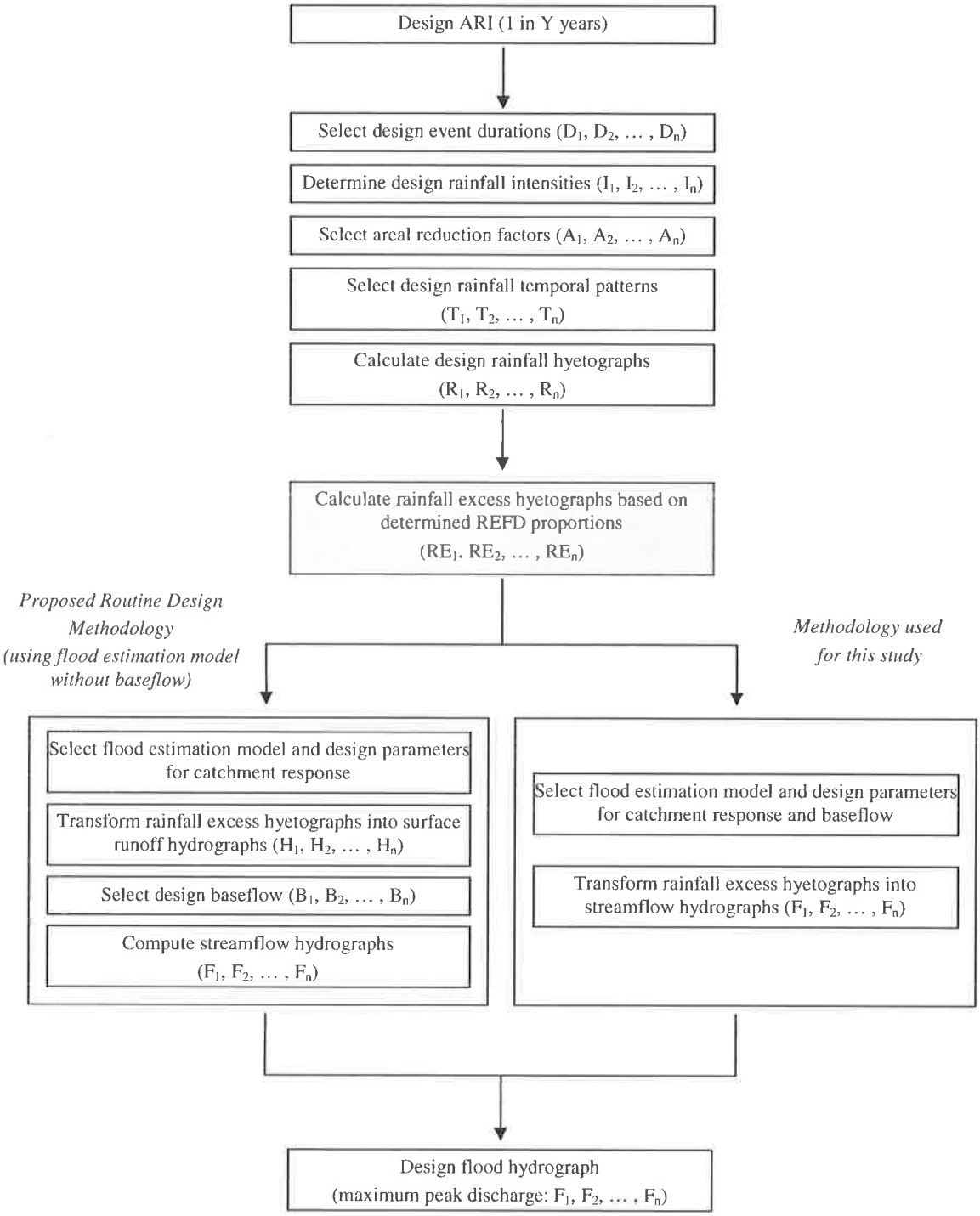

Figure 1.9 Proposed routine design methodology.

For routine design flood estimation the generation of design rainfall occurs as outlined in Section 1.2.1. Then, instead of selecting a design initial loss value, the REFD proportions are used to convert the design rainfall directly to design rainfall excess. The remainder of the design rainfall is assumed to infiltrate into the soil. With the use of the REFD proportions, the proposed design methodology can follow one of two paths. The left hand path shows the standard process as used in ARR (1987) where the rainfall excess is routed to the catchment outlet and design baseflow is added to the surface runoff hydrograph to determine the streamflow hydrograph. The right hand path shows the methodology that was used in this study, which used a flood estimation model with an infiltration and sub-surface flow component to eliminate the need to select a design value of baseflow. This allowed the surface runoff hydrographs to be transformed directly into streamflow hydrographs. A flood frequency distribution can then be determined.

1.5.3 Study Outline

In the following chapter, a number of stochastic rainfall models are investigated to determine the best possible options for use in this study. This review highlighted the difficulties in obtaining a reliable rainfall model that could adequately reproduce the observed statistical properties of rainfall at a variety of time scales. As such, an alternative stochastic rainfall model was developed and validated, which has the potential to be used for a wide variety of purposes in addition to the current study. This is discussed in Chapters 3 to 5. Following this, methods for generating potential evaporation for use in the calibration of a catchment water balance model and a model to stochastically generate evaporation were examined, as discussed in Chapter 6. The developed model is then linked with the stochastic rainfall model.

A number of catchment water balance models were reviewed to select an appropriate model. Of these, one was chosen. Chapter 7 describes the chosen model and the modifications made to better reproduce observed runoff records. The model was then calibrated to a number of study sites. Chapter 8 outlines the use of the stochastic rainfall and evaporation models as input into a continuous catchment simulation. The synthetic rainfall and rainfall excess was then analysed and REFD proportions determined. These were then used in conjunction with the current design flood estimation approach to derive a flood frequency distribution. Comparisons with observed flood records were used to validate the approach. Conclusions from this study and recommendations for future research are provided in Chapter 9.

2. REVIEW OF RAINFALL GENERATION MODELS

Rainfall is the major factor that affects the volume of runoff from a catchment. During design flood estimation, the rainfall intensity directly controls the maximum peak flow that can occur. Rainfall is therefore an important quantity and needs to be accurately represented. This chapter considers the requirements of a rainfall simulation model for engineering design flood estimation and then reviews a number of existing models for this purpose. The review of these is then used to support the development of a new stochastic model suitable for the continuous simulation used in this study.

2.1 REQUIREMENTS OF RAINFALL SIMULATION MODELS FOR DESIGN

The generation of rainfall is characterised by three basic phases, namely the creation of saturation conditions in the atmosphere, a cooling phase (change of water vapour to liquid) and the growth of small water droplets to precipitable size (Eagleson, 1970). The dynamic, thermodynamic and cloud microphysical processes all operate and interact on a variety of scales (microscale, mesoscale and synoptic) resulting in a highly non-stationary and time-space variable process that could be considered chaotic. The numerous and complex atmospheric processes that lead to rainfall make it one of the most difficult meteorological phenomenon to model or predict.

Deterministic models assume that from the present state of a system the future characteristics of the system, in this case rainfall, can be predicted with certainty. Due to numerous deficiencies in the current knowledge of atmospheric physics attempts to deterministically model rainfall have met with limited success. Therefore, for engineering design purposes deterministic models are of limited practical use, which has led to the development of stochastic rainfall models. Stochastic models assume that from the present state of a system, the probability of a future state of this system can be determined. Cho (1985) argued that the assumption that rainfall can be described as a stochastic process is justified and is of more practical use than deterministic models.

A stochastic approach to rainfall generation is considered the most effective method for providing an engineering description of rainfall. The following presents a discussion of

stochastic models used to model rainfall. It is important that the model can replicate a variety of observed statistical characteristics, including extreme events, as these determine the design rainfall levels and the aggregated statistics as these control the water balance.

The majority of stochastic rainfall models developed to date have been point models, representing the essential observed features of the rainfall time series at a single location. The general theory of point processes is outlined by Cox and Isham (1980), with a detailed summary of the mathematical structure of these processes and their use in rainfall models provided by Waymire and Gupta (1981a, 1981b, 1981c). Several approaches have dominated the development of point rainfall models, with each approach based on alternative assumptions for modelling the rainfall process, these being:

(a) the use of a point process or a *marked* point process where intensity and/or duration is assigned to each event. The rainfall process is described as a continuous point process with an assumed underlying rainfall pattern consisting of sub-events, which when super-imposed attempt to model the aggregated historical rainfall record. Parameter estimates are usually obtained using aggregated historical rainfall records and inferring the properties of the underlying sub-events from observed discrete data. Some event-based calibration has also been undertaken. Single point process models based on the Poisson process and its subsequent generalisation to produce clustered point process models are the most commonly used;

(b) the use of Markov time-series methods with a discrete time scale. The assumption is made that successive intervals are not independent and the model predicts the "state" (wet or dry) of an interval based on the previous interval(s). The use of transitional probability matrices or fitted Markov chains are employed to predict the wet and dry states, with a separate distribution used to determine rainfall depth during the wet intervals. Procedures using Markov processes and transitional probability matrices have also been developed for continuous time scales; and

(c) The assumption of an event-based nature of rainfall that consists of alternating dry and wet periods. Independent events are identified in the historical data as sequences of rainfall separated by more than a specified minimum inter-event dry period. Probability distributions are used to describe the rainfall occurrence for the length of the dry (inter-event) periods, the wet (event duration) periods and the depth/intensity

of each event. Once the total event rainfall has been modelled it is redistributed over the duration of the event, defining internal temporal characteristics.

These three approaches were considered to be the most suitable type of model needed for this study and are discussed in more detail in the following section. Particular attention is paid to each model's potential to reproduce extreme statistics such as Intensity-Frequency-Duration (IFD) statistics, a feature that is essential for flood estimation applications and design. Also, as these statistics are not generally used during calibration they provide a valuable check on the credibility of a model. Attention is also given to the ability to represent the aggregated statistics at a variety of time scales. It is important that a model has the ability to reproduce the statistics of the temporal structure of rainfall at other levels of aggregation in addition to that at which it was calibrated.

2.2 SINGLE POINT PROCESS MODELS OF RAINFALL

Point rainfall can be considered as "a random time series of discrete storm events which under certain restrictions may be assumed to be mutually independent and in which the average time between events is large with respect to the average duration of the events themselves" (Eagleson, 1978b). By examining the restrictions for mutual independency, synthetic rainfall sequences can be simulated by modelling the data as a series of individual events. Stochastic models using the Poisson process in conjunction with varying representations for event depth have been developed to do this.

The Poisson process (Ang and Tang, 1975) assumes that an event can occur randomly at any point within a continuous time scale and that the occurrence(s) of an event in a given time interval (δt) is statistically independent of an event in any other non-overlapping interval. The probability of an occurrence in δt is proportional to the size of δt and can be given by $\nu \delta t$, where ν is the mean rate of occurrence of the event (assumed to be constant). A series of single Poisson arrivals has been widely used to describe a process for the temporal evolution of independent rainfall events. These are generally *marked models* and have been developed with models of intensity with varying complexity.

The least complex of these models is shown in Figure 2.1. Event duration and depth are described by an instantaneous burst of intensity (U_i) and hence the inter-event time (t_a) is the

time between these bursts. A two-parameter gamma distribution (Todorovic and Yevjevich, 1967) and an exponential distribution with annually periodic mean depth (Todorovic, 1968; Todorovic and Yevjevich, 1969) have been used to model U. Through calibration to observed independent events at hourly and daily time scales it was shown that there is a loss of statistical information about the rainfall events with these relatively large scales. Use of a smaller time unit is important, particularly when considering floods from small catchments.

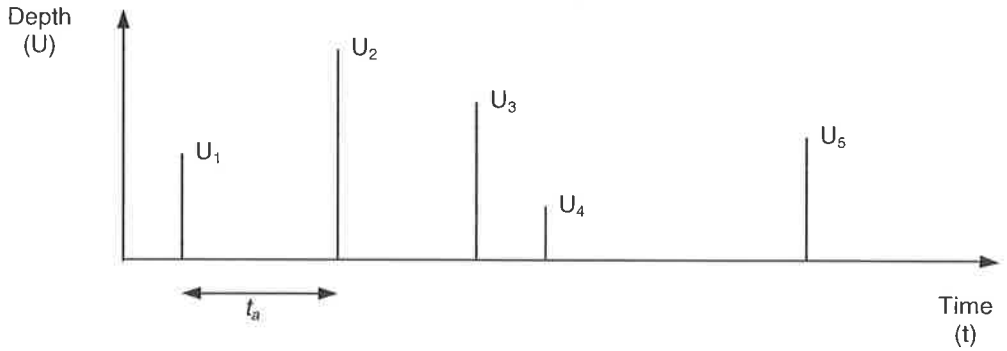

Figure 2.1 Single Poisson Arrival Model / Poisson White Noise Model (adapted from Rodriguez-Iturbe *et al.*, 1984).

In contrast to Todorovic and Yevjevich (1969), Rodriguez-Iturbe *et al.* (1984) derived equations for the second-order moments for aggregated rainfall and used these to estimate ν and the parameters for U. The model, named the Poisson White Noise (PWN) model, was fitted to hourly and daily data for each month. Analysis of model performance showed that the PWN model was inadequate for representing the rainfall process at either time scale and that the estimated model parameters were dependent on the scale at which the rainfall process was described and can not be transformed to other scales.

Eagleson (1978b) suggested that the rainfall occurrence pattern could be modelled as a sequence of non-overlapping rectangular pulses. Grayman and Eagleson (1969) and Eagleson (1972) combined a marked point process of Poisson arrivals with independent and identically distributed (exponentially) random variables for the event duration (t_d) and average intensity (i) of each event. This model, referred to as the Independent Poisson Marks (IPM) model, was calibrated using independent events. Eagleson (1978b) produced a similar model (Figure 2.2) but explicitly defined the inter-event time (t_a) by an exponential distribution and assumed a two-parameter gamma distribution for the event depth (Todorovic and Yevjevich, 1967; Ison *et al.*, 1971). This was calibrated using independent events from ten-minute data

and used successfully to generate frequency curves for annual rainfall.

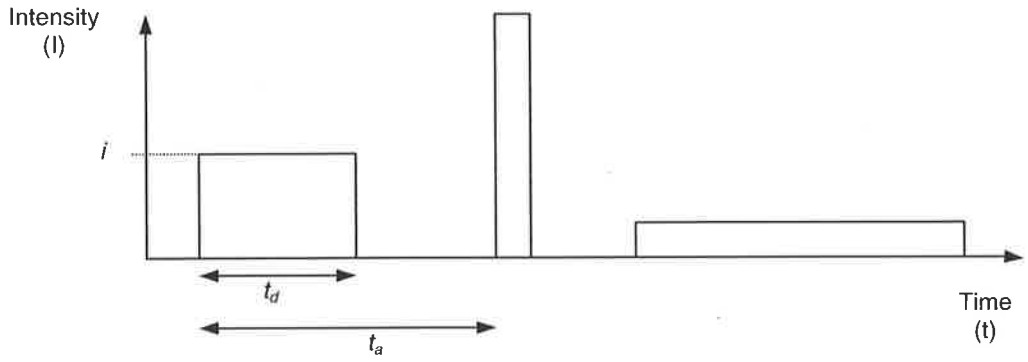

Figure 2.2 Independent Poisson Marks (IPM) Model
(adapted from Eagleson, 1978b).

The IPM model has been used to derive flood frequency distributions (Carlson and Fox, 1976; Hebson and Wood, 1982; Diaz-Granados *et al.*, 1984; Beven, 1987). Using the exponential, gamma and bivariate exponential distributions for t_d and i, Bacchi *et al.* (1989) and Burlando and Rosso (1993) analysed the performance of this model type in simulating Intensity-Frequency-Duration (IFD) statistics. Only the bivariate exponential model showed satisfactory results. However, Burlando and Rosso (1993) suggested that a more complex formulation for a model of the rainfall process is required.

The Poisson Rectangular Pulses (PRP) model (Figure 2.3), similar to the models of Eagleson (1972) and Eagleson (1978b), was studied in detail by Rodriguez-Iturbe *et al.* (1984, 1987a, 1987b).

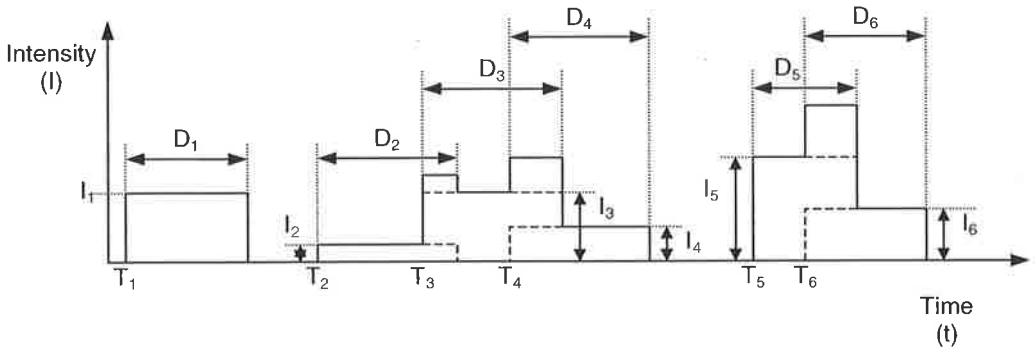

Figure 2.3 Poisson Rectangular Pulses Model
(adapted from Rodriguez-Iturbe *et al.*, 1984).

Poisson arrivals denote the occurrence of rainfall events (T_i), each with duration (D_i) and intensity (I_i). The model allows these events to overlap producing a superimposed event with varying intensity. This allows calibration to be performed using aggregated records without the need to determine independent events. Statistical comparisons indicated reasonable results, but the overall model performance needed improvement. As for the PWN model, it appeared that the structure of statistical dependence was closely linked to the time scale of the aggregated record.

Burlando and Rosso (1993) showed theoretically that there was no improvement in the estimation of extreme events by using the PRP model in preference to the IPM model. It was also suggested that as the above Poisson models do not provide an adequate description of the natural rainfall process through a continuum of scales, nor provide a real description of the internal structure (variation of intensity) of an event, that "their use should be confined to applications where a simple mathematical structure is requested in order to derive analytically the properties of the processes which are mainly driven by rainfall, than to simulation problems". To better define the internal structure of events clustered point process models for rainfall have been developed that by their nature, effectively produce a disaggregated event.

2.3 Clustered Point Process Models of Rainfall

Clustered point process models are an extension of the Poisson arrival process. The general structure begins with a point process mechanism generating a series of cluster centres or *storm origins*, which define the location of rainfall events within a continuous time interval. For each storm origin a series of points or *rain cells* are formed by a subsidiary process and distributed at or following the storm origin in a specified way. The process then consists of the superposition of these separate clusters of rain cells to define the overall event. Assigning a rainfall cell to the storm origin varies between models.

Models of rainfall based on clustered point process models have been developed in part for the purpose of aggregating and disaggregating temporal rainfall records through a continuum of scales (Burlando and Rosso, 1993). Le Cam (1961) first produced a stochastic description of rainfall using the cluster process approach. Since then, a great deal of research has been undertaken utilising this methodology, particularly using the Neyman-Scott (N-S) and Bartlett-Lewis (B-L) processes.

2.3.1 The Neyman-Scott Point Process

The Neyman-Scott (N-S) point process was developed to model the spatial variation of galaxies by Neyman and Scott (1958) and has been used to model earthquake phenomena (Vere-Jones, 1970). Kavvas and Delleur (1975) first applied this process to rainfall by investigating a Neyman-Scott White Noise (N-SWN) model (Figure 2.4). This model assumes that each storm origin (T_i) arrives according to a Poisson process and has an associated number (C_i, $C_i \geq 1$) of rain cells from an assumed distribution. The distance of each rain cell from T_i is an independent and identically distributed random variable ($X_i = \{X_{i,1}, X_{i,2}, \cdots, X_{i,C_i}\}$). No rain cell is located at T_i and each cell has depth defined by a random variable ($U_i = \{U_{i,1}, U_{i,2}, \cdots, U_{i,C_i}\}$), representing an instantaneous burst.

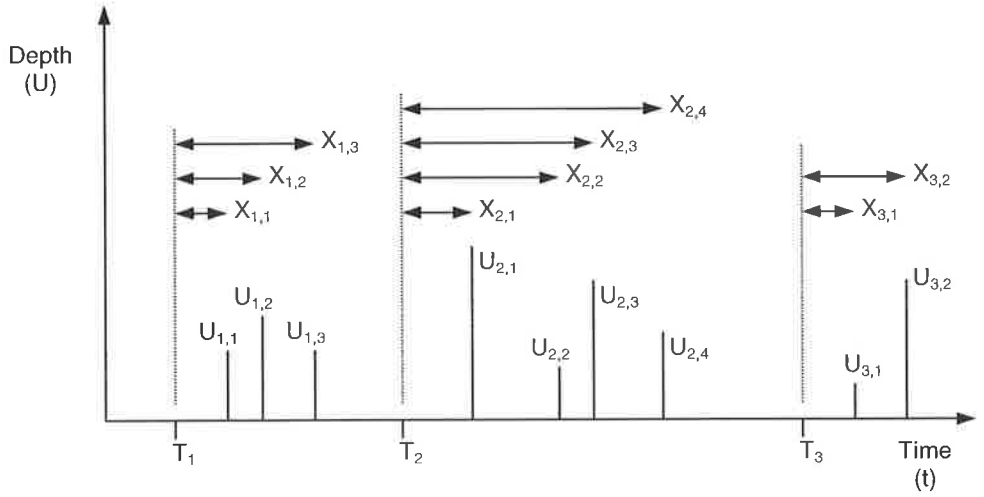

Figure 2.4 Neyman-Scott White Noise (N-SWN) Model
(adapted from Rodriguez-Iturbe *et al.*, 1984).

Kavvas and Delleur (1975, 1981), using a geometric distribution for C and a negative exponential distribution for X_i, showed that the exceedance probabilities of a N-S process fitted equally well or better than those of the Poisson models. However, while the N-SWN may have the potential to preserve the explicit dependence structure and marginal probabilities of the rainfall process, it was explained that because it was developed without any seasonal component, it is only of practical use for stationary rainfall occurrences. Extending the work of Kavvas and Delleur (1981), Rodriguez-Iturbe *et al.* (1984) derived the second-order moments for the aggregated rainfall data. Describing X_i as an exponential

distribution and calibrating to hourly and daily data, the model was shown to provide a more appropriate representation of the rainfall process than the PWN and PRP models.

Foufoula-Georgiou and Guttorp (1986, 1987) analysed event-based data and concluded that the application of the N-SWN model should be restricted to the time scale of the available aggregated rainfall record. The previous research suggested that this scale dependency applies to any rainfall model with instantaneous bursts described by a N-S process, irrespective of the distribution or dependence structure of the bursts. The simplistic view of instantaneous rainfall bursts did not provide an adequate fit to some observed rainfall series and a more complex formulation is required. The above researchers stated that physically interpreting components of the rainfall model by describing a primary process (a frontal system) with a secondary process (rainbands), while appealing is untenable as these physical processes do not change with the discretisation scale. A sensitivity analysis of the choice of cluster size distribution by Foufoula-Georgiou and Guttorp (1986, 1987) showed the representation of this variable greatly influenced the characteristics of the generated rainfall sequences. A negative binomial distribution was shown to be more appropriate than either the geometric or Poisson distribution. While good agreement with observed rainfall was reported, the conclusion was made that as the N-S model does not provide an adequate description of the underlying rainfall generating mechanism and that the selection of one cluster size distribution over another based on physical considerations is not possible. This does not allow physical meanings to be associated to the model parameters.

2.3.2 The Bartlett-Lewis Point Process

The Bartlett-Lewis (B-L) point process was developed for traffic studies (Bartlett, 1963) and to predict computer failure times (Lewis, 1964). This process has been used by Rodriguez-Iturbe *et al.* (1987a) for modelling rainfall in a rectangular pulses model form (Section 2.3.3). The B- L process involves storm origins (T_i) arriving according to a Poisson process as with the N-S point process. However, for each storm origin a number of rain cells ($C_i, C_i \geq 1$) also arrive according to a separate Poisson process. Each event begins with the arrival of a rain cell at T_i. The intervals between successive rain cells ($X_i = \{X_{i,1}, X_{i,2}, \cdots, X_{i,C_i}\}$) are independent and identically distributed by an exponential distribution. The process of rain cell generation continues for each storm origin until a storm duration (SD_i), generally described by an exponential distribution, is reached.

2.3.3 Neyman-Scott and Bartlett-Lewis Rectangular Pulses Models

As mentioned above Rodriguez-Iturbe *et al.* (1987a) extended the N-S and B-L processes by attaching a rectangular pulse of duration ($D_i = \{D_{i,1}, D_{i,2}, \cdots, D_{i,C_i}\}$) and intensity ($I_i = \{I_{i,1}, I_{i,2}, \cdots, I_{i,C_i}\}$) to each rain cell, producing the Neyman-Scott Rectangular Pulse (N-SRP) and Bartlett-Lewis Rectangular Pulse (B-LRP) models (Figure 2.5 and Figure 2.6).

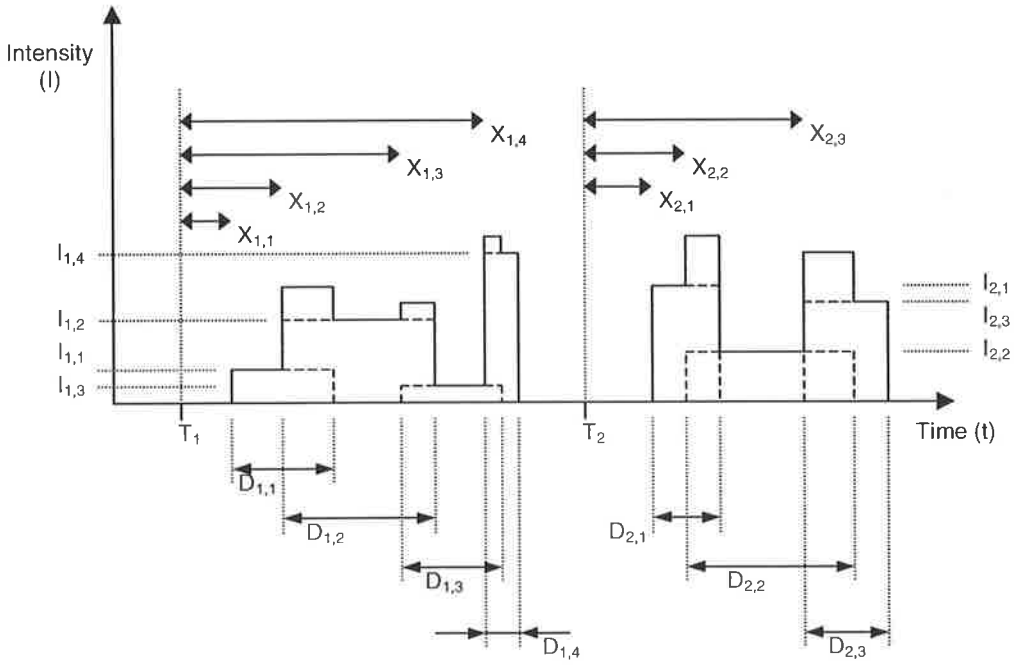

Figure 2.5 The Neyman-Scott Rectangular Pulses (N-SRP) Model.

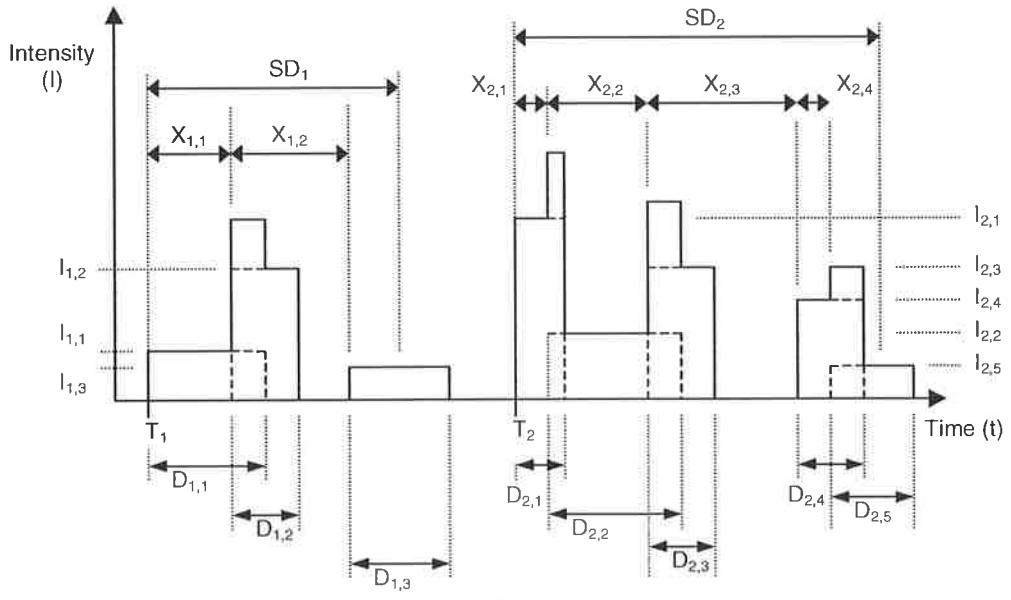

Figure 2.6 The Bartlett-Lewis Rectangular Pulses (B-LRP) Model.

These models provide a more realistic description of rainfall intensity and duration. D_i and I_i are generally described using exponential distributions which are independently associated with each rain cell and are independent of all other rain cells and storm origins. Both of these models are fitted to aggregated rainfall data, and the parameters for the distribution functions of D_i, I_i and C_i are the same for all events such that the stochastic description of the rectangular pulses is invariant.

Rodriguez-Iturbe *et al.* (1987a, 1987b) determined the second-order moments of the rainfall process for aggregated data for both the N-SRP and B-LRP models, and an expression for the probability of an arbitrary interval being dry for the B-LRP model. The distribution of C in the B-LRP model was assumed to be geometric, while Poisson and geometric distributions were suggested as alternatives in the N-SRP model. Rodriguez-Iturbe *et al.* (1987b) evaluated these alternatives and observed no significant difference between the models when applied to hourly data, from which it was concluded that a geometric or Poisson description had no general bias on the statistics. General overestimation of the proportion of dry intervals at aggregation levels greater than one hour was apparent, although both models adequately preserved other statistics at all aggregation levels (1 to 24 hours). Extreme values were reproduced satisfactorily for return periods of up to 20 years.

Burlando and Rosso (1993) compared the N-SRP and B-LRP models with the previously discussed Poisson models (Section 2.2) and concluded that the N-SRP and B-LRP models perform better at reproducing the continuous rainfall process. A fine temporal resolution of homogenous and stationary data is necessary for calibration, with the B-LRP model being very sensitive to data quality. An analysis of IFD statistics showed discrepancies at higher return periods. The N-SRP model overestimated for short durations and underestimated for longer ones, with the reverse for the B-LRP model. Similar results were found for the N-SRP model by Cowpertwait (1991a,b), who reported an overall underestimation of extreme events, particularly for return periods greater than ten years. Cowpertwait (1991a,b) derived an expression for the probability that an arbitrary interval is dry; results from the calibration to hourly data for each month suggested that improvement is required to satisfactorily reproduce summer dry spell sequences. Both Cowpertwait (1991b) and Burlando and Rosso (1993) concluded that the N-SRP model could not reproduce the probabilities and characteristics of small rainfall events. The latter suggested that this was one of a number of major limitations with the N-SRP modelling approach.

Analysis of rainfall data and characteristics by many researchers has shown a strong influence from climatic variations on the parameters of these models. Variations have been incorporated into the model structures of the N-SRP and B-LRP models to improve the approach and overcome model limitations. Rodriguez-Iturbe *et al.* (1988) modified the B-LRP model (MB-LRP) to incorporate variation into the structural characteristics of events. A gamma distribution was used to randomly vary the mean rain cell duration parameter between events. Application to hourly data showed improvements in reproducing the dry interval probabilities. However, historical extremes were shown to be severely underestimated for return periods greater than five years. The MB-LRP model appears to produce less satisfactory extremes than the B-LRP model of Rodriguez-Iturbe *et al.* (1987b). Islam *et al.* (1990) also calibrated the MB-LRP model to hourly data and the results suggested that the model-estimated statistics at various aggregation levels need improvement for both the dry interval probabilities and extreme value statistics.

Burlando and Rosso (1991) questioned the improvements to the B-LRP model (Rodriguez-Iturbe *et al.*, 1988; Islam *et al.*, 1990). Using hourly data it was shown that the MB-LRP model did not overcome the inadequacies of the B-LRP model. Comparisons with the N-SRP model showed a better performance than both the B-LRP and MB-LRP models. While the B-LRP model may allow for an easier mathematical framework and a larger availability of theoretical relationships for parameter estimation, the N-SRP has been shown to produce more satisfactory results if the parameters can be estimated accurately (Burlando and Rosso, 1991).

Entekhabi *et al.* (1989) also used a gamma distribution to randomly vary the mean rain cell duration parameter between events in the N-SRP model (MN-SRP). Using hourly data, the proportion of dry days compared favourably with historical records but improvements were needed in the simulation of extreme aggregated rainfall totals. Troch *et al.* (1991) applied the MN-SRP model to study rainfall characteristics of five-minute data, observing that the model performed poorly in preserving the historical dry interval probabilities.

In response to the varied results obtained using the MB-LRP model, Velghe *et al.* (1994) evaluated this model, together with the MN-SRP, N-SRP and MB-LRP models. Using hourly data, it was concluded that the modified models show improvement in the representation of the dry interval probabilities and historical extremes. However, due to higher complexities in parameter estimation, they do not preserve the second-order properties of the rainfall process

as well as the unmodified models. The importance of the distribution choice for C in both the N-SRP and MN-SRP models confirmed the work of Foufoula-Georgiou and Guttorp (1986, 1987). While the modified models show a general improvement in the representation of the rainfall series, they do not adequately reproduce the historical data, especially at higher return periods (greater than 15 years). It was emphasised that the improved results reported were based on one data set and that using other historical series, such as Islam *et al.* (1990) or Burlando and Rosso (1991), may produce different conclusions as to the suitability of cluster models for rainfall modelling. The B-L process and particularly the MB-LRP model was found to be very sensitive to the different sets of moment equations used for calibration, which is considered a drawback for applying this model in hydrologic simulation studies. Changing equations to improve the performance of one aspect of the model tends to be to the detriment of the performance in other areas.

In the application of the N-SRP model to sewer rehabilitation studies, Cowpertwait *et al.* (1996a, 1996b) used wet transition probabilities to produce considerable improvement to the reproduction of historical dry spell sequences and dry day proportions. However, in extreme value analysis poor results were shown, particularly for return periods greater than five years. An over-simplification in the parameterisation of the model was suggested as the possible cause. Cowpertwait (1998) addressed this issue by deriving a third-moment function and using a gamma distribution to define I_i. Using hourly data, improvements to the reproduction of extreme values and other statistics were shown.

In generalising the N-SRP model, Cowpertwait (1994) allowed multiple rain cell types to occur within the same event (GN-SRP(n), which indicates a generalised N-SRP model with n cell types). A GN-SRP(2) was investigated with the two cell types described as heavy short-duration cells and light long-duration cells. Using a geometric distribution with parameters varying over the year for C_i, the second-order aggregated properties were derived including a one hour wet transition probability. Overestimation of this probability was reported and it was emphasised that the practical implication of a consistent error such as this must be assessed before the model can be applied to actual hydrological problems. Extreme value analysis showed a satisfactory reproduction of the one hour extremes, but overestimation at the 24 hour level, particularly for return periods greater than five years. Comparisons with the N-SRP model show the GN-SRP(2) to be superior, but still requiring some improvement.

Onof and Wheater (1993, 1995) used a gamma distribution to randomise rain cell duration in the B-LRP model. Analytical results showed this random-parameter B-LRP (RPB-LRP) overestimated the auto-correlation statistics and mean inter-event times but improved the proportion of dry intervals. The simulation of hourly data confirmed these results. Major discrepancies with the average event duration and number of events per month were evident, as well as the overestimation of extreme values for return periods greater than two years. For some parameters, seasonal variation was applied using polynomials (up to degree 12). A two-stage optimisation was then applied to overcome major problems in parameter identification and this produced improvements to the average event duration. Onof and Wheater (1994b) incorporated monthly seasonality into this model and while it reproduced the observed rainfall depth statistics at all time scales, it showed poor temporal representation of events and overestimated the proportion of dry intervals.

Onof and Wheater (1994a) then applied a superposition of a jitter process on each rectangular pulse of the RPB-LRP model as a more realistic representation of the rainfall process to improve the overestimation of the auto-correlations (Onof and Wheater, 1993). A gamma distribution was used to represent D and improvements in the reproduction of extreme events and auto-correlations were achieved for hourly/daily data. Difficulties were encountered in estimating parameters and the development of methods to reduce the number of parameters was suggested.

Verhoest *et al.* (1997) examined the applicability of the B-LRP, MB-LRP and RPB-LRP models for design rainfall estimation. A severe underestimation of extreme rainfall events, particularly for shorter durations was reported in addition to an underestimation of event durations.

2.3.4 Combination Models

A number of researchers have combined the cluster models with other models. Morrissey and Krajewski (1993), using hourly data, showed that the N-SRP and the MN-SRP models were generally unsuited for modelling tropical rainfall. A new model, combining the properties of the N-SRP model with a PWN model, was developed. This was found to give more realistic representations of tropical rainfall and better reproduction of occurrence statistics.

Gyasi-Agyei and Willgoose (1997) combined the B-LRP model with an auto-regressive jitter

process, using 15 minute data, showing improved results for some aggregated statistics that were not used in calibration. However, aggregation levels greater than 24 hours were not examined and no IFD or extreme value analysis was reported. Gyasi-Agyei and Willgoose (1999) generalised this hybrid model by replacing the B-LRP model with a binary chain model (both B-L and Markov chains considered), reproducing various aggregated statistics over a range of time scales.

Istok and Boersma (1989) developed a Poisson cluster model with a negative exponential distribution for both T_i and C_i. An event is located at the start of each cluster. A non-stationary auto-regressive process described the hourly rainfall depths within events. The duration of events and time between events within clusters are described with identical logarithmic negative mixture distributions. Using hourly data it was shown that the model reproduces the seasonal pattern of the number of event occurrences, the auto-correlation functions and the marginal and conditional distributions for the event characteristics. However, the intensity was consistently overestimated and maximum event intensities require improvement.

2.4 Markov Time-Series Rainfall Models

2.4.1 Discrete Markov Chain Models

The assumption of independence between successive rainfall events is used in many rainfall models. The difficulty associated with determining independent events from historic records for model calibration increases with successively finer resolutions of data. The dependence between successive intervals increases with finer resolutions, such that at aggregation levels of 24 hours or less successive depths may not be independent. Because of the dependence between the states of successive intervals (dry or wet) and the assumption that the rainfall process can be described as a binary series (zero representing a dry interval, one representing a wet interval), one of the simplest probabilistic models capable of representing the process and any dependence structure is a Markov chain model.

A first-order Markov chain model, known as a simple Markov chain, is a discrete time-series approach where rainfall occurrence is described by a two state (wet or dry) series. It is used where the probability of the state at one time interval is clearly influenced more by the previous state than by the entire history of states, where the dependence is limited to the effect

of one time interval on the next (Wiser, 1965). The probabilistic structure is completely determined by its initial probability distribution and transition matrix. This transition matrix is defined by:

$$P = \begin{bmatrix} q_0 & p_0 \\ q_1 & p_1 \end{bmatrix} \tag{2.1}$$

where:

p_0 = the probability that the ith interval is wet given the (i-1)th interval is dry

= $pr[X_i = 1 | X_{i-1} = 0]$;

p_1 = the probability that the ith interval is wet given the (i-1)th interval is wet

= $pr[X_i = 1 | X_{i-1} = 1]$;

q_0 = $1 - p_0$;

q_1 = $1 - p_1$; and

i = $1, 2, \ldots .$

The present state of the interval i is dependent only on the state of i-1. The need to identify independent events is eliminated and the model is applicable at any time scale. The transition probabilities can be estimated using the equivalent proportions taken from the historical data.

Gabriel and Neumann (1962) were the first to develop and calibrate a two-state, first-order Markov chain model using daily rainfall sequences, extending earlier work by Gabriel and Neumann (1957). Many of the Markov chain models used have been first-order models and have been applied to determine the probabilities for wet and dry sequences (Weiss, 1964; Caskey, 1963; Hopkins and Robillard, 1964; Feyerherm and Bark, 1967; Smith and Schreiber, 1973; Haan *et al.*, 1976; Buishand, 1978; Stern and Coe, 1984). This has direct application for determining the probabilities of rainfall or drought regimes. Most of this research has been applied using daily data, although some hourly records have been used. Seasonality has generally been incorporated into the matrix probabilities for these and almost all other Markov chain models. Results have shown an inadequacy of the first-order Markov chain model to represent prolonged wet or dry sequences and even shorter sequence lengths of around seven days. They were also unable to adequately describe the number of wet days per month, with a tendency to underestimate wet day frequency in relatively dry months, and as a result, overestimate the proportion of dry days.

While many first-order Markov chains have not incorporated a model for depth, some have defined more than two states, one dry and the remainder wet with each wet state differentiated by increasing depths of rainfall. Alternatively, a separate model has been used to represent the depth of a wet state. The model of Haan *et al.* (1976) incorporated seven states, the sizes of which were found by geometric progression. Actual depths within the six wet states were determined using a uniform (states one to five) and shifted exponential distributions (state six). While the model satisfactorily reproduced the statistics of wet and dry sequences it overestimated rainfall amounts within each state.

In a second-order Markov chain, the state of i is dependent on the two previous states, i-1 and i-2 and so on for higher-order Markov chains. Higher-order Markov chain models have been used by Feyerherm and Bark (1967), Eidsvik (1980) and Stern and Coe (1984) to achieve improved results. Improvements have also been achieved by making extensions of the first-order Markov chain models. Wiser (1965) applied three modifications using Polya models to describe various levels of persistence through sequences of wet and dry days. Although higher-order chains may have produced similar outcomes, these modified models effectively specify relations between the parameters of the higher-order chains, thus reducing the total number of parameters that need to be estimated. Improvements were shown by fitting to sequences that were unable to be successfully fitted using a simple Markov chain.

Pattison (1965) suggested that the failure of a first-order Markov chain to describe the transition between sequences of wet and dry hours is because the occurrence of a dry hour at the end of a wet hour sequence is assumed to be the start of a sequence of dry hours. This may be unrealistic as there may be short periods of dry hours occurring within sequences of wet hours. A combination of a sixth-order and first-order Markov chain model was developed. If the state of the present hour t was wet, then the model used a first-order dependence to determine the state of hour $t+1$. However, if the state of the present hour t was dry, then the model used a sixth-order dependence to determine the state of hour $t+1$. A 20-state chain, with uniform depth distribution for each state was used. The analysis of rainfall cycles (cycles start after a six-hour dry period, continuing until the end of another six-hour dry period following rain) showed an overestimation of the inter-event times.

During comparisons with other models, Smith and Schreiber (1973) showed the Markov chain produced superior results than an independent Bernoulli model (Section 2.5.1) for modelling daily thunderstorm rainfall. It was concluded that while daily thunderstorm rainfall

may not occur as a simple Markov chain, some of the stochastic properties of this rainfall process can be adequately described. However, as with most applications of this model, problems with the representation of extended wet and dry sequences were apparent. Buishand (1978) compared the Markov chain model with an alternating renewal model (Section 2.5.2), reporting that the alternating renewal model gave better estimations of the proportion of short length dry sequences. However, in a similar comparison Woolhiser and Roldan (1982, 1986) found the first-order Markov chain model with a mixed exponential distribution for depth preferable for simulating daily rainfall.

Models incorporating more than two states are referred to as transition probability matrices as they do more than just determine whether the next interval is wet or dry. However, they are based on the same Markov matrix technique. Srikanthan and McMahon (1985) developed transition probability matrix (TPM) models for the generation of daily, hourly and six-minute data, applying these extensively to locations around Australia. The daily model consisted of a TPM with a maximum of seven states (one dry, up to six wet) for each month, the number of states determined using maximum likelihood techniques. Depths within each state were generated using a Box-Cox transformation with a normally distributed random variable for the largest wet state and a linear distribution for the other states. Comparisons of various statistics showed reasonable reproduction although improvement is required to adequately reproduce the monthly and annual means and standard deviations at many sites.

The hourly model used daily and hourly TPMs combined with a time dependent two-state second-order Markov chain. Using the daily TPM, the state (wet or dry) of the current day is determined and if wet, the type of wet day. Two types of wet days were defined based on a rainfall threshold and the time dependent Markov chain was used to model the rainfall occurrence probability over a day. Each wet day type had a set of hourly TPMs from which the hourly data was generated. Calibrating the model to each month required in excess of 1 000 parameters to be estimated. While reasonable reproduction of examined statistics was obtained, the results appeared less successful than the daily model.

The six-minute rainfall model consisted of a daily TPM with hourly second-order Markov chain, and both hourly and six-minute TPMs. Developed in a similar way to the hourly model but with various types of wet hours it produced reasonable results but underestimated the wet sequence statistics. The need to use even more parameters than for the hourly model limits the practical application of this model.

Boughton and Hill (1997) applied a variant of the Srikanthan and McMahon (1985) TPM method, using a log-Boughton distribution (Boughton, 1980) for the rainfall in the largest state, to provide daily rainfall inputs to a design flood estimation method based on continuous simulation. The model performed satisfactorily in relation to flood estimates but was unable to reproduce sustained dry periods, and thus did not preserve annual totals. Boughton (2000a) extended this approach by proposing that an empirical adjustment factor, based on the observed mean annual rainfall and the generated annual rainfall for a particular year, be applied to the daily totals produced by the TPM model of Srikanthan and McMahon (1985). The adjustment factor was found by trial and error and used to improve the underestimation of the observed standard deviations of annual totals produced by the model.

2.4.2 Markov Process Models

Green (1964) described the characteristics of a discrete daily rainfall sequence based on a continuous two-state Markov process. In the Markov process model the duration of successive dry and wet intervals are independent and exponentially distributed. Recursive formulas for the full set of first and higher order Markov chain transition probabilities for the daily process were derived. The model improved the first-order Markov chain model representation of observed daily rainfall.

From the work of Green (1964), Hutchinson (1990) developed a three-state Markov process with state 0 defined as a dry spell that is always succeeded by state 1, state 1 defined as a transition dry spell that is succeeded by either state 0 or state 2 and state 2 defined as a wet spell that is always succeeded by state 1. Three parameters describe the mean duration of each of the three states and the fourth the state transition matrix, which contains the probabilities that state 0 or state 2 will follow state 1. Due to the shorter mean durations of states 1 and 2 relative to state 0, the model produces rainfall events as a cluster of showers, similar to the clustered point process models. However, duration is incorporated directly into the model structure, which produces sequentially occurring showers without overlap. A mixed geometric distribution was used to describe the duration of dry periods. As in Green (1964), recurrence formulae for the probabilities of the length of wet sequences was derived and verified using hourly data. A two-parameter auto-correlated exponential intensity process was associated with the wet periods within each event. Although the distributions of wet periods were not as well matched as the dry periods, the model was shown to perform better than the B-LRP model.

Rajagopalan *et al.* (1996) presented a two state, first-order Markov model for daily rainfall occurrences, assuming a non-stationary transitional probability matrix with transition probabilities fitted using non-parametric techniques that varied over the year to account for seasonality. The model performance was verified using an analysis of the frequency structure of the events, with many statistics comparing well. A limitation of the non-parametric density estimation approach is the inability to extrapolate daily precipitation values beyond the largest recorded value.

2.5 EVENT-BASED MODELS

2.5.1 Independent Occurrence Models

The Bernoulli model is one of the simplest event-based stochastic models. The potential occurrence or recurrence of a rainfall event is evaluated through a sequence of repeated trials where there are only two possible outcomes to each trial (wet or dry). The trials are assumed to be statistically independent where the probability of one event in a time interval δt is p (constant probability of occurrence) and that the arrival of another event in this interval is negligible. The derivation of the basic sequence of Bernoulli trials leads to the use of a binomial distribution (Ang and Tang, 1975) to define the probability of having $X = x$ events in a total time $t = n * \delta t$.

Although a binomial model has been suggested for use in determining the design capacity of flood-control systems to withstand critical magnitude flood events (Benjamin and Cornell, 1970), it has not been extensively used for the identification of rainfall event sequences. Smith and Schreiber (1973) evaluated its use for this purpose, showing that the distribution did not provide an accurate model due to the inadequacy of the assumption of independent sequential rainfall events.

In many situations, including the modelling and subsequent simulation of rainfall, it is neither possible nor convenient to identify individual discrete trials to determine when events may occur. In addition, the independence assumption for successive rainfall events in the Bernoulli model is only valid for instantaneous arrivals (zero duration) as an event of finite duration may overlap into, and therefore reduce, the length of the subsequent interval.

2.5.2 Alternating Renewal Models

Alternating renewal models have a structure that explicitly models alternate wet and dry periods; the wet periods are referred to as events (Figure 2.7). The approach assumes independence between successive events. A minimum separation criterion is defined for the historical record to make this assumption valid for calibration. The rainfall process is defined completely by probability distributions for the dry inter-event times and wet event durations, together with a distribution for intensity/depth. The simulation process then samples alternate inter-event times and event durations from the probability distributions. For each event, the total depth is distributed using a disaggregation scheme.

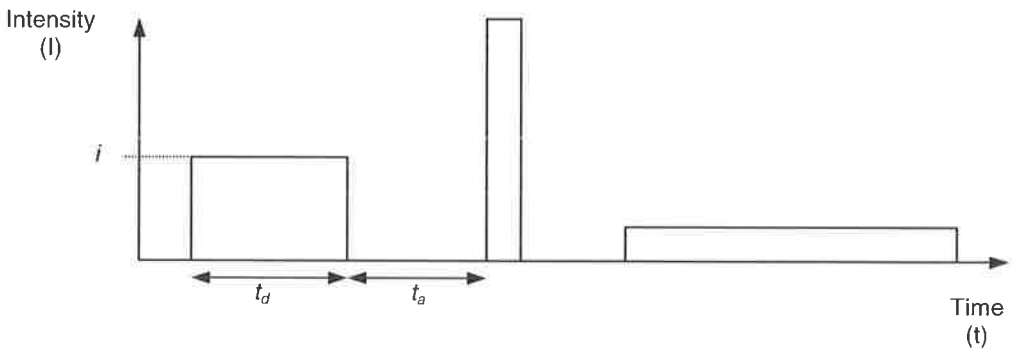

Figure 2.7 Alternating renewal Model.

Green (1964) was one of the first researchers to use this model structure, calibrating an exponential distribution using daily wet and dry sequences. Findings were compared to those of Gabriel and Neumann (1957, 1962) showing that the renewal model was preferable to the Markov chain model for some sites with neither model providing better results at others. Green (1965) disputed the findings and conclusions of Gabriel and Neumann (1962) and Weiss (1964), by showing that the geometric memory of the first-order Markov chain is not adequate for describing long or extended dry or wet sequences, as the persistence effects are considered negligible beyond one day. If they are not negligible for a particular site and are taken into account by another model, such as the alternating renewal model (Green, 1964), an improved representation of the observed data will result.

Surpassing the work of Green (1964), Grace and Eagleson (1966, 1967) calibrated to rainfall event data and synthesised short time increment sequences. The inter-event time, event duration and total depth were treated as random variables with a two-hour minimum inter-event time separating independent events. The Weibull distribution was chosen for both the

distributions of inter-event times and event durations. A beta distribution was fitted to the residuals from a linear regression of depth against duration, enabling a conditional relationship between the two variables to be incorporated. Urn models were used in synthesising the interior of events. Using a similar method, Sariahmed and Kisiel (1968) attempted to represent summer thunderstorm occurrences for use in a watershed model for flood forecasting. The inter-event times, event durations, event depths and daily totals were calculated using a minimum inter-event time of three hours. A Weibull distribution was fitted to both the inter-event times and event durations. The model was shown to produce reasonable results.

Smith and Karr (1983) developed a renewal Cox process with Markovian intensity (RCM) for the rainfall process. This is a Cox-type process (doubly stochastic Poisson process for which the event occurrence rate varies randomly over time in addition to the parameter function of the Poisson process) and was chosen after an analysis of the rainfall event occurrences showed the overall plausibility of renewal models for modelling rainfall. The model was suggested to represent an observed clustering of wet and dry periods without the need to assume a cluster model that is defined by a storm front with subsequent rain cells. The two-state Markovian nature of the intensity process is based on the assumption that the clustering of the rainfall events are described by alternating wet and dry periods. It was shown that the rainfall process can be effectively modelled for data with small correlations between inter-event times, overcoming a limitation of the point process models (Section 2.2 and 2.3).

Small and Morgan (1986) developed and evaluated the relationship between a two-state renewal process and a two-state Markov chain. A gamma distribution was assumed for the inter-event times and an exponential for the event durations. The ability of either model to adequately represent the rainfall process was found to be site dependent.

Acreman (1990) developed a 22 parameter, two-season hourly event-based rainfall model. Any continuous sequence of wet hours was defined as an event. An analysis of the correlations of inter-event times and event durations indicated that these events were independent. A generalised Pareto distribution was fitted to the inter-event times and an exponential distribution to the event durations. Dependence between duration and depth was observed and incorporated by dividing the depths into 16 classes according to their duration, with the duration within each class represented using a gamma distribution. Event profiles were modelled using a beta distribution to define the average shape of observed rainfall

profiles for each season, with a lag-one correlation model used to reproduce the observed correlation between successive wet hours. Comparison between simulated and historical mean monthly totals showed consistent underestimation in one season and overestimation for the other. Comparisons were made with observed maximum depths at various aggregation levels and with rainfall frequency curves generated in the Flood Studies Report (NERC, 1975). In general the model performed well, but appeared to overestimate rainfall depths for all return periods at higher aggregation levels (12 to 48 hours).

Wong (1996) used a transformed gamma distribution (first-order Markov model with Wilson-Hilferty transformation) to generate inter-event times and event durations using monthly and yearly parameters. To generate the rainfall depth, the mean, standard deviation and coefficient of skewness of observed bursts for nine durations (0.5, 1, 3, 6, 9, 12, 18, 24 and 72 hours) were calculated. Event depths for other durations were linearly interpolated but a procedure to extrapolate depths for durations greater than 72 hours was not reported. The statistics of the simulated inter-event times and event durations compared reasonably with the historical values but the annual totals were overestimated and a number of very long and unrealistic event durations (in the order of 1 000 hours) were generated. Also, using statistics obtained from the analysis of rainfall bursts to generate total event depth is inconsistent because the bursts do not represent actual events.

In a non-seasonal model, Lambert and Kuczera (1996) described the distribution of inter-event times using a two-parameter gamma distribution, the event durations using a modified exponential distribution and the rainfall intensity using a generalised Pareto distribution with its parameters conditioned on event duration. Temporal variation was introduced into each event using a random walk in the dimensionless depth-time space and a truncated log-normal distribution. The model was found to produce good predictions of the IFD data for short to medium duration events but underestimated them for longer durations.

2.5.3 Combination Models

Smith (1987) generalised the Markov chain and a Bernoulli trial model to produce a Markov Bernoulli Model for daily rainfall occurrences, defined as a sequence of Bernoulli trials with randomised success probability. The randomised success probability was a seasonal, two-state Markov chain. Nine parameters were required and model performance was compared with the standard Markov chain and Bernoulli trial models using daily data. Wet-dry

sequences with three precipitation thresholds (0.01, 0.1 and 1.0 inches) to define a wet day were examined, with results indicating a strong dependency on the threshold chosen. For the highest threshold it was shown that there is little improvement from the simple Bernoulli trail models, while for the two lower thresholds, the Markov Bernoulli model performed better.

2.6 EVALUATION OF MODELS

The clustered point process models of point rainfall have been developed more recently than the Markov Chain and alternating renewal models, forming a large part of the recent literature. In order to determine the most suitable type of model the following aspects were considered in terms of their effect on design flood estimation:

(a) the potential of each type of model based on reported and validated results;

(b) data requirements and the effect of missing data;

(c) parameter estimation and calibration techniques; and

(d) calibration of continuous rainfall models with aggregated rainfall data.

It was concluded that model choice is dependent on the intended application.

As seen in the previous sections, models attempt to characterise the rainfall process in different ways. Provided a model generates rainfall data that preserves the statistical characteristics of the observed data, or at least those properties required for a particular application, the process generating assumptions may not be important. Stern and Coe (1984) emphasised the importance of matching the model performance to the intended application. Acreman (1990) provided similar arguments in addition to suggesting that while actual rainfall depends on the climatic and meteorological regime, selection of an appropriate process model depends on the length of the time interval over which the rainfall depth has been measured or aggregated. The degree of dependence between the successive intervals is higher in hourly records than in daily records, allowing the dependency assumption of the various models to be matched to the available data, intended application and required aggregation level. For example, determining the number of days in a growing season does not require short time interval data to be used, whereas design flood estimation involving flood frequency analysis requires a finer resolution to ensure a flood peak is not missed.

2.6.1 Examination of Validated Results

Many of the models discussed have not been rigorously validated. A model must be capable of reproducing and preserving more than just the statistics and characteristics used in its calibration (Cowpertwait, 1994). Effective validation techniques include the analysis of extreme values through IFD statistics and an examination of the dry probabilities. Of the models discussed in this section that have been validated, many have performed poorly in at least one aspect.

Poor rainfall simulation will carry through into applications that utilise the synthetic data. The effect may be dependent on the particular characteristic(s) that is important to the application. For example, poor reproduction of dry probability statistics can have a serious impact on the infiltration process and hence rainfall-runoff calculations, as the model may generate unreliable runoff output after varying inter-event times. Haan *et al.* (1976) showed a case where overestimation of rainfall resulted in the overestimation of runoff and underestimation of reservoir size in a streamflow generation model. Hydrological models that are sensitive to the distribution of wet and dry periods, such as catchment infiltration models, can be adversely affected by the inability of a rainfall model to adequately represent the time history of the rainfall process. In this instance, the values of initial loss, one of the most influential parameters estimated for design, may be inaccurately determined. The dry probability statistics is an important property for a rainfall model. Failure to represent this distribution will result in poor rainfall simulation (Velghe *at al.*, 1994), which indicates an overall inability of the model to capture the general temporal structure of the observed rainfall events.

Overall model suitability for a particular location must also be considered. When considering a rainfall model for Australian conditions it is important to recognise that a large percentage of Australia lies within tropical and subtropical zones. A model suitable for tropical areas is important although few within the literature have modelled such conditions. In fact, very few models have been applied to Australian data. A number of models presented are based on the Poisson process, which models rainfall by assuming the arrival rates of events with zero (or insignificant) duration in relation to dry inter-event periods (Eagleson, 1978b). However, some researchers have indicated that this assumption may not be valid. Acreman (1987) stated that in Britain, the average event duration is around 20% of the average inter-event times making the Poisson assumption less acceptable. A similar percentage is observed for

the wet season in tropical Australia.

The N-SRP and B-LRP models are said to be capable of replicating a variety of rainfall statistics over a range of rainfall aggregation levels including the mean, variance and lag auto correlation. However, the results published for aggregation levels other than those used in calibration do not always support this statement. Although advances and improvements have been made with regard to the replication of particular rainfall statistics using these models, each improvement has often led to a less satisfactory replication of other statistics, most commonly the extreme values and dry probabilities.

Morrissey and Krajewski (1993) suggested that the clustered point process models are not able to reproduce the characteristics of tropical rainfall and hence cannot adequately represent the tropical rainfall process. Morrissey and Krajewski (1993) speculated that the reason for the failure of these models lies in the physically different rainfall process for mid-latitude and tropical rainfall. The process associated with mid-latitude rainfall, as reproduced using point process models, is driven by frontal systems occurring on synoptic time scales. However, tropical rainfall consists of frequent small scale convective events and occasional large scale convective cloud clusters, which has a fundamentally different structure to the point process from which the occurrence statistics are calculated. An event-based approach appears superior in terms of reproducing tropical rainfall because individual events are modelled and the model can be more easily changed to approximate the local rainfall process.

Markov models appear to provide a simple mathematical model of the rainfall process but the dependence structure can not adequately describe long-term persistence, not even over a few hours, without using a large number of parameters. A general observation by many researchers is that the first and higher-order Markov Chain models may not be adequate for use in calculating probabilities for prolonged dry periods. This is particularly important for modelling highly seasonal rainfall.

Less research has been conducted using alternating renewal models, but despite this, there is physical appeal as these models use actual observed events from the rainfall record for calibration rather than assume a rainfall process model. The models have a more intuitive physical interpretation and parameter meaning and identification. A number of authors have reported reasonable results for these models.

An advantage of the alternating renewal models and Markov chain models is the ability to

incorporate a dependency of rainfall intensity on event duration. Assuming independence of intensity with respect to duration can lead to difficulties in matching observed duration and intensity statistics, as was found by Hutchinson (1990). The cluster models assume independence between intensity and duration, although the data generally shows this dependency exists (Grace and Eagleson, 1966, 1967; Acreman, 1990; Lambert and Kuczera, 1996).

2.6.2 Difficulties with Missing Rainfall Segments

Most rainfall records are only long enough to contain a representative sample of low magnitude, high frequency rainfall events. This may be sufficient for applications where lower ARI values are important or a representative year can be employed, but in general using the records in this form makes analysis difficult.

Missing data within historical rainfall records can also present a serious problem by decreasing the likelihood of observing higher ARI events. The amount missing can affect the type of model structure selected for consideration. Few researchers have published how to adequately deal with this. Cowpertwait (1991a) described a replacement strategy to handle missing data. Missing daily data within a particular month was replaced with data from the same month within a different year but where the monthly totals were similar. If many months were missing then the whole year was deleted or if only a few data were missing those values were replaced by zero. Although this approach may be adequate for some data sets, there is no confidence that this approach will be adequate to compensate for significant missing or rejected data.

Large portions of recorded data generally need to be discarded in order to calibrate a rainfall model that utilises a method based on aggregated statistics. The higher the proportion of missing data, the more likely the underestimation of the aggregated statistics becomes. Katz and Parlange (1995) and Gyasi-Agyei (1999) ignore and discard months with any missing data. As a result, valuable information could be lost, particularly where there is limited data in the first place. For some months of the year Gyasi-Agyei (1999) discarded up to half of the available data. This may reduce the ability to include any observed higher ARI events, and may even mean significant events are discarded. With an event-based approach, discarding rainfall events or inter-event times containing missing intervals should introduce no significant bias into the calibration provided the occurrence of these missing intervals is

random. Therefore, if part of a month of data is missing it does not invalidate the remaining quality data for that month. This allows more data to be used in calibration of model parameters of the various probability distributions.

With a Markov approach, high levels of missing data significantly lowers the chance of determining the persistence between successive intervals and hence model parameters. This may lead to difficulties in representing the number of wet days in dry months (Srikanthan and McMahon, 1985).

2.6.3 Parameter Estimation and Calibration Techniques

A small number of parameters needed to calibrate a model is generally considered preferable, but using more parameters may not be a drawback if these parameters are intuitive and easily estimated.

Many researchers have indicated that parameters for the cluster models are difficult to estimate, partly because they are not intuitive or easily observed from the data. Although the parameters of the clustered point processes have been given a physical interpretation, such as the duration of a rain cell, they are not readily determined from a rainfall hyetograph. Also, the usual physical interpretation of each cluster of rectangular pulses as a sequence of showers is an approximation, since pulses from within each cluster and from within different clusters may overlap in time. Foufoula-Georgiou and Guttorp (1986) suggested that since the N-S model does not provide an adequate description of the underlying rainfall generating process, no physical meaning should be attached to the parameters. Onof and Wheater (1994b) showed for the RPB-LRP that as the number of parameters increased, the identification problem became more difficult and alternative identification strategies gave significantly different values for the same parameter. Khaliq and Cunnane (1996) showed that the high variability of some parameters for the MB-LRP means that various values of the parameters can give rise to similar analytical model values, making optimisation more difficult. In this case, a complex optimisation procedure using a number of different statistic sets was required to address the problem of parameter stability and sensitivity.

Markov models that use a number of wet states differentiated by increasing depths of rainfall have a large number of parameters that need to be estimated. The distribution of rainfall depth within each state also requires estimation. This often makes these models difficult to

calibrate for sites that have limited historical data. In the case of Pattison (1965), the large number of states and hence parameters for calibration was a major drawback, particularly as many of these parameters do not provide any additional information about the depth process than could be obtained through the use of other rainfall depth models. While the structure of the Markov models is valid at all time scales, to produce short-increment rainfall data a large number of parameters must be used, along with a high-order chain to account for the dependence between successive intervals, or a disaggregation process for the sub-division of the fixed interval rainfall depth.

Alternating renewal models apply an intuitive process and use parameters that are generally easily estimated. Because they are event-based models, the simulated event durations may vary significantly between events and a disaggregation method is required to produce short-increment data at the required time scale. The properties of observed rainfall event profiles can be used to disaggregate the total event rainfall, as opposed to disaggregating the rainfall depth in each time interval into smaller intervals such as from daily time scales to hourly time scales. This allows for a better reproduction of the observed temporal pattern of the rainfall within each event.

The availability of a useable calibration technique is an important consideration for model selection. Two major techniques, the method of moments and the method of maximum likelihood have been widely used. Foufoula-Georgiou and Lettenmaier (1987) compared the method of moments with the maximum likelihood method for estimating the parameters of a daily Markov Renewal Model and concluded that the latter gave better results. A disadvantage of clustered point process models is that they are relatively intractable mathematically so that maximum likelihood estimation of parameters from observations at regular time intervals is generally not feasible (Hutchinson, 1990).

For very dry regions, calibrating a model using data that occurs within a specified period such as one or two months may significantly limit the number of data points available for fitting the model. This also applies to the tropical locations where there are very few wet days for some months of the year. In such locations, Srikanthan and McMahon (1985) found the mean, standard deviation and skewness values were not satisfactorily preserved during the dry season for a Markov chain model. If the number of wet days per month are few, then the length of the historical data for these months may not be sufficient to adequately estimate model parameters.

2.6.4 Calibrating Continuous Models Using Discrete Rainfall Data

While clustered point process models are calibrated using aggregated rainfall data, the methodology is based on a continuous process and the discreteness of the data has not been taken into account. Chang *et al.* (1984) reported that the continuous N-S model is inappropriate for calibration using aggregated data. Foufoula-Georgiou and Lettenmaier (1986) suggested that the problem is the result of the inappropriate assumption that a continuous-time point process, used to model the rainfall, can be calibrated against an aggregated record. Foufoula-Georgiou and Lettenmaier (1986) further showed this to be the case for all continuous-time stochastic models. They concluded that using aggregated rainfall data to calibrate continuous-time point process models introduced severe biases in parameter estimation that can result in misleading interpretations regarding observed rainfall clustering. As such, calibrating continuous models using aggregated data is not recommended even where the aggregation is hourly. Markov models assume a discrete basis for the rainfall process that incorporates aggregated data directly into parameter estimation. Parameter estimation is more straightforward for event-based models, which if continuous, more easily allows the incorporation of estimation procedures to account for aggregated data.

2.6.5 Model Choice

From the above discussion an event-based model of an alternating renewal type was selected as the most appropriate model to use for this study. When discussing models of precipitation, Eagleson (1978b) stated, "...that for reasons of physical validity an engineering model of this process must retain those natural features which are important to the problem at hand, while for the economy of computation and for clarity of behaviour it should omit those features deemed unessential". Models of rainfall must reflect the natural occurrence, not attempt to shape the process into what it is thought it should be. Models should not contain too much information, to enable them to be easily calibrated. This was an important factor considered in electing to pursue an alternating renewal model in the development of an alternative method for engineering design. As the rainfall sequences are described simply by alternate wet and dry periods, the process is less complicated than other models, but most importantly the events required to calibrate the model are easily observable in the available historical data. High percentages of missing data within available rainfall records were also an issue. The use of an event-based calibration technique in preference to one that employs aggregated statistics was considered more robust in terms of accommodating the extent of missing data.

3. DEVELOPMENT OF A NEW STOCHASTIC RAINFALL MODEL

Rainfall is the major factor that affects the level of runoff from a catchment. Therefore, it is important that a rainfall model can effectively reproduce the statistical properties of the observed rainfall to ensure a reasonable representation of the catchment water balance. Key statistical factors that a model needs to adequately reproduce include:

(a) the inter-event time, which defines when evaporation can occur and therefore establishes the amount of moisture that will be removed from the soil before the next event begins. The antecedent moisture conditions prior to an event are directly connected to these inter-event dry periods;

(b) the event duration, which partially determines the beginning and end of the infiltration process;

(c) the event depth, which determines the maximum peak and the total volume of runoff, in addition to the water available for infiltration and groundwater recharge; and

(d) the temporal distribution of event depth, which determines the maximum peak of the runoff hydrograph.

An alternating renewal model was selected for this study, as discussed in the previous chapter. This chapter describes the development of a new alternating renewal model and its calibration using data from a wide range of sites with varying climatic conditions to show the validity of the model across a range of Australian climatic zones. This is an important aspect of model development and one that has not been extensively undertaken by other researchers.

3.1 Model Outline and Essential Elements

The rainfall model developed for this study involved two stages. The first stage was to develop probability distributions for three random variables: the inter-event time (t_a), the event duration (t_d) and the average event intensity (i), with the event depth (d) defined as the product of i and t_d. Figure 3.1(a) shows these variables on a time series of rectangular rainfall pulses. The second stage involved determining the temporal distribution of rainfall

within each event using a disaggregation scheme as shown in Figure 3.1(b). This disaggregation scheme uses the gross characteristics of each rainfall event (t_d and i) to produce a hyetograph, based on a conditional random walk that generates a dimensionless mass curve. Dry periods were allowed to occur within an event, indicated by t_{idp} in Figure 3.1(b). The disaggregation scheme is discussed further in Chapter 5.

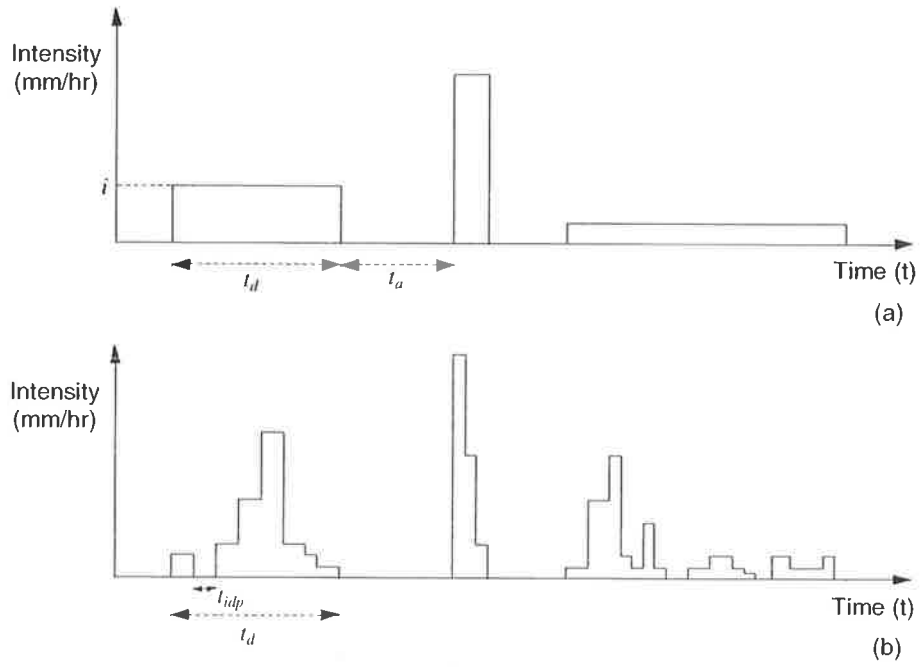

Figure 3.1 Model of precipitation event series:
(a) generation of a time series of rectangular rainfall pulses or events; and
(b) a random shaped hyetograph produced by the disaggregation scheme.

The model developed in this study is to be used in conjunction with a catchment water balance model, which in turn can be incorporated into design flood estimation. The temporal scale at which rainfall is generated by the model is an important factor and is dependant on the intended application. For flood frequency analysis short resolution data is important for calibration and simulation to ensure that flood peaks are not missed. In addition, on small catchments runoff may occur quickly and the outflow hydrograph may not be well described if the overall temporal resolution is too large.

The available data directly affects the methodology for defining how the alternating sequences of wet and dry periods will be handled by the model. There is an extensive network of daily rainfall gauges located in major cities and regional centres around Australia. This data is readily available from the Bureau of Meteorology and other government departments, with

good quality records of 50 to 100 years in length available for many sites. Daily rainfall data has been used to calibrate rainfall models that generate both daily and sub-daily rainfall. The generation of sub-daily rainfall using these models requires the disaggregation of the daily record, but if little information about the temporal rainfall characteristics at lower resolutions is known for the site then there is no certainty that the disaggregation is reasonable. Ideally data recorded at high resolutions should be used for both calibration and determining appropriate disaggregation procedures. Pluviograph data at a time scale of six-minutes is available for selected Australian locations from the Australian Bureau of Meteorology. This data was used to facilitate the simulation of long sequences of events at the six-minute time scale.

3.2 AVAILABLE DATA

Australia is a large and relatively arid continent with 50 percent of the land area having a median annual rainfall of less than 300 millimetres and 80 percent less than 600 millimetres (Bureau of Meteorology, 1983). The climate is dominated by dry, sinking air of a sub-tropical high pressure belt which seasonally alternates between the north and south (Bureau of Meteorology, 2001). Classification of Australian regional areas into categories based on various climatic conditions has a long history, beginning as early as 1865 (Sturman and Tapper, 1996) and was based primarily on annual rainfall totals. Since then other factors have been considered including rainfall variability, rainfall seasonal distribution, temperature and humidity to produce classifications such as those shown in Figure 3.2.

A diverse range of zones is evident, from tropical regions in the north, through arid and subtropical expanses in the middle latitudes, to temperate regions in the south. Data for this study has been chosen in part by the availability of pluviograph data but also to test the model over the range of climatic conditions and seasonal rainfall patterns. Therefore, at least one data set has been selected for each zone and full details of each site is shown in Appendix A.1. The zone and rainfall classification, seasonal characteristics and rainfall variability at each location, based on information from the Bureau of Meteorology (1983, 2001), are described in Table 3.1.

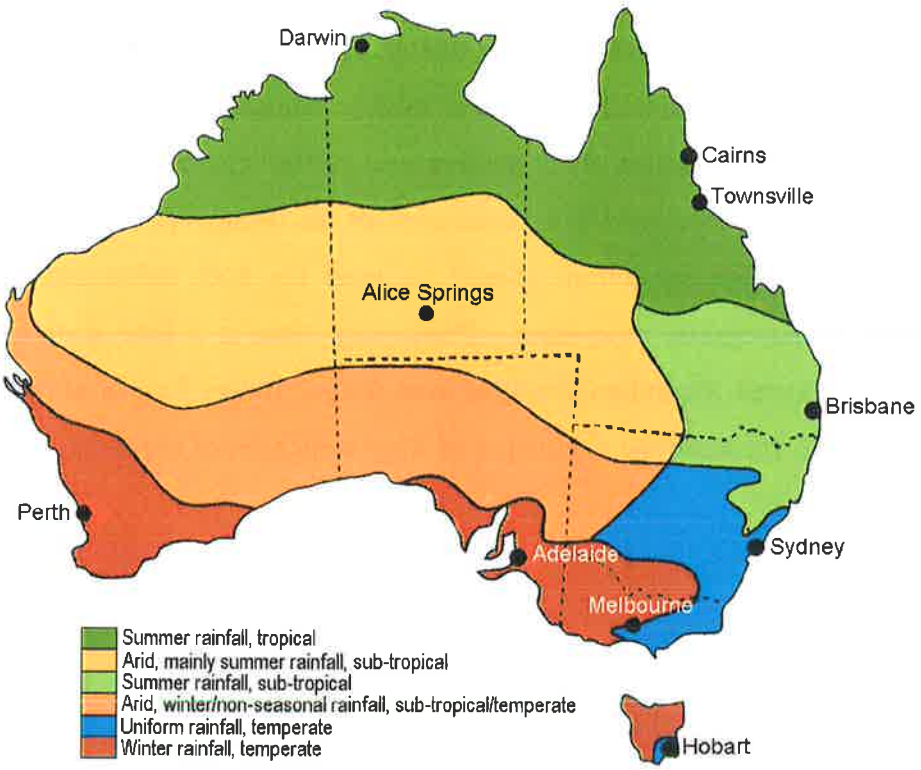

Figure 3.2 Location of pluviograph sites within climatic zones
(Source: Bureau of Meteorology, 1983, 2001).

Figure 3.3 to Figure 3.5 show the changes in rainfall variability over the year, described as Low (L), Low-Medium (L-M), Medium (M), Medium-High (M-H), High (H), Very High (VH), Extreme (E) and Very Extreme (E+), for dominant summer rainfall, dominant winter rainfall and uniform rainfall, respectively. The rainfall variability over the year for all sites is shown in Appendix A.2. This information highlights the difficulty in developing a model that can produce synthetic sequences of rainfall to replicate the statistical properties of the observed data for any location within Australia.

In obtaining data from the various sites a problem of fragmented data and short records soon became evident. Although the pluviograph data sets obtained were considered to be of a high quality, a perfect data set is rare and the record inevitably contains missing periods of data. In some cases up to 10% of the total depth was either missing or unusable due to the recorder being inactive or incorrectly recording (refer to Table A.2, Appendix A.1 for missing proportions from each site). As indicated in Section 2.6.5, the choice of an alternating renewal model was influenced by its ability to accommodate high percentages of missing data in available records.

Table 3.1 Pluviograph site climatic zones and rainfall characteristics (Source: Bureau of Meteorology, 1983, 2001).

Location	Zone Classification	Rainfall Classification	Rainfall Variability		Seasonal Characteristics	
			Summer	Winter	Summer	Winter
Cairns	Tropical	Summer	Medium to Very High	Medium to High	Hot, humid with heavy periodic rain	Warm to mild with dry periods
Darwin			Low to Medium	Extreme		
Townsville			High to Very High	Very High to Extreme		
Alice Springs	Sub-tropical	Arid (Summer)	Very High to Extreme	Extreme	Hot to extreme, irregular rain	Mild to warm, dry
Brisbane		Summer	Medium to High	High to Very High	Hot, humid, heavy periodic rain	Mild, light irregular rain
Adelaide	Temperate	Winter	High to Very High	Low to Medium	Warm to hot, light, irregular rain	Cool to cold, moderate rain
Melbourne			Medium to High			
Perth			High to Extreme			Cool to mild, moderate to heavy rain
Hobart	Temperate	Uniform (Non-seasonal)	Medium to High	Low to Medium	Warm to hot	Cool to Cold
Sydney				High		

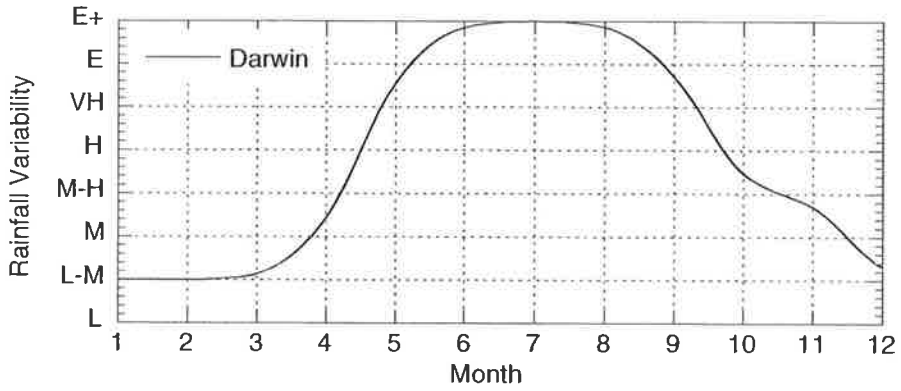

Figure 3.3 Typical rainfall variability for a location with dominant Summer rainfall.

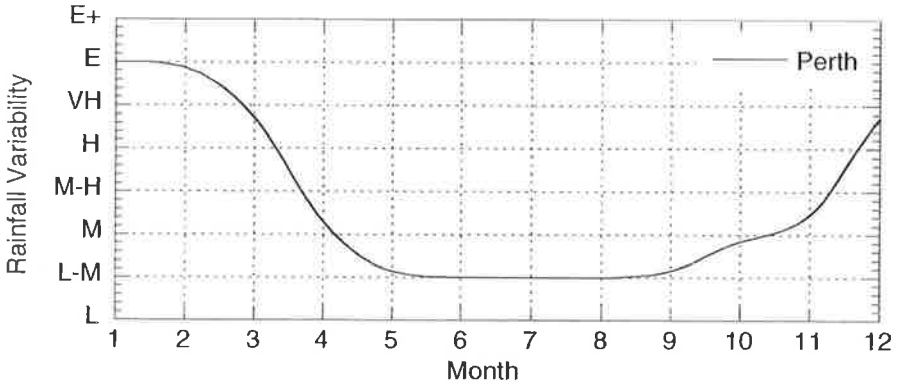

Figure 3.4 Typical rainfall variability for a location with dominant Winter rainfall.

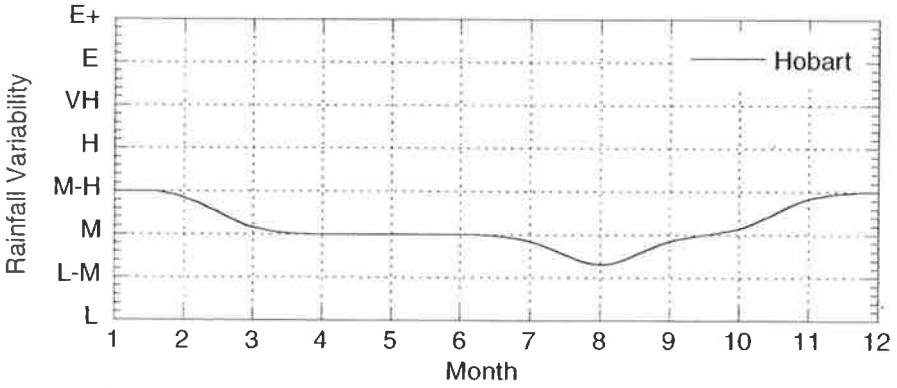

Figure 3.5 Typical rainfall variability for a location with uniform rainfall.

3.3 INDEPENDENCE OF EVENTS

In order to utilise an alternating renewal approach with event-based calibration the historical rainfall record needed to be separated into a series of independent events. To achieve this, a minimum inter-event time (t_{min}) value needed to be established in such a way that it could be assumed that successive events were not correlated. The requirement that each rainfall event used during calibration is independent ensures that inter-event times and rainfall events can be calibrated and simulated independently. This leads to the question which has caused much conjecture among researchers: what constitutes an event?

3.3.1 Previous Research

Researchers have used a wide range of values for t_{min} to separate independent events. The selection of t_{min} depends on a number of factors, including the choice of rainfall model, the assumed distribution of inter-event times and the temporal resolution of the available data. The longer the length of these intervals (larger temporal resolution), the longer inter-event times need to be to ensure that they are not part of an ongoing event. For high resolution data, sequences of a small number of dry periods may be contained within a longer event. These dry periods are short in relation to the total length of the wet periods and may not be long enough to consider the wet periods on either side as independent. Some researchers have assumed that a single dry interval at the recorded aggregation level is enough to separate independent events, while other researchers have used an arbitrarily specified length of time or a time determined by some significance test.

For daily data, Green (1964) and Todorovic and Yevjevich (1969) defined an event as any sequence of wet days surrounded by at least a single dry day. The latter research expanded this theory to temporal scales of less that one day, defining an independent event in an hourly record as an uninterrupted sequence of wet hours surrounded by at least one dry hour, effectively assuming t_{min} of one hour. Yen and Chow (1980), Acreman (1990) and Cameron *et al.* (1999) also used a value of one hour when using hourly data and Marien and Vandewiele (1986) used a t_{min} of ten minutes for ten minute data. Other researchers have defined independent events as continuous wet sequences separated by multiple dry intervals in

the data. For example, Huff (1967) used a t_{min} of six hours for 15 minute data.

Grace and Eagleson (1966, 1967), using ten minute data, calculated t_{min} from the historical record by way of a rank correlation coefficient at a selected significance level. This resulted in a t_{min} of two hours for north-eastern U.S.A. and three hours for Arizona. Eagleson (1978b) used a t_{min} of two hours for ten minute data for Boston, Massachusetts. Sariahmed and Kisiel (1968) confirmed the work of Grace and Eagleson (1966, 1967) by using the rank correlation coefficient as a basis for determining dependence on five-minute data and obtained a t_{min} of three hours. Rao and Chenchayya (1974) also used this method.

Restrepo-Posada and Eagleson (1982) contradicted the earlier work of Grace and Eagleson (1966, 1967) by suggesting that the correlation of ranked rainfall depth values cannot be used to identify independent events. They argued that since there are three variables associated with rainfall events (inter-event time, event duration and total event depth), zero correlation between subsequent event depths alone does not guarantee that corresponding event arrivals are independent. Restrepo-Posada and Eagleson (1982) suggested that if only one of the three variables defining the rainfall time series was to be used to ensure event independence it should be the inter-event time, as the independence of inter-event times has a greater physical link to event independence than that of event depths. To analyse the inter-event times, the arrival of independent events was assumed to follow a Poisson process which is analogous to assuming that the distribution of inter-event times follows an exponential distribution. The analysis then followed the procedure of Grace and Eagleson (1966, 1967) to obtain a range of t_{min} values for a number of sites. Bonta and Rao (1988) confirmed this method as a better choice over the rank correlation method, calculating a t_{min} of 9.5 hours using hourly data. It has also been used for the selection of design events by Huber *et al.* (1986), who used a t_{min} of 19 hours for hourly data when calibrating a model for input into a stormwater management model.

Koutsoyiannis and Xanthopoulos (1990), Koutsoyiannis and Foufoula-Georgiou (1993) and Koutsoyiannis and Pachakis (1996) have developed rainfall models based on a Poisson process, where the time between independent events must follow an exponential distribution and hence t_{min} is determined to satisfy this assumption. Koutsoyiannis and Xanthopoulos (1990) found that t_{min} ranged from five to seven hours for hourly data. Koutsoyiannis and

Foufoula-Georgiou (1993) and Koutsoyiannis and Pachakis (1996) determined a t_{min} of seven hours, based on a Kolmogorov-Smirnov test of the exponential distribution.

In a different approach, Robinson and Sivapalan (1997) selected a t_{min} of seven hours so that each event in the three years of data examined, corresponded approximately to an identifiable synoptic (frontal) event on weather charts.

3.3.2 Determining a Minimum Inter-event Time for Australian Data

Determining a minimum inter-event time using the methods of Restrepo-Posada and Eagleson (1982) or Koutsoyiannis and Foufoula-Georgiou (1993) can be considered satisfactory when the distribution of the inter-event times is exponential (or can be reasonably assumed to be so). However, if the historical data is not representable by an exponential distribution then these methods are not satisfactory. Lambert and Kuczera (1996, 1998) suggested that an exponential distribution was not necessarily appropriate for modelling the inter-event times in Australia.

A check of the probability distribution most appropriate for a set of observed data, such as the inter-event times, can be obtained visually using *probability paper*, which can be constructed for a range of specific probability distributions (Ang and Tang, 1975). A straight line plot on a given probability paper will provide a good indication that the plotted values can be represented by the specific distribution of the probability paper. However, it is generally preferable to plot the data on *general probability paper*, by defining a standard variate that is appropriate to the distribution being examined but that is independent of the actual values of the parameter values (Ang and Tang, 1975). For the exponential distribution, this standard variate can be defined as $\ln(1-F(x))$, where $F(x)$ represents the cumulative probability of each inter-event time value within a sorted (lowest to highest) set of values and is defined (Ang and Tang, 1975) as:

$$F(x) = \frac{m}{N+1} \tag{3.1}$$

where:

N = Number of inter-event times; and

m = Rank of each inter-event time within the sorted set.

Using this method, if an exponential distribution is appropriate for the inter-event times, the data should plot as a straight line.

An examination of inter-event times (Figure 3.6) from the Melbourne data shows that for a t_{min} of up to 12 hours an exponential distribution can not satisfactorily represent the data. Similar results are obtained for the other Australian sites as shown in Appendix B.1. To confirm that an exponential trend does not exist, a seven-hour minimum time as in Koutsoyiannis and Foufoula-Georgiou (1993) is used to examine the distribution of inter-event times for individual months (Figure 3.7 and Figure 3.8). These figures show that the monthly inter-event times could not be adequately modelled using an exponential distribution. Therefore, the selection of t_{min} using the method proposed by Koutsoyiannis and Xanthopoulos (1990) or Koutsoyiannis and Foufoula-Georgiou (1993) (exponential distribution assumption) was not considered appropriate for Australian data and an alternative method for selecting or verifying a t_{min} needed to be sought.

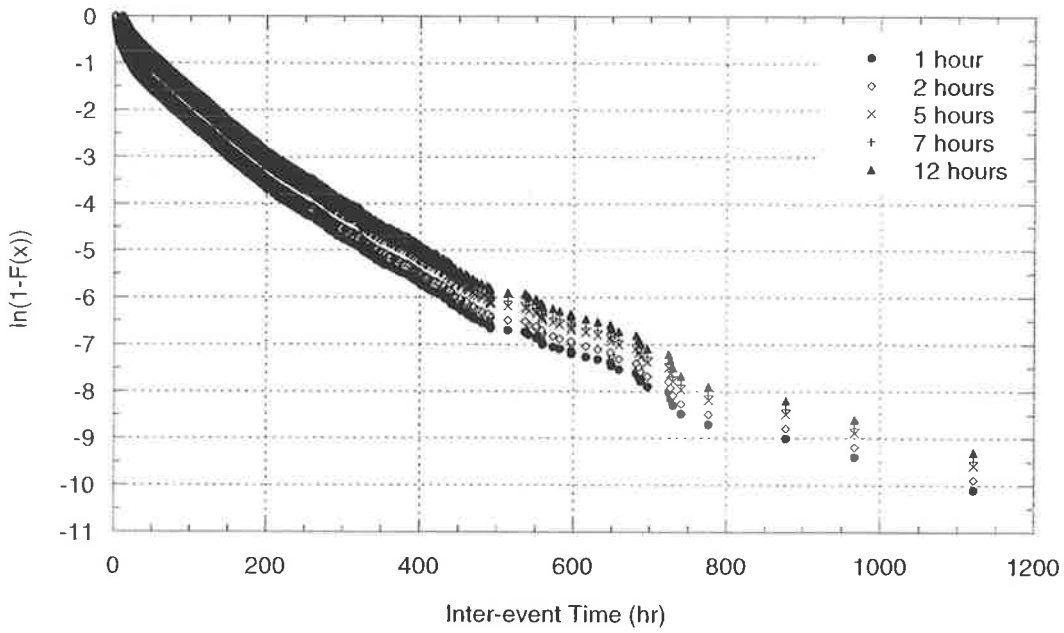

Figure 3.6 Distribution shape comparison of inter-event times obtained using various values of t_{min} for Melbourne.

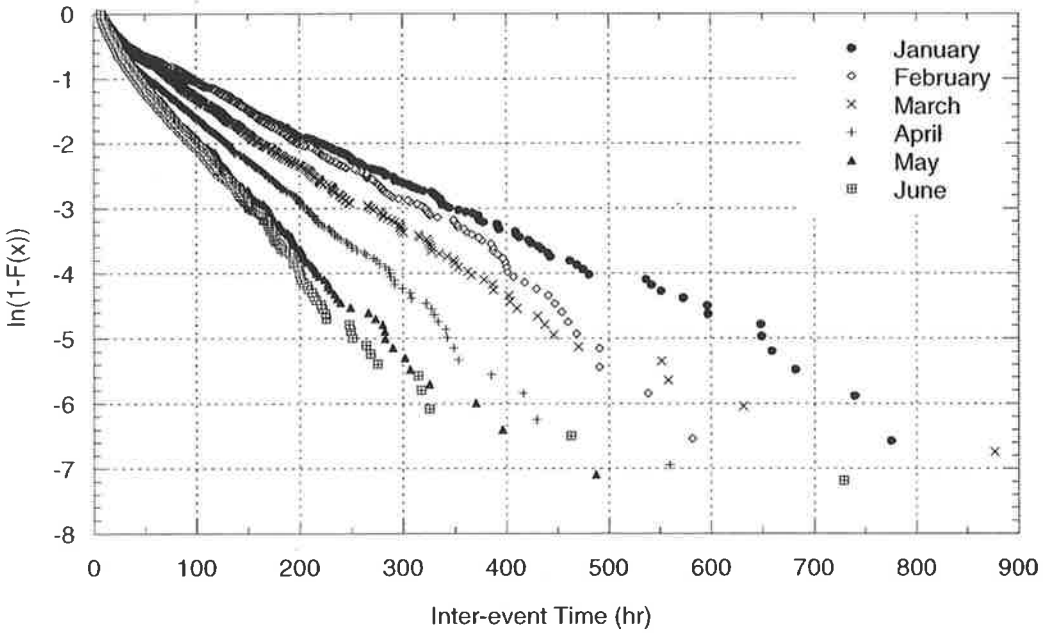

Figure 3.7 Distribution shape comparison of inter-event times with a seven hour t_{min} for Melbourne in months January to June.

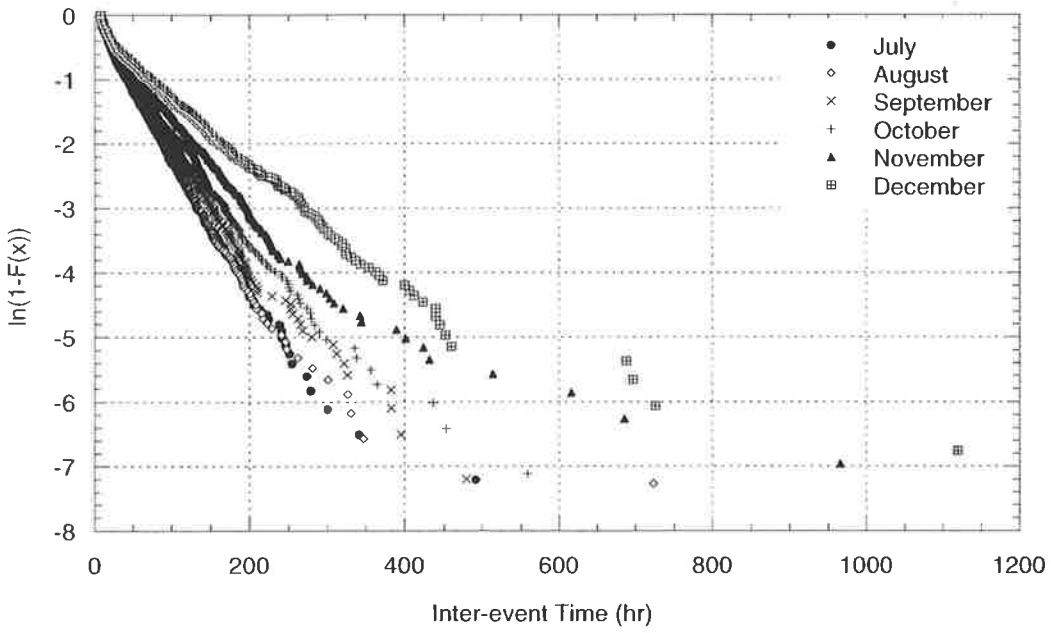

Figure 3.8 Distribution shape comparison of inter-event times with a seven hour t_{min} for Melbourne in months July to December.

The approach to selecting a t_{min} to model the inter-event times for this study involved selecting a value for t_{min} and then fitting a general probability distribution to the events obtained from the data using this assumed t_{min}. A two-hour minimum value for the inter-event time was initially assumed from the work of Eagleson (1978b), and independence was assumed based on this criteria. However, in light of the t_{min} suggested by Koutsoyiannis and Xanthopoulos (1990), Koutsoyiannis and Foufoula-Georgiou (1993) and Koutsoyiannis and Pachakis (1996), a t_{min} of two hours may not have been large enough to ensure independence. Therefore, an examination of various correlation statistics was used to substantiate the assumption of two hours for t_{min}.

3.3.3 Correlation Criteria to Validate t_{min} Selection

Consideration of the correlation between various quantities can aid in validating an independence assumption and hence assist in verifying a value for t_{min}. Two methods were used to evaluate correlation:

(a) the auto-correlation test; and

(b) the rank correlation test.

Auto-Correlation

The auto-correlation was calculated for successive inter-event times, event durations and event depths at six-minute intervals. A lag 20 auto-correlation at this temporal resolution is equivalent to two hours and will provide the correlation between recorded rainfall intervals that are two hours apart. The auto-correlation coefficient (r_k) between n events in a series and for a lag k between the events in question, is defined (McMahon and Mein, 1986) as:

$$r_k = \frac{\frac{1}{n-k}\sum_{i=1}^{n-k} x_i\, x_{i+k} - \frac{1}{(n-k)^2}\sum_{i=1}^{n-k} x_i \sum_{i=1}^{n-k} x_{i+k}}{\left[\frac{1}{n-k}\sum_{i=1}^{n-k} x_i^2 - \frac{1}{(n-k)^2}\left(\sum_{i=1}^{n-k} x_i\right)^2\right]^{0.5}\left[\frac{1}{n-k}\sum_{i=1}^{n-k} x_{i+k}^2 - \frac{1}{(n-k)^2}\left(\sum_{i=1}^{n-k} x_{i+k}\right)^2\right]^{0.5}} \qquad (3.2)$$

Rank Correlation

Rank correlation was calculated for successive inter-event times, event durations and event depths using the Spearman-Rank correlation coefficient. This is a non-parametric correlation coefficient that requires no assumptions regarding the underlying distribution. The concept of non-parametric correlation is that each value (x_i) in a sorted (lowest to highest) set of observed values ($x_1, x_2, \cdots, x_n$) is replaced by its rank or position ($R_1, R_2, \cdots, R_n$) among the sample and any linear correlation between the ranks can be determined.

The Spearman-Rank correlation coefficient (r_s) is defined (Press *et al.*, 1992) as:

$$r_s = \frac{\sum_i (R_i - \overline{R})(S_i - \overline{S})}{\sqrt{\sum_i (R_i - \overline{R})^2}\sqrt{\sum_i (S_i - \overline{S})^2}} \tag{3.3}$$

where:

R_i = Rank of the inter-event times (t_{ai})

$(t_{a1}, t_{a2}, \cdots, t_{aN}) \equiv (R_1, R_2, \cdots, R_N)$;

$\overline{R}$ = Mean of R;

S_i = Rank of the inter-event times ($t_{a(i-1)}$)

$(t_{a0}, t_{a1}, \cdots, t_{a(N-1)}) \equiv (S_1, S_2, \cdots, S_N)$; and

$\overline{S}$ = Mean of S.

The significance of a non-zero value of r_s can be tested by computing (Press *et al.*, 1992):

$$t = r_s \sqrt{\frac{N-2}{1-r_s^2}} \tag{3.4}$$

where:

N = Number of points.

The value of t is distributed approximately as a Student's distribution with $N-2$ degrees of freedom.

Table 3.2 shows the auto-correlation and Spearman-Rank correlation coefficients for varying t_{min} for Melbourne. Values for other Australian sites are shown in Appendix B.2. With a

correlation value of one meaning perfect correlation it can be seen that a minimum inter-event time of two hours has little observable correlation between successive inter-event times, event durations and event depths. Values for t_{min} greater than two hours were examined but made little difference to the auto-correlations reported in Appendix B.2.

Table 3.2 Auto-correlation and Spearman-Rank correlation coefficients for varying inter-event times for Melbourne.

Minimum Inter-Event Time (hr)	Inter-event Times		Event Durations		Event Depths	
	Auto-correlation	Spearman-Rank	Auto-correlation	Spearman-Rank	Auto-correlation	Spearman-Rank
1	0.075	0.086	0.055	0.059	0.051	0.065
2	0.073	0.073	0.042	0.043	0.051	0.062
5	0.074	0.050	0.024	0.031	0.033	0.056
7	0.070	0.045	0.040	0.035	0.037	0.052
12	0.082	0.046	0.009	0.020	0.029	0.022

To validate the use of an even lower minimum inter-event time to define independence between events, the lag 10 and lag 20 auto-correlation values at a six-minute temporal scale were calculated for each site, which correspond to a time interval of one hour and two hours respectively. Table 3.3 shows there was an observable decrease in the correlation level from the one hour interval to the two hour interval, with a reasonably low correlation level obtained for the two hour interval.

Table 3.3 Lag 10 (one hour) and lag 20 (two hours) values for six-minute data.

Location	Lag 10	Lag 20
Adelaide	0.178	0.118
Alice Springs	0.198	0.141
Brisbane	0.187	0.126
Cairns	0.260	0.184
Darwin	0.109	0.066
Hobart	0.305	0.227
Melbourne	0.206	0.132
Perth	0.157	0.114
Sydney	0.263	0.175
Townsville	0.250	0.152

The lag 10 and lag 20 values were also calculated for each month at each site to examine any effects of seasonal rainfall patterns upon the correlation. For Melbourne the monthly values ranged from 0.18 to 0.24 for the lag 10 (one hour) correlation and were within a range of 0.10 to 0.16 for the lag 20 (two hour) correlation. The reduction of the correlation and the range

was very significant for some months and supported the use of a two hour t_{min} over a one hour t_{min}. The lag 20 correlation value was considered to be representative of very small correlations. The full range of values for Melbourne and the other sites are shown in Appendix B.3. For some sites very large differences in correlation values were observed between months, which confirm the conclusions of Bonta and Rao (1988) that t_{min} varies over the year.

The purpose of the rainfall simulation model is to produce a synthetic rainfall data set with the same statistical characteristics of the observed data. The size of t_{min} should not be critical for this use provided that the statistical properties of the observed time series are preserved. Acreman (1990) likewise concluded that separation criteria for independent events was not critical, providing realistic rainfall sequences can be generated. In addition, the larger t_{min} the smaller the number of events that will be extracted from the record, leading to a smaller sample size from which the statistical properties of the chosen probability distribution can be determined. The effect of increasing t_{min} on the number of events is seen in Appendix B.2. The reduction in event numbers is a serious consideration when starting with short historical records.

Based on the above correlation analysis, the assumption was made that a t_{min} of two hours is sufficient to separate independent events within Australian rainfall data.

3.4 Development of Inter-Event Time and Event Duration Models

The development of a model to generate inter-event time and event duration data involved:

(a) reviewing previous research and its applicability to Australian data from which a suitable distribution was chosen;

(b) incorporating into the chosen distribution a method to account for the seasonal effects on the inter-event time and event duration data;

(c) determining the calibrated parameters for the distribution by comparing the fitted distributions to the observed data; and

(d) validating the model by comparing observed and simulated statistics that were not used in the calibration process.

3.4.1 Previous Research

As discussed in Section 3.3.1, the distribution of the time between independent events is often assumed to follow an exponential distribution. This assumption has been applied to models utilising a Poisson arrival formulation (such as the single Poisson arrival models and the clustered point process models) and for many alternating renewal and event-based models. Other distributions used in an event based modelling approach have included a Weibull distribution (Grace and Eagleson, 1967; Sariahmed and Kisiel, 1968), a negative exponential (Grayman and Eagleson, 1969), a truncated geometric distribution (Roldan and Woohiser, 1982), a gamma distribution (Small and Morgan, 1986; Foufoula-Georgiou and Lettenmaier, 1987; Lambert and Kuczera, 1996), a generalised Pareto distribution (Acreman, 1990), a transformed gamma distribution (Wong, 1996) and a generalised exponential distribution (Lambert and Kuczera, 1998).

The distribution of event duration is also often assumed to follow an exponential distribution (Eagleson, 1978b; Small and Morgan, 1986; Bacchi *et al.*, 1989; Burlando and Rosso, 1993; Acreman, 1990). Other distributions that have been used include a Weibull distribution (Grace and Eagleson, 1966, 1967; Sariahmed and Kisiel, 1968), a negative exponential distribution (Grayman and Eagleson, 1969), a truncated negative binomial distribution (Roldan and Woohiser, 1982), a gamma distribution (Bacchi *et al.*, 1989; Burlando and Rosso, 1993), a bivariate exponential distribution (Bacchi *et al.*, 1989; Burlando and Rosso, 1993), a geometric distribution (Wong, 1996), a modified exponential distribution (Lambert and Kuczera, 1996), a shifted exponential distribution (Robinson and Sivapalan, 1997) and a generalised exponential distribution (Lambert and Kuczera, 1998).

The inappropriateness of the exponential distribution for representing the inter-event times has been discussed in Section 3.3.2. In addition, the use of an exponential distribution for event duration is not suited in terms of representing the distribution of historical Australian data. Figure 3.9 shows that event duration distributions for Adelaide, Brisbane and Melbourne are not exponential. The distributions for all sites are shown in Appendix B.3 and Appendix D.1. Of the distributions used to model event duration, the generalised exponential distribution (Lambert and Kuczera, 1998) has shown the most potential.

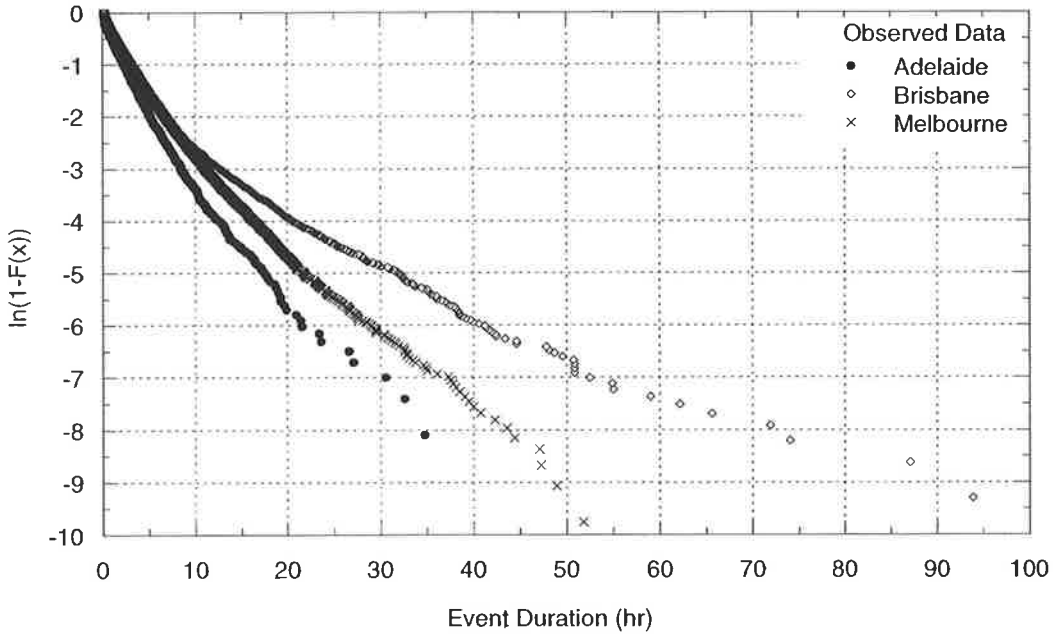

Figure 3.9 Distribution of event duration for Adelaide, Brisbane and Melbourne.

3.4.2 Selection of Distribution

The generalised exponential distribution (Lambert and Kuczera, 1998) is defined as:

$$F(x \mid \theta_t) = P(X \le x \mid \theta_t) = 1 - \exp[-g(x,\theta_t)] \qquad x>0 \qquad (3.5)$$

where:

X = independently distributed random variable (inter-event times or event durations);

t = time at the start of the inter-event time or event duration (years);

θ_t = a vector of distribution parameters dependent on t; and

$g(x,\theta_t)$ = kernel function producing the selected distribution type.

The exponential distribution can be used by selecting $g(x,\theta_t) = \frac{x}{\theta_t}$.

The generalised exponential distribution provides flexibility by allowing different kernels to be used. The kernel can be any function that is a non-decreasing function of x such that for $x_1 < x_2$ the kernel satisfies $g(x_1,\theta_1) \le g(x_2,\theta_2)$, that passes through (0,0) and that approaches infinity as $x \to \infty$. This provides the ability to use functions for the inter-event times and event durations that more appropriately describe these distributions.

The generalised exponential distribution can be re-expressed as:

$$\ln[1-F(x\,|\,\theta_t)] = -\,g(x,\theta_t) \tag{3.6}$$

which allows graphical identification of the appropriate kernel.

The probability density function of the generalised exponential distribution can be expressed (Lambert and Kuczera, 1998) as:

$$\ln(f(x\,|\,\theta_t)) = \ln\left(\frac{dg}{dx}\right) - g(x,\theta_t) \tag{3.7}$$

The generalised exponential distribution was used to simulate the random variables t_a and t_d, which define the location and length of the event pulses shown in Figure 3.1(a).

3.4.3 Model Calibration Techniques

The two most commonly used calibration methods for parameter estimation are the method of moments and the method of maximum likelihood.

The method of moments can yield simple expressions for parameter estimation but it tends to give parameter estimates with larger variances than those calculated using the method of maximum likelihood (Foufoula-Georgiou and Guttorp, 1987).

A disadvantage of the method of moments is discussed by Foufoula-Georgiou and Guttorp (1987) for the Neyman-Scott White Noise (N-SWN) model. Estimates for some of the parameters were found to be unstable with small changes in an empirical moment estimate leading to large changes in the estimated parameter values. This created high variability in one of the parameters of this model. The method of moments is sometimes used for its quality of preserving the low-order moments, which is important for models that are used as the input to hydrological simulations. However, as empirical moments have large variability it is more important to validate the structure of the model against available data rather than choose particular empirical moments and preserve these during a simulation (Foufoula-Georgiou and Guttorp, 1987).

The sensitivity of the method of moments estimate equations is also illustrated by Foufoula-Georgiou and Guttorp (1986), where two methods of fitting the N-SWN model were

compared, yielding models with very similar moments but quite different estimated parameters values. This severely limits the physical interpretability of the parameters and illustrates the need for independent checking of the components of the stochastic model that is being calibrated.

The method of maximum likelihood is generally attributed to statistician R.A. Fisher. It is a well respected method since it yields asymptotically efficient estimators (Foufoula-Georgiou and Guttorp, 1987). However, the form of the likelihood expression can be complicated. Unlike the method of moments, it provides a procedure for deriving the point estimator of the parameter directly and often has the minimum variance (asymptotically), particularly for a large sample size *n* and is hence considered the "best" estimate (Ang and Tang, 1975). It has the ability to evaluate lower order moments using the theoretical formulae, allowing these to be compared with the corresponding sample moments from the data, without having an in-built dependence on these measures.

The method of maximum likelihood was chosen for this study because of its robustness and the ability to independently compare lower order moments which can assist in checking the validity of the model structure.

Method of Maximum Likelihood

If a random variable (*X*) with observed sample values $(x_1, x_2, \cdots, x_n)$ has a density function $f(x;\theta_t)$, then by the principle of maximum likelihood the value of θ_t is calculated to maximise the likelihood of obtaining the observed values.

The likelihood of obtaining a particular sample value x_i can be assumed to be proportional to the value of the probability density function evaluated at x_i (Ang and Tang, 1975). Therefore, assuming random and independent sampling, the likelihood of obtaining *n* independent observations $x_1, x_2, \cdots, x_n$ is:

$$L(x_1, x_2, \cdots, x_n) = f(x_1;\theta) f(x_2;\theta) \cdots f(x_n;\theta) \tag{3.8}$$

which is the likelihood function of observing the set $x_1, x_2, \cdots, x_n$. The value of θ_t that maximises the likelihood function is obtained by either differentiating the likelihood function with respect to θ_t and equating the derivative with zero or by numerically maximising the

likelihood. The latter of these methods was adopted here.

During estimation, the likelihood function can become so small that on a computer it is indistinguishable from zero due to its multiplicative nature. For this reason maximising the logarithm of the likelihood function is generally preferred as this format is additive. The logarithm of the likelihood function is defined as:

$$\ln[L(x_1, x_2, \cdots, x_n)] = \ln[f(x_1;\theta)] + \ln[f(x_2;\theta)] + \cdots + \ln[f(x_n;\theta)] \quad (3.9)$$

3.4.4 Development of the Likelihood Function

Equation 3.7 allows a simple construction of the logarithmic likelihood function needed to estimate θ_t. However, this equation is only applicable when the exact start and finish times of each inter-event time and event duration is available. The recorded rainfall data used in this study had depths accumulated over discrete intervals of six minutes. Therefore, the exact time that an inter-event time commences and finishes is unknown. Similarly, the exact time that each rainfall event commences and finishes is unknown. Adjustments must be made to the formulation of the likelihood function to account for this uncertainty and avoid an inappropriate use of aggregated data to calibrate a continuous model (refer Section 2.6.4).

Figure 3.10(a) shows an observed inter-event time, surrounded by two rainfall events and Figure 3.10(b) demonstrates how this inter-event time would be recorded by a pluviograph (t_{arec}). A similar scenario is seen for a recorded rainfall event (t_{drec}). Event durations may be either greater than or less than one interval in length. Figure 3.11(a) and Figure 3.12(a) show observed events surrounded by two inter-event periods and Figure 3.11(b) and Figure 3.12(b) show how this rainfall event would be recorded by a pluviograph.

Considering the inter-event time shown in Figure 3.10, zero rainfall would be reported in intervals two to four. But the inter-event time starts during the first interval and finishes during the fifth interval and t_a may be between three to five intervals in length. Ignoring any constraints imposed on the minimum inter-event time, this suggests that t_a may be underestimated by up to 12 minutes.

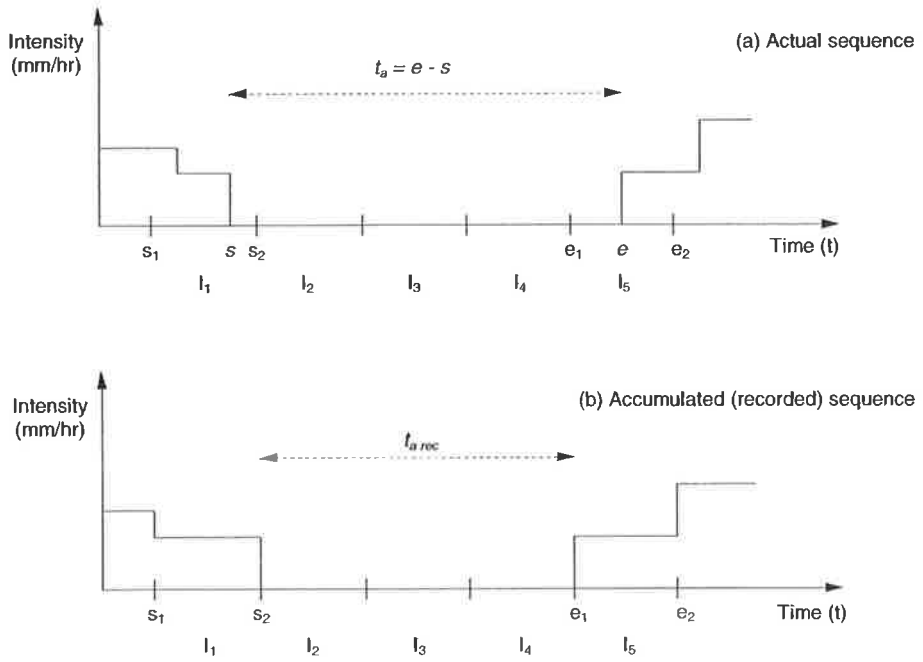

Figure 3.10 Difference between an actual and a recorded inter-event time.

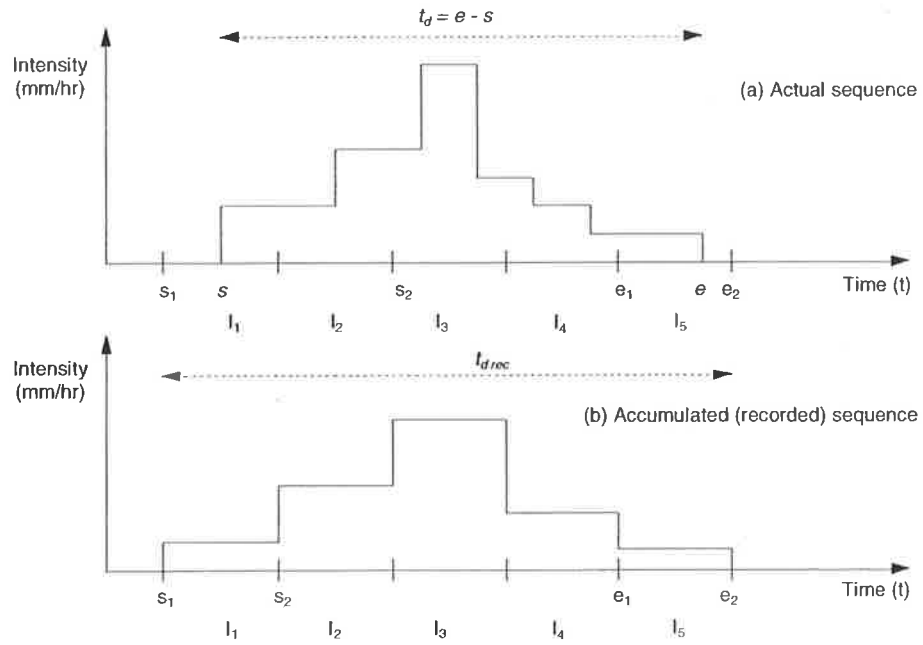

Figure 3.11 Difference between an actual and a recorded rainfall event (t_d >6 minutes) (adapted from Lambert and Kuczera, 1998).

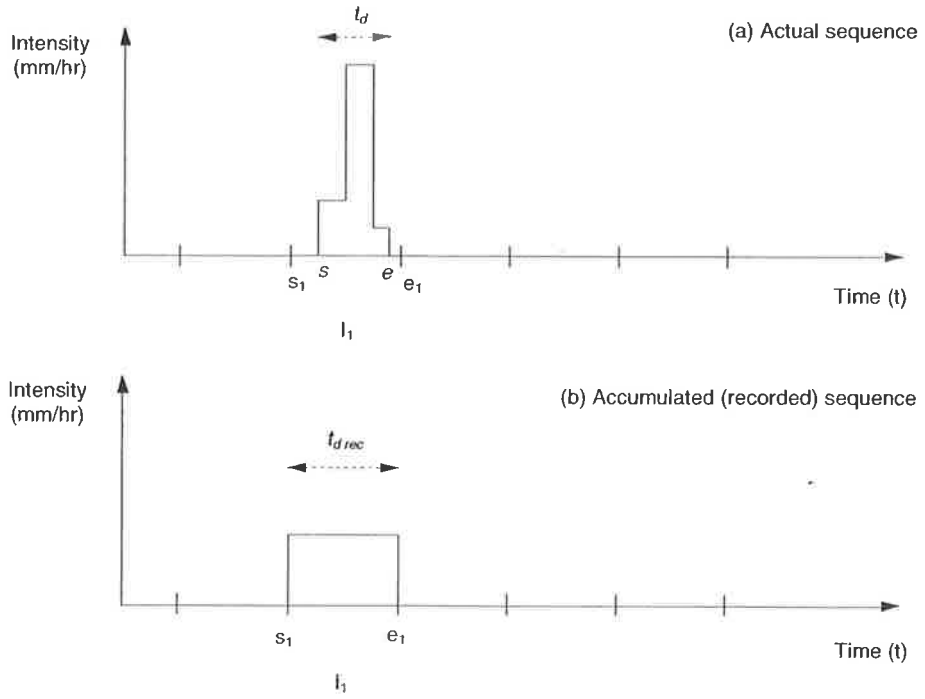

Figure 3.12 Difference between an actual and a recorded rainfall event ($t_d < 6$ minutes) (adapted from Lambert and Kuczera, 1998).

Similarly, for the event duration shown in Figure 3.11, a positive rainfall depth is recorded in intervals one to five but as the event begins in the first interval and finishes in the fifth its length may be overestimated by up to 12 minutes. For a short duration event that begins and ends in the same interval as shown in Figure 3.12, the event may be overestimated by up to six minutes (the length of the interval).

For the data examined in this study between 30 to 40 percent of the event durations are less than 60 minutes, which suggested that uncertainty in the start and end times would affect a significant number of the short duration events. These discrepancies in the start and end times needed to be accommodated in the likelihood function. This is particularly important where the critical event durations of any model using simulated rainfall data are less than one hour, which is a likely situation for the rapid response of small urban catchments.

These discrepancies were accommodated by deriving an expression for the likelihood function of the generalised exponential distribution (Equation 3.5) for each of the following scenarios:

(a) inter-event time,

$$L(t_a;\theta)=\left(1-\exp[-g(t_{arec}+\frac{3}{2}\times 0.1,\theta_t)]\right)-\left(1-\exp[-g(t_{arec}+\frac{1}{2}\times 0.1,\theta_t)]\right); \quad (3.10)$$

(b) event durations greater than one interval in length,

$$L(t_d;\theta)=\left(1-\exp[-g(t_{drec}-\frac{1}{2}\times 0.1,\theta_t)]\right)-\left(1-\exp[-g(t_{drec}-\frac{3}{2}\times 0.1,\theta_t)]\right); \quad (3.11)$$

(c) event durations of one single interval,

$$L(t_d;\theta)=\left(1-\exp[-g(\frac{t_{drec}}{2}\times 0.1,\theta_t)]\right). \quad (3.12)$$

where t_a and t_d are in hours and the pluviograph recording interval is 0.1 hours or six minutes. The full derivation of these equations is shown in Appendix C.

3.4.5 Selection of Kernel Function

As discussed in Section 3.4.2, the generalised exponential distribution allows the graphical identification of a suitable kernel function to represent the observed data. To determine a suitable kernel, an analysis was undertaken by fitting the data with a generalised Pareto kernel, a power law kernel and combination of generalised Pareto and power law kernels.

Generalised Pareto Distribution and Kernel

The Generalised Pareto Distribution (GPD) has a scale parameter (θ_1) and a shape parameter (θ_2) with a probability density function (Rosbjerg *et al.*, 1992) defined as:

$$f(x)=\frac{1}{\theta_1}\left(1-\theta_2\frac{x}{\theta_1}\right)^{\frac{1}{\theta_2}-1} \qquad \theta_2\neq 0 \quad (3.13a)$$

$$f(x)=\frac{1}{\theta_1}e^{\frac{-x}{\theta_1}} \qquad \theta_2=0 \quad (3.13b)$$

and a cumulative distribution function defined as:

$$F(x)=1-\left(1-\theta_2\frac{x}{\theta_1}\right)^{\frac{1}{\theta_2}} \qquad \theta_2\neq 0 \qquad (3.14a)$$

$$F(x)=1-e^{\frac{-x}{\theta_1}} \qquad \theta_2=0 \qquad (3.14b)$$

For $\theta_2=0$ the GPD is equivalent to the exponential distribution and for $\theta_2<0$ the Pareto distribution (PD) is obtained. When compared to an exponential distribution, the GPD has a longer tail for $\theta_2<0$ and a shorter tail for $\theta_2>0$. The random variable x has no upper limit for $\theta_2<0: 0\leq x<\infty$ but an upper limit exists when $\theta_2>0: 0\leq x\leq\frac{\theta_1}{\theta_2}$.

Using equations (3.6) and (3.14a, b) the kernel for the GPD is:

$$\ln\left[1-F(x|\theta_t)\right]=-g(x,\theta_t)=-\frac{1}{\theta_2}\ln\left(1-\theta_2\frac{x}{\theta_1}\right) \qquad \theta_1<0,\ \theta_2>0 \qquad (3.15)$$

Power Law Kernel

A two parameter (θ_3 and θ_4) power law kernel has been defined by Lambert and Kuczera (1998) as:

$$\ln\left[1-F(x|\theta_t)\right]=-g(x,\theta_t)=\theta_3 x^{\theta_4} \qquad \theta_3>0,\ \theta_4>0 \qquad (3.16)$$

Generalised Pareto and Power Law Kernel Combination

A GPD-Power Law combination kernel was produced by combining Equations (3.15) and (3.16) to produce:

$$\ln\left[1-F(x)\right]=\frac{1}{\theta_1}\ln\left(1-\theta_1\frac{x}{\theta_2}\right)-\theta_3 x^{\theta_4} \qquad \theta_1<0,\ \theta_2>0,\theta_3>0,\theta_4>0 \qquad (3.17)$$

The parameter ranges shown above are required to ensure that the cumulative distribution function is monotonically increasing and hence provides a valid probability distribution.

Kernel Choice

The probability plots for each of the above kernel functions fitted to the Melbourne inter-event time and event duration (for March) are shown in Figure 3.13 and Figure 3.14.

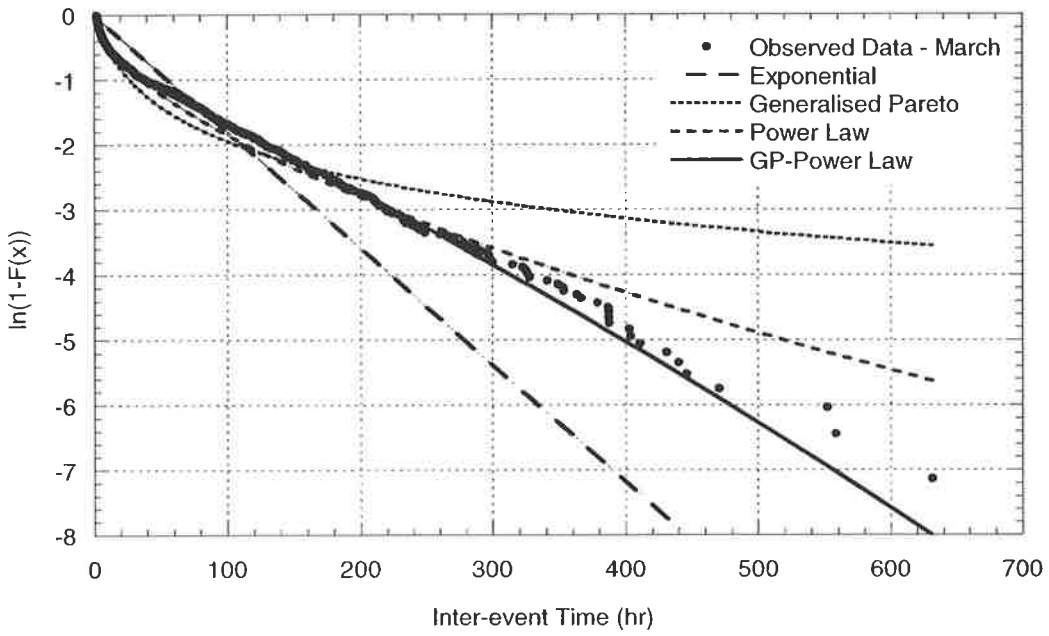

Figure 3.13 Fitted kernels to inter-event time data from Melbourne in March.

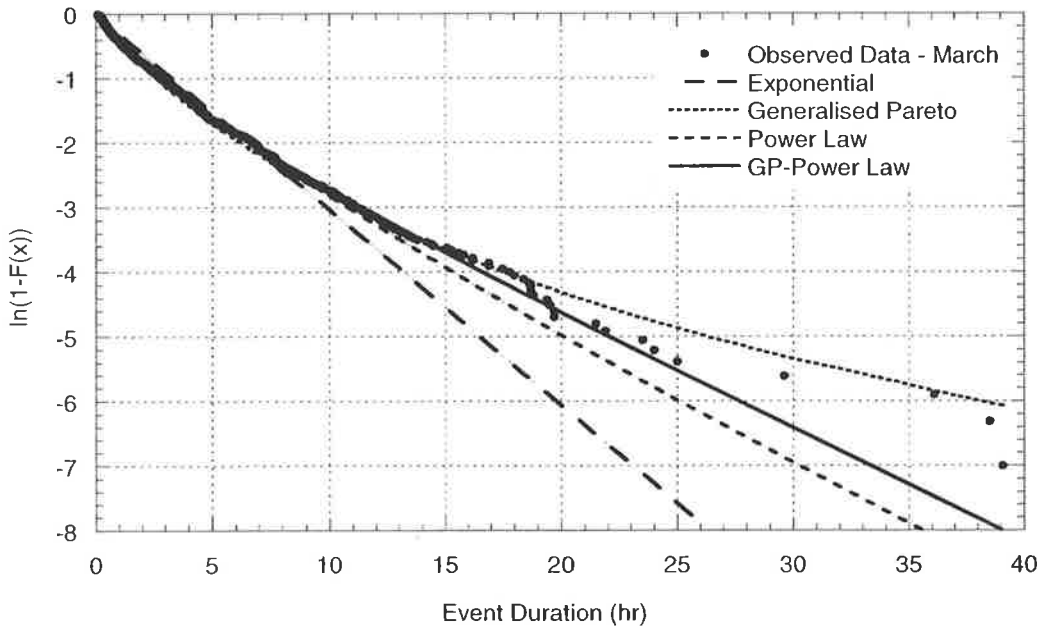

Figure 3.14 Fitted kernels to event duration data from Melbourne in March.

The representation of the data using these kernels to the remaining months is shown in Appendix B.3 and Appendix D.2. For the inter-event times the GP-Power Law kernel is the only kernel that adequately represents the entire shape of the probability distribution. The probability plots, presented in an exponential probability format, clearly indicate that the random variables are not exponentially distributed and that the GP-Power kernel distribution provides an adequate fit, particularly to the concave shape of the distribution for the lower data values. This kernel also best fits the event duration data, particularly the longer events.

In the kernel formulation the value of the inter-event time can be equal to zero. Since all inter-event times must be greater than two hours (t_{min}), to calibrate the distribution the observed inter-event times are determined from the rainfall record and this data series minus the minimum inter-event time value (t_{min}) is used. When simulating inter-event times a value of two hours (t_{min}) must be added to the value sampled from the calibrated probability distribution.

3.4.6 Seasonality

Seasonal variations in inter-event time and event duration occur over the year. For some sites the seasonal trends in the inter-event time data are very pronounced, particularly where the rainfall is highly seasonal as it is in tropical locations such as Darwin (Figure 3.15). Other locations such as Sydney (Figure 3.16) have more uniform rainfall characteristics and a less pronounced seasonal inter-event time fluctuation. For event duration data, a single seasonal cycle is visible in the Perth data (Figure 3.17) and an apparent multi-cycle fluctuation is seen in the Brisbane data (Figure 3.18), which also shows that where more than one yearly cycle is present its effect can be less obvious. Appendix B.5 and Appendix D.4 show the seasonal trends for all the Australian sites. Seasonal trends in the event duration data are generally less pronounced.

Two methods were considered to incorporate seasonality. The first was to determine parameters for the entire data set and then, using these as a starting point, apply an harmonic variation of these parameters over the year using a Fourier series type equation. The second method was to fit the distribution parameters over smaller periods of the year such as seasons or months.

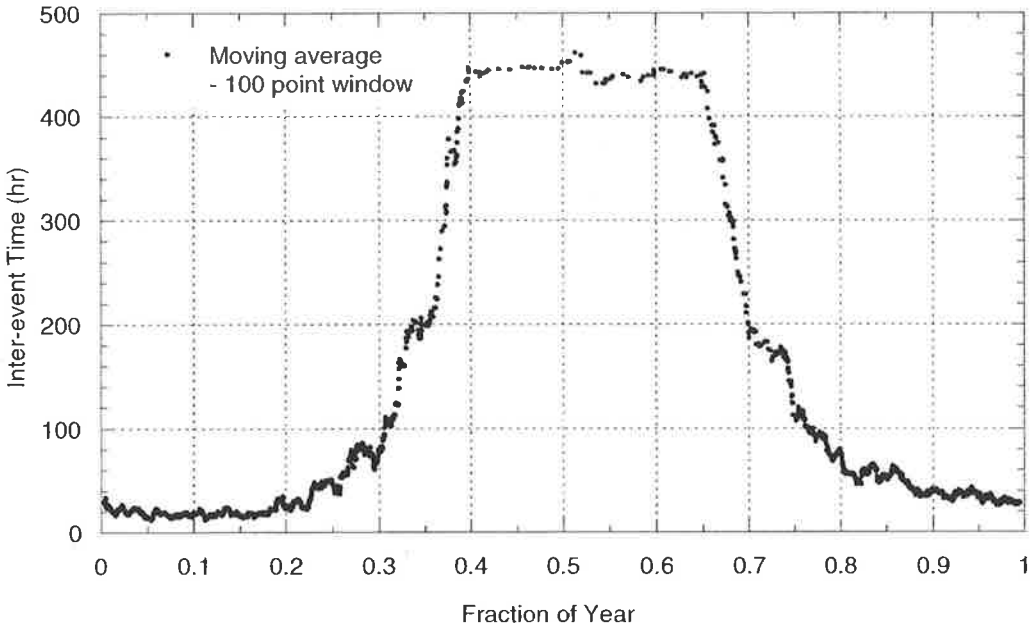

Figure 3.15 Moving average of Darwin inter-event time data.

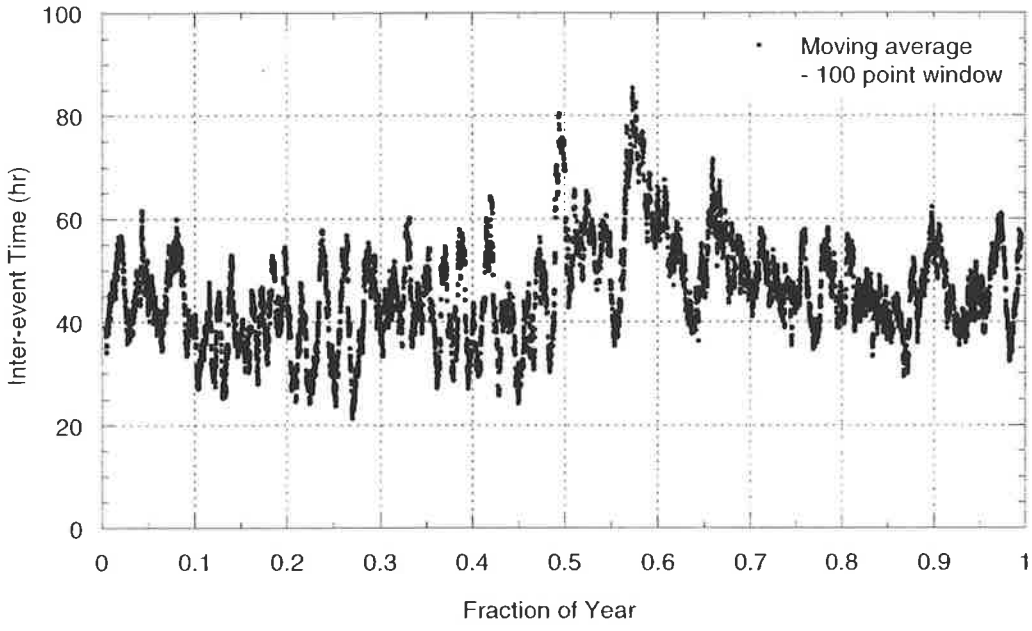

Figure 3.16 Moving average of Sydney inter-event time data.

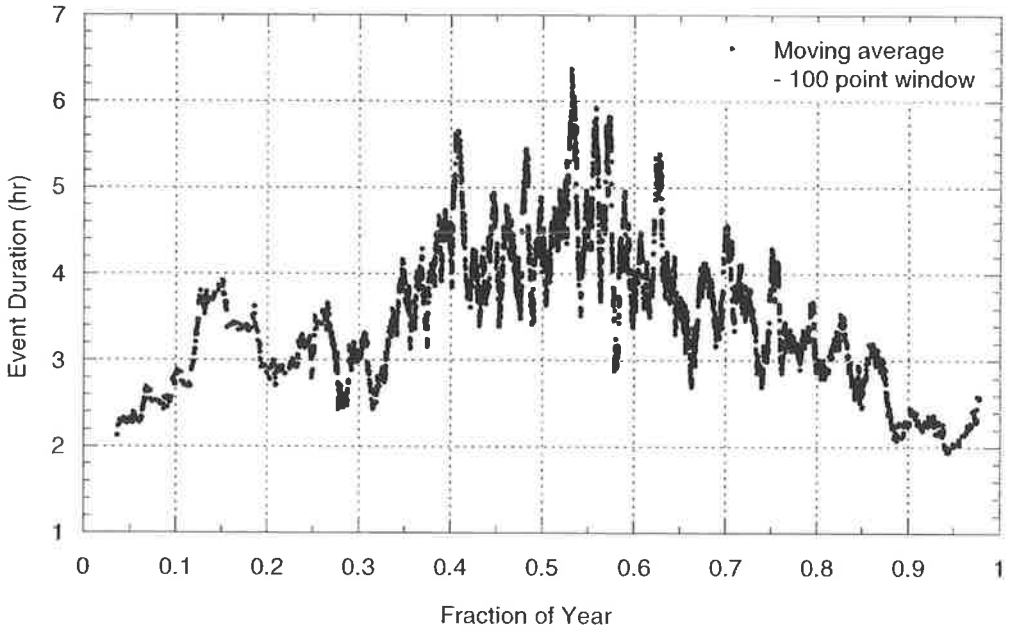

Figure 3.17 Moving average of Perth event duration data.

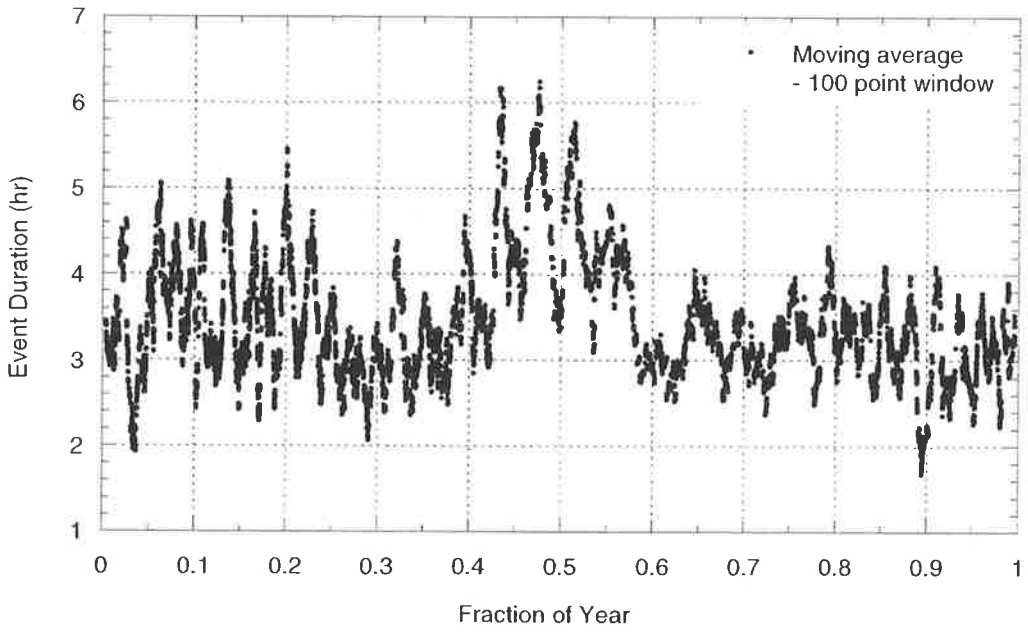

Figure 3.18 Moving average of Brisbane event duration data.

Harmonic Variation

The harmonic variation on the parameters was carried out according to:

$$\theta = \theta_0 + \sum_{k=1}^{n} \alpha_k \sin\left(2\pi k\,(t + \phi_k)\right) \tag{3.18}$$

where:

t = time (years);

n = number of harmonics; and

α_k, ϕ_k = parameters.

The choice of seasonal variation can depend on a number of factors. If there is a gradual change in the distributions of the inter-event time and event duration over the year, such as in areas that have a uniform rainfall distribution with no distinct rainfall season, then an harmonic variation may be the most effective. The advantages of using an harmonic variation on one or more of the parameters include a reduction in the total number of parameters required compared to applying the model to each month of the year, avoiding the problem of events overlapping months and eliminating the problem of high sampling variability if there are small numbers of events in any particular month. Hopkins and Robillard (1964) recommend the use of a continuous seasonal variation rather than discrete monthly steps to allow for any non-stationary effects in the data within each month.

Monthly/Seasonal Parameters

Locations where more than one yearly cycle exists may be more easily represented using monthly parameters. Similarly, in areas where there are sudden transitions from the wet season to the dry season, using monthly parameters may allow the extreme differences between the different seasons to be adequately represented. However, small event sample sizes in dry months may make calibrating the distributions for monthly parameters difficult and a seasonal model may be more appropriate.

A seasonal model requires the seasons to be defined and problems may arise for those months in which the season changes. A similar problem exists with a monthly model as there is no reason for the cyclic changes to occur at the change of a month.

Without the addition of a seasonal component to the representation of inter-event times and

event durations, the GP-Power Law kernel with four parameters (θ_1 to θ_4) is referred to as the *base model*. This model and any subsequent addition of seasonal variation is described here using a sequence of four numbers. The position of each number (one to four) represents each of the four parameters (θ_1 to θ_4) of the distribution and the number itself represents the number of harmonics that have been added to each of the parameters. For example, the base model is referenced as "0000" while the addition of a single harmonic to, for example parameter θ_3, is referred to as "0010".

Figure 3.19 and Figure 3.20 show the probability distribution with no harmonic variations (model 0000) and with a single harmonic on one parameter (model 0010) fitted to the March inter-event time and event duration data for Melbourne. During simulation a probability is generated and then the inter-event time or event duration is determined. Therefore, the differences between the observed data and the fitted curve on the horizontal (time) axis are the most important (refer Figure 3.19). Without harmonics, the model fails to reproduce the strong seasonal dependence on this variable. The addition of only one harmonic to θ_3 for the distribution of inter-event times, gives a significantly improved fit. It is not possible to show a smooth probability distribution for a particular month when an harmonic variation is applied to one or more parameters as the gradual changes in the parameter values over the year produce a gradually changing probability distribution. Therefore, the distribution has been calculated using the midpoint of each month to give a representation of the distribution shape during that month. As the single harmonic produces a gradual change in the parameter value over the year some months may have a noticeable improvement of the representation by the addition of this harmonic but some may show little or no improvement. This is apparent for the event duration data where improvement is only seen in the tail of the distribution. For the mid-length event durations the representation is not as good as the fit without harmonics. Appendix B.6 and Appendix D.5 show the calibration of the GP-Power Law kernel without harmonics and with one harmonic applied to the inter-event time and event duration data respectively, for all months of the year for Melbourne.

Figure 3.21 and Figure 3.22 show fitted probability distributions where parameters have been calibrated for each month. It can be seen that this approach provides an increased flexibility for fitting the distribution to the observed data.

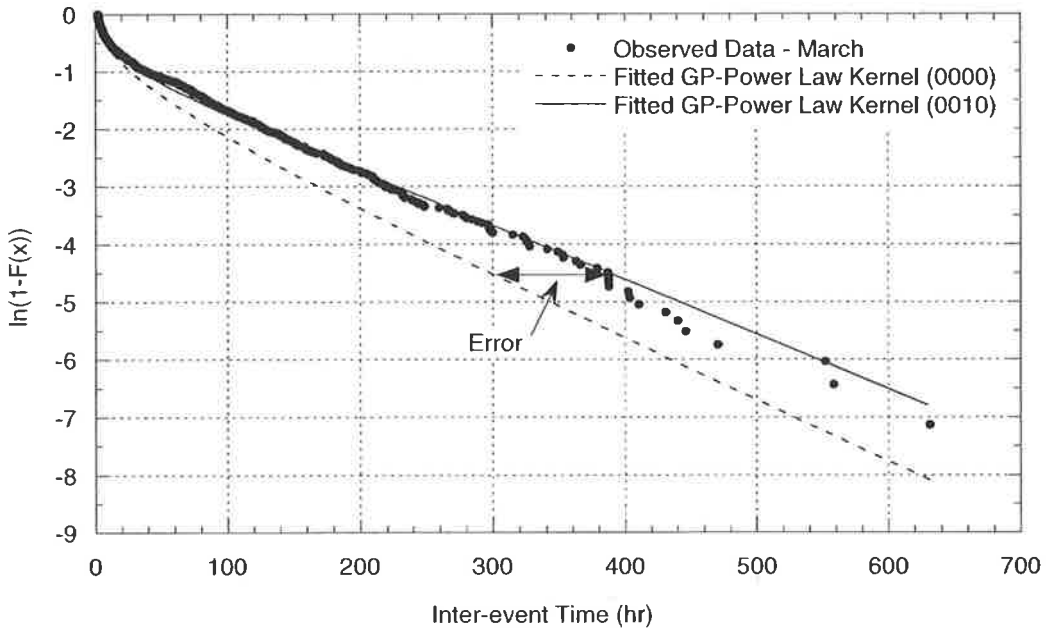

Figure 3.19 GP-Power Law kernel (with and without harmonic variation) fitted to the inter-event time data for Melbourne in March.

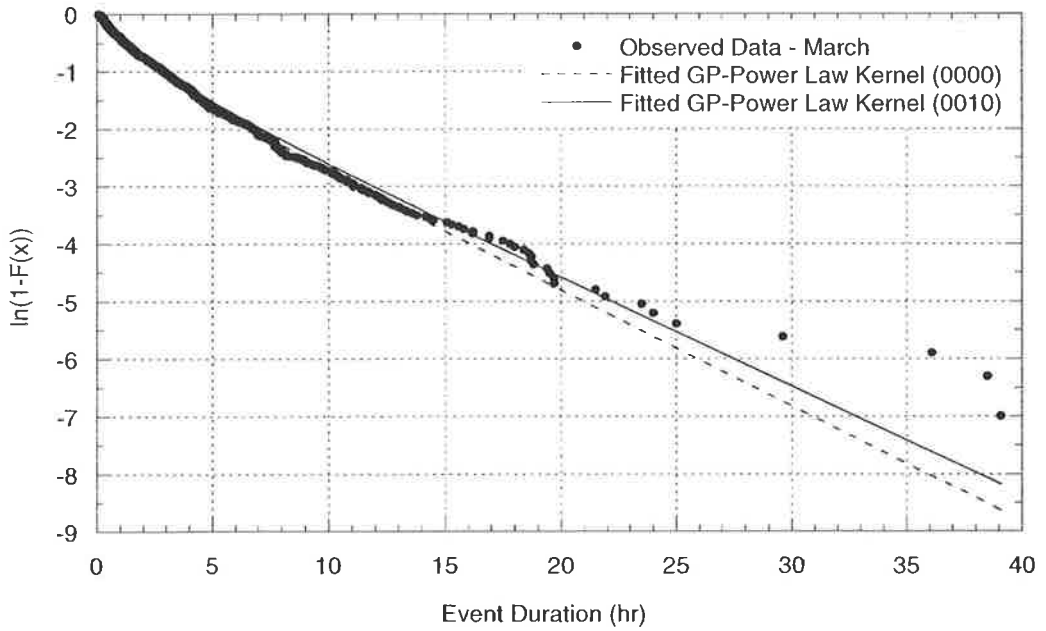

Figure 3.20 GP-Power Law kernel (with and without harmonic variation) fitted to the event duration data for Melbourne in March.

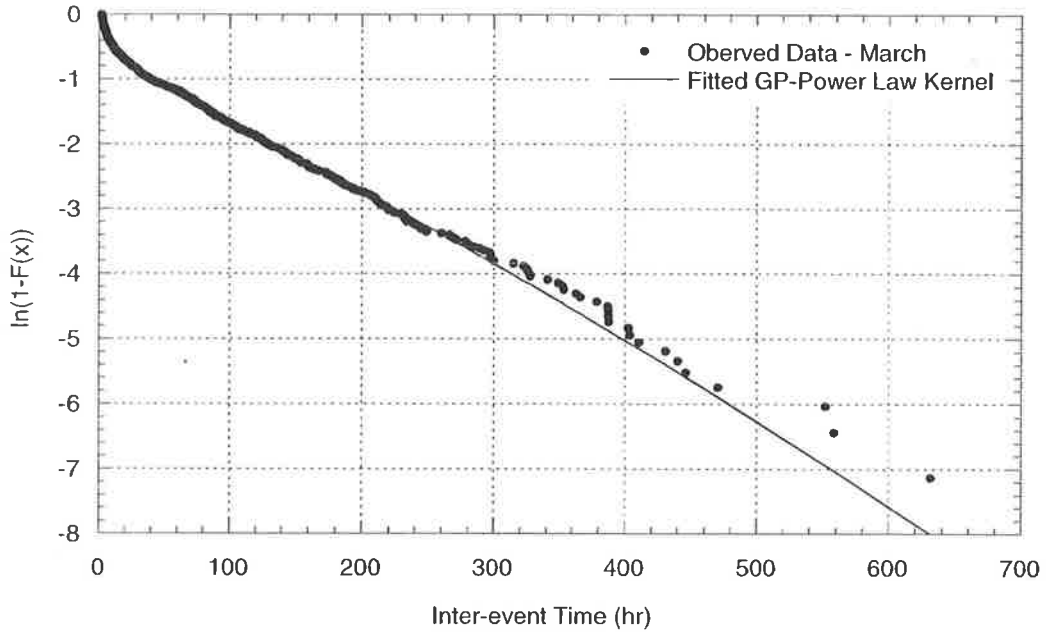

Figure 3.21 GP-Power Law kernel fitted to monthly inter-event time data for Melbourne in March.

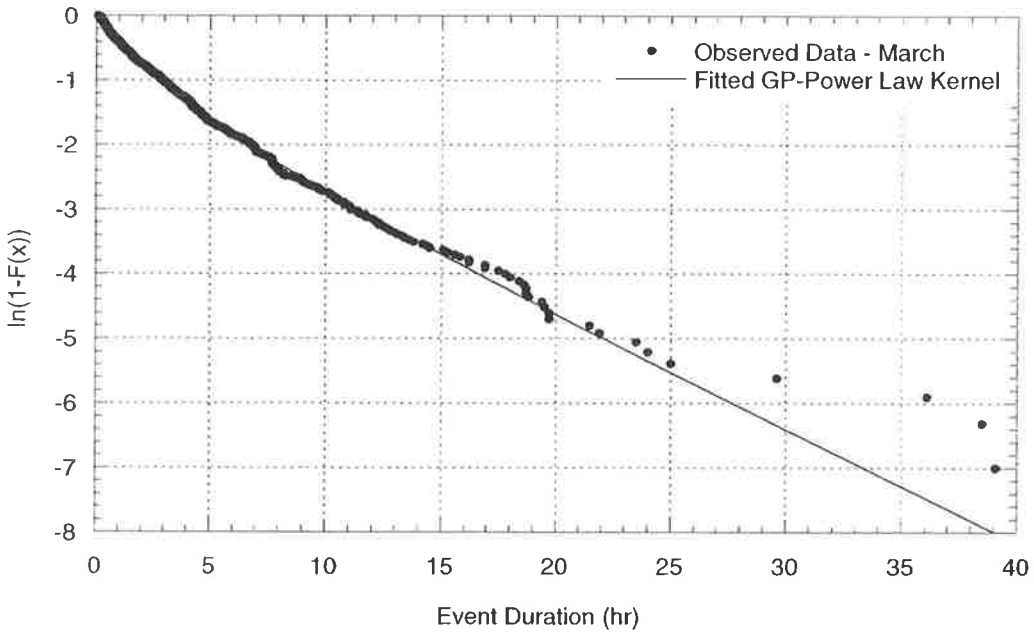

Figure 3.22 GP-Power Law kernel fitted to monthly event duration data for Melbourne in March.

A monthly approach increases the likelihood of obtaining a good representation of the observed data through the kernel function being able to accommodate significant differences in the distribution shape of the data. Although this means that more parameters are required to fit the model to each site, the parameters are generally easily calibrated. The fits for remaining months for both the inter-event time and event duration data are contained in Appendix B.8 and Appendix D.7 respectively.

3.4.7 Spectral Analysis

While seasonal variations can be observed in the moving averages of the inter-event time and event duration data it is not always clear how many cycles are present and which are the most important. A spectral analysis was used to provide an indication of the presence and level of seasonal variations in the data and enable the identification of the level of harmonic variation that should be incorporated into the model. For example, if one dominant cycle is present in the data then it is likely that the addition of one harmonic to one or more of the parameters will adequately reproduce this variation over the year.

Method for Unevenly Sampled Data

The majority of spectral analysis techniques deal with evenly sampled data. However, as with many scientific observations, recorded rainfall data consists of unevenly sampled data. The Lomb method (Press *et al.*, 1992) allows a spectral analysis to be undertaken for unevenly sampled data. The Lomb normalised periodogram (spectral power as a function of angular frequency $\omega \equiv 2\pi f > 0$) evaluates the data and sines and cosines at the times (t_i) that are actually recorded. If there are N data points ($h_i = h(t_i), i=1,\ldots,N$) with mean ($\bar{h}$) and variance ($\sigma^2$) then the periodogram is defined as:

$$P_N(\omega) \equiv \frac{1}{2\sigma^2}\left\{\frac{\left[\sum_j (h_j - \bar{h})\cos\omega(t_j - \tau)\right]^2}{\sum_j \cos^2\omega(t_j - \tau)} + \frac{\left[\sum_j (h_j - \bar{h})\sin\omega(t_j - \tau)\right]^2}{\sum_j \sin^2\omega(t_j - \tau)}\right\} \qquad (3.19)$$

where τ is defined by the relation $\tan(2\omega\tau) = \dfrac{\sum_j \sin 2\omega t_j}{\sum_j \cos 2\omega t_j}$.

The method weights the data on a per point basis instead of on a per time interval basis.

Uneven sampling can introduce serious error in the latter.

A property of the Lomb normalised periodogram is that the viability of the null hypothesis (that data values are independent Gaussian random values) can be rigorously and quantitatively tested to answer the question of how significant is the peak in the spectrum at $P_N(\omega)$? This enables confidence levels to be attached to the values of the spectrum. Press *et al.* (1992) indicate that if M independent frequencies are examined, the probability of a peak value of $P_N(\omega)$ larger than a value z is:

$$P(Z>z) \equiv 1-(1-e^{-z})^M \tag{3.20}$$

under the assumption that the data comes from an independent Gaussian process. When the probability is small, Equation (3.20) can be rewritten as:

$$P(Z>z) \approx M\, e^{-z} \tag{3.21}$$

such that the probability scales linearly with M. Probability levels considered here were 0.1, 0.01and 0.001 (the 10%, 1% and 0.1% levels). A reasonable estimate was considered to be $M = 2\frac{F}{ofac}$, where F is the number of frequencies examined and *ofac* is an over-sampling factor.

The lowest independent frequency examined is the inverse of the span of the input data $\frac{1}{T} = \frac{1}{\max_i(t_i) - \min_i(t_i)}$ which is the frequency for a complete yearly cycle. In general, higher independent frequencies would be multiples of $\frac{1}{T}$ but because the interest is with the statistical significance of any peak, the method requires over-sampling to generate intervals at less than $\frac{1}{T}$ so that sample points lie close to the top of any peak. Therefore, a value of seven was assumed for *ofac* in this study. A maximum frequency (f_{hi}) is specified and the number of independent frequencies evaluated (Press *et al.*, 1992) is:

$$N_P = \frac{ofac \times \frac{f_{hi}}{f_c} N}{2} \tag{3.22}$$

where:

f_c = Nyquist frequency.

Results

Non-dimensionalised results of the spectral analysis of the inter-event time data for Melbourne and the event duration data for Perth are shown in Figure 3.23 and Figure 3.24.

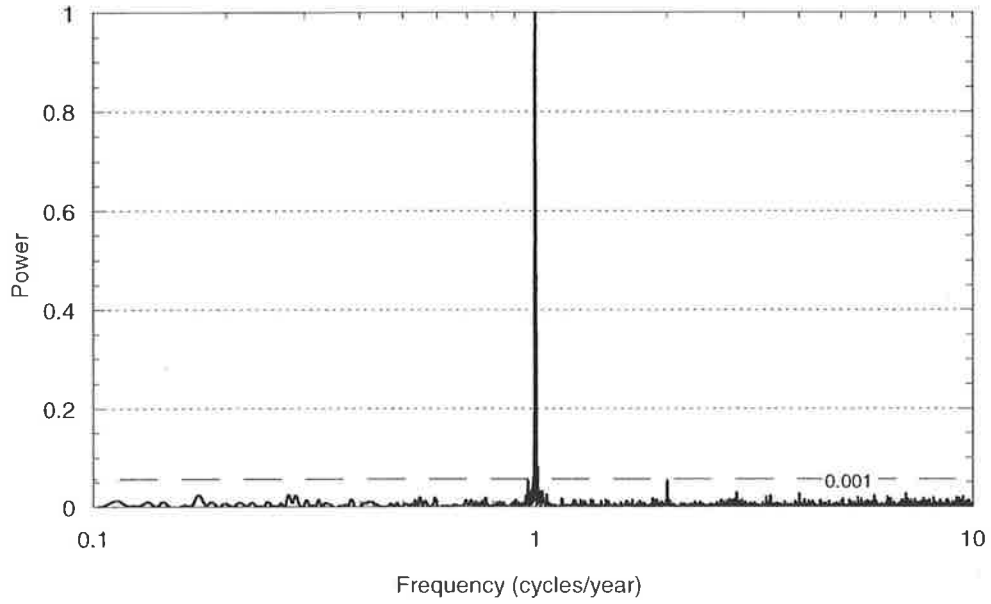

Figure 3.23 Spectral analysis of Melbourne inter-event time data.

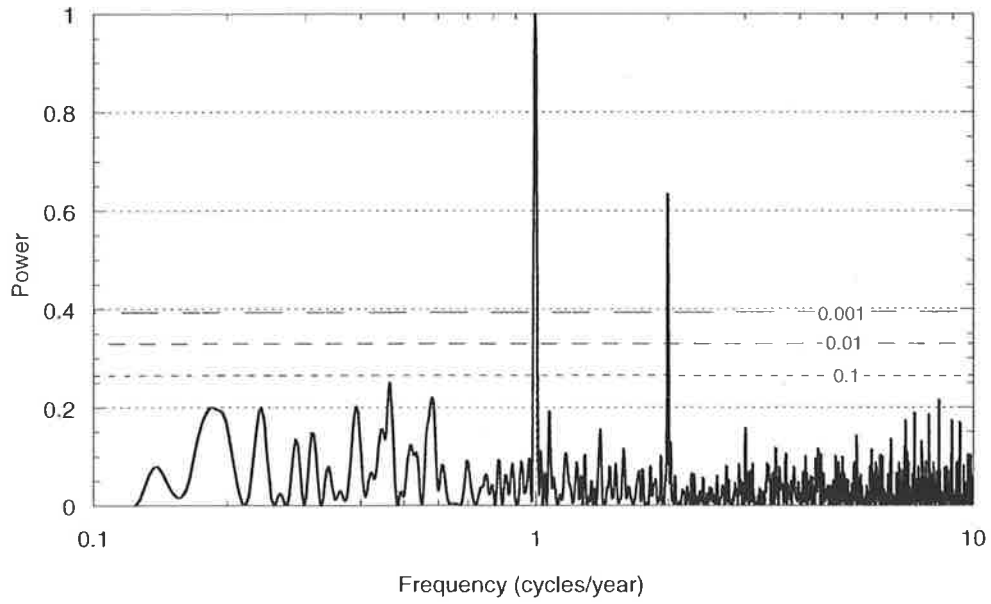

Figure 3.24 Spectral analysis of Perth event duration data.

These figures also include probability levels (0.1, 0.01 and 0.001) that are shown depending on the size of the highest frequency. A dominant spike can be seen at a frequency of one cycle per year in the inter-event time data for Melbourne. This highly significant one cycle per year periodic variation in the inter-event time data is visible at many of the sites. In contrast, the event duration data for Perth shows two important cycles at one and two cycles per year. This suggests that two harmonics may be required for one or more of the parameters of the model to adequately reflect this type of cycle variation.

The results for all sites are shown in Appendix B.4 and Appendix D.3. For each of the locations, the analysis shows that the inter-event fluctuations have a dominant frequency of one cycle per year. For Adelaide, Alice Springs, Brisbane and Perth this is the only significant frequency. Cairns and Hobart show a second significant frequency of two cycles per year. These are less significant in relation to the single yearly cycle, but still surpass the 0.01 significance level and approaches the 0.001 level. Darwin and Townsville both have significant frequencies of two cycles per year and a lesser but still significant spike that surpasses the 0.001 level at three cycles per year. The Sydney data also shows a very significant frequency of one cycle per year in addition to a spike that is greater than the 0.1 significance level at approximately 4.5 cycles per year.

Analysis of the event duration data does not show any particular frequency to be consistently important for all sites. A frequency of one cycle per year dominates the spectrum for Alice Springs, Cairns, Perth and Sydney, and is significant at the 0.1 level for Hobart. Cairns also has a significant frequency at two cycles per year. For Darwin and Townsville a frequency of two cycles per year is the most dominant and Darwin also has significant frequencies at one and three cycles per year. The frequency of three cycles per year is the most important for Brisbane. For Adelaide there are a number of significant frequencies at approximately one cycle per year while the Alice Springs and Melbourne data shows longer term cyclic variations in the event duration data.

This analysis aids in the determination of the level of seasonal variation present in the data and the number of harmonics that may be required for the parameters in the model. For example, the event duration data for Alice Springs showed one significant frequency at one cycle per year and for Brisbane one significant frequency at three cycles per year. When harmonic variations were fitted to the parameters of the model, one harmonic was required for

Alice Springs (Figure 3.25a) and three harmonics for Brisbane (Figure 3.25b) on θ_1 to fit the model to the observed seasonal variation. (Alice Springs also required one harmonic on θ_2 and θ_3, and Brisbane required one harmonic on θ_2.)

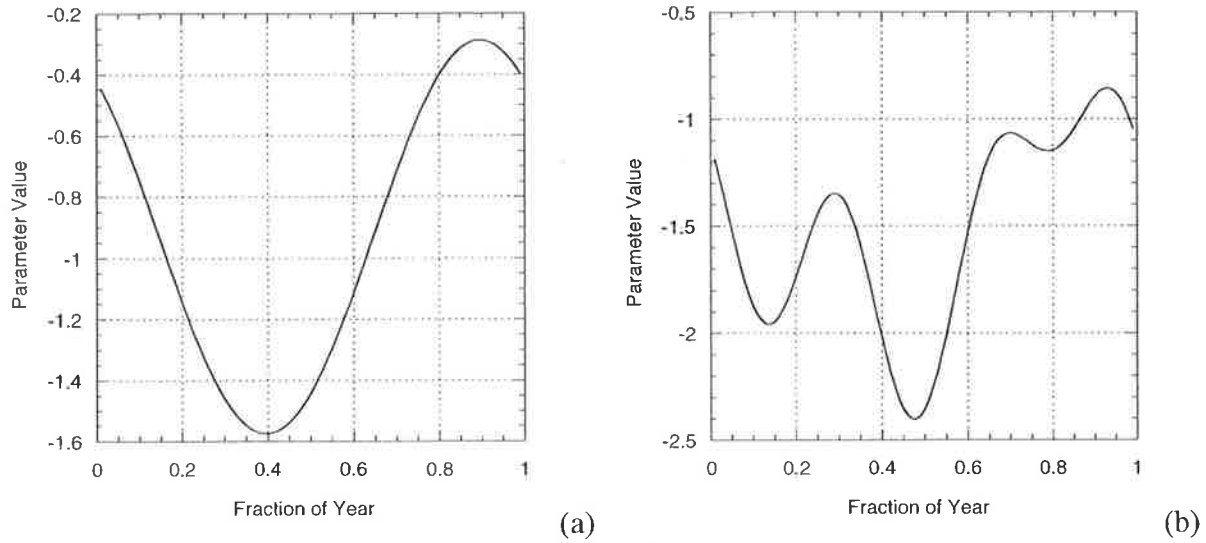

Figure 3.25 Seasonal variation of parameter θ_1 of the event duration model: (a) Alice Springs (one harmonic); (b) Brisbane (three harmonics).

3.4.8 Description of Parameter Estimation Search Methods

Three search methods were used to determine the parameters of the GP-Power Law kernel for the inter-event time and event duration data. These were:

(a) Direct search downhill Simplex method of Nelder and Mead (1965) (Press *et al.*, 1992);

(b) Powell's method (Press *et al.*, 1992); and

(c) Shuffled complex evolution (SCE) method (Duan *et al.*, 1992; Kuczera, 1997).

Using these methods in combination was found to be the most likely approach to detect the global optimum.

Some methods only require the evaluation of the function to be minimised while others require evaluations of the derivatives of the function as well. Those calculating the derivatives are considered more powerful (Press *et al.*, 1992) but this is not always enough to compensate for the extra calculations required. The downhill simplex method and Powell's method are both local-type direct search optimisation methods. The simplex method moves

downhill in a straight forward manner and makes no special assumptions about the function. It requires only function evaluations and is robust, but can be slow and it is not efficient in terms of the number of function evaluations required. Powell's method is generally faster in most applications but it is more suited to problems requiring small computational effort.

Powell's method is a direction-set method and the method of choice when derivatives are not easily calculated, as the choice of successive directions does not involve the explicit calculation of the function's gradient. From a starting point and at each stage, a direction is chosen along the function's surface to minimise. The method consists of prescriptions for updating the set of directions as the method proceeds. This can be inefficient, depending on the surface structure, taking many steps to reach the minimum. Local search methods are limited in that they are generally not capable of handling the presence of multiple local optima and can have convergence problems when locating the global optimum (Duan *et al.*, 1992).

The SCE search method is a global optimisation procedure which conducts multiple concurrent searches within the parameter space. Each search is based on a complex (or set) of parameters, which are initially randomly selected from the search space. At each iteration, a simplex is randomly selected from each complex and allowed to evolve in a downhill direction using a probabilistic variant of the simplex search above. The main strength of the algorithm comes from the periodic shuffling and reforming of the complexes that allows global sharing of information about the objective function.

Because of its ability to locate the global optima, this study utilised the SCE search method initially and the search was continued using either a simplex method search or a Powell's method search. In this way, the best possible parameter set was obtained. Parameter estimation for the inter-event time, event duration and average event intensity was carried out in logarithmic space to ensure that parameter constraints were satisfied.

3.4.9 Statistical Evaluation of Incorporated Seasonal Variations

The addition of harmonic variations to one or more of the four parameters of the GP-Power Law kernel allows the kernel to accommodate seasonal changes. However, while seasonal variations in the inter-event times and event durations may be seen in the data, the level to which this variation is incorporated into the model must be assessed. If too many harmonic variations are added to the parameters, the level of seasonal variation and hence the model

may become over-determined from a statistical viewpoint. This means that a model with less harmonics can produce a representation that is just as good statistically as one with a higher number of harmonics.

There are a number of criteria available to statistically choose between models, based on the statistical significance of changes in the value of the maximum likelihood. Three that have been frequently used are the Likelihood Ratio Test (LRT), Bayesian Information Criterion (BIC) and Akaike Information Criterion (AIC). These three tests were used to evaluate the changes in the maximum likelihood estimates from the addition of harmonics during calibration and attempts to identify the most statistically efficient level of seasonal variation required.

Likelihood Ratio Test (LRT)

Asymptotic likelihood ratio theory can be used to evaluate the significance of changes in likelihood resulting from the addition of more parameters to nested models. If $\log l_n\left(\hat{\theta}\right)$ is the maximised log-likelihood for a particular model with n parameters, then it can be shown (Bickel and Doksum, 1977) that:

$$\log\left(\frac{l_n(\hat{\theta})}{l_{(n-k)}(\hat{\theta})}\right) < \frac{1}{2}\chi^2(f,\alpha)k \tag{3.23}$$

where:

$\chi^2(f,\alpha)$ = chi-squared variate;

α = exceedance probability;

f = number of degrees of freedom; and

k = difference in the number of parameters between models.

Table 3.4 shows the $\chi^2(f,\alpha)$ for $\alpha = 0.95$. This test applies only to nested models. The null hypothesis is a reduced model in which some of the parameters are fixed at predetermined values such as zero. This method of model evaluation has been used by Woolhiser and Pegram (1979), Woolhiser and Roldan (1982, 1986), Woolhiser and Osborn (1985) and Lambert and Kuczera (1998).

Table 3.4 Chi-square variates ($\alpha = 0.95$).

Degrees of Freedom (f)	$\frac{1}{2}\chi^2(n,\alpha)$
2	3.0
4	4.7
6	6.3
8	7.8
10	9.2

Bayesian Information Criterion (BIC)

The Bayesian framework for hypothesis testing uses Bayes factors to quantify the evidence for one hypothesized model against another (Kass and Raftery, 1995). The Bayesian Information Criterion (BIC) provides an approximation to the Bayes factor and has widely been used as a statistical model selection criterion (Katz and Parlange, 1995; Jimoh and Webster, 1996). It is defined (Volinsky and Raftery, 2000) as:

$$BIC = -2[l_j(\hat{\theta}_j) - l_0(\hat{\theta}_0)] + (n_j - n_0)\log(N) \tag{3.24}$$

where $l_j(\hat{\theta}_j)$ and $l_0(\hat{\theta}_0)$ are the maximised log-likelihood values for models M_j and M_0 with sample size N. The two models are parameterised by an n_j dimensional vector θ_j, and an n_0 dimensional vector θ_0, respectively.

Bayes factors can be applied to both non-nested models and nested models, whereas the application of non-Bayesian significance tests to non-nested models is difficult (Kass and Raftery, 1994). If $BIC < 0$, then M_j is favoured over M_0, and the more negative BIC is, then the more that M_j is favoured. Therefore, two models can be compared by taking the difference of their BIC values, when each is compared to a base model, for example, M_0.

If M_0 is nested within M_j, then $2[l_j(\hat{\theta}_j) - l_0(\hat{\theta}_0)]$ is the standard LRT statistic for testing M_0 against M_j, and $(n_j - n_0)$ is the difference in the number of model parameters associated within that test.

Raftery (1995) provides a scheme to determine the significance in the differences between the BIC values of different models. This is shown in Table 3.5.

Table 3.5 Significance of Bayesian Information Criterion values (from Raftery, 1995).

BIC difference	Significance
0-2	Weak
2-6	Positive
6-10	Strong
>10	Very Strong

Akaike Information Criterion (AIC)

Akaike (1974) suggested alternative criterion that could be used to objectively choose between models. The model chosen should be the one which minimises the Akaike information criterion (AIC), defined (Kass and Raftery, 1994) as:

$$AIC = -2[l_j(\hat{\theta}_j)] + 2n_j \tag{3.25}$$

where $l_j(\hat{\theta}_j)$ is the maximised log-likelihood for model M_j, parameterised by an n_j dimensional vector θ_j.

This has been used for model evaluation by Eidsvik (1980), Woolhiser and Roldan (1982), Woolhiser and Osborn (1985), Katz and Parlange (1995) and Jimoh and Webster (1996). Eidsvik (1980) found that using the AIC to identify one model from another was unnecessarily complicated and models with a large number of parameters were often chosen. Kass and Raftery (1994) also indicated that the AIC tends to overestimate the number of parameters required, even for large data sets.

Results

Various parameter and harmonic combinations were examined in addition to a monthly model where the GP-Power Law kernel was calibrated to each month. Analysis of the likelihood values for each model for seasonal variation, in conjunction with the LRT, BIC and AIC tests, aided in the decision as to which model best represented each location in terms of parameter efficiency.

Table 3.6 shows the significance of maximum likelihood estimates using the LRT, BIC and AIC tests when compared with the "0000" model for the Melbourne data. The "0010" seasonal model (shown in bold) was the most efficient for both the inter-event times and event

durations. However, there is a significant difference between the BIC of the monthly inter-event time model and that of the "0000" harmonic model. In addition, although the "0010" harmonic model is the most efficient for the event durations, its significance is weak and the additional parameters provide only a small improvement.

These results also show how the addition of an harmonic to the optimum combination can result in a less suitable choice via these tests. In some instances the optimum model chosen was not the same for each statistical test as different tests may select different models. For example, in Table 3.6 the LRT test results for the "0010" model do not identify this model as the optimum. However, the values are very close to the optimum model values.

Table 3.6 Likelihood test results for Melbourne.

	No. of Parameters	$\log l_n(\hat{\theta})$	BIC	LRT	AIC
Inter-Event Time					
0000	4	-131875.5	-	-	263759.0
0010	6	-131515.8	**-710.8**	**359.7**	**263043.6**
1010	8	-131515.0	-703.8	360.5	263046.0
month	48	-131477.2	-607.8	-	263050.4
Event Duration					
0000	4	-76865.2	-	-	153738.4
0010	6	-76859.8	**-2.3**	**5.4**	**153731.6**
1010	8	-76858.3	3.1	6.9	153732.6
month	48	-76830.4	116.8	-	153756.8

Appendix B.7 and Appendix D.6 contain the likelihood estimates for various harmonic combinations and the model chosen for each site. Only the combinations that produced improved models over the "0000" model are shown. In general, it was most important to fit harmonics to the parameters θ_1 and θ_3 as these had the most influence on improving the likelihood estimate and obtaining a better representation of the data. There appears to be a large correlation between the parameters θ_3 and θ_4 such that the addition of any harmonics to θ_4 after θ_3 had little effect on the likelihood, and θ_3 produced the most improvement from the "0000" model.

In a number of cases the monthly models appeared to have an excessive number of parameters as judged by these tests. For example, in Table 3.6 the monthly model shows a significant improvement over the "0000" model for the inter-event time data but does not for the event duration data. Ultimately, the validation of the results from the model simulation must have

the biggest influence on model choice, that is, even if statistical tests indicate that a monthly model is not required, if the results using a model with harmonic variation are not satisfactory then the extra computational effort of determining monthly parameters is warranted.

3.4.10 Validation by Simulation

The accuracy of the calibrated model was validated by comparing the observed inter-event times and event durations to those produced by a 250 year simulation. Simulated distributions for the monthly estimated parameter-based model and the harmonic parameter-based model are shown in Figure 3.26 to Figure 3.29. The reproduction of both seasonal models over the year is discussed further in Section 5.1. In general the models described by monthly parameters produced better simulated distributions than those that used harmonic variation to account for seasonality.

Although the statistical tests used in this section to evaluate the harmonic and monthly models generally favoured the harmonic models over the monthly models, the results of the simulation favour the use of monthly models. It must be emphasised that an over-determined model is not a drawback provided the parameters can be estimated. The structure of the event-based alternating renewal model developed in this study allows for the straightforward calibration of parameters because the calibrated events are easily observable in the historical data. Because the main focus in this study is goodness-of-fit and an adequate representation of the observed data rather than parsimony, the monthly models were preferred for the representation of both the inter-event time and event duration data.

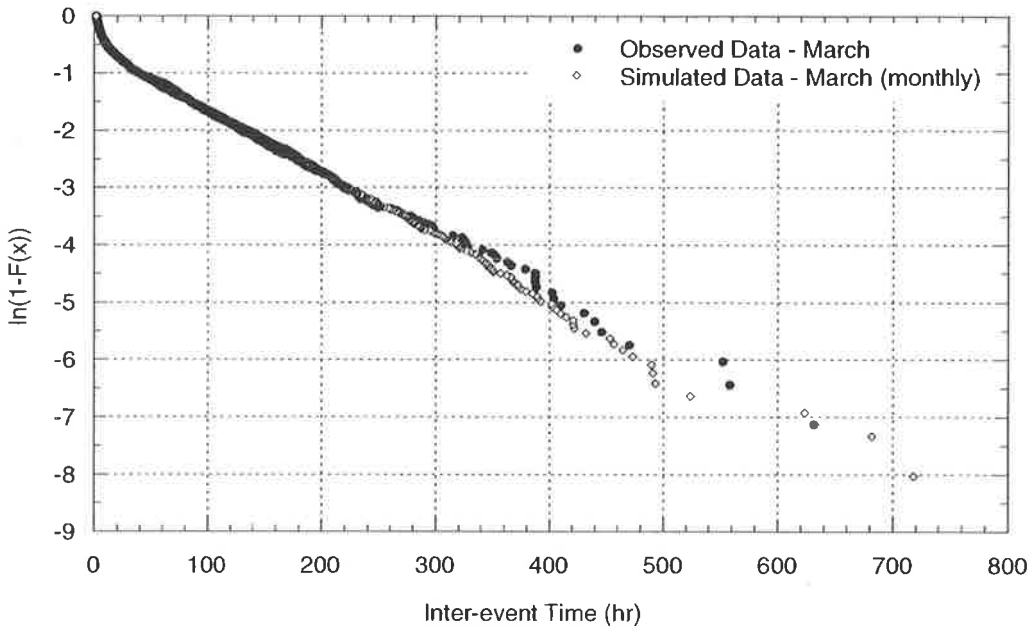

Figure 3.26 Observed and simulated inter-event times using a monthly parameter-based model for Melbourne in March.

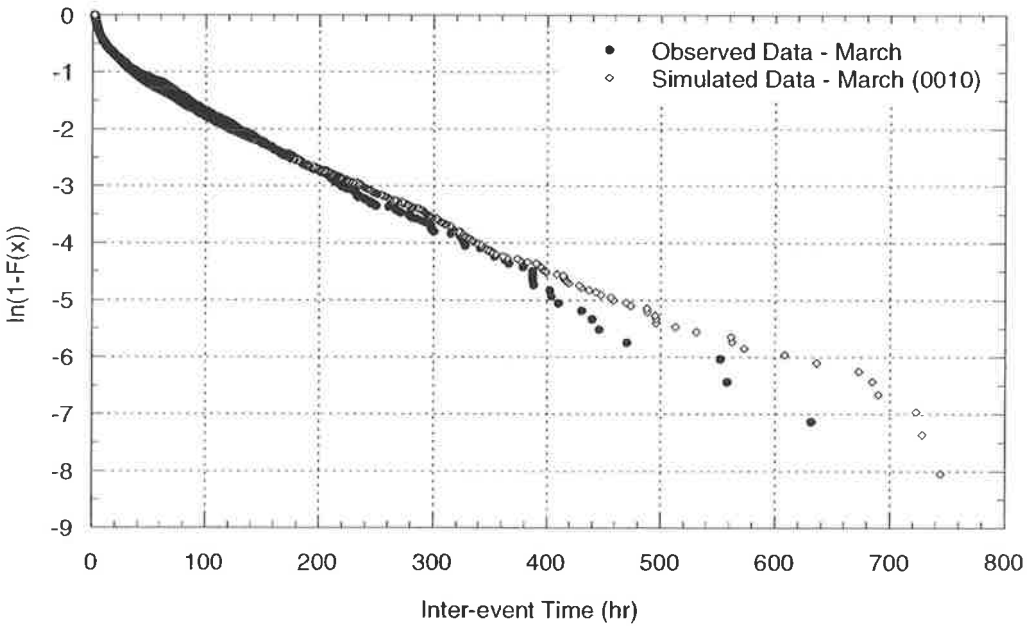

Figure 3.27 Observed and simulated inter-event times using an harmonic parameter-based model (0010) for Melbourne in March.

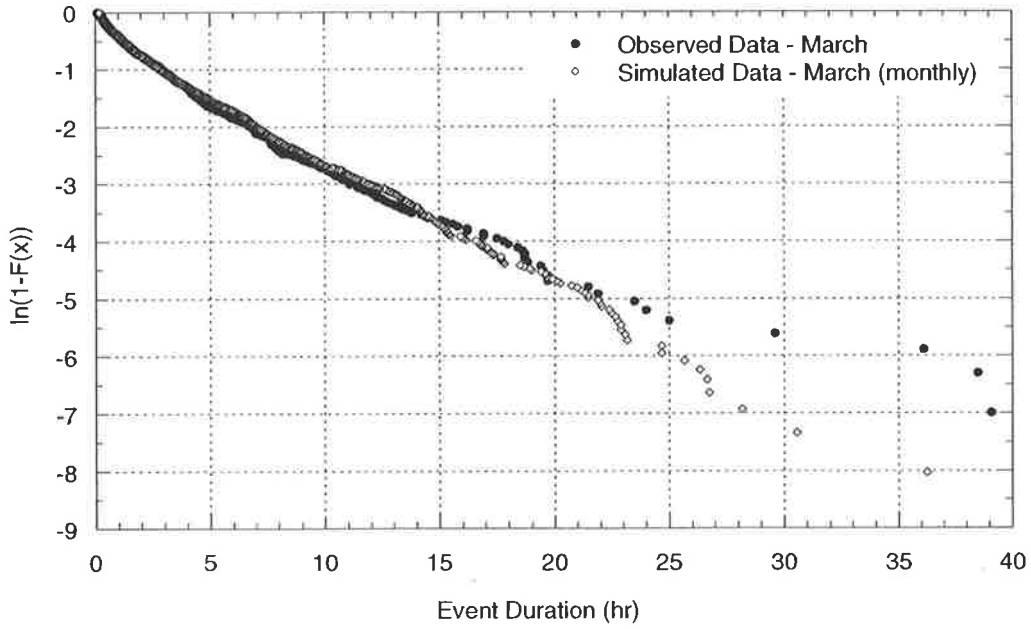

Figure 3.28 Observed and simulated event durations using a monthly parameter-based model for Melbourne in March.

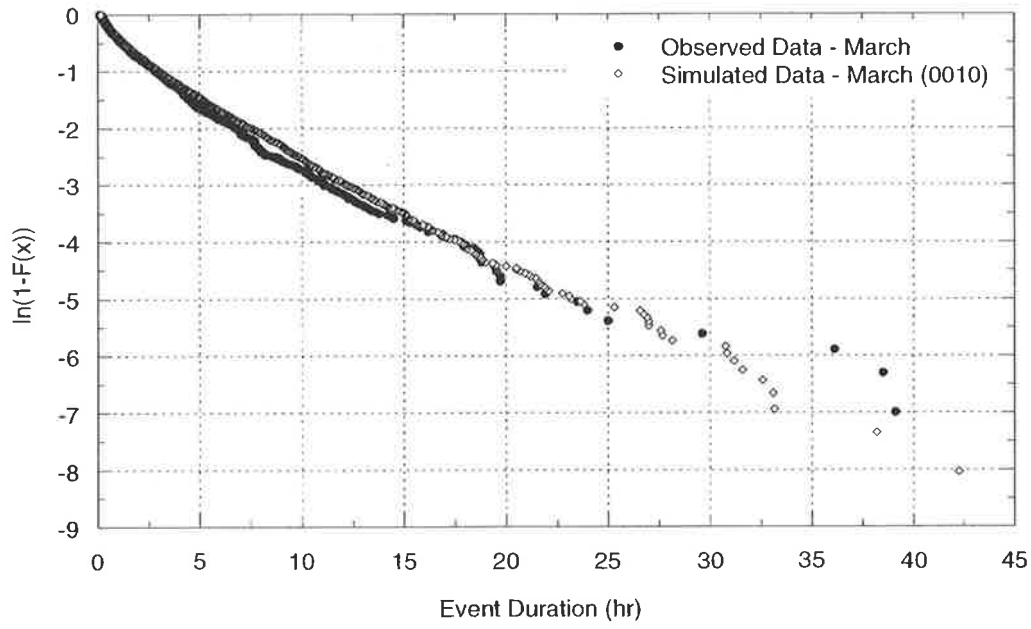

Figure 3.29 Observed and simulated event durations using an harmonic parameter-based model (0010) for Melbourne in March.

3.5 Development of an Average Event Intensity Model

A probability distribution was needed that would describe the average event intensity (i) as defined in Figure 3.1(a). The development of a model to describe this variable involved:

(a) reviewing previous research from which a suitable distribution was chosen;

(b) incorporating into the chosen distribution a method to account for observed dependence between average event intensity and event duration;

(c) incorporating into the chosen distribution a method to account for the seasonal effects on the average event intensity and its relationship with event duration; and

(d) evaluating the calibrated distribution parameters by validating the marginal distributions of the simulated data with the observed data.

3.5.1 Previous Research

In event-based rainfall models, there have been numerous probability models used to describe the distribution of inter-event times and event durations. Similarly, the average event intensity and depth has been modelled using a variety of distributions including the gamma distribution (Eagleson, 1978b; Acreman, 1990; Koutsoyiannis and Foufoula-Georgiou, 1993; Robinson and Sivapalan, 1997), the Weibull distribution (Grace and Eagleson, 1966, 1967) and the generalised Pareto distribution (Van Montfort and Witter, 1986; Lambert and Kuczera, 1996; Cameron *et al.*, 1999).

Figure 3.30 shows the distribution of average event intensity for Brisbane, Darwin and Melbourne. These distributions exhibit a similar concave nature to those of the inter-event times and event durations. This concavity is one of the reasons for the use of the generalised Pareto (GP) distribution to describe rainfall depths by Van Montfort and Witter (1986). The GP distribution, described in Section 3.4.5, also has the desirable property of having an upper limit when the standard deviation is less than the mean. This reduces the possibility of generating unrealistic combinations of events with large average rainfall intensities and long durations. For these reasons, the generalised Pareto distribution (Rosbjerg *et al.*, 1992) was chosen to model the average event intensity. The distributions for all sites are shown in Appendix E.1.

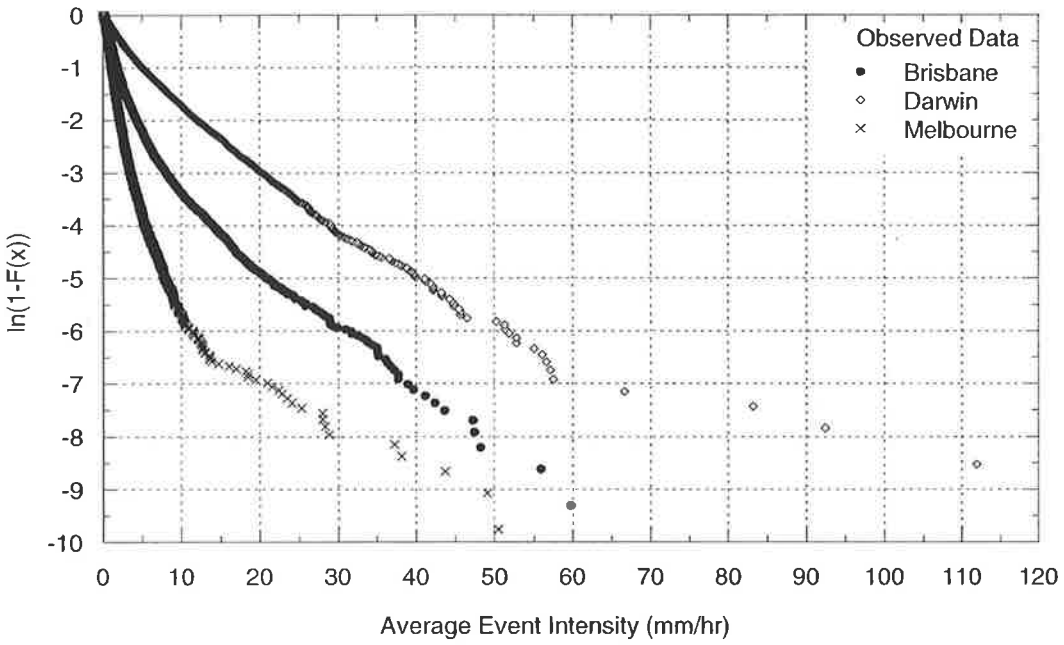

Figure 3.30 Distribution of average event intensity for Brisbane, Darwin and Melbourne.

3.5.2 Conditional Relationship with Event Duration

The conditional relationship between average event intensity and event duration, along with the importance of modelling this relationship successfully, has been well established and incorporated into event-based models of point rainfall (Grace and Eagleson, 1966, 1967; Acreman, 1990; Lambert and Kuczera, 1996; Robinson and Sivapalan, 1997; Cameron *et al.*, 1999). An examination of the historical data used for this study found this relationship to be clearly observable, as shown for Melbourne in Figure 3.31, with the remainder of the sites shown in Appendix E.4. Figure 3.32 shows this relationship on a logarithmic plot where the low average intensity and duration events can be more clearly observed.

It is also observed that shorter duration events generally have higher intensities than longer duration events, although, for durations greater than 20 hours, the mean intensity often reverses its declining trend and starts to increase. The rainfall model must be able to reproduce the average event intensity, as well as adequately represent its dependency on the event duration.

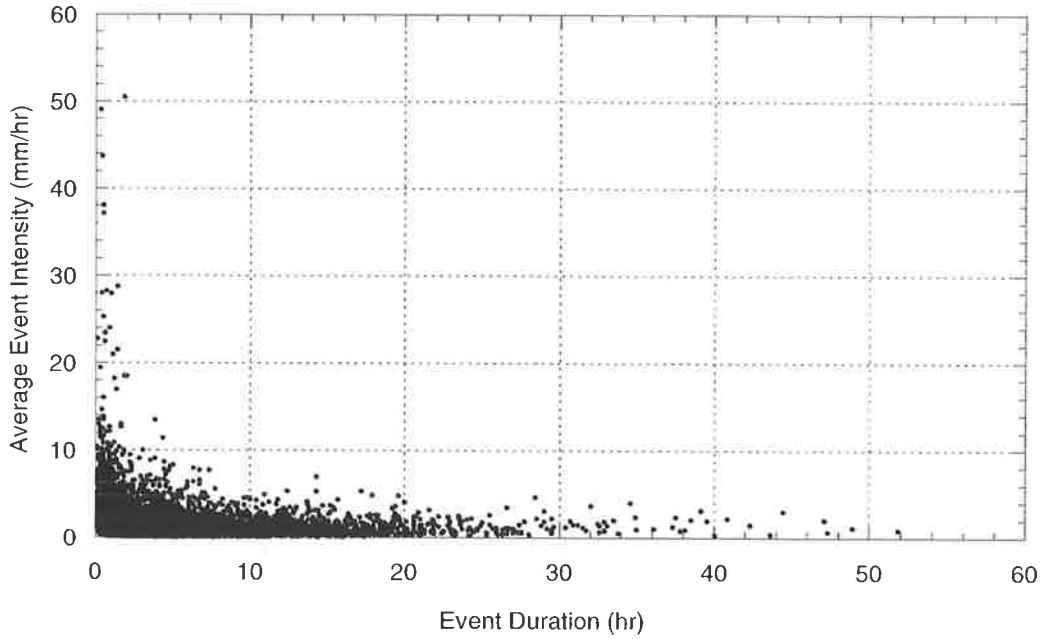

Figure 3.31 Relationship between average event intensity and event duration for Melbourne.

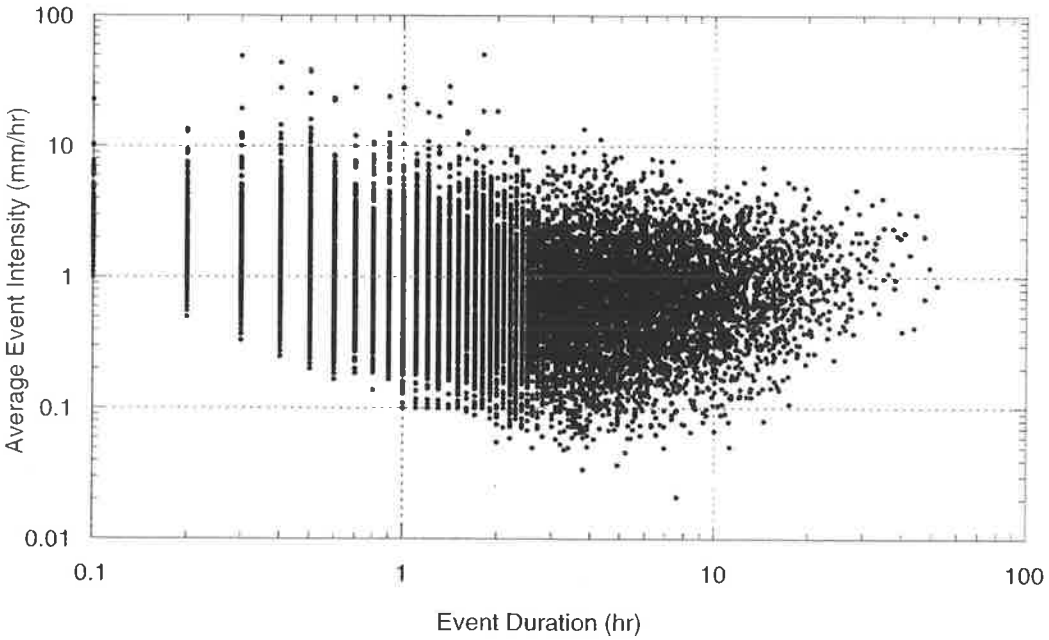

Figure 3.32 Logarithmic relationship between average event intensity and event duration for Melbourne.

3.5.3 Conditional Probability Model of Average Rainfall Intensity

The parameters of the GP probability distribution kernel chosen to represent the average event intensity can be related to the mean and standard deviation of average event intensity conditioned on event duration. In this way, the dependence of intensity upon event duration can be incorporated into the model. The mean and variance of this distribution is defined (Rosbjerg *et al.*, 1992) as:

$$\mu = E[X] = \frac{\theta_1}{1+\theta_2} \qquad \theta_2 > -1 \qquad (3.26a)$$

$$\sigma^2 = Var[X] = \frac{\theta_1^2}{(1+\theta_2)^2(1+2\theta_2)} \qquad \theta_2 > -\frac{1}{2} \qquad (3.26b)$$

Using these equations, the parameters θ_1 and θ_2 can be solved using the sample mean ($\hat{\mu}$) and variance ($\hat{\sigma}^2$) by the following:

$$\hat{\theta}_1 = \frac{1}{2}\hat{\mu}\left(\frac{\hat{\mu}^2}{\hat{\sigma}^2}+1\right) \qquad (3.27a)$$

$$\hat{\theta}_2 = \frac{1}{2}\left(\frac{\hat{\mu}^2}{\hat{\sigma}^2}-1\right) \qquad (3.27b)$$

3.5.4 Conditional Function for Model Parameters

It is clear from Figure 3.32 that both $\hat{\mu}$ and $\hat{\sigma}$ depend on $\ln(t_d)$. This dependence is denoted by the function $\hat{\mu} = f_{\hat{\mu}}(\ln(t_d))$ and $\hat{\sigma} = f_{\hat{\sigma}}(\ln(t_d))$. In order to determine what type of conditional function would best describe the relationship between the mean and standard deviation of average event intensity and event duration, a moving average of average event intensity against event duration using a window size of 50 points was undertaken. The outcome of this process is shown in Figure 3.33 and Figure 3.34 for the Melbourne and Brisbane data. This gives an indication of how the mean of the average event intensity changes with increasing event duration. It is interesting that the basic shape is similar for both these cities, as it is for the remaining sites shown in Appendix E.5, even though the climates are very different.

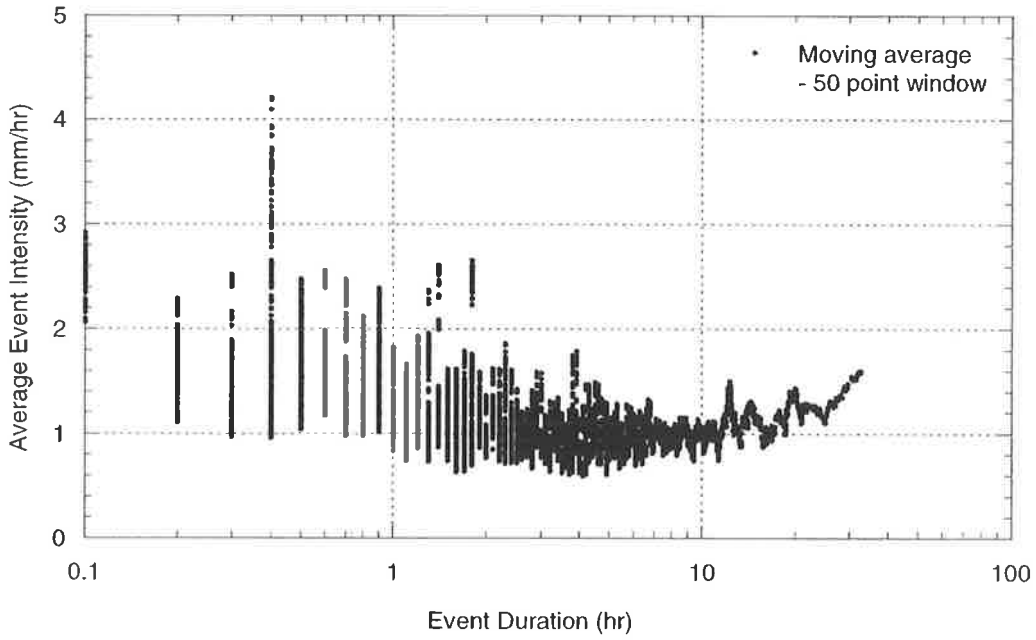

Figure 3.33 Moving average of average event intensity with event duration for Melbourne.

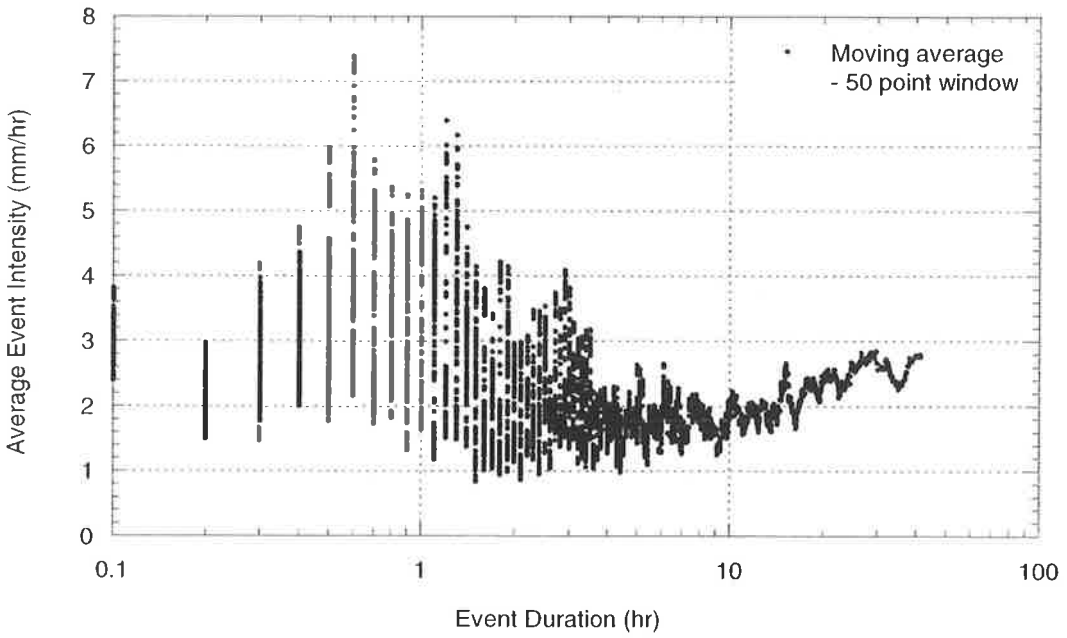

Figure 3.34 Moving average of average event intensity with event duration for Brisbane.

Mean and Standard Deviation Function Development

From observations of the shape of the moving average of average event intensity, a cubic polynomial function was selected to represent the mean and standard deviation of average event intensity. To prevent the increase in the intensity from persisting for the longer durations, which would produce unrealistic combinations of event duration and average event intensity, a cut-off duration was chosen beyond which the function remained constant. This duration was chosen from visual inspection of the data. However, through simulation it was found that this function was unable to adequately reproduce the Intensity-Frequency-Duration (IFD) statistics, as the conditional relationship between event duration and average event intensity was not adequately modelled. Difficulties with the calibration of parameters were also encountered, particularly when trying to incorporate seasonal variations (Section 3.5.5). It was concluded that the function chosen was not flexible enough to represent the changes in intensity with event duration while at the same time remain easily calibrated.

As an alternative, two broken line functions were defined to represent the relationship between event duration and average intensity. While these may be more parameter intensive, they were the most flexible option for the representation of average event intensity moments. For a given event duration, these functions yield the conditional mean and standard deviation of the average event intensity, from which the two GP parameters can be computed. Both functions are continuous and consist of a series of straight line segments to represent the changes in variation of the mean and standard deviation of average event intensity as the event duration increases. The number of segments was chosen to minimise the number of parameters while at the same time adequately describing the relationship (the shape of the curve).

The conditional functions defined for Melbourne are shown in Figure 3.35 and Figure 3.36. Also shown is the broken line function used to represent the changes in mean and standard deviation of average event intensity with event duration. Each point is the mean or standard deviation of intensity of 50 events. These points were calculated by ranking all rainfall events in order of increasing event duration and averaging the mean and standard deviation of average event intensity for successive groups of 50 events. The mean event duration of each group of 50 points was used for plotting purposes. The conditional functions for all sites are shown in Appendix E.6.

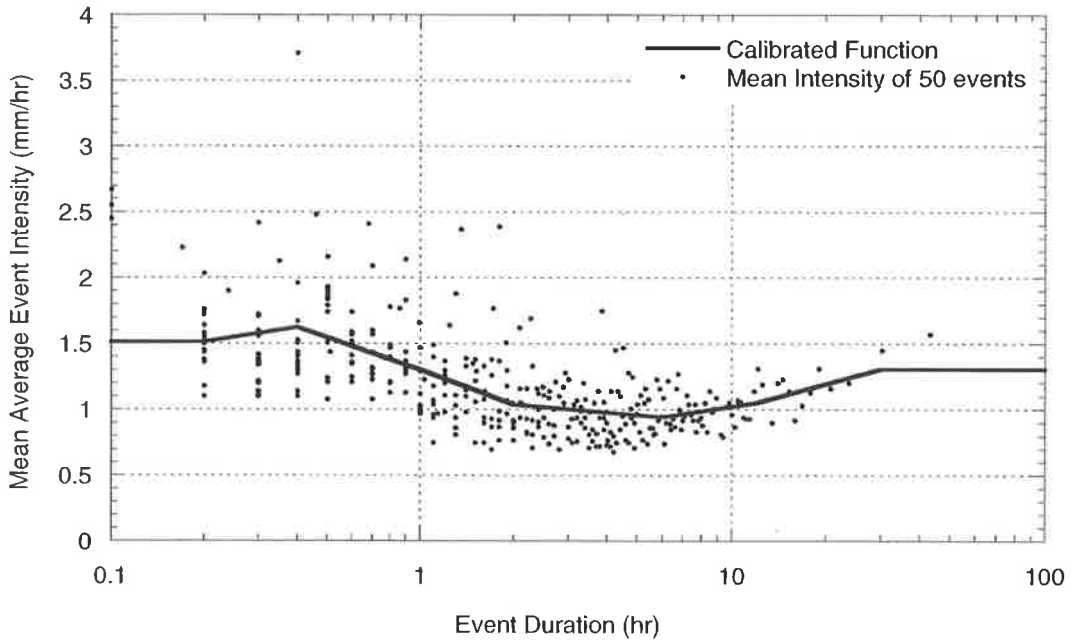

Figure 3.35 Variation of the mean average rainfall intensity with event duration for Melbourne.

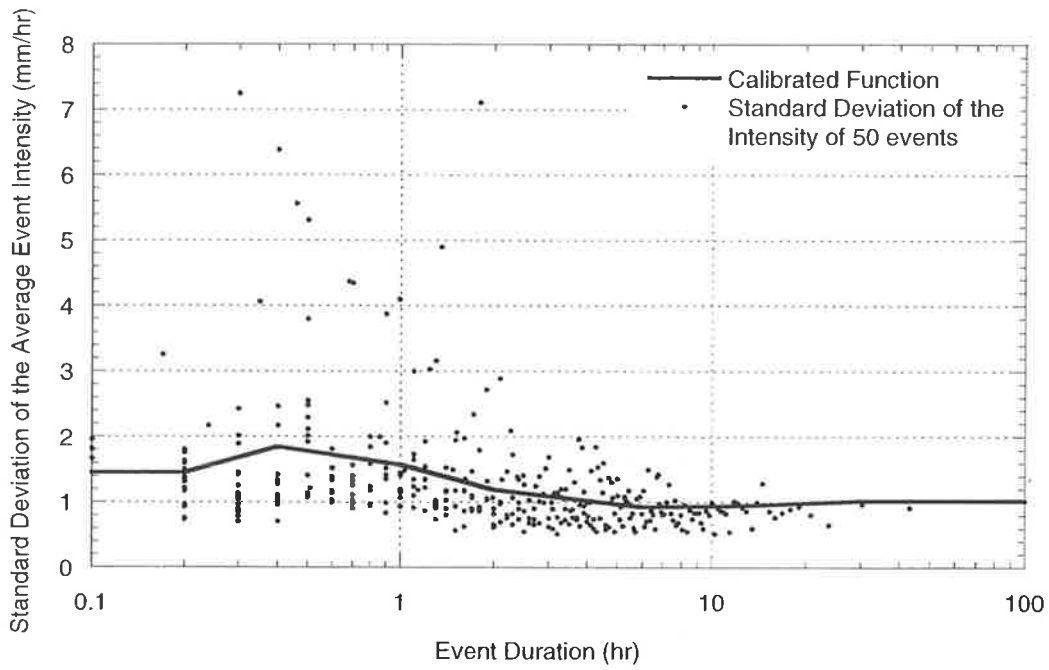

Figure 3.36 Variation of the standard deviation of the average rainfall intensity with event duration for Melbourne.

3.5.5 Seasonality

As with inter-event time and event duration, seasonal variations in the average event intensity occur over the year. A moving average of average event intensity over the year for Melbourne (Figure 3.37) and Cairns (Figure 3.38) demonstrates this. Appendix E.3 shows the seasonal trends for all the Australian sites.

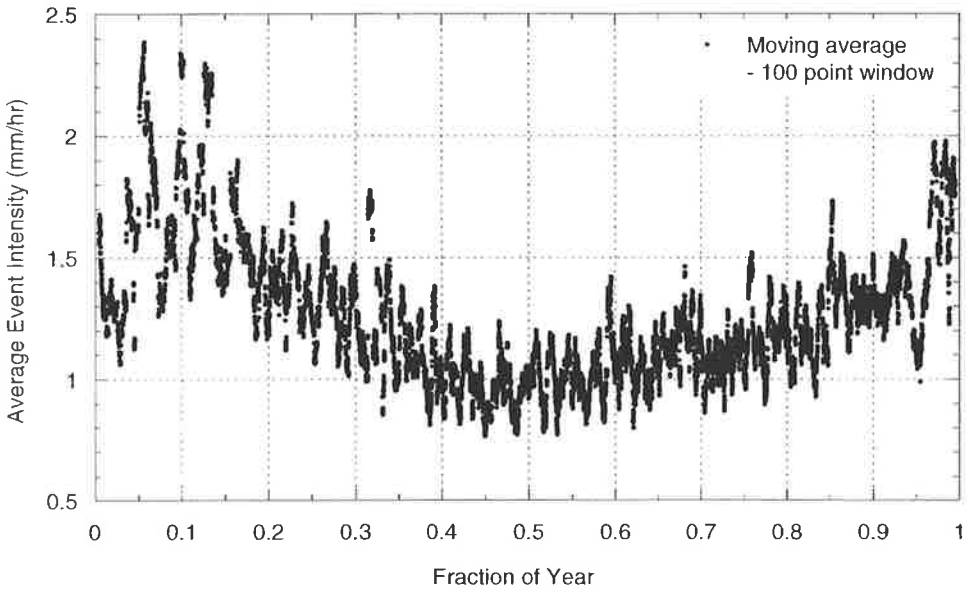

Figure 3.37 Moving average of Melbourne average event intensity data.

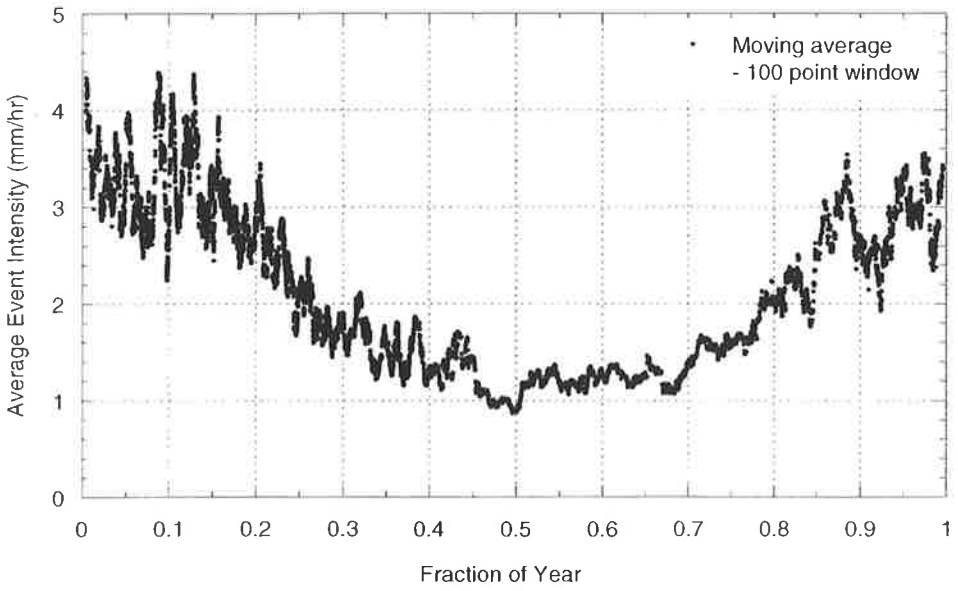

Figure 3.38 Moving average of Cairns average event intensity data.

3.5.6 Spectral Analysis

A spectral analysis of the average event intensity data was undertaken. Figure 3.39 shows the results for Melbourne where there is one main spike of importance at one cycle per year, and Figure 3.40 shows the result for Darwin where there are a number of spikes of importance, the greatest of which is at two cycles per year, but again a one cycle per year trend can be seen.

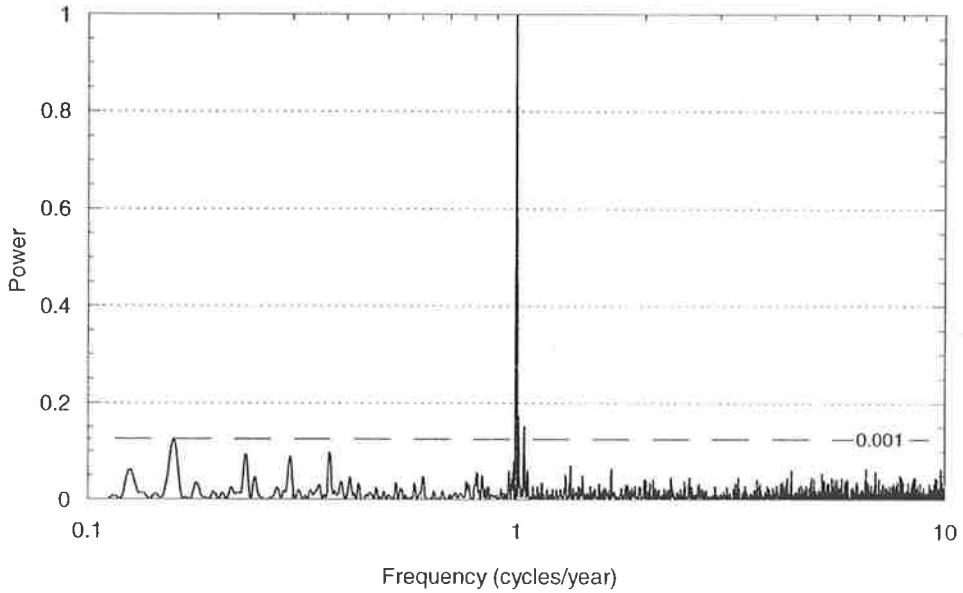

Figure 3.39 Spectral analysis of Melbourne average event intensity data.

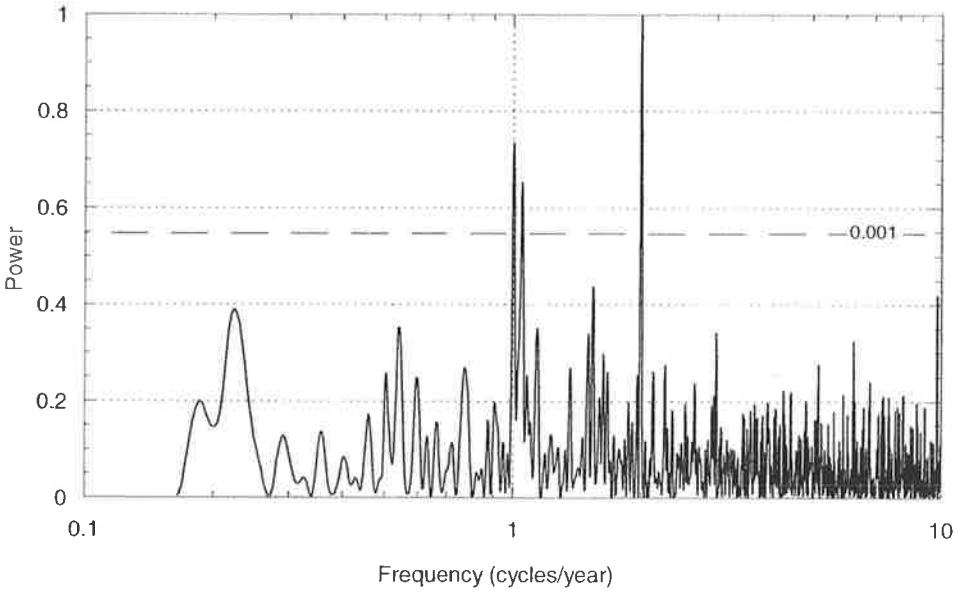

Figure 3.40 Spectral analysis of Darwin average event intensity data.

A similar result can be seen for Adelaide as shown in Appendix E.2, along with the results from the other sites. While all sites have significant frequencies of one cycle per year, Brisbane, Cairns and Perth also have significant frequencies of two cycles per year. As with the inter-event time and event duration data, this analysis provides an indication of how many seasonal cycles there are within the year to assist in selecting an appropriate method for accommodating this seasonality.

3.5.7 Incorporation of Seasonal Variation

The seasonality in the data is characterised as the large variation in the observed values of the mean and standard deviation of average intensity. These seasonal changes were incorporated into the model by allowing the values of the parameters to vary (if required) between months. A set of values for the year was obtained first to determine reasonable starting points for the parameters. Figure 3.41 and Figure 3.42 show the fit over the whole year together with the adjustment of this curve for two selected months of the year for Melbourne. These curves represent the extremes in the seasonal relationship.

Results for the remainder of the locations are shown in Appendix E.7. Locations with uniform rainfall often have less seasonal variations in this relationship. For locations in the tropics the higher intensity values occur mainly during the rainy season (summer) and the lower intensity values for the same durations during the dry season (winter). The opposite occurs for locations with predominantly winter rainfall, although the standard deviations are often larger in the summer months.

While the use of the broken line method requires a large number of parameters to be estimated, the use of an harmonic variation such as for the inter-event times and event durations was considered. However, the use of harmonics was not able to represent the extremes over the year and in general underestimated the IFD statistics. Harmonic modifications to accommodate seasonal variation were not used further in this study.

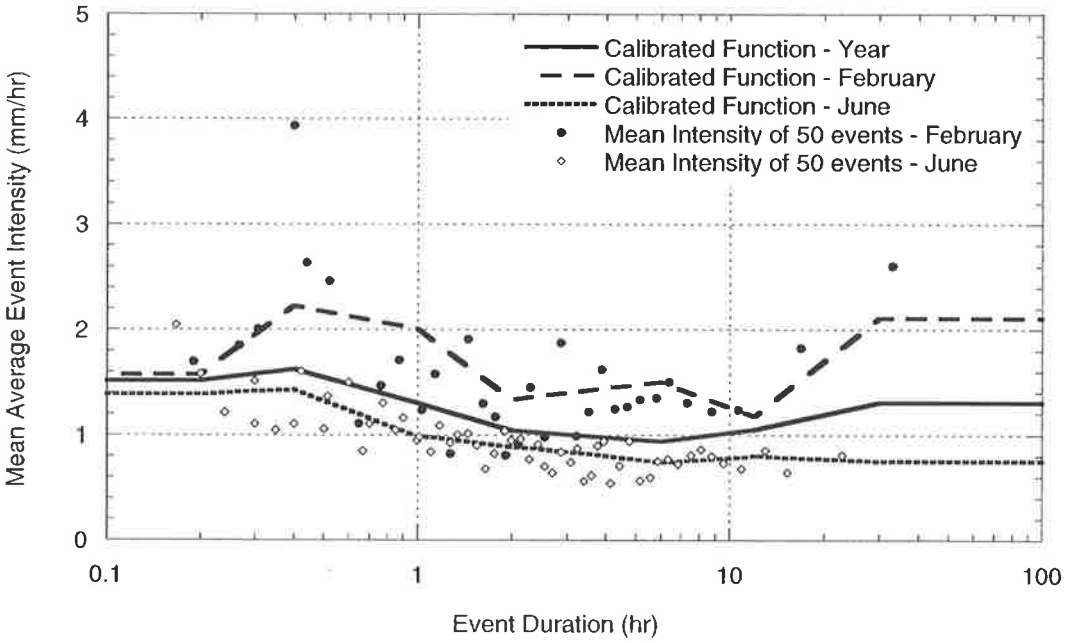

Figure 3.41 Extremes of seasonal differences in the variation of the mean average rainfall intensity with event duration for Melbourne.

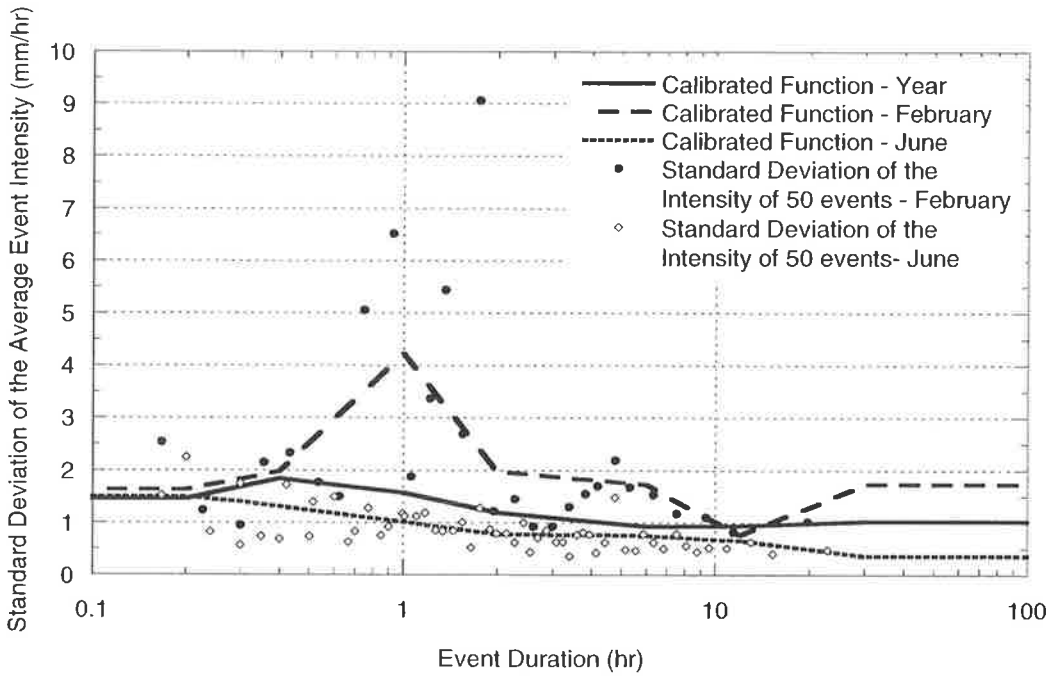

Figure 3.42 Extremes of seasonal differences in the variation of the standard deviation of the average rainfall intensity with event duration for Melbourne.

3.5.8 Validation by Simulation

The calibrated parameters of the monthly average event intensity model were validated by comparing the observed marginal distribution to that generated by a 250 year simulation. Figure 3.43 and Figure 3.44 show the simulated distributions obtained using the monthly and harmonic variation event duration models respectively for Melbourne in March. These results are discussed further in Chapter 5.

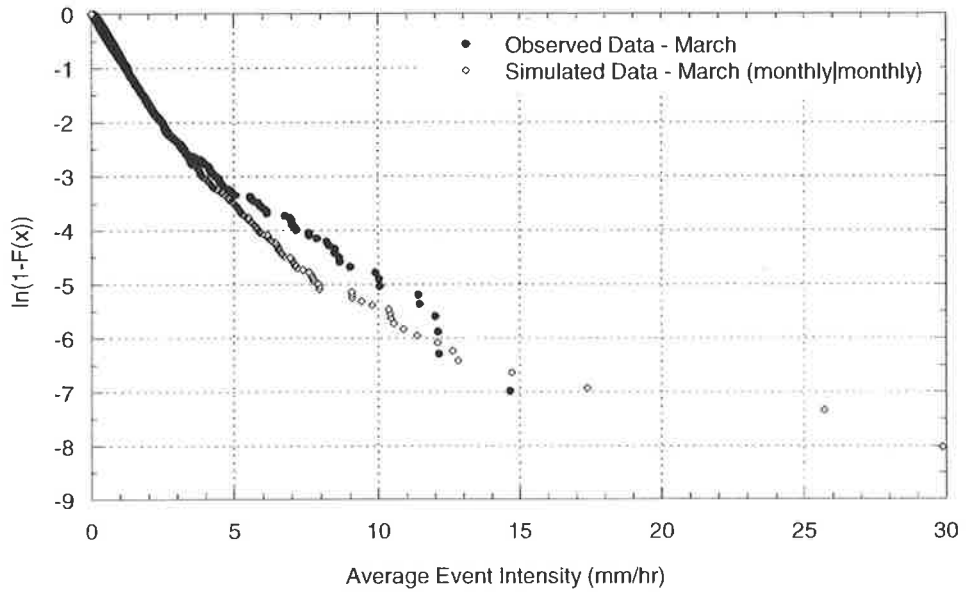

Figure 3.43 Observed and simulated marginal distributions of average event intensity using a monthly parameter-based event duration model for Melbourne in March.

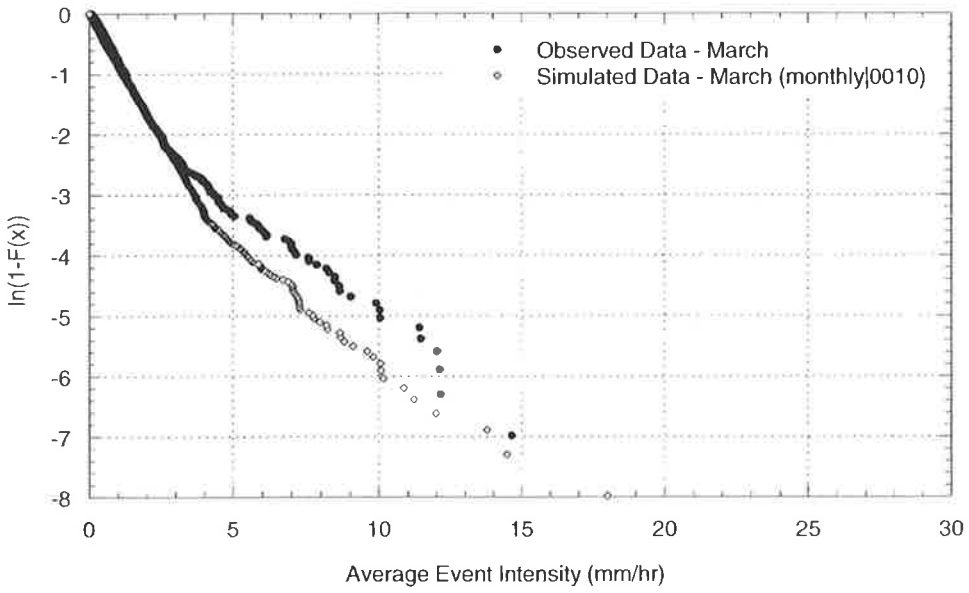

Figure 3.44 Observed and simulated marginal distributions of average event intensity using an harmonic parameter-based event duration model (0010) for Melbourne in March.

3.6 CONCLUDING REMARKS

In this chapter the first stage in the development of an event-based alternating renewal model for the simulation of synthetic rainfall has been presented. The model uses a generalised exponential distribution with a combination of the generalised Pareto and Power Law kernels to represent the inter-event times and event durations and a generalised Pareto distribution for the average event intensity, conditioned upon the event duration. These random variables describe the gross characteristics of the rainfall process, representable by a series of rectangular pulses. The seasonal variation in the observed inter-event times, event durations and the average event intensity was shown to be significant and this was incorporated into the model in two ways. Firstly, the parameters of each distribution were calibrated using data for the relevant month. Secondly, an harmonic variation was applied to the parameters, allowing them to vary over the year. Although the harmonic models were generally statistically preferred, the monthly models produced a better representation of the observed distributions during simulation and are the preferred option. In the following chapter, a model is developed to disaggregate the simulated rainfall pulses into a hyetograph.

4. DEVELOPMENT OF A RAINFALL PULSE DISAGGREGATION MODEL

Stage one of the rainfall model generates a series of rainfall events in the form of rectangular pulses, as shown in Figure 3.1(a), which represent generated rainfall events passing over a rain gauge. However, as with actual events, each generated event may actually consist of a series of cells that produce intra-event wet and dry periods as the event moves over the gauge. This would produce a temporal distribution similar to that shown in Figure 3.1(b) that needs to be simulated using a disaggregation scheme.

When using synthetic rainfall events as the input for hydrological applications or other models such as infiltration, erosion, or the transport of chemicals and sediment from agricultural fields, it is important that the temporal distribution of the rainfall is able to be realistically reproduced. Some of the above models can be sensitive to the distribution of total event rainfall over temporal resolutions as small as five minutes (Woolhiser and Osborn, 1985).

Australian Rainfall and Runoff (ARR, 1987) suggest that the rainfall temporal pattern can have a major impact on the size of a flood event. Many authors, including Askew (1975), Cordery *et al.* (1984), Lambourne and Stephenson (1987) and Viessman *et al.* (1989), have demonstrated the effect that different assumed temporal patterns can have on a flood peak. ARR (1987) shows that flood peaks can vary by up to 50 percent as a result of using different derived patterns for the temporal variation of rainfall, and that at the extreme ranges for the patterns computed flood peaks vary dramatically for individually observed heavy rainfalls. Beran (1973) suggested that the effect of the assumed temporal distribution of rainfall on the computed design floods, while being less than that of the assumptions for rainfall loss, is still very important. Yen and Chow (1980) emphasised the importance of the effect of the temporal rainfall distribution for determining runoff from small basins (25-50 km^2) in comparison to larger catchments. This was suggested because the time of concentration on large catchments may be sufficiently long to reduce, but not eliminate, the effect of the rainfall temporal pattern on the runoff hydrograph.

4.1 PREVIOUS RESEARCH

In design flood estimation the typical methods for deriving a temporal distribution of a design event are deterministic and have no probability associated with their application. This is in contrast to the perceptible stochastic nature of the phenomenon (Koutsoyiannis, 1994). The temporal patterns of observed events exhibit a high degree of variability and a general method for describing this variability is desired. As such the derivation of temporal patterns for use with design rainfall has received a great deal of attention, resulting in numerous methods and procedures for describing the distribution of rainfall depth over time. Some have been developed for the distribution of rainfall over an entire event, while others to distribute the intense rainfall burst generally used in design. The range of models based on both a non-probabilistic and probabilistic approach were investigated to select an appropriate model and are discussed in the following.

4.1.1 Non-Probabilistic Disaggregation

Non-probabilistic disaggregation is carried out by deterministically distributing the total rainfall depth over the event using pre-calculated temporal patterns. The simplest temporal patterns use a pre-selected time distribution curve with a uniform, triangular, trapezoidal or bimodal profile. Of these, the uniform profile (Todorovic and Yevjevich, 1967; Ison *et al.*, 1971; Eagleson, 1978b) is the most basic and is generally accepted as being unrealistic.

Grayman and Eagleson (1969) used an isosceles triangular profile with the peak adjusted to preserve the total depth for each event. Yen and Chow (1980) also used a triangular profile to distribute rainfall events, showing that it was able to produce runoff hydrographs with comparable or better accuracy than the uniform and trapezoid distributions. It was also shown that the effect of the distributed event duration on the shape of the non-dimensional hyetograph was not significant. Rahman *et al.* (1998) reported that the triangular profile is inadequate in reflecting the actual time variations of events. Lambourne and Stephenson (1987) investigated the effects that bimodal, triangular and uniformly distributed rainfall patterns for complete events and intense bursts had on the runoff peak and volume, up to an ARI of five years. The bimodal profile was shown to better represent the peak discharges and volumes.

An alternative method for rainfall disaggregation is the use of non-dimensionalised mass

curves. While they may be constructed using a probabilistic basis the application is purely deterministic and no probability can generally be associated with such curves. Keifer and Chu (1957) produced a synthetic storm pattern for Chicago for use with any design storm of any given duration. This pattern, often referred to as the Chicago pattern, was derived from rate-duration-frequency curves in conjunction with the statistical averages of the most important characteristics affecting the peak runoff rate for a complete event, namely the total rainfall within the maximum period or storm burst period, the amount of antecedent rainfall and the location of the peak rainfall intensity. The pattern has been used in design applications for other locations (Watson, 1981), but has received criticism. Watson (1981) indicated that the pattern is too peaked, resulting in a greater proportion of rainfall occurring at the peak intensity than normally occurs during real events.

Liou (1970) developed a disaggregation model to use with a continuous simulation approach. In this model, hourly rainfall was disaggregated into 15-minute averages using one of four explicit distributions. The choice of distribution for a particular hour was based on a comparison of the precipitation for that hour with that of the previous and succeeding hours.

The U.S. Soil Conservation Service (SCS) (1972, 1985) derived synthetic temporal patterns from an analysis of observed event data, enabling rainfall hyetographs to be specified for events of 6 and 24 hours duration. Four sets of the 24 hour duration temporal patterns were developed for each of four defined geographical locations within the United States and a single pattern was defined for the six hour duration event.

The current design temporal patterns stated in ARR (1987) are based on a non-probabilistic approach. Australia has been divided into eight zones on the basis of climatology and expected differences in temporal patterns, with the boundaries generally following major drainage divides (ARR, 1987). Pilgrim *et al.* (1969), Pilgrim and Cordery (1975) and Cordery *et al.* (1984) describe the methodology used to define the temporal patterns for each of these zones. The methodology involves ranking the time intervals within intense rainfall bursts by the depth of rainfall in each; this is repeated for many intense bursts within each region. By averaging the ranks for each interval, a pattern of average variability and the most likely sequence of intensities are obtained. For each design duration two patterns are provided, one for an ARI of less than 30 years and one for 30 years or greater. This is the only attempt to associate a probability to the patterns. In fact, ARR states that the only valid use for these

patterns is for converting a design rainfall of a selected ARI into a design flood of the same ARI, which implies that they are ARI neutral. Pilgrim and Cordery (1975) and ARR (1987) suggest that the patterns embody average variability but should not be considered as typical patterns for most regions and durations.

Ormsbee (1989) developed a discrete distribution approach for disaggregating to intervals of 20 minutes. The model was based on an assumption that the distribution of rainfall within the central hour of a three hour moving sequence was proportional to the hourly distribution of rainfall over the three hour sequence. A continuous distribution approach was also developed using a similar assumption. A probability distribution was developed for the rainfall distribution so that disaggregation to any time resolution between 1 to 30 hours could be obtained. The model was tested by aggregating and then disaggregating 5 and 15 minute data. In general the model performed better on the 15 minute data. The effect of the temporal pattern model on hydrologic design was evaluated using generated runoff statistics for small urbanised watersheds. The model was shown to produce results better than those from a uniform rainfall distribution. Its performance was also assessed by comparing observed and predicted peak discharge flows. The disaggregation model showed an improvement to the case of uniformly distributed rainfall, but underestimated the observed historical peak flows.

4.1.2 Probabilistic Disaggregation

The alternative to using a fixed or non-probabilistic temporal pattern is to develop a probabilistic description for this variable. This may be undertaken by deriving a series of non-dimensionalised mass curves with a probability level assigned to each. These curves can be determined from a probabilistic analysis of historical events. Huff (1967) developed a series of temporal pattern curves for use on complete events in Illinois, along with areas of similar climate and topography. Recorded event distribution patterns were characterised by mass curves and classified into four groups depending on whether the heaviest rainfall occurred in the first, second, third or fourth quarter of the total event period. In each group, nine probability curves, from 10% to 90% at 10% increments were determined. From each curve a design event hyetograph can be constructed. These *Huff curves* have been used as design rainfall hyetograph inputs into hydrologic models (Bonta and Rao, 1988) and as a probabilistic input to derive flood probability distributions (Beran, 1973).

While this method involves a probabilistic approach, the determination of a resulting design

flood is obscure (Koutosyiannis, 1994). The Huff curves do not represent the actual patterns for a certain probability of exceedance but are matched to the statistics of an ensemble of patterns, which means that the curves exhibit less variability than would actually be observed between the patterns of individual events (Rahman *et al.*, 1998). In addition, the representation of the real event process by these smooth curves is poor as the burst characteristics of observed events are not reflected (Koutosyiannis, 1994).

Hashino (1986) theoretically derived a stochastic event pattern to preserve the stochastic properties of actual event hyetographs. A bivariate exponential density function was used to derive equations to describe two design patterns, one with peak rainfall intensity at the centre of an event, the other with peak rainfall at the end of the event. The patterns were described by three parameters, the reduced variate of the peak rainfall intensity, the auto-correlation index (related to the auto-correlation coefficient of the rainfall intensities) and the conditional probability of rainfall intensity at time t, given the rainfall intensity at time $t-1$ ($P(I_t|I_{t-1})$). This assumes that rainfall intensity actually decreases monotonically away from the peak. This assumption limits the method for situations where the actual process is represented by this assumption, which is not always the case.

Rahman *et al.* (2001) assumed that the temporal patterns for *storm cores* (the most intense periods of rainfall within an event) were dependent only on the total event duration. Observed events were transformed into dimensionless mass curves, defined by ten equal time increments, and separated into two groups, those up to 12 hours duration and those less than 12 hours. Within each group, the curves were sequentially numbered. During Monte Carlo simulation to derive flood frequency curves, the temporal pattern was sampled from the appropriate duration group using a uniform distribution.

Other methods involve the disaggregation of rainfall events using probability distributions for various random variables that can be used to define characteristics of the observed data. These methods produce a unique hyetograph for each event.

Woolhiser and Osborn (1985) developed a probabilistic model to disaggregate thunderstorm rainfall at a point using a non-dimensionalised mass curve approach. The dimensionless duration was divided into ten equal time increments and the depth increments re-scaled to a range of zero to one. The expected value of the kth re-scaled increment given the $(k-1)$ th

increment was assumed to be a linear function of that increment. The marginal distribution of the first element and the conditional distribution of subsequent elements (kth given $(k-1)$ th) was described using a beta distribution. No intra-event dry periods were included within the disaggregation of events, which is reasonable given the nature of thunderstorm rainfall. The sequence of re-scaled increments were then modelled as a non-homogeneous Markov chain in discrete time in order to calibrate the model using thunderstorm data from south-east Arizona. The model required 26 parameters but the use of polynomial approximations for a number of parameters was suggested to reduce this number. A 13 parameter model was used and it was shown that the dependence between successive increments was sufficiently strong to validly include this dependency in the model. Dimensionless events were simulated and compared against the simulated and observed cumulative marginal distributions of re-scaled increments with reasonable agreement.

The concept of normalised mass curves has since been applied by Koutsoyiannis and Foufoula-Georgiou (1993), who produced a four parameter model to disaggregate total event rainfall into any desired resolution, with reasonable results. Robinson and Sivapalan (1997) also used normalised mass curves to describe the temporal pattern of rainfall intensity for use in determining flood frequency distributions. A stochastic model was developed to produce curves that satisfied the statistical characteristics of the observed data. The model utilised a multiplicative structure with continual disaggregation of the normalised event duration until the desired time scale was reached. The mass curve ordinates at each successive disaggregation level were drawn from a beta distribution. The stochastically generated curves were then converted to within-storm temporal patterns of rainfall intensity.

Marien and Vandewiele (1986) divided observed rainfall sequences into events using a minimum inter-event time of ten minutes. Each event of duration D and total depth R was then sub-divided into N partial events with durations $D_1, D_2, \cdots, D_N$ and depths $R_1, R_2, \cdots, R_N$, to represent the rise and fall of rainfall intensity within each event. The changes in rainfall intensity during each of these partial events was then represented using isosceles triangular profiles. Conditional probability models were derived for each partial event parameter, namely $P[N \mid R = r, D = d]$, $P[D_1, D_2, \cdots, D_N \mid R = r, D = d, N = n]$ and $P[R_1, R_2, \cdots, R_N \mid R = r, D = d, N = n, D_1 = d_1, \cdots, D_N = d_n]$.

Beven (1987) obtained a mean event profile from averaging the summer and winter profiles given in the U.K. Flood Studies Report (NERC, 1975). Individual event profiles were then modelled by adding a random component to the mean profile for each hour of rain in the form of a first-order Markov process, then re-scaling to preserve the total event rainfall. It was found that using the mean rainstorm intensity for each hour alone did not yield a sufficient number of high peaks to reasonably represent the flood characteristics. It was concluded that variations in rainfall intensity within events may need to be well represented to obtain a true determination of flood peaks.

Acreman (1987) treated rainfall temporal distribution as a random element where individual event profiles were equivalent to a population density function that describes the average of all profiles present in a number of sample histograms. The total event rainfall was divided into depths of 0.5mm that were distributed within the profile using a normal distribution to govern the probability of occurrence at any time during the event.

Ormsbee (1989) modified the non-probabilistic discrete disaggregation model in order to use it in a discrete stochastic model. The model was again based on the assumption that the distribution of rainfall within the central hour of a three hour moving sequence was proportional to the hourly distribution of the rainfall over the three hour sequence. It was assumed that the volume of rainfall in any hour occurred in discrete amounts of 0.01 inch, and a probability function for the occurrence of these discrete rainfall pulses in each of the three 20 minute time intervals within the central hour were developed. Once the probability function for a particular hour was developed, the total volume of rainfall was disaggregated into N pulses of 0.01 inches and each pulse was then assigned to one of the three time intervals using the developed functions and a sequence of N random numbers sampled from a uniform probability distribution.

Ormsbee (1989) also developed a continuous stochastic disaggregation model. As with the discrete stochastic disaggregation model, rainfall was assumed to occur in discrete amounts of 0.01 inch and was distributed over the central hour of a three hour sequence, based on the knowledge of the three hours. The central hour was separated into N intervals of δn (the selected time interval for the disaggregated rainfall). A probability density function was developed for the time of occurrence of the ith time interval in the central hour. This changed from hour to hour depending on the shape of the three hour series to reflect the changing

dependence of rainfall within different shaped three hourly sequences. The total depth was divided into N pulses which were assigned randomly to the intervals using a uniform distribution. This method has since been used by Cowpertwait (1991b) and Cowpertwait *et al.* (1996b) with the modification that the depth of the discrete rainfall pulses was determined as a random variable. The model was fitted to a set of one-minute data at a number of sites where it was considered to perform well.

Acreman (1990) examined the rainfall profiles of events of varying duration and showed that the profiles are independent of duration, which suggests that the average standardised profile can be considered constant across event duration. A beta distribution was used to describe the average shape of all rainfall profiles for each season. To obtain a profile for a given event, the relative proportions of the total rainfall depth in each hour was determined by random sampling from a beta distribution. A lag-one auto-correlation model was used to reproduce the observed correlation between successive hours.

Koutsoyiannis and Xanthopoulos (1990) developed a single-site dynamic disaggregation model that transformed monthly rainfall into events and hourly amounts. The distribution of rainfall in a given hour of an event was either a gamma or Weibull with its parameters dependent on the duration of the event and the position of the current hour within the total event. The number of parameters varied from 4 to 12, depending on the accuracy desired. The 12 parameter disaggregation of rainfall data from two stations gave satisfactory results. Statistics and distribution functions computed from synthetic samples derived by the model matched well with the theoretical expectations.

Boughton (2000b) defined a disaggregation model in terms of the fraction of the daily total that occurs in the hour of maximum rainfall (R). The values of R were obtained from Victorian pluviograph records. The records were processed into 9am to 9am daily blocks and only days with total rainfall greater than 15 mm were selected for analysis. For each value of R, an average set of values for the remaining 23 fractions of the daily total were defined. Clusters of fractions from each set of 24 fractions were then determined in order to preserve the average values of the highest two, three, six and twelve hour fractions. These clusters were then randomly arranged over the day to reproduce the natural variations in 9am to 9am rainfall. During simulation a value of R is selected from the distribution of R based on the pluviograph records. This value is then associated with its determined set of 24 fractions and

the clusters required to maintain the average multi-hour fractions. These fractions are multiplied by the daily total to give the hourly rainfalls, which are arranged into a daily temporal pattern. While this model may provide a reasonable distribution of rainfall over a day, it is not clear how the day to day relationship is accommodated if a number of consecutive days are wet.

Menabde and Sivapalan (2000) showed that for a Melbourne 25 year six-minute pluviograph record, the calculated ensemble-averaged power spectrum of all events with durations greater than 6.4 hours produced an exponent greater than one, indicating that the events exhibit stochastically self-affine rather than self-similar properties. A bounded random cascade model (a special form of the multiplicative random cascade model) was then used to produce random, intra-event hyetographs. Breakdown coefficients were used to analyse the scaling properties of intra-event rainfall. This method is applicable to both self-affine and self-similar events. A breakdown coefficient was then constructed as a random variable and its probability density function for a number of event durations was determined and fitted to a symmetric beta distribution, with its parameter dependent on event duration. Comparisons between observed and simulated extreme intensities for events of 30 minutes duration showed good results. However, it would be desirable to view results such as IFD and aggregated statistics over a range of durations before the method was considered applicable to a range of event durations.

4.1.3 Evaluation of Models

Given the decision in Chapter 2 to use an event-based rainfall model, the use of disaggregation models that disaggregate fixed time intervals into smaller intervals, rather than disaggregating an event, is not appropriate. A probabilistic approach is considered essential to account for the joint probability of the temporal rainfall distribution with other rainfall producing variables. The use of a dimensionless mass curve has been widely used and was considered a good basis for the simulation of fine resolution temporal patterns for events of varying duration. Figure 4.1 shows the variability in 20 non-dimensionalised rainfall events from Melbourne. The dimensionless mass curve approach was seen as a potentially useful method for accommodating the large variability in the shape of the temporal distribution in events found in the historical data and was chosen for further consideration.

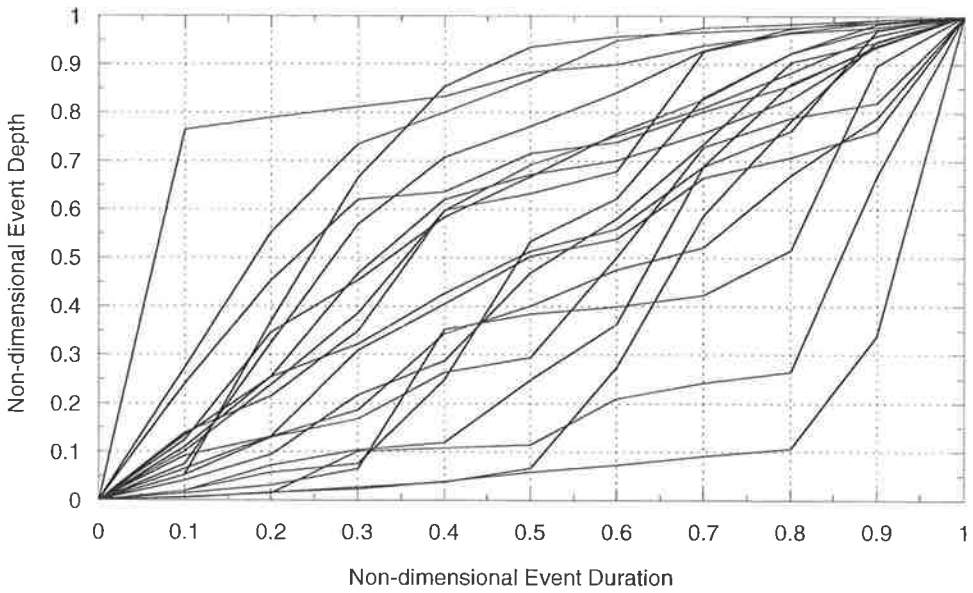

Figure 4.1 Variability in the temporal distribution of rainfall in non-dimensional events.

4.2 DEVELOPMENT OF THE RAINFALL PULSE DISAGGREGATION MODEL

The disaggregation model used in this study utilises a dimensionless mass curve. It is assumed that the probabilistic evolution of traces within the dimensionless mass curve can be described by a self-similar, discrete stochastic process that describes how each rainfall trace moves from one point in time to the next. The trace may either jump upwards indicating rainfall, or remain horizontal implying an intra-event dry period. The self-similarity concept, where events are expected to exhibit similarities in their internal structure despite their different duration or total event depths has been applied by a number of researchers including Woolhiser and Osborn (1985) and Koutsoyiannis and Foufoula-Georgiou (1993). Self-similarity provides the ability to simulate high resolution temporal patterns for long duration events.

4.2.1 Non-Dimensional Mass Curve

For each event, duration is non-dimensionalised as $\tau = t/t_d$ where t is the time since the start of the event, t_d is the total event duration and $0 < t < t_d$. Depth is non-dimensionalised as $\delta = \frac{d(t)}{d(t_d)}$ where $d(t)$ is the cumulative rainfall up to time t. Therefore, all rainfall traces

must:

(a) lie within the limits $0 \leq \delta \leq 1$ and $0 \leq \tau \leq 1$;

(b) begin at (0,0) and end at (1,1); and

(c) have a non-negative slope.

If τ is initially divided into n finite intervals, τ_k is taken as corresponding to k/n and δ_k to $\frac{d(\tau_k t_d)}{d(t_d)}$ with $1 < k < n$. In this study, n was set to ten, creating the ability to reduce the initial ten intervals to sequentially smaller decimal based intervals for longer duration events.

An analysis of historical events of various durations was undertaken to measure the reasonableness of the self-similarity assumption. Figure 4.2 shows a comparison of averaged dimensionless observed event profiles for various ranges of event durations for Melbourne and Figure 4.3 shows these for Perth. For Perth the curves are virtually coincident and while the curves for Melbourne are slightly spread they are still reasonably similar. The curves for all sites are shown in Appendix F.1, with each having a similar relationship. For some sites there are few events that have a duration greater than 25 hours. For these sites, all events with durations greater than 15 hours have been grouped together. This suggests that the assumption of self-similarity is reasonable as a first approximation and that the same set of parameters can be used for all events, regardless of event duration. If these averaged profiles showed a stronger dependence upon duration, a self-affine approach similar to Menabde and Sivapalan (2000) could be investigated (refer Section 4.1.2).

The characteristics of the rainfall jumps on the dimensionless mass curve and the total intra-event dry periods are evaluated separately for each observed event. The wet part of all observed events is mapped onto a dimensionless mass curve and the statistical moments of each successive jump, conditioned on the jump origin, are estimated. The total intra-event dry period for all events is then determined. When a temporal pattern is generated for each simulated event the rainfall jumps and dry periods are again treated separately. The dry periods are randomly mixed within the generated jump distribution using a non-replacement sampling scheme to produce the simulated hyetograph. Because of this process, the intra-event rainfall can be conceptualised as a conditional random walk on a dimensionless mass curve for the rainfall event. Each of these processes is discussed in the following sections.

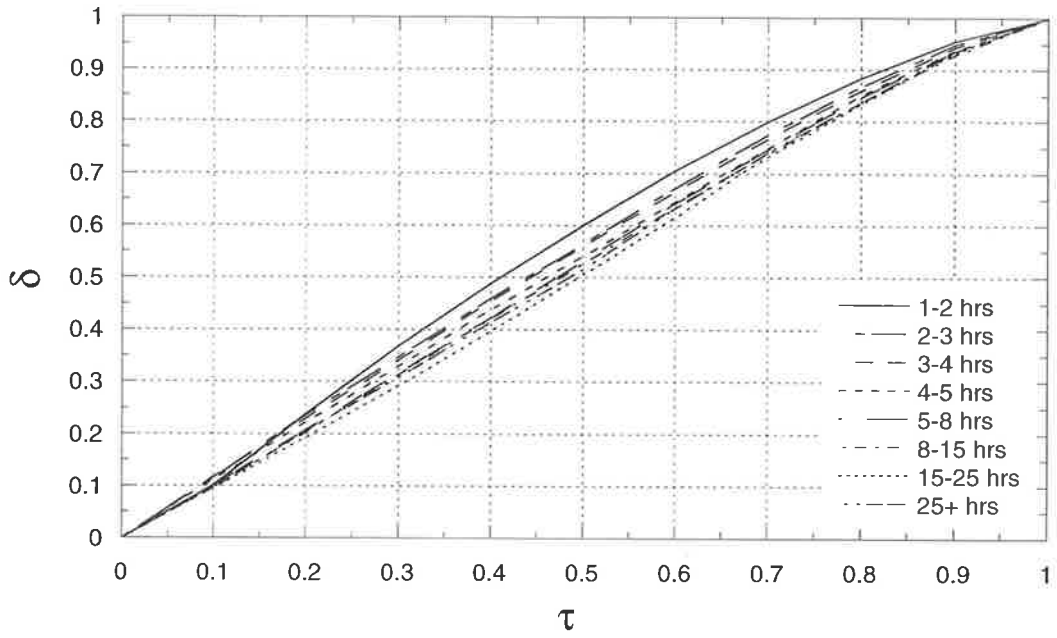

Figure 4.2 Comparison of averaged observed event profiles for varying event durations for Melbourne.

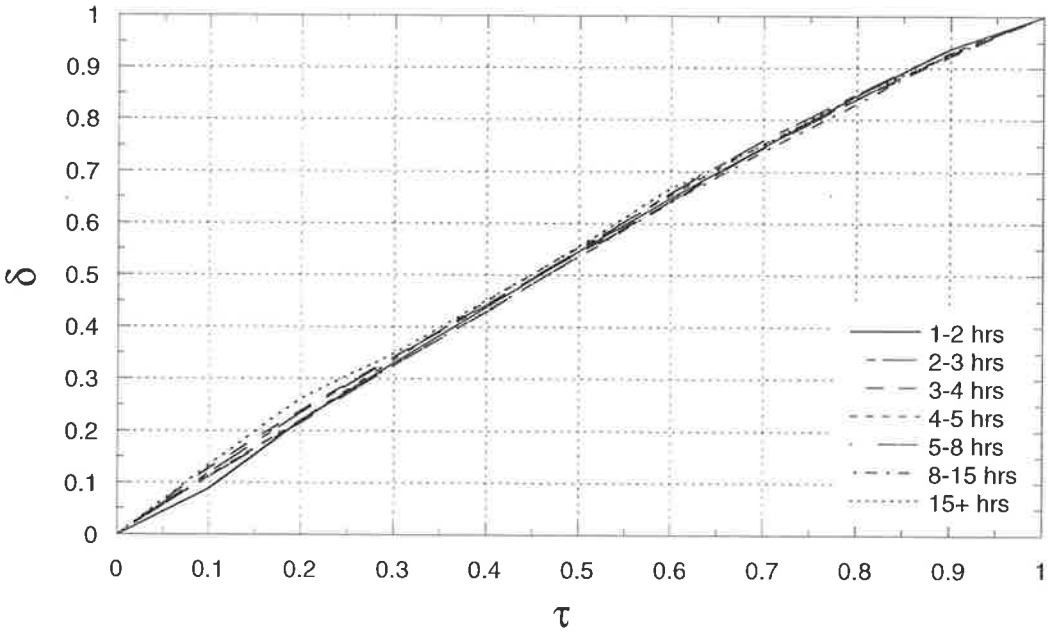

Figure 4.3 Comparison of averaged observed event profiles for varying event durations for Perth.

4.2.2 Intra-Event Rainfall Distribution Determination

A histogram of all observed jumps in each tenth of the dimensionless event duration was examined. This is shown for Melbourne in Figure 4.4 with the shape of the histogram suggesting that a log-normal distribution can be assumed. Similar shaped histograms were obtained for all sites as shown in Appendix F.2.

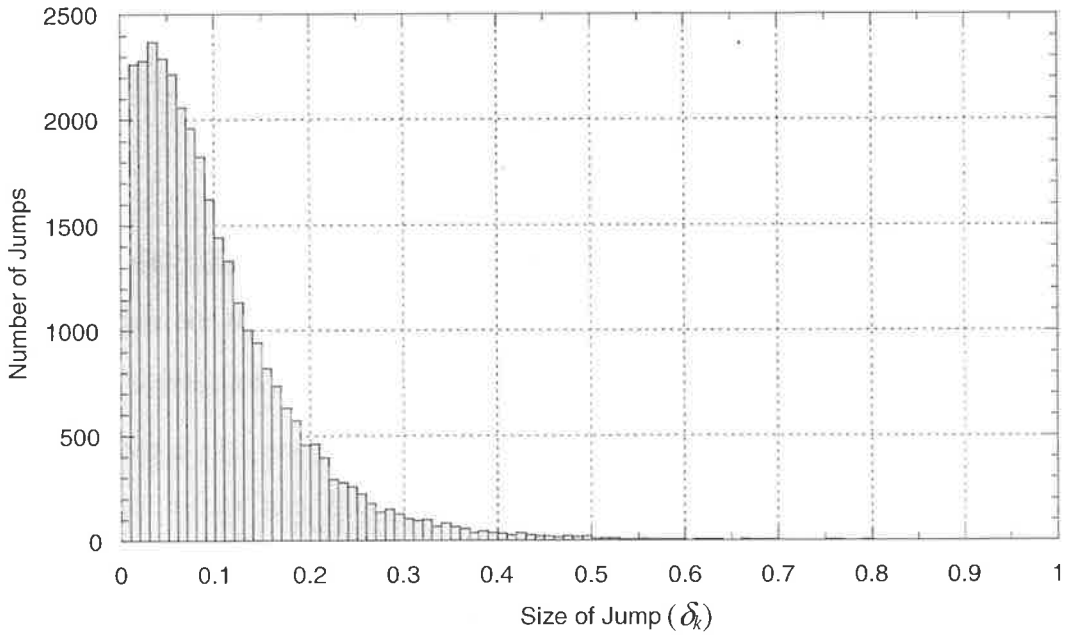

Figure 4.4 Distribution of jumps for Melbourne.

The first jump within a rainfall event (δ_1) will be from the origin and can be sampled from its marginal probability distribution. The probability distribution of subsequent jumps however, δ_{k-1} to δ_k for $k>1$, will depend on the jump origin δ_{k-1}. The jump distribution model works directly with the non-dimensionalised depth, using relationships for the conditional jump mean and standard deviation, which are dependent on the remaining portion of the non-dimensional depth. This eliminates the need to re-scale the depth increments as was done in Woolhiser and Osborn (1985). The δ range available to the jump from time τ_{k-1} to τ_k is $1-\delta_{k-1}$, so as δ_{k-1} approaches 1.0 the size of the jump becomes more constrained. The conditional probability density function $f\left(x=\delta_k-\delta_{k-1}\middle|\delta_{k-1}\le\delta_k\le 1\right)$ describes the probability of jumping from $(\tau_{k-1},\delta_{k-1})$to (τ_k,δ_k) for $k=2,\cdots,n-1$.

The size of the jump $x=\delta_k-\delta_{k-1}$ from time τ_{k-1} to τ_k can be described by the following

truncated (at $1-\delta_{k-1}$) log-normal distribution:

$$f_X(x) = \frac{1}{P_{1-\delta_k} x\zeta\sqrt{2\pi}} \exp\left[-\frac{1}{2}\left(\frac{\ln x - \lambda}{\zeta}\right)^2\right] \qquad 0 \le x < 1-\delta_{k-1} \qquad (4.1)$$

where:

$$P_{1-\delta_k} = \int_0^{1-\delta_k} \frac{1}{x\zeta\sqrt{2\pi}} e^{-\frac{1}{2}\left(\frac{\ln x-\lambda}{\zeta}\right)^2} dx;$$

$\lambda = E(\ln X)$, the mean of $\ln x$; and

$\zeta = \sqrt{Var(\ln X)}$, the standard deviation of $\ln x$.

Sampling from a truncated log-normal distribution is straightforward. The jump (x) is sampled from a log-normal distribution with parameters λ and ζ. If the sampled value is greater than the upper limit $(1-\delta_{k-1})$, the value is re-sampled. Each successive jump is based on the current position within the dimensionless time-depth space and constrained by the amount of dimensionless depth remaining. Since a jump can never equal the total dimensionless depth remaining it will never quite reach $\delta = 1$. If, in the unlikely event, after the second or third jump the δ value exceeds 0.99 the small amount of rainfall that is left is distributed over the remaining time periods so that $\delta = 1$ when $\tau = 1$. Thus the remaining intervals are not considered as dry periods but periods of very low intensity rainfall. Events of this nature can be observed in Figure 4.1. Assuming otherwise would violate the model assumptions used to identify independent events. The parameters λ and ζ depend on the jump origin δ_{k-1}, and during the mapping of each observed event into the dimensionless mass curve the statistical moments of each jump conditioned on the jump origin were estimated. The parameters λ and ζ were found to be suitably described by the following parabolic curves, chosen to ensure that λ and ζ converge to 0 as δ_{k-1} approaches 1:

$$\lambda = (1-\delta_{k-1})(\lambda_1 + \lambda_2\delta_{k-1}) \qquad (4.2)$$

$$\zeta = (1-\delta_{k-1})(\zeta_1 + \zeta_2\delta_{k-1}) \qquad (4.3)$$

The parameters λ_1, λ_2, ζ_1 and ζ_2 were fitted to the data using weighted least squares. The weights are dependent on the sample size of the data used to define the jump mean and

standard deviation at different values of δ_i. Figure 4.5 and Figure 4.6 show the fits of these functions to the data from Melbourne. It must be noted that the outlying points have very few values (and hence low weight) associated with them. The fitted functions for all sites are shown in Appendix F.3.

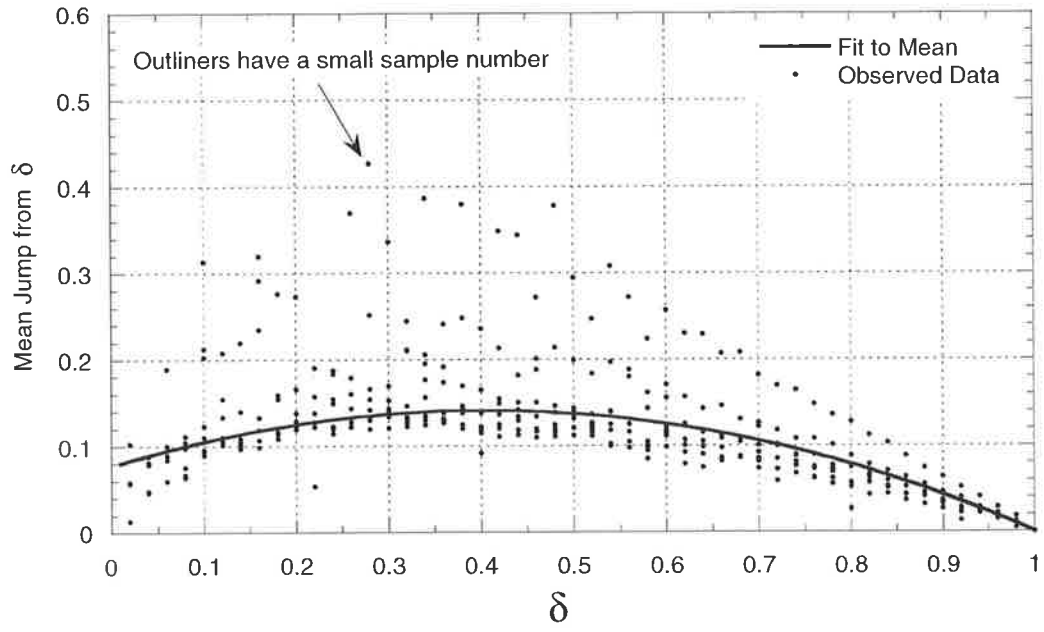

Figure 4.5 Variation of the mean jump from δ for Melbourne.

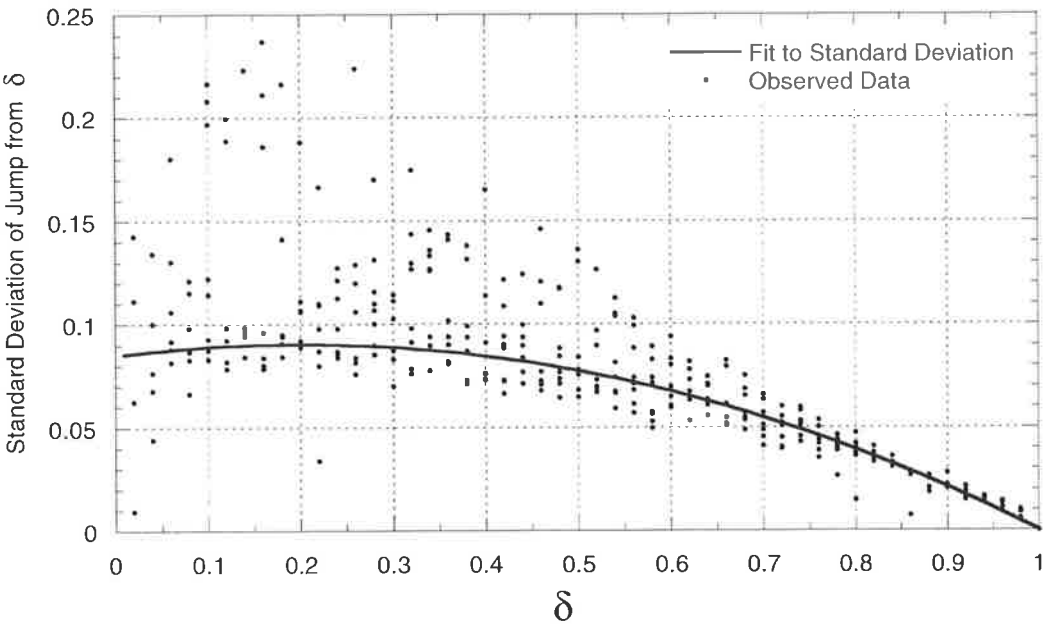

Figure 4.6 Variation of the standard deviation of the jump from δ for Melbourne.

The six parameters that require estimation for the jump distribution component of the disaggregation model, these being the parameters of the parabolic curves along with the mean and standard deviation of the first jump from the origin, are shown in Table 4.1.

Table 4.1 Jump distribution parameters.

	First Jump from Origin		Subsequent Jumps			
	μ	σ	λ_1	λ_2	ζ_1	ζ_2
Adelaide	0.089	0.078	0.070	0.395	0.073	0.144
Alice Springs	0.119	0.133	0.096	0.375	0.109	0.105
Brisbane	0.116	0.115	0.087	0.404	0.101	0.156
Cairns	0.099	0.105	0.080	0.403	0.096	0.177
Darwin	0.153	0.172	0.114	0.393	0.126	0.146
Hobart	0.097	0.082	0.077	0.398	0.074	0.147
Melbourne	0.106	0.096	0.078	0.394	0.085	0.140
Perth	0.111	0.108	0.081	0.369	0.093	0.151
Sydney	0.103	0.100	0.081	0.402	0.093	0.115
Townsville	0.107	0.123	0.090	0.426	0.112	0.162

Although these cities are in different climatic regions, the jump distribution parameters are remarkably similar. This is seen further in Figure 4.7 to Figure 4.10 where the sites are loosely grouped according to climate region. The similarity in the jump distribution parameters over the variation of regions as shown provides significant potential for regionalisation to sites where there is little or no data.

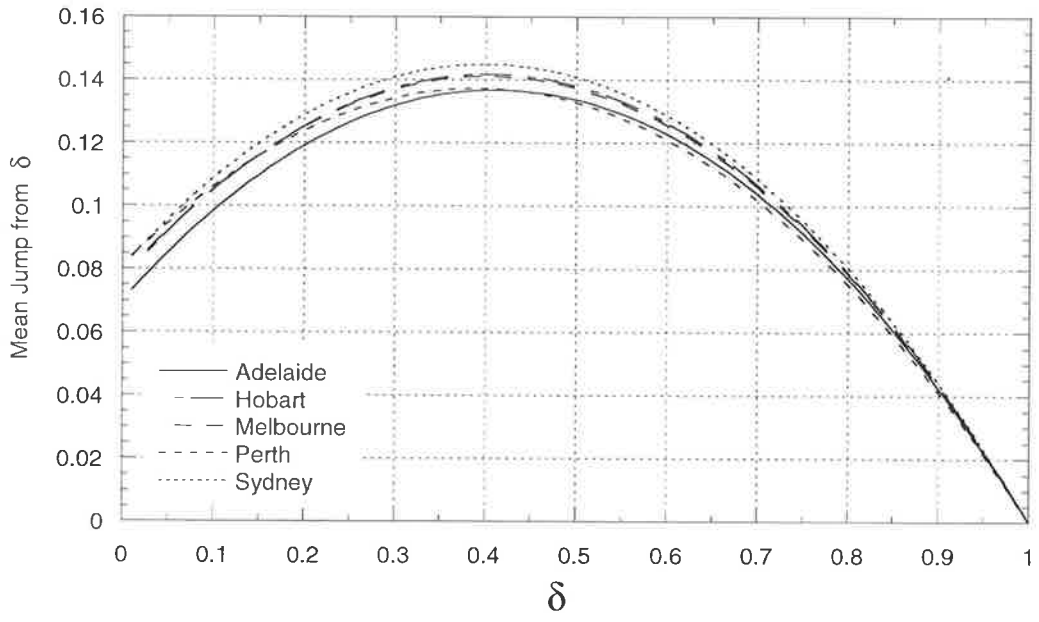

Figure 4.7 Comparison of the variation in the mean jump from δ for Adelaide, Hobart, Melbourne, Perth and Sydney.

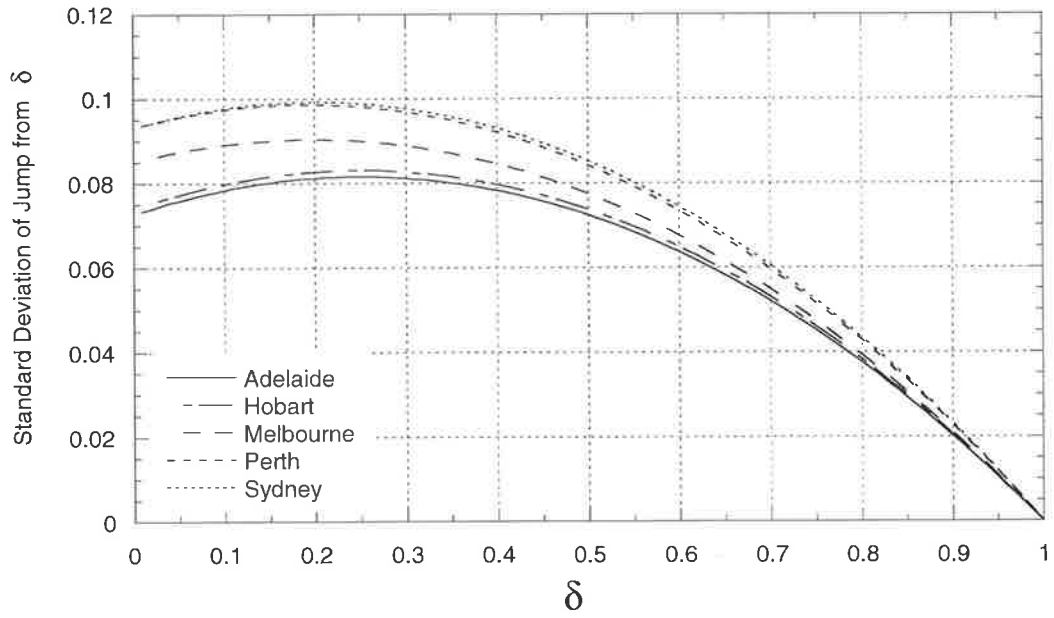

Figure 4.8 Comparison of the variation in the standard deviation of the jump from δ for Adelaide, Hobart, Melbourne, Perth and Sydney.

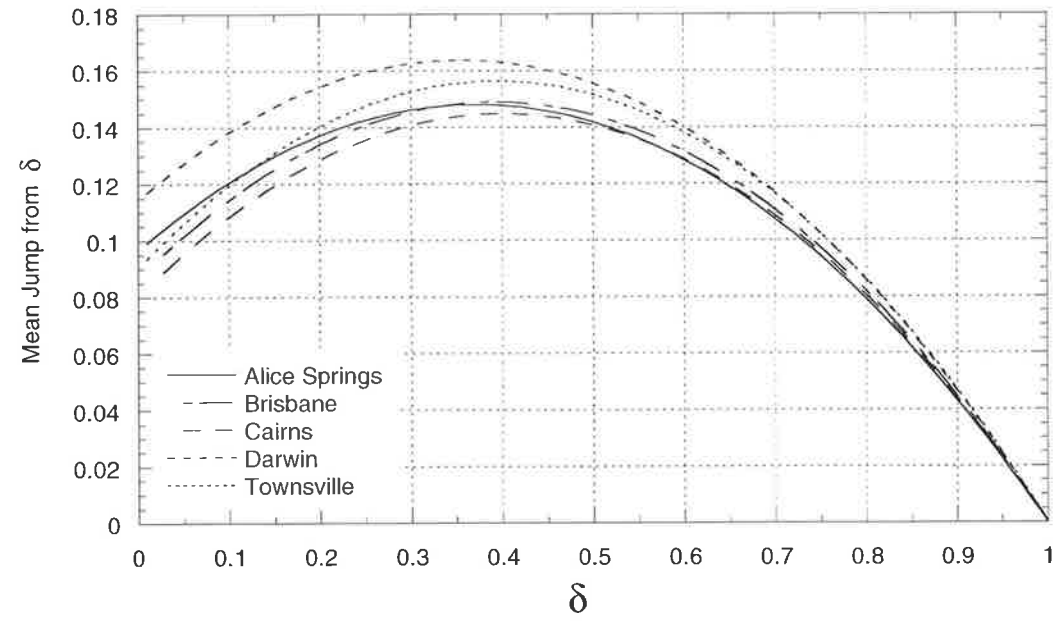

Figure 4.9 Comparison of the variation in the mean jump from δ for Alice Springs, Brisbane, Cairns, Darwin and Townsville.

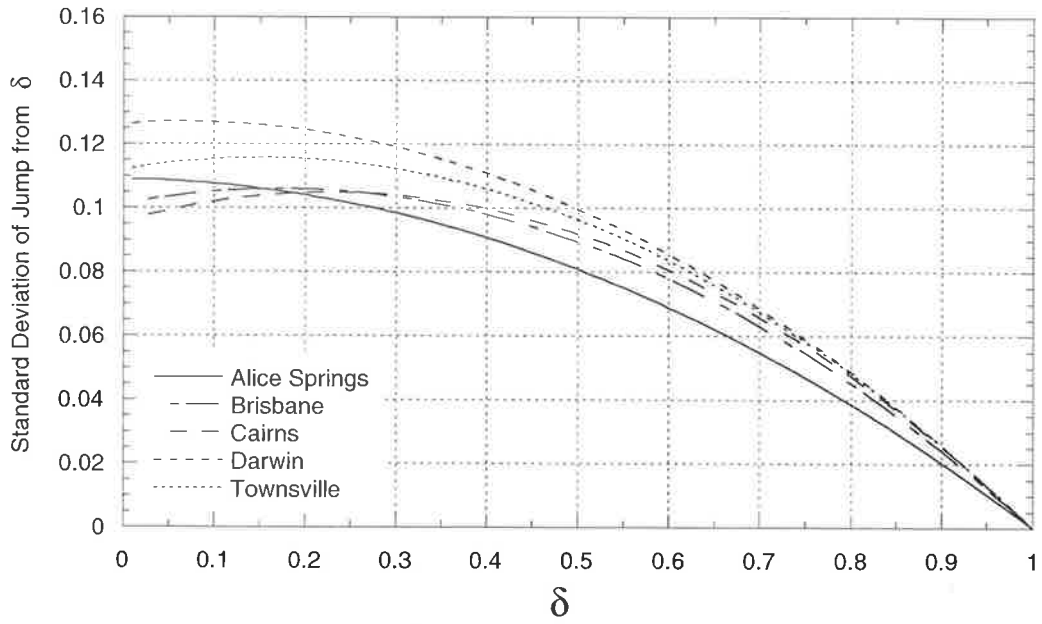

Figure 4.10 Comparison of the variation in the standard deviation of the jump from δ for Alice Springs, Brisbane, Cairns, Darwin and Townsville.

4.2.3 Intra-Event Dry Period Distribution Determination

The intra-event dry fraction (P) of an event is defined as the proportion of dry increments within an event. A histogram of the intra-event dry fractions for Melbourne is shown in Figure 4.11 and all sites are shown in Appendix F.4.

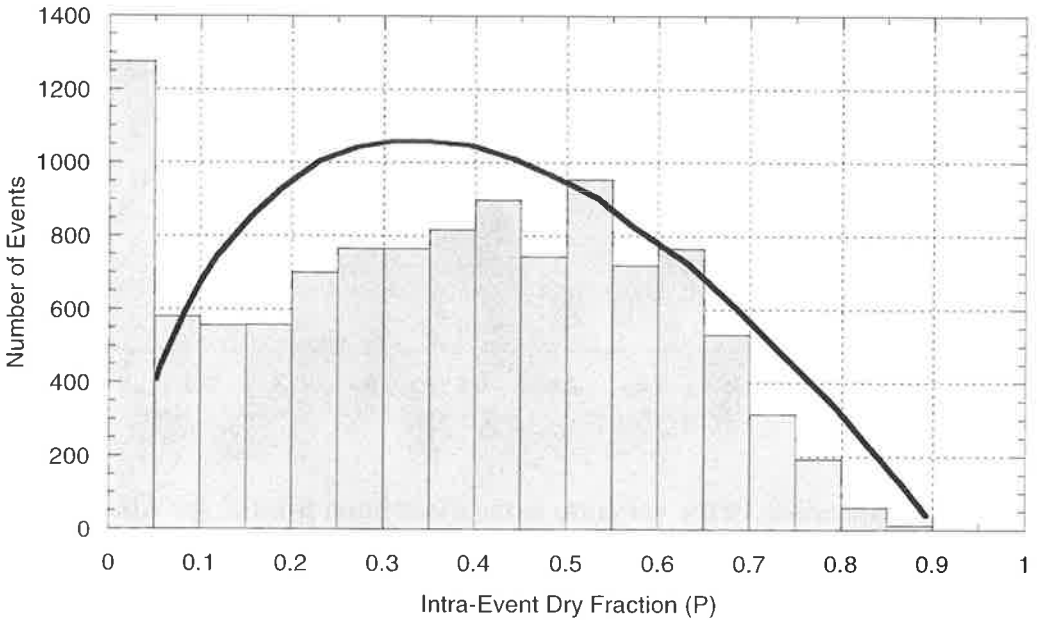

Figure 4.11 Distribution of intra-event dry fractions for Melbourne.

This shows that there are a significant number of events with a low P (P_L, $P < 0.05$). A beta distribution (shape parameters μ and σ) is often used to model data with upper and lower bounds. The shape of the distribution of P for higher values (P_H, $P > 0.05$) indicates it could be modelled using this distribution with a lower limit of 0.05 and an upper limit (P_{MAX}) defined as the maximum P observed in the data. A uniform distribution was used to model events classified as P_L.

There are four parameters that require estimation for the intra-event dry fraction distribution component of the disaggregation model, these being parameters of the beta distribution, the probability of P_L and P_{MAX}. These fitted parameters are shown in Table 4.2 and the fitted distribution for Melbourne is also shown in Figure 4.11.

Table 4.2 Intra-event dry fraction distribution parameters.

	Prob(P_L)	Prob(P_H)		P_{MAX}
		μ	σ	
Adelaide	0.128	0.471	0.202	0.905
Alice Springs	0.262	0.359	0.187	0.818
Brisbane	0.113	0.415	0.196	0.905
Cairns	0.152	0.418	0.189	0.905
Darwin	0.210	0.373	0.191	0.900
Hobart	0.144	0.396	0.186	0.905
Melbourne	0.115	0.407	0.191	0.895
Perth	0.128	0.444	0.188	0.905
Sydney	0.121	0.406	0.188	0.868
Townsville	0.189	0.371	0.193	0.897

As was the case for the jump distribution parameters, the intra-event dry fraction distribution parameters are similar across the different locations. The only obvious exception is with the P_L for Darwin and Alice Springs, which are likely to experience more intense events such that once it begins raining there are not many intra-event dry periods. In Darwin, intense events often occur in the afternoons during the wet season, resulting in independent events with short intra-event dry periods on each day. Figure 4.12 and Figure 4.13 compare the probability density function for the beta distribution using the parameters in Table 4.2. Melbourne, Brisbane and Sydney have very similar distributions, as do Townsville and Darwin. The distributions for Perth and Cairns are also similar. Although the distributions for all sites do not display the same level of similarity that was observable for the jump distributions, similarities exist that may allow some regionalisation of these parameters.

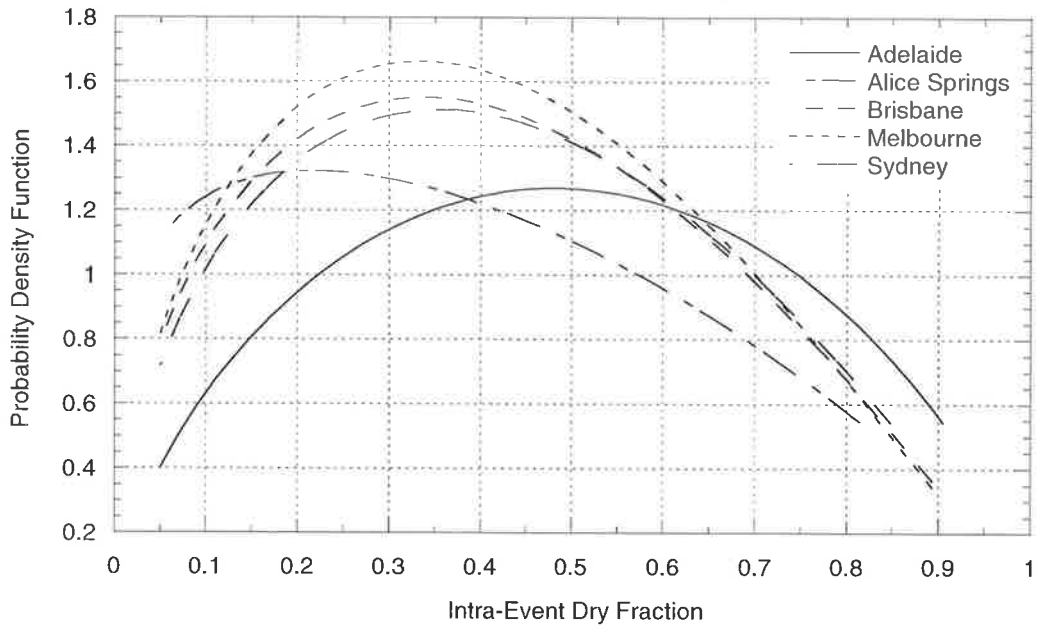

Figure 4.12 Comparison of the Beta distribution probability density function for Adelaide, Alice Springs, Brisbane, Melbourne and Sydney.

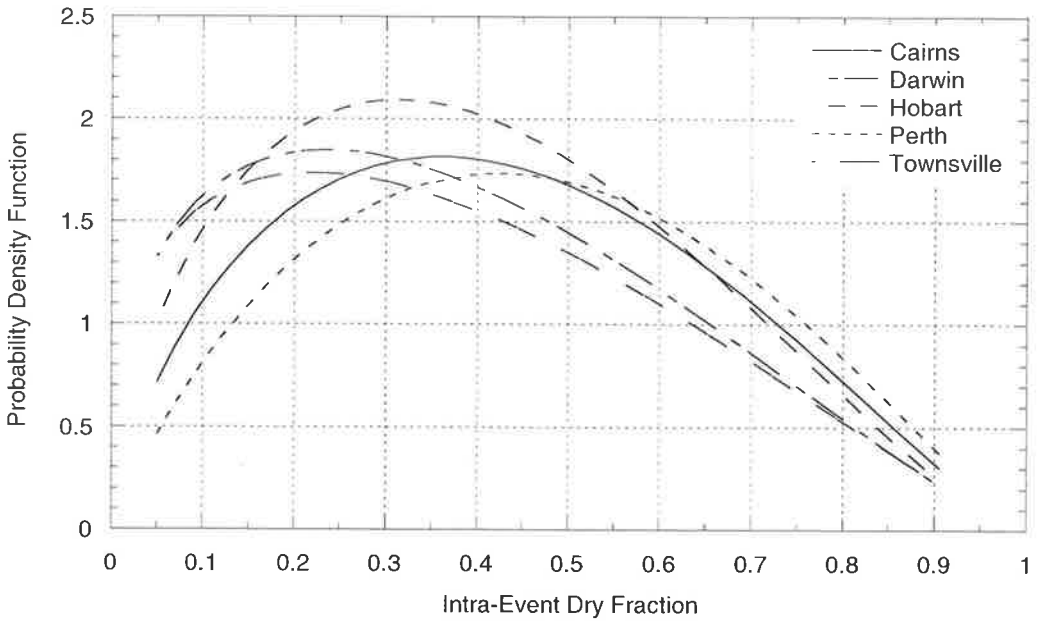

Figure 4.13 Comparison of the Beta distribution probability density function for Cairns, Darwin, Hobart, Perth and Townsville.

4.2.4 Self-Similarity of Parameters

To confirm the self-similarity between the temporal profiles of non-dimensional events and consequently to support the use of the non-dimensionalised mass curve approach, disaggregation parameters were estimated for events of different durations at the same site. Table 4.3 shows this comparison for the jump distribution parameters and Table 4.4 for the intra-event dry fraction parameters for Melbourne. For the jump distribution parameters it can be seen that the values obtained for the varying duration events are very similar and are also close to the fitted parameters obtained for the entire record. Figure 4.14 and Figure 4.15 also show the fitted functions for the jump parameters. The fitted parameters for the mean jump are very similar and those for the standard deviation of the jump are not too different. From these results it was concluded that the use of the dimensionless mass curve with parameters not dependent upon event duration is reasonable.

Table 4.3 Jump distribution parameters for varying duration events for Melbourne.

	First Jump from Origin		Subsequent Jumps			
	μ	σ	λ_1	λ_2	ζ_1	ζ_2
All Events	0.106	0.096	0.078	0.394	0.085	0.140
1-2 hrs	0.101	0.107	0.095	0.406	0.097	0.142
2-3 hrs	0.115	0.107	0.080	0.390	0.086	0.146
3-4 hrs	0.117	0.103	0.074	0.394	0.084	0.127
4-5 hrs	0.112	0.095	0.071	0.386	0.076	0.129
5-8 hrs	0.101	0.085	0.069	0.391	0.065	0.141
8-15 hrs	0.097	0.071	0.067	0.392	0.067	0.127
15+ hrs	0.095	0.056	0.056	0.408	0.044	0.148

Table 4.4 Intra-event dry fraction distribution parameters for varying duration events for Melbourne.

	Prob(P_L)	Prob(P_H)		P_{MAX}
		μ	σ	
Fitted Parameters	0.115	0.407	0.191	0.895
1-2 hrs	0.343	0.357	0.194	0.846
2-3 hrs	0.132	0.434	0.202	0.864
3-4 hrs	0.065	0.432	0.193	0.872
4-5 hrs	0.051	0.435	0.182	0.884
5-8 hrs	0.037	0.429	0.184	0.895
8-15 hrs	0.032	0.398	0.174	0.800
15+ hrs	0.026	0.341	0.152	0.726

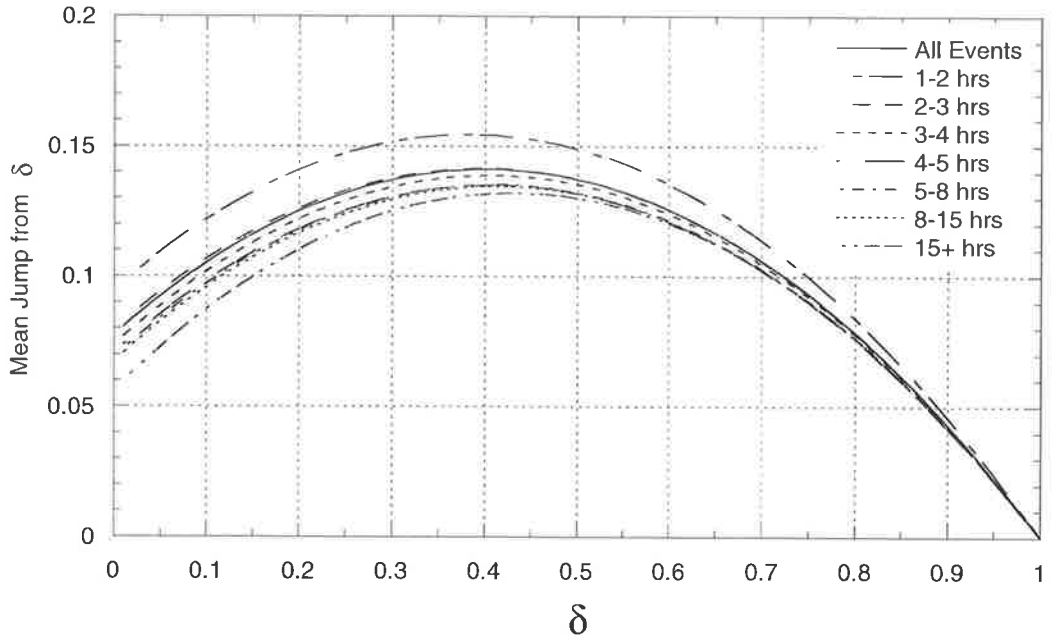

Figure 4.14 Variation of the mean jump from δ during events of varying duration for Melbourne.

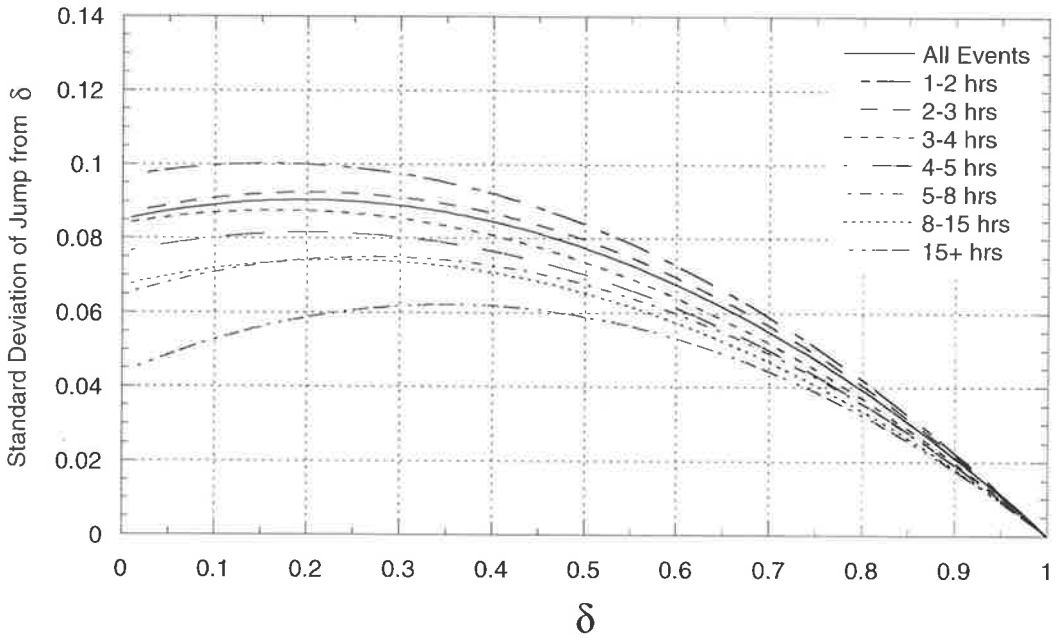

Figure 4.15 Variation of the standard deviation of the jump from δ during events of varying duration for Melbourne.

However, while the intra-event dry fraction parameters for the beta distribution and for P_{MAX} are very similar, the value of P_L noticeably decreases with increasing event duration. This indicates that there may be some differences between the intra-event dry period characteristics of shorter events compared to longer ones. It was observed that for longer duration events a large portion of the event consists of intra-event dry periods. Therefore, the probability of having a small number of intra-event dry periods for long duration events is low. Figure 4.16 compares the probability density function of the beta distribution using the parameters from Table 4.4. These show that the functions appear dependent on the event duration. However, the significance of the extent of this dependency needs to be assessed in terms of its effect on the success of the synthetic rainfall series to replicate the observed rainfall characteristics, such as aggregated statistics, to determine the need to undertake further investigation to address any lack of self similarity.

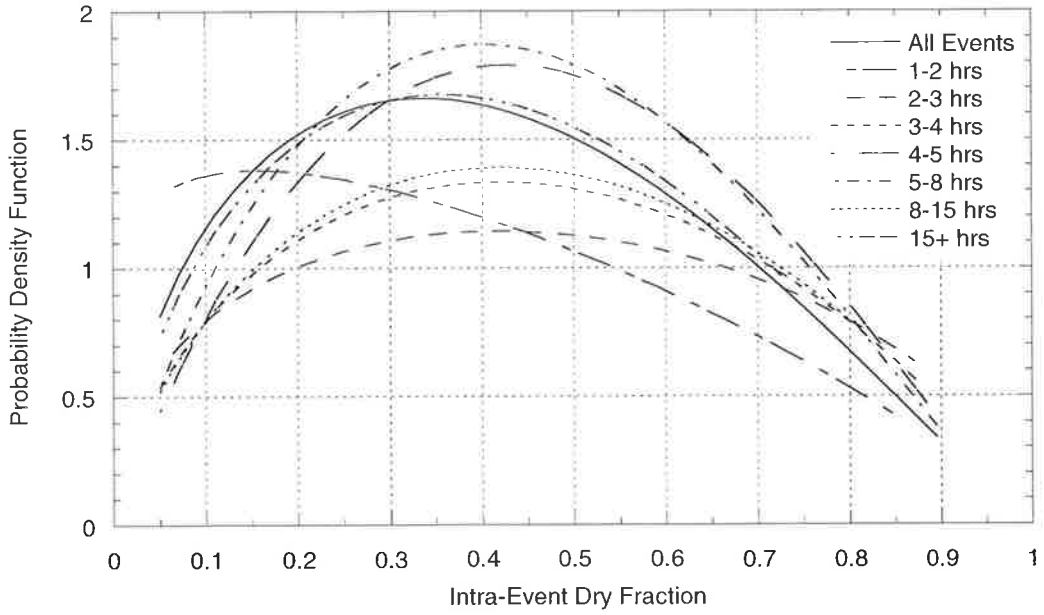

Figure 4.16 Comparison of the Beta distribution probability density function for events with varying duration for Melbourne.

4.3 DISAGGREGATION OF SIMULATED RAINFALL PULSES

Using the generated total event depth, the disaggregation model initially allocates rainfall depths for each time decile of the event. Then, by the assumption of self similarity, each of these decile depths is disaggregated into a further ten depths. This process continues until the time increments are less than or equal to six minutes. The same parameters that were applied to profile the total event duration into deciles, are used to generate the profiles for each subsequent decile. This is an extension from Woolhiser and Osborn (1985) who only consider ten intervals and assumed that the intensity remains constant within each interval, regardless of the actual event duration. Therefore, for a long duration event the intervals remained relatively large (for example, a 10 hour event results in a disaggregated event with one hour intervals).

Once the temporal pattern of wet increments had been determined, the distribution of dry increments was evaluated and inserted. The following steps were followed in the assignment of an intra-event dry fraction:

(a) events of duration less than 0.5 hours were assumed to have no dry increments;

(b) for events greater than 0.5 hours, the probability of a particular event having either an high (P_H) or low (P_L) intra-event dry fraction was determined by sampling from a uniform distribution between 0 and 1, with P_L as described in Table 4.2;

(c) an event that was classified as P_L then had its P value sampled from a uniform distribution between 0 and 0.05; and

(d) an event that was classified as P_H then had its P value sampled from a generalised beta distribution, with a lower limit of 0.05 and upper limit of P_{MAX}, using calibrated parameters.

To produce the entire temporal distribution of rainfall within a rainfall event, the simulated wet and dry periods were then combined by random assignment without replacement, subject to the constraints that no intra-event dry period could exceed two hours and that the first and last elements must be wet. The following example illustrates the steps undertaken:

(a) if a particular event is one hundred six-minute increments long and the intra-event dry fraction is determined to be 20%, this results in 20 (20% of 100 increments) six-minute

increments being dry;

(b) the first increment of the event must be wet. The six-minute rainfall depth placed in this increment corresponds to the first six-minute increment of rainfall determined by the jump distribution;

(c) this reduces the number of available increments to be allocated to 98 and the number of available wet increments to 78, allowing for the fact that the last rainfall increment must be wet. A uniform random number is then sampled and if this number is less than 20/98 then the second increment is dry; if not, the second increment is wet; and

(d) this then reduces the number of either wet or dry increments to be assigned. The process continues until all of the increments have been allocated with the final increment being wet.

Figure 4.17 presents an example of two simulated rainfall traces as dimensionless mass curves.

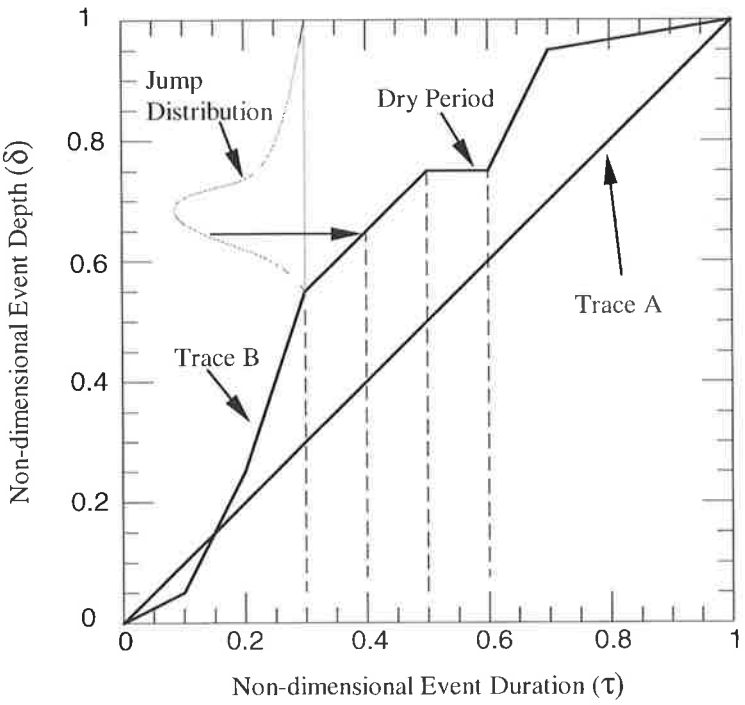

Figure 4.17 A non-dimensional description of the rainfall temporal pattern.

Trace A follows the straight line $\delta = \tau$, depicting uniformly distributed rainfall with time and no intra-event dry periods, whereas trace B depicts an event in which a large initial burst of rainfall is followed by lighter rainfall and contains a dry period within the event. Also shown

for trace B is the conditional jump distribution process. When the random walk is at $\tau = 0.3$, it must jump to a new time $\tau = 0.4$ by sampling from a truncated log-normal jump distribution.

4.3.1 Non-Dimensional Mass Curve Comparison

In Section 4.2.1, a comparison between the average dimensionless mass curve of events of varying durations was undertaken. This was to establish that self-similarity is a reasonable approximation. As a result, parameters that are independent of event duration and depth were determined. To confirm whether the disaggregation process reproduced the observed self-similarity, an analysis was undertaken of events of varying durations to determine an average non-dimensionalised mass curve. These were then compared with the original non-dimensionalised curves as shown in Figure 4.18 for Melbourne and Figure 4.19 for Perth. Results for all sites are shown in Appendix F.5. It can be seen that the self-similarity property is reasonably well reproduced. However, a discrepancy in the period $\tau = 0.7-0.9$ is noticeable, in that the simulated curves are much flatter than the observed, with a steeper step between $\tau = 0.9-1.0$. This pattern appears to occur independently of event duration.

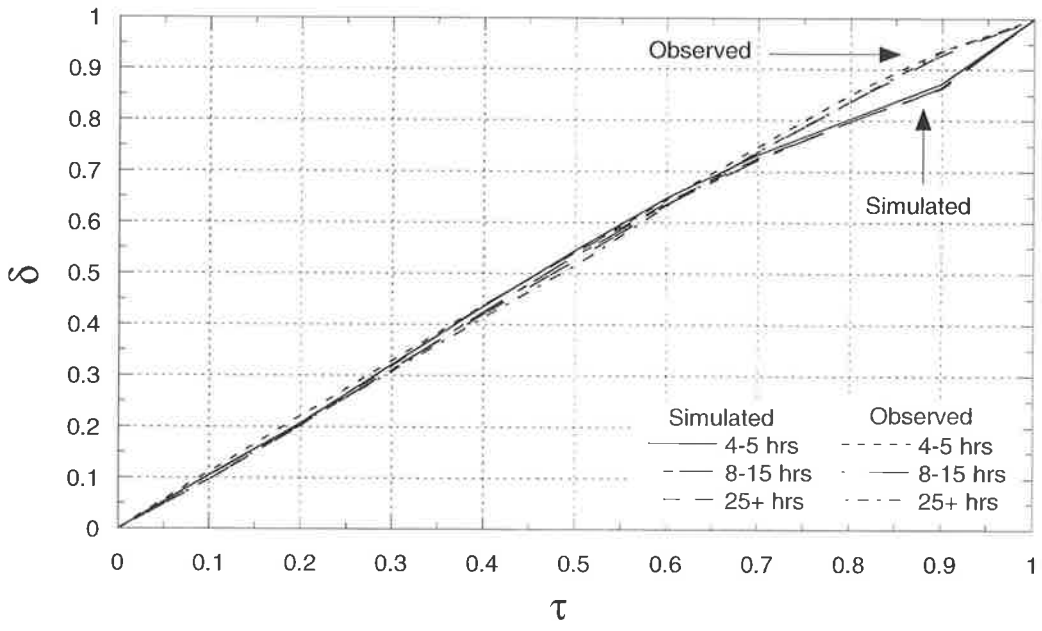

Figure 4.18 Comparison of simulated and observed event profiles for varying event durations for Melbourne.

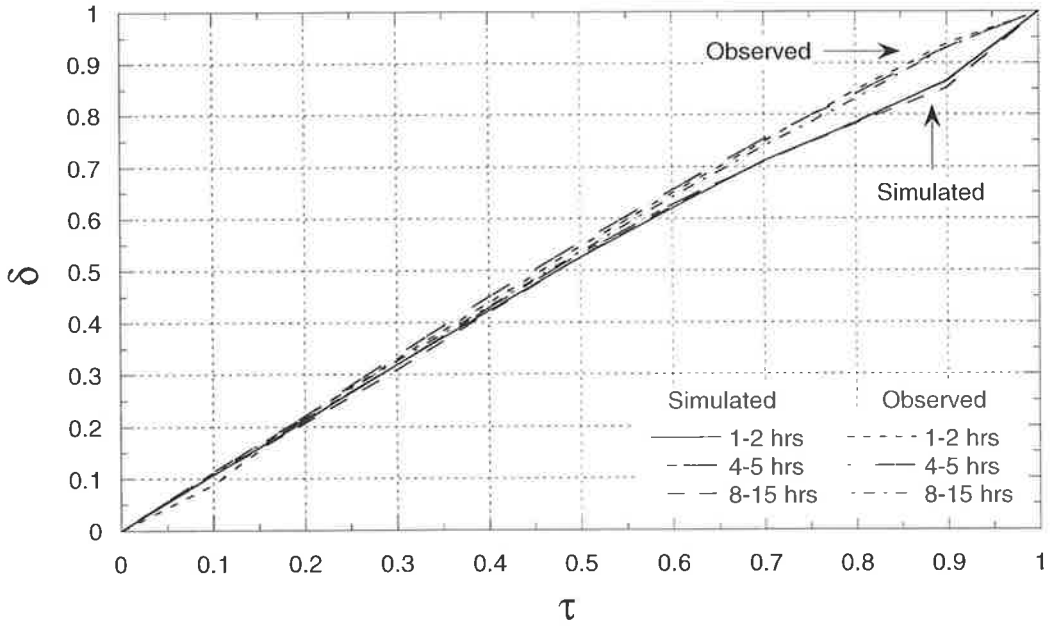

Figure 4.19 Comparison of simulated and observed event profiles for varying event durations for Perth.

One possible reason for this is that the standard deviation of the jump from δ (as shown in Figure 4.6 for Melbourne) decreases as τ increases. Therefore, there may not be enough variability in the jumps in this range and the jumps are small. As such, there is less rainfall during the period $\tau = 0.7-0.9$ than would normally occur but once $\tau = 0.9$, the remainder of the non-dimensionalised depth must fall before $\tau = 1.0$ and hence the curve is steep. Another cause may be the simplistic approach to determine wet or dry increments, which appears to have a bias towards dry increments occurring later in an event.

4.4 Concluding Remarks

This chapter has discussed the development of a probabilistic rainfall pulse model. A comparison of non-dimensionalised mass curves between events of varying durations showed that an assumption of self-similarity between events was reasonable as a first approximation. The model uses a constrained random walk on a dimensionless mass curve to describe the temporal distribution of intra-event rainfall.

The characteristics of the rainfall jumps on the dimensionless mass curve and the total intra-event dry periods were evaluated separately for each event during both the calibration of parameters and the simulation of the intra-event hyetograph. A truncated log-normal

distribution provided an adequate representation of the rainfall jumps. The parameters for the first jump within a rainfall event were taken from the marginal distribution, with each successive jump dependent on its current position on the dimensionless mass curve. The successive jumps were described using parabolic curves, which were found to be very similar across the varied Australian climatic regions considered. This offers significant potential for regionalisation and application of this approach to areas with limited or no data.

The proportion of dry increments within an event or the intra-event dry fraction (P) was represented using a uniform distribution for $0 \le P \le 0.05$ and a beta distribution for $0.05 < P \le P_H$ where P_H is the maximum dry fraction observed in the historical data. The parameters for the proportion of intra-event dry increments were also very similar between locations despite the differences in climatic conditions. The only exceptions were Darwin and Alice Springs, which experience more intense events than most of Australia, such that once it begins raining there are not many intra-event dry periods. Despite this, the method offers considerable potential for regionalisation.

A comparison of simulated and observed average event profiles showed the self-similarity property to be reasonably well produced. However, within the dimensionless depth (δ) range of 0.7 to 1.0 discrepancies were noticed and were independent of event duration. This is possibly attributable to the parabolic functions used to represent the conditional jumps, in particular, the fact that the standard deviation decreases significantly as the dimensionless depth approaches one. There may not be enough variability in the jumps in this range, resulting in smaller jumps that cause the trace to flatten relative to the observed historical record. Because the remaining δ at a dimensionless time (τ) of 0.9 must fall before 1.0, this portion of the curve is steeper than in the observed record. Increasing the variability of the jumps in the upper regions of the dimensionless mass curve may be an option for correcting this. Because the validation of the total rainfall model is carried out using statistics not used in its calibration, the effect of this disaggregation discrepancy will be tested at a higher level. This study did not seek to make further improvements to the disaggregation model but the opportunity for improvement was noted should the overall rainfall model be unable to adequately reproduce key observed statistics.

5. VALIDATION OF THE STOCHASTIC RAINFALL MODEL

This chapter provides a rigorous examination of many aspects of the performance of the rainfall model and its suitability for use in developing the design flood estimation procedure outlined in Chapter 1.

An examination of the observed and simulated probability distributions for inter-event time, event duration and marginal average event intensity is presented. While these probability distributions are used to calibrate and subsequently simulate rainfall, this comparison provides a level of confirmation that the observed distributions are being effectively reproduced by the simulation. For the marginal average event intensity, a comparison is made between the model outputs dependent on both a monthly and harmonic event duration model.

Successful calibration is a necessary but not sufficient requirement for demonstrating model credibility. The robustness of a model can be best illustrated when it is validated by examining properties that are not used in its calibration (Cowpertwait, 1994; Cowpertwait *et al.*, 1996a). This is an important step in model development because it can reveal structural inadequacies in the model methodology and assumptions. The ability of the point rainfall model to simulate rainfall statistics that are not used in its calibration is further considered in this chapter.

Intensity-Frequency-Duration (IFD) curves, aggregated statistics and the probability distribution of annual totals, which are not used to calibrate the model, are examined. While many researchers have considered the effective reproduction of aggregated statistics as a measure of a model's credibility, these statistics have often been used to calibrate the models. The reproduction of these statistics for durations longer than 24 hours is rarely considered, nor is the effectiveness of a model to reproduce extreme values. When extreme values have been checked many models have shown poor results for higher Average Recurrence Intervals (ARI).

5.1 Probability Distributions of Characteristic Event Variables

A comparison between the observed and simulated inter-event time and event duration probability distributions provides confirmation that the simulation is adequately reproducing these calibrated parameters. This is an important first step in model validation. The distributions for these variables were calibrated on a monthly basis, which results in a large number of parameters that require estimation. To reduce the number of parameters, the use of harmonic functions to vary the distribution parameters over the year was examined. The development of these functions and the statistically preferred harmonic model for each site was discussed in Chapter 3. Presented in the following is a comparison of the distributions of inter-event time and event duration variables generated using both the monthly and harmonic models, along with an examination of the effect of the harmonic and monthly event duration distributions on reproducing the marginal average event intensity distribution.

Figure 5.1 (Sydney in April) shows that the inter-event time distribution is well represented using the monthly model but not by the harmonic model, particularly in the tail of the distribution. Most of the months and sites modelled showed this type of relationship, that is, the monthly model produced much better results than the harmonic model. However, Figure 5.2 (Sydney in June) shows a situation where both models produce a very similar representation. Some cases, such as shown in Figure 5.3 (Alice Springs in August), exhibit a more complex observed probability distribution that is different to the "typical" distribution shape. This form of distribution can only be produced using a monthly fitted model. In a small number of cases observed probability distributions were reproduced more reliably using the harmonic model, such as Figure 5.4 (Cairns in May). In this instance, the result may indicate some seasonal variations in the properties of the inter-event times occur within a month, which may occur during the transition months between seasons. Harmonic models were able to represent these monthly variations because the parameters of the distribution change smoothly over the year, whereas the parameters of the monthly model are fixed for the month and cannot accommodate intra-month variations in the distribution of inter-event times.

Difficulties in fitting a distribution to a particular month occurred for Darwin where there are less than 20 rainfall events recorded during the June to July dry season for over 40 years of record. This small number of data points is not enough to calibrate and produce a meaningful

monthly probability distribution. Theoretically the harmonic model should be able to overcome this issue as it is calibrated using all available data points and is based on seasonal changes over the entire year. However, the observed variation of inter-event times over the year was so great, as a result of the vastly different rainfall patterns in the wet and dry seasons, that the harmonic model was not able to effectively represent this in order to overcome the problem of a small number of data points. Overall, the monthly model provided the most reliable and meaningful representation of the inter-event time distributions for each site. The observed and simulated distributions of the inter-event times for all sites are shown in Appendix G.

A similar result was observed for the representation of event duration distributions, with the distributions being better represented for each site and month using the monthly model as seen in Figure 5.5 (Perth in July). Again, the harmonic model was unable to reproduce the more complex probability distributions for some months, as shown in Figure 5.6 (Alice Springs in May). The observed and simulated distributions of event duration for all sites are shown in Appendix H.

The simulated marginal distributions of average event intensity using both the monthly and harmonic event duration models were also compared to determine the effect of event duration distribution on the marginal average event intensity. Overall, the simulated average event intensity distributions adequately reproduced the observed distributions. The only exception was in the tail of some of the monthly marginal distributions. However, this may be a result of the limited length of available Australian data resulting in an insufficient number of extreme events to allow an effective comparison. Typically, less than 0.1 percent of the total events for each month lie in the tail of the marginal average event intensity distribution.

The distributions using the different event duration models are generally similar in shape such as in Figure 5.7 (Melbourne in December). In a small number of cases, for example in Figure 5.8 (Melbourne in October), the marginal average event intensity produced using the harmonic event duration model was better. Overall, the monthly model was generally better at producing the observed tails of the distribution. The small differences between the monthly and the harmonic event duration model indicates that where the duration model is reasonable the type of model has little effect on the marginal distribution of average event intensity. However, the IFD and aggregated statistics produced using the harmonic model of event

duration were less than satisfactory, which suggests that the choice of the average event intensity distribution is important for overall model results. The observed and simulated distributions of the marginal average event intensity for all sites are shown in Appendix I.

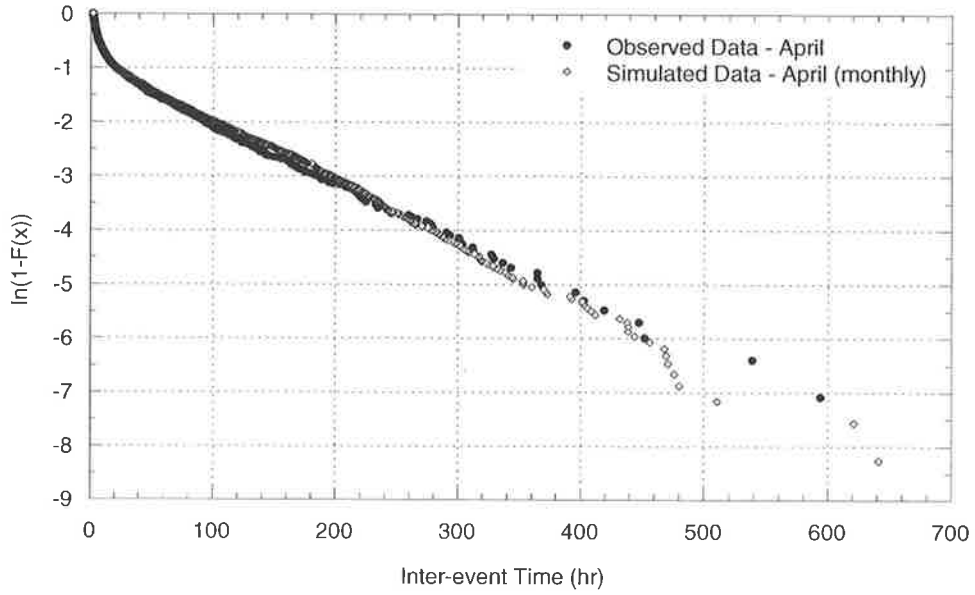

(a)

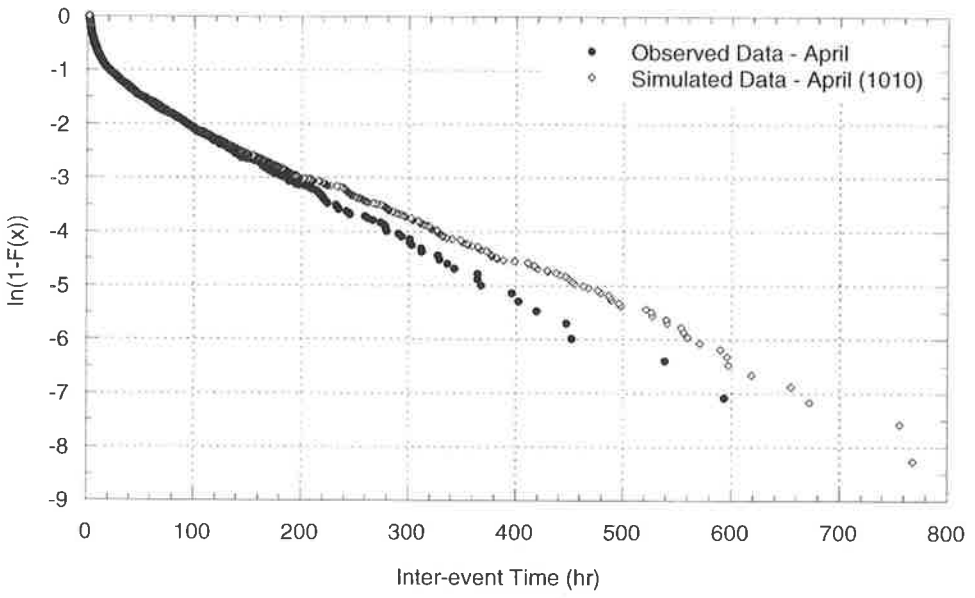

(b)

Figure 5.1 Observed and simulated inter-event time distributions for Sydney in April: (a) Monthly model; (b) Harmonic model 1010.

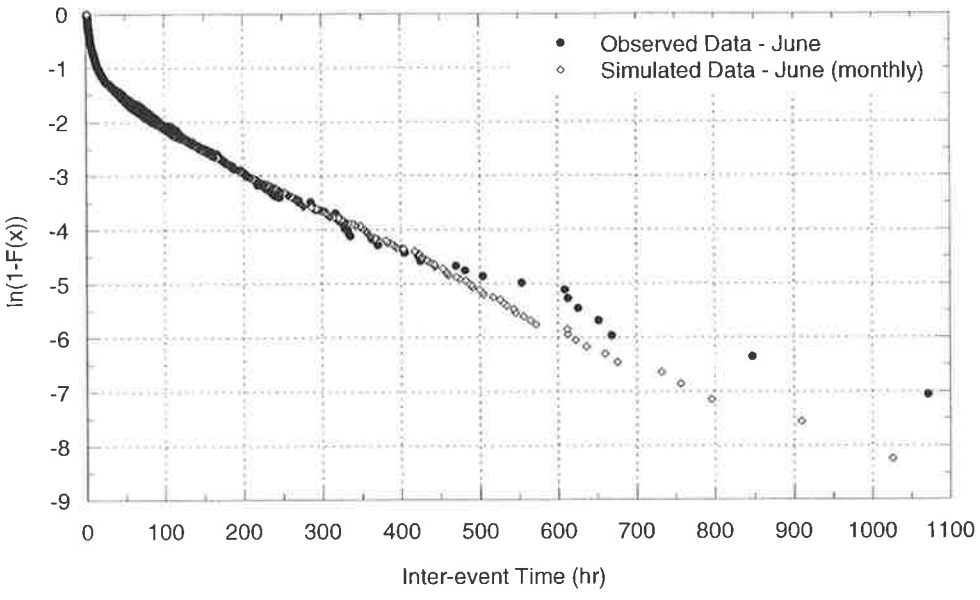

(a)

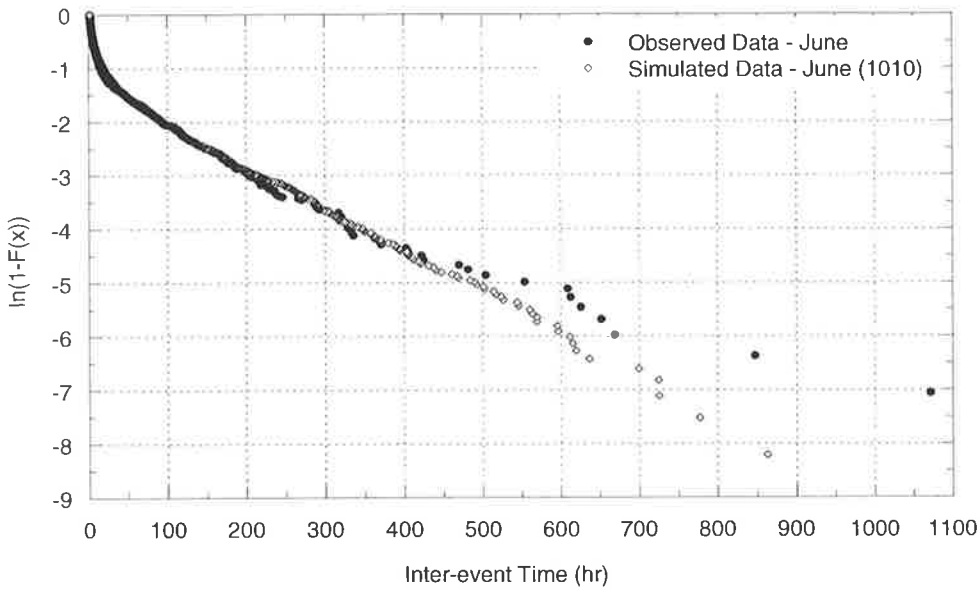

(b)

Figure 5.2 Observed and simulated inter-event time distributions for Sydney in June: (a) Monthly model; (b) Harmonic model 1010.

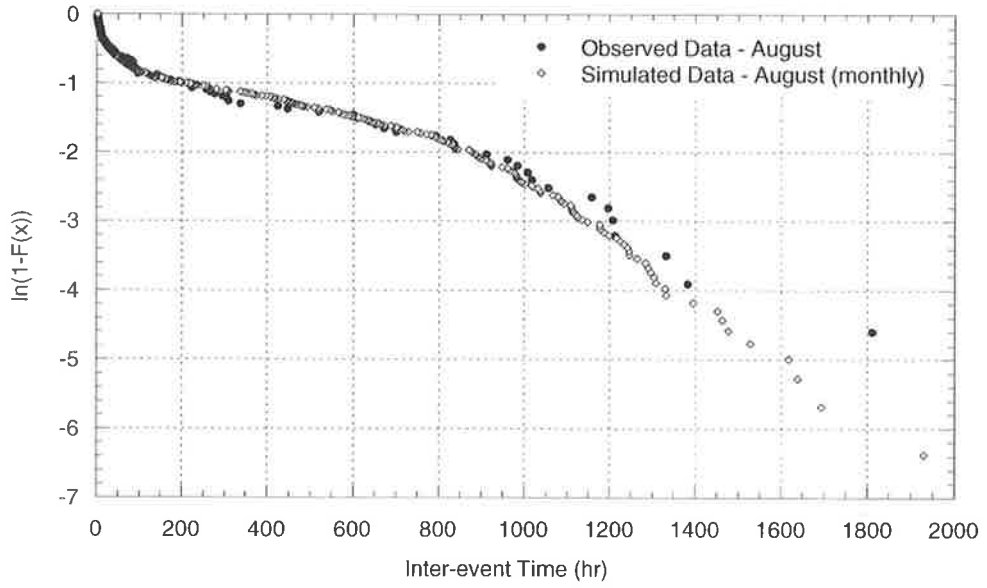

(a)

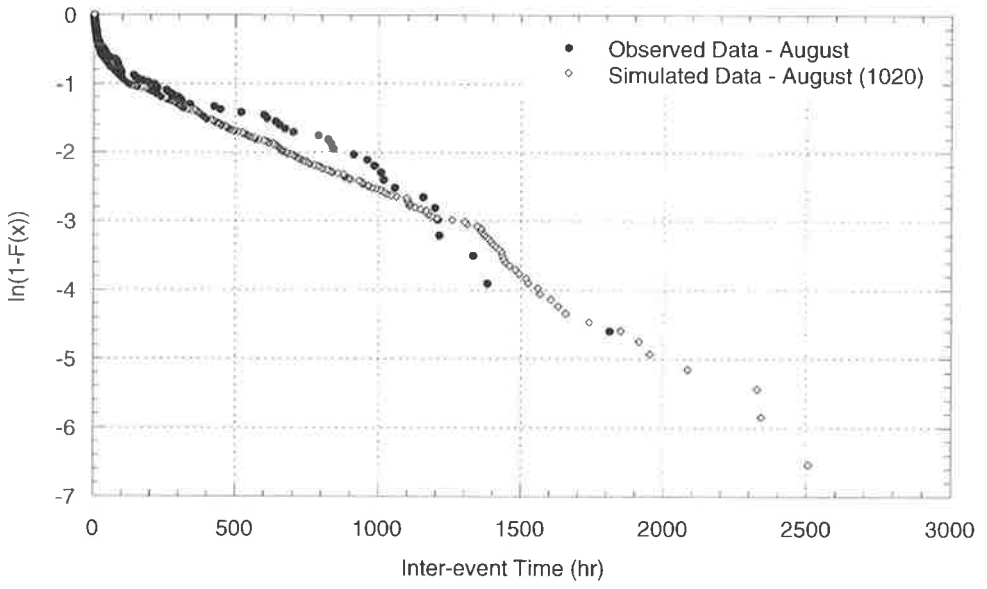

(b)

Figure 5.3 Observed and simulated inter-event time distributions for Alice Springs in August: (a) Monthly model; (b) Harmonic model 1020.

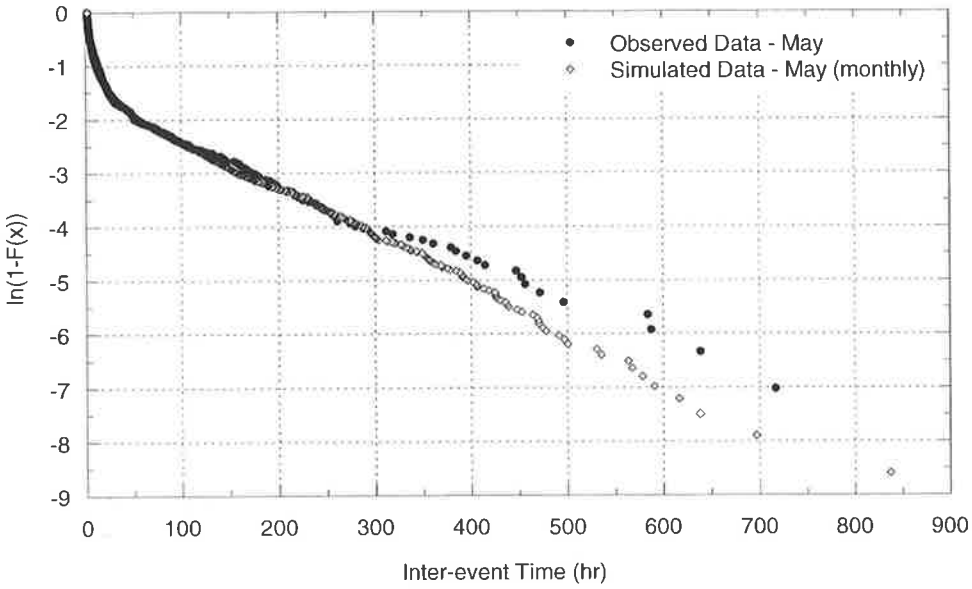

(a)

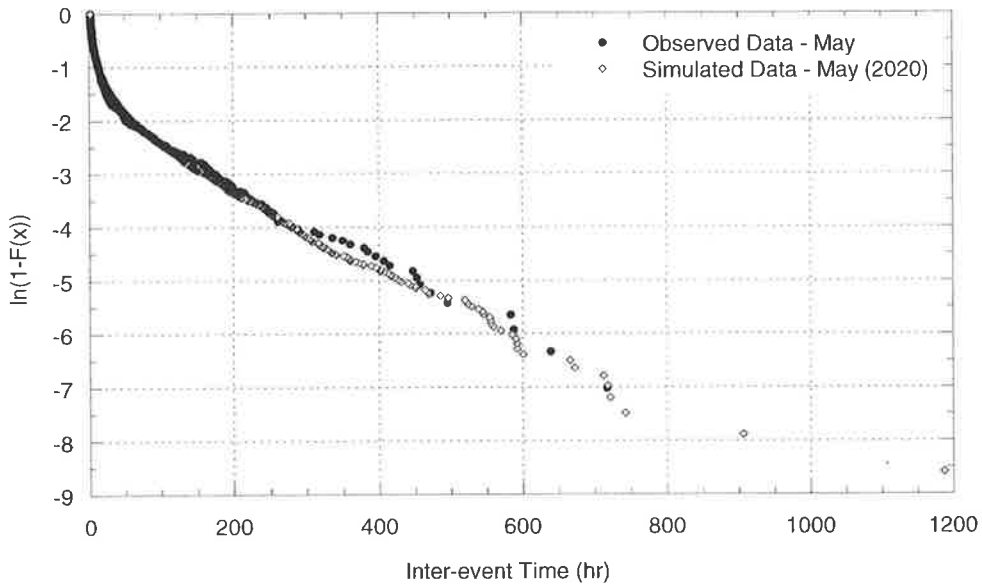

(b)

Figure 5.4 Observed and simulated inter-event time distributions for Cairns in May: (a) Monthly model; (b) Harmonic model 2020.

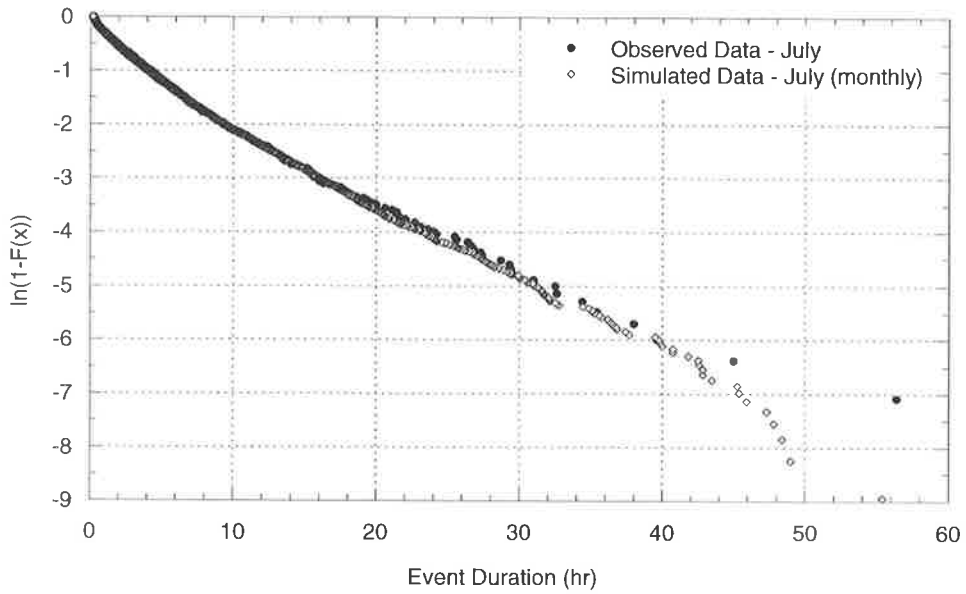

(a)

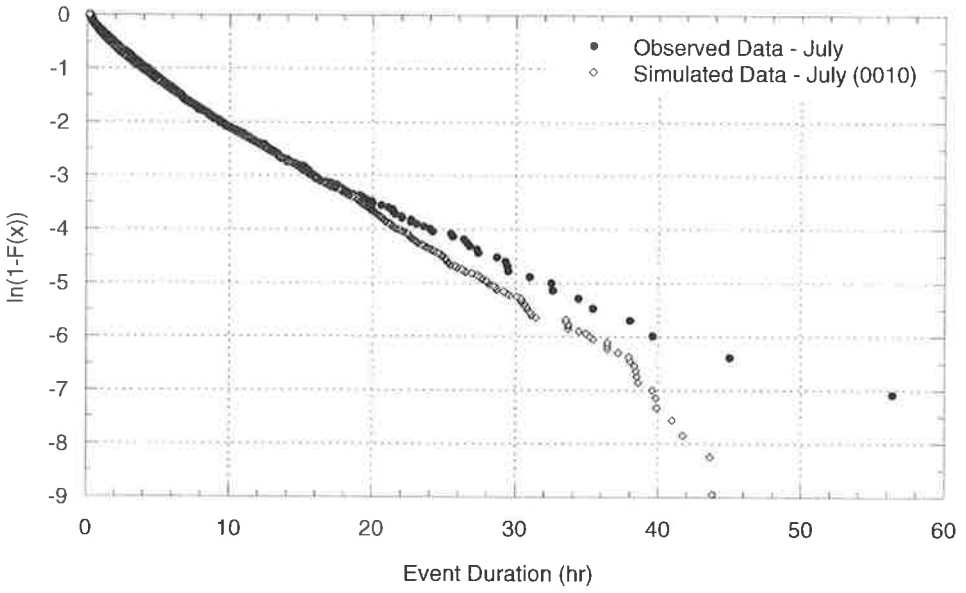

(b)

Figure 5.5 Observed and simulated event duration distributions for Perth in July: (a) Monthly model; (b) Harmonic model 0010.

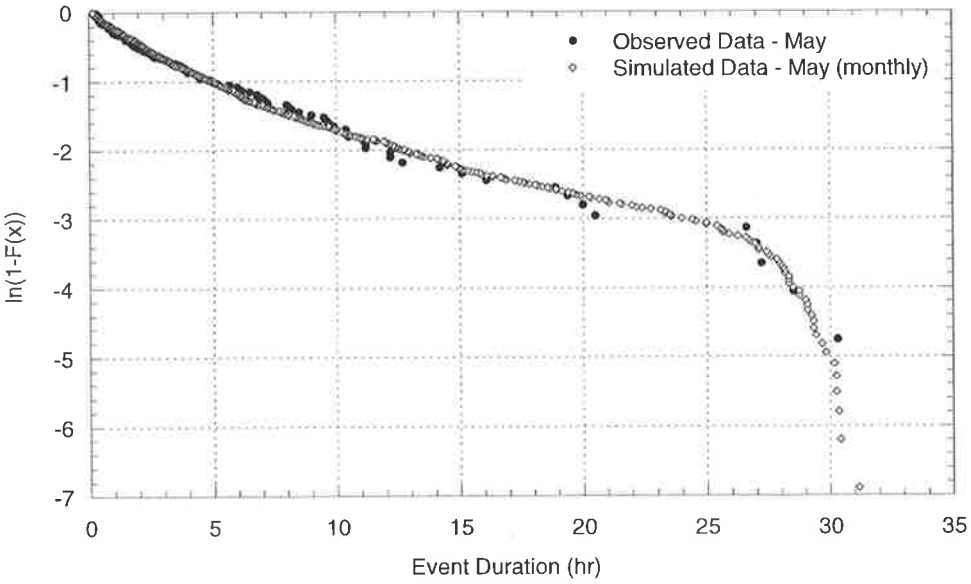

(a)

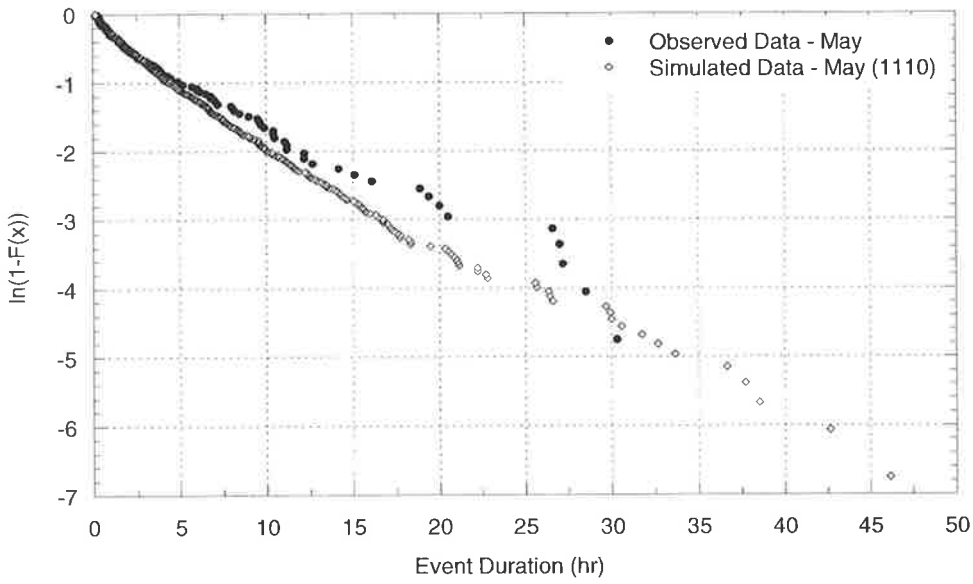

(b)

Figure 5.6 Observed and simulated event duration distributions for Alice Springs in May: (a) Monthly model; (b) Harmonic model 1110.

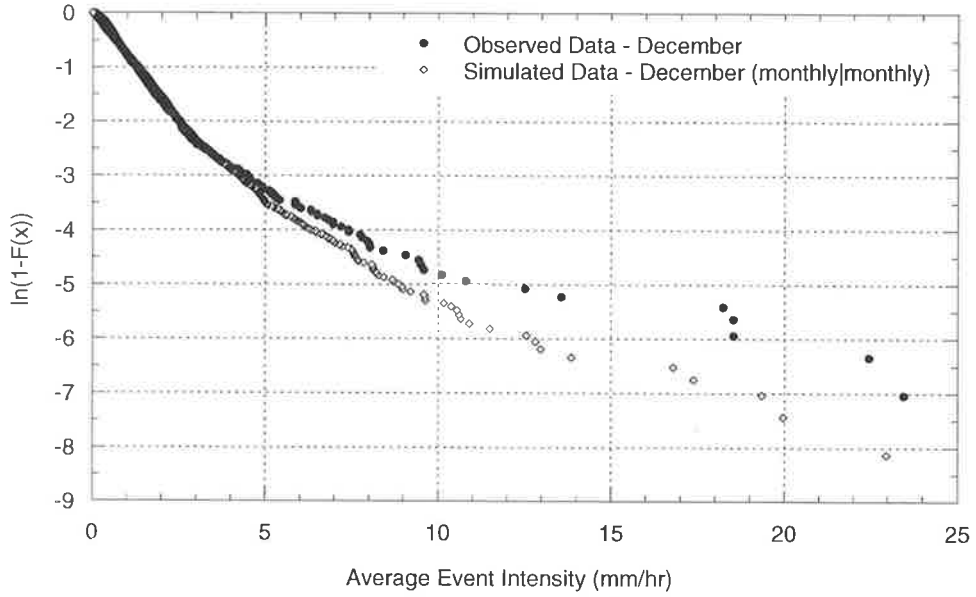

(a)

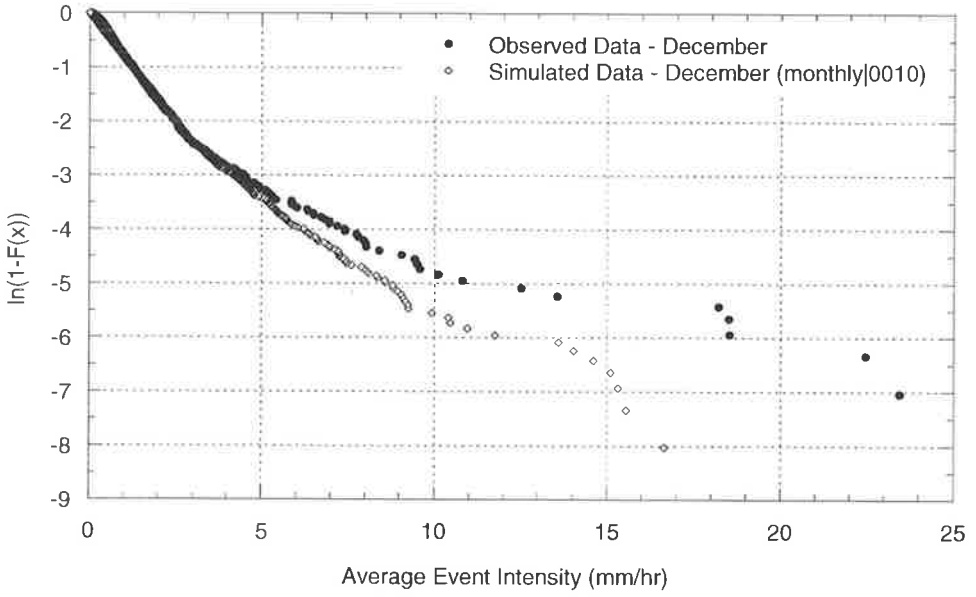

(b)

Figure 5.7 Observed and simulated marginal average event intensity distributions for Melbourne in December: Event duration: (a) monthly model; (b) harmonic model 0010.

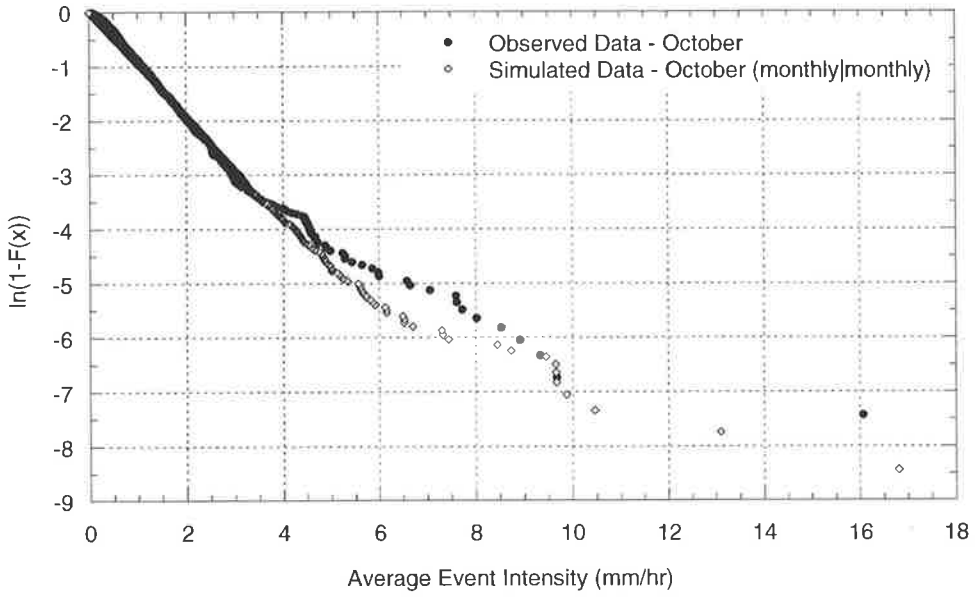

(a)

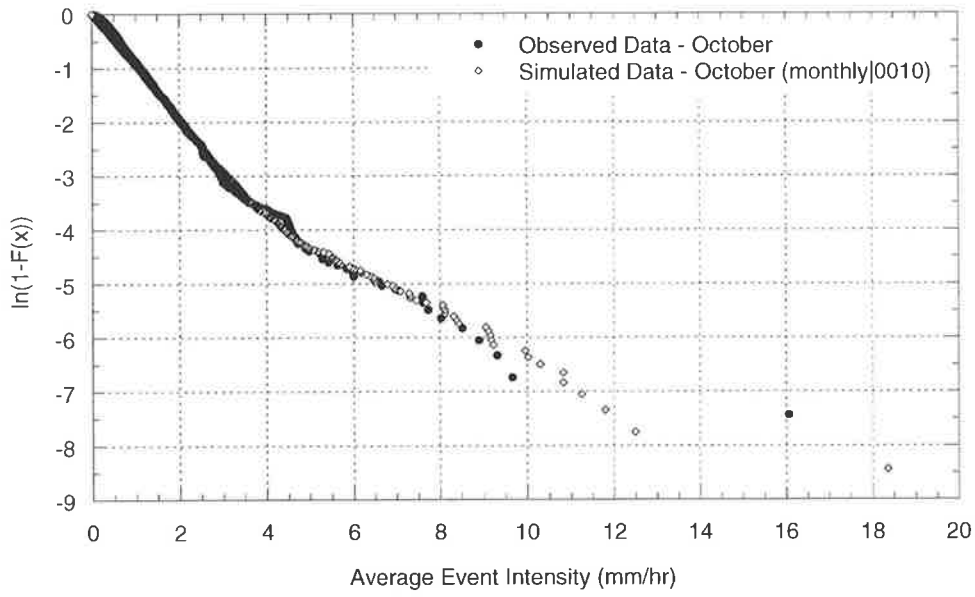

(b)

Figure 5.8 Observed and simulated marginal average event intensity distributions for Melbourne in October: Event duration: (a) monthly model; (b) harmonic model 0010.

5.2 INTENSITY-FREQUENCY-DURATION STATISTICS ANALYSIS

A comparison of observed and simulated IFD curves provides a rigorous test of the ability of a model to simulate the temporal nature of rainfall. These statistics are also an important quantity that needs to be able to be reproduced successfully if a model is to be used with confidence in design flood applications. IFD curves are obtained by moving windows of a fixed duration incrementally through each year and determining the annual maximum rainfall depths for each of these windows. A frequency analysis can then be undertaken on these annual maxima for the various durations to produce the IFD curves. This is a standard method to determine the statistics of extreme rainfall over different durations for use in engineering design. Evaluated separately in the following are the replication of the observed annual maximum probability distributions, short duration (1 and 3 hour) IFD curves and the long duration (12, 24 and 72 hour) IFD curves. Because the monthly model for the inter-event time and event duration distributions was found to perform better in Section 5.1, the monthly model simulations were used to produce the simulated IFD curves.

5.2.1 Annual Maximum Probability Distributions

The observed and simulated annual maximum probability distributions for 1, 3, 12, 24 and 72 hour duration IFD rainfall were calculated for all sites. For most locations including Melbourne (Figure 5.9), the simulated IFD curves, shown as a solid line, compare very well with the observed IFD curves. This suggests that the rainfall model can adequately simulate random bursts of high intensity over a range of durations. However, for some locations, particularly in tropical and arid areas, more deviation of the simulated distributions from the observed was noticeable. For Alice Springs (Figure 5.10) it can be seen that for higher duration events (12-72 hours) the simulated distributions do not have enough variation in the annual maximum intensity, which results in intensities that are too high for low probabilities and too low for high probabilities. The IFD curves for Cairns (Figure 5.11) show similar deviations for the higher duration events although the lower duration events tend to be overestimated for the higher probabilities. The statistical significance of the departures from the observed distribution is discussed in Section 5.2.2. Appendix J.1 contains the annual maximum probability distributions for all locations.

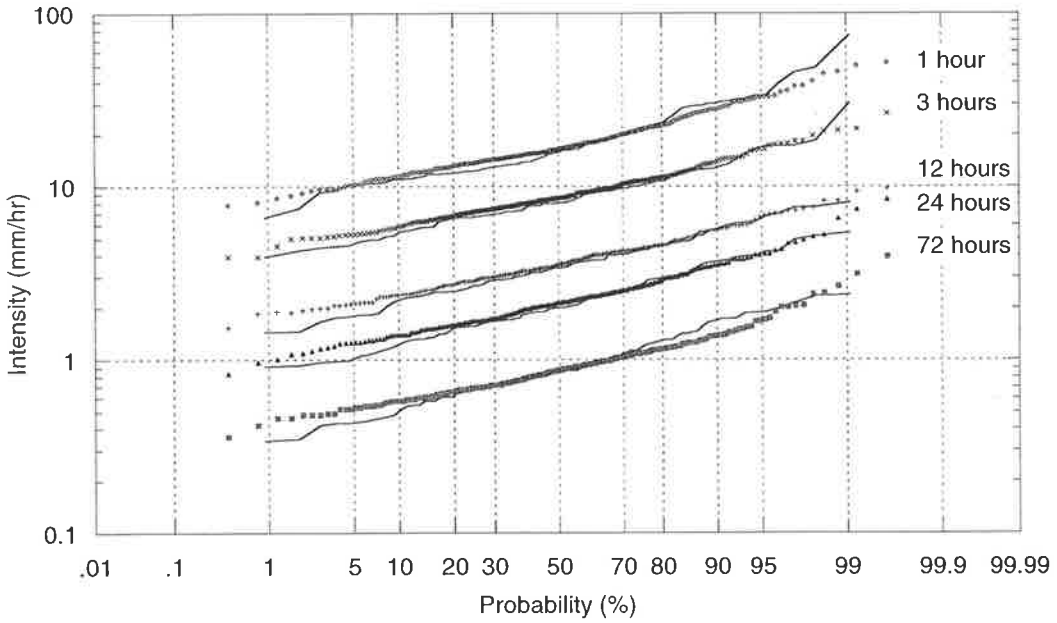

Figure 5.9 Simulated and observed IFD probability distributions for Melbourne.

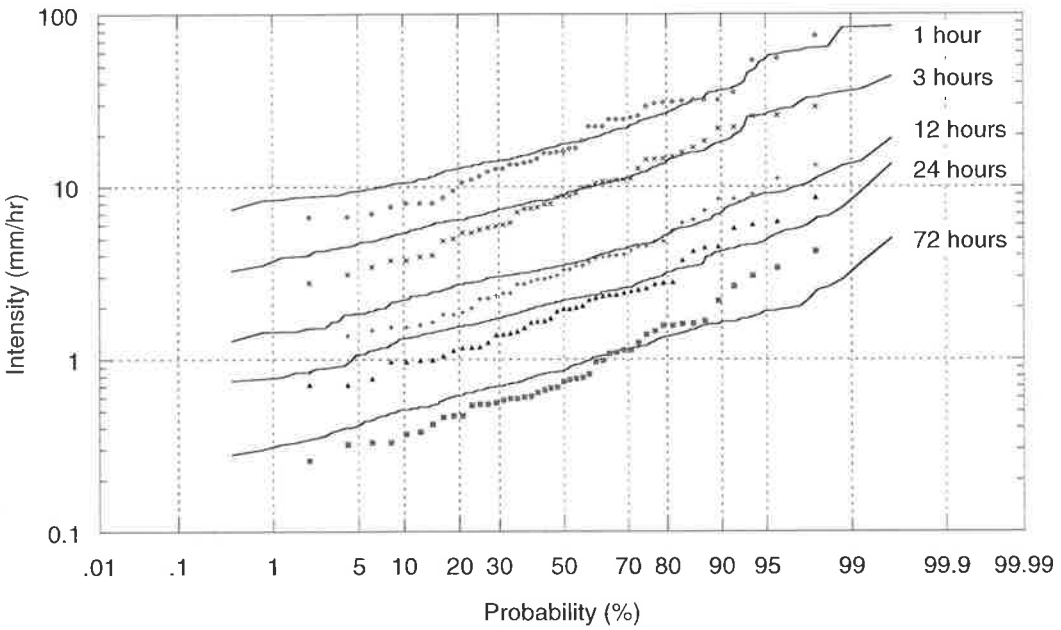

Figure 5.10 Simulated and observed IFD probability distributions for Alice Springs.

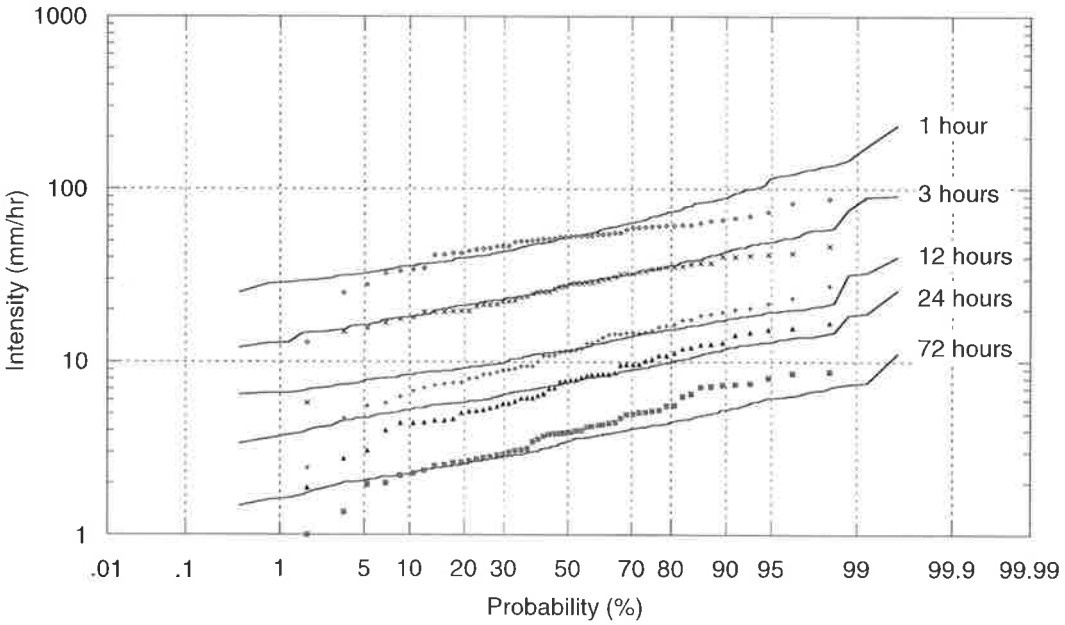

Figure 5.11 Simulated and observed IFD probability distributions for Cairns.

5.2.2 Short-Duration IFD Analysis

Successful simulation of short duration IFD curves, taken as one to three hours, depends on the ability of the temporal pattern generator to replicate the random bursts that occur during rainfall events. For example, the annual maximum one hour duration rainfall intensity may not be produced by a one hour event but by a burst within a longer duration event. A frequency analysis was carried out on both the observed and simulated annual maxima for one and three hour durations and a generalised exponential value (GEV) distribution was then fitted to this data to obtain an IFD curve. The approximate 90 percent probability limits were also determined to assess the significance of the deviations between the distributions discussed in Section 5.2.1.

Figure 5.12(a) shows the frequency analysis of the one hour observed IFD data for Melbourne and Figure 5.12(b) the simulated one hour IFD data. The IFD rainfall intensity is plotted against the logarithm of the ARI to exaggerate the tail of the probability distribution. In both cases the GEV distribution fits well to the data. A comparison of the observed and simulated fitted IFD distributions for one hour, along with the Australian Rainfall and Runoff (ARR, 1987) IFD data for this site and duration is shown in Figure 5.12(c). While the simulated distribution is lower than the observed distribution, the expected value of the simulated

distribution is contained within the 90% confidence limits of the observed distribution, with the 90% confidence limits for both distributions overlapping for most ARIs. It is interesting to note that the ARR (1987) IFD data is lower than that observed in the pluviograph data, which is based on over 100 years of data. A similar analysis for a three hour duration (Figure 5.13) shows that the simulated distribution and its 90% confidence limit are contained within the observed confidence limits. The fitted GEV distributions for the observed and simulated data, along with a comparison of these curves for one and three hours at all locations is contained in Appendix J.1.

The observed one and three hour duration IFD curves for Alice Springs (Figure 5.14 and Figure 5.17) and Sydney (Figure 5.15 and Figure 5.18) are well reproduced by the simulation. However, for Cairns (Figure 5.16 and Figure 5.19) it can be seen that the simulated IFD overestimates the observed distribution. In Section 5.2.1 it was noted that the simulated short duration annual maximum probability distributions for Cairns overestimated the observed data, which has been clearly reflected in Figure 5.16 and Figure 5.19. While the GEV distribution produces a good representation of the observed IFD data obtained from 57 years of pluviograph record (refer to Appendix J.1.5) it can be seen that the ARR (1987) IFD data is also significantly higher than this observed IFD data.

At other sites, the one hour IFD distributions for Adelaide and Perth are well reproduced by the simulation. Brisbane and Darwin (Figure J.21 and J.31, Appendix J.1) are slightly overestimated although the confidence limits partially overlap. For Hobart and Townsville the simulated IFD curves are overestimated although for Townsville it can be seen (Figure J.56, Appendix J.1) that the ARR (1987) IFD values are much higher than the observed IFD data based on the pluviograph record.

The observed three hour duration IFD statistics for Adelaide, Brisbane, Darwin, and Townsville are well reproduced by the simulation. The results for Perth are similar to those for Cairns in that the ARR (1987) IFD values are contained well within the confidence limits of the simulation but the observed IFD curves are lower. The IFD curves for Hobart (Figure J.37, Appendix J.1) are overestimated.

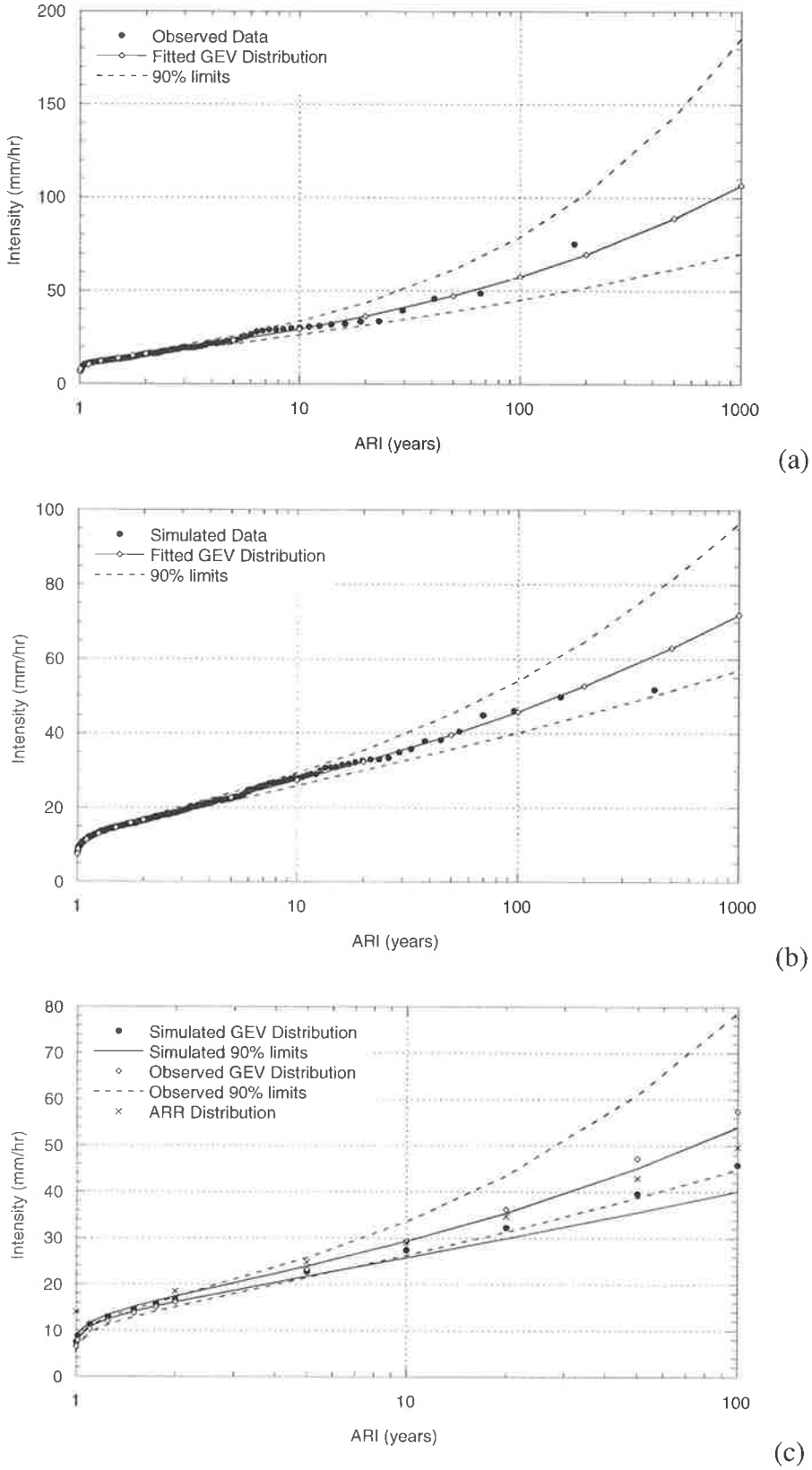

Figure 5.12 1 hour Melbourne IFD analysis:
(a) Fitted GEV distribution to observed IFD data;
(b) Fitted GEV distribution to simulated IFD data; and
(c) Simulated and observed IFD curves.

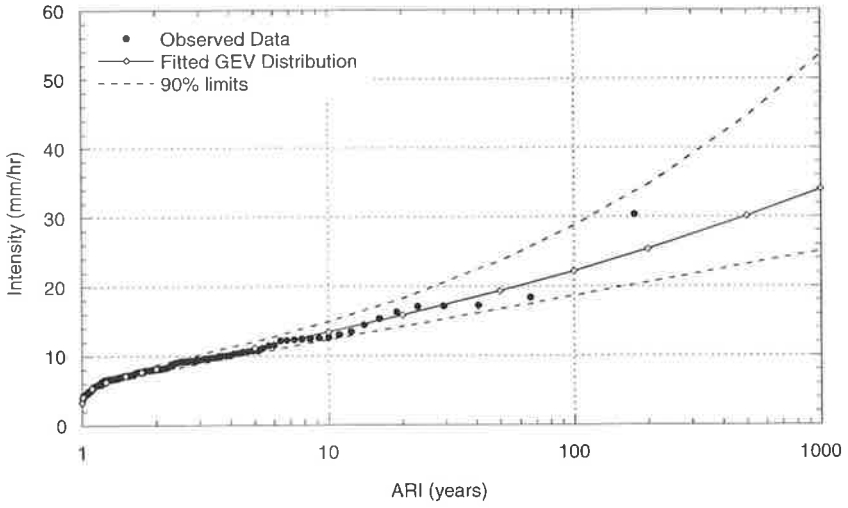

(a)

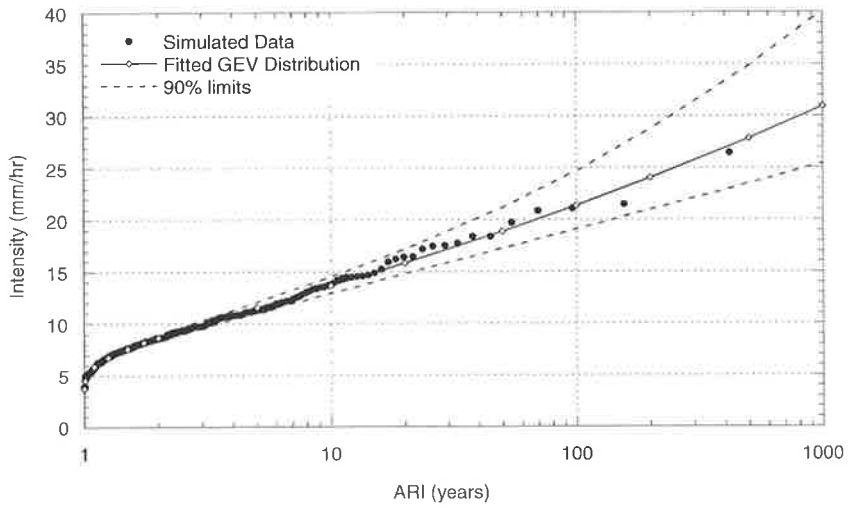

(b)

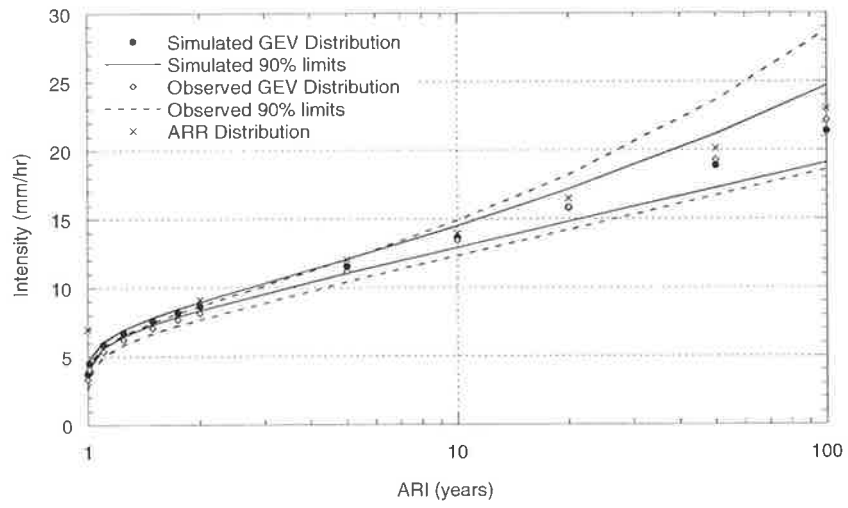

(c)

Figure 5.13 3 hour Melbourne IFD analysis:
(a) Fitted GEV distribution to observed IFD data;
(b) Fitted GEV distribution to simulated IFD data; and
(c) Simulated and observed IFD curves.

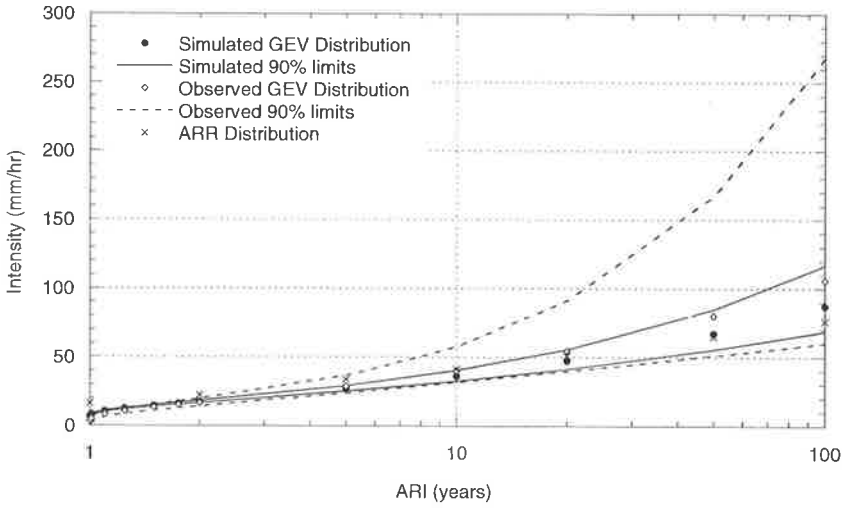

Figure 5.14 Simulated and observed 1 hour IFD curves for Alice Springs.

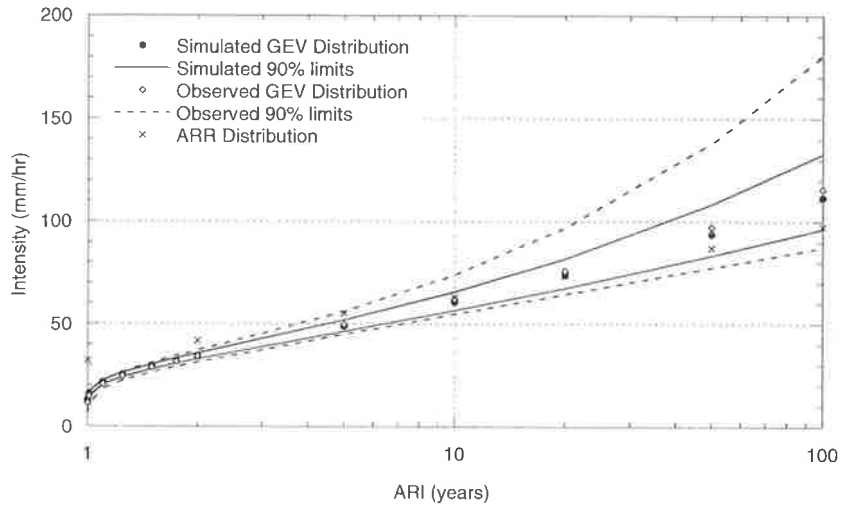

Figure 5.15 Simulated and observed 1 hour IFD curves for Sydney.

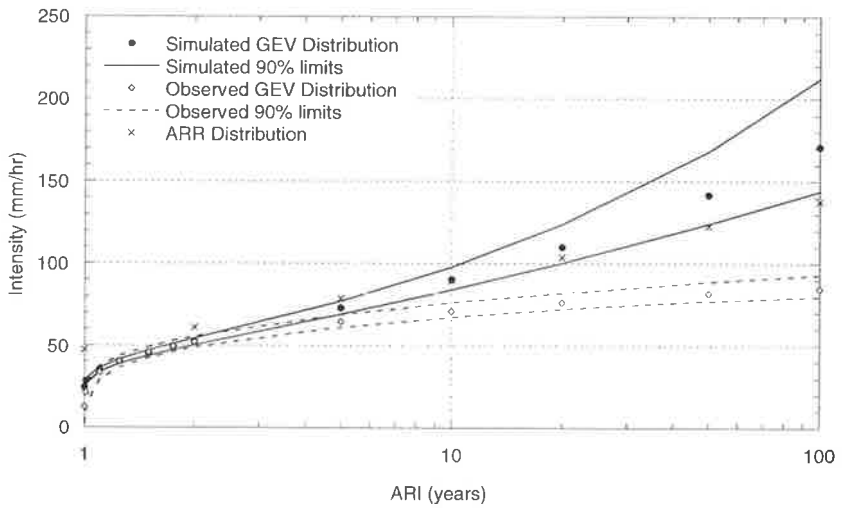

Figure 5.16 Simulated and observed 1 hour IFD curves for Cairns.

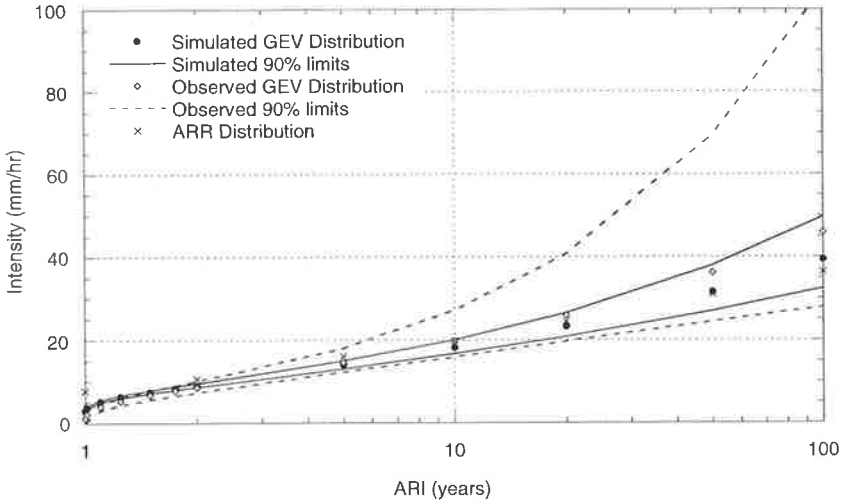

Figure 5.17 Simulated and observed 3 hour IFD curves for Alice Springs.

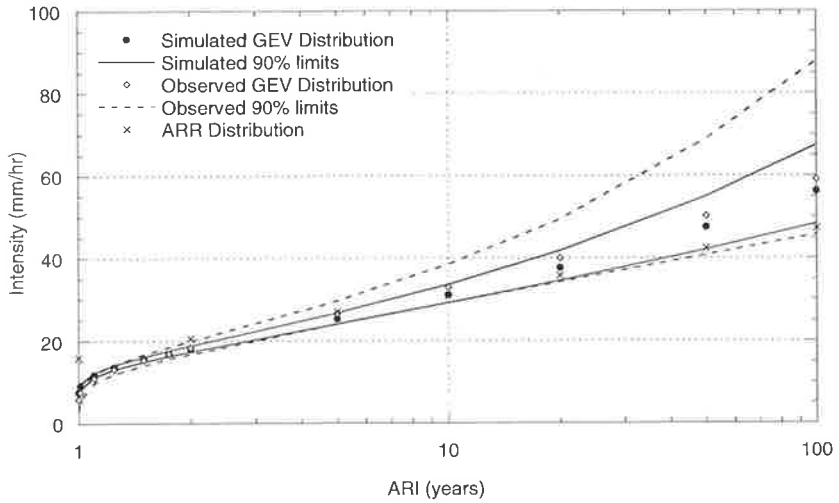

Figure 5.18 Simulated and observed 3 hour IFD curves for Sydney.

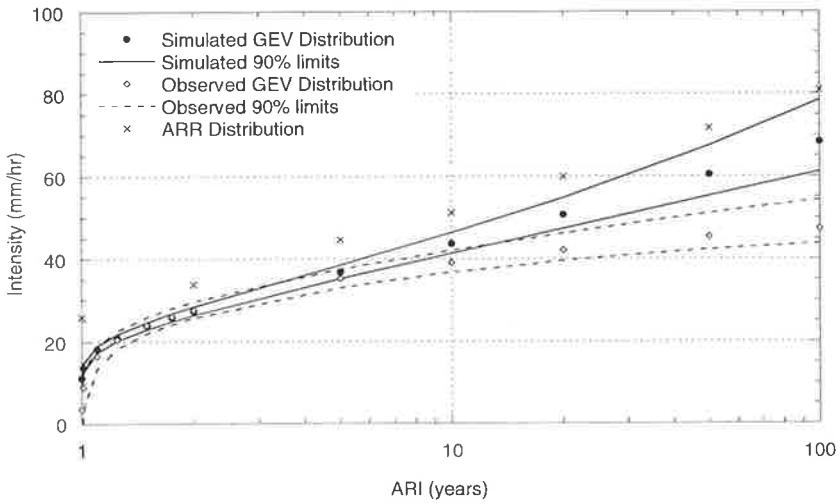

Figure 5.19 Simulated and observed 3 hour IFD curves for Cairns.

5.2.3 Long-Duration IFD Analysis

In contrast to the short duration IFD, successful simulation of the long duration IFD curves such as 12, 24 and 72 hours depends to a large extent on how well the intensity-duration relationship has been modelled. Lambert and Kuczera (1996) found that adequate modelling of the rainfall intensity for long duration events was important for simulating long duration IFD curves.

The frequency analysis of the 12 hour observed IFD data for Melbourne, with the fitted generalised exponential distribution GEV distribution and its approximate 90% probability limits is shown in Figure 5.20(a). Figure 5.20(b) shows this for the simulated 12 hour IFD data. In both cases the GEV distribution represents the data well. A comparison of the observed and simulated fitted IFD distributions for 12 hours is shown in Figure 5.20(c) along with the ARR (1987) IFD data for this site and duration. For this duration, the observed and ARR (1987) data overlap and the simulated distribution and probability limits show good agreement with the observed. Similar results were obtained for a duration of 24 hours (Figure 5.21) and 72 hours (Figure 5.22). While the simulated GEV distribution and confidence limits are in the lower part of the observed limits, they still indicate good agreement.

The fitted GEV distributions for the observed and simulated data and the comparison of these curves for 12, 24 and 72 hours at all locations is contained in Appendix J.1. The 12 hour observed IFD distributions were well produced for all sites including Alice Springs (Figure 5.23), Cairns (Figure 5.24) and Sydney (Figure 5.25).

The 24 hour duration IFD curves for Alice Springs (Figure 5.26), Cairns (Figure 5.27) and Sydney (Figure 5.28) were also satisfactorily produced, although the simulated curves are in the lower section of the observed 90 % confidence limits reflecting a general trend for the GEV distribution to slightly overestimate the actual simulated data at high ARIs. It is also noted that the ARR 24 hour IFD values for Cairns are much higher than the observed IFD distributions.

The 24 hour duration IFD curves were well produced for Adelaide, Brisbane, Hobart, Perth and Townsville but were slightly underestimated for Darwin (Figure 5.29) although the simulated confidence limits do contain the ARR (1987) IFD values.

The 72 hour duration IFD curves for Alice Springs (Figure 5.30), Cairns (Figure 5.31) and Sydney (Figure 5.32) were underestimated, although the simulated IFD curve confidence limits for Sydney do overlap the observed limits. The observed curves were well reproduced for Adelaide, Hobart and Perth, with Brisbane slightly underestimated.

As for the 24 hour duration IFD for Cairns, the ARR (1987) 72 hour IFD values are much higher than the observed IFD distribution. Townsville is similar although in this case the simulated IFD curves reflect those from the observed pluviograph data (Figure 5.33).

Differences between the ARR (1987) and observed IFD distributions have been noted for a number of sites for a variety of burst durations. ARR (1987) describes the method used to determine the rainfall intensity for six specific combinations of duration and ARI, namely durations of 1, 12 and 72 hours and ARIs of 2 and 50 years. The intensities were derived in the late 1970s to early 1980s, at which time there was a good coverage of daily rainfall gauges but very few long-term six-minute pluviograph records. The statistical analysis that was undertaken assumed that the period of observed record available at each station was representative of long term conditions at that station. A requirement was that each of the pluviograph records used needed to have a minimum of six years of data. It is quite possible that under- or over-estimation of the higher ARI intensities in particular may have occurred because this length of record was not sufficient to record the long term conditions. In addition, daily rainfall stations only required 30 years of data to be included in the analysis, which in some areas may not be long enough to establish accurate estimates of higher ARI intensities for long duration bursts. Walsh (1991) showed that the ARR (1987) IFD intensities may underestimate the observed intensities at a range of sites in New South Wales by as much as 10 to 20% for an ARI of 50 years and 30 to 40% for an ARI of 100 years.

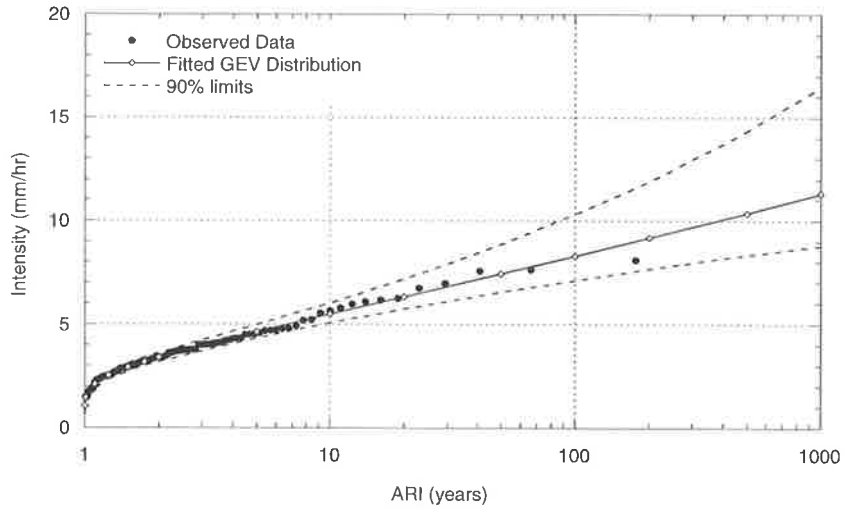

(a)

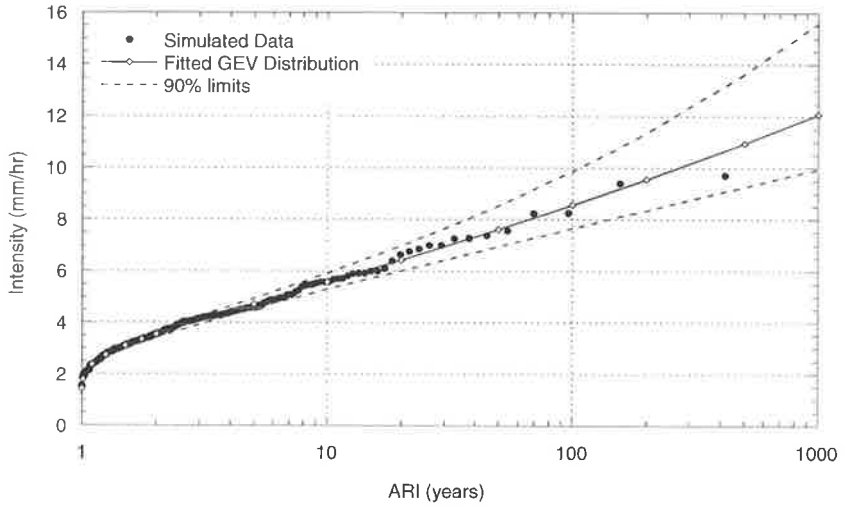

(b)

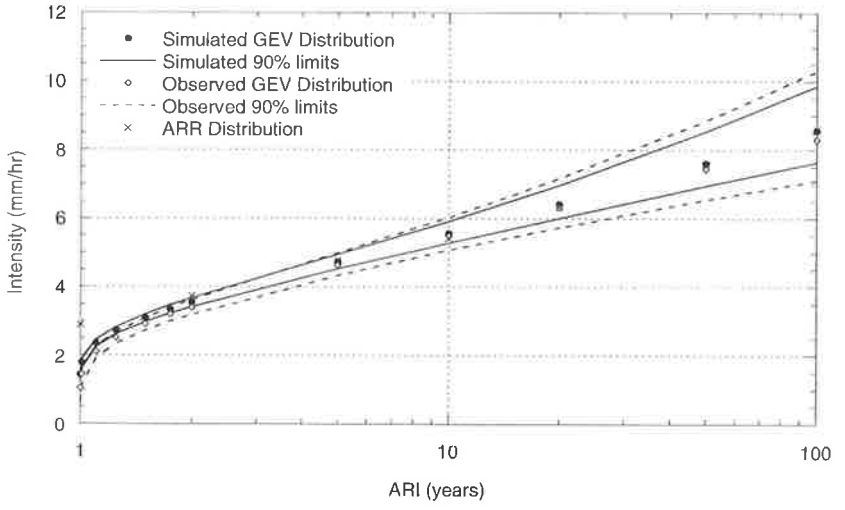

(c)

Figure 5.20 12 hour Melbourne IFD analysis:
(a) Fitted GEV distribution to observed IFD data;
(b) Fitted GEV distribution to simulated IFD data; and
(c) Simulated and observed IFD curves.

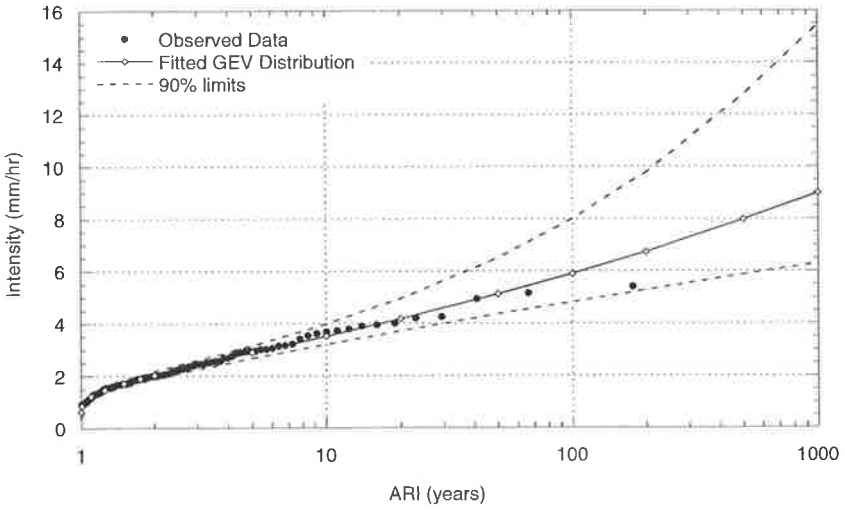

(a)

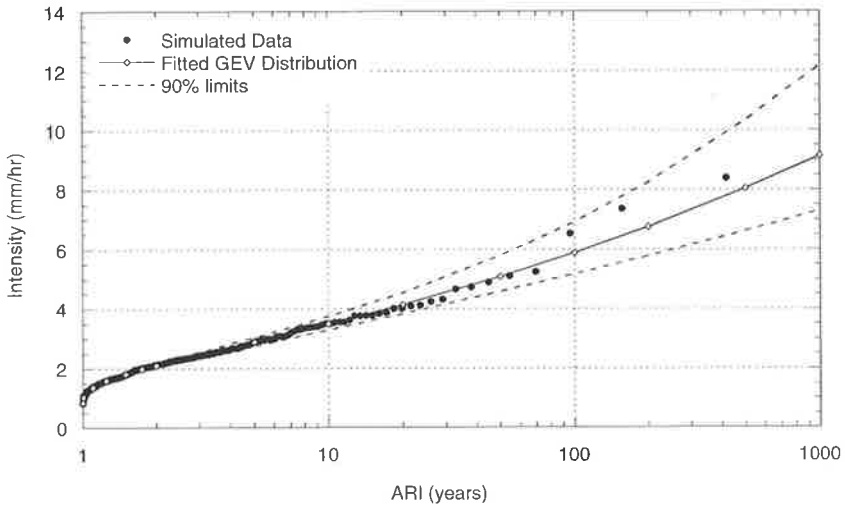

(b)

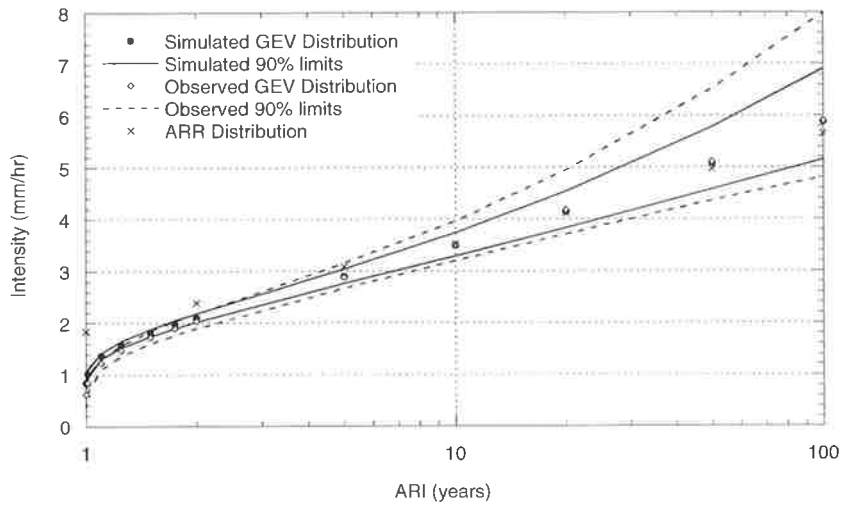

(c)

Figure 5.21 24 hour Melbourne IFD analysis:
(a) Fitted GEV distribution to observed IFD data;
(b) Fitted GEV distribution to simulated IFD data; and
(c) Simulated and observed IFD curves.

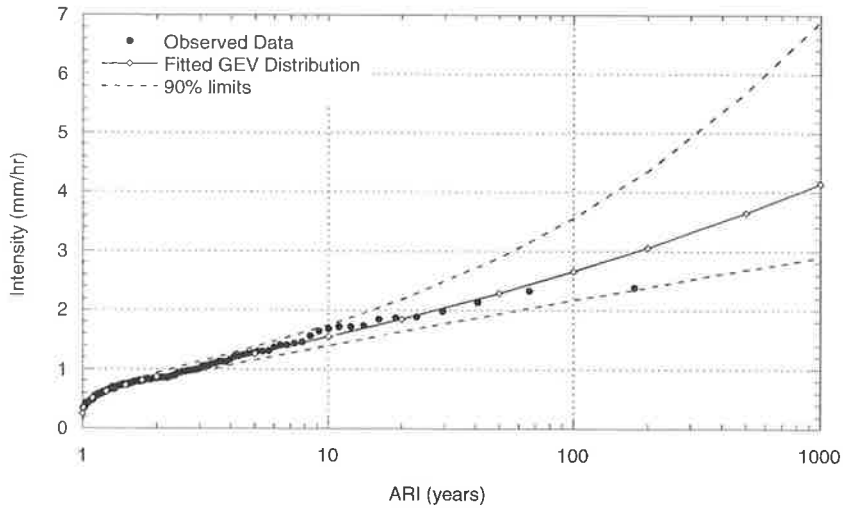

(a)

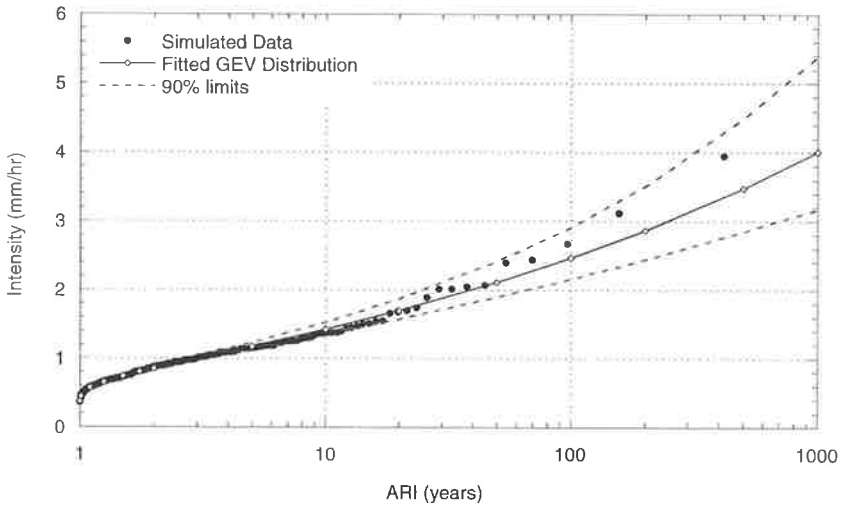

(b)

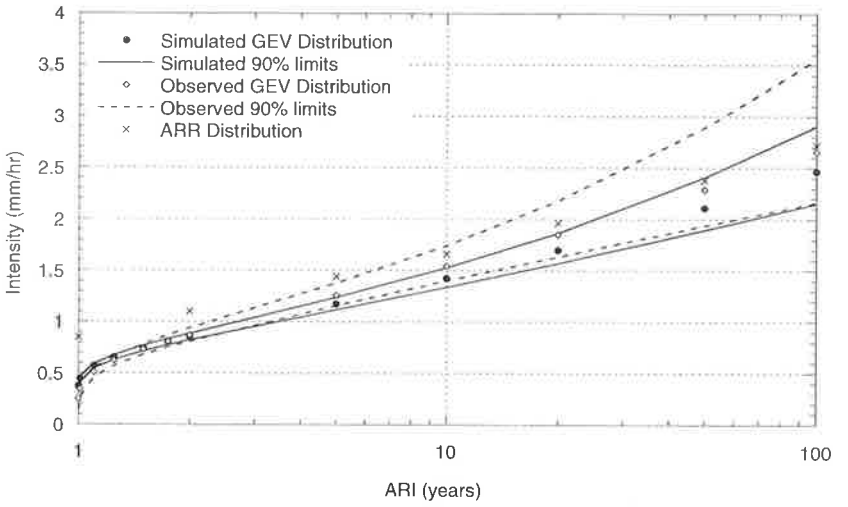

(c)

Figure 5.22 72 hour Melbourne IFD analysis:
(a) Fitted GEV distribution to observed IFD data;
(b) Fitted GEV distribution to simulated IFD data; and
(c) Simulated and observed IFD curves.

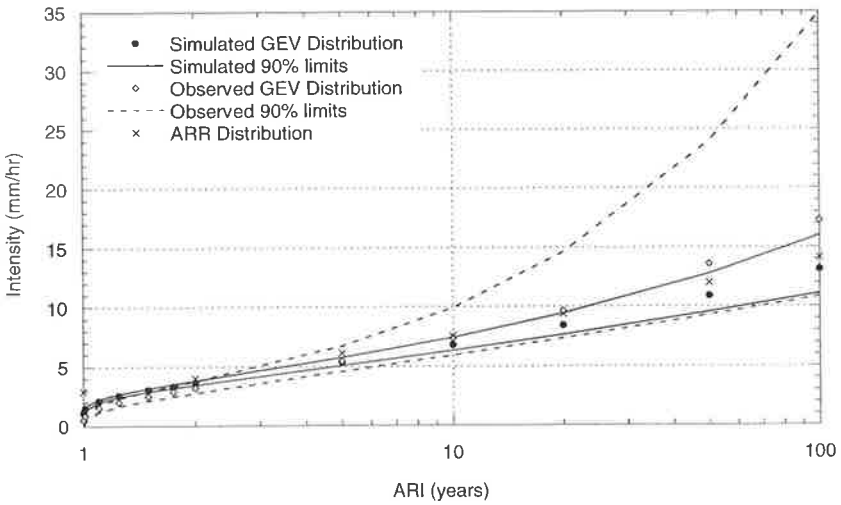

Figure 5.23 Simulated and observed 12 hour IFD curves for Alice Springs.

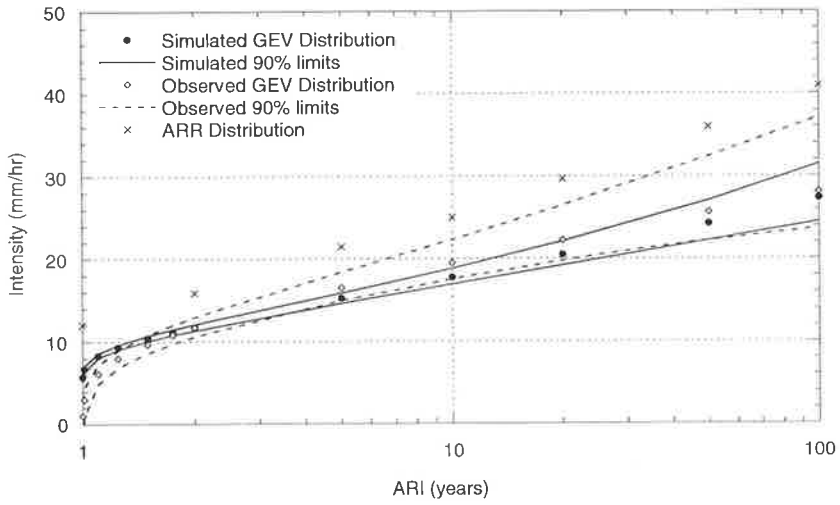

Figure 5.24 Simulated and observed 12 hour IFD curves for Cairns.

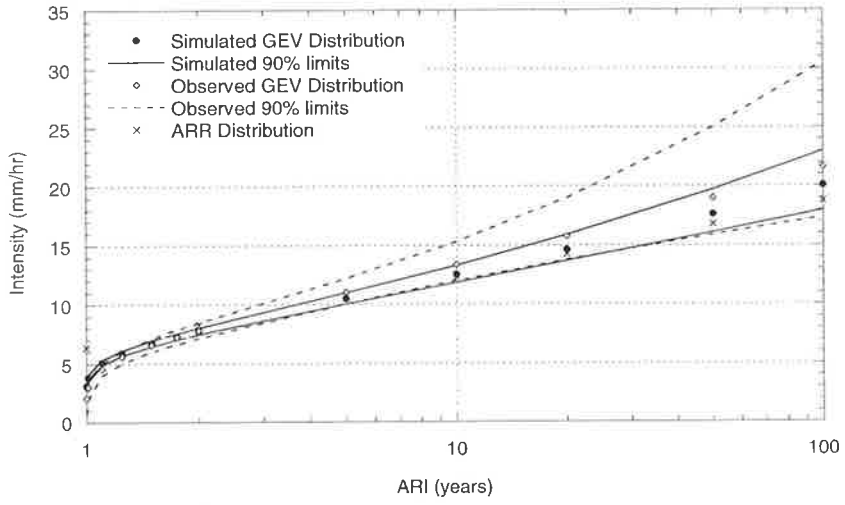

Figure 5.25 Simulated and observed 12 hour IFD curves for Sydney.

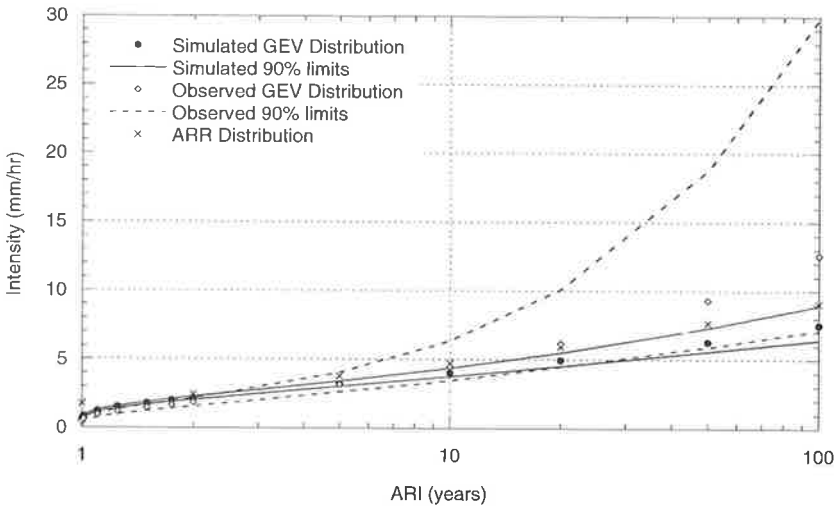

Figure 5.26 Simulated and observed 24 hour IFD curves for Alice Springs.

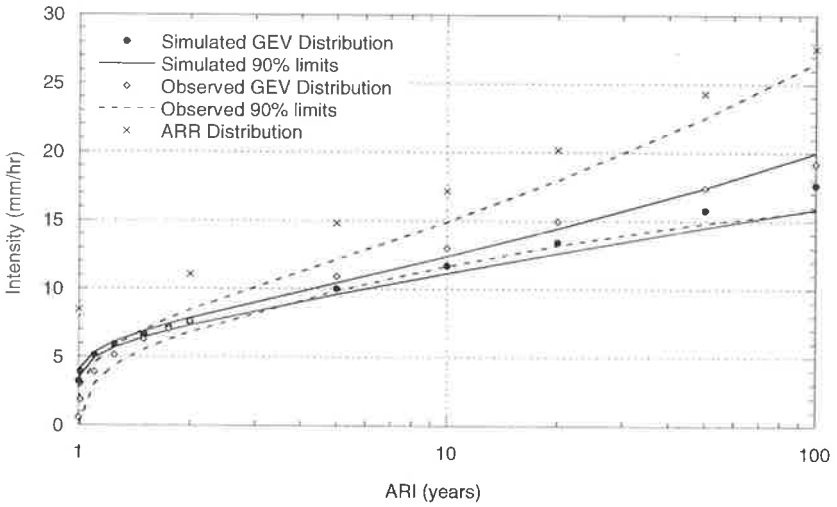

Figure 5.27 Simulated and observed 24 hour IFD curves for Cairns.

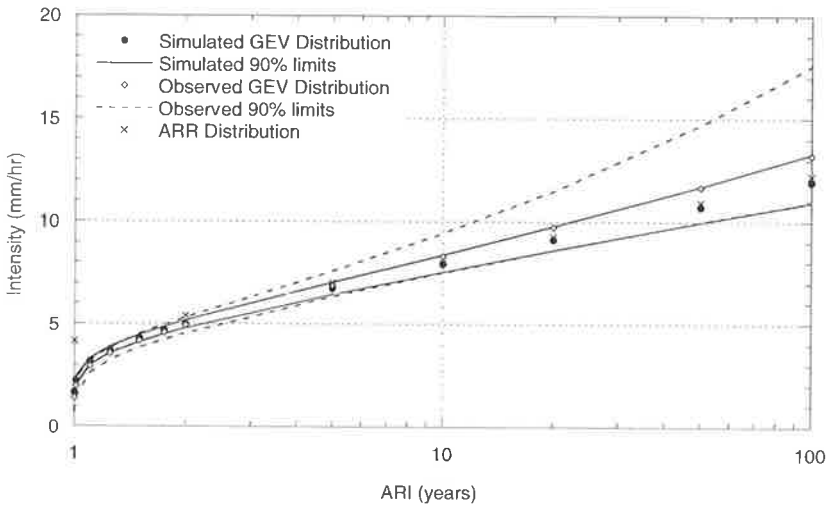

Figure 5.28 Simulated and observed 24 hour IFD curves for Sydney.

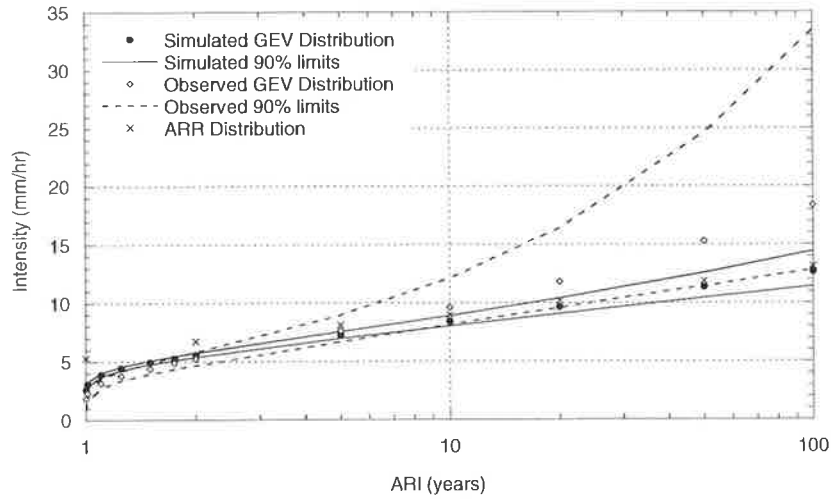

Figure 5.29 Simulated and observed 24 hour IFD curves for Darwin.

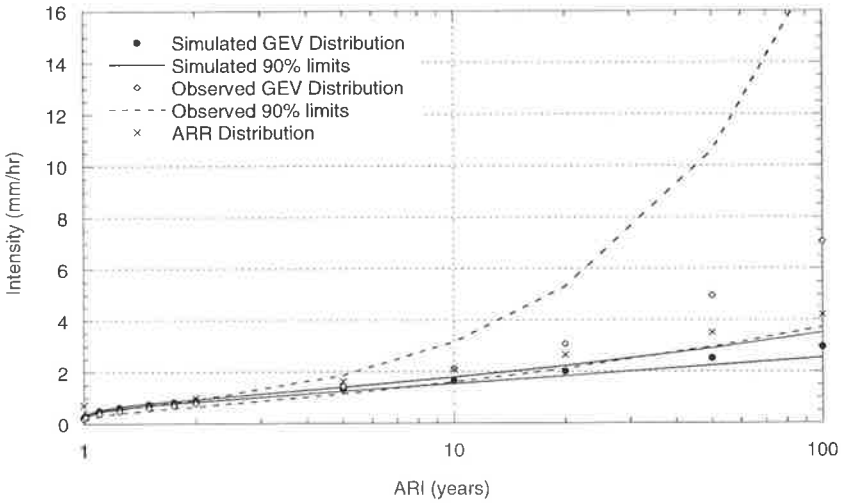

Figure 5.30 Simulated and observed 72 hour IFD curves for Alice Springs.

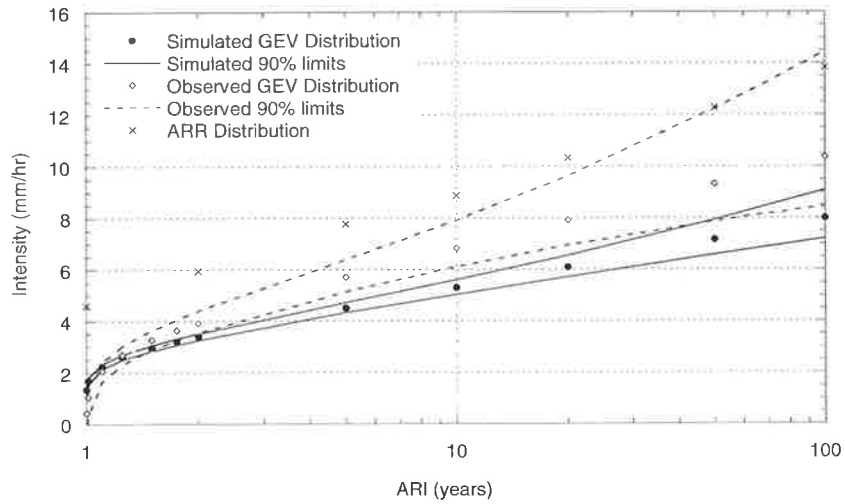

Figure 5.31 Simulated and observed 72 hour IFD curves for Cairns.

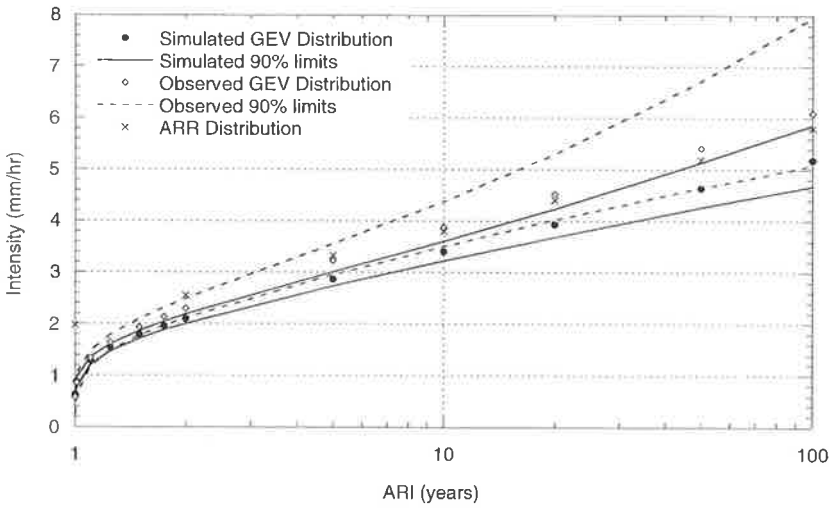

Figure 5.32 Simulated and observed 72 hour IFD curves for Sydney.

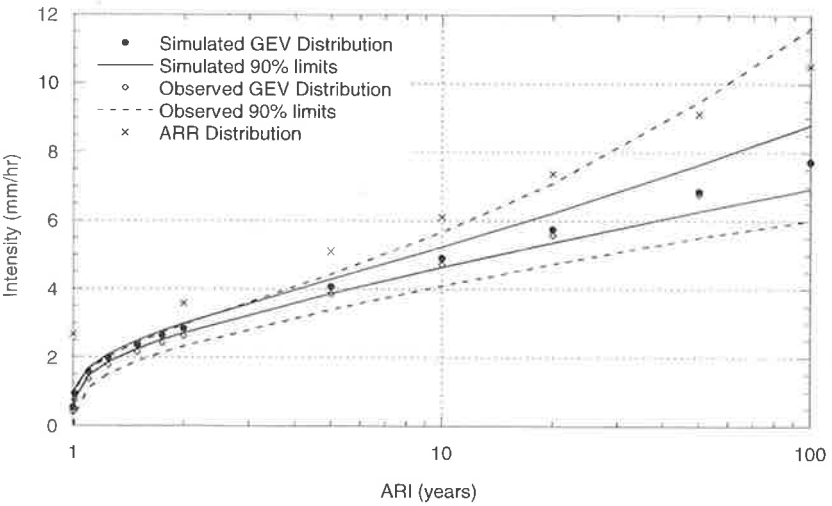

Figure 5.33 Simulated and observed 72 hour IFD curves for Townsville.

5.3 AGGREGATED STATISTICS

Another important function of the rainfall model is to simulate aggregated rainfall statistics. The mean, standard deviation, dry probability and lag one auto-correlation at several aggregation levels (1, 6, 12 and 24 hours and monthly) were examined. For durations less than a day the pluviograph record has been used to obtain the observed statistics, with missing values ignored. The absence of small amounts of data from a month does not warrant the exclusion of the whole month of data when calculating the aggregation statistics at levels less than 24 hours, as has been done by some researchers (Section 2.6.2). Daily rainfall data recorded at each site has been used to calculate statistics for durations of 24 hours or greater. These records are generally free of missing data and hence provide an unbiased estimate of these statistics.

Table 5.1 contains the observed and simulated annual mean and standard deviation for each site. In general the means are well reproduced, with the differences between the simulated and observed values less than the observed standard deviation. The underestimation of the observed standard deviation at some locations is discussed further in Section 5.4.

Table 5.1 Comparison of observed and simulated annual mean and standard deviation statistics.

Location	Mean (mm)		Standard Deviation (mm)	
	Observed	Simulated	Observed	Simulated
Adelaide	450	469 (4)[1]	106	89
Alice Springs	276	306 (11)	140	105
Brisbane	1146	1133 (1)	355	252
Cairns	1993	2018 (1)	524	393
Darwin	1702	1730 (2)	380	303
Hobart	621	680 (10)	140	132
Melbourne	657	673 (2)	129	118
Perth	870	833 (4)	160	151
Sydney	1224	1237 (1)	332	278
Townsville	1133	1161 (2)	441	315

[1] The value in brackets is the difference between the observed and simulated annual means as a percentage of the observed value.

Appendix J.2 contains the observed and simulated aggregated statistics at 1, 6, 12 and 24 hours and monthly time scales for each month of the year. A comparison between the mean and standard deviation of the observed and simulated depths at various aggregation levels for Melbourne is shown in Figure 5.34 to Figure 5.37. It can be seen for this site that the

simulation adequately reproduced the observed mean and standard deviation of depths at a number of aggregation levels.

The observed mean rainfall is reasonably well reproduced by the simulation for all sites for all durations. The standard deviation of the observed depth at 1, 6 and 12 hours is satisfactorily reproduced at all sites. For 24 hour durations, sites in tropical areas (Brisbane, Cairns, Darwin and Townsville) tend to have a significantly underestimated standard deviation for wet season months. This is also the case for Alice Springs for the higher rainfall summer months and Sydney for approximately half of the year. For Adelaide, Hobart and Perth, the standard deviations are considered satisfactory.

Figure 5.38 to Figure 5.40 show the dry probability and lag one auto-correlation statistics at a 6, 12 and 24 hour aggregation level for each month of the year for Melbourne. It can bee seen that these statistics are well reproduced, as is the case for all other sites and durations. The dry season in tropical locations was clearly evident although at the 24 hour and monthly time scale it was slightly underestimated for Cairns and Darwin. The dry summers in Perth and Adelaide were also adequately reproduced. The lag one auto-correlation values at 1, 6 and 12 hour durations were satisfactorily reproduced for all sites. However, in some instances the variation in the 24 hour and monthly values suggest the need to consider further improvements for the model.

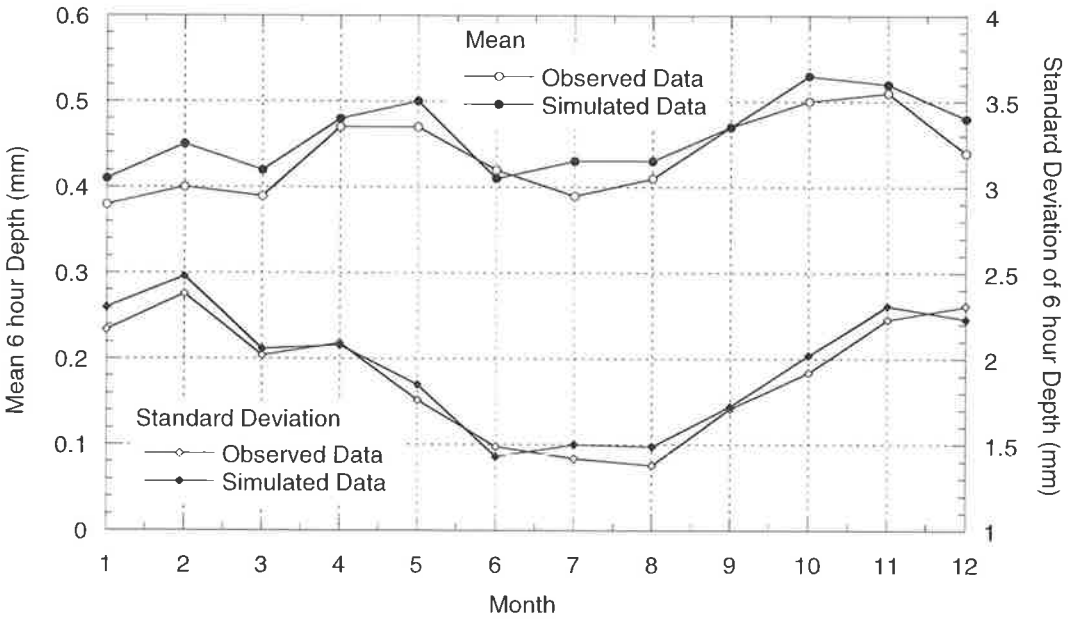

Figure 5.34 Mean and standard deviation of 6 hour depth for Melbourne.

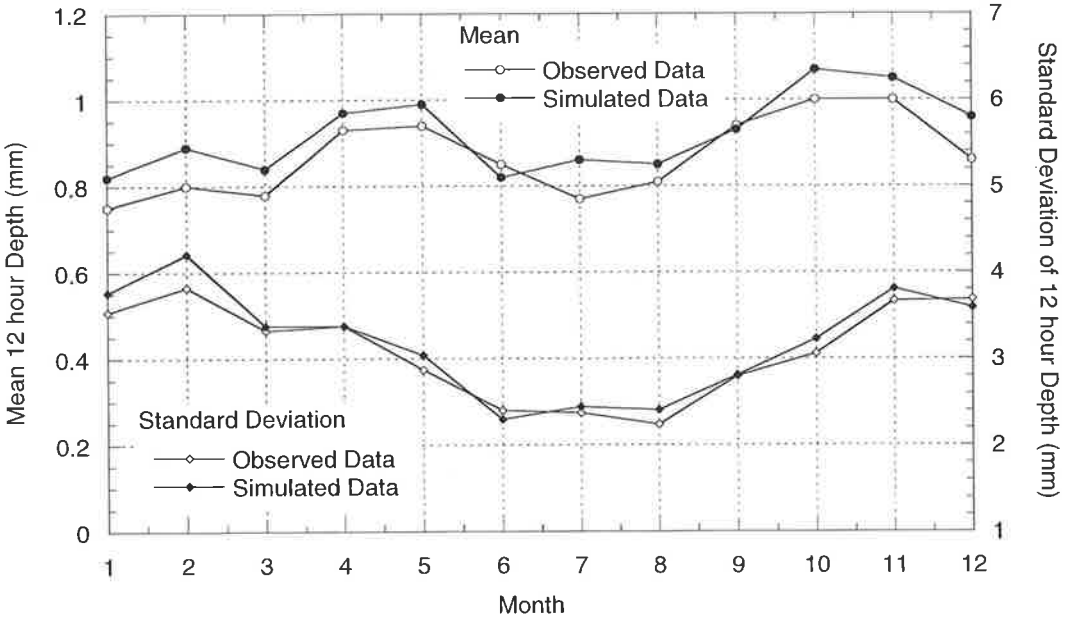

Figure 5.35 Mean and standard deviation of 12 hour depth for Melbourne.

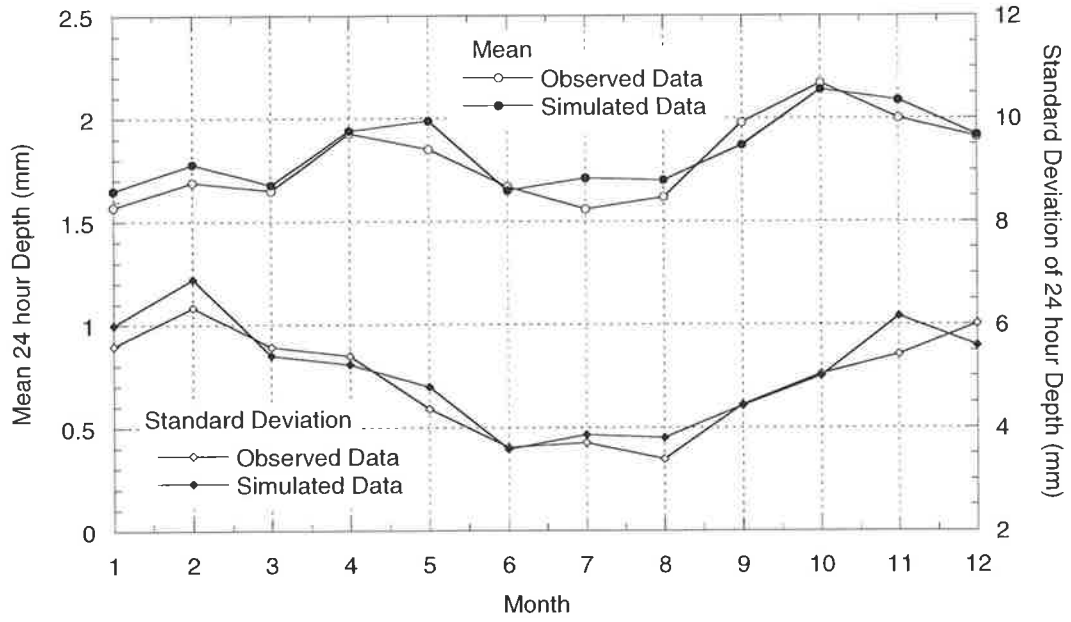

Figure 5.36 Mean and standard deviation of 24 hour depth for Melbourne.

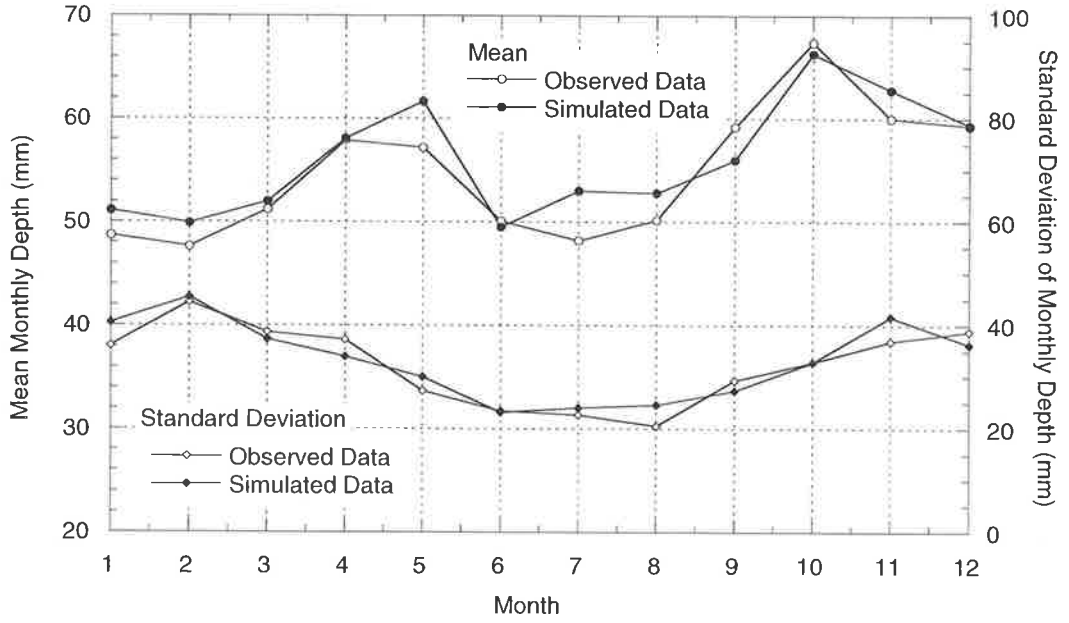

Figure 5.37 Mean and standard deviation of monthly depth for Melbourne.

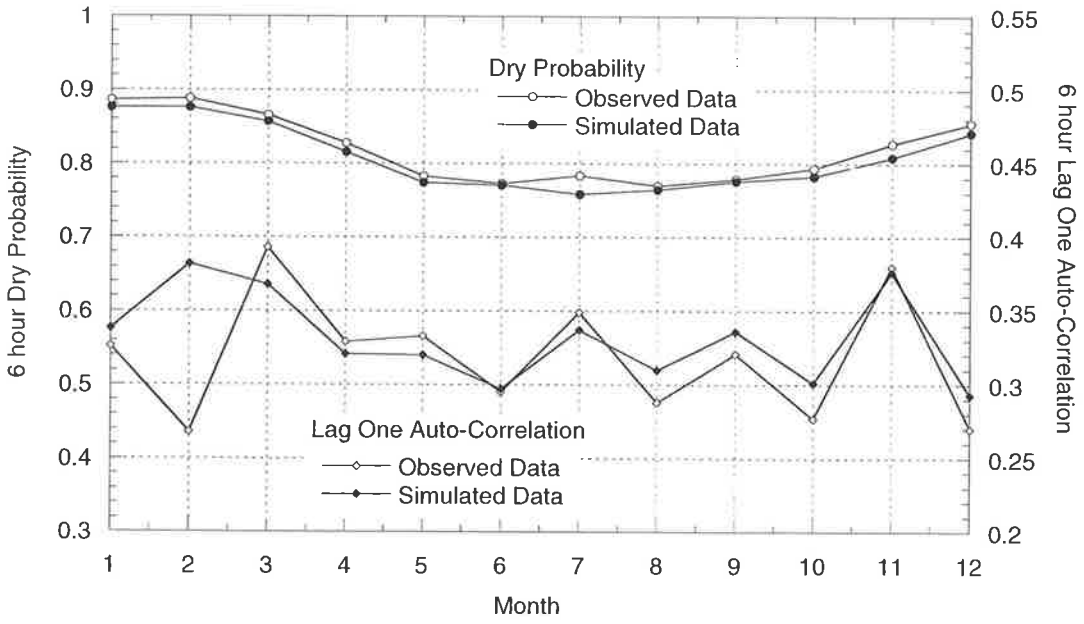

Figure 5.38 6 hour dry probability and lag one auto-correlation for Melbourne.

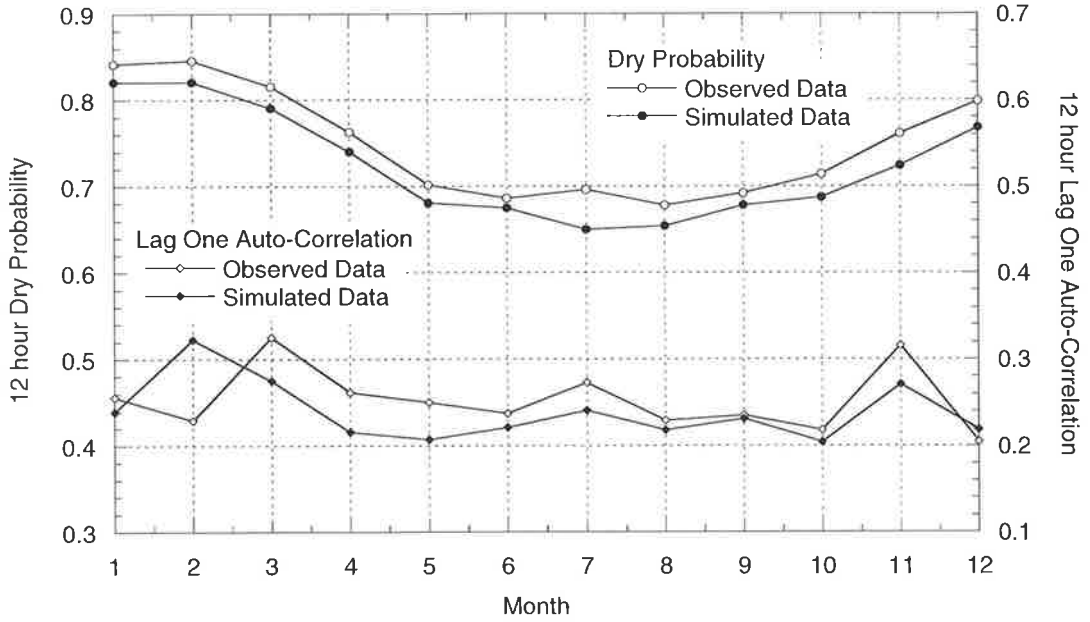

Figure 5.39 12 hour dry probability and lag one auto-correlation for Melbourne.

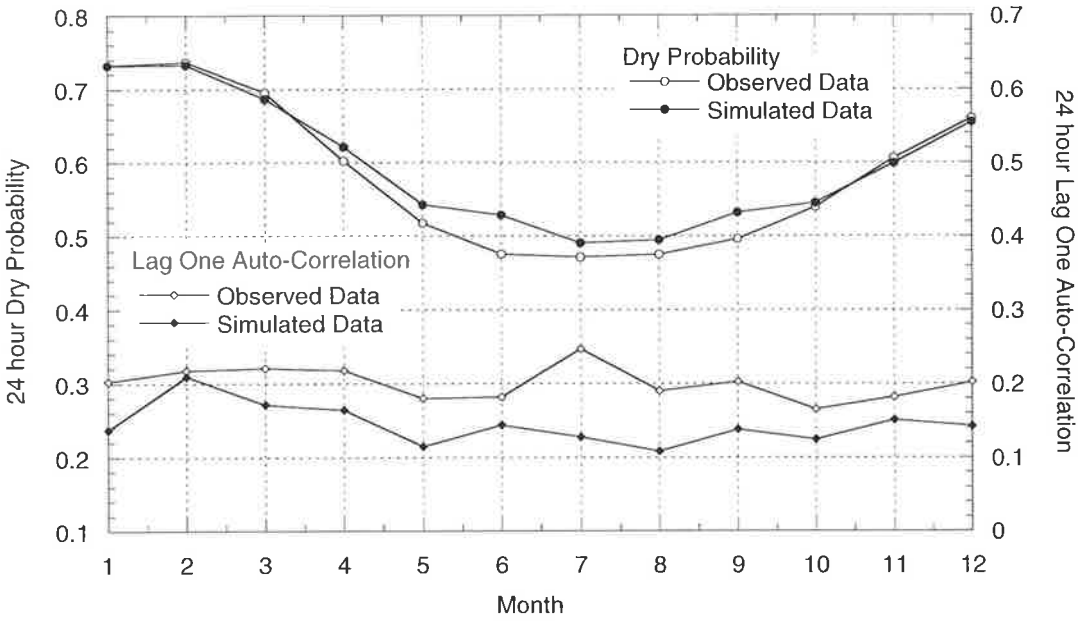

Figure 5.40 24 hour dry probability and lag one auto-correlation for Melbourne.

5.4 Probability Distribution of Annual Totals

As discussed in the previous section, the mean annual rainfall was satisfactorily reproduced for most sites but the standard deviation was underestimated for tropical and arid areas. The probability distribution of annual rainfall is shown for Alice Springs (Figure 5.41), Brisbane (Figure 5.42), Melbourne (Figure 5.43) and Perth (Figure 5.44). While the median rainfall is well approximated, the reduced slope of the simulated distribution for Alice Springs and Brisbane is a reflection of the model underestimating the annual standard deviation and hence the rainfall variability for these sites. The annual variability is well reproduced for Melbourne and Perth where the standard deviation was adequately reproduced by the model. Comparisons between the observed and simulated annual rainfall probability distributions for all sites are contained in Appendix J.3, with the results showing similar trends for the other tropical/arid climates.

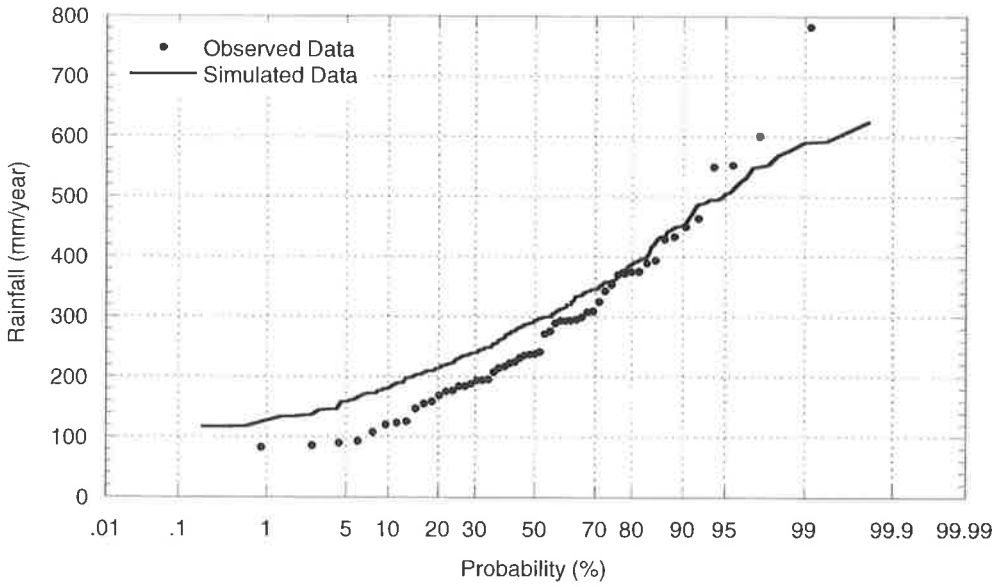

Figure 5.41 Probability distribution of annual rainfall for Alice Springs.

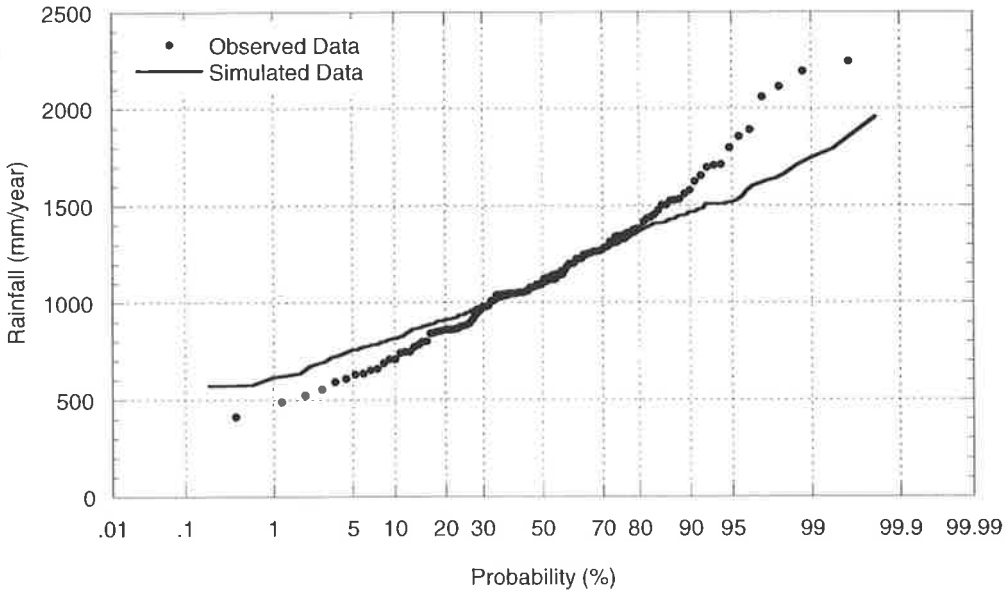

Figure 5.42 Probability distribution of annual rainfall for Brisbane.

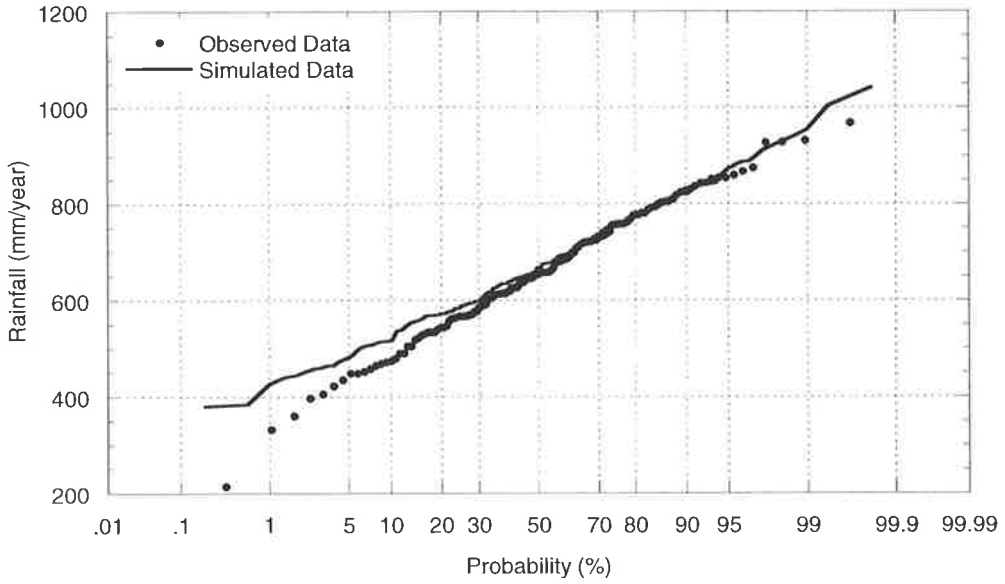

Figure 5.43 Probability distribution of annual rainfall for Melbourne.

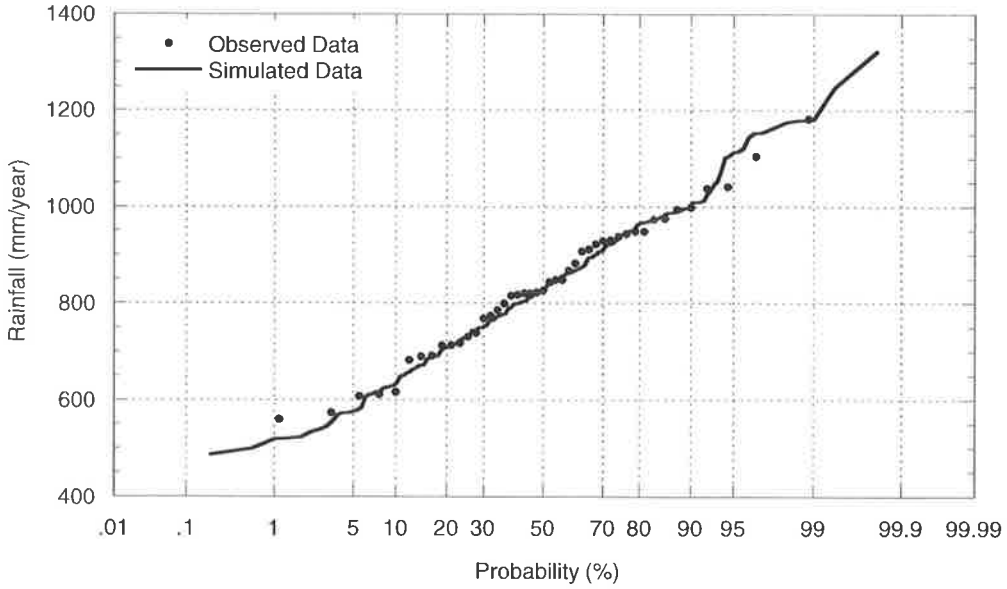

Figure 5.44 Probability distribution of annual rainfall for Perth.

This underestimation of the standard deviation of annual rainfall affects most models that aggregate statistics. The model only allows for seasonal variation in the probability distributions affecting rainfall depth and its timing. It does not allow for inter-annual persistence which may result in fewer and less intense events in drought years and a higher number of more intense events in other years. For example, periods of lower and higher annual rainfall can be seen for Brisbane in Figure 5.45 and Alice Springs in Figure 5.46.

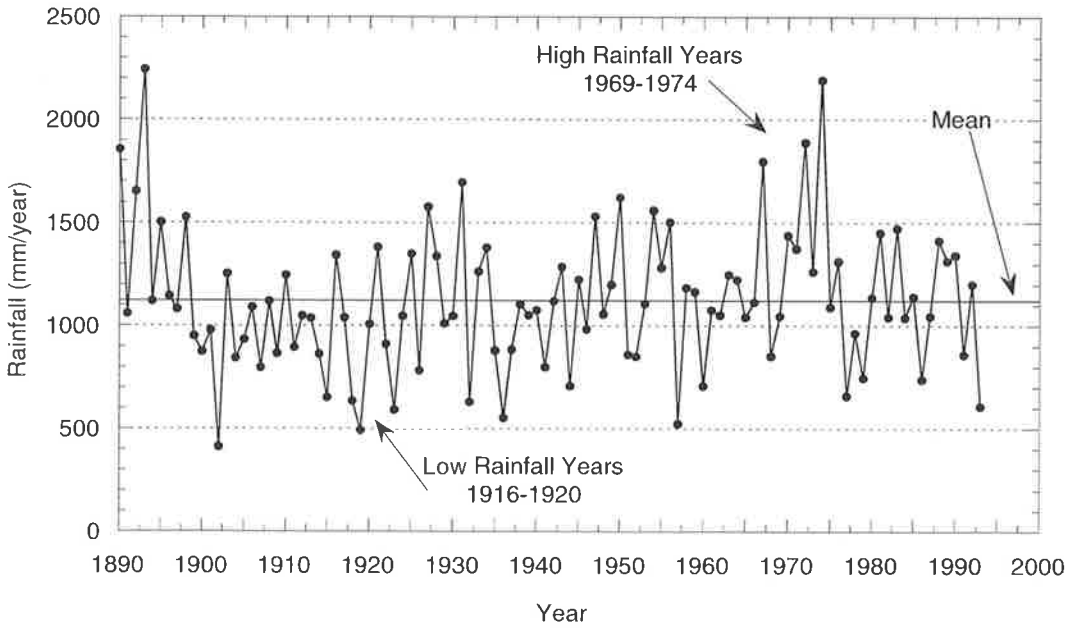

Figure 5.45 Observed annual rainfall totals for Brisbane.

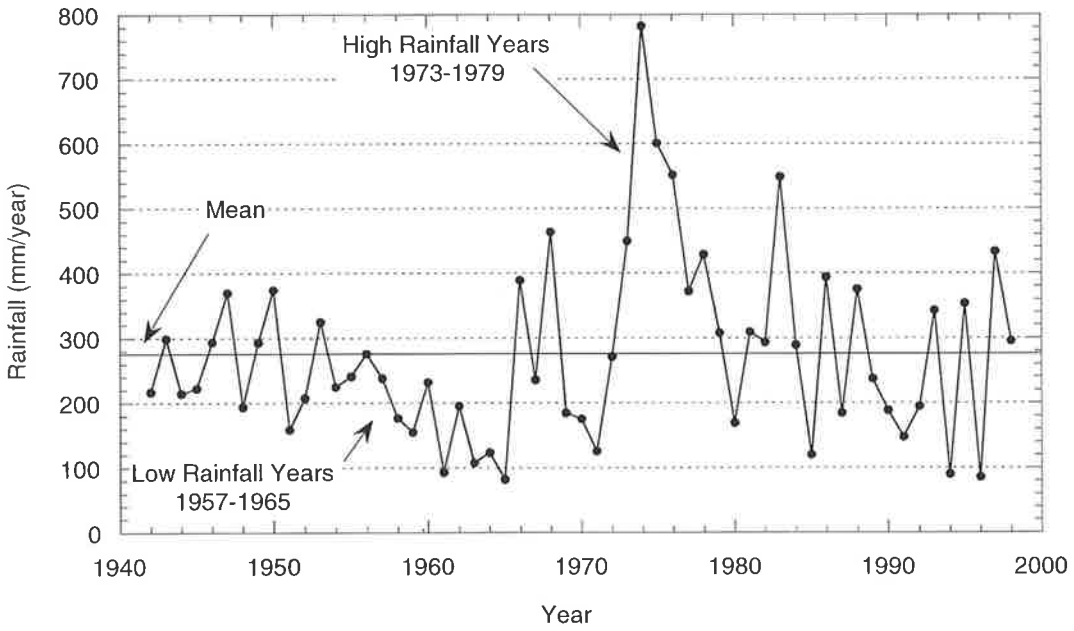

Figure 5.46 Observed annual rainfall totals for Alice Springs.

The work of Thyer and Kuczera (2000) provides some insight into these findings for the tropical regions. A hidden state Markov model of annual rainfall was developed and strong evidence was presented that inter-annual persistence exists in Sydney and Brisbane rainfall. The tropical oceans affect the rainfall regimes for both Brisbane and Sydney, along with other tropical locations. It was speculated that inter-annual modulations in the tropical oceans such as ENSO and the Inter-Pacific Oscillation may be responsible for the persistence. In contrast, no credible evidence was found that the annual rainfall in Melbourne exhibits inter-annual persistence, possibly because the rainfall regime is dominated by weather systems originating in the Southern Ocean rather than the tropical oceans.

The results shown here indicate that persistence in inter-annual rainfall may also be important at other locations, in particular arid regions. The variability of the rainfall regime at these locations is well documented (Bureau of Meteorology, 1983). The mechanisms behind persistence are worth pursuing to provide an improved representation of rainfall for these arid locations. Recently, Frost *et al.* (2000) has demonstrated that conditioning rainfall model parameters on whether the current year is *wet* or *dry* may largely rectify this problem.

5.5 CONCLUDING REMARKS

The generation of synthetic rainfall using the stochastic model developed in this study was overall successful. While the validation shows that some specific aspects of the simulated data require improvement for individual locations, the data produced at any one site is not unsatisfactory.

The IFD validation was important in guiding model development. The inclusion of seasonal dependence in the intensity-duration relationship proved to be very important in the reproduction of IFD statistics, particularly for tropical sites where there are very high intensity storms during the wet summer season. Without the addition of seasonal dependence, reliable simulation of extreme rainfall would not be possible for tropical and sub-tropical zones, especially those that experience heavy monsoonal summer rainfall and little rainfall in the remainder of the year. About one quarter of Australia lies within this tropical and sub-tropical zone and as such being able to reproduce the IFD for such areas is important.

The successful reproduction of the short duration IFD at most sites suggests that the disaggregation procedure is effective and that the current deficiencies identified in Chapter 4 do not have a significant impact on the overall model results. At some sites where the IFD curves were overestimated, the use of an auto-correlation function similar to that used by Acreman (1990) during disaggregation may improve the results.

For the successful reproduction of the longer duration IFD, the model of average event intensity is considered satisfactory even though at some sites these IFD curves, particularly for 72 hours, were underestimated. Improvements to the distribution of the average event intensity model are warranted to address this. Calibration can be difficult because of the need to define breakpoints (Section 3.5.4) along with an often low sample size of event data for each month, making the choice of a reasonable distribution difficult. An investigation into a more general function, such as a higher order polynomial, is justified. By improving the distribution of average event intensity, an improved reproduction of the long duration IFD at some sites should be possible.

The aggregated statistics were generally well produced. The seasonal variation in the mean, standard deviation and dry probability in the simulation corresponded well to the observed.

This indicates in part the success of the distributions of inter-event times over the year in producing more events and hence shorter dry times at appropriate times of the year. The use of an auto-correlation function similar to that used by Acreman (1990) during the disaggregation procedure may improve the reproduction of the lag-one auto-correlation statistics. The underestimation of the standard deviation of annual rainfall and hence the ability to closely reproduce the rainfall variability (that is, the slope of the annual probability distribution), suggests the need to incorporate inter-annual variability into the model. It was observed that this was not only required for tropical climates as has been suggested by Thyer and Kuczera (2000), but also for arid climates.

The reproduction of the inter-event time and event duration distributions using the monthly models was successful for all sites. In general, the harmonic models produced less satisfactory results, except for locations where it is likely that data within each month is non-stationary, such as would occur where there are sharp changes in the rainfall occurrence due to the change of seasons in tropical locations (wet to dry or dry to wet). For most months and sites, the shape of the marginal average event intensity distribution using either the monthly or harmonic model for event duration was similar, although for both models, the tail of the distribution was not always adequately reproduced. Improvements to the distribution of average event intensity may address this.

In conclusion, the stochastic model of rainfall developed in this study was considered to be a very suitable tool for use as input into a water balance model and the subsequent determination of rainfall excess.

6. GENERATION OF STOCHASTIC EVAPORATION DATA

The stochastic generation of rainfall represents the first step of the proposed engineering design flood estimation methodology. Evaporation is the second major factor, following rainfall, that can affect the water balance and therefore reliable estimates are needed to accurately simulate the rainfall-runoff process. Soil moisture loss as a result of evaporation affects the initial rainfall loss from an event and can have a major influence on both the peak and volume of the resulting flood hydrograph.

Evaporation data is needed to calibrate the catchment water balance model. Pan evaporation data is ideally used but where it is not available the potential evaporation must be generated. This section considers both the generation of potential evaporation for use in calibrating the catchment water balance model, and the development of a stochastic model that can be used to generate evaporation concurrently with rainfall for use in continuous simulation of the water balance of a catchment.

6.1 EVAPORATION PROCESS

Evaporation is the transfer of moisture into the atmosphere, whether from a free water surface, a soil surface or by the process of transpiration from plants. Liquid water is converted to water vapour and removed from the evaporating surface. The rate at which water vapour enters the atmosphere from an evaporating surface depends on meteorological conditions and the type of surface, that is, under the same conditions different surfaces may have large variations in the rates of evaporation. The transfer of water from the soil surface and plants is the most important factor in the development of a catchment water balance model.

Evaporation is an important component of the hydrologic cycle and accurate estimates are essential for hydrologic water-balance calculations used for irrigation and water resources planning and management. Although the term evapotranspiration (ET) is often used interchangeably with evaporation, this term is intended to emphasise the transfer of water from land surfaces with plants. As such it can be considered a combination of two separate processes: evaporation, where water is lost from the soil surface; and transpiration, where

water is lost from vegetation (Chow *et al.*, 1988). These processes occur simultaneously and there is no way of easily distinguishing between them or calculating the relative proportions (Allen *et al.*, 1998). Aside from the water availability in the top layers of the soil, the evaporation from a vegetation covered soil is mainly determined by the fraction of solar radiation reaching the soil surface. This fraction decreases as the level of vegetation cover increases. When vegetation cover is low, water is predominantly lost by soil evaporation, but for densely vegetated areas transpiration becomes the main process (Allen *et al.*, 1998).

The water balance models examined and the model developed in this study are typically used in catchments consisting mainly of vegetated surfaces, as opposed to open water bodies. As such, evaporation in this study refers to the combination of both processes, evaporation from a soil surface and transpiration from plants.

6.1.1 Evaporation from a Soil Surface

The loss of water from the soil surface depends on the nature of the surface, the soil type, prevailing weather conditions, the amount of moisture already in the soil and the height of the water table (Hounam, 1961). Under the same weather conditions, evaporation from a saturated soil is approximately equal to that from a free water surface. Direct solar radiation and to a lesser extent, the ambient temperature of the air, provide the energy to change the water from liquid to vapour (Allen *et al.*, 1998). The driving force to remove water vapour from the evaporating surface is the difference between the water vapour pressure at the evaporating surface and the surrounding atmosphere. As evaporation proceeds, the surrounding air gradually becomes saturated and the process will slow down and potentially stop if the moist air is not transferred to the atmosphere; this is significantly dependent on wind speed (Allen *et al.*, 1998). Therefore, solar radiation, air temperature, air humidity and wind speed are climatological parameters to consider when assessing the evaporation process.

When the evaporating surface is the soil surface, the degree of shading by the vegetation canopy and the amount of water available at the evaporating surface are other factors that affect the evaporation process. Frequent rain and upward transportation of water from a shallow water table wet the soil surface. When the soil is able to supply water fast enough to satisfy the evaporation demand, the evaporation from the soil is determined only by the meteorological conditions, but where the interval between rains becomes large and the ability of the soil to conduct moisture to the surface is small, the surface layer gradually dries out.

Under these circumstances the limited availability of water is the controlling influence on soil evaporation. In the absence of any supply of water to the soil surface, evaporation decreases rapidly and may cease completely within a few days (Chow *et al.*, 1988; Allen *et al.*, 1998).

6.1.2 Transpiration

Transpiration consists of the vaporisation of liquid water contained in plant tissue and the removal of this liquid to the atmosphere. The moisture is lost through the stomata in leaves of plants (Chow *et al.*, 1988; Allen *et al.*, 1998). Transpiration, like direct evaporation, depends on the energy supply, the vapour pressure gradient and wind speed. As such it is a function of radiation, air temperature, air humidity and wind. In addition, the soil water content and the ability of the soil to conduct water to the roots also affects the transpiration rate. The rate is also influenced by the type of vegetation as different vegetation types have different transpiration rates. The variation of the transpiration rate when a soil is drying out has been widely investigated. Veihmeyer and Hendrickson (1955) suggest that transpiration continues at or near the potential level whilst the soil is drying out almost until the wilting point is reached. An opposing view is that the transpiration rate begins to decrease below the potential rate as soon as the moisture content of the soil begins to decrease.

6.2 Factors Affecting Evaporation

Potential evaporation (E_p) is the maximum amount of water that can evaporate or transpire from a surface where water availability is not limiting. Actual evaporation is the amount of water that crosses an interface into the air. This is generally constrained by the atmospheric conditions during wet periods and by the soil moisture/plant physiology during dry periods. Weather parameters, vegetation characteristics, land management and environmental aspects are also factors that affect evaporation and transpiration. The meteorological factors that provide energy for vaporisation and removal of water vapour from the evaporating surface are described in the following.

6.2.1 Solar Radiation

The level of potential evaporation is determined by the amount of energy available to vaporise water. Solar radiation is the largest energy source and is able to convert large quantities of liquid water into water vapour. The potential amount of radiation that can reach the

evaporating surface is determined by the location and the time of year as the potential radiation differs at various latitudes and in different seasons due to the different position of the sun. The actual solar radiation reaching the evaporating surface depends on the turbidity of the atmosphere and the presence of clouds, which reflect and absorb major parts of the radiation (Shuttleworth, 1993; Allen *et al.*, 1998). When assessing the effect of solar radiation on E_p, it must be remembered that solar energy is also used to heat the atmosphere and the soil and not all is available to vaporise water.

6.2.2 Air Temperature

The air temperature is dependent on the solar radiation absorbed by the atmosphere and the heat emitted by the earth. The heat of the surrounding air exerts a controlling influence on the rate of E_p from the vegetative surface (Allen *et al.*, 1998). As such, the loss of water by E_p is greater in warm weather than in cool weather.

6.2.3 Air Humidity

While the energy supply from the sun and surrounding air is the main driving force for the vaporisation of water, the difference between the water vapour pressure at the evaporating surface and the surrounding air is the determining factor for the vapour removal (Shuttleworth, 1993; Allen *et al.*, 1998). Well-watered areas in hot dry arid regions consume large amounts of water due to the abundance of energy and the drying (desiccating) power of the atmosphere. In humid, tropical regions, notwithstanding the high energy input, the air is already close to saturation, so that less additional water can be stored and hence the E_p rate is lower than in arid areas.

6.2.4 Wind Speed

Wind and air turbulence transfers large quantities of air over the evaporating surface to assist the process of vapour removal. As water vaporises, the air above the evaporating surface gradually becomes saturated and if this air is not continuously replaced with drier air the E_p rate decreases (Allen *et al.*, 1998). Wind speed affects the E_p rate to a far lesser extent in humid conditions than under arid conditions where small variations in wind speed may result in large variations in the E_p rate. In humid conditions, the high humidity of the air and the

presence of clouds cause the E_p rate to be lower. Under hot dry conditions, the E_p rate is high due to the dryness of the air and the amount of direct radiation and heat energy available, which means that a significant amount of water vapour can be stored in the air with wind promoting the transport of water and allowing more water vapour to be taken up.

6.3 CALCULATING EVAPORATION

In many rainfall-runoff models the actual evaporation (E_a) is determined as a function of the soil moisture status and model parameters representing plant-controlled rates of transpiration with atmospherically controlled rates of evaporation. A commonly used method for Australia is the Denmead and Shaw (1962) relationship which has been simplified and used by researchers including Nathan and McMahon (1990a), Chiew *et al.* (1996) and Sumner *et al.* (1997). In this method, E_a (mm/day) is calculated using the following:

$$E_a = \min\left(E_{\max} \frac{\theta}{\theta_{fc}}, E_p \right) \tag{6.1}$$

where:

$\frac{\theta}{\theta_{fc}}$ = soil moisture ratio;

$E_{\max}$ = maximum plant controlled transpiration rate (mm/day); and

E_p = potential evaporation or upper constraint on the value of E_a (mm/day).

The soil moisture ratio is usually defined as the ratio of the soil moisture level (θ) to a parameter representation of the field capacity (θ_{fc}).

The potential evaporation can be calculated in two ways. The first is by using pan evaporation. This is based on evaporation from an open water surface and provides an index of the integrated effects on E_p from radiation, air temperature, air humidity and wind. However, a soil and vegetated surface produces significant differences in the water loss than that from an open water surface. Despite this, pan evaporation has often been used successfully to estimate E_p for vegetated surfaces by applying a pan coefficient (Raghuwanshi and Wallender, 1998).

When pan evaporation is not available or it is difficult to obtain accurate field measurements, E_p is commonly computed from weather and climate data. There are a number of different methods such as temperature based, radiation and combination methods. Each requires various climatological and physical parameters to be known, some of which are measured directly while others are derived using direct or empirical relationships from commonly measured data. Three possible models are discussed in the following sections, namely the Penman-Monteith model (Monteith, 1965), the Morton model (Morton, 1983) and the Priestley-Taylor model (Priestley and Taylor, 1972).

6.3.1 Penman-Monteith Combination Method

Penman (1948) developed an approach that uses a combination of energy balance methods and mass transfer methods to compute evaporation from open water surfaces based on standard climatological records of sunshine, temperature, humidity and wind speed. Monteith (1965) then incorporated canopy resistance to describe the influence of plants on the water flux through roots, stems and leaves to produce the Penman-Monteith model, which has been widely used to estimate E_p from land surfaces (Lemeur and Zhang, 1990; Crago and Brutsaert, 1992; Stannard, 1993; Federer *et al.*, 1996; Vorosmarty *et al.*, 1998; Dias and Kan, 1999; Biftu and Gan, 2000). E_p (mm/day) is defined (Allen *et al.*, 1998) as:

$$\lambda E_p = \frac{\Delta (R_n - G) + \rho_a c_p \dfrac{(e_s - e_a)}{r_a}}{\Delta + \gamma \left(1 + \dfrac{r_s}{r_a} \right)} \tag{6.2}$$

where:

R_n = net radiation flux at the surface (kJ m^{-2} d^{-1});

G = soil heat flux (kJ m^{-2} d^{-1});

$(e_s - e_a)$ = vapour pressure deficit of the air (kPa);

ρ_a = mean air density at constant pressure (kg m^{-3});

c_p = specific heat of the air (kJ kg^{-1} $°C^{-1}$);

Δ = slope of the saturation vapour pressure temperature relationship (kPa $°C^{-1}$);

λ = latent heat of vaporisation (kJ kg^{-1});

γ = psychrometric constant (kPa $°C^{-1}$); and

r_s, r_a = bulk surface and aerodynamic resistances.

The equation has subsequently been modified by Smith (1991) and Allen *et al.* (1998) to provide a standard method for the United Nations Food and Agriculture Organisation (FAO) for determining crop evapotranspiration (ET_0) or evaporation from highly vegetated surfaces. This model can be used for comparisons of evapotranspiration (mm/day) between different seasons or regions. ET_0 (mm/day) is defined (Smith, 1991; Allen *et al.*, 1998) as:

$$ET_0 = \frac{0.408\Delta(R_n - G) + \gamma \frac{900}{T+273} u_2 (e_s - e_a)}{\Delta + \gamma (1 + 0.34 u_2)} \tag{6.3}$$

where:

R_n = net radiation at the vegetated surface (MJ m^{-2} d^{-1}) ;

G = soil heat flux (MJ m^{-2} d^{-1});

T = mean daily temperature at 2m height (°C);

u_2 = wind speed at 2m height (m s^{-1}); and

900 = constant (kJ^{-1} kg K).

There is often an insufficient length of records for many of the meteorological variables, such as wind speed, at Australian climate stations. This, coupled with the lack of information on the canopy resistance of common vegetation types, precludes the widespread use of the Penman-Monteith model for the calibration of catchment water balance models.

6.3.2 Morton Complementary Method

The evapotranspiration model (CRAE) by Morton (1983) was developed using a complementary relationship between the actual and potential evapotranspiration, based on the interaction between evapotranspiration response and humidity of the overpassing air for a large uniform closed system. This complementary relationship is defined (Chiew and Jayasuriya, 1990) as:

$$E_a + E_p = 2E_w \tag{6.4}$$

where:

E_a = actual evapotranspiration (mm/day), from an area so large that the transfer of

heat and water vapour is controlled by the evaporability of the lower atmosphere;

E_p = potential evapotranspiration (mm/day), occurring from a continuously moist surface with an area so small that the fluxes of heat and water vapour from the surface have no significant effect on the evaporability of the overpassing air; and

E_w = wet environment evapotranspiration (mm/day), occurring if the availability of water is not a limiting factor.

Under this relationship, in arid conditions where there is no available water to supply the soil-plant system, $E_a = 0$ and E_p is at its maximum rate because the air is hot and dry. As water becomes available, E_a increases and this increase causes the overpassing air to become cooler and more humid, producing an equivalent decrease in E_p. When the supply increases sufficiently, the values of E_a and E_p converge to that of E_w (Chiew and Jayasuriya, 1990).

Morton (1983) defined two simultaneous equations to calculate E_p, the first representing the energy balance and the second the vapour transfer, as:

$$E_p = R_n - [\gamma P f_a + 4\varepsilon\sigma (T_p + 273)^3] (T_p - T) \tag{6.5}$$

$$E_p = f_a (e_p - e_s) \tag{6.6}$$

where:

R_n = net radiation for soil-plant surfaces at air temperature (kJ m^{-2} d^{-1});

T_p, T = equilibrium and air temperatures (°C);

P = atmospheric pressure (kPa);

f_a = vapour transfer coefficient (kJ m^{-2} kPa^{-1});

ε = surface emissivity;

σ = Stefan-Boltzmann constant (4903 x 10^9 kJ m^{-2} $°K^{-4}$ d^{-1});

e_p = saturation vapour pressure at equilibrium temperature (kPa); and

e_s = saturation vapour pressure in the air (kPa).

The Priestley-Taylor (1972) equation was modified to produce as expression for E_w (mm/day) defined (Morton, 1983) as:

$$E_w = b_1 + b_2 \left(1 + \frac{\gamma P}{\Delta_p}\right)^{-1} R_{np} \tag{6.7}$$

where:

R_{np} = net radiation for soil-plant surfaces at T_p (kJ m^{-2} d^{-1});

Δ_p = slope of the saturation vapour pressure curve at T_p (kPa $°C^{-1}$); and

b_1, b_2 = constants.

The derivation of R_{np} includes the use of a measure for the albedo. The albedo, or canopy reflection coefficient, is the fraction of solar radiation reflected by the surface. This is dependent on transient features such as the direction of the solar beam, the proportion of diffuse radiation and land cover because tall vegetation usually reflects less solar radiation than short vegetation (Shuttleworth, 1993). The albedo for this model is determined using derived equations (Morton, 1983) for the zenith value of snow-free clear sky albedo, the zenith value of clear sky albedo and the clear sky albedo, which were calibrated using data from the northern hemisphere.

The model has been used to derive potential evapotranspiration for use in rainfall-runoff modelling by Nathan and McMahon (1990a; 1990b), Chiew and Jayasuriya (1990), Jayasuriya *et al.* (1990), Chiew and McMahon (1991) and Chiew and McMahon (1993a; 1993b; 1993c) for Australian locations, and by Lemeur and Zhang (1990). Recently the Bureau of Meteorology (2001) has used this method to generate annual areal and point evapotranspiration estimates for Australia.

6.3.3 Priestley-Taylor Method

The Priestley-Taylor method (Priestley and Taylor, 1972) for calculating potential evaporation (mm/day) under conditions of minimal advection is a radiation based model and can be written (Bates, 2000a) as:

$$E_p = \frac{\alpha (R_n + G)\Delta}{\lambda(\Delta + \gamma)} \tag{6.8}$$

where:

R_n = net radiation at the surface (MJ m^{-2} d^{-1});

G = soil heat flux (MJ m^{-2} d^{-1});

α = constant, equal to 1.3 for Australian conditions (Bates, 2000c);

Δ = slope of the saturation vapour pressure versus temperature curve (kPa $°C^{-1}$);

λ = latent heat of vaporisation of water (MJ kg^{-1}); and

γ = psychrometric constant (kPa $°C^{-1}$);

The Priestley-Taylor method has been used by Sumner *et al.* (1997) for calculating E_p for use in rainfall-runoff modelling in Australia and also by Federer *et al.* (1996), Eichinger *et al.* (1996) and Dias and Kan (1999).

6.3.4 Method Selection

The wet environment evapotranspiration model of Morton (1983) is derived without a requirement for wind data, making it a better alternative to the Penman-Monteith model. While the Morton (1983) method has been widely used in Australia it is not always recommended for all locations and time scales. Large differences between the Morton model and the Priestley-Taylor model have been observed (Bates, 2000b). Bates (2000b) indicates that while the Morton approach appears to work well on a monthly or larger time scale, as in Bureau of Meteorology (2001), it does not always perform well on a daily time scale where temperature and humidity values fluctuate. The changes in albedo incorporated into the method are related to snow and highly seasonal vegetation growth in a northern hemispherical environment rather than the Australian environment. For these reasons, the Priestley-Taylor method was used to generate potential evaporation in this study when it was required.

6.4 Application of the Priestley-Taylor Method

6.4.1 Generation of Solar Radiation Data (R_n)

The net input of radiation at the surface (R_n in equation 6.8) is defined by Shuttleworth (1993) as:

$$R_n = R_{ns} + R_{nl} \tag{6.9}$$

where:

R_{ns} = net incoming short wave radiation (MJ m^{-2} d^{-1}); and

R_{nl} = outgoing long wave radiation (MJ m^{-2} d^{-1}).

R_n is normally positive during the day and negative during the night with the total daily value for R_n almost always positive over a 24 hour period, except in extreme conditions at high latitudes.

Shortwave Radiation (R_{ns})

As radiation penetrates the atmosphere a proportion is scattered, reflected or absorbed by atmospheric gases, clouds and dust. The amount of radiation that reaches the ground is known as the total global radiation (R_s). Because the sun emits energy by means of electromagnetic waves characterised by short wavelengths, R_s is also referred to as shortwave radiation. Estimates of the amount of incoming R_s that reaches the ground (R_{ns}) and is not reflected can be obtained (Smith, 1991; Allen *et al.*, 1998) from the following:

$$R_{ns} = (1-\alpha_l) R_s \tag{6.10}$$

where:

R_s = total global radiation (MJ m^{-2} d^{-1}); and

α_l = albedo.

Shuttleworth (1993) and Allen *et al.* (1998) recommend an albedo value of 0.23 as an overall average value for grassland or green vegetation cover. Forest conditions have a slightly lower α_l of approximately 0.17 and the open water α_l is considered to be about 0.08.

Daily total global solar radiation is not widely monitored in Australia and often has to be estimated, spatially interpolated or extrapolated using relationships between solar radiation and sunshine hours, cloudiness or a normalised rainfall index. For areas where R_s is not available, it can be calculated using the Angstrom formula which relates solar radiation to extraterrestrial radiation and measured sunshine hours (Smith, 1991; Shuttleworth, 1993; Allen *et al.*, 1998) by:

$$R_s = \left(a_s + b_s \frac{n}{N} \right) R_a \tag{6.11}$$

where:

R_a = extraterrestrial radiation (MJ m^{-2} d^{-1});

n = actual duration of sunshine (hours);

N = maximum possible duration of sunshine (hours);

a_s = is the regression constant expressing the fraction of extraterrestrial radiation reaching the earth on overcast days ($n=0$); and

$a_s + b_s$ = fraction of extraterrestrial radiation reaching the earth on clear days ($n=N$).

The Angstrom values a_s and b_s vary according to atmospheric conditions (humidity, dust) and the solar declination (latitude, month). Where solar radiation data and calibrated values for a_s and b_s are unavailable, the recommended values of $a_s=0.25$ and $b_s=0.5$ (Shuttleworth, 1993; Allen *et al.*, 1998) can be used.

The amount of daylight hours is dependent on the 23.5° angle of the earth's rotational axis relative to its orbital plane (Dingman, 1994). The maximum possible sunshine duration or daylight hours (N) can be calculated (Smith, 1991; Allen *et al.*, 1998) using:

$$N = \frac{24\,\omega_s}{\pi} \tag{6.12}$$

where:

ω_s = sunset hour angle (rad)

= $\arccos\left(-\tan(\phi)\tan(\delta)\right)$;

ϕ = latitude (rad); and

δ = solar declination (rad).

The solar declination, the latitude at which the sun is directly overhead at solar noon, changes between +23.5° and -23.5° as the earth revolves around the sun and is defined (Allen *et al.*, 1998) as:

$$\delta = 0.409 \sin\left(\frac{2\pi}{365} J - 1.39\right) \tag{6.13}$$

where:

J = day number of the year.

The extraterrestrial radiation (R_a) is the radiation striking a surface perpendicular to the sun's

rays at the top of the earth's atmosphere. The intensity of this radiation is determined by the angle between the direction of the sun's rays and the normal to the surface of the atmosphere, which is dependent on the latitude and time of year. R_a can be calculated (Smith, 1991; Allen *et al.*, 1998) as:

$$R_a = \frac{24(60)}{\pi} G_{sc}\, d_r \left[\omega_s \sin(\phi)\sin(\delta) + \cos(\phi)\cos(\delta)\sin(\omega_s)\right] \tag{6.14}$$

where:

G_{sc} = solar constant (0.0820 MJ m^{-2} min^{-1}); and

d_r = inverse relative distance of the Earth-Sun.

The inverse relative distance for the Earth-Sun (d_r) can be estimated (Allen *et al.*, 1998) using:

$$d_r = 1 + 0.033\cos\left(\frac{2\pi}{365} J\right) \tag{6.15}$$

Alternatively, R_s can be calculated (Bates, 2000c) from:

$$R_s = \left[a_{alt} + (1 - a_{alt})\frac{n}{N}\right] R_o \tag{6.16}$$

where:

R_o = clear day radiation at the surface (MJ m^{-2} d^{-1}); and

a_{alt} = 0.34.

Longwave radiation ***(R_{nl})***

The solar radiation absorbed by the earth is converted to heat energy which is lost by several processes including the emission of radiation. Because the earth is at a much lower temperature than the sun it emits radiative energy with wavelengths longer than those from the sun. Therefore, the terrestrial radiation is referred to as longwave radiation, which is absorbed by the atmosphere or lost into space. The longwave radiation received by the atmosphere contributes to an increase in temperature and, as a consequence, the atmosphere radiates energy, some of which hits the earth's surface. This results in the earth's surface emitting and receiving longwave radiation. The difference between outgoing and incoming longwave radiation is the net longwave radiation. As the outgoing longwave radiation is

almost always greater than the incoming longwave radiation, it represents an energy loss.

Net outgoing long wave radiation (R_{nl}) (MJ m^{-2} d^{-1}) can be calculated (Shuttleworth, 1993) using the following:

$$R_{nl} = -f\varepsilon'\sigma(T_m + 273.2)^4 \tag{6.17}$$

where:

f = adjustment for cloud cover;

ε' = net emissivity between the atmosphere and the ground surface;

σ = Stefan-Boltzmann constant (4.903 x 10^9 MJ m^{-2} $°K^{-4}$ d^{-1}); and

T_m = mean daily air temperature (°C).

The cloudiness factor can be estimated (Shuttleworth, 1993) with solar radiation data using:

$$f = a_c \frac{R_s}{R_o} + b_c \tag{6.18}$$

where $a_c = 1.35$ and $b_c = -0.35$ for arid areas and $a_c = 1.0$ and $b_c = 0.0$ for humid areas. The arid set of values are generally used for Australian conditions (Bates, 2000a).

Where only sunshine data is available, the cloudiness factor can be estimated (Shuttleworth, 1993) using:

$$f = c_c \frac{n}{N} + d_c \tag{6.19}$$

where $c_c = 0.8$ and $d_c = 0.2$ for Australian conditions (Bates, 2000a).

When data for the vapour pressure at dew point (e_d) is available the net emissivity (ε') can be estimated (Shuttleworth, 1993) using:

$$\varepsilon' = a_e + b_e \sqrt{e_d} \tag{6.20}$$

where:

a_e, b_e = correlation coefficients.

For humid conditions and high latitudes $a_e = 0.44$ and $b_e = -0.25$, for semiarid conditions and the tropics $a_e = 0.34$ and $b_e = -0.14$ (Shuttleworth, 1993).

If no humidity data is available the net emissivity can be estimated (Shuttleworth, 1993) using:

$$\varepsilon' = 0.261 \exp\left(-7.77 x 10^{-4} T_m^2\right) - 0.02 \qquad (6.21)$$

where:

T_m = mean daily air temperature (°C).

6.4.2 Soil Heat Flux (G)

The soil heat flux (G) is the energy that is used to heat the soil. It is positive when the soil is warming and negative when the soil is cooling. Although the heat flux is small compared to the R_n and may be often ignored, the amount of energy gained or lost by the soil in this process should theoretically be subtracted or added to R_n when estimating evaporation (as shown in Equation 6.8). Smith (1991) and Shuttleworth (1993) state that the magnitude of daily soil heat flux over 10-30 day periods is relatively small and can be neglected as it is negligible over time periods of a day or less.

6.4.3 Vapour Pressure Curve (Δ)

The slope of the saturation vapour pressure curve (Δ) is important in the description of vaporisation and hence evaporation and is defined (Smith, 1991) as:

$$\Delta = \frac{4098 e_s}{(237.3 + T_m)^2} \qquad (6.22)$$

where:

e_s = saturation vapour pressure (kPa).

The transformation of water molecules between liquid and vapour is dependent on a minimum energy level. If air is thermally enclosed above an evaporating surface, the transfer of water molecules between the evaporating surface and the air will reach equilibrium. At this point the air has become saturated and cannot store more water and the corresponding water vapour pressure exerted is the saturation vapour pressure (e_s). As the temperature rises, the storage capacity of the air increases and hence the saturation vapour pressure also increases. This relationship can be expressed (Smith, 1991) by the following:

$$e_s = 0.6108 \exp\left[\frac{17.27 T_m}{237.3 + T_m}\right] \tag{6.23}$$

where:

T_m = mean daily air temperature (°C).

It is recommended (Allen *et al.*, 1998) that the mean of the daily maximum air temperature (T_{max}) and the daily minimum air temperature (T_{min}) be used in the calculations of e_s and Δ. Therefore T_m should be used as:

$$T_m = \frac{T_{max} + T_{min}}{2} \tag{6.24}$$

6.4.4 Latent Heat of Vaporisation (L)

The latent heat of vaporisation (L) is a measure of the energy required to change a unit mass of water from liquid to water vapour at constant pressure and temperature. Since L varies slightly over normal temperature ranges, a standardised value (at 20°C) of 2.45 MJ kg^{-1} can been adopted (Smith, 1991).

6.4.5 Psychrometric Constant (γ)

The psychrometric constant (γ) is given (Smith, 1991) by:

$$\gamma = 0.00163 \frac{P}{L} \tag{6.25}$$

where:

P = atmospheric pressure (kPa); and

L = latent heat of vaporisation (MJ kg^{-1}).

The atmospheric pressure (P) is the pressure exerted by the weight of the earth's atmosphere. Assuming conditions of 20°C or 293K and P at sea level equal to 101.3 kPa, P can be calculated for any elevation (Smith, 1991) from the following:

$$P = 101.3\left(\frac{293 - 0.0065 z}{293}\right)^{5.26} \tag{6.26}$$

where:

z = height above sea level (m).

6.5 Analysis of Potential and Pan Evaporation

In Equation 6.11 the daily solar radiation (R_s) is related to observed daily sunshine hours. In this section an analysis of this relationship is undertaken for four locations: Alice Springs (station number 015590), Perth (009034), Sydney (066037) and Townsville (032040), to confirm that the solar radiation can be represented in this way. These are located in different regions around Australia and have concurrent records of sunshine hours and solar radiation.

A comparison of observed pan evaporation data with generated potential evaporation is also presented to determine whether they both provide a similar measure of evaporation and could therefore be used relatively interchangeably.

6.5.1 Generation of Radiation by Sunshine Hours

Solar radiation data calculated using sunshine data and Equation (6.11) was compared with data measured directly by the Bureau of Meteorology for each of the four above mentioned locations. The results are shown in Figure 6.1 and Figure 6.2. It can be seen by the values of the coefficient of determination (R^2) and the coefficient of efficiency (E), that the relationships are good. Therefore, the use of sunshine data in the calculation of solar radiation was considered a reliable approach to use in this study.

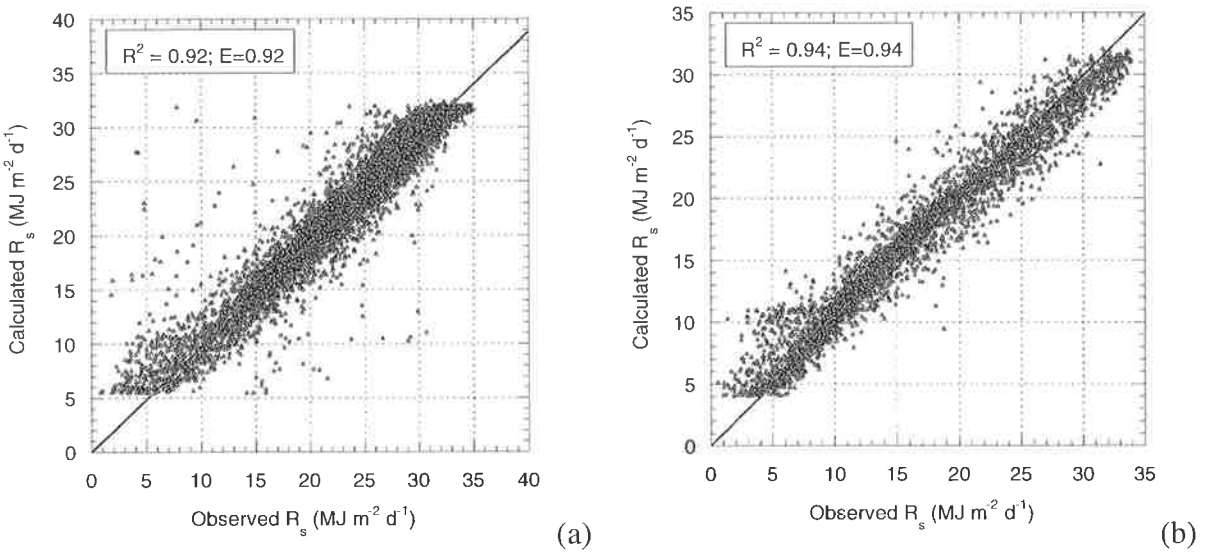

Figure 6.1 Observed and calculated solar radiation data: (a) Alice Springs; (b) Perth.

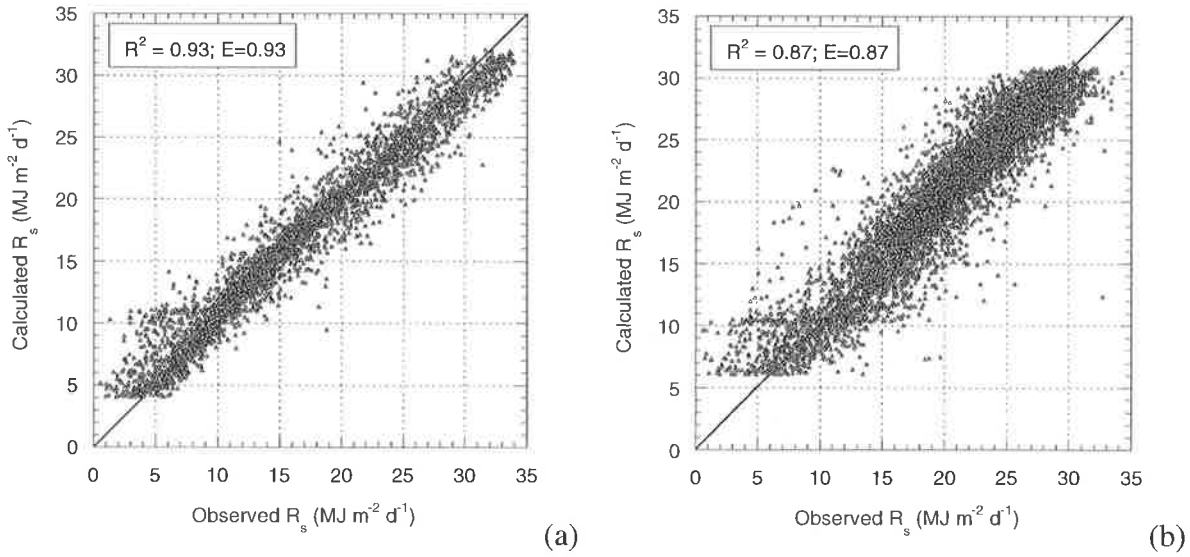

Figure 6.2 Observed and calculated solar radiation data: (a) Sydney; (b) Townsville.

6.5.2 Comparison of Potential and Pan Evaporation

The Priestley-Taylor method described in Section 6.4 was used to generate potential evaporation. At the chosen locations 20 to 40 years of concurrent sunshine hours data and daily temperature data was available. There were periods of missing record at most sites. To infill missing temperature records a linear relationship was formed with a nearby site, while missing sunshine hours records were estimated from a fitted third order polynomial (Chiew and McMahon, 1991) between sunshine hours data and cloud cover data at the same location.

The regression equations developed for Perth (009034) for daily maximum and minimum temperature are shown in Figure 6.3 and Figure 6.4 and for sunshine hours in Figure 6.5. The location details, level of missing data and regression equations used for all sites are shown in Appendix K.1.

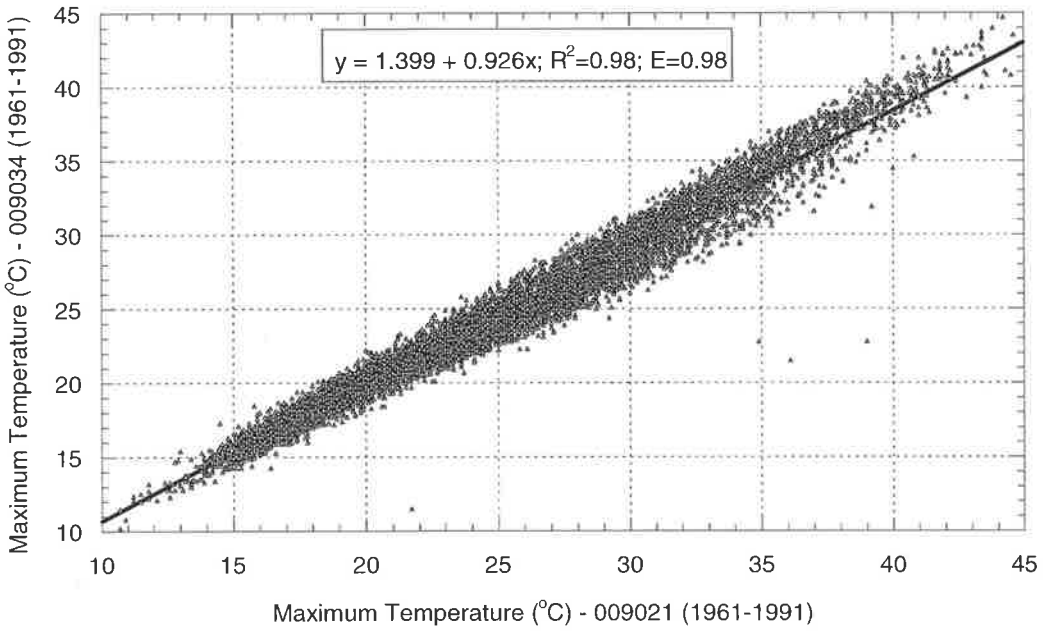

Figure 6.3 Perth: Regression between maximum daily temperatures for Perth Regional Office (009034) and Perth Airport (009021).

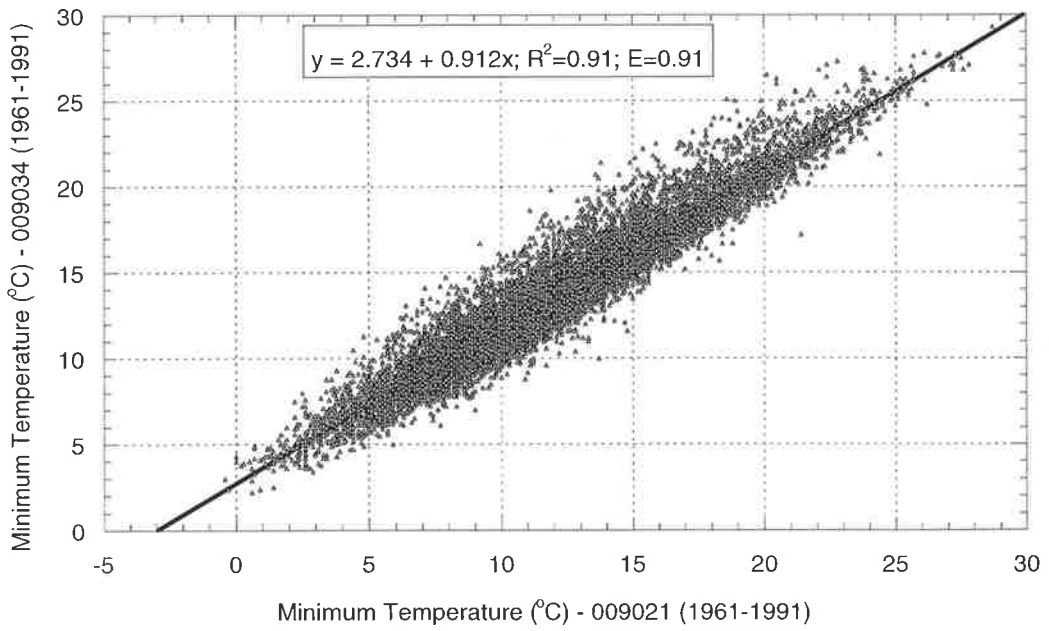

Figure 6.4 Perth: Regression between minimum daily temperatures for Perth Regional Office (009034) and Perth Airport (009021).

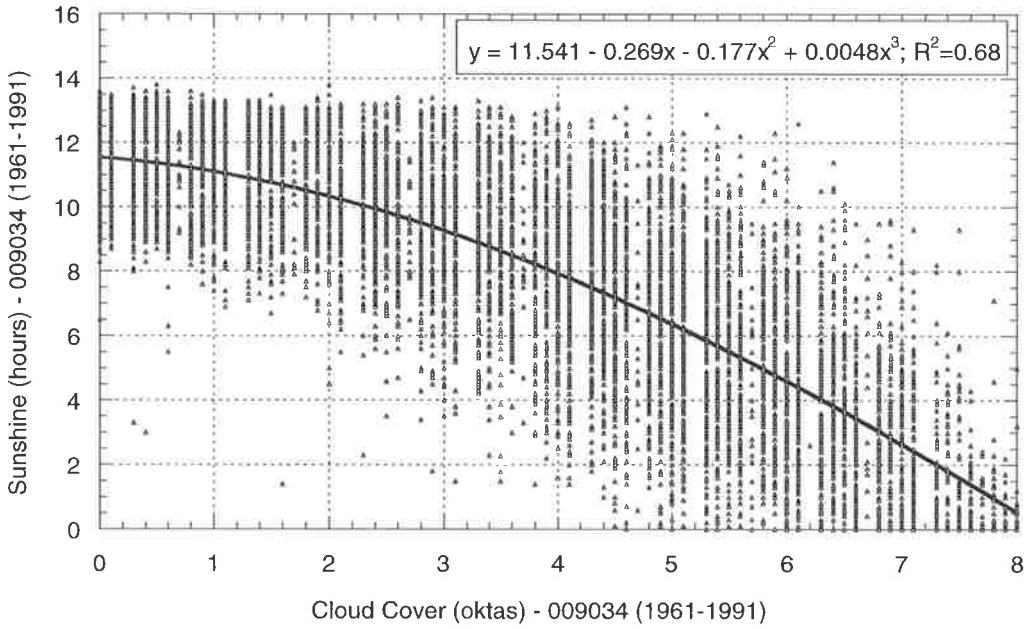

Figure 6.5 Perth: Regression between sunshine and cloud cover for Perth Regional Office (009034).

The potential evaporation was generated using the records of sunshine hours and temperature. As no humidity data was available, Equation 6.21 was used for the net emissivity. Figure 6.6 shows a comparison between the generated potential evaporation and the pan evaporation observed at the same location. This shows that both the pan and potential evaporation are nearly equivalent measures of evaporation with the pan evaporation having a slightly higher and wider spread of values. A proportional factor, calculated as the ratio of the potential to the pan evaporation, was applied to the pan evaporation as shown in Figure 6.7. It can be seen that the pan and potential evaporation overlap and in general can effectively be used interchangeably for a measure of evaporation. Similar results were found for all sites, with the evaporation comparisons shown in Appendix K.1.

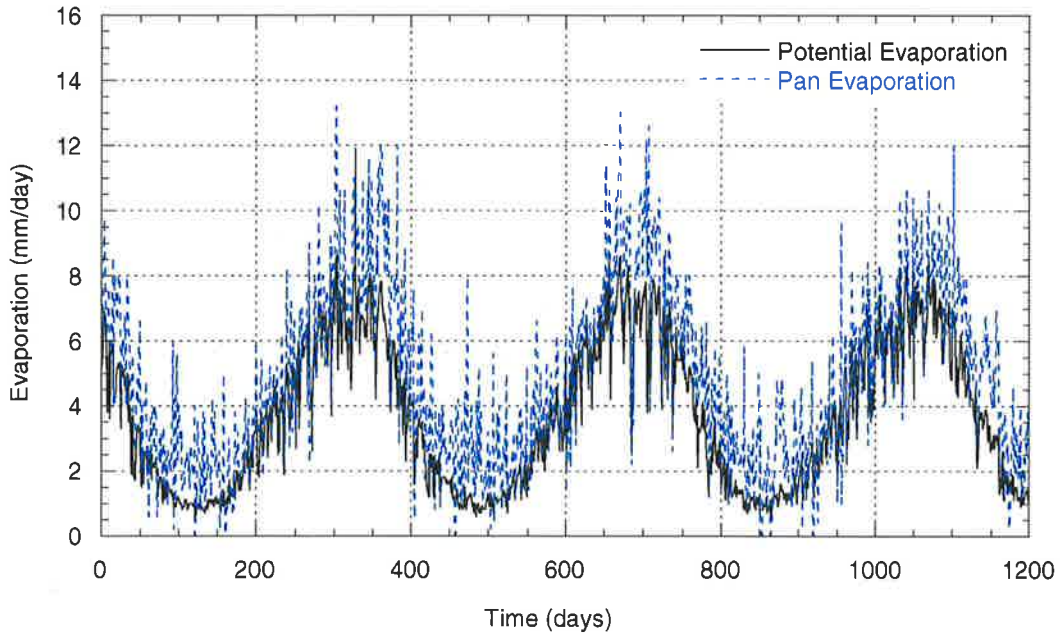

Figure 6.6 Comparison between generated potential and pan evaporation for Perth (009034) (21/2/1974 - 5/6/1977).

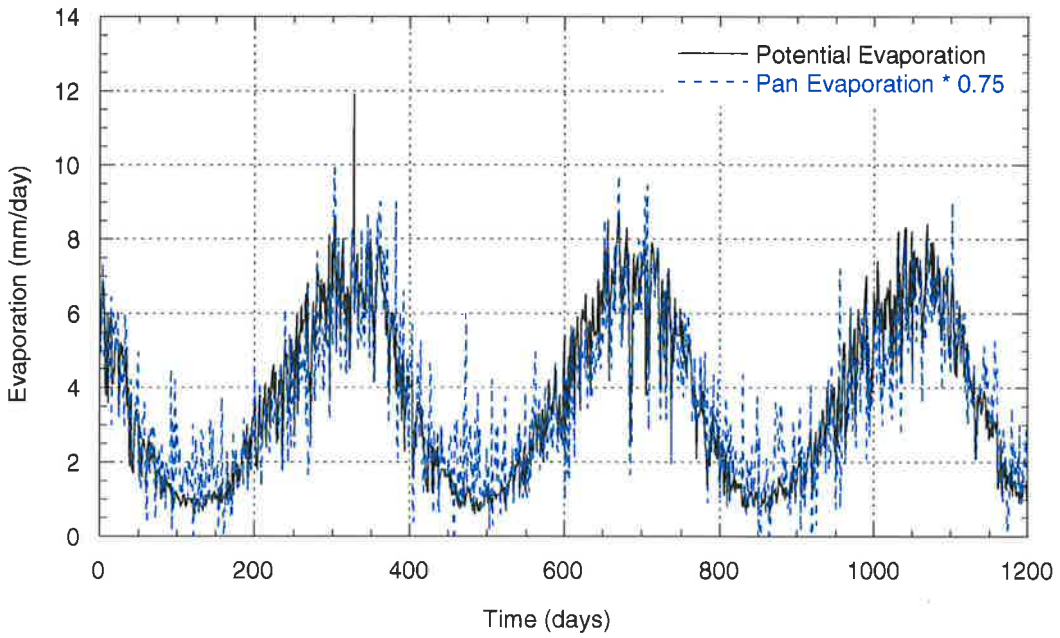

Figure 6.7 Comparison between generated potential and reduced pan evaporation for Perth (009034) (21/2/1974 - 5/6/1977).

6.6 STOCHASTIC MODEL OF EVAPORATION

A number of stochastic models were considered for generating evaporation at the required six-minute level. Evaporation may be generated using models at a higher time scale which then needs to be disaggregated to the desired time scale, or alternatively, models that generate evaporation at the required six-minute resolution may be used. As evaporation data is rarely available at time scales of less than a day, only daily models were investigated. A number of daily models for evaporation are discussed in the following, along with the development of the model used for this study. Validation of the model was carried out by comparing observed and simulated evaporation for a number of sites.

6.6.1 Review of Daily Models for Evaporation

Evaporation has a significant influence on the operation of many hydrological and agricultural systems. However, in comparison to the development of rainfall models, very little research has been undertaken to stochastically generate synthetic models of evaporation, particularly at a daily time scale. Evaporation can either be simulated on its own, or temperature and sunshine or net radiation can be simulated and used to determine potential evaporation. Despite the method used, the cross correlation between variables and in particular between evaporation and rainfall must be preserved (Srikanthan and McMahon, 1985).

Jones *et al.* (1972) developed a simple model to simulate daily evaporation in conjunction with models for rainfall, temperature and soil moisture. Jones *et al.* (1972) suggested that evaporation could be represented as a normal distribution with parameters described by polynomial equations relating to the time of year and the state (wet or dry) of the present and preceding day. It has been shown (Srikanthan and McMahon, 1985) that evaporation on a particular day is highly correlated to that of the previous day, with evaporation data generally being skewed. Neither of these characteristics were taken into account by Jones *et al.* (1972) which is a drawback of the model.

Nicks and Harp (1980) generated daily air temperature and solar radiation data using a lag one Markov model, assuming a normal distribution for both variables. From the generated records of solar radiation and temperature, monthly evaporation was calculated using the Jensen-Haise model (Jensen and Haise, 1963) and was found to adequately reproduce the

mean monthly evaporation calculated from historical temperature and solar radiation data. Srikanthan and McMahon (1985) subsequently suggested that with modifications to account for skewness this model could be used to model daily evaporation.

Srikanthan and McMahon (1985) then developed a first-order Markov model that used a Wilson-Hilferty transformation (Wilson-Hilferty, 1931) to account for skewness or a normal distribution if the simulated skewness was less than 0.1. The parameters of the model were defined by the mean, standard deviation, skewness and lag one auto correlation of daily evaporation, dependent on the state (wet or dry) of the current and preceding days. The model adequately reproduced the observed data although the monthly and annual standard deviations were underestimated.

The lag one Markov model of Srikanthan and McMahon (1985) is easily calibrated using either pan or potential estimates of evaporation. The other models require more parameters and due to lack of available data would have proved to be difficult to calibrate for use in this study. For this reason the lag one Markov model was pursued further.

6.6.2 Description of Model used for this Study

Examination of the available pan and potential evaporation data showed that the daily values are generally dependent on the evaporation on the previous day, as can be seen in Figure 6.8. Figure 6.9, which shows this relationship for January and June, displays a noticeable definite difference in the values of evaporation for different periods of the year. Appendix K.2 contains these relationships for all sites. This further supports the use of the lag one Markov model (Srikanthan and McMahon, 1985) for generating daily evaporation for this study.

The daily evaporation data was divided into four classes described by the following:

(1) dry day followed by a dry day - P(D|D);

(2) dry day followed by a wet day - P(D|W);

(3) wet day followed by a dry day - P(W|D); and

(4) wet day followed by a wet day - P(W|W).

To calibrate the model, the mean, standard deviation, skewness and lag one auto correlation was calculated for each evaporation class in each month.

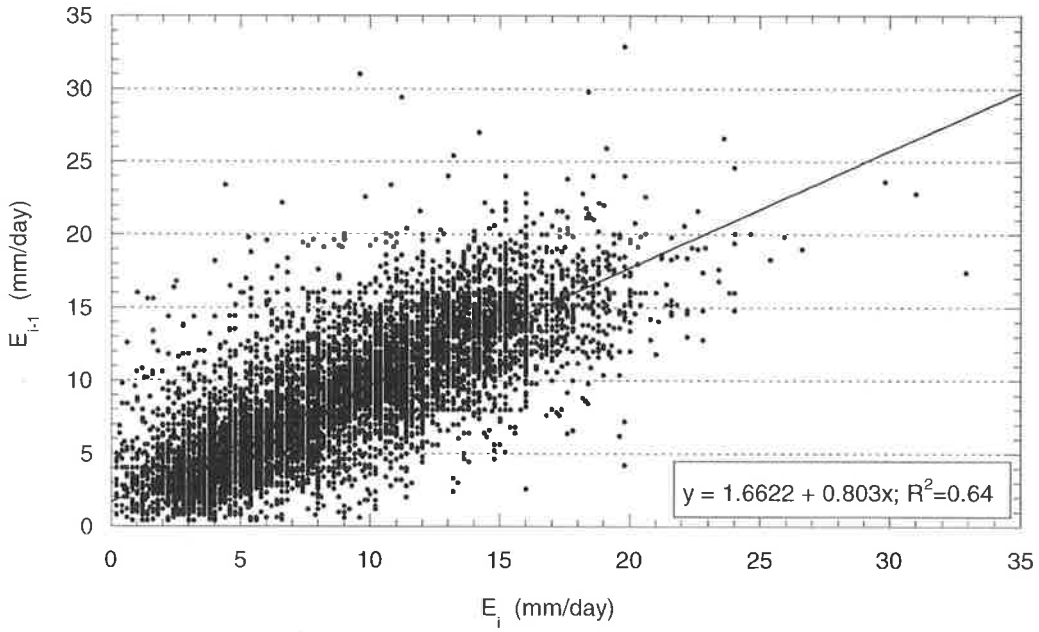

Figure 6.8 Evaporation on current and previous day for Alice Springs (015590).

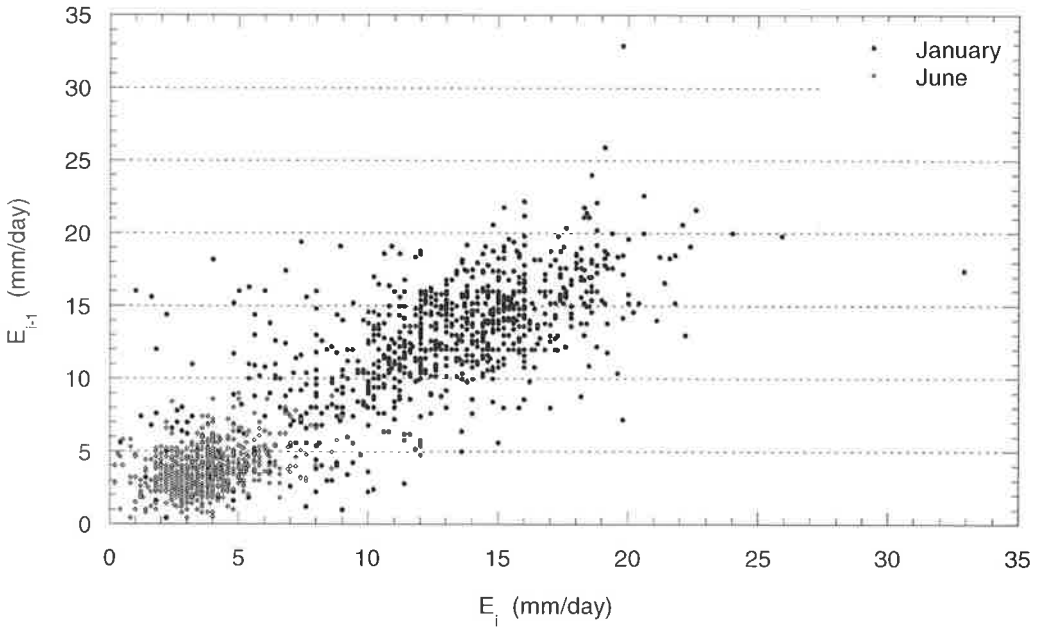

Figure 6.9 Evaporation on current and previous day in January and June for Alice Springs (015590).

Table 6.1 shows the daily evaporation values for Alice Springs in January and June. It can be seen that the values vary depending on the time of the year and for each of the different classes. Similar seasonal variations were found for the other sites.

Table 6.1 Calibrated parameters (daily evaporation statistics) for the Lag One Markov Model of Evaporation for Alice Springs in January and June.

Month	Class	Mean (mm)	Standard Deviation (mm)	Skewness	Lag One Auto-Correlation	Number of Points
January	P(D|D)	14.030	3.219	0.361	0.634	667
	P(D|W)	11.167	3.736	0.225	0.304	73
	P(W|D)	10.944	3.896	-0.030	0.581	75
	P(W|W)	5.886	3.564	0.663	0.280	85
June	P(D|D)	3.793	1.280	0.974	0.375	748
	P(D|W)	3.139	1.571	0.084	0.411	44
	P(W|D)	2.787	1.167	-0.113	0.319	45
	P(W|W)	1.228	0.896	0.859	-0.081	29

To generate daily evaporation the state (wet or dry) of the current and previous day must first be obtained from the simulated rainfall. Using this combination of states, the evaporation is then calculated by applying a random number sampled from a normal distribution to the calibrated parameters. If the absolute value of the observed skewness for that combination of states in that month was greater than 0.1, the random number was transformed using the Wilson-Hilferty transformation (Wilson and Hilferty, 1931). If it was less than or equal to 0.1 the random number was not transformed. The equations for the model were defined (Srikanthan and McMahon, 1985) as:

$$E_t = \overline{E} + r_1\left(E_{t-1} - \overline{E}\right) + S\left(1 - r_1^2\right)^{\frac{1}{2}}\varepsilon_t \tag{6.27}$$

$$\varepsilon_t = \frac{2\left(\left(1 + \frac{g\eta_t}{6} - \frac{g^2}{36}\right)^3 - 1\right)}{g} \qquad |\gamma| > 0.1 \tag{6.28}$$

$$\varepsilon_t = \eta_t \qquad |\gamma| \le 0.1 \tag{6.28}$$

$$g = \frac{\left(1 - r_1^3\right)\gamma}{\left(1 - r_1^2\right)^{1.5}} \tag{6.29}$$

where:

E_t, E_{t-1} = evaporation in day t and $t-1$ (mm);

$\overline{E}$ = mean daily evaporation (mm);

S = standard deviation of the daily evaporation (mm);

γ = skewness of the daily evaporation (mm);

r_1 = lag one auto-correlation of the daily evaporation (mm);

ε_t = random number with mean zero, variance one and skewness g;

η_t = normally distributed random number with mean zero and variance one; and

g = is the skewness of random numbers ε_t.

6.6.3 Continuous Simulation of Rainfall and Evaporation

The stochastic model for simulating daily evaporation was linked to the stochastic rainfall model. As rainfall was generated, the level of evaporation was calculated dependent on the states of the current and previous days. In order to confirm that the combined stochastic rainfall and evaporation models where producing reasonable estimates of evaporation a comparison between the simulated and observed statistics was undertaken for Alice Springs, Perth, Sydney and Townsville. For each of these sites the observed statistics were calculated from the available pan evaporation records.

Table 6.2 shows a comparison of the annual statistics for each site. The means compare well although the standard deviations are underestimated. Table 6.3 shows the daily statistics and Table 6.4 the monthly statistics of the observed and simulated evaporation for Townsville. The monthly standard deviations are underestimated for some months but all other statistics are satisfactory. Appendix K.3 shows the results for all sites.

The results produced are consistent with those shown by Srikanthan and McMahon (1985) who used a transitional probability matrix to generate rainfall states and in which the annual and monthly standard deviations were also underestimated. However, the results shown here confirm that the stochastic evaporation model performs well in conjunction with the stochastic rainfall model. In addition, the rainfall model produces an appropriate number of dry and wet days, which is a relationship not used during calibration.

Table 6.2 Annual statistics for observed and simulated evaporation.

Site	Mean (mm)		Standard Deviation (mm)	
	Observed	Simulated	Observed	Simulated
Alice Springs	3072	3103	429	181
Perth	1774	1780	160	119
Sydney	1795	1780	103	121
Townsville	2625	2622	200	163

Table 6.3 Daily observed and simulated evaporation statistics for Townsville.

Month	Mean (mm)		Standard Deviation (mm)		Skewness		Lag One Auto-Correlation	
	Observed	Simulated	Observed	Simulated	Observed	Simulated	Observed	Simulated
1	8.3	8.2	2.8	2.7	-0.6	-0.6	0.53	0.37
2	7.3	7.2	2.5	2.5	-0.2	-0.2	0.45	0.32
3	7.0	7.0	2.3	2.2	-0.3	-0.3	0.45	0.31
4	6.6	6.6	2.1	2.0	-0.2	-0.2	0.43	0.27
5	5.6	5.6	1.8	1.7	0.0	0.1	0.40	0.26
6	5.1	5.0	1.7	1.6	0.5	0.2	0.19	0.12
7	5.3	5.4	1.7	1.7	0.4	0.5	0.27	0.17
8	6.2	6.3	1.8	1.8	0.2	0.2	0.37	0.25
9	7.7	7.8	2.0	2.0	0.2	0.3	0.37	0.22
10	8.9	9.0	2.1	1.9	-0.1	-0.1	0.37	0.23
11	9.2	9.3	2.2	2.1	-0.3	-0.4	0.38	0.24
12	9.0	9.0	2.6	2.4	-0.6	-0.6	0.52	0.35

Table 6.4 Monthly observed and simulated evaporation statistics for Townsville.

Month	Mean (mm)		Standard Deviation (mm)	
	Observed	Simulated	Observed	Simulated
1	258	263	49	23
2	206	201	35	22
3	217	216	29	22
4	198	199	28	19
5	173	173	25	17
6	152	151	16	13
7	165	168	19	15
8	194	193	19	18
9	232	234	25	20
10	277	277	27	22
11	276	279	30	23
12	278	268	38	26

6.7 DISAGGREGATION OF DAILY EVAPORATION

The daily evaporation data generated by the above model needed to be disaggregated to a six-minute resolution for use with the stochastic rainfall in a continuous simulation of the catchment water balance. For general application, the distribution function applied to daily evaporation needed to be independent of the evaporating surface, location and time of year even though the diurnal pattern of evaporation is known to be strongly influenced by these and other weather patterns (Fleming, 1970). Evaporation from natural surfaces (other than lakes or other large bodies of water) was investigated by Fleming (1970) who developed non-dimensional functions for the distribution of total daily evaporation over the day, for two cases: clear days and cloudy days. Clear days were generally considered to have the highest periods of evaporation and the largest magnitude of diurnal range. Overcast days were considered to have lower evaporation values because sunshine is broken during the day. This results in more diurnally fluctuating evaporation rates.

The functions used to disaggregate daily evaporation on clear and cloudy days are described in the following sections. To use these calculation, estimates of sunrise, sunset and daily sunshine hours were also required. A method for calculating these is also discussed.

6.7.1 Clear Day Evaporation

Fleming (1970) used relationships for the energy balance from an evaporating surface and the partition of available energy into sensible and latent heat, assuming a diurnal cycle and that the radiation components of the relationships dominate. A dimensionless distribution function for evaporation was derived using average daylight evaporation and time as a proportion of day length. The evaporation rate (ER) in mm/hour was given by the following:

$$ER = EVI * AvDE \tag{6.30}$$

where:

$AvDE$ = ratio of the 24 hour evaporation to the number of sunshine hours;

EVI = dimensionless evaporation index

= $\max[(2.78 - (7.73 + A)^{0.5}), 0]$;

A = $31.4(D_{hr})^2 - 33.6(D_{hr}) + 2.23$; and

D_{hr} = ratio of the time from sunrise to the number of sunshine hours.

This technique removed most of the variation due to seasonal conditions and also reduced some of the variation due to atmospheric conditions. Fleming (1970) examined available data and showed that evaporation does not usually commence before $D_{hr} = 0.07$ and ceases when $D_{hr} = 1.0$. The equation for the EVI is based on a hyperbola with base length of 0.93, a peak height of 1.80 and an area under the curve equal to 1.00. Figure 6.10 shows this relationship for two arbitrary days, one in January when the evaporation and daylight hours are high and one in June when evaporation and daylight hours are low.

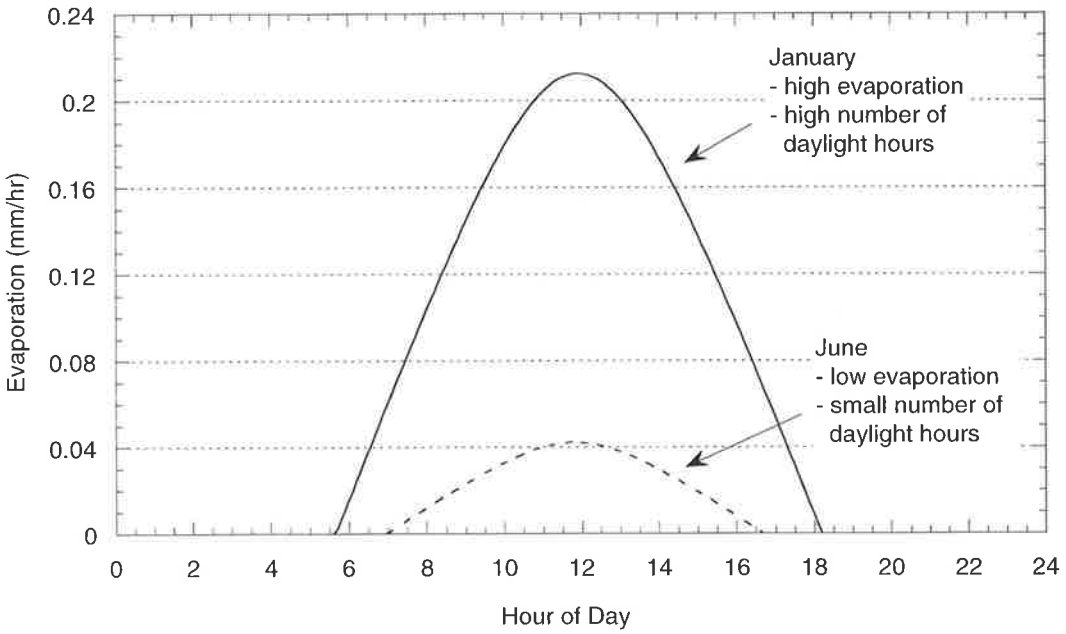

Figure 6.10 Diurnal distribution of evaporation over a clear day in January and June for Alice Springs.

6.7.2 Cloudy Day Evaporation

On cloudy days radiant energy levels may widely fluctuate unless the cloud cover is so thick as to reduce radiation to a very low level (Fleming, 1970). Fleming (1970) suggested that evaporation rates are more evenly distributed over cloudy days with randomly distributed peaks determined by cloudiness and wind speed patterns. A simple truncated triangle function was suggested to distribute evaporation over cloudy days described by the following:

$$EVI = 0 \qquad 0 \le D_{hr} \le 0.060 \qquad (6.31)$$

$$EVI = 6.75(D_{hr} - 0.060) \qquad 0.061 \le D_{hr} \le 0.26 \qquad (6.32)$$

$$EVI = 1.35 \qquad 0.261 \leq D_{hr} \leq 0.80 \qquad (6.33)$$

$$EVI = 1.35 - 6.75(D_{hr} - 0.80) \qquad 0.81 \leq D_{hr} \leq 1.0 \qquad (6.34)$$

This was obtained from examination of average non-dimensional distributions of evaporation on cloudy days. Figure 6.11 shows this relationship for two arbitrary days, one in January when the evaporation and daylight hours are high and one in June when evaporation and daylight hours are low. While the evaporation for January is higher than that for June it can be seen, as would be expected, that when compared to Figure 6.10 that the peak evaporation on the cloudy day is much lower than on the clear day.

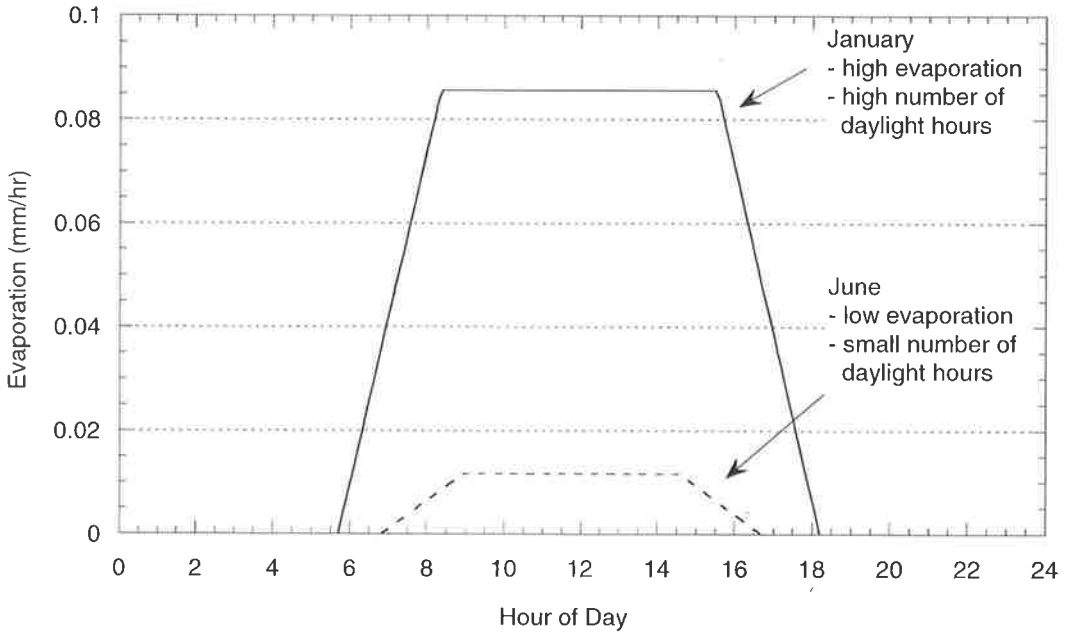

Figure 6.11 Diurnal distribution of evaporation over a cloudy day in January and June for Alice Springs.

6.7.3 Sunshine Calculations

To use the disaggregation function described above, estimates of sunrise, sunset and daily sunshine hours were needed. As discussed in Section 6.4.1, the maximum possible sunshine duration or daylight hours (N) can be then be calculated (Allen *et al.*, 1998) using:

$$N = \frac{24\omega_s}{\pi} \qquad (6.35)$$

where:

ω_s = sunset hour angle (rad)

= $\arccos(-\tan(\phi)\tan(\delta))$;

ϕ = latitude (rad); and

δ = solar declination (rad).

Kepler discovered that the earth's tangential speed varies, getting faster when the earth is closer to the sun and slowing down when farther away. Because of this variation in speed, the time it takes for the sun to get to the same position overhead varies throughout the year. This variation is called the equation of time (US Department of Commerce, 2000). In astronomical terms it is defined as the difference between the mean solar time and the apparent solar time. Solar noon calculations account for the equation of time as well as the longitudinal position of the observer within the local time zone. The equation of time is described (US Department of Commerce, 2000) as:

$$eqtime = 229.18*(0.000075 + 0.001868\cos(\Gamma) - 0.032077\sin(\Gamma) - 0.0014615\cos(2\Gamma) - 0.040849\sin(2\Gamma)) \quad (6.36)$$

where:

Γ = day angle (rad)

= $\frac{2\pi(J-1)}{365}$; and

J = day number.

Using the equation of time, solar noon in Greenwich Mean Time (GMT) at a given location can be calculated (US Department of Commerce, 2000) using the following:

$$solarNoon = 720 + 4*longitude - eqtime \quad (6.37)$$

The theoretical time for sunrise and sunset is then:

$$Sunrise = solarNoon - \frac{N}{2} \quad (6.38a)$$

$$Sunset = solarNoon + \frac{N}{2} \quad (6.38b)$$

The actual times for sunrise and sunset will depend on a number of factors including

atmospheric variation and orography (that is mountains and hills). Atmospheric variation, which may occur on a daily or seasonal basis, is due to variations in the density of the atmosphere with respect to elevation that may effect the refraction path of the light. A location at sea level with an ideal horizon is assumed for the calculations. However, the values calculated using these equations were considered satisfactory and deviations were not likely to affect results significantly because the total daily evaporation remains constant, irrespective of the sunrise and sunset times.

There was no clear relationship between the state of the day and whether it was clear or cloudy and little research appears to have been done in this area. For this study, a day with rainfall was assumed to be cloudy and all other days were assumed to be clear. The disaggregated evaporation data was then suitable for use in the catchment water balance model.

6.8 Concluding Remarks

This chapter has evaluated methods for stochastically generating evaporation data in conjunction with rainfall and for calculating evaporation from observed sunshine hours and temperature records to calibrate a deterministic water balance model.

The combination of rainfall and evaporation models to generate concurrent data at a six-minute time scale has been rarely undertaken by previous researchers. However, this study has demonstrated successful generation of synthetic evaporation using the developed model in conjunction with the stochastic rainfall model. This evaporation model, which can be calibrated using either pan or potential evaporation, generates synthetic data conditioned upon the state (wet or dry) of the current day, preceding day and the time of year. This is then disaggregated to a six-minute time scale using relationships based on clear and cloudy day evaporation. The stochastic rainfall model is not a state-based model and thereby effectively tests characteristics of both the evaporation and rainfall models. The simulated evaporation statistics successfully replicated the observed statistics, which also indicated that the rainfall model was capable of producing an appropriate number of wet and dry days.

A number of methods for calculating potential evaporation were investigated and the Priestley-Taylor (Priestley and Taylor, 1972) method was subsequently chosen. Use of this model with hours of sunshine data in place of radiation data was examined and found to be

valid for a number of sites in different climatic regions. The pan and calculated potential evaporation were observed to be proportional and with the use of a multiplying factor can be effectively used interchangeably for a measure of evaporation.

The stochastic model of evaporation was considered, in conjunction with the stochastic rainfall model, to be a suitable tool for generating the input for a water balance model for determining the subsequent rainfall excess.

7. MODEL OF THE CATCHMENT WATER BALANCE

Estimation of surface runoff or rainfall excess from rainfall is the next component in the proposed method for design flood estimation for engineering design. Using rainfall, streamflow and evaporation records as input data, the development of a catchment water balance model that will represent water movement through a catchment and into streams is presented in the following sections. Such a model must be complex enough to capture and replicate the physical processes without being overly complex, which can result in calibration difficulties. Using the catchment model together with the stochastic models for rainfall and evaporation (discussed in Chapters 3 to 6), long continuous simulations of a number of catchments were undertaken and are discussed in Chapter 8.

Catchment water balance models were evaluated using a number of criteria that included the capability to describe the physical processes, the number of parameters required and the ease of calibration. Very little work appears in the literature that deals with the optimisation of catchment water balance models using comparisons with daily values of flow. Most, even when using daily inputs of rainfall, aggregate the predicted flow to monthly time scales before comparing with observed data. This restricted the ability to determine whether current models would be satisfactory for flood estimation applications.

7.1 Review of Catchment Water Balance Processes and Models

A catchment water balance accounts for all water entering and leaving a catchment. Figure 7.1 shows the hydrological cycle of a catchment with the major inputs, outputs, storage and movement mechanisms. These mechanisms are discussed in the following along with a presentation of the detailed analysis of modelling approaches that were considered for this study.

7.1.1 Components of the Catchment Water Balance

At the beginning of an event rainfall loss occurs via mechanisms such as interception by trees and other vegetation, infiltration into the soil and the storage of water in small ground depressions (Chapter 1). Water that is collected in storage can either be retained for a long period of time (retention storage) and depleted by evaporation or held for a much shorter time

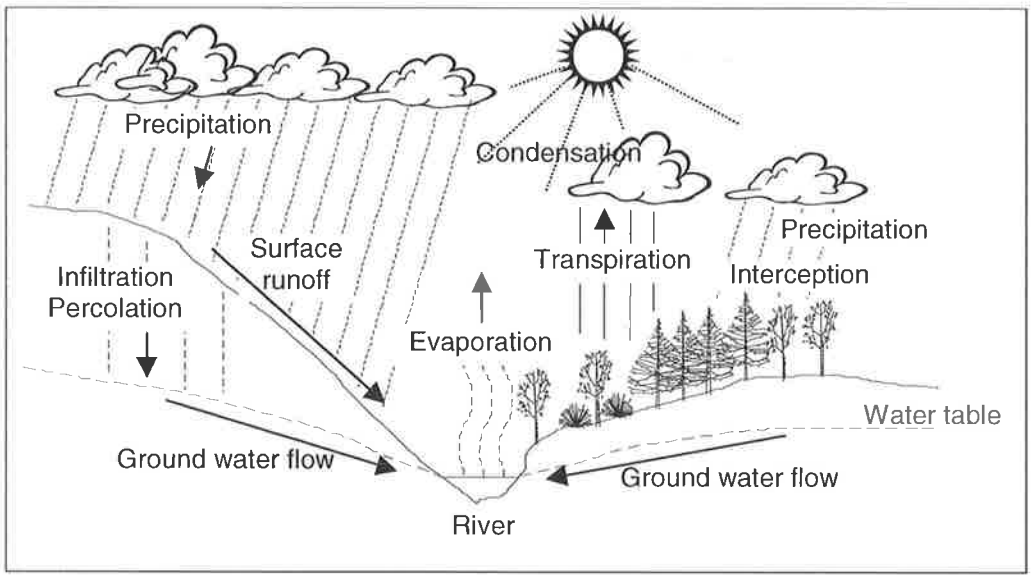

Figure 7.1 The hydrological cycle.

(detention storage) and depleted by movement away from the storage location (Chow *et al.*, 1988). There are two major types of runoff processes, the movement of water into a stream channel along surface and sub-surface flow paths and the movement of water through a stream channel network to produce an event hydrograph.

The mechanisms by which water stored at the ground surface travels to the stream system can be classified as:

(a) surface or overland flow across the land;

(b) sub-surface or unsaturated flow through the unsaturated soil near the land surface; or

(c) groundwater flow through saturated aquifers.

Some or all of these mechanisms may operate simultaneously on a given watershed and the relative importance of individual mechanisms may fluctuate seasonally or even during a single rainfall event depending on the antecedent catchment wetness and the climatic, topographic and geologic conditions of the catchment.

The movement of water through a stream network is discussed in Chapter 8. All the above surface and sub-surface processes contribute to this flow. However, during a rainfall event channel interception also occurs, where rain falls directly on a stream to become incorporated in channel flow. Runoff from this source occurs in all events and in all regions and is usually an insignificant component of the total event flow. However, channel interception can

constitute a larger fraction of the event response and peak discharge when an intense rain falls on a very dry watershed (Dingman, 1994).

Surface Runoff (Overland flow)

Surface runoff is the result of a complex interaction between rainfall and the land surface. Also referred to as overland flow or rainfall excess, it occurs on a sloping surface that is either impermeable or saturated from above or below.

The classical theory of surface runoff generation was developed by Horton (1933) who described Hortonian overland flow as the runoff resulting from above ground saturation. Horton (1933) stated that "Neglecting interception by vegetation, surface runoff is that part of the rainfall which is not absorbed by the soil by infiltration" and considered surface runoff to take the form of a sheet flow whose depth increases as flow accumulates down a slope until it discharges into a stream channel. It was considered that when the rainfall intensity exceeds the infiltration capacity of the soil or the surface onto which it is falling, surface runoff and overland flow will occur. At this time it was postulated that this was the primary, if not only, mechanism responsible for event response. Horton (1933) suggested that overland flow due to saturation from above would occur from virtually an entire catchment. This view has since been modified through the proposition of the partial-area concept (Betson, 1964) whereby event response occurring as Hortonian overland flow will originate from only a limited contributing area that generally remains constant within a catchment and within a rainfall event (Dingman, 1994). It is now accepted that Hortonian overland flow rarely occurs on natural surfaces since typical rainfall intensities are less than the infiltration capacities of many soils. The theory is more applicable to impervious surfaces in urban areas and natural surfaces with thin soil layers and low infiltration capacities such as in arid and semiarid lands (Chow *et al.*, 1988; Dingman, 1994).

Saturation overland flow is overland flow that occurs due to saturation from below (Dingman, 1994) and is produced when sub-surface flow (discussed below) saturates the soil near the bottom of a slope and overland flow then occurs as rain falls onto saturated soil (Chow *et al.*, 1988). It differs from Hortonian overland flow in that it is produced by saturation from below and occurs primarily at, but is not restricted to, the bottom of hill slopes and near stream banks. Saturation overland flow is also contributed to by return flow. The importance of near-stream saturation overland flow as a stream-response mechanism in humid regions has been well established (Dingman, 1994). The variable-source-area concept (Dunne *et al.*,

1975) is based on the presumption that within a catchment the extent of areas saturated from below can vary over time, in order to better reflect the overall catchment wetness. This mechanism goes some way to describing the temporal variability of the proportion of rainfall excess that results from a certain amount of rainfall, which has been observed in many regions (Dingman, 1994). The variable source area generally expands during a rainfall event and contracts thereafter (Chow *et al.*, 1988). This mechanism is considered the most appropriate for event response in humid regions.

Sub-Surface and Groundwater Flow

Groundwater flow, or baseflow, is generally considered the main source of water for a stream between rainfall events. This water infiltrates the soil during a rainfall event and moves through groundwater reservoirs with residence times that are large enough not to contribute significantly to an event response (Dingman, 1994). However, when the infiltration capacity of the soil exceeds the rainfall intensity, sub-surface flow may become a more significant mechanism for the transport of water to a stream (Dingman, 1994). While the velocities are usually lower than those of surface flow, hence contributing a less significant portion of a rainfall event to the stream, flow through root holes in forested soil can be more rapid (Chow *et al.*, 1988). Sub-surface flow is generally a more important runoff mechanism that needs to be considered in humid regions.

7.1.2 Types of Modelling Approaches

Modelling approaches for the estimation of runoff output from rainfall and evaporation inputs can be broadly classified into the following types:

(a) black box models;

(b) process models; and

(c) conceptual models.

Black Box Models

Black box modelling approaches generally use empirical equations that relate the inputs and outputs. These may be simple polynomial functions (Chiew *et al.*, 1993) such as

$$R = a + b r + c r^2 + d r^3 + e r^4 \qquad (7.1)$$

where:

R = runoff (mm);

r = rainfall (mm); and

a - e = parameters.

In this type of model, only the rainfall input and runoff output have physical meanings.

A more complex black box type model is a time series model such as the IHACRES (Jakeman and Hornberger, 1993; Chiew *et al.*, 1993), which is defined as:

$$R_i = -a_1 R_{i-1} - a_2 R_{i-2} + b_0 EX_i + b_1 EX_{i-1} \qquad (7.2)$$

where:

R_i = runoff in time period i (mm);

EX_i = rainfall excess in time period i (mm); and

$a_{1,2}, b_{0,1}$ = parameters.

The rainfall excess is calculated by a non-linear relationship incorporating rainfall, catchment wetness and temperature in current and preceding time periods. While the components of the model are given physical interpretations, the parameters are not quantities that can be physically measured or interpreted for particular site conditions. Chiew *et al.* (1993) found that black box models such as the IHACRES model did not satisfactorily estimate daily runoff.

Process Models

Process models attempt to simulate the hydrological processes for a catchment and generally describe the movement of water within catchments using either numerical solutions of partial differential equations governing various physical processes or experimentally derived empirical equations representing flow processes (Jayatilaka *et al.*, 1998). An example is the Systeme Hydrologique Europeen (SHE) model (Abbott *et al.*, 1986a, 1986b), which is a deterministic, distributed and physically-based model. This model uses an orthogonal grid network in the horizontal dimension and columns comprising a series of nodes in the vertical dimension at each grid cell to allow for the spatial variation of catchment parameters, hydrometeorological input and hydrologic response with the nodes in the vertical scale representing various soil zones.

Other process type models have included the IHDM model (Beven *et al.*, 1987) and the TOPOG (Vertessy *et al.*, 1994) model. Process models require the use of many parameters.

Generally data limitations and the difficulty in relating theoretical equations that describe hydrologic processes to large scale catchments means that the use of these models is not justified (Chiew *et al.*, 1993; Jayatilaka and Connell, 1995). In Australia, data is limited and a simple model with easily calibrated parameters is preferred for engineering design work.

Conceptual Models

Conceptual models provide a simpler approach. The catchment is conceptualised by a number of interconnected storages with mathematical functions describing the movement of water into, between and out of them. They attempt to represent catchment physical processes but often include black box treatment where empirical equations and parameters are used to describe a process (Chiew *et al.*, 1993). Conceptual rainfall-runoff models simulate the physical processes that comprise the land phase of the hydrologic cycle. The transformation is modelled by a set of transfer functions that generally link several interconnected conceptual water stores. The parameter estimates for the model must be obtained by fitting computed hydrographs to observed hydrographs as direct physical measurements of the parameters are either difficult or impossible.

There are numerous conceptual models in use, varying from simple daily rainfall-runoff models such as the SFB model (Boughton, 1984) to complex models such as MODHYDROLOG (Chiew and McMahon, 1993a, 1994). In these models, an accurate estimate of the antecedent catchment conditions (or the initial loss) prior to rainfall events is obtained through a continuous account of the catchment soil water. Because of the large number of conceptual models available, an examination of alternative approaches in this study was restricted to models that have been extensively tested on Australian catchments. The conceptual flow mechanisms in such models are more likely to be appropriate for Australian hydrological conditions.

The *Streamflow-Infiltration-Baseflow (SFB) Model* was initially developed by Boughton (1984) as a simple method for estimating the water yield on ungauged catchments. This lumped conceptual model is illustrated in Figure 7.2. The model has three parameters, a surface storage capacity (S), a daily infiltration capacity (F) and a baseflow factor (B). These parameters can be related to physical catchment characteristics and the model uses rainfall (P) and evaporation (E) as required input data.

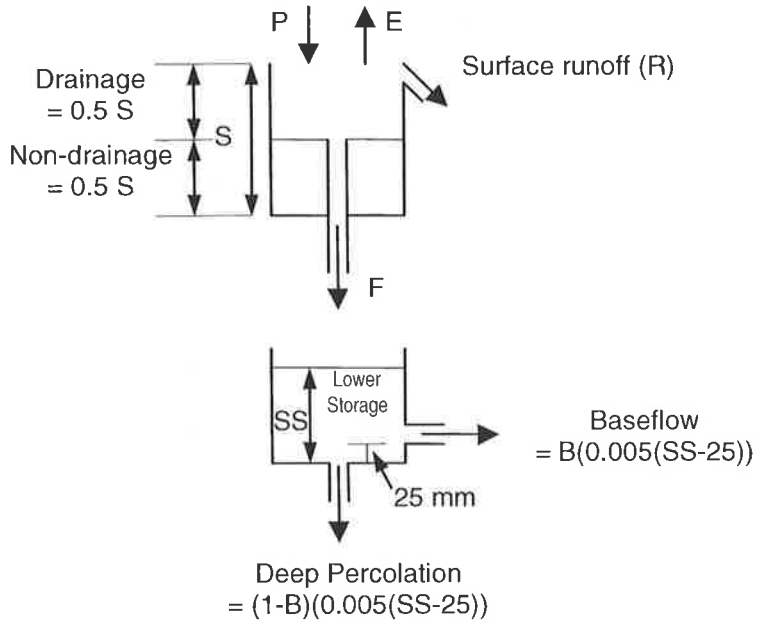

Figure 7.2 Streamflow-Infiltration-Baseflow (SFB) Model
(adapted from Nathan and McMahon, 1990a).

Rainfall is added and evaporation subtracted from the surface store, which has two components. The first is an upper drainage store that represents soil moisture levels between saturation and field capacity and it also represents the loss of any rainfall by interception or ponding. A lower non-drainage store represents soil moisture levels between field capacity and the wilting point. Once the surface store is full, runoff (R) is generated. When the surface store is full, evaporation will occur at the potential rate. However, when the non-drainage component of the surface store is not full, evaporation is estimated as a function of the water remaining in storage. When the drainage component of the surface store contains water, drainage into a sub-surface store can occur at a maximum rate of F mm/day. Once a minimum water level is reached in this sub-surface store (often 25 mm), baseflow and deep percolation can occur at a fixed fraction of 0.005 of the water remaining in the store. The baseflow parameter (B) determines how much of this water appears as baseflow and how much is lost to deep percolation.

The SFB model has been extensively applied to Australian catchments by researchers including Boyd *et al.* (1986), Nathan and McMahon (1990a, 1990b), Chiew *et al.* (1993), Sumner *et al.* (1997), Ye *et al.* (1997) and Thyer *et al.* (1999). In addition, modifications have been made by some of these researchers such as that shown in Figure 7.3.

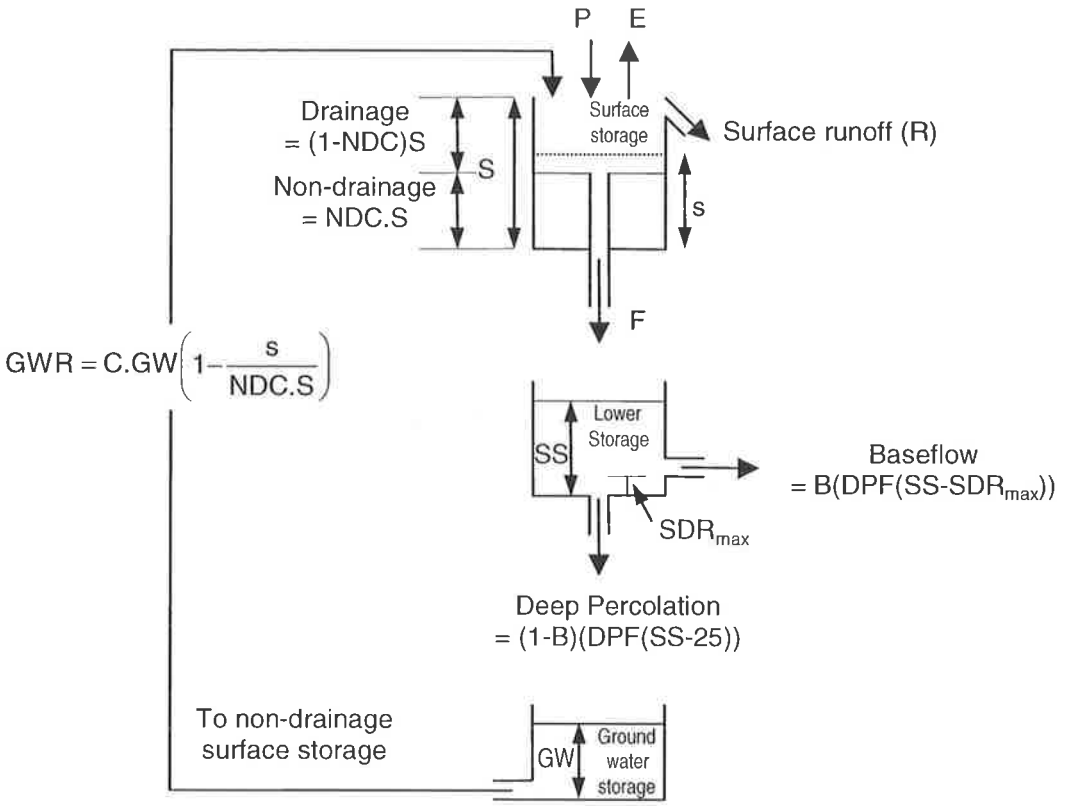

Figure 7.3 Modified Streamflow-Infiltration-Baseflow (SFB) Model (adapted from Sumner *et al.*, 1997).

The first modification of the original model involved calibrating the previously constant parameters that controlled the drainage and non-drainage proportions of the surface store and the sub-surface depletion rate. A non-drainage component (NDC) parameter was then defined as the proportion of the surface store that is non-draining. Nathan and McMahon (1990a, 1990b) applied the original and this modified model to 33 catchments in New South Wales and Victoria and showed that the value of NDC and DPF varied considerably between catchments. Sumner *et al.* (1997) allowed the minimum threshold value before baseflow occurs to vary and showed that this varies quite significantly between catchments, ranging from no minimum water content to over 80 mm on one catchment. In the original formulation of the model, if B<1 then water was assumed to be lost to deep percolation and accumulated in an unrestricted groundwater store, resulting in an open water balance. Sumner *et al.* (1997) commented that in many Australian catchments, deep rooted vegetation draws on such stores. Therefore, an additional conceptual process was added to the model that allowed groundwater storage to contribute to the evaporation process by refilling the non-drainage component of the surface storage at a rate proportional to the deficit in that store. Results presented by researchers using this model have showed good representation of the process for

monthly and annual yield applications.

The *Australian Water Balance Model (AWBM)* is a saturation overland flow model developed by Boughton (1993, 2000a) and Boughton and Carroll (1993). Shown in Figure 7.4, it incorporates an explicit water balance model which uses recorded rainfall and estimates of evaporation to simulate losses and runoff from a catchment area.

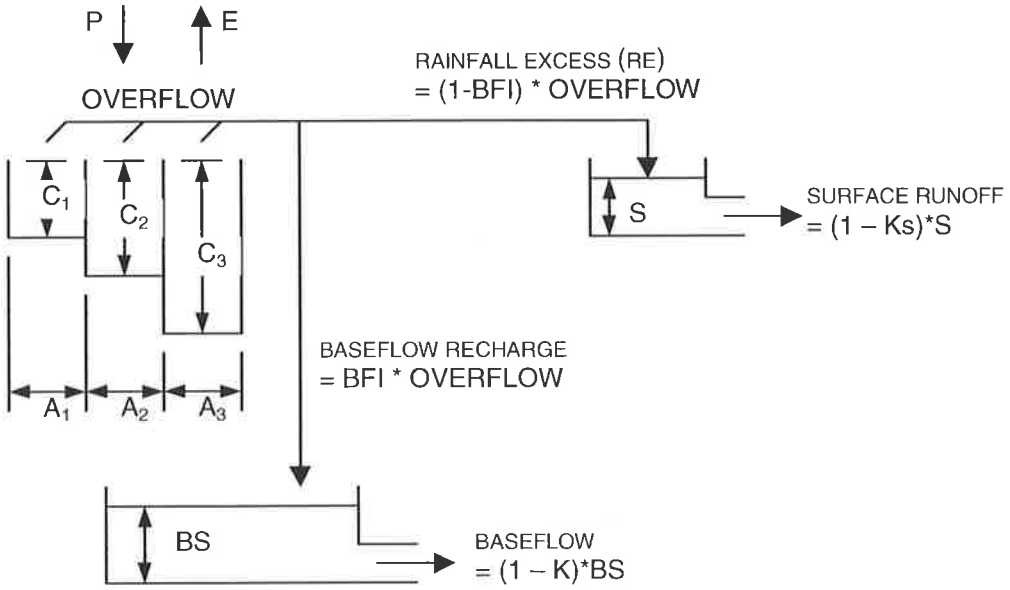

Figure 7.4 The Australian Water Balance Model (AWBM) (adapted from Boughton, 1993).

The AWBM allows for spatial variability of the catchment by using three surface stores. These storage capacities (C1, C2 and C3) represent partial areas of a catchment (A1, A2 and A3), which allows the simulation of partial area runoff. The initial loss from each partial area is therefore dependent on the storage available in each of the surface stores at the commencement of the rainfall event and any evaporation that occurs during the event. The water balance of each surface store is calculated independently of the others. As with the SFB model, rainfall is added and evaporation subtracted from these surface stores. If the value of moisture in the store exceeds the capacity of the store, the moisture in excess of the capacity becomes runoff. Part of the runoff from each store becomes recharge of the baseflow store (if there is a baseflow component in the streamflow) with the remainder becoming rainfall excess. This means that water only infiltrates to the lower soil store when surface runoff occurs, in contrast to the SFB model where infiltration can occur at any time so long as there is sufficient water in the surface store.

A baseflow index (BFI), defined as the ratio of the amount of baseflow to the total amount of streamflow, controls the recharge to the baseflow store. This store volume is then reduced at each time step by the proportion of the water remaining in the store using a baseflow recession constant (K). Surface runoff routing is carried out using a single store with a linear discharge function, similar to the baseflow store. All surface runoff enters the surface routing store with discharge from this store occurring in the same manner as the baseflow store, with a surface runoff recession constant (Ks). This routing simulates the delay of surface runoff reaching the outlet of a medium to large catchment and allows a more meaningful comparison between observed and predicted streamflow values.

While the model was originally developed for both water yield and flood studies, it has quickly become widely accepted for water yield studies (Sharifi and Boyd, 1994; James *et al.*, 1999). Its use in flood studies has progressed much more slowly. More recently it has been applied with some success in a number of flood estimation studies including Boughton and Hill (1997), Boughton *et al.* (1999) and Boughton *et al.* (2000).

MODHYDROLOG (Chiew *et al.*, 1993) is another model that has been applied to Australian catchments. It is a complex conceptual model that incorporates a number of soil stores and flow paths. Chiew and McMahon (1994) showed that a number of model parameters can be related to catchment characteristics. While it is purported to be physically based and produce good results when estimating catchment yield (Chiew *et al.*, 1993), it requires the estimation of 19 parameters. Therefore, its application is restricted to areas with a reasonable length of good quality data. In many Australian locations data is limited and therefore calibration can be difficult. For these reasons and because other models with fewer parameters have been shown to produce reasonable results, it has not been pursued further for use in this study.

7.1.3 Model Choice

The main deficiencies with most previous Australian research examined is that the surface routing stores used have not often allowed successful comparisons between observed and predicted results at a daily time scale, with monthly time scales generally preferred. While this is acceptable for studies involving yield, a smaller time scale is required for it to be used for design flood applications. In addition, many of the published parameters are only suitable for use at monthly time scales as they do not produce the shape and peaks of observed hydrographs when comparisons are made at a daily scale.

Before a choice of model was made for this study, both the AWBM (Boughton, 2000a) and modified SFB model (Sumner *et al.*, 1997) were calibrated to a number of catchments. From these initial results, the AWBM model was found to be the more flexible. With an identified potential for improvement to obtain a suitable relationship between observed and predicted streamflow hydrographs, this model was chosen.

7.2 Development and Calibration of a Catchment Water Balance Model

In this section, the catchment water balance developed for this study and the method used for calibration is described. Following this, the characteristics of the catchments used to calibrate the model are described. One of the major limitations to calibrating each component of the process is the lack of available data and often high levels of missing data within the available records. The methods used to estimate missing values and for confirming data consistency are presented and discussed, along with the results of the water balance model calibration.

7.2.1 The Modified AWBM

A number of modifications were made to the original AWBM. The features of the modified model are shown in Figure 7.5, with the parameters and units defined in Table 7.1. The algorithm developed for this model is contained in Appendix L1.

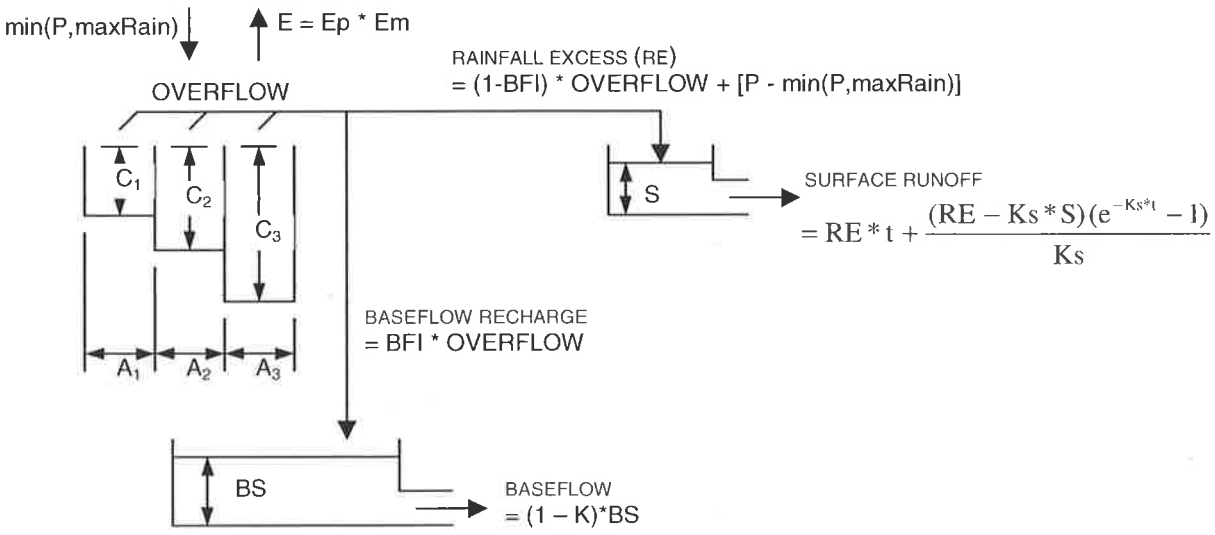

Figure 7.5 The modified AWBM.

Table 7.1 Description of modified AWBM parameters.

Parameter Description	Symbol	Units
Rainfall	P	mm
Capacity of surface store 1	C1	mm
Capacity of surface store 2	C2	mm
Capacity of surface store 3	C3	mm
Partial area of store 1	A1	-
Partial area of store 2	A2	-
Partial area of store 3	A3	-
Evaporation multiplier	Em	-
Actual evaporation	E	mm
Baseflow infiltration index	BFI	-
Surface routing store coefficient	Ks	-
Sub-surface routing store coefficient	K	-
Maximum daily infiltration	maxRain	mm
Current water level in sub-surface store	BS	mm
Current water level in surface routing store	S	mm
Rainfall excess	RE	mm

The original AWBM was modified to explicitly calculate the size of the soil stores and partial areas as opposed to using an average soil store capacity. In previous research a linear store in the same form as that used to determine baseflow has sometimes been incorporated. A linear store is required in order to simulate routing of the surface runoff and allow better comparisons with the observed streamflow. However, this form of representation of the linear store was found to produce poor results because the value of the discharge constant Ks does not always remain small. To improve the representation of the observed hydrograph, in particular the recession immediately following the peak, a different formulation was required. From first principles a function for the operation of the linear store was derived to allow a delay between the occurrence of surface runoff and its appearance as streamflow, which also allowed for fast runoff from small catchments. The full derivation of this equation is contained in Appendix L2 and is defined as:

$$Q = RE * t + (RE - Ks * S)\left(\frac{e^{-Ks*t} - 1}{Ks}\right) \qquad Ks > 0 \qquad (7.3)$$

where :

Q = surface runoff at time period t (mm);

RE = rainfall excess entering the store at time period t (mm);

Ks = recession constant;

S = height of water in the store at the start of time period t; and

t = time step in hours.

Lindsey and Farnsworth (1997) suggested that a limitation of the use of mean monthly values for evaporation is the large day-to-day variance in evaporation during Spring and Autumn. In addition, the seasons may begin early in some years and late in others, causing serious errors in the estimates of evaporation and hence the resulting water balance. Significant variations from the mean monthly values may also occur at any time during the year. For example, during a rainy period in the middle of Summer evaporation may be suppressed by lower temperatures and high humidity, or alternatively, hot and dry periods may cause the evaporation to be very high during some years. Both of these situations can cause significant deviations from the daily average evaporation values for a month (Lindsey and Farnsworth, 1997). To accommodate these deviations, the AWBM was modified to accommodate inputs of daily evaporation, as opposed to a monthly average, using either pan evaporation or potential evaporation (refer Chapter 6).

In the SFB model a wilting point is specified and potential evaporation can be converted to actual evaporation using Equation 6.1. However, as groundwater recharge in the AWBM can not occur from the soil stores directly, there is no requirement to calculate actual evaporation by this equation. This means that the actual value of evaporation (E) is not reduced when there is moisture stress. To accommodate some reduction, an evaporation multiplier (Em) was used to convert both the pan or potential evaporation to actual evaporation. If the reduction of evaporation during moisture stress is identified as being important at particular sites, then the model could be modified to incorporate this process. However, the use of Em in this study was considered satisfactory.

It was identified that during the simulation of some large events (high rainfall and runoff) a large amount of the rainfall entered the soil stores and not enough runoff was taking place. To address this problem a maximum rainfall depth ($maxRain$) was used such that any daily rainfall above this amount moved directly into the surface store and was not able to contribute to baseflow. The use of this parameter was based on the concept of infiltration curves (Chow *et al.*, 1988) where a given soil has a maximum or potential infiltration depth and was defined as:

$$maxRain = (1-BFI)*Overflow+[P-\min(P,maxRain)] \qquad (7.4)$$

where :

BFI = baseflow infiltration index;

Overflow = rainfall depth in excess of available depth within surface stores during period *t* (mm); and

P = rainfall during time period *t* (mm).

Although the use of this parameter provides a very simplified implementation of the infiltration curve concept, it did allow a better representation of some of the higher runoff events.

7.2.2 Description of Study Catchments

Many of alternative design flood estimation techniques developed recently in Australia have been tested on Victorian and some New South Wales catchments. This study sought to test the approach on a number of catchments in different states with varying conditions. Six catchments were chosen, two in Victoria to allow reference with previous studies and one each in South Australia, Queensland, Tasmania and New South Wales. Figure 7.6 shows the location of each of these catchments.

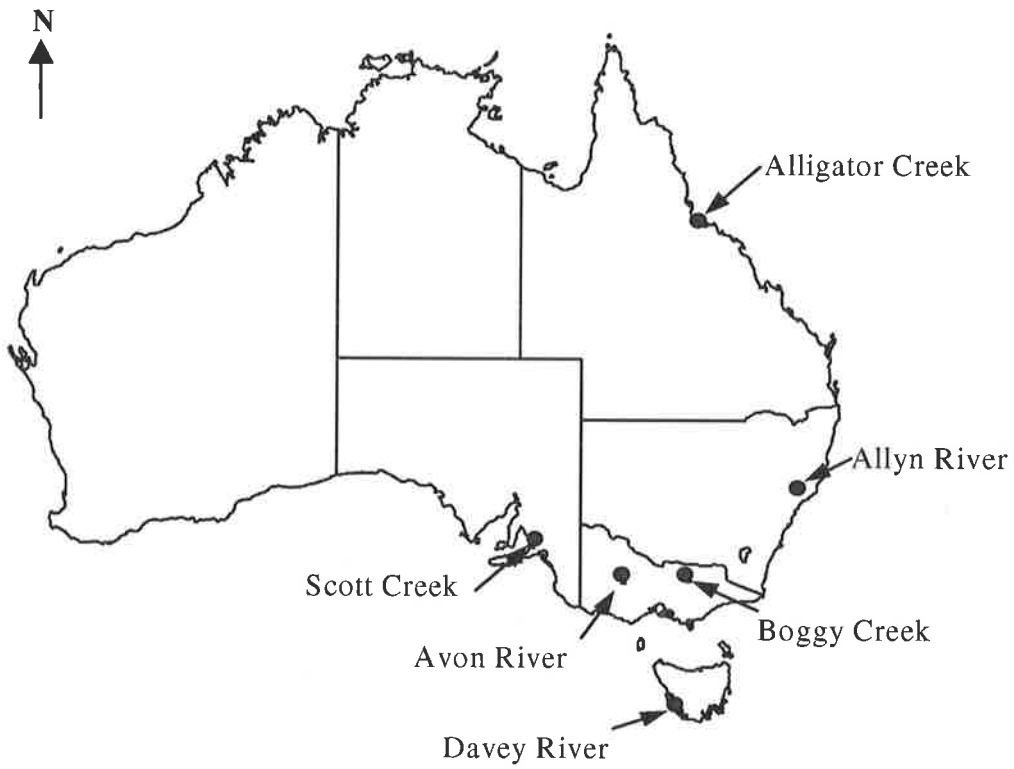

Figure 7.6 Location of study catchments.

Alligator Creek, Queensland

Alligator Creek enters Cleveland Bay approximately 10 km south-east of Townsville in northern Queensland. The catchment draining to the streamflow gauging site at Allendale, station number 118106, is 69 km^2 and consists primarily of national park where the average height of native vegetation is 15 m. The climate is tropical with distinct wet and dry seasons with most rainfall occurring in the summer months and evaporation is high throughout the year. The topography ranges from 1 200 m in the steep hills at the top of the catchment to 10 m in the slight slopes near the gauging station. The average annual rainfall is 1 135 mm and the average annual runoff is 480 mm.

Allyn River, New South Wales

The Allyn River catchment is a sub-catchment of the Lower Hunter River, joining the Patterson River before entering north of Newcastle in New South Wales. A large portion of the upper catchment is in State Forest and National Park, and is heavily timbered. The remainder is open forest, cleared grazing land and some arable land close to the river. Elevation ranges from 1 500 m at the Barrington tops in the northern part of the catchment to 250 m at the gauging station at Halton, station number 210022. Rainfall largely occurs during Summer and large orographic effects over the catchment controls the distribution of rainfall, with heavier rainfall occurring at higher elevations. Summers are warm and winters cool to cold with an occasional snow fall. The catchment has an area of 205 km^2, average annual rainfall of 1 440 mm and average annual runoff of 350 mm.

Avon River, Victoria

The Avon River catchment is a sub-catchment of the Wimmera Basin and is located in south-western Victoria. It is a mainly rural catchment with grazing and timber the major land uses. The climate of the catchment is temperate with high evaporation in Summer. Annual rainfall is relatively low and occurs mainly between late Autumn and early Spring. The topography ranges from hills of moderate relief to open plains in the lower reaches. Catchment elevation ranges from 500 m in the top of the catchment to 220 m at the streamflow gauging at Beazleys Bridge, station number 415224. The catchment has an area of 259 km^2, average annual rainfall of 566 mm and an average runoff of 52 mm.

Boggy Creek, Victoria

The Boggy Creek catchment is a sub-catchment of the Ovens River and is located in north-eastern Victoria. It is a mainly rural area with state forests occupying a large portion of the catchment. The climate is temperate with high evaporation during the summer months with the majority of the annual rainfall occurring from late autumn to early spring. The topography ranges from steep hills in the west and east, grading to undulating slopes around the creek itself. Catchment elevation ranges from 900 m at the top of the catchment to 190 m at the streamflow gauging station at Angleside, station number 403226. The catchment has an area of 108 km^2, average annual rainfall of 1 100 mm and average annual runoff of 290 mm.

Davey River, Tasmania

The Davey River catchment is located in the Southwest National Park in Tasmania, flowing into Payne Bay at Port Davey approximately 125 km south west of Hobart. The catchment draining to the streamflow gauging site downstream of Crossing River, station number 307001, is 686 km^2 and the topography contains steep hills and ranges. Catchment elevation ranges from 1 100 m in the upper reaches of the catchment, to 250 m at the gauging station. The climate is temperate with most rainfall occurring during cool to cold Winters. The catchment has an average annual rainfall of 2 730 mm and average annual runoff of 2 000 mm.

Scott Creek, South Australia

The Scott Creek catchment is a sub-catchment of the Onkaparinga River and is located in the Mount Lofty Ranges approximately 25km south-east of Adelaide. It is a mainly rural catchment with native vegetation and grazing the major land use. The climate of the catchment is typically temperate with high maximum daily temperatures and high evaporation in summer. Rainfall is seasonal, occurring mainly in Winter and Spring. The topography ranges from steep to rolling hills in the west and east, grading to undulating slopes around the creek itself. Catchment elevation ranges from 500 m at the top of the catchment to 220 m at the streamflow gauging station at Scott Bottom, station number 503502. The catchment has an area of 26.7 km^2, average annual rainfall of 992 mm and average annual runoff of 150 mm.

7.2.3 Available Data

The lack of data availability at time scales of less than a day for all inputs, generally precludes

calibration at sub-daily time scales. As such, calibration was undertaken at a daily time scale.

Streamflow

There were varying lengths of daily streamflow data available for each of the catchments, as described in Table 7.2. These records were of good quality and very little data were missing. Full details of the location of each gauging station is contained in Appendix M.

Table 7.2 Available data for each of the study catchments.

Catchment	Years of data at streamflow gauging	Missing (%)
Alligator Creek[1]	24	-
Allyn River[2]	10	0.8
Avon River[3]	14	-
Boggy Creek[3]	17	-
Davey River[2]	17	2.0
Scott Creek[4]	24	-

Data Source: [1] Queensland Department for Natural Resources; [2] Chiew and McMahon (1993a); [3] Boughton (2000a); [4] South Australian Department for Water Resources.

Rainfall

For each of the catchments, the spatial representation of daily rainfall was considered. In each case a number of sites were required to adequately represent this spatial variability. Table 7.3 shows the proportion of each station used to calculate the catchment average rainfall and Appendix M contains details of the location of each gauge, the quality of each data set and the proportions accumulated or missing.

Table 7.3 Contribution of rainfall stations to catchment average rainfall for each catchment.

Catchment	Contributing Rainfall Gauge(s)	Proportions
Alligator Creek	032040[1]	0.10[3]
	033028	0.90
Allyn River	complied dataset[2]	-
Avon River	079086[1]	0.40[4]
	079079	0.60
Boggy Creek	082032[1]	0.17[5]
	082033	0.47
	083031	0.13
	083032	0.23
Davey River	complied dataset[2]	-
Scott Creek	023709[1]	0.44[3]
	023727	0.41
	023734	0.15

Data Source: [1] Bureau of Meteorology; [2] Chiew and McMahon (1993a).
Proportions: [3] Chiew and McMahon (1993a); [4] Mein *et al.* (1995); [5] Hill *et al.* (1996a).

The exceptions were the Allyn and Davey River catchments where catchment average rainfall was obtained directly and rainfall factors of 1.3 and 1.2 were applied to the catchment average rainfall at these locations respectively, to account for rainfall gradients as described in Sumner *et al.* (1997).

Evaporation

Examination of pan evaporation stations for each catchment showed that estimates of daily evaporation were available at all but the Allyn and Davey River catchments. For these sites, daily potential evaporation was calculated by the method described in Chapter 6, using records of temperature and sunshine hours. All data was obtained from the Bureau of Meteorology. Appendix M contains details of the location of each record, the quality of each data set and the proportions accumulated or missing.

7.2.4 Estimation of Missing Data

The majority of data sources contain missing segments. Missing data in daily rainfall and pan evaporation records may occur in two forms: when a value has not been recorded on a particular day but the cumulative total has been recorded on a subsequent day; or where the data is missing due to a recording error.

The first type are referred to as accumulated records and may be disaggregated over the total number of days missing data using proportions from a nearby site. In this study, the choice of site was made by developing a linear relationship between the data from the station in question with nearby sites and using the neighbouring site that was best able to reproduce records for the days when data was not available. This assessment was carried out by examining the coefficient of determination (R^2) and the coefficient of efficiency (E).

The coefficient of determination is the square of the Pearson's product moment correlation coefficient and describes the proportion of the total variance in the observed data that can be explained by the model, in this case, the linear relationship described above. R^2 is defined (Legates and McCabe, 1999) as:

$$R^2 = \left\{ \frac{\sum_{i=1}^{N} (O_i - \overline{O})(P_i - \overline{P})}{\left[\sum_{i=1}^{N} (O_i - \overline{O})^2\right]^{0.5} \left[\sum_{i=1}^{N} (P_i - \overline{P})^2\right]^{0.5}} \right\}^2 \qquad (7.5)$$

where:

O_i = ith observed data point;

$\overline{O}$ = mean of the observed data;

P_i = ith observed data point; and

$\overline{P}$ = mean of the predicted data.

The value of R^2 ranges from 0.0 to 1.0 with values close to 1.0 indicating better correlation.

While a high value of R^2 only indicates high correlation it does not necessarily mean that the predicted values are equal to the observed values. For this reason the coefficient of efficiency is often considered a better comparison tool because it is sensitive to differences in the observed and predicted means and variances. This is defined (Legates and McCabe, 1999) as:

$$E = 1.0 - \frac{\sum_{i=1}^{N}(O_i - P_i)^2}{\sum_{i=1}^{N}(O_i - \overline{O})^2} \tag{7.6}$$

E ranges from minus infinity to 1.0, with values close to 1.0 again indicating a good approximation of the observed data by the model. A value of E less than zero indicates that $\overline{O}$ is a better predictor than P_i (Legates and McCabe, 1999).

For rainfall data that is completely missing due to instrument failure or another record generating fault, a number of methods have been developed to calculate the missing values.

The *station-average* method uses nearby gauges to estimate the missing point rainfall ($\hat{P}$) on a given day at the gauge of interest using (McCuen, 1998):

$$\hat{P} = \frac{1}{n}\sum_{i=1}^{n} P_i \tag{7.7}$$

where:

P_i = rainfall at gauge i.

While this is a simple method it may not be accurate when the total annual rainfall at any of the n regional gauges differs from the annual rainfall at the gauge of interest by more than

10% (McCuen, 1998).

The *normal-ratio method* uses the annual average rainfall of n regional gauges to derive weights to calculate the rainfall on a particular day at the gauge of interest using (McCuen, 1998):

$$\hat{P} = \sum_{i=1}^{n} \omega_i P_i \tag{7.8}$$

where:

$\omega_i = \frac{A_x}{nA_i}$;

A_x = average annual rainfall at the station of interest; and

A_i = average annual rainfall at gauge i.

If differences between the average annual rainfall at the gauges are larger than 10% then this method is preferred (McCuen, 1998). Chiew and McMahon (1993a) have used this method to infill missing records for a number of Australian sites.

The *quadrant method* takes into account the closeness of other regional gauges to the gauge of interest when calculating missing rainfall. The method assumes that the rainfall at gauges located close to each other are not independent of the rainfall at the unknown point. Weights are assigned to each gauge, which decrease as the distance from the gauge in question increases. To estimate the rainfall on a given day, the region surrounding the site is divided into four quadrants. The gauge in each quadrant that is closest to the gauge of interest is used to ensure that the gauges used to estimate the missing rainfall are independent (McCuen, 1998). For each quadrant that contains a gauge, the weight for each gauge is given (McCuen, 1998) by:

$$\omega_i = \frac{1}{d_i^2 \sum_{j=1}^{4} \frac{1}{d_j^2}} \tag{7.9}$$

where:

d_i = distance between gauge i and the gauge of interest.

A difficulty with the use of the data available for this study was that there were limited nearby

sites that could be used to infill a missing record. In addition, many of these sites also had large quantities of missing or accumulated data, making the use of the above methods difficult. As such, an alternative method was used that involved establishing a linear relationship between the site with missing data and a nearby site, similar to that for estimating missing temperature records in Section 6.5. If more than one neighbouring site was available then the site with the better correlation values of R^2 and E was used. Often, more than one site was used to complete the record of interest because of large quantities of missing data from the neighbouring sites. Missing values of pan evaporation were also calculated using this method. Missing values in records of sunshine hours were calculated using cloud cover data as described in Section 6.5.

Results for Study Sites

The correlation between the rainfall gauges with a missing or accumulated record and those used to calculate the missing values or distribute the record over a period was generally good for all sites and catchments. Figure 7.7 shows the relationship between sites in the Avon River catchment and Figure 7.8 between sites in the Boggy Creek catchment. In both cases, the description of the relationship between the sites as linear was considered satisfactory. Figure 7.9 suggests that the relationship between the two sites in the Alligator Creek catchment was not as good as for other sites. However, in this case, there was very little missing data from this site, with mainly accumulated data, so the relationship was considered acceptable.

The correlation between pan evaporation stations was generally lower than for the rainfall stations, although satisfactory relationships were obtained. Figure 7.10 to Figure 7.12 show these relationships for stations representing evaporation for the Avon River, Boggy Creek and Scott Creek catchments.

Appendix M contains location details of the reference sites used for each of the rainfall and evaporation gauges within the study catchments and the relationships developed to de-accumulate or calculate this missing data. The regression relationships developed for the temperature and sunshine hours data to allow the subsequent generation of potential evaporation are also shown.

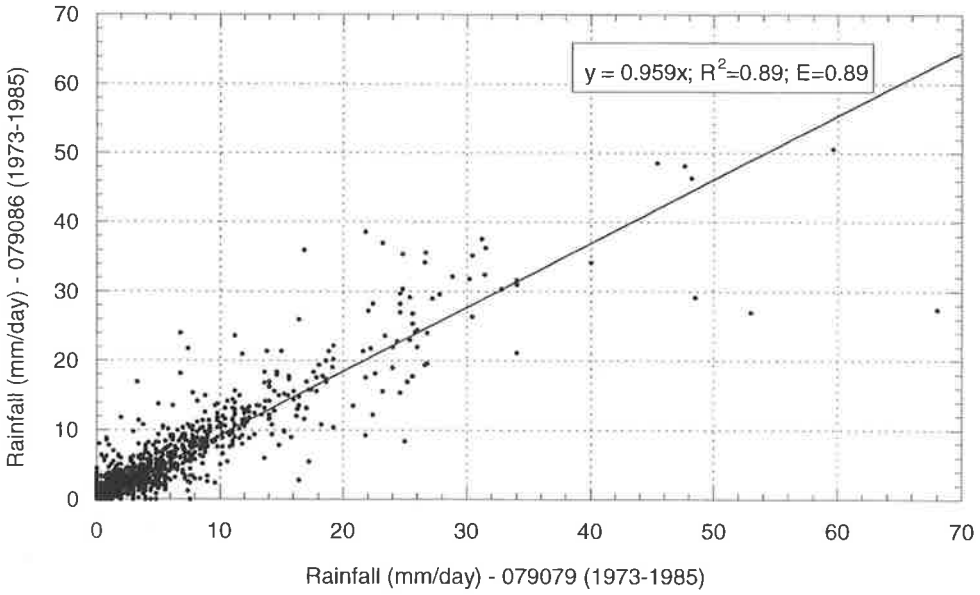

Figure 7.7 Avon River catchment: linear relationship between rainfall data from Tottington (079079) and Supple (079086).

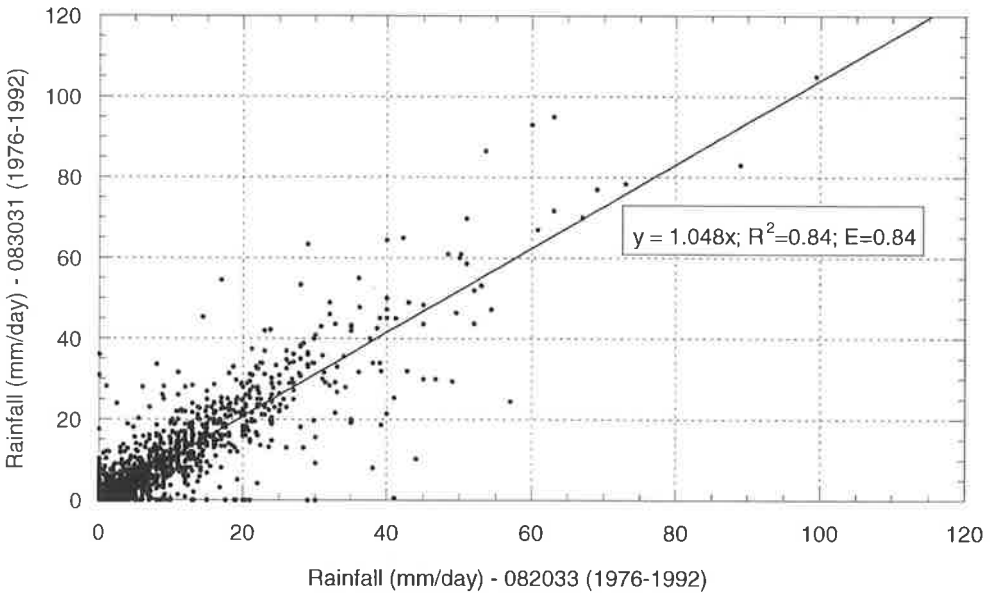

Figure 7.8 Boggy Creek catchment: linear relationship between rainfall data from sites Myrrhee (082033) and Whitfield (083031).

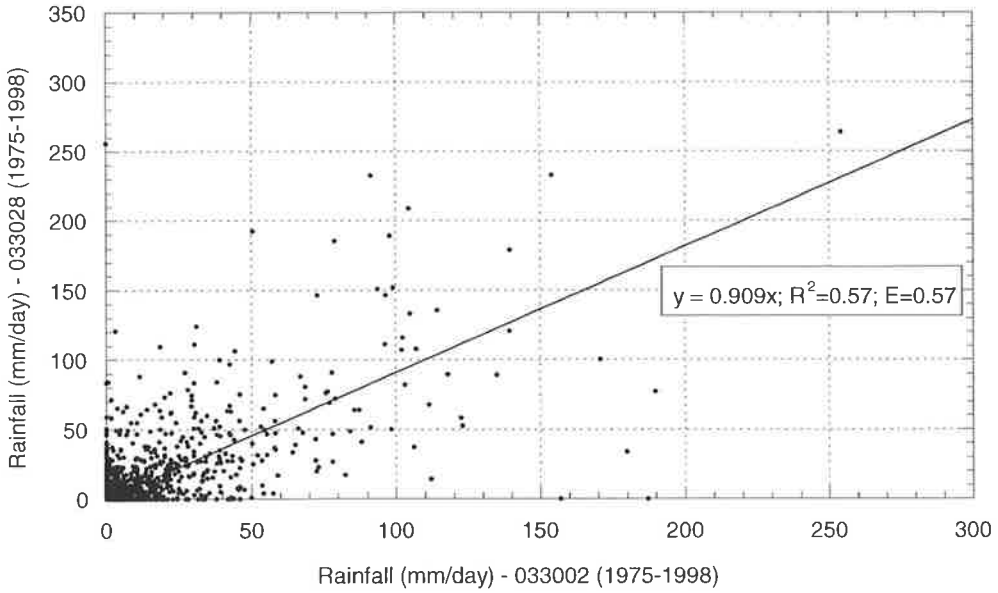

Figure 7.9 Alligator Creek catchment: linear relationship between rainfall data from sites Ayr Research Station (033002) and Giru Post Office (033028).

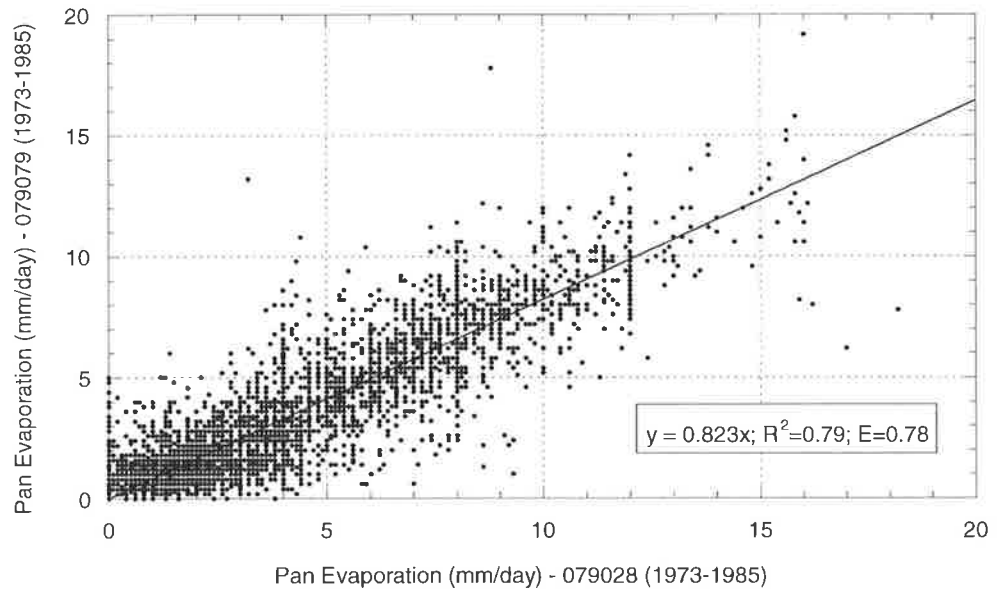

Figure 7.10 Avon River catchment: linear relationship between pan evaporation data from sites Longerenong (079028) and Tottington (079079).

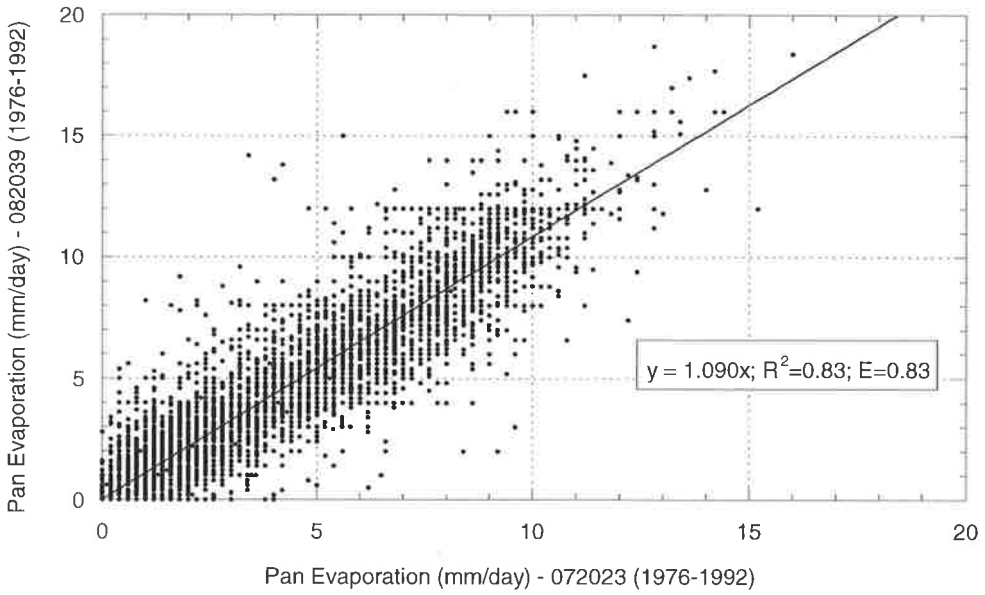

Figure 7.11 Boggy Creek catchment: linear relationship between pan evaporation data from sites Hume Reservoir (072023) and Rutherglen (082039).

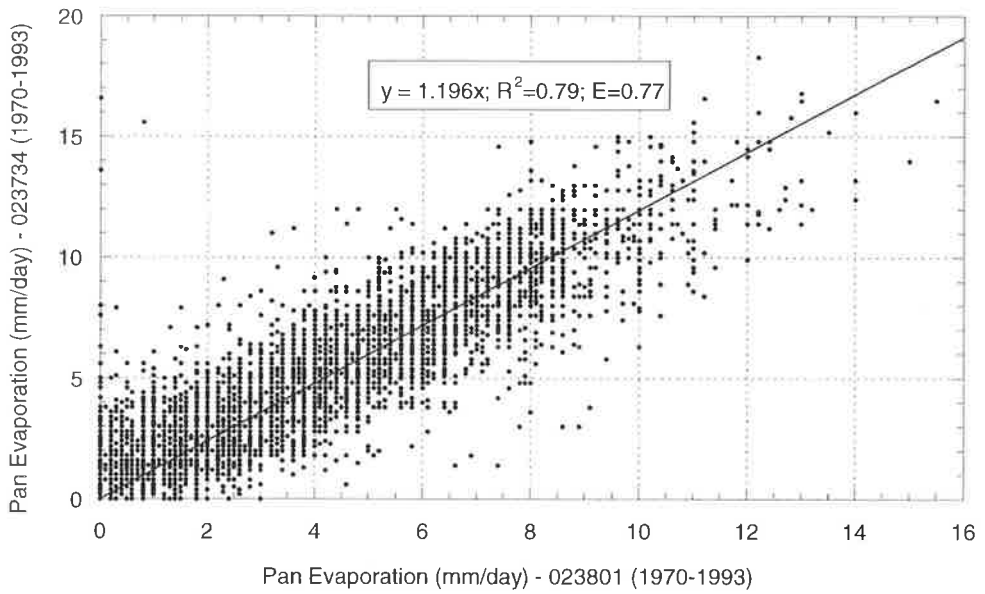

Figure 7.12 Scott Creek catchment: linear relationship between pan evaporation data from sites Lenswood Research Centre (023801) and Mount Bold Reservoir (023734).

7.2.5 Data Consistency

To identify the occurrence, magnitude and nature of trends within long time series records the double mass curve technique (Grayson *et al.*, 1996) is often used. It is constructed by plotting the accumulated values of two time series against each other. A break in slope or a gradual change in curvature will reveal a change in the constant proportionality between the two sets of data. This indicates the presence of a trend such as changes in measured rainfall due to the growth of obstructive vegetation at a site. Grayson *et al.* (1996) suggests that a double mass curve is only useful if the two variables being accumulated are proportional and that at least one of the data sets is stationary over the period examined. The method is often used to establish the presence of changes within rainfall or evaporation records and adjustments can subsequently be made to affected data sets to ensure consistency of record.

In this study the consistency of each rainfall and evaporation record was confirmed by constructing a double mass curve with a neighbouring site. Figure 7.13 and Figure 7.14 show this curve with a fitted linear relationship for rainfall stations used for the Alligator Creek and Scott Creek catchments respectively. Figure 7.15 and Figure 7.16 show similar results for evaporation stations for the same study catchments. Appendix M contains the results from the period of record examined.

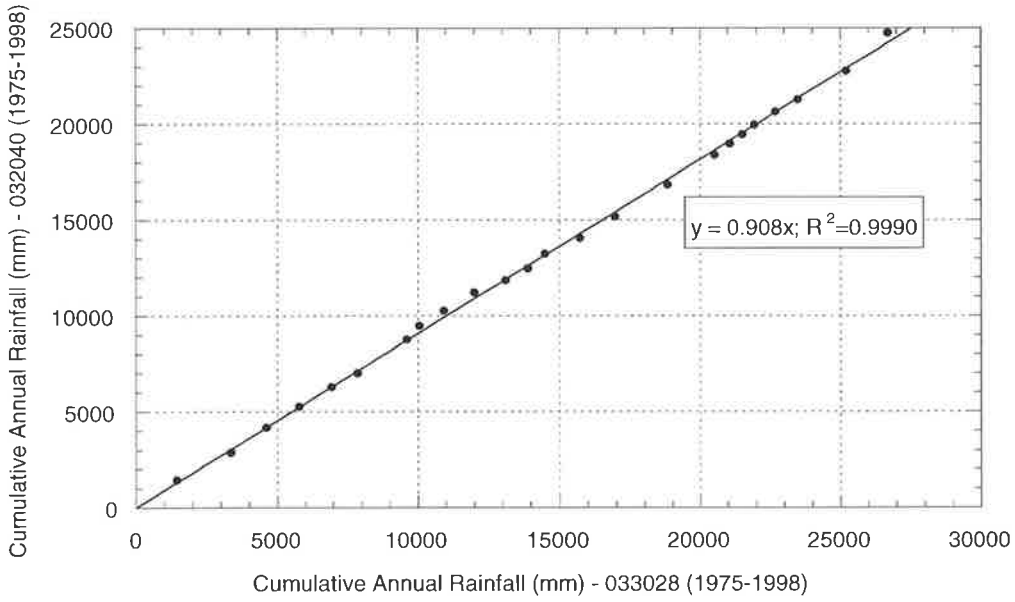

Figure 7.13 Alligator Creek catchment: double mass curve analysis between rainfall data for sites Giru Post Office (033028) and Townsville Airport (032040).

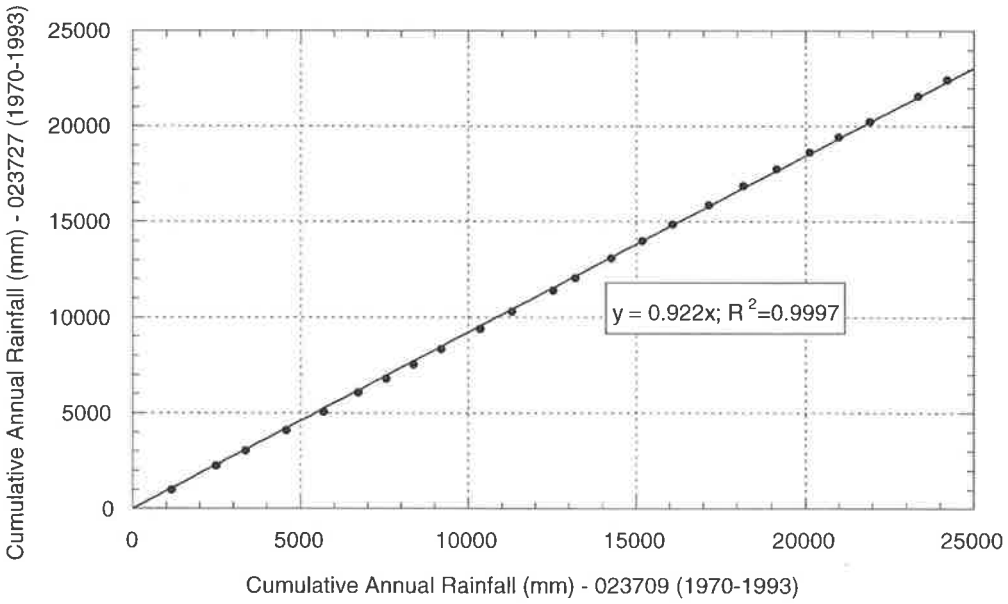

Figure 7.14 Scott Creek catchment: double mass curve analysis between rainfall data from sites Cherry Gardens (023709) and Longwood (023727).

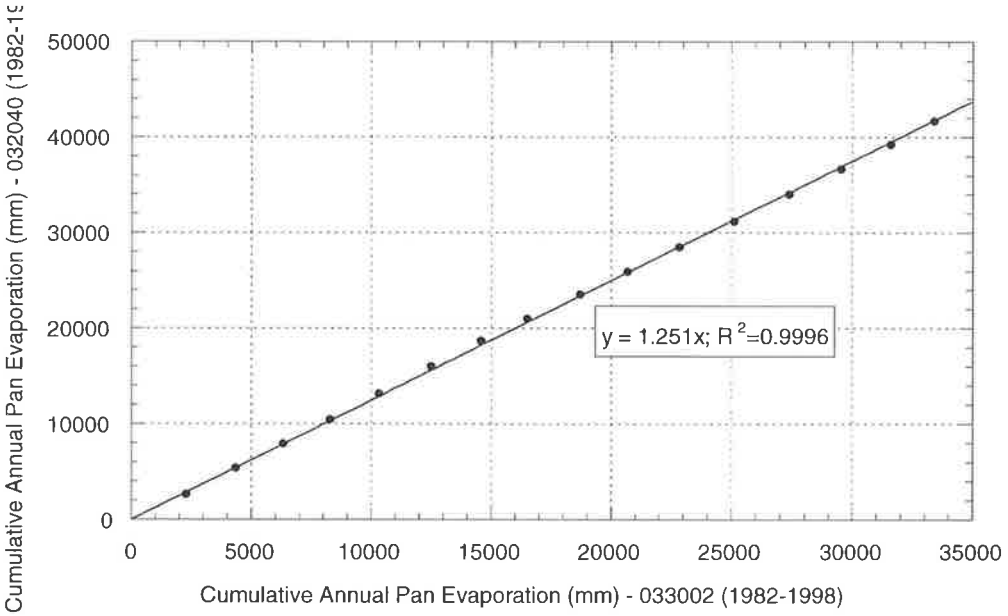

Figure 7.15 Alligator Creek catchment: double mass curve analysis between pan evaporation data from sites Ayr Research Station (033002) and Townsville Airport (032040).

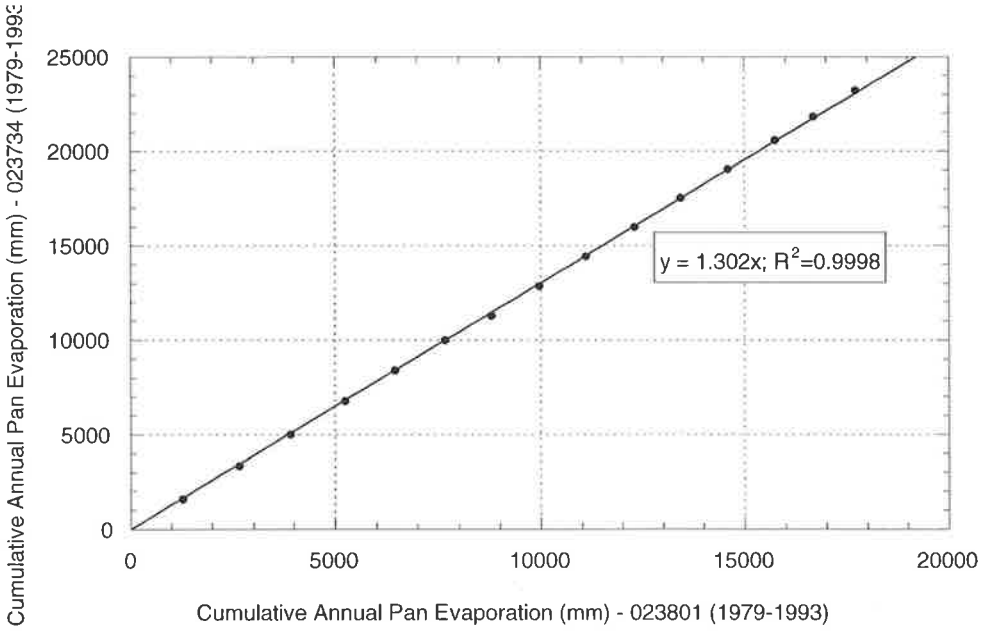

Figure 7.16 Scott Creek catchment: double mass curve between pan evaporation data from sites Lenswood Research Centre (023801) and Mount Bold Reservoir (023734).

7.2.6 Calibration Method and Error Model

Calibration of the modified AWBM was carried out using the SCE algorithm (refer Section 3.4.8) in the NLFIT program (Kuczera, 1994a). NLFIT is a Bayesian non-linear regression program (Kuczera, 1983a, 1983b) to which specific model algorithms can be added and subsequently calibrated. The daily runoff values and the maximum daily runoff values in each month were simultaneously calibrated. The latter is often undertaken when comparisons of total monthly flows are carried out (Boughton and Hill, 1997; Boughton *et al.*, 1999) to ensure maximum daily flows are represented. It was used in this study to provide a second validity check for the model.

The *least squares error model* is widely used to describe errors in conceptual rainfall runoff models. A consequence of this error model is that model parameters are calibrated by searching the parameters which minimise the sum of squares of the residuals (Kuczera, 1994a; Sumner *et al.*, 1997), the residual being the difference between the observed and predicted data. In this case there are two responses and the relationship between the observed and predicted data was defined (Kuczera, 1994a) as:

$$Q_i^d = \hat{Q}_i^d + \varepsilon_i^d \qquad i=1,\cdots,n \qquad (7.10a)$$

$$Q_j^m = \hat{Q}_j^m + \varepsilon_j^m \qquad j=1,\cdots,m \qquad (7.10b)$$

where :

Q_i^d = observed daily runoff on day i;

$\hat{Q}_i^d$ = predicted daily runoff on day i;

ε_i^d = residual or random error in daily runoff on day i;

n = number of observations in the daily runoff response;

Q_j^m = observed daily runoff in month j;

$\hat{Q}_j^m$ = predicted daily runoff in month j;

ε_j^m = residual or random error in daily runoff of month j; and

m = number of observations in the maximum daily runoff in each month response.

The residuals are estimates of ε (Kuczera, 1994a). The least squares model assumes that the expected value of ε is zero, the variance of ε is constant and that the residuals are statistically independent. There are a number of diagnostic methods to check these assumptions including:

(a) predicted response versus standardised residual plot; and

(b) residual auto-correlation plot.

If the least squares model is adequate, the points of each predicted response versus standardised residual plot should appear to be normally scattered and contained largely within a parallel band (Kuczera, 1994a). An auto-correlation plot displays the time dependence between residuals. If most of the auto-correlation at various lag times lies within the 95% confidence limits for white noise the assumption that the residuals are statistically independent can be confirmed (Kuczera, 1994a). In order to ensure that both responses considered here were concurrent, the method used to define the maximum daily runoff values in each month data meant that there was no correlation between the residuals. Therefore, only the auto-correlation between the residuals of the daily runoff response was considered.

If the residual versus predicted response relationship does not display randomly scattered behaviour, a Box-Cox transformation (Box and Cox, 1964) can be used to stabilise the variance of the residuals to produce a more satisfactory pattern. The general Box-Cox transformation of an observed response is defined as:

$$q_i = \frac{(Q_i + K)^{\lambda} - 1}{\lambda} \qquad \lambda \neq 0 \qquad (7.11)$$

where :

λ, K = transformation parameters; and

q_i = transformed response at time *i*.

The predicted response is transformed using the same transformation, which produces a transformed residual at time *i* defined as $q_i - \hat{q}_i$. When λ=1 the transformation is linear and has no effect on the response data. As λ is reduced below 1, the transformation tends to decrease the scatter of residuals for large predicted responses and increase the scatter for small predicted responses (Kuczera, 1994a). The residual variance can be approximately stabilised by trial and error and two values of λ (λ_1, λ_2), one for each response, were chosen here.

An auto-regressive (*AR*) model can be applied to the residuals to remove any time dependence and ensure that the auto-correlation between residuals lies within the 95% confidence limits for white noise. A general *AR* model with *p* parameters and the transformed residual at time *i*, is defined (Kuczera, 1994a) as:

$$q_i - \hat{q}_i = \phi_1 (q_{i-1} - \hat{q}_{i-1}) + \cdots + \phi_p (q_{i-p} - \hat{q}_{i-p}) + \varepsilon_i \qquad (7.12)$$

where :

$\phi_1, \cdots, \phi_p$ = auto-regressive parameters for an $AR(p)$ model; and

ε_i = random independent disturbance at time *i*.

In order to simultaneously calibrate the daily runoff values and the maximum daily runoff values in each month, the error model was generalised. This generalisation is done within NLFIT using a generalised least squares approach. In the context of this application the generalised least squares is implemented by dividing for each response the sum of the squares of the disturbances ε_τ by an estimate of the disturbance variance, thereby standardising or nondimensionalising the disturbances. It is then meaningful to add these standardised sum-of-squares terms together to form a joint objective function.

7.2.7 Calibration Results

The calibration of the modified AWBM was undertaken using the complete sets of rainfall

and evaporation for each catchment. The fitted model parameters and initial conditions for each of the soil stores are shown in Table 7.4. An initialisation period of three months was used to remove the effects of initial store conditions on the parameter estimates. The appropriateness of the calibrated parameters was assessed by comparing the values predicted by the model against the observed daily runoff.

Table 7.4 Calibrated parameter values and initial conditions for study catchments.

Model Parameter Values						
	Alligator Creek	Allyn River	Avon River	Boggy Creek	Davey River	Scott Creek
C1 (mm)	28.9	49.5	17.7	9.9	5.4	17.4
C2 (mm)	189.2	126.4	94.5	180.5	173.7	206.6
C3 (mm)	357.1	223.7	173.4	405.9	434.0	520.8
A1	0.177	0.282	0.075	0.084	0.746	0.108
A2	0.568	0.335	0.676	0.485	0.134	0.464
A3	0.255	0.383	0.249	0.431	0.120	0.428
Em	0.58	1.35	0.997	0.70	1.26	0.93
BFI	0.34	0.39	0.18	0.40	0.70	0.37
Ks	6.10	2.44	1.17	0.35	1.93	2.20
K	0.52	0.21	0.999	0.98	0.540	0.95
maxRain (mm)	148.6	133.2	200.0	95.1	78.4	59.6
Initial Conditions						
Initial C1 (mm)	10	0	0	7.5	0	0
Initial C2 (mm)	100	50	50	100	20	50
Initial C3 (mm)	200	100	100	200	150	100
Initial BS (mm)	0	0	0	0	0	0
Initial S (mm)	0	0	0	0	0	0

Figure 7.17 and Figure 7.18 show these for Alligator Creek, Figure 7.19 and Figure 7.20 for Allyn River and Figure 7.21 and Figure 7.22 for Avon River. The observed rainfall is also shown and this indicates numerous events that did not produce a runoff response. This type of pattern often makes the water balance of the catchment more difficult to model and on occasions, small events such as in Figure 7.18 and Figure 7.22, are not reproduced by the model. However, the reproduction of the runoff traces for these sites is considered satisfactory.

Figure 7.23 and Figure 7.24 show the observed and predicted daily runoff for Boggy Creek Similarly, Figure 7.25 and Figure 7.26 shows these comparisons for Davey River and Figure 7.27 and Figure 7.28 for Scott Creek respectively. The reproduction of the observed runoff is very good for these sites. Boggy Creek and Scott Creek each produce a runoff response to almost all rainfall events and there is observable streamflow for most of the year, unlike

Alligator Creek and Avon River where the streams are dry for much of the year. Davey River has observable streamflow throughout the year and responses to each rainfall event.

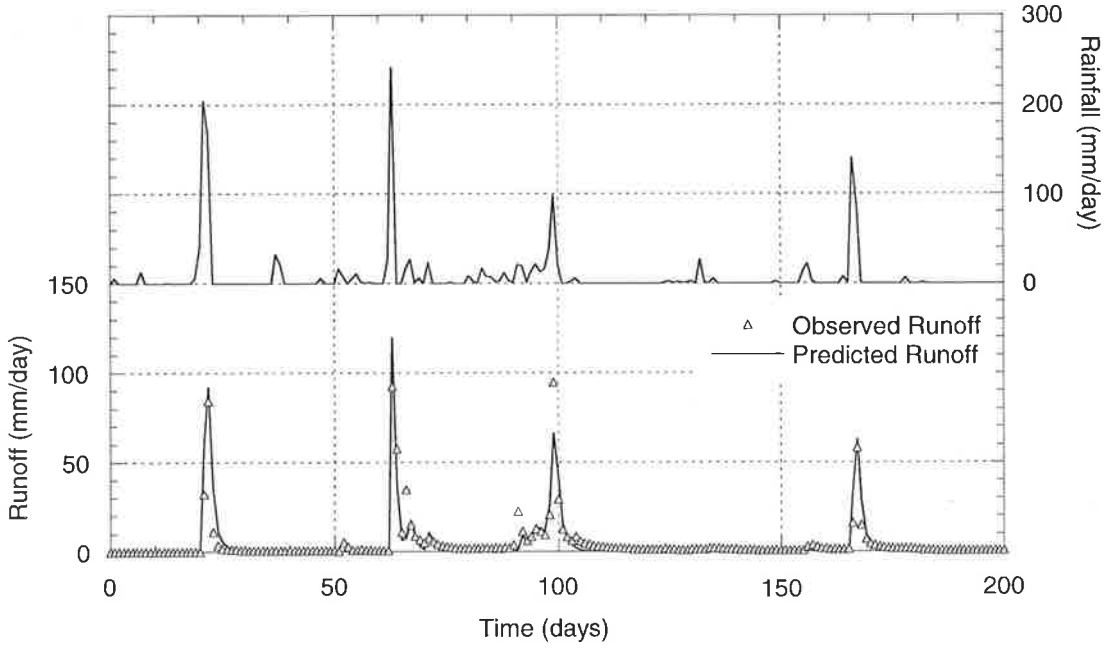

Figure 7.17 Alligator Creek: Observed and predicted runoff - 30/11/1976 to 18/6/1977 ($\lambda_1 = 0.95$; AR(1) = 0.30; AR(2) = 0.05; $\lambda_2 = 0.95$).

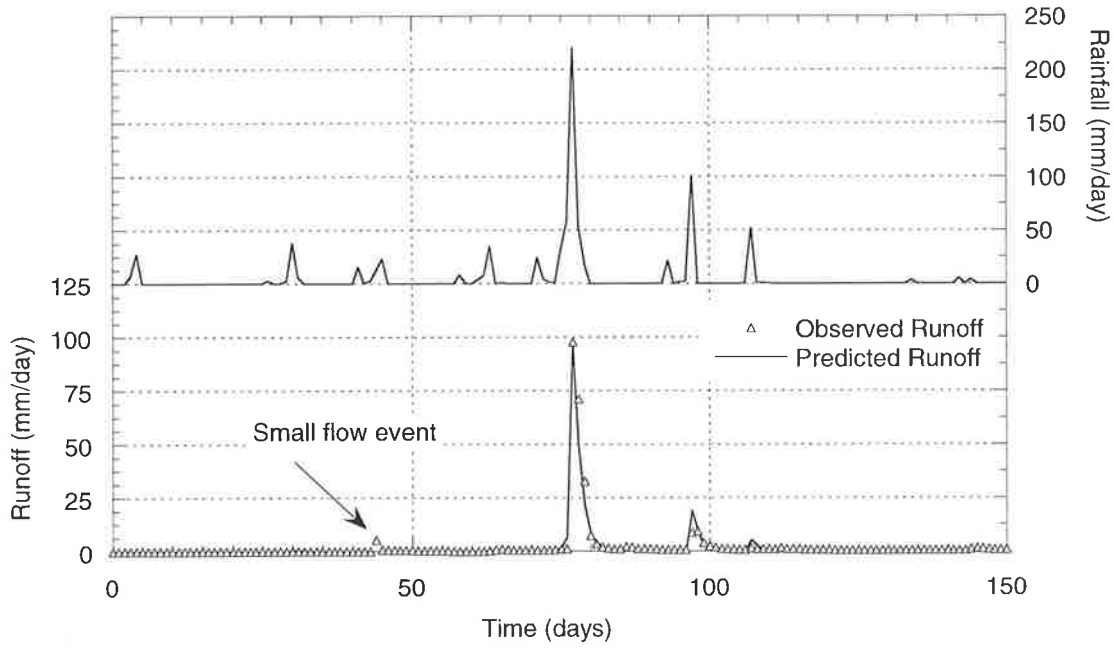

Figure 7.18 Alligator Creek: Observed and predicted runoff - 22/10/1995 to 20/3/1996 ($\lambda_1 = 0.95$; AR(1) = 0.30; AR(2) = 0.05; $\lambda_2 = 0.95$).

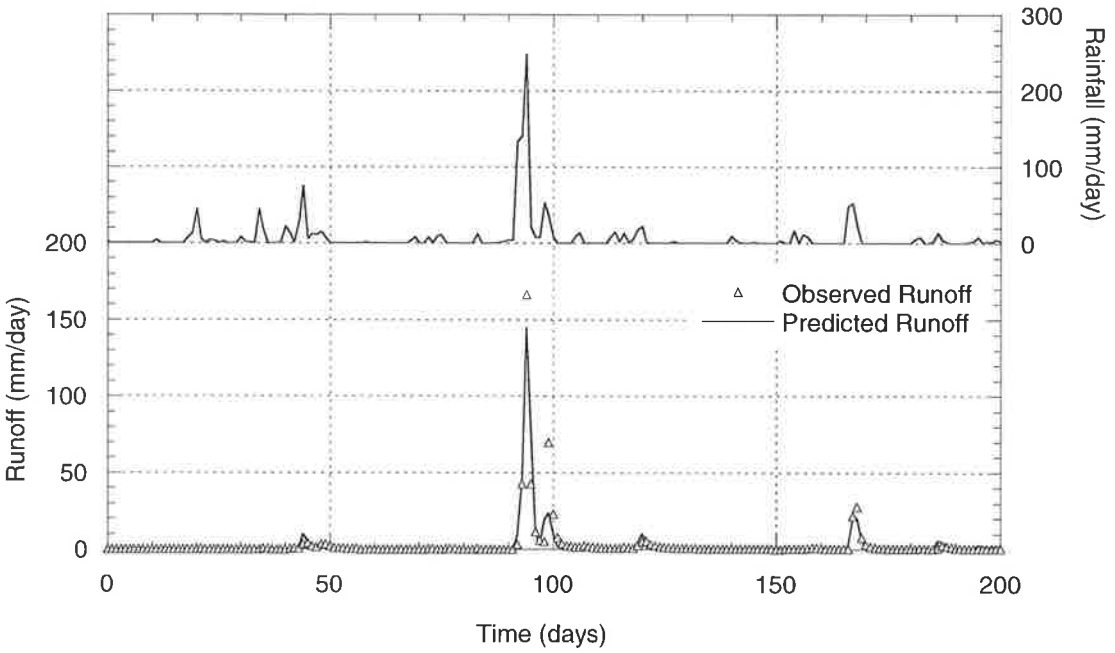

Figure 7.19 Allyn River: Observed and predicted runoff - 16/12/1977 to 4/7/1978 (λ_1 = 0.80; AR(1) = 0.20; AR(2) = 0.10; λ_2 = 1.00).

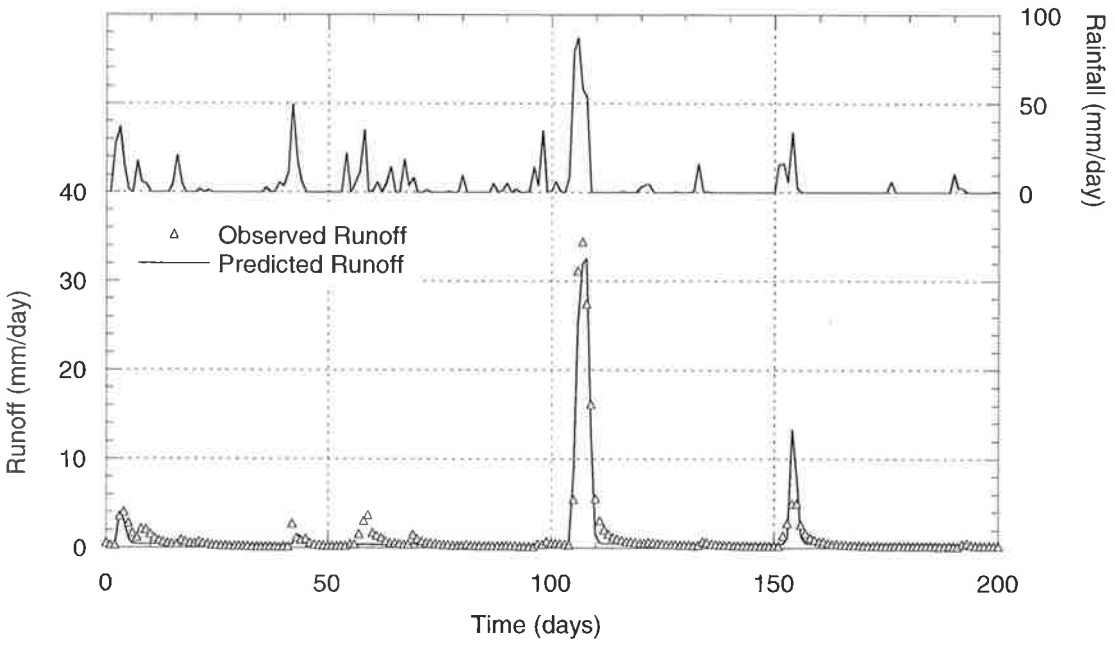

Figure 7.20 Allyn River: Observed and predicted runoff - 20/1/1979 to 8/8/1979 (λ_1 = 0.80; AR(1) = 0.20; AR(2) = 0.10; λ_2 = 1.00).

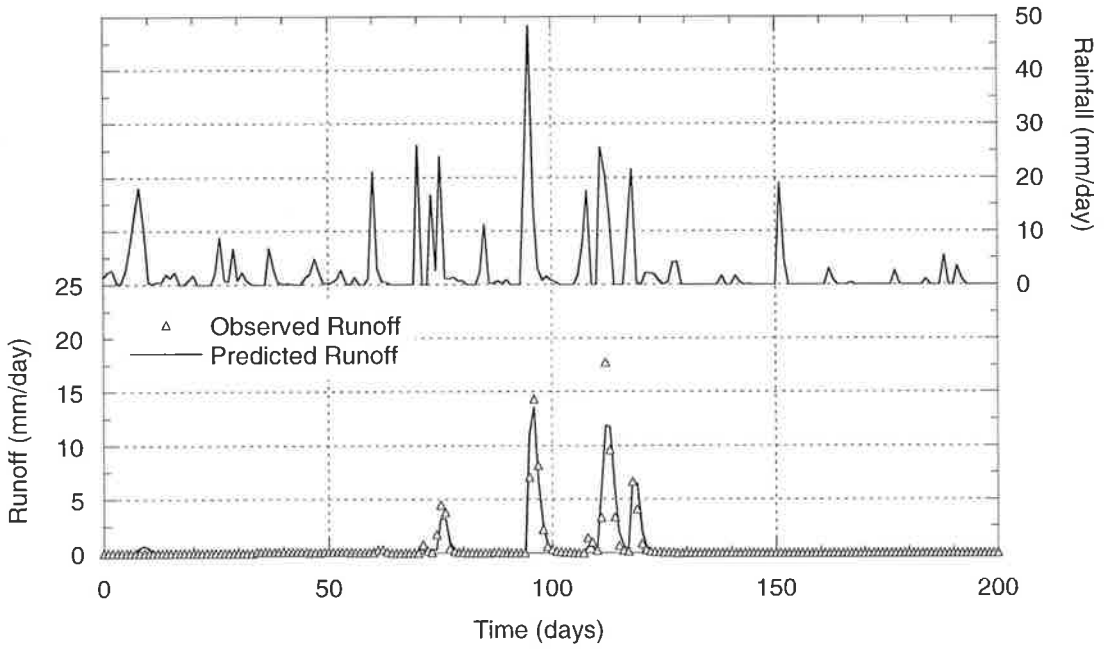

Figure 7.21 Avon River: Observed and predicted runoff - 4/7/1975 to 20/1/1976 (λ_1 = 1.50; AR(1) = -0.40; λ_2 = 1.50).

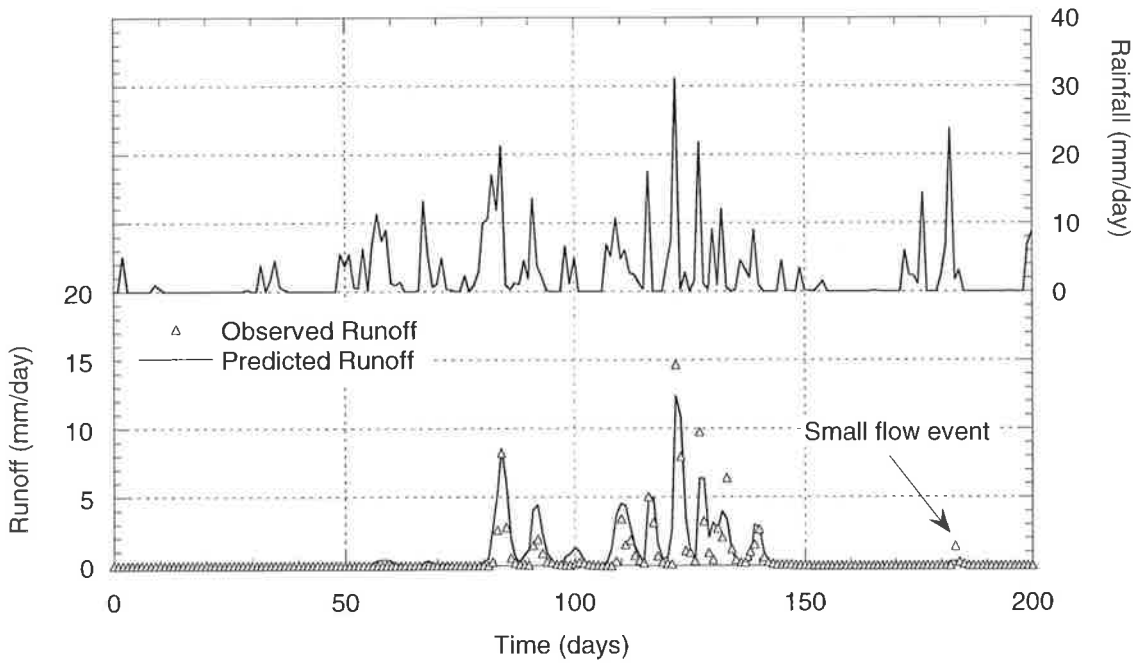

Figure 7.22 Avon River: Observed and predicted runoff - 3/4/1981 to 20/10/1981 (λ_1 = 1.50; AR(1) = -0.40; λ_2 = 1.50).

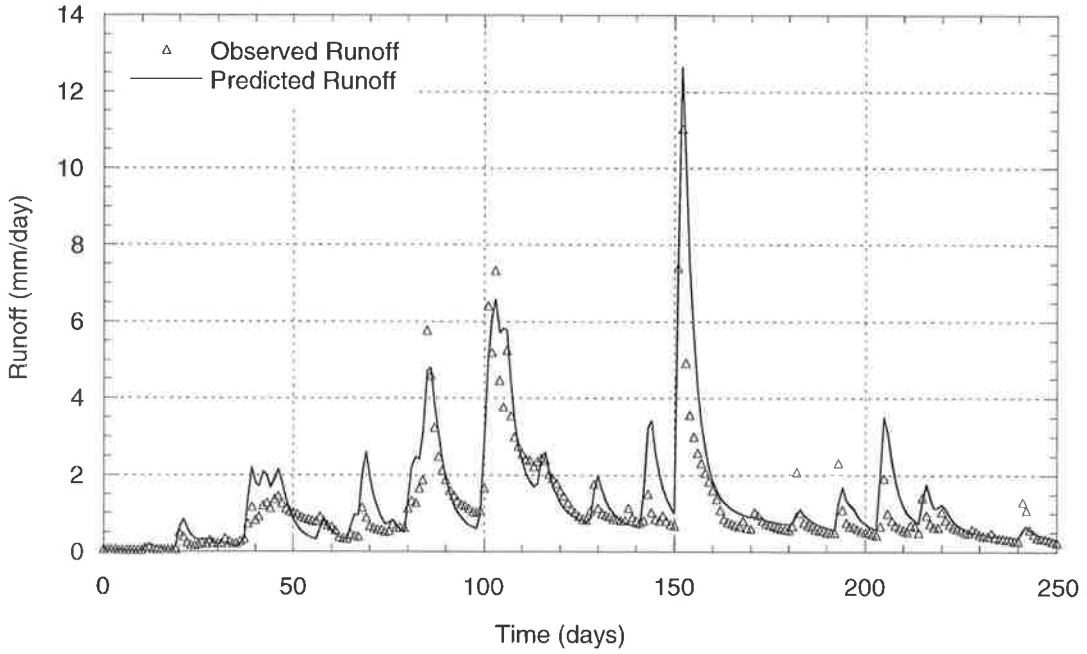

Figure 7.23 Boggy Creek: Observed and predicted runoff - 29/4/1978 to 4/1/1979 ($\lambda_1 = 0.70$; AR(1) = 0.50; $\lambda_2 = 1.25$).

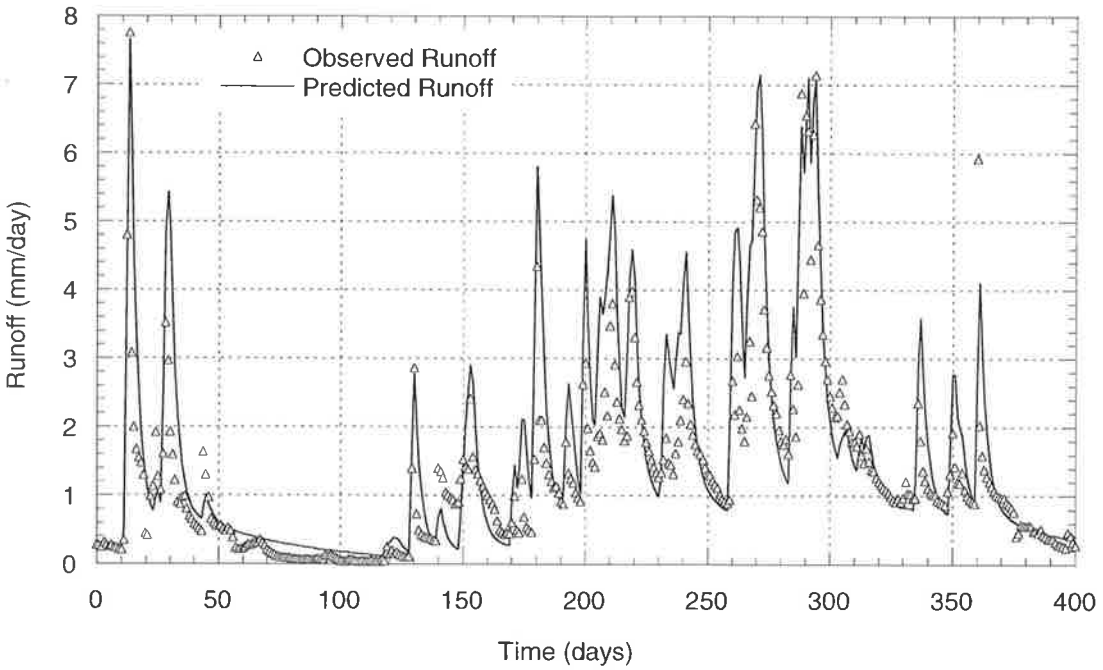

Figure 7.24 Boggy Creek: Observed and predicted runoff - 12/11/1988 to 17/12/1989 ($\lambda_1 = 0.70$; AR(1) = 0.50; $\lambda_2 = 1.25$).

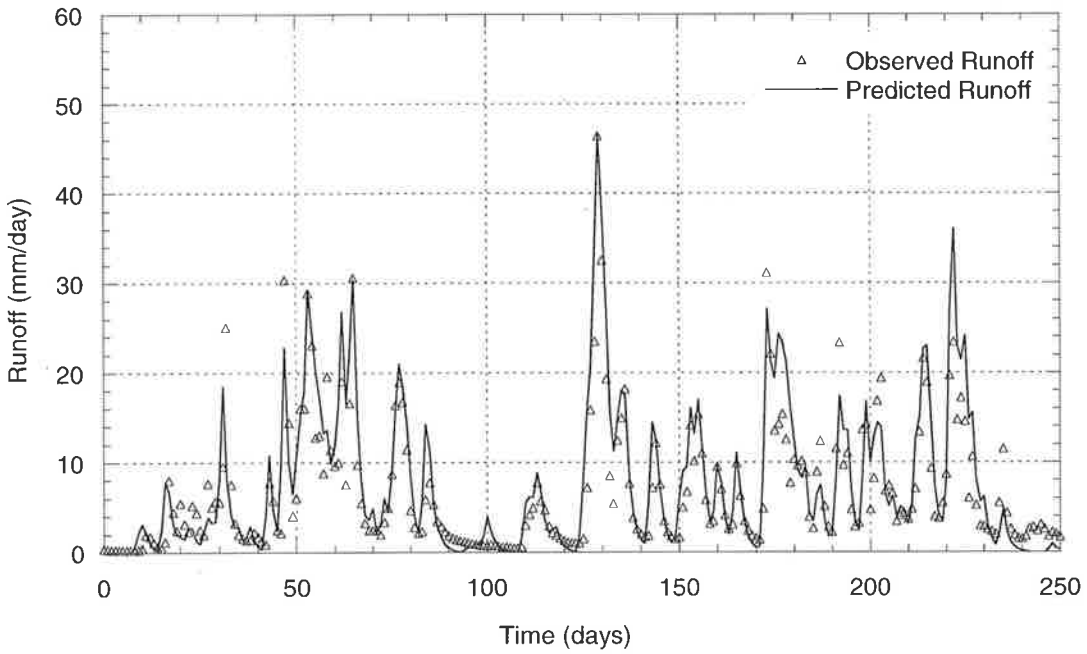

Figure 7.25 Davey River: Observed and predicted runoff - 23/2/1981 to 31/10/1981 (λ_1 = 0.95; AR(1) = 0.55; AR(2) = -0.05; λ_2 = 1.20).

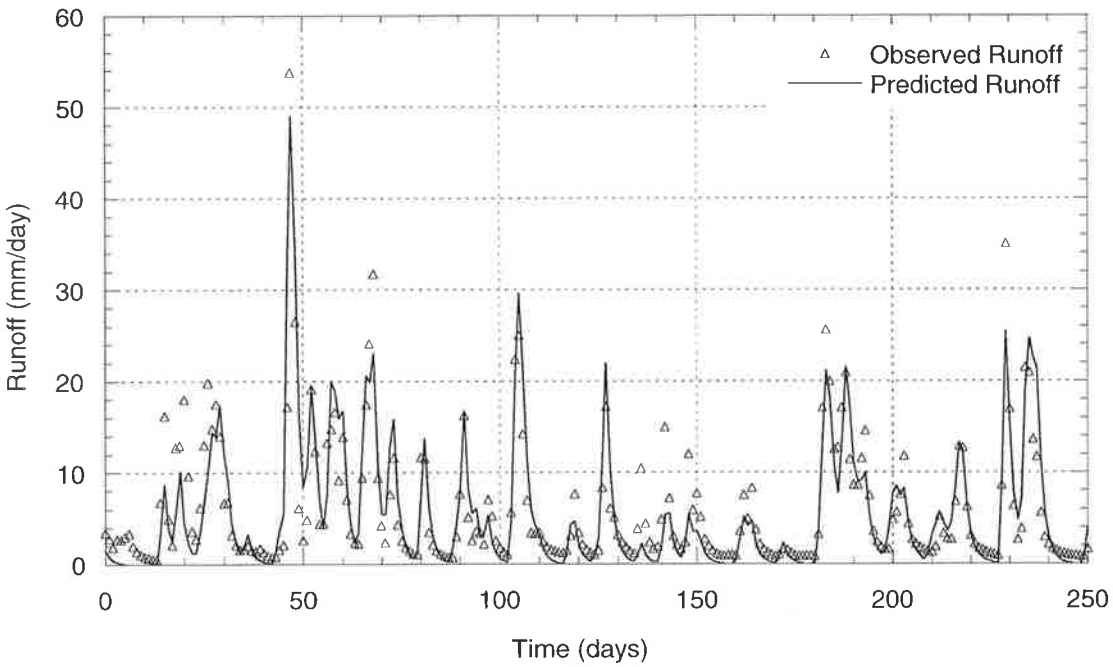

Figure 7.26 Davey River: Observed and predicted runoff - 24/11/1986 to 1/8/1987 (λ_1 = 0.95; AR(1) = 0.55; AR(2) = -0.05; λ_2 = 1.20).

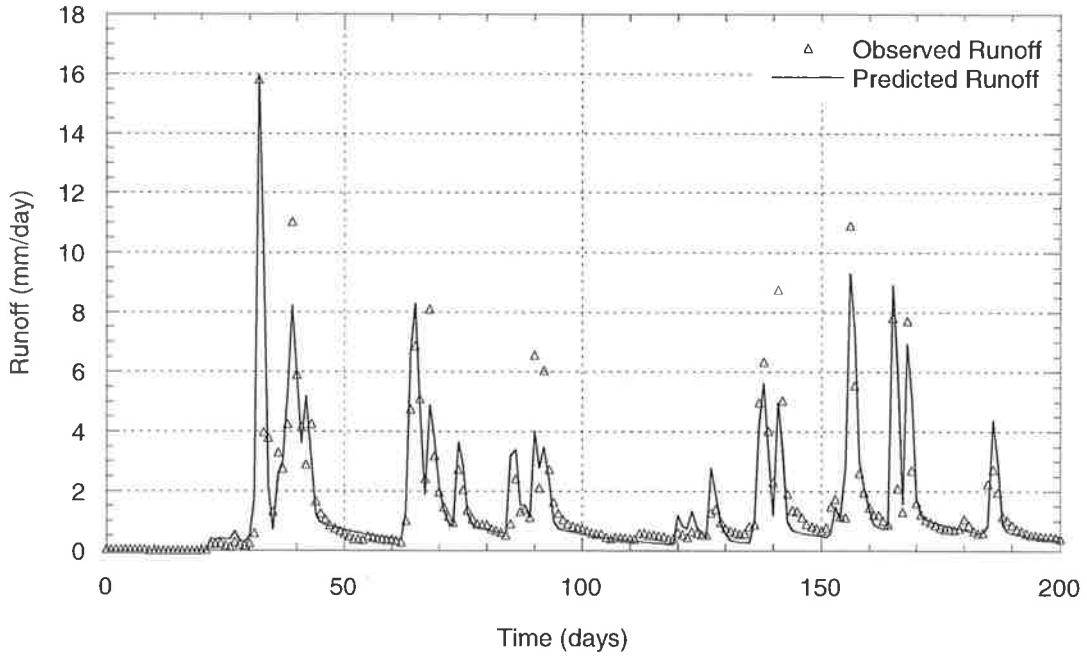

Figure 7.27 Scott Creek: Observed and predicted runoff - 26/3/1971 to 12/10/1971 ($\lambda_1 = 0.90$; AR(1) = 0.20; $\lambda_2 = 1.25$).

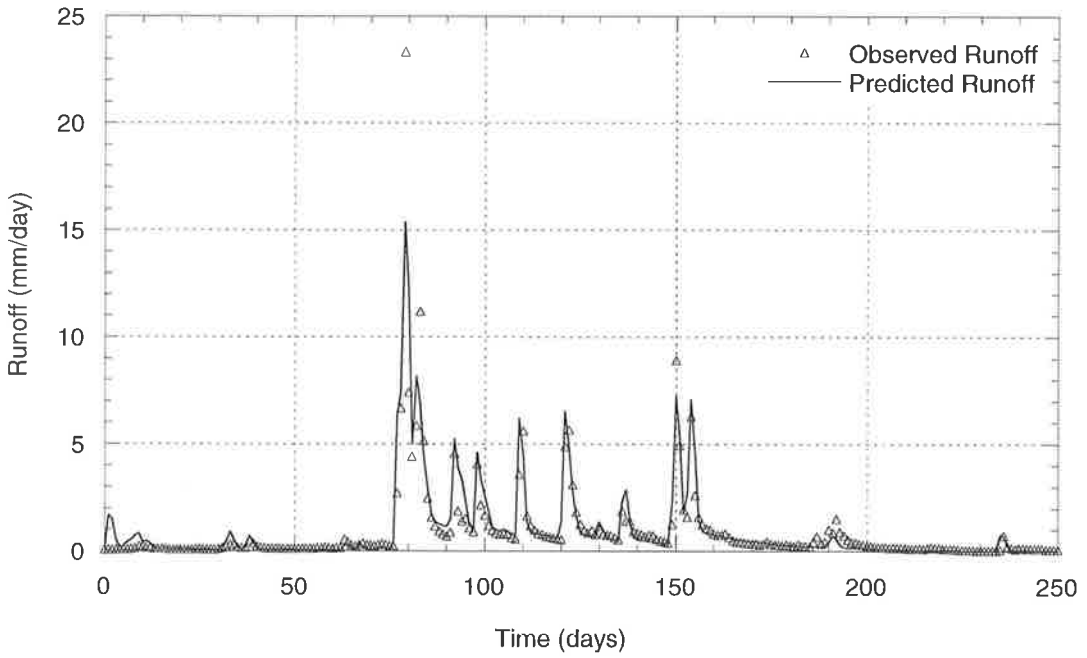

Figure 7.28 Scott Creek: Observed and predicted runoff - 16/4/1986 to 22/12/1986 ($\lambda_1 = 0.90$; AR(1) = 0.20; $\lambda_2 = 1.25$).

The addition of the alternative surface routing equation to the AWBM aided significantly in the calibration of the model to Scott Creek. Because of the small catchment area, surface runoff response is fast and this parameter allowed the model to capture the often steep recessions after the peaks. Appendix M shows the observed and predicted daily runoff for four events at each location, further demonstrating the ability of the model to reproduce the observed data.

Figure 7.29 to Figure 7.34 show the relationship between the observed and predicted daily runoff and maximum daily runoff in each month. It can be seen that the R^2 and E values obtained for each site are reasonable. The model often underestimates the higher runoff values, which is a limitation of this and other lumped models when there are more low runoff values than high runoff values. During calibration, the parameters were determined to obtain the best representation of the entire time series, which may sometimes be to the detriment of obtaining a good representation of the higher runoff values. The higher values of the Box Cox $\lambda(\lambda_1, \lambda_2)$ parameters used below, attempted to compensate for this as much as possible, without overestimating the lower runoff values and hence the antecedent moisture conditions before subsequent rainfall events.

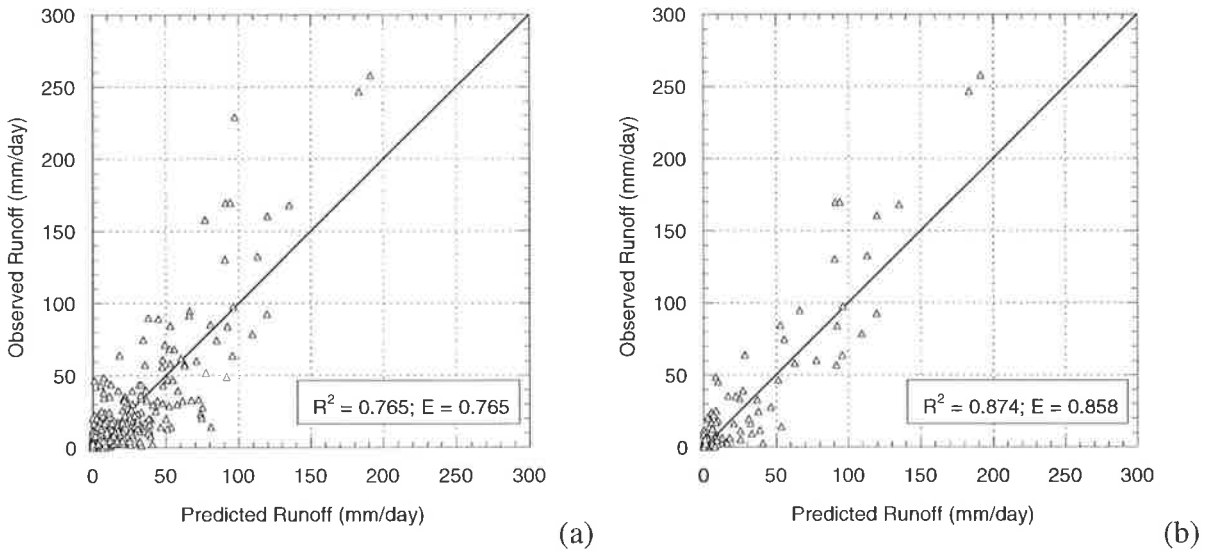

Figure 7.29 Comparison of observed and predicted data for Alligator Creek: (a) Daily runoff values; (b) Maximum daily runoff in each month (λ_1 = 0.95; AR(1) = 0.30; AR(2) = 0.05; λ_2 = 0.95).

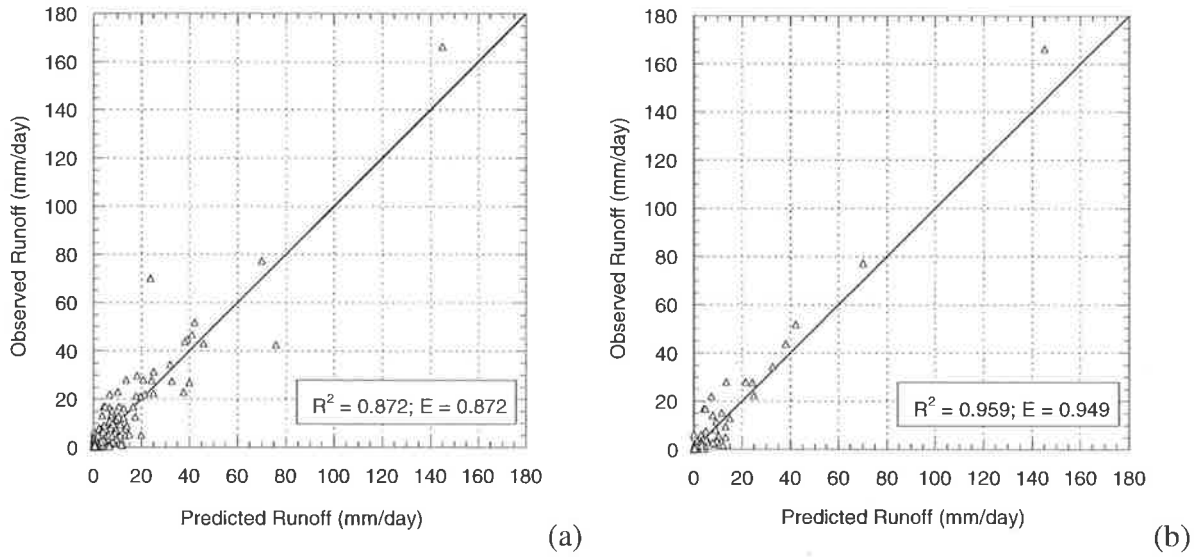

Figure 7.30 Comparison of observed and predicted data for Allyn River:
(a) Daily runoff values; (b) Maximum daily runoff in each month
(λ_1 = 0.80; AR(1) = 0.20; AR(2) = 0.10; λ_2 = 1.00).

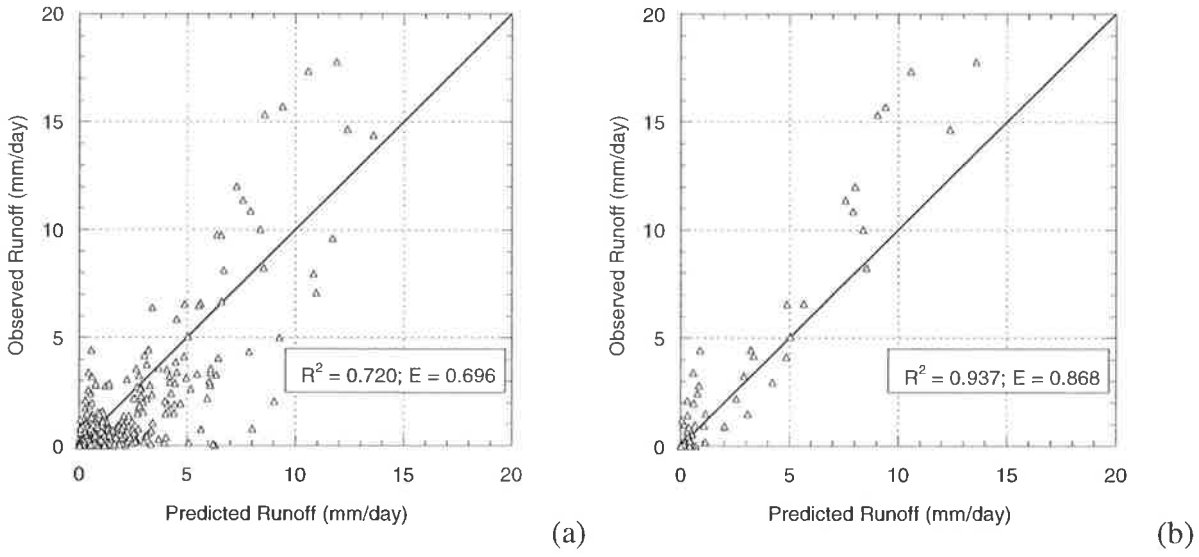

Figure 7.31 Comparison of observed and predicted data for Avon River:
(a) Daily runoff values; (b) Maximum daily runoff in each month
(λ_1 = 1.50; AR(1) = -0.40; λ_2 = 1.50).

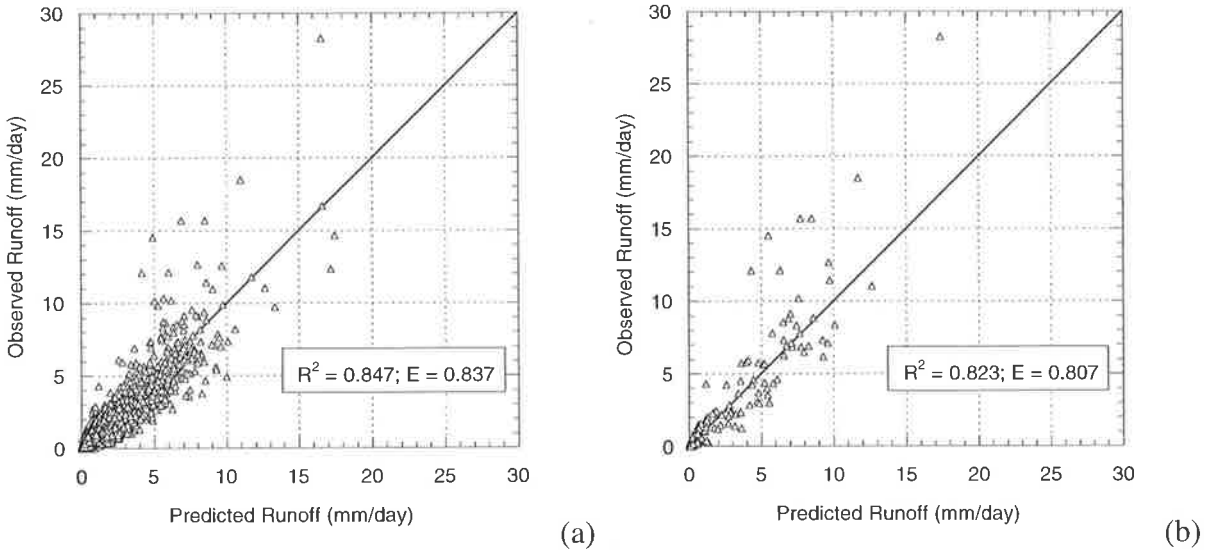

Figure 7.32 Comparison of observed and predicted data for Boggy Creek: (a) Daily runoff values; (b) Maximum daily runoff in each month ($\lambda_1 = 0.70$; AR(1) = 0.50; $\lambda_2 = 1.25$).

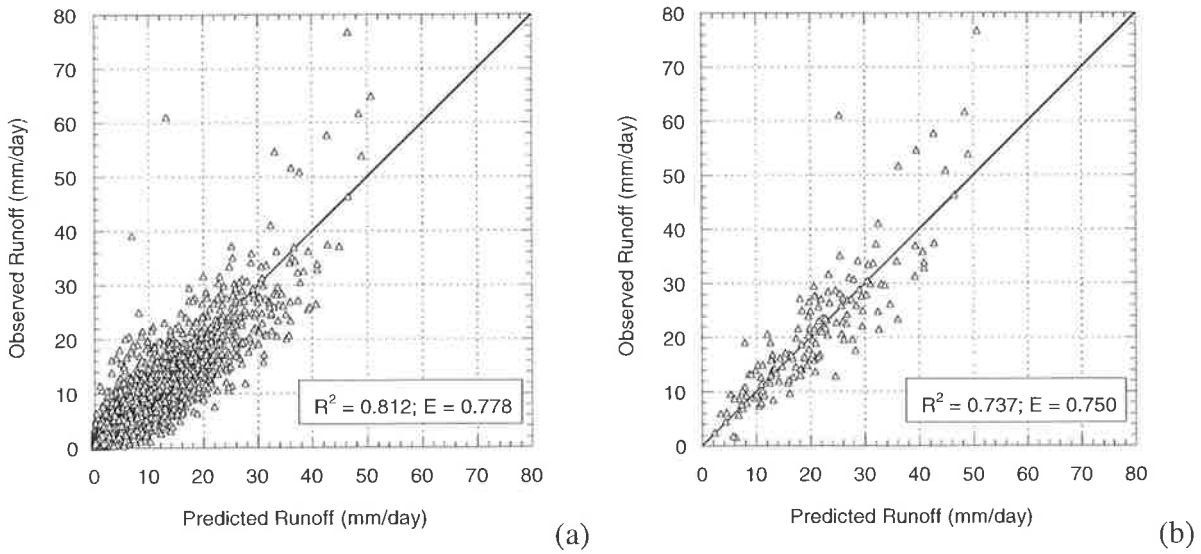

Figure 7.33 Comparison of observed and predicted data for Davey River: (a) Daily runoff values; (b) Maximum daily runoff in each month ($\lambda_1 = 0.95$; AR(1) = 0.55; AR(2) = -0.05; $\lambda_2 = 1.20$).

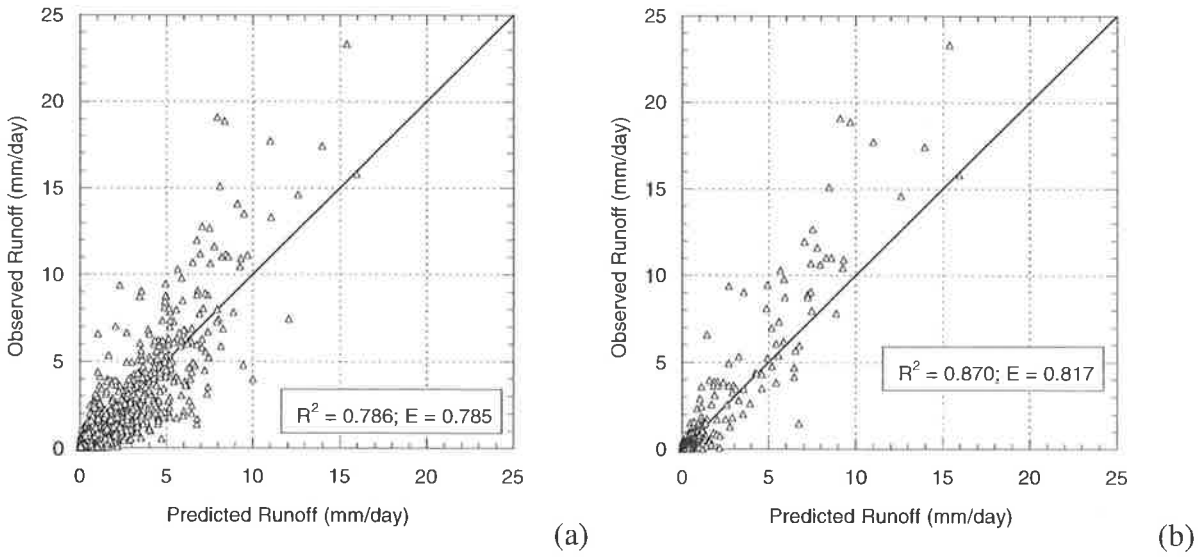

Figure 7.34 Comparison of observed and predicted data for Scott Creek: (a) Daily runoff values; (b) Maximum daily runoff in each month ($\lambda_1 = 0.90$; AR(1) = 0.20; $\lambda_2 = 1.25$).

It should be noted that Sumner *et al.* (1997) fitted the SFB model to data from Alligator Creek, Allyn River, Davey River and Scott Creek with comparisons between observed and predicted runoff made at a monthly time scale. The results presented here for Scott Creek show more satisfactory values of R^2 and E for comparisons at a daily time scale than that achieved by Sumner *et al.* (1997). The results in Sumner *et al.* (1997) are slightly better for the Allyn River and Davey River and are similar to those shown here for Alligator Creek. This suggests that the results produced here for comparisons at a daily scale are satisfactory and the catchment water balance model is considered capable of adequately reproducing the observed data.

Table 7.5 summarises the values of the Box-Cox transformation parameters (λ_1, λ_2) adopted to improve the representation of residuals and the peak values of both responses.

Table 7.5 Error model parameters.

Site	Daily Flow			Daily Maximum Monthly Flows
	λ_1	AR(1)	AR(2)	λ_2
Alligator Creek	0.95	0.30	0.05	0.95
Allyn River	0.80	0.20	0.10	1.00
Avon River	1.50	-0.40	-	1.50
Boggy Creek	0.70	0.50	-	1.25
Davey River	0.95	0.55	-0.05	1.20
Scott Creek	0.90	0.20	-	1.25

These values were chosen based on an analysis of the objective function, the distribution of residuals and the predicted runoff. A value of $\lambda = 1.0$ results in no transformation, $\lambda < 1.0$ places more emphasis on lower runoff values and $\lambda > 1.0$ on the higher runoff values.

For most sites, values of $\lambda_1 < 1.0$ were chosen for the residuals of the daily runoff, the exception being Avon River where a value of $\lambda_1 > 1.0$ was required. For Alligator Creek and Avon River, runoff is highly seasonal and the records contain small numbers of high-peaked runoff events. Since the model is to be used for design flood estimation it was important to obtain a good representation of the peak daily runoff values. This was not achieved with lower values of λ_1, even though the distribution of residuals (Figure 7.35 for Alligator Creek) is not uniform. The distribution of daily runoff residuals is given for Boggy Creek in Figure 7.36 and for Scott Creek in Figure 7.37. Although a lower value of λ_1 may reduce the spread of residuals further, a compromise between the representation of the residuals and representing the higher runoff values within the daily runoff response was required.

A value of $\lambda_2 > 1.0$ was required for the residuals of the maximum daily runoff in each month at almost all sites to ensure that the highest runoff values were reproduced. Figure 7.38 to Figure 7.40 show the predicted maximum daily runoff in each month versus standardised residual for the Allyn River, Davey River and Scott Creek. While the distribution of residuals does not appear uniform, the results are considered reasonable, particularly because there were limited data points and it was important to obtain a good representation of the higher runoff values. This was often at the expense of the lower values.

Appendix M shows the distribution of residuals for both the daily runoff and maximum daily runoff in each month for each site.

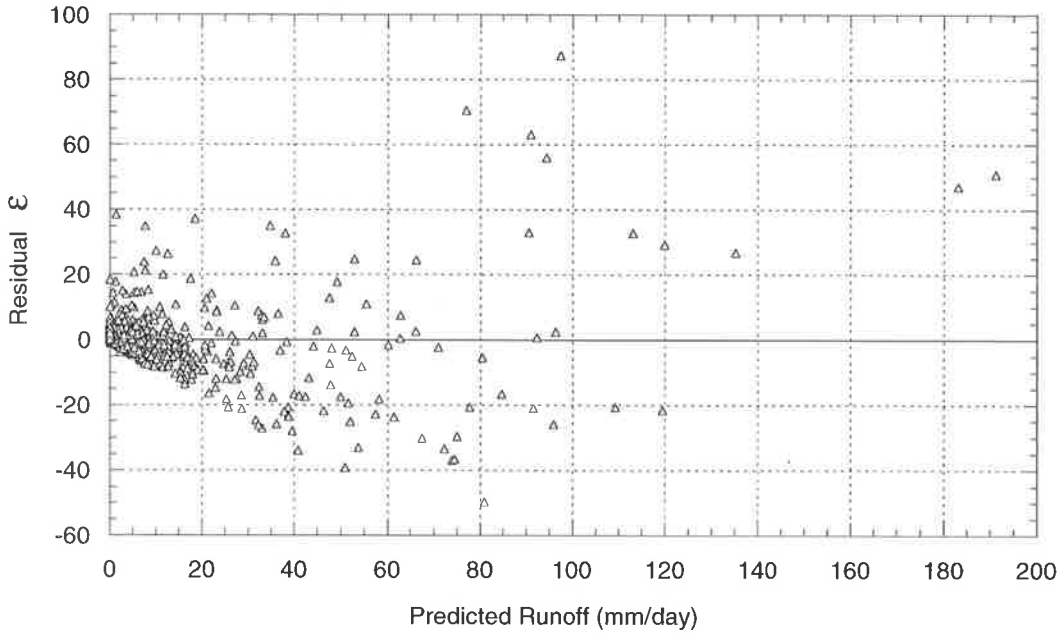

Figure 7.35 Alligator Creek: Predicted daily runoff versus residual ($\lambda_1 = 0.95$; AR(1) = 0.30; AR(2) = 0.05; $\lambda_2 = 0.95$).

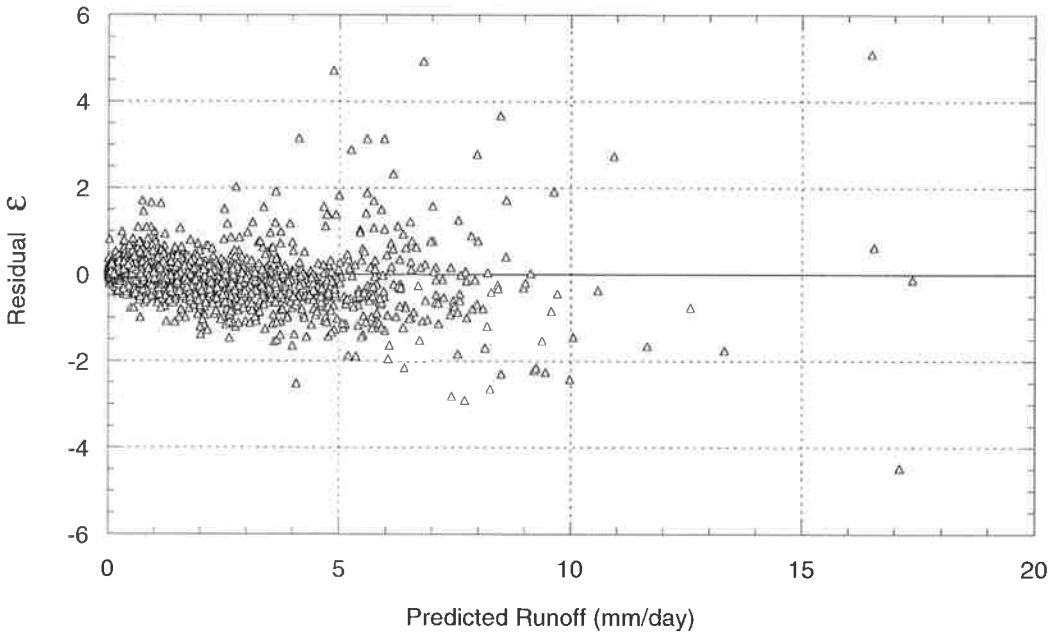

Figure 7.36 Boggy Creek: Predicted daily runoff versus residual ($\lambda_1 = 0.70$; AR(1) = 0.50; $\lambda_2 = 1.25$).

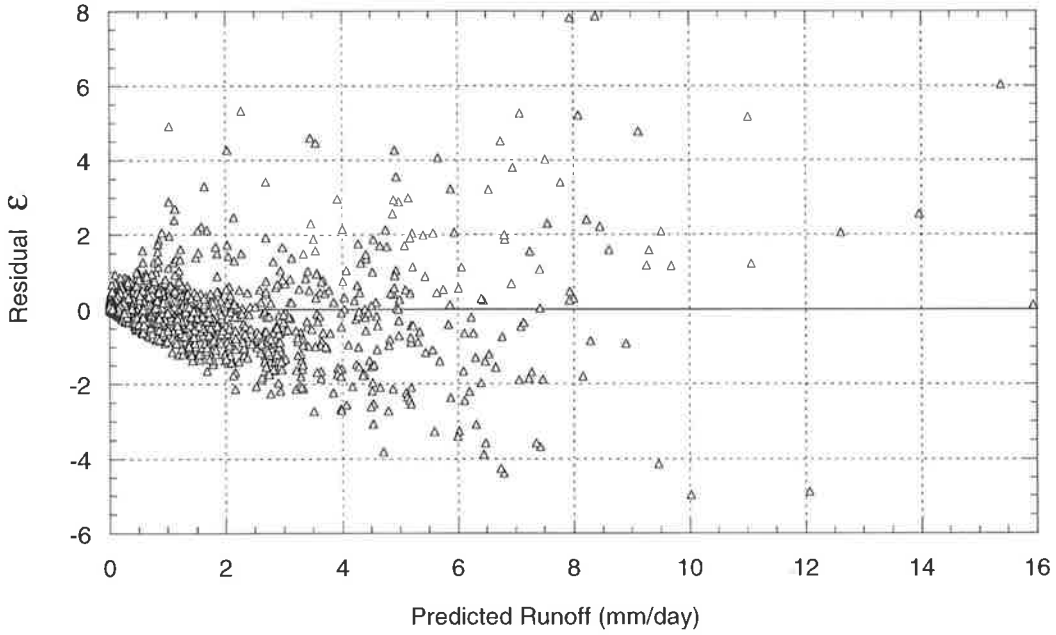

Figure 7.37 Scott Creek: Predicted daily runoff versus residual ($\lambda_1 = 0.90$; AR(1) = 0.20; $\lambda_2 = 1.25$).

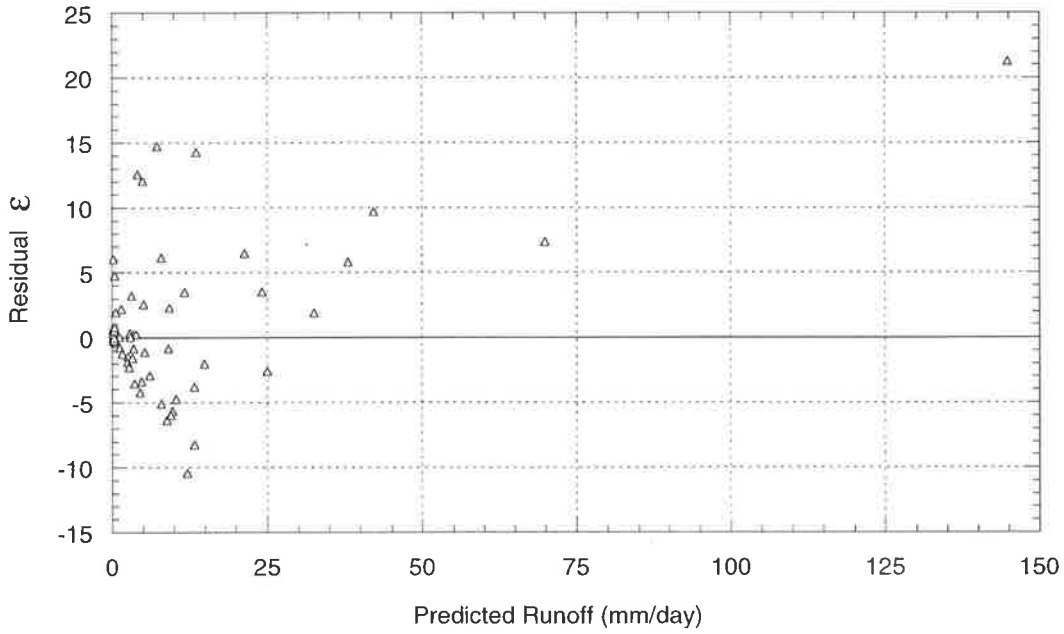

Figure 7.38 Allyn River: Predicted maximum daily runoff in each month versus residual ($\lambda_1 = 0.80$; AR(1) = 0.20; AR(2) = 0.10; $\lambda_2 = 1.00$).

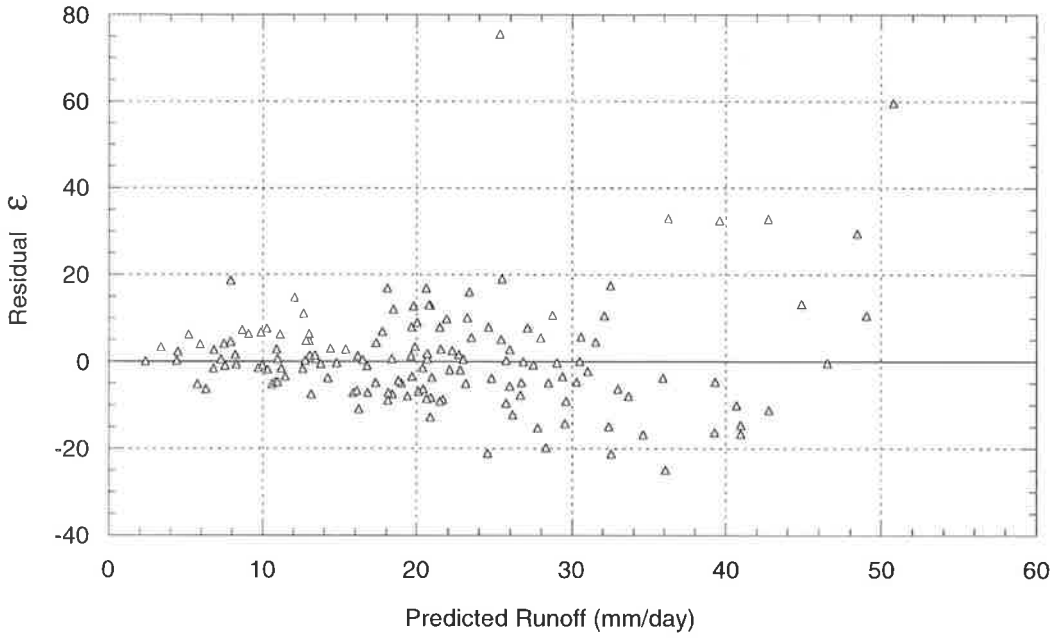

Figure 7.39 Davey River: Predicted maximum daily runoff in each month versus residual ($\lambda_1 = 0.95$; AR(1) = 0.55; AR(2) = -0.05; $\lambda_2 = 1.20$).

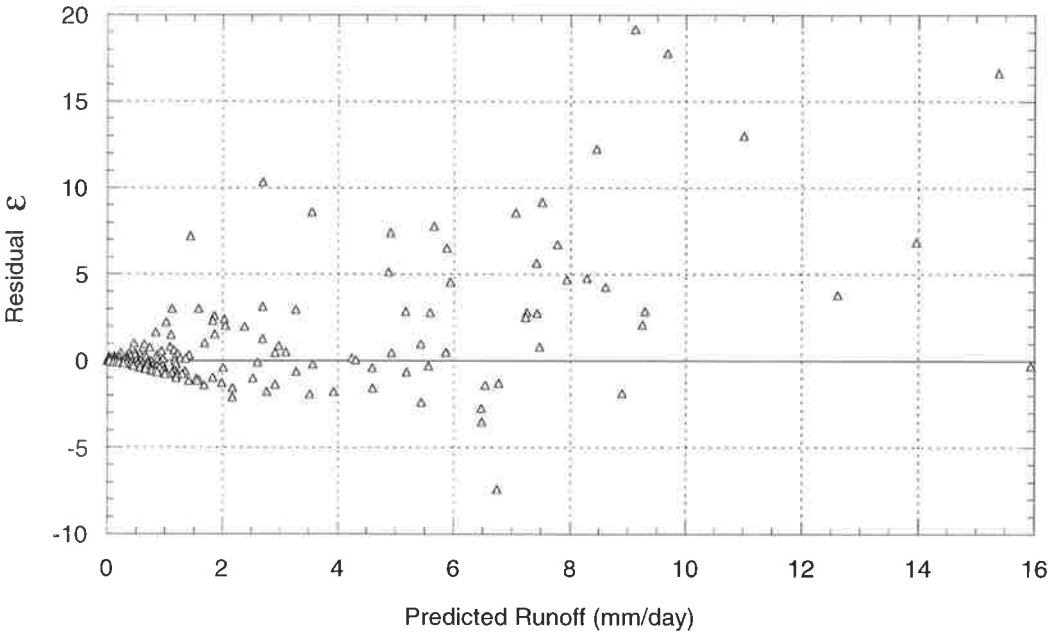

Figure 7.40 Scott Creek: Predicted maximum daily runoff in each month versus residual ($\lambda_1 = 0.90$; AR(1) = 0.20; $\lambda_2 = 1.25$).

Auto-regressive (AR) parameters were applied to the residuals of the daily runoff sequence to remove the observed correlation. The parameters applied for each catchment can be seen in Table 7.5. For Alligator Creek, an AR(2) model was required to ensure that the observed correlation between the residuals is within the 95% confidence limits of white noise as shown in Figure 7.41. The Allyn River also required an AR(2) model, with the resulting auto-correlation shown in Figure 7.42. The correlation at a lag of three days in the data from this site indicates that an AR(3) model may be required. However, the addition of the extra parameter made little difference to the residuals or the parameter values.

A negative AR(1) parameter was required for Avon River, because in contrast to the other sites where the residuals showed positive correlation, negative correlation was observed here. The resulting residual auto-correlation can be seen in Figure 7.43. For Scott Creek, shown in Figure 7.44, a single AR(1) model was required and although for this site the observed correlation is outside the 95% limits on white noise, the addition of an AR(2) parameter did not improve the fit of the model to the data. Appendix M shows the auto-correlation between residuals for all sites. An AR(1) parameter was also used for Boggy Creek, while Davey River required an AR(2) model to adequately account for the auto-correlation.

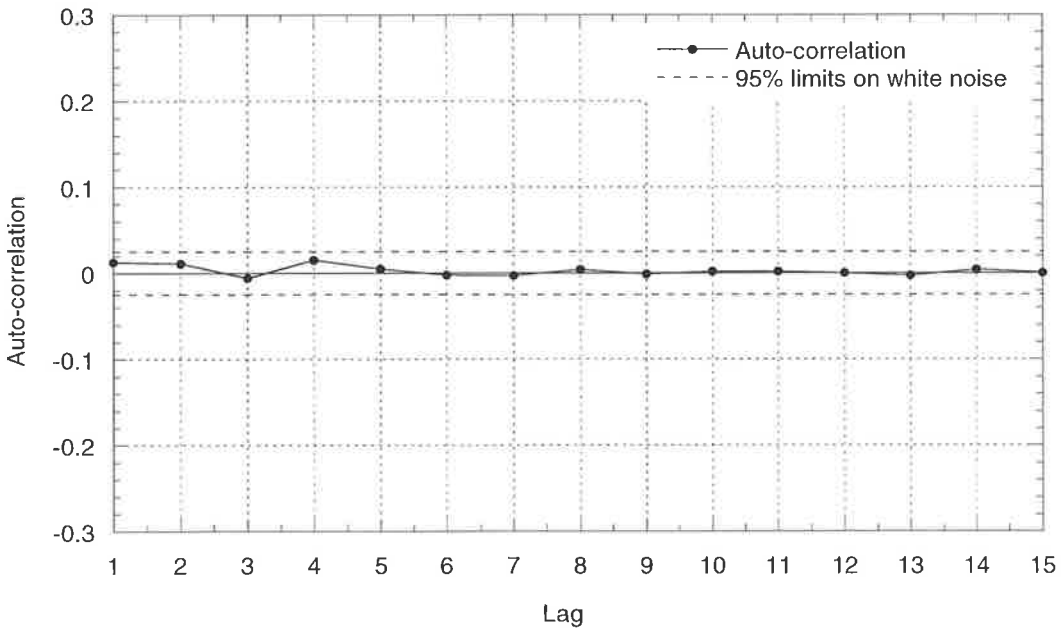

Figure 7.41 Alligator Creek: Auto-correlation of daily runoff residuals ($\lambda_1 = 0.95$; AR(1) = 0.30; AR(2) = 0.05; $\lambda_2 = 0.95$).

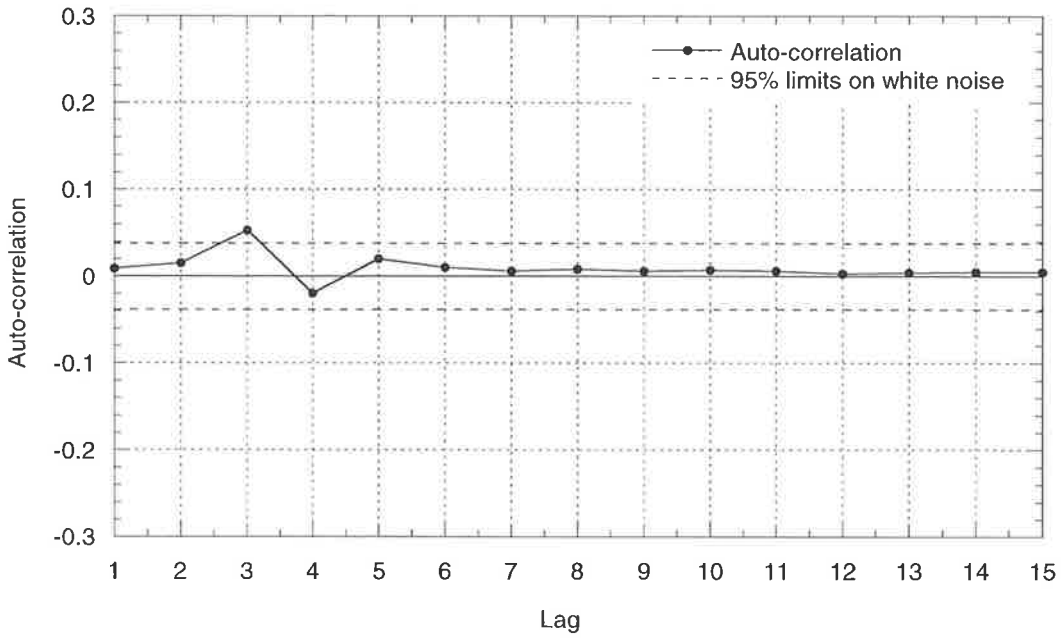

Figure 7.42 Allyn River: Auto-correlation of daily runoff residuals (λ_1 = 0.80; AR(1) = 0.20; AR(2) = 0.10; λ_2 = 1.00).

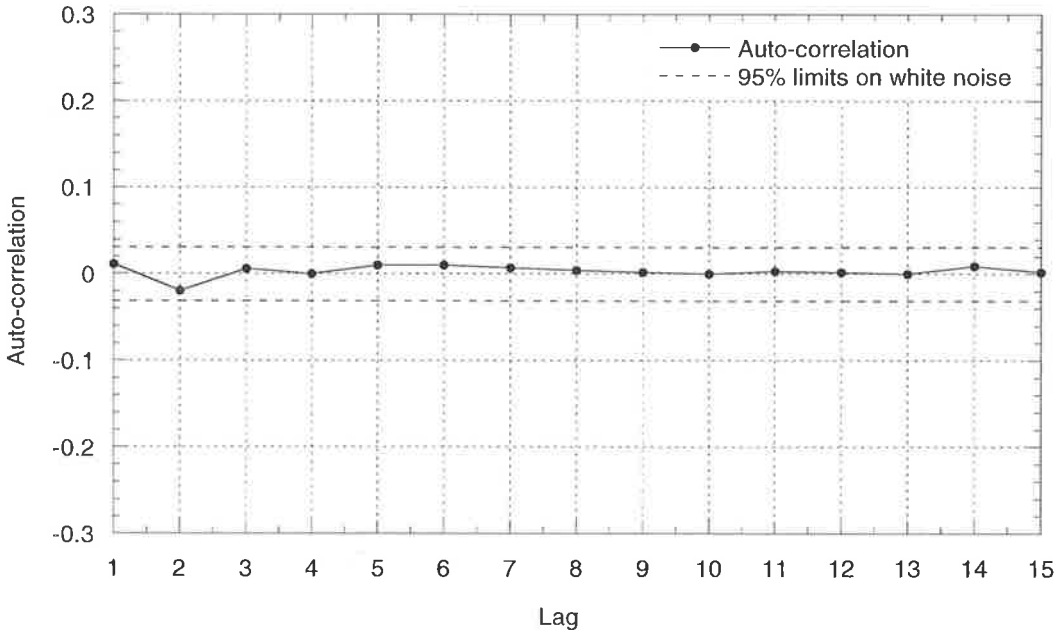

Figure 7.43 Avon River: Auto-correlation of daily runoff residuals (λ_1 = 1.50; AR(1) = -0.40; λ_2 = 1.50).

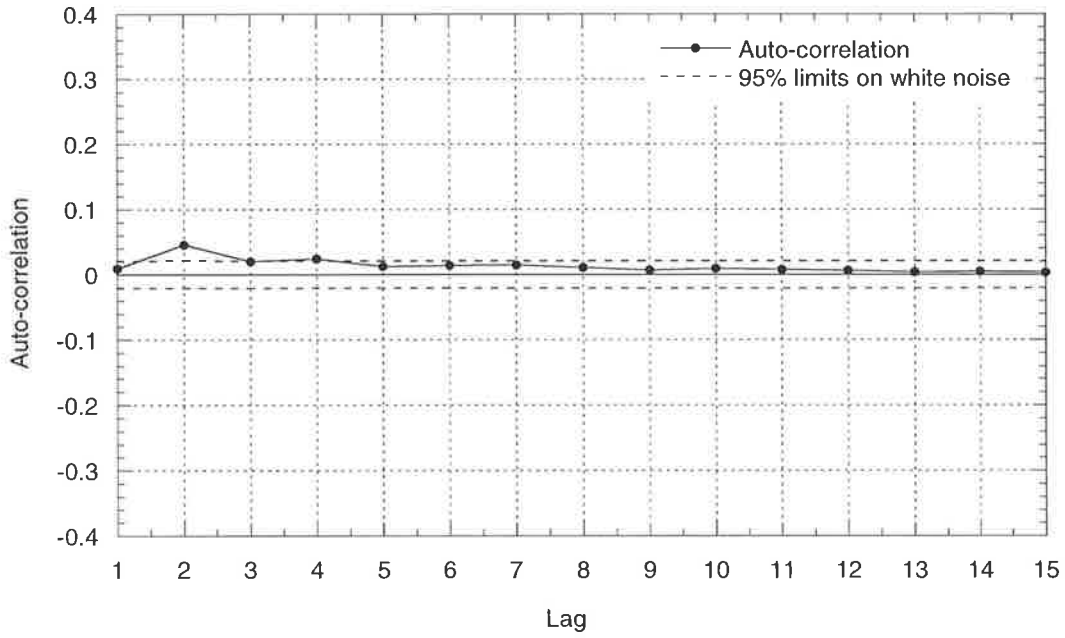

Figure 7.44 Scott Creek: Auto-correlation of daily runoff residuals ($\lambda_1 = 0.90$; AR(1) = 0.20; $\lambda_2 = 1.25$).

7.3 CATCHMENT WATER BALANCE SIMULATION AT SMALL TIME SCALES

The water balance model developed in this chapter has been calibrated using daily streamflow, rainfall and evaporation data. In the next chapter, this will be combined with the stochastic rainfall and evaporation models to generate rainfall excess at a six-minute time scale. Before this is undertaken it is desirable to ensure that the parameters obtained at the daily time scale are transferable to the six-minute time scale.

There is generally limited sub-daily streamflow data available for extended periods and often the closest rainfall pluviograph records are not located on the catchment or the period of record is not concurrent with that of the streamflow. However, in the case of Boggy Creek a pluviograph is located at Whitfield, one of the daily rainfall gauges used to determine the catchment rainfall, and this record is concurrent with most of the daily streamflow. To test the use of the model at a six-minute time scale, the daily catchment average rainfall was disaggregated using the proportion of rainfall occurring within each six-minute increment in the Whitfield pluviograph record. If no rainfall occurred at the pluviograph site or the data was missing, the daily rainfall was distributed uniformly over the day. The catchment water balance model was then calibrated using this disaggregated daily rainfall record. Table 7.6 shows that the parameters obtained are similar to those using the daily rainfall data.

Table 7.6 Boggy Creek: Comparison between calibrated parameter values and initial conditions using daily and six-minute rainfall.

Model Parameter Values		
	Daily Rainfall	Six-Minute Rainfall
C1 (mm)	9.9	6.8
C2 (mm)	180.5	183.9
C3 (mm)	405.9	402.8
A1	0.084	0.087
A2	0.485	0.482
A3	0.431	0.431
Em	0.70	0.70
BFI	0.40	0.40
Ks	0.35	0.39
K	0.98	0.978
maxRain (mm)	95.1	95.0
Initial Conditions		
Initial C1 (mm)	7.5	0
Initial C2 (mm)	100	100
Initial C3 (mm)	200	200
Initial BS (mm)	0	0
Initial S (mm)	0	0

Comparison between the observed and predicted daily runoff shown in Figure 7.45 and Figure 7.46 indicate that the reproduction of the observed runoff is very good and that the use of six-minute rainfall actually improves the reproduction of some peaks in these and two other events shown in Appendix M.

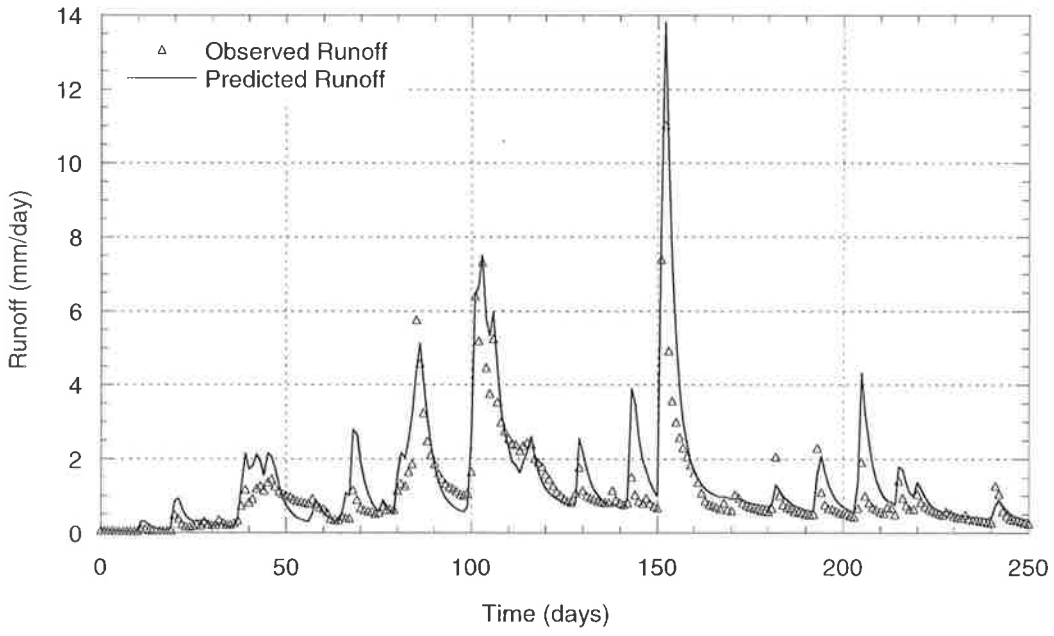

Figure 7.45 Boggy Creek: Observed and predicted runoff: 29/4/1978 to 4/1/1979 (six-minute rainfall) ($\lambda_1 = 0.75$; AR(1) = 0.60; AR(2) = 0.10; $\lambda_2 = 1.20$).

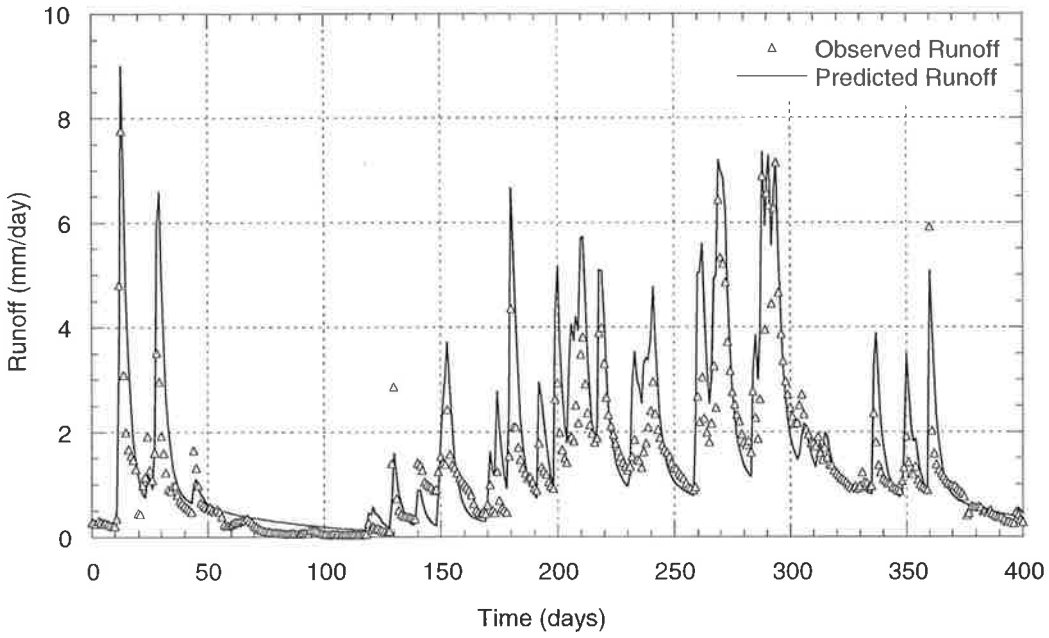

Figure 7.46 Boggy Creek: Observed and predicted runoff: 12/11/1988 to 17/12/1989 (six-minute rainfall) ($\lambda_1 = 0.75$; AR(1) = 0.60; AR(2) = 0.10; $\lambda_2 = 1.20$).

Figure 7.47 shows the relationship between the observed and predicted daily runoff and the maximum daily runoff in each month. The R^2 and E values obtained are reasonable and slightly better than those obtained using daily rainfall.

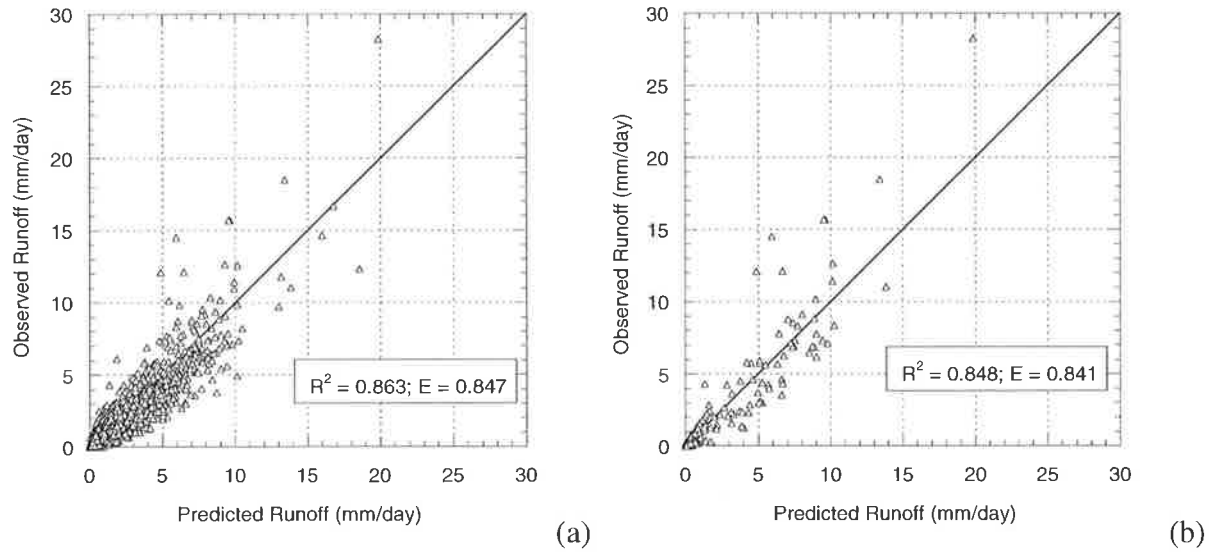

Figure 7.47 Comparison of observed and predicted data for Boggy Creek: (a) Daily runoff values; (b) Maximum daily runoff in each month (six-minute rainfall) ($\lambda_1 = 0.75$; AR(1) = 0.60; AR(2) = 0.10; $\lambda_2 = 1.20$).

As previously, the Box-Cox transformation parameters (λ_1 and λ_2) for the daily runoff and maximum daily runoff in each month were varied. Values of $\lambda_1 = 0.75$ and $\lambda_2 = 1.20$ were used to improve the representation of the residuals for both responses as shown in Figure 7.48 and Figure 7.49 respectively. These values are similar to those used for the calibration with daily rainfall in Table 7.5.

When calibration was undertaken using daily rainfall, the auto-correlation at a lag of two was outside the 95% confidence limits for white noise. Although an AR(2) parameter applied to the daily runoff residuals did not make a significant difference to the residuals or the parameter values, it made a more significant difference when six-minute rainfall was used. An AR(1) parameter equal to 0.6 and an AR(2) parameter equal to 0.1 were applied and the results in Figure 7.50 show the auto-correlation between residuals to be within the 95% confidence limits for white noise.

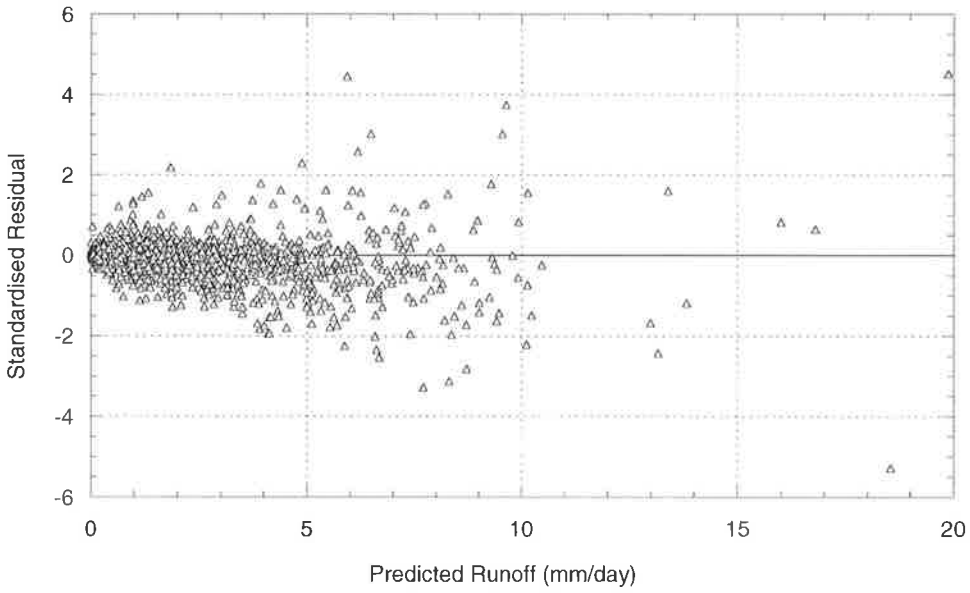

Figure 7.48 Boggy Creek: Predicted daily runoff versus residual (six-minute rainfall) ($\lambda_1 = 0.75$; AR(1) = 0.60; AR(2) = 0.10; $\lambda_2 = 1.20$).

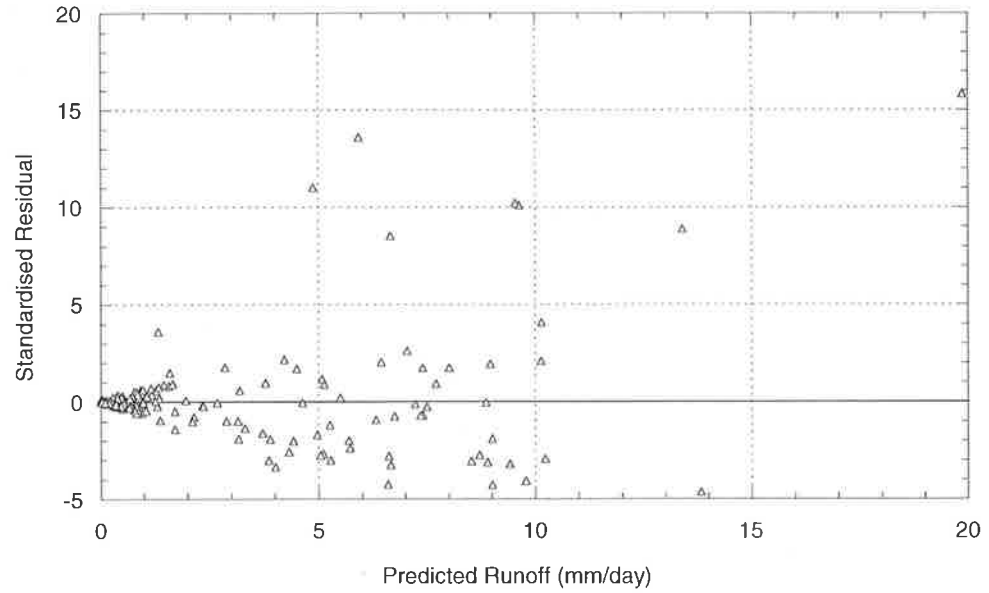

Figure 7.49 Boggy Creek: Predicted maximum daily runoff in each month versus residual (six-minute rainfall) ($\lambda_1 = 0.75$; AR(1) = 0.60; AR(2) = 0.10; $\lambda_2 = 1.20$).

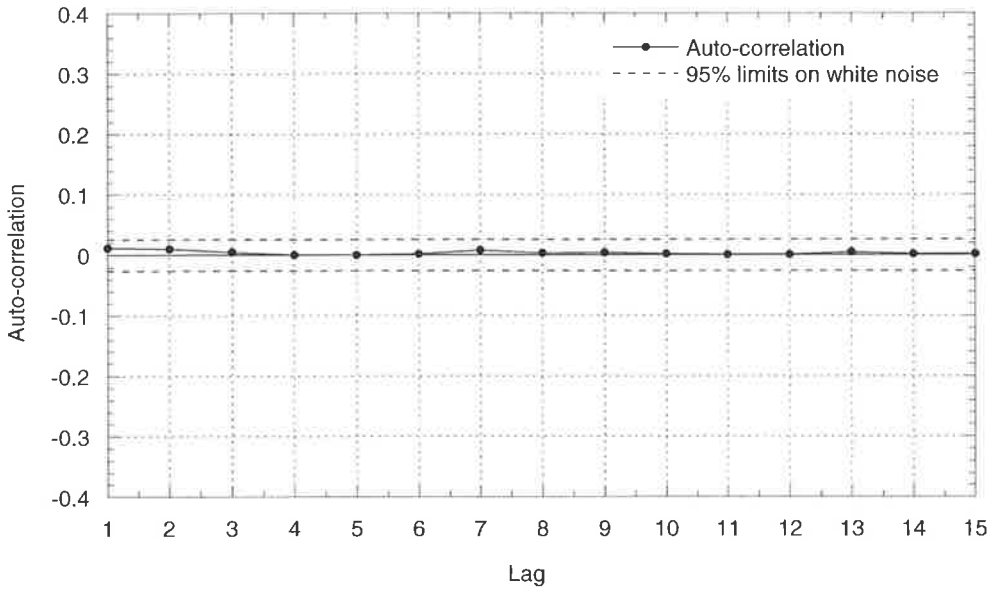

Figure 7.50 Boggy Creek: Auto-correlation of daily runoff residuals (six-minute rainfall) ($\lambda_1 = 0.75$; AR(1) = 0.60; AR(2) = 0.10; $\lambda_2 = 1.20$).

The parameters for the water balance model, obtained by calibrating with daily rainfall disaggregated to a six-minute time scale were similar to those obtained from calibration using daily rainfall alone, with both sets of parameters providing a reasonable reproduction of the observed runoff. This suggests that parameters obtained from a calibration with daily rainfall

are suitable for use in a continuous simulation where the rainfall input is at a six-minute time scale. Therefore, further use of the catchment water balance model in this study was undertaken with parameters calibrated using daily rainfall.

7.4 Concluding Remarks

The results from calibrating the modified Australian Water Balance Model indicate its suitability for modelling the catchment water balance and the generation of rainfall excess for this study. In each case, the predicted runoff replicated the observed runoff adequately and the values of R^2 and E in the comparison of observed and predicted daily runoff was considered very good for this time scale. Comparison of the predicted maximum daily runoff in a month generally showed a good reproduction of the observed runoff. Using the routing store in the form derived in this chapter allowed better comparisons with the observed runoff, in particular improved representation of the recession immediately following the peak. Comparison of the results from the observed and predicted runoff for Alligator Creek and Scott Creek at a daily time scale showed a better representation in terms of the R^2 and E than that produced by Sumner *et al.* (1997) for comparisons at a monthly time scale, highlighting the success of this routing store.

The chosen Box-Cox transformation parameters were generally able to reduce the variance of the residuals. In some cases, lower values than those chosen may have reduced the variance further but higher values of the Box-Cox transformation parameters were required to adequately reproduce the higher runoff events. This was identified as important for design flood estimation, particularly for Alligator Creek and Avon River where runoff is highly seasonal and the record contains a small number of runoff events. For the Alligator Creek catchment these are very high-peaked runoff events. The auto-regressive models applied to the residuals were able to generally reduce the correlation between residuals to within the 95% confidence limits on white noise.

The catchment water balance model developed here has been shown to provide a suitable deterministic model for converting rainfall into rainfall excess. In addition, it has been shown that parameters calibrated at a daily time scale are suitable for use at a six-minute time scale and thus can be used in conjunction with the stochastic rainfall and evaporation model developed in previous chapters.

8. DESIGN FLOOD ESTIMATION USING RAINFALL EXCESS FREQUENCY DURATION PROPORTIONS

The preceding chapters have discussed the following aspects of this study:

- the development of a stochastic rainfall model to simulate synthetic rainfall that has the same statistical characteristics of observed data;
- the combination of the rainfall model with a stochastic evaporation model to generate daily evaporation, conditional on the rainfall state (wet or dry), which is then disaggregated to the same time scale as the rainfall; and
- the development of a conceptual catchment water balance model that combined with the rainfall and evaporation inputs, produces a continuous simulation model that can be used to generate long concurrent series of rainfall and rainfall excess.

As introduced in Chapter 1, a technique for eliminating the need to select a value of initial loss when calculating design flood frequency distributions is being examined. This chapter develops such a technique by examining the relationship between the Intensity-Frequency-Duration (IFD) curves of the simulated rainfall and the Rainfall Excess-Frequency-Duration (REFD) of the simulated rainfall excess. This relationship is then described in terms of REFD proportions (the ratio of the REFD to the IFD) for a design event of a given duration and Average Recurrence Interval (ARI). The REFD proportions enable the design rainfall to be converted directly to design rainfall excess, in effect providing a proportional loss model with zero initial loss. This improves the design flood estimation approach by eliminating a sensitive input parameter, but retains the overall simplicity of use of the design method. Validation of this approach was undertaken using the rainfall excess calculated from the REFD proportions as input into a flood estimation model to determine a flood frequency distribution, which was then compared with observed distributions.

Validation of this method is presented for four of the sites calibrated using the catchment water balance model in Chapter 7, these being Alligator Creek (Queensland), Avon River (Victoria), Boggy Creek (Victoria) and Scott Creek (South Australia). Difficulties exist in applying this method at the other two sites because of a lack of observed rainfall-runoff events, which are needed to effectively calibrate the flood estimation model.

8.1 DEVELOPMENT OF REFD PROPORTIONS FROM CONTINUOUS SIMULATION

The stochastic rainfall and evaporation models, together with the catchment water balance model were used to simulate 250 years of synthetic rainfall and rainfall excess data for each study catchment. A description of the pluviograph data used for each site is provided below. The IFD and REFD curves for the simulated rainfall and rainfall excess respectively, were determined using the same windowing technique and frequency analysis method described in Section 5.2. The relationship between these curves was then examined in order to establish a means of converting the IFD to REFD during design.

8.1.1 Available Pluviograph Data

The aggregated and IFD statistics of the available pluviograph data were compared with those of the catchment average rainfall and the Australian Rainfall and Runoff (ARR, 1987) design IFD curves respectively. If the statistics were consistent, no adjustments to the simulated data was required. However, the pluviograph was not always located on the catchment and in one case it was a considerable distance away. In this instance the simulated rainfall data based on the pluviograph record required modification to adequately reproduce the observed statistical characteristics of the catchment average rainfall and IFD relationships.

The pluviograph data used to simulate rainfall for the Boggy Creek, Alligator Creek and Avon River catchments required no adjustment. For Boggy Creek, a six-minute pluviograph station is co-located with one of the daily rainfall gauges used to determine the catchment average rainfall which is located at Whitfield (083031). This record has approximately 30 years of data. For Alligator Creek there is a pluviograph at Townsville (032040), which is located outside and approximately 20 km from the catchment with 46 years of data. For Avon River there is a pluviograph at Tottington (079079), which is located within the catchment and has approximately 28 years of data.

The closest six-minute pluviograph station to the Scott Creek catchment having a reasonable length of record, approximately 28 years of data, is at Williamstown (023763), which is 45 km from the catchment. Comparison of the statistics revealed that higher rainfall occurs at the Scott Creek catchment than at the pluviograph site and that the IFD bursts are more intense, particularly at higher durations. This difference was accounted for by increasing the simulated average event intensity at higher event durations. The average event intensity was

increased by 5% for event durations less than six hours and by 60% for event durations greater than six hours. The simulated aggregated statistics were validated using the observed statistics from the catchment average rainfall data at a daily, monthly and annual scale. In addition to the mean and standard deviation, it was important to ensure that the dry probability statistics were well reproduced as this significantly affects the level of initial loss. The simulated IFD characteristics were also compared with the ARR (1987) IFD curves and the reproduction was considered satisfactory across all burst durations for both sites. In the absence of a more satisfactory method to generate statistically suitable six-minute rainfall at these sites this approach was considered reasonable. A comparison of simulated rainfall and the catchment average rainfall statistics for each site is contained in Appendix N.

8.1.2 Generation and Analysis of Rainfall Excess

The modified AWBM catchment water balance model was then used with the calibrated parameters from Chapter 7 to generate 250 years of synthetic rainfall excess. A frequency analysis of this synthetic rainfall excess was undertaken using a generalised exponential distribution (GEV) to represent the annual maxima. Figure 8.1 to Figure 8.8 show the fitted distribution for 3 and 72 hours at Alligator Creek, 3 and 24 hours at Boggy Creek, 1 and 24 hours at Scott Creek and 1 and 72 hours at Avon River respectively. Because the synthetic rainfall excess is only 250 years in length, little reliance should be placed on the simulated data for ARI values greater than 100 years. Fitted distributions for all durations are shown in Appendix N and are considered satisfactory.

8.1.3 Analysis of Rainfall IFD and REFD Distributions

In order to identify a relationship between the IFD and REFD curves, the fitted distributions were compared. These are shown for durations of 1, 3, 12, 24 and 72 hours for each site in Figure 8.9 to Figure 8.12. As can be seen, for each duration the shape of the rainfall excess REFD curve and the rainfall IFD curve has a similar pattern for increasing ARI. Therefore, establishing a similar relationship for all sites between the two curves appeared plausible. The form of scaling required to transform rainfall into rainfall excess, the ratio of the REFD curve to the rainfall IFD curve was examined for each duration. Figure 8.13 shows this relationship for Boggy Creek. The left vertical axis shows this ratio as the proportion of rainfall excess that will occur for a given duration. The right vertical axis presents the relationship in terms of the amount of rainfall that will become loss. For ARIs between 5 and

100 years, this relationship appears to be relatively constant and varies little with duration.

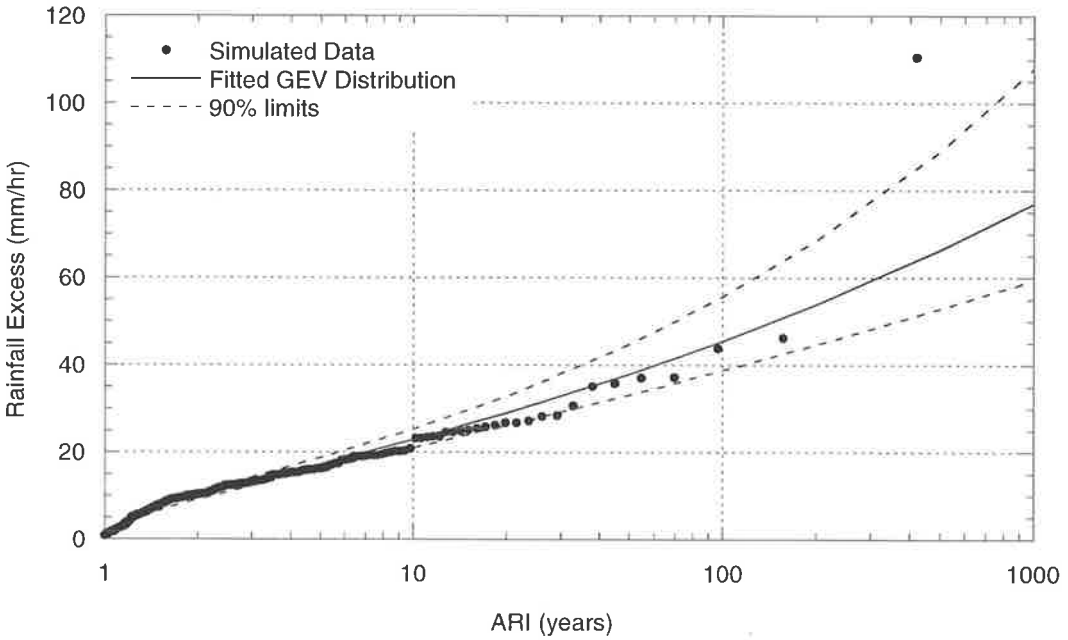

Figure 8.1 Alligator Creek: Fitted GEV distribution to 3 hour simulated REFD data.

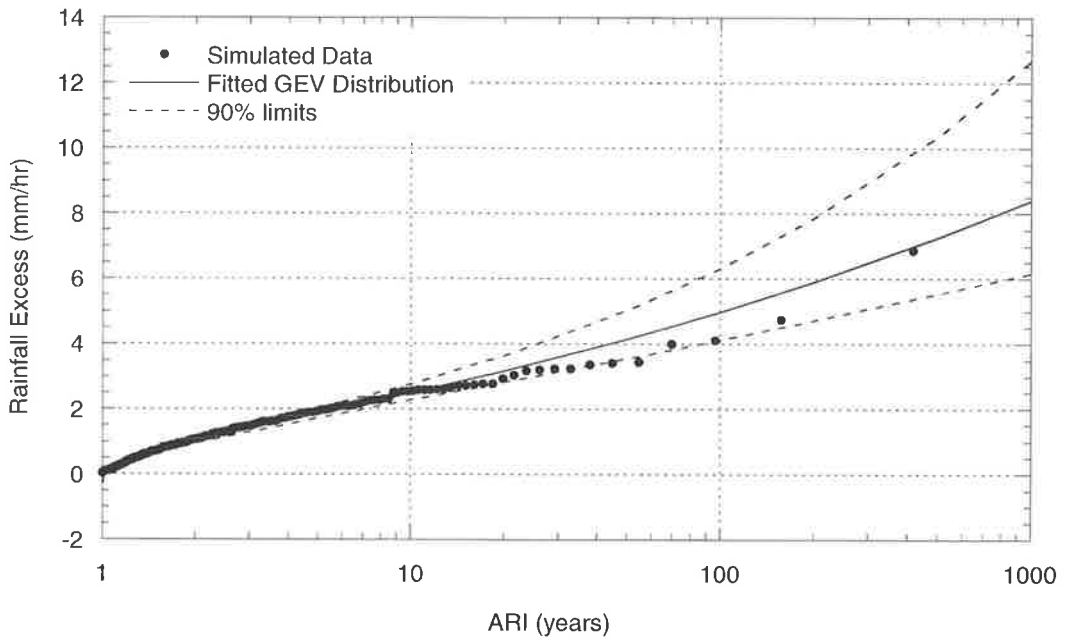

Figure 8.2 Alligator Creek: Fitted GEV distribution to 72 hour simulated REFD data.

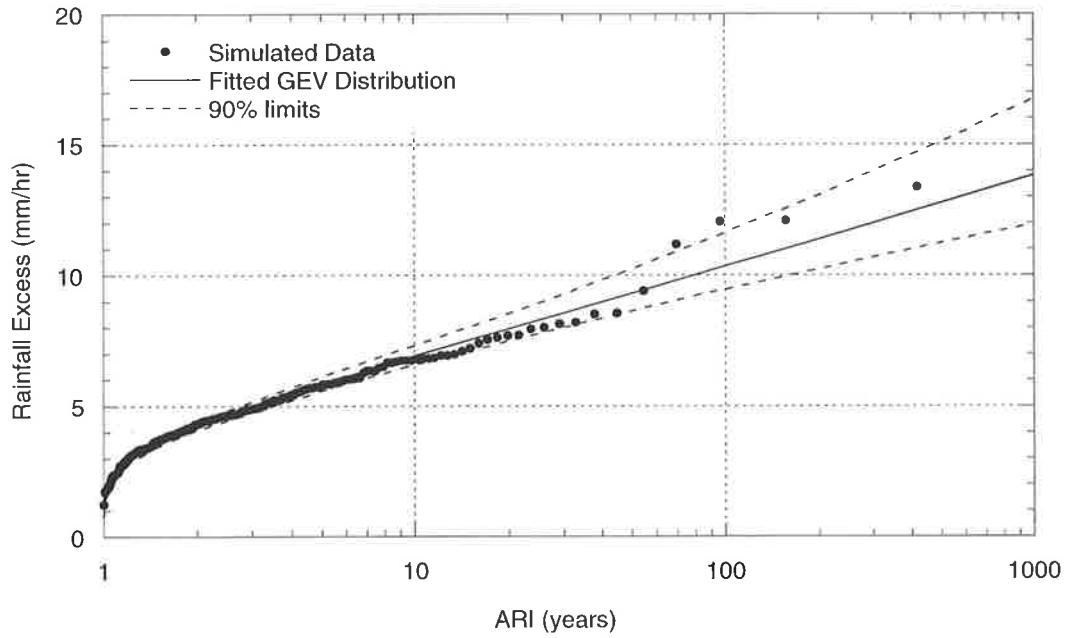

Figure 8.3 Boggy Creek: Fitted GEV distribution to 3 hour simulated REFD data.

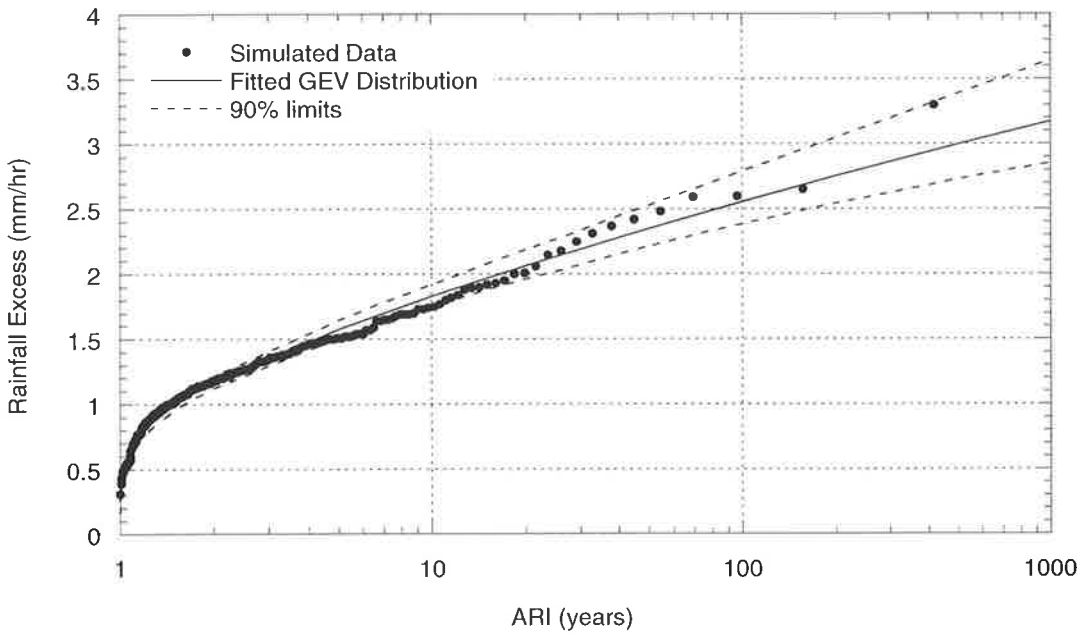

Figure 8.4 Boggy Creek: Fitted GEV distribution to 24 hour simulated REFD data.

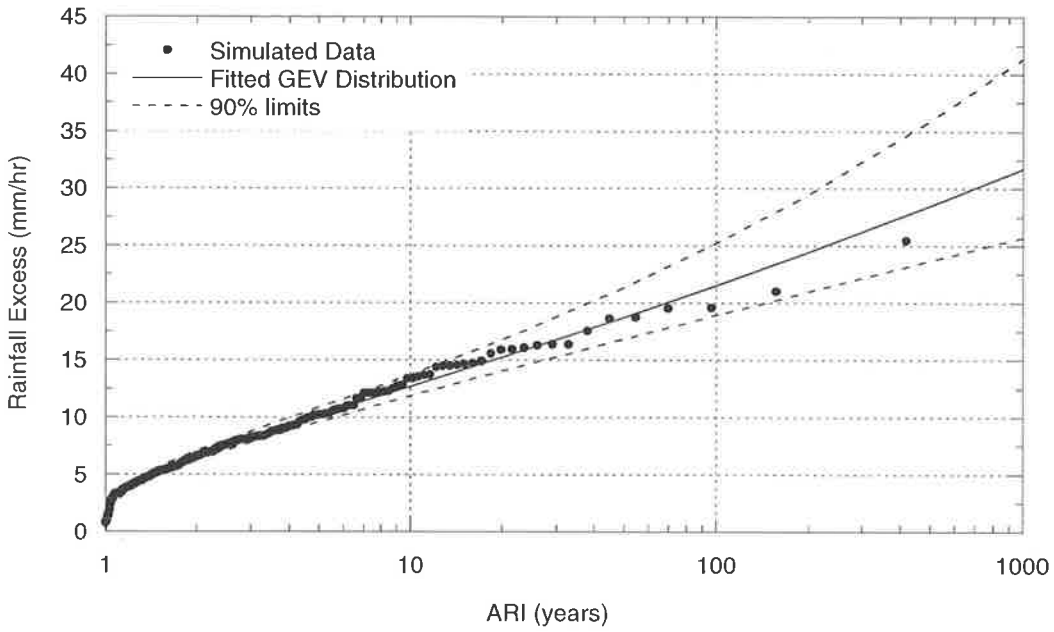

Figure 8.5 Scott Creek: Fitted GEV distribution to 1 hour simulated REFD data.

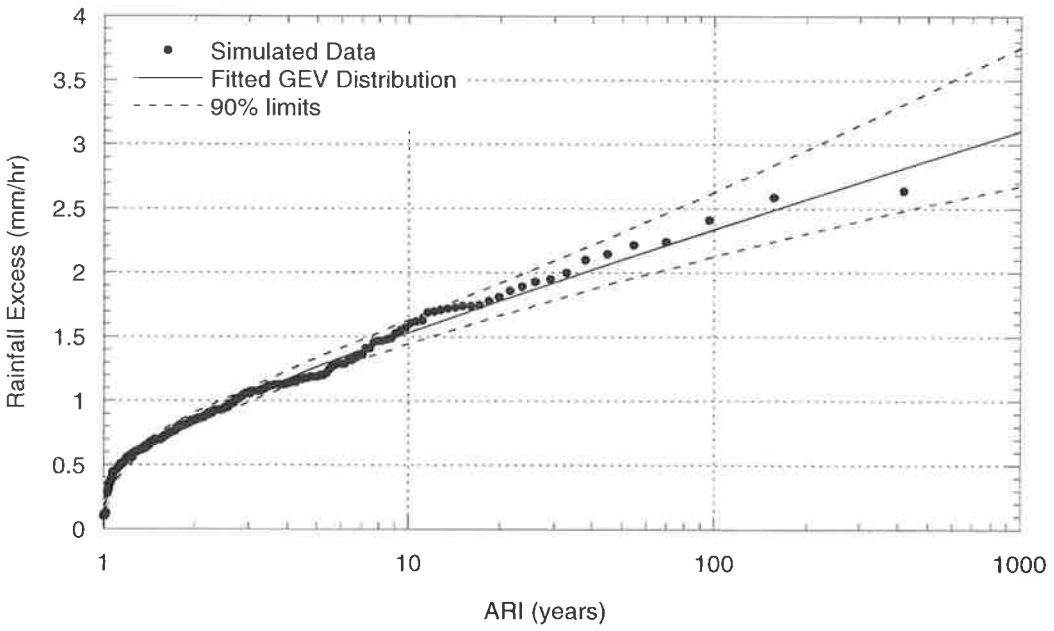

Figure 8.6 Scott Creek: Fitted GEV distribution to 24 hour simulated REFD data.

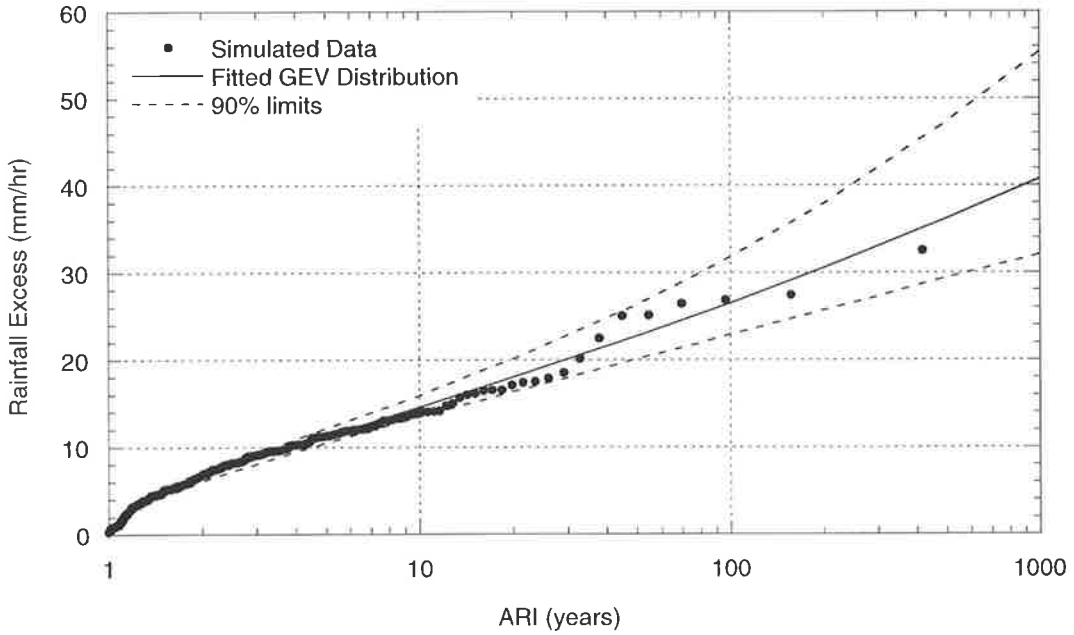

Figure 8.7 Avon River: Fitted GEV distribution to 1 hour simulated REFD data.

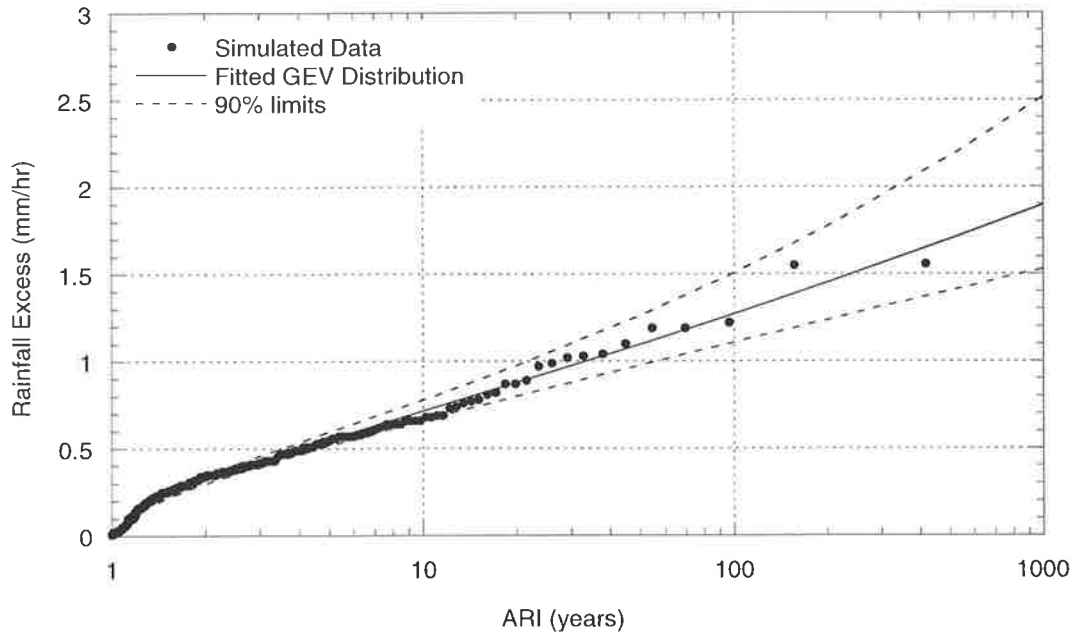

Figure 8.8 Avon River: Fitted GEV distribution to 72 hour simulated REFD data.

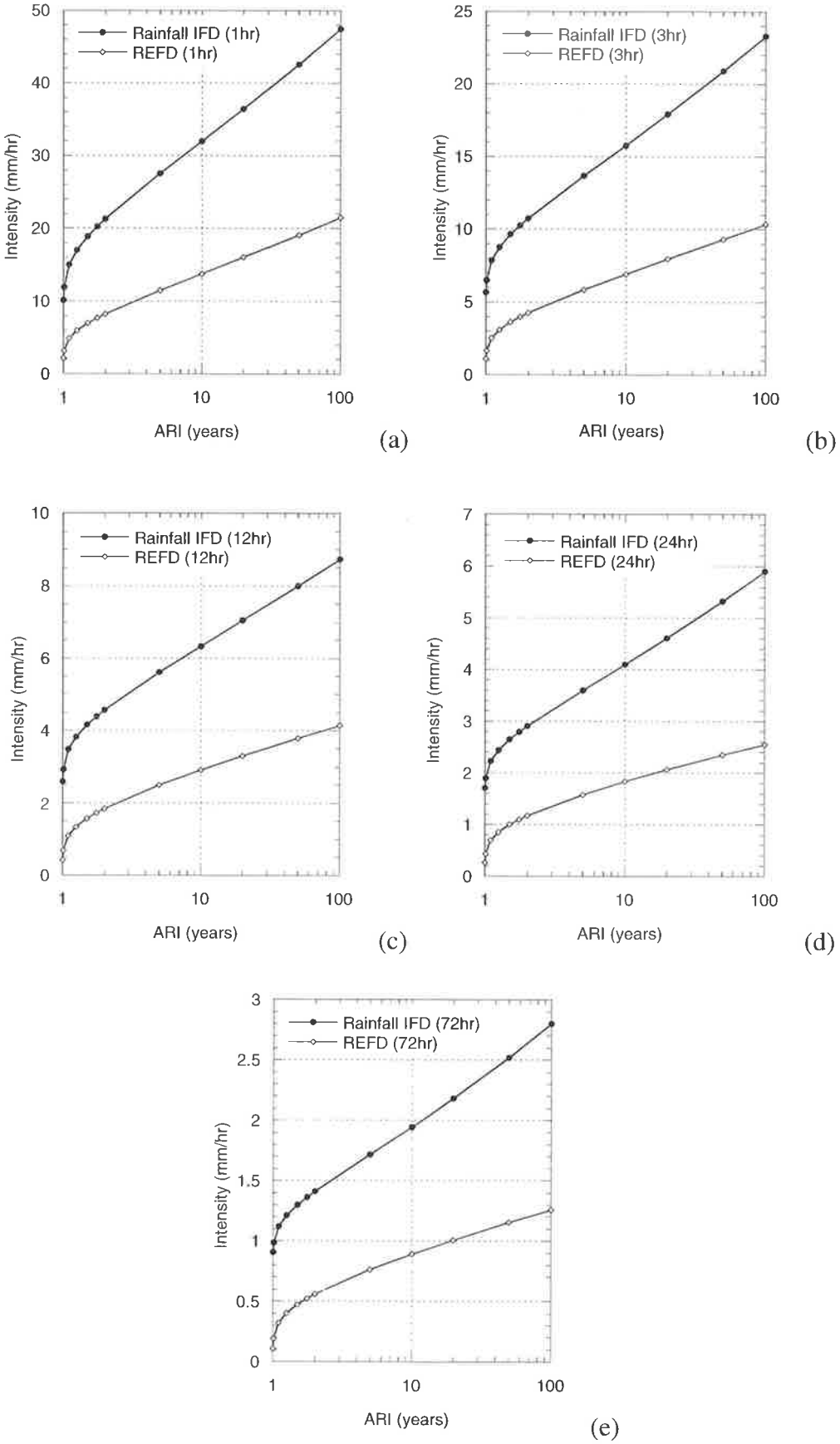

Figure 8.9 Rainfall IFD and REFD distributions for Boggy Creek catchment: (a) 1 hour; (b) 3 hours; (c) 12 hours; (d) 24 hours; (e) 72 hours.

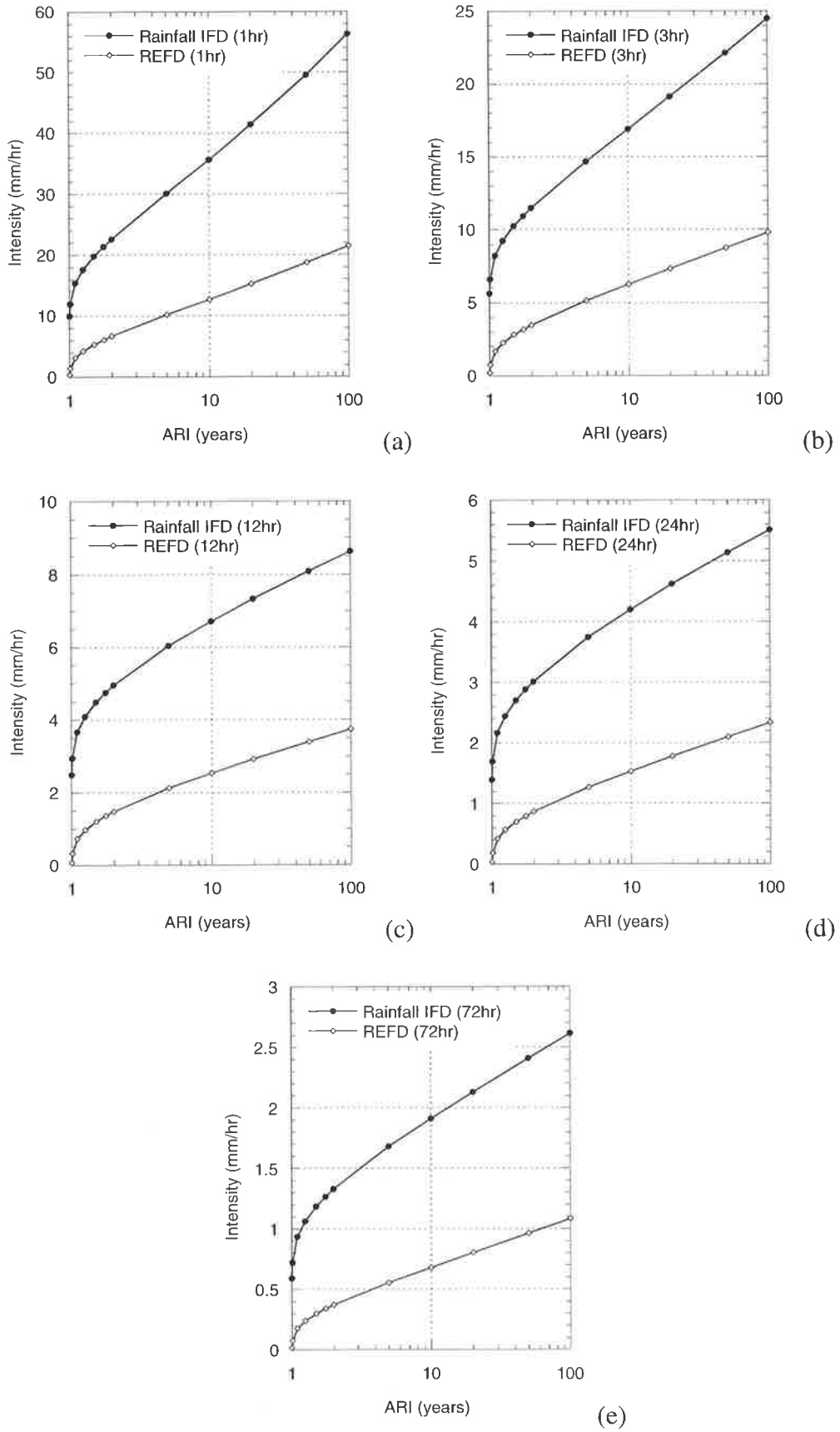

Figure 8.10 Rainfall IFD and REFD distributions for Scott Creek catchment: (a) 1 hour; (b) 3 hours; (c) 12 hours; (d) 24 hours; (e) 72 hours.

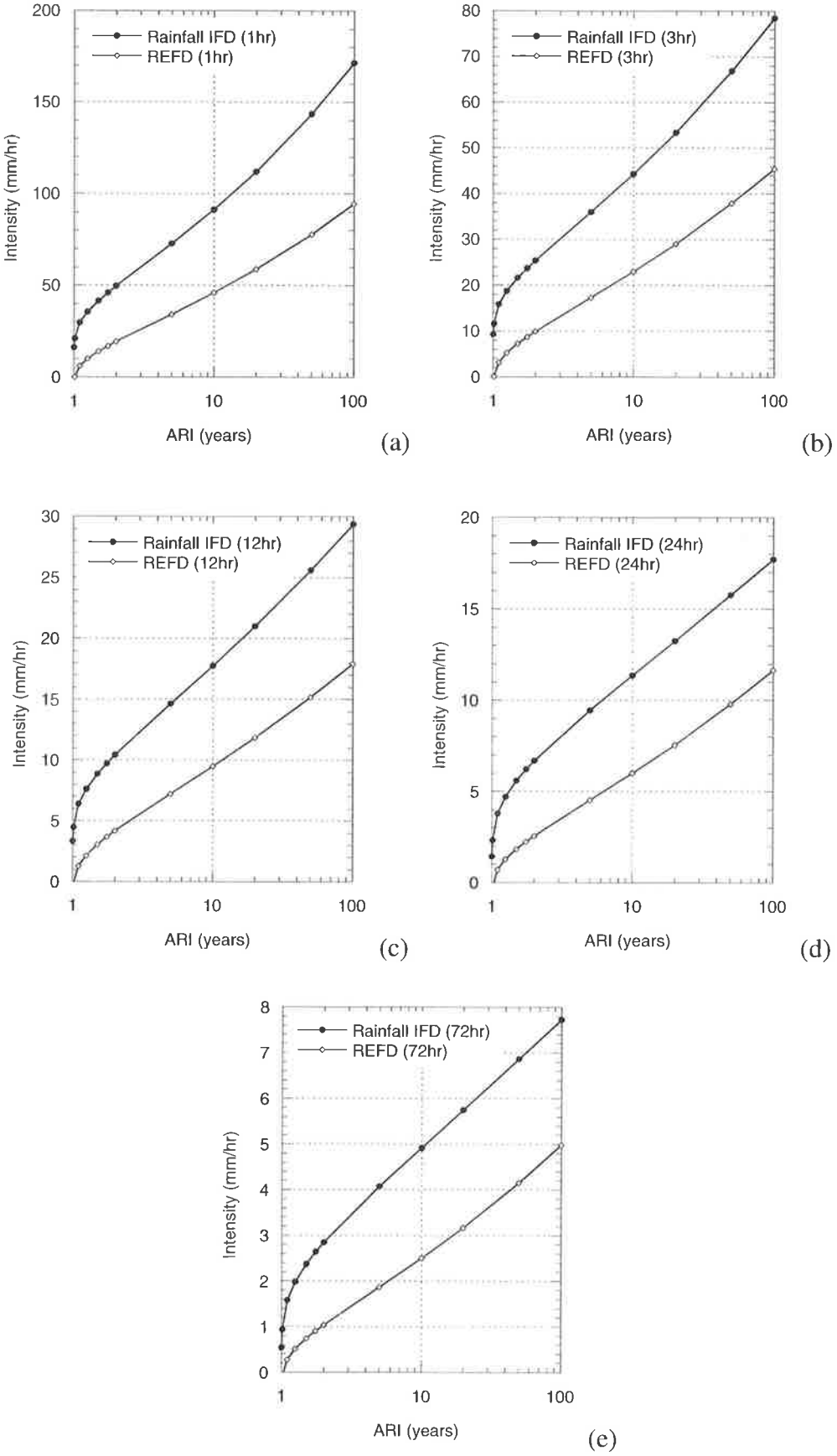

Figure 8.11 Rainfall IFD and REFD distributions for Alligator Creek catchment: (a) 1 hour; (b) 3 hours; (c) 12 hours; (d) 24 hours; (e) 72 hours.

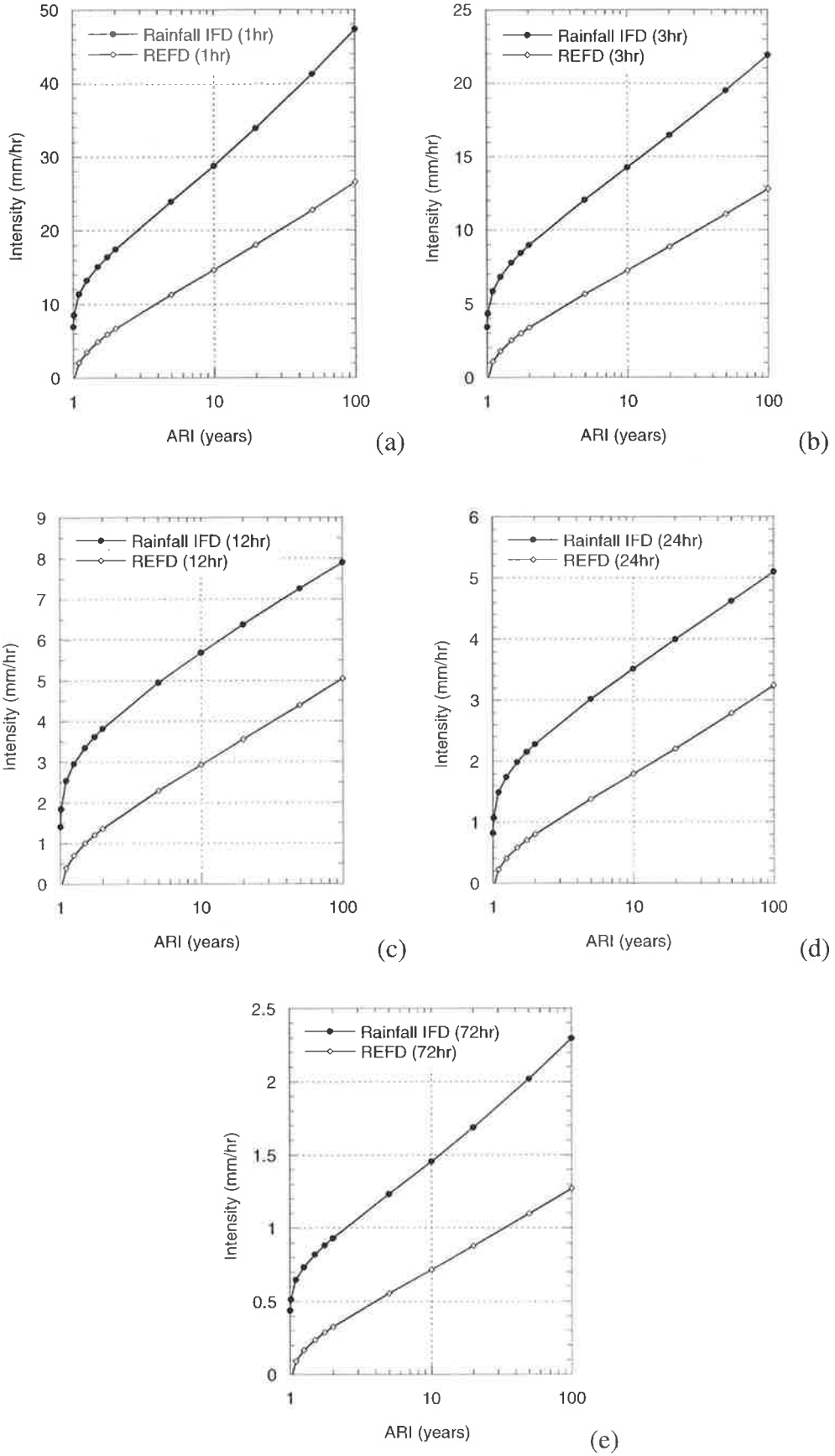

Figure 8.12 Rainfall IFD and REFD distributions for Avon River catchment: (a) 1 hour; (b) 3 hours; (c) 12 hours; (d) 24 hours; (e) 72 hours.

The ratio of the curves for Scott Creek is shown in Figure 8.14. For each ARI the relationship is relatively constant with duration and as the ARI increases from 2 to 100 years, the ratio of rainfall to rainfall excess increases slowly. For Scott Creek and Boggy Creek, the REFD proportions suggest the possibility of using a fixed REFD proportion for all higher ARI design considerations. Figure 8.15 and Figure 8.16 show the curve ratios for Alligator Creek and Avon River respectively. For these sites it can be seen that this relationship increases, and hence loss decreases, steadily with ARI. However, for each ARI the relationship is relatively constant with duration.

The AWBM partitions overflow from the surface stores into surface runoff and sub-surface recharge using a baseflow infiltration index (BFI). Therefore, 1-BFI defines the maximum surface runoff that can occur for a given rainfall event, provided the rainfall is less than maxRain. In this latter case, a higher proportion of rainfall may become surface runoff, although it is likely that the REFD proportions would approach 1-BFI. For Alligator Creek (Figure 8.15) the REFD proportions are close to 1-BFI at an ARI of 100 years. For Avon River (Figure 8.16) the REFD proportions are still increasing at an ARI of 100 years and may approach the 1-BFI level at higher ARI values.

For Boggy Creek (Figure 8.13) and Scott Creek (Figure 8.14) the REFD proportions are more constant and conceivably may not reach the 1-BFI level even at ARIs much large than 100 years. Because the simulated rainfall excess was only 250 years in length, it was thought that this was perhaps not long enough to gain meaningful values for ARIs of 100 years. However, the REFD proportions from longer simulations of 1 000 years for these two sites produced almost identical results. It would appear that the surface storages are not close to capacity prior to higher ARI events and hence more initial loss occurs during these higher ARI events than may occur for Alligator Creek and Avon River. In these cases, there may be a maximum proportion of the rainfall that can become runoff. In addition, if the sub-surface storages at these sites are sufficiently reactive, a large proportion of total flow may occur by this mechanism. Further investigation into the mechanisms that cause the higher runoff events may be warranted.

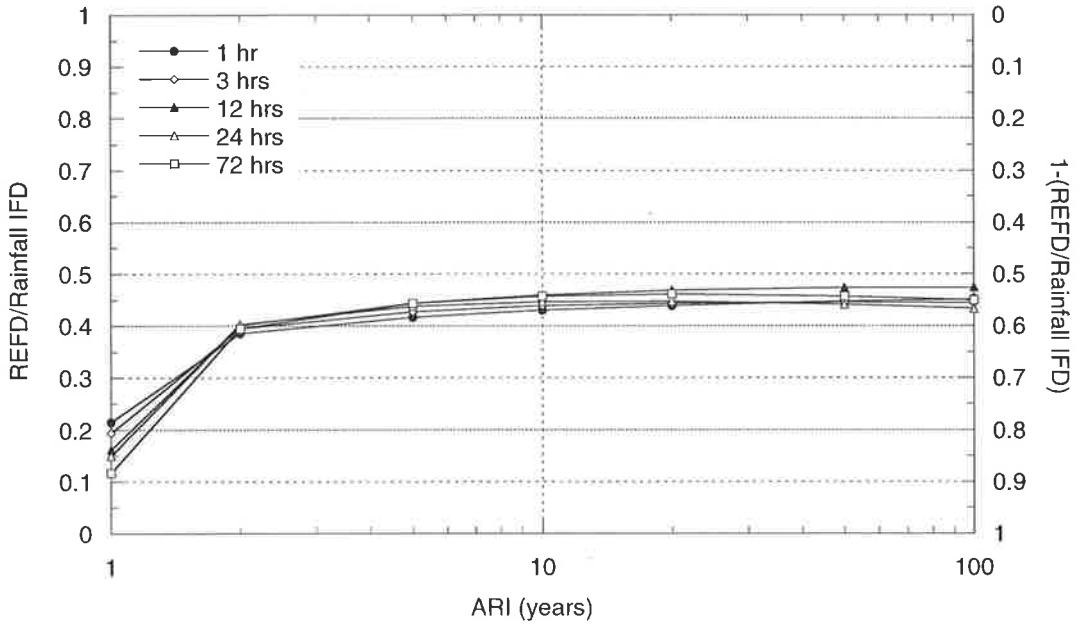

Figure 8.13 Proportional loss-frequency curve for Boggy Creek catchment.

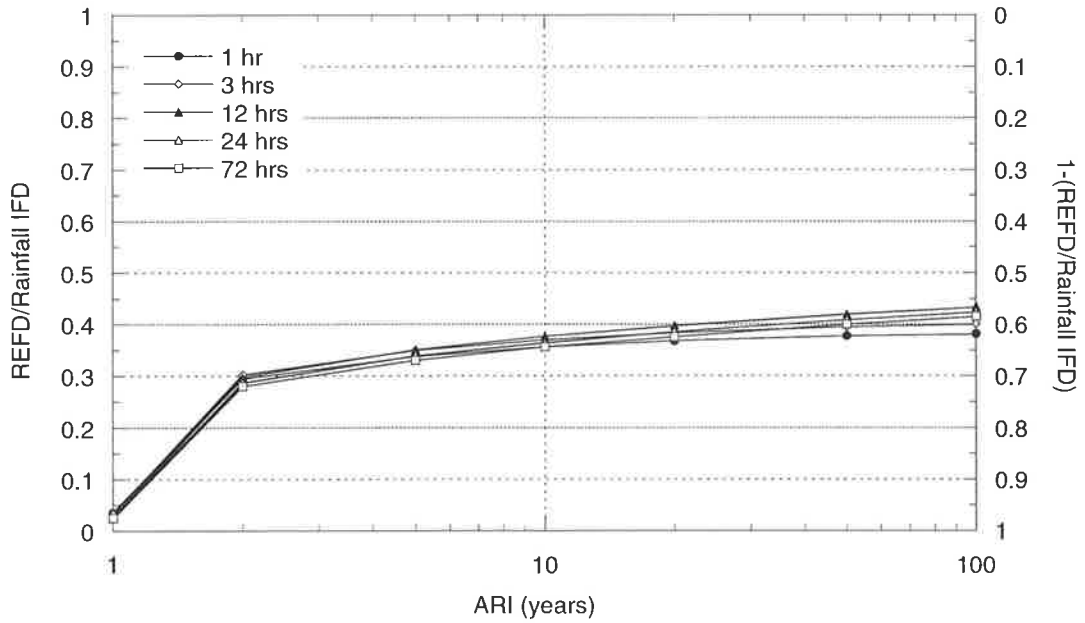

Figure 8.14 Proportional loss-frequency curve for Scott Creek catchment.

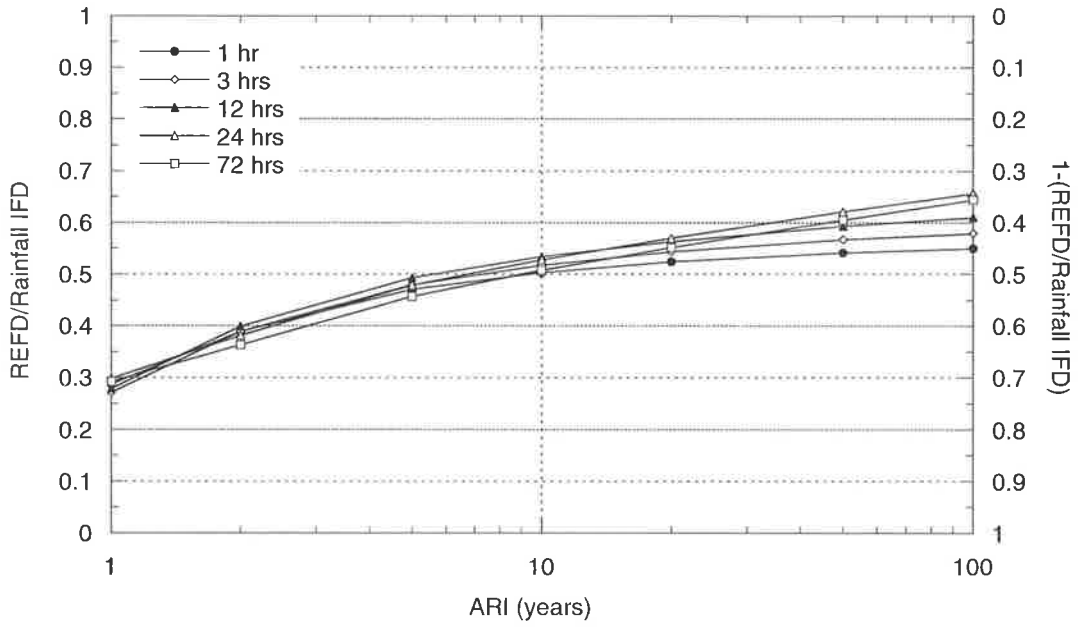

Figure 8.15 Proportional loss-frequency curve for Alligator Creek catchment.

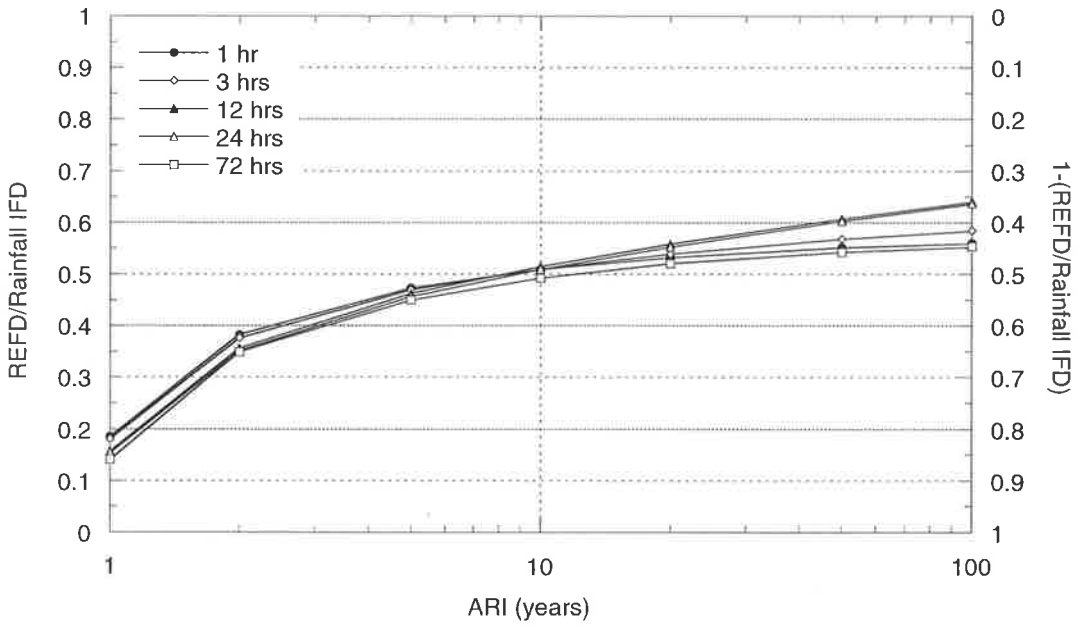

Figure 8.16 Proportional loss-frequency curve for Avon River catchment.

The amount of surface runoff is related to the storage properties of the catchment and the levels of baseflow. Because initial loss is taken into account during continuous simulation by the surface stores, it is clear from the generally increasing nature of the REFD proportions with ARI that the initial loss and hence the level of surface runoff is dependent upon ARI. For smaller ARI events, the level of water is lower in the stores indicating that higher levels of initial loss are occurring while for higher ARI events, the stores are able to hold less of the incident rainfall and more run off occurs. In current design flood estimation the ARI of the initial loss is not considered. However, these results suggest that it should be taken into account.

The ratio of REFD to the rainfall IFD can be defined as a set of proportional loss-frequency curves, which define the separation of the design rainfall into rainfall excess and infiltration, or loss, that occurs after runoff has commenced. It was proposed that these curves could be used in a runoff-routing model, which is effectively the equivalent of assuming a proportional loss model for the entire rainfall burst. This approach removes the need to assume an initial loss because it has already been taken into account within the continuous simulation of rainfall excess and hence within the REFD curves. The suitability of this approach is further examined in Section 8.3.

8.2 Selection and Calibration of a Flood Estimation Model

To validate the use of the proportional loss-frequency curves developed in the previous section, a flood estimation model such as a unit hydrograph or runoff-routing model must be chosen and calibrated. The proportional loss-frequency curves can then be used to transform the rainfall into rainfall excess, which is then routed through the catchment to the outlet using the chosen model. The flood frequency distribution can then be determined and compared to the observed distribution. In this section, some of the available models are discussed, including the one selected for use in this study. The results from the calibration of the chosen model using observed flood events and associated concurrent rainfall data are then presented.

8.2.1 Unit-Hydrograph Methods

A unit hydrograph is defined (ARR, 1987) as the hydrograph resulting from a unit depth of rainfall excess produced by an event of uniform intensity and specified duration occurring

over a catchment. The unit depth is generally taken as 1 mm. The unit hydrograph is applied to the rainfall excess hyetograph to estimate the hydrograph of the surface runoff. Baseflow must then be added to produce the total runoff hydrograph. This method assumes that the catchment response behaviour is linear. The unit hydrograph for a catchment is generally derived from large flood events to ensure this assumption is met (ARR, 1987). Minimisation procedures are used to derive a unit hydrograph, which involves matrix manipulation of a series of equations to relate the ordinates of the surface runoff hydrograph to the rainfall excess hyetograph and unit graph.

There are a number of advantages of using unit hydrographs, compared to runoff-routing models, in that the procedure is relatively simple to apply and is based on the integrated response of the catchment so that no assumptions are required regarding storage effects. Alternative unit hydrographs can be derived for different types of conditions on a catchment or for different antecedent moisture conditions. However, the method is limited to a linear response, which is adequate for large events on most catchments (ARR, 1987) but may not always be a reasonable description of the actual rainfall-runoff process, particularly if large storages such as dams or reservoirs are present within the catchment. Also, the unit hydrograph is derived for gauging station locations, so that if a flood estimate is required at a different location within the catchment, it must be adjusted.

8.2.2 Runoff-Routing Methods

The estimation of a flood hydrograph by runoff-routing involves the routing of rainfall excess through a model that represents the catchment storage characteristics. This method provides an alternative to the use of a unit hydrograph as it is not restricted by the assumption of linear behaviour that may result in underestimation of the peaks for major flood events (ARR, 1987). Other advantages of runoff-routing models over unit hydrograph methods include the use of the actual stream network, which results in a better representation of the spatial distribution of catchment storage, and the ability to include the effects of any significant storages such as dams or reservoirs.

Developing a runoff-routing approach involves the selection of an appropriate conceptual model of catchment storage, development of a storage model network and the calibration of model parameters for the catchment concerned. The complexity of these models can often lead to difficulties in parameter estimation during calibration. The storage model network for

a particular catchment is determined by sub-dividing the catchment into a series of sub-catchments that contain major tributaries or reaches of the stream. Model parameters are calibrated using available flood records and concurrent rainfall data. Discussed in the following are a number of runoff-routing models commonly used in Australia. The output from a model can be either the surface runoff hydrograph at the catchment outlet to which baseflow must be estimated and added, or the total runoff hydrograph if baseflow is incorporated into the model and is routed through the catchment storage with the rainfall excess (ARR, 1987).

RORB

The RORB runoff-routing model (Laurenson and Mein, 1985, 1990) is widely used and recommended for Australian design flood estimation (ARR, 1987). RORB is structured so that each sub-catchment between specified nodes of the storage model network is represented by a non-linear concentrated storage that is assumed to have a storage discharge relationship described (ARR, 1987; Walsh, 1991) by the following:

$$S = 3600\, k\, Q^{m} \tag{8.1}$$

where:

S = storage (m^3);

Q = outflow discharge (m^3/s);

m = exponent parameter; and

k = empirical coefficient.

The parameter m is a measure of the non-linear behavioural properties of the catchment and is dependent on the size of the flood plain storage. The greater this storage and the closer the value of m is to 1.0, the closer the catchment response is to a linear system (ARR, 1987). The coefficient k is determined for each sub-catchment by the product of a catchment parameter (k_c) applicable to the entire catchment and a relative delay time ratio (k_r) applicable to each sub-catchment. The value of k_c is the more important of the two parameters of k when attempting to reproduce observed hydrographs. Small values of k_c will result in a decreased delay of catchment runoff and hence an increase in peak discharge (Walsh, 1991).

Two alternative loss models are used to model loss to determine the rainfall excess

hyetograph, an initial loss followed by either a runoff coefficient or a constant loss rate. Baseflow must be estimated separately and added to the surface runoff hydrograph.

Watershed Bounded Network Model (WBNM)

The structure of the WBNM (Boyd *et al.*, 1979a; 1979b; 1987) is similar to RORB, but is based on more detailed consideration of geomorphological relations. For each sub-catchment defined within the model network, the WBNM uses a storage to route the rainfall excess to the sub-catchment outlet and a second *transmission* storage to route any upstream runoff through the catchment. Because the characteristics and delay times of each storage type is different, the resulting model behaviour is physically realistic (ARR, 1987). The storage used to route the rainfall excess on a given sub-catchment is described (ARR, 1987) as:

$$S = K_B Q \tag{8.2}$$

where:

K_B = storage parameter (hours)

$= c A^{0.57} Q^{-0.23}$;

A = sub-catchment area (km^2);

Q = outflow discharge at downstream end of the sub-catchment(m^3/s); and

c = empirical coefficient that applies to all sub-catchments.

The corresponding transmission storage parameter (K_I) for routing upstream runoff is equal to $0.6 K_B$ (ARR, 1987). Because there is only the parameter c to calibrate, ARR (1987) considers this model easier to apply than RORB. Both models produce similar results and as with RORB, baseflow must be calculated separately and added to the surface runoff hydrograph.

KinDog

KinDog (Kuczera *et al.*, 2000) is a kinematic runoff-routing catchment model based on the Field-Williams Kinematic Catchment Model (Field and Williams, 1983, 1987). It conceptualises rainfall excess as Hortonian overland flow routed through a non-linear storage into a channel. Infiltration recharges a sub-surface linear store which then simulates the baseflow or the sub-surface event-flow process. Flow in channels is modelled using a kinematic wave. The model incorporates both the initial loss-continuing loss and initial loss-proportional loss models to determine infiltration. Initial loss does not infiltrate but is

removed from the system. Because the model incorporates sub-surface flow, there is no need for baseflow separation, nor to add baseflow to a design event.

The parameters that require calibration relate to the following components of the model:

- channel conveyance (C_r and m);
- surface supply (C_s and γ);
- infiltration (initial loss and continuing loss (CL) or proportional loss (PL)); and
- sub-surface supply (C_g).

The kinematic wave approximation for flow through the channel equates the friction and bed slopes and then uses Manning's equation to define the discharge as:

$$Q = K S^{0.5} \tag{8.3}$$

where:

S = bed slope;

K = channel conveyance (m^3/s)

= $C_r A_r^m$;

m = channel conveyance exponent;

C_r = channel conveyance coefficient ($m^{(3-2m)}s^{-1}$); and

A_r = flow area (m^2).

The rate of surface supply (S_s) is related to the depth of water stored on the hillslope by:

$$h_s = C_s B_\gamma S_s^\gamma$$

where:

C_s = surface supply parameter ($m^{(1-2\gamma)}s^{\gamma}$); and

γ = hillslope flow exponent.

The rate of sub-surface supply (s_g) is related to the depth of the sub-surface store (h_g) by:

$$h_g = C_g B s_g \tag{8.4}$$

where:

C_g = sub-surface supply parameter (sm^{-1}); and

B = width of the catchment element (m).

The different components of the model influence the ability to reproduce an observed hydrograph in different ways. C_r influences the timing of the hydrograph peak, C_s the peak flow and C_g the recession limb.

The advantages of KinDog over other established models such as RORB is that it incorporates sub-surface flow directly and explicitly distinguishes between hillslope runoff and channel flow. In addition, overbank flow along channels can be modelled using *difference conveyance relationships* that may allow a more reliable extrapolation to extreme events (Kuczera, 2001).

Discussion of Runoff-Routing Models

Runoff-routing models and unit hydrograph methods are the two main approaches recommended in ARR (1987). Guided by this, the review options were limited to these. However, it is also noted that there are models, such as the US Army Corps HEC-1 model, which combine both techniques in the same model. There are a number of advantages of using runoff-routing models over unit hydrograph methods, particularly as the arrangement of a catchment storage network provides a realistic physical basis to take account of the characteristics of a given catchment (ARR, 1987). Hydrographs can be determined at almost any location within the catchment and catchment changes such as additional storages or urbanisation can be easily incorporated. Also, the non-linearity of catchment response can be modelled along with the spatial variation of rainfall over a catchment. However, while the models have an overall physical realism, they all incorporate assumed relationships (such as the power law relation that provides for non-linear response) that may differ from observed rainfall-runoff behaviour (ARR, 1987). Data errors can have a greater effect on a non-linear model, especially if the design events being investigated are much larger than the events available for calibration (ARR, 1987).

In recent design flood estimation studies, Boughton (2000a) applied a combination of the unit hydrograph method and a runoff-routing model. Each hour of rainfall excess had its arrival at the catchment outlet spread into a fixed pattern in the manner of a unit hydrograph. The spatial pattern of rainfall excess was then routed to the catchment outlet using a single non-linear concentrated storage in a form similar to Equation (8.1), to determine the hourly hydrograph of runoff. Rahman *et al.* (2001) also used a single non-linear storage model.

8.2.3 Model Choice

Of the models discussed, the KinDog (Kuczera *et al.*, 2000) was chosen as the rainfall-routing model for this study. This choice was made as this model allows sub-surface flow to be routed through the catchment, removing the need to separate observed streamflow into surface runoff and baseflow to calibrate the model, and the need to determine the baseflow to generate the total runoff hydrograph. The generation of baseflow for design situations introduces uncertainty into the appropriateness of the selected ARI of the resulting flood event, as discussed in Section 8.3.1. The KinDog model has been tested on a number of Australian catchments with good results (Kuczera, 2002).

8.2.4 Runoff-Routing Model Calibration

The study catchments were each divided into a series of nodes and associated sub-catchments. For example, Scott Creek catchment was defined by 7 sub-catchments as shown in Figure 8.17. Each node defines the upper end of the main stream length of a sub-catchment and the drainage paths within the catchment. Node 1 defines the outlet and location of the streamflow gauging station. Node P defines the relative position of the rainfall pluviograph. Appendix O contains a map of each catchment, catchment layouts, sub-catchment areas, main stream lengths and elevation of nodes.

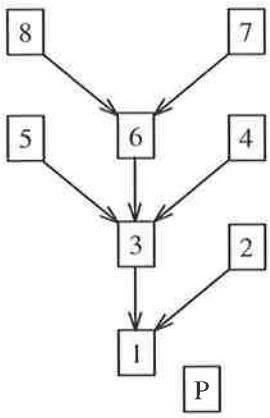

Figure 8.17 Layout of sub-catchments in the Scott Creek catchment.

For each catchment, a number of flood events with the associated high resolution pluviograph data were used to calibrate the model with the aim of determining common, event independent parameters for the catchment. Of the six common KinDog model parameters, two were assumed to have fixed values for the four catchments. Kuczera (2001) recommends that the channel conveyance exponent parameter m=1.4 and the hillslope flow exponent

$\gamma=0.5$ because of high correlation with C_r and C_s respectively. Table 8.1 shows the values of the six common model parameters obtained for each catchment. Although the model allows different parameters to be used for each sub-catchment, in this study the parameters determined were applied over the entire catchment to assist with simplicity of application to design situations.

Table 8.1 Common model parameter values obtained from concurrent calibration of events.

	Alligator Creek	Avon River	Boggy Creek	Scott Creek
Cs	0.40	0.46	1.05	0.80
γ	0.50	0.50	0.50	0.50
Cg	50	990	1800	600
PL	0.43	0.28	0.54	0.34
Cr	9.00	4.70	19.0	10.0
m	1.40	1.40	1.40	1.40

The final KinDog parameter that needs to be calibrated is initial loss, which is event specific. Because rainfall pluviographs are not usually located near the catchment outlet, the rainfall event may move over the pluviograph location at a different time to when it moves over the catchment. Therefore, a hydrograph offset adjustment factor was used to adjust the rainfall and streamflow so that the records were concurrent. Another adjustment factor for specific events is a rainfall multiplier, which is used to allow the event rainfall to be increased or decreased. This may be required to address the issue of spatial variability of rainfall over a catchment, particularly where there is a high rainfall gradient, as is the case for Scott Creek and Avon River. Table 8.2 shows the initial loss parameter obtained and the adjustment factors for rainfall and the hydrograph used for each catchment.

There were five flood events from the Boggy Creek catchment suitable for calibration, the most of any site. The results from two of these events are shown in Figure 8.18 to Figure 8.19. It must be emphasised that because model parameters were obtained from the concurrent calibration of a number of events, the resulting parameters and relationships between the observed and predicted outflow may not be as good as if each event was calibrated independently, allowing different parameters to be found for each event. However, as can be observed in the figures, this approach results in a set of event independent parameters that can be used for a range of simulated events, while still providing an adequate representation of actual events.

Table 8.2 Event dependent parameters and adjustment factors obtained from concurrent calibration of events.

Catchment	Event	Initial Loss (mm)	Hydrograph Offset (hrs)	Rainfall Multiplier
Alligator Creek	1977	20	-2.00	0.57
	1978	50	-4.30	1.96
	1990	27	-0.75	0.55
Avon River	1973	9.0	-3.00	1.41
	1975	0.0	-5.00	0.92
	1981	8.2	-3.00	1.22
	1983	2.8	-5.00	0.94
Boggy Creek	1978	0.0	-1.75	1.00
	1979	11.5	-1.25	1.07
	1980	0.0	-1.39	0.825
	1981	14.0	-4.75	1.33
	1983	0.25	0.75	1.23
Scott Creek	1992	8.5	-1.00	1.10
	1995(1)	25.0	-1.15	2.15
	1995(2)	0.0	-1.46	0.98
	1996	0.0	0.00	0.85

Four flood events were available for the Scott Creek and Avon River catchments. The calibrated parameters produce a satisfactory representation of each event, as shown for two events in Figure 8.20 and Figure 8.21 for Scott Creek and Figure 8.22 and Figure 8.23 for the Avon River. There were only three flood events with associated high resolution pluviograph data for Alligator Creek. Other flood events were available in the streamflow gauging record, but unfortunately the associated rainfall data was not satisfactory. Figure 8.24 and Figure 8.25 show the results for two of these events. Although the recession curves for this site are not as well reproduced as for Boggy Creek and Scott Creek, the flood peaks at the Alligator Creek gauging station are much higher and have been reproduced using the calibrated parameters. It was considered important that these peaks were predicted adequately.

In Table 8.2, it can be seen that there were large differences in the value of the hydrograph offset parameter between events at the same site. This may be due to a number of factors. For tropical locations, rainfall events can be caused by a number of mechanisms including cyclonic activity, which may result in rainfall events approaching and moving over a catchment from varying directions. Hence, rainfall may be recorded at different intervals relative to the actual start of each event over a catchment. The speed of rainfall events may also be a factor, with some events moving more slowly over a catchment than others, causing timing differences. Timing errors are another factor that is widely acknowledged to have caused differences between the observed hydrograph trace or rainfall and the actual times at

which they occurred. These errors were particularly prevalent in the 1970s and 1980s when chart recorders (for example, circular or strip charts) attached to clocks were used. These clocks were not always reliable and discrepancies often occurred, particularly because the clocks were generally re-set during each site visit.

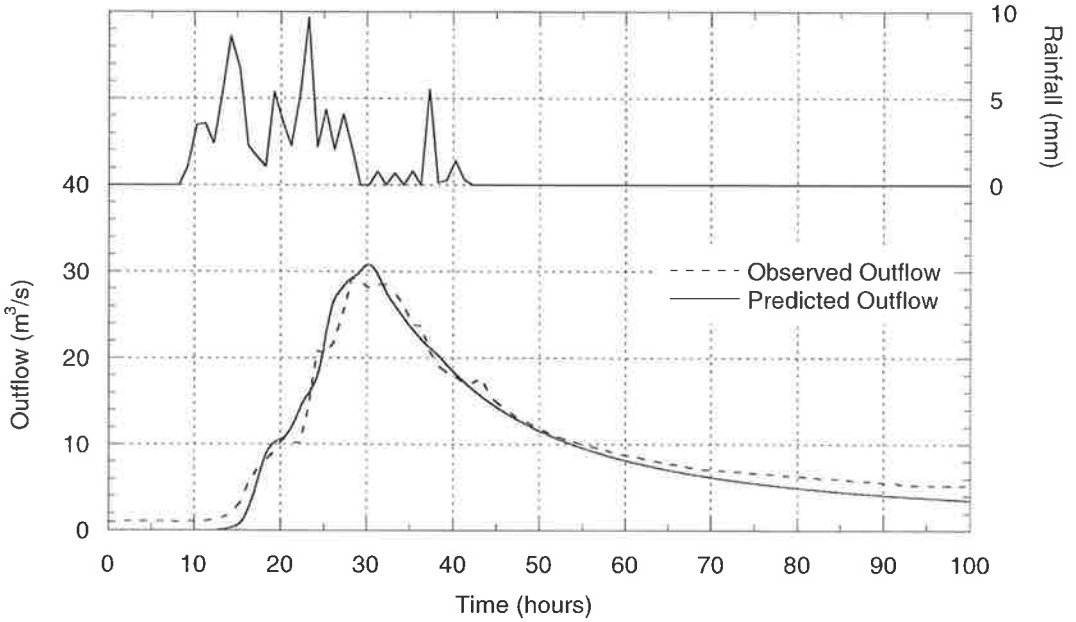

Figure 8.18 Boggy Creek: Calibration of event from 26/9/1978 to 30/9/1978.

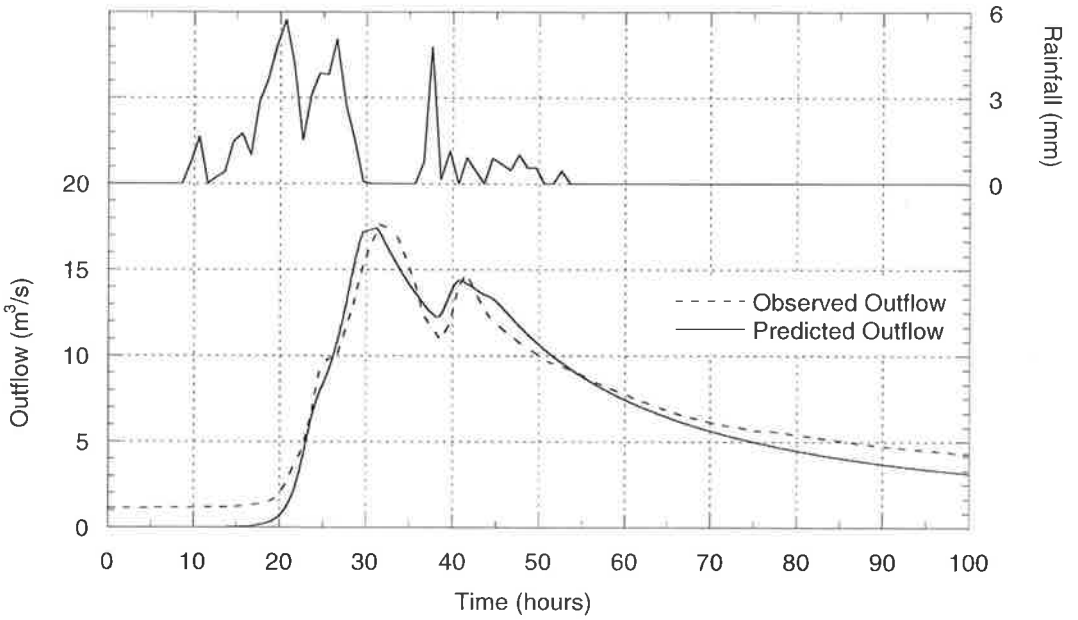

Figure 8.19 Boggy Creek: Calibration of event from 27/7/1980 to 29/7/1980.

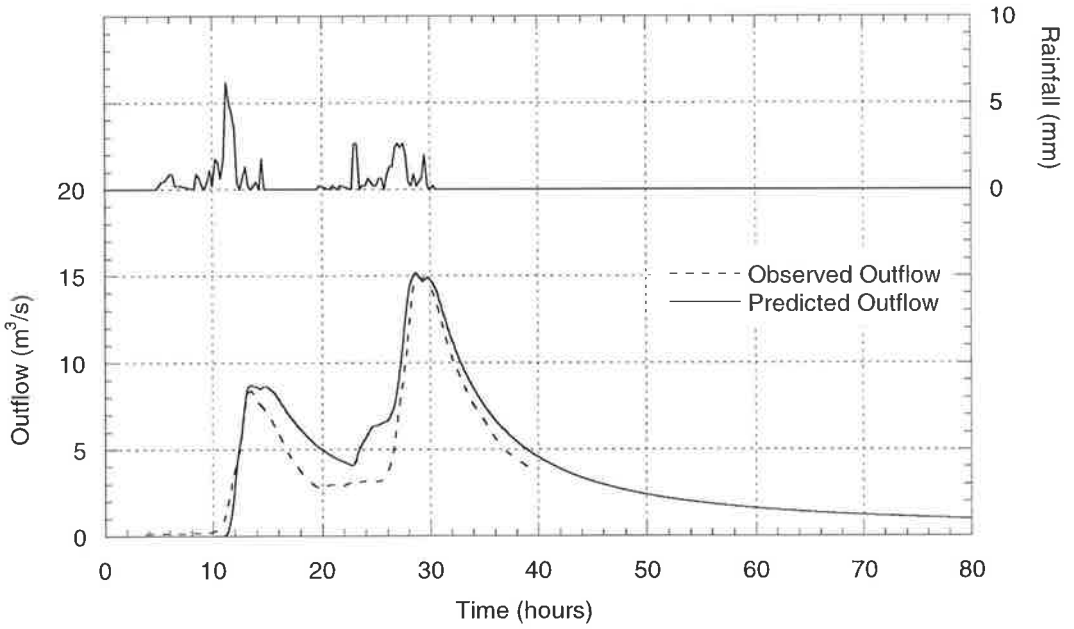

Figure 8.20 Scott Creek: Calibration of event from 29/8/1992 to 30/9/1992.

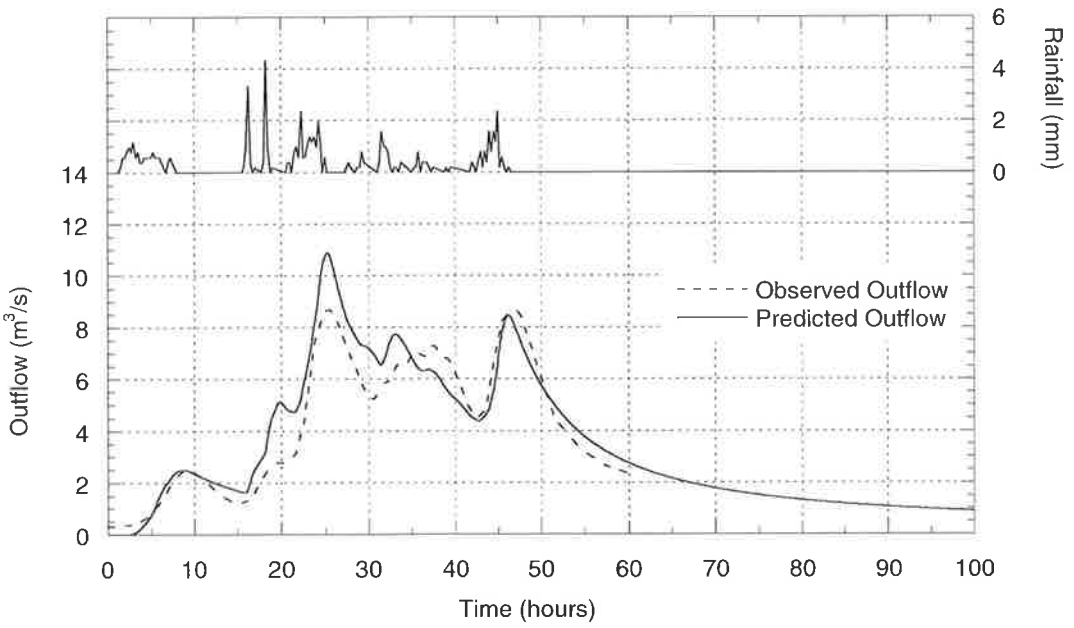

Figure 8.21 Scott Creek: Calibration of event from 21/7/1995 to 23/7/1995.

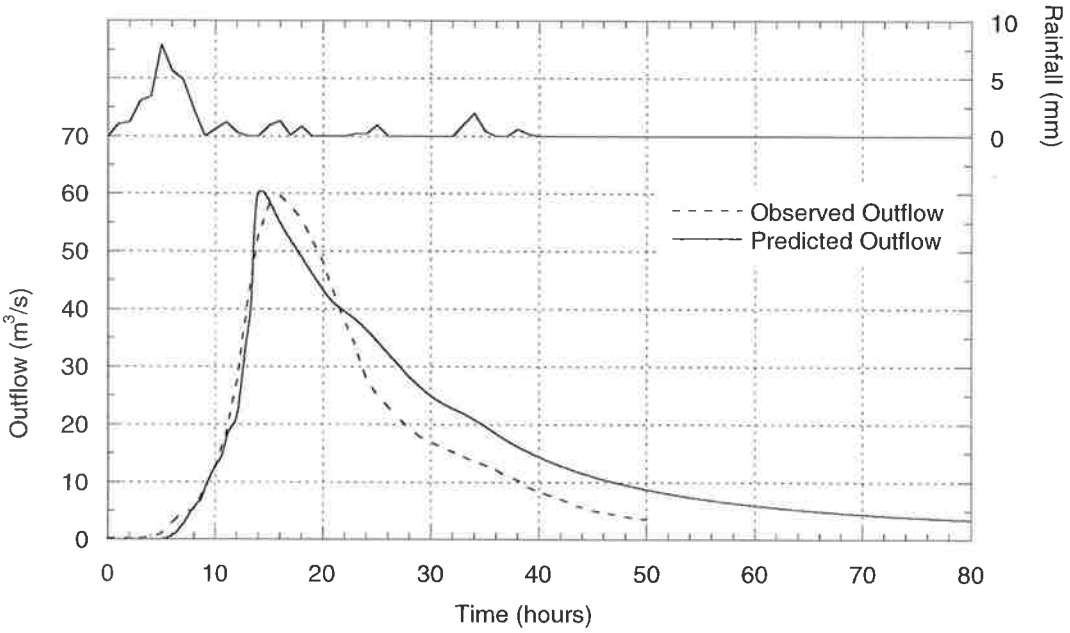

Figure 8.22 Avon River: Calibration of event from 31/8/1973 to 2/9/1973.

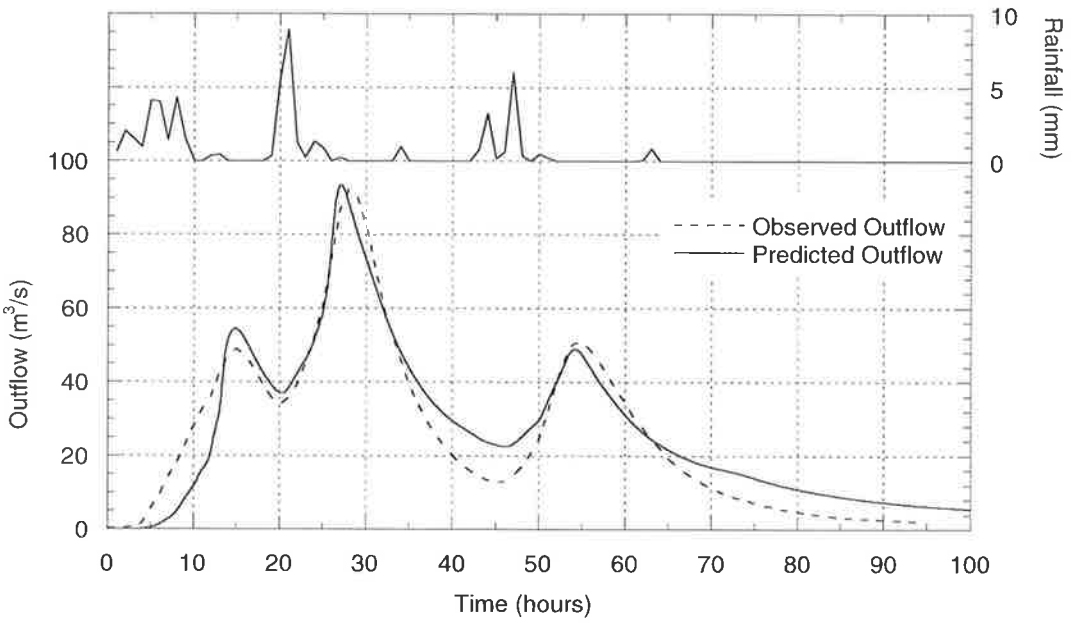

Figure 8.23 Avon River: Calibration of event from 23/10/1975 to 26/10/1975.

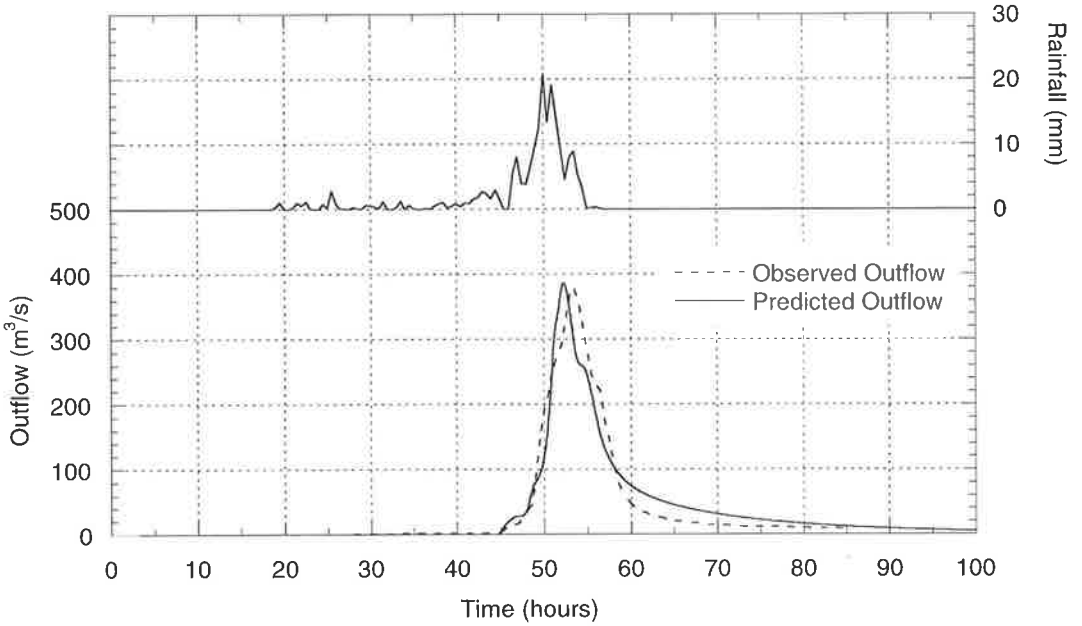

Figure 8.24 Alligator Creek: Calibration of event from 30/1/1977 to 2/2/1977.

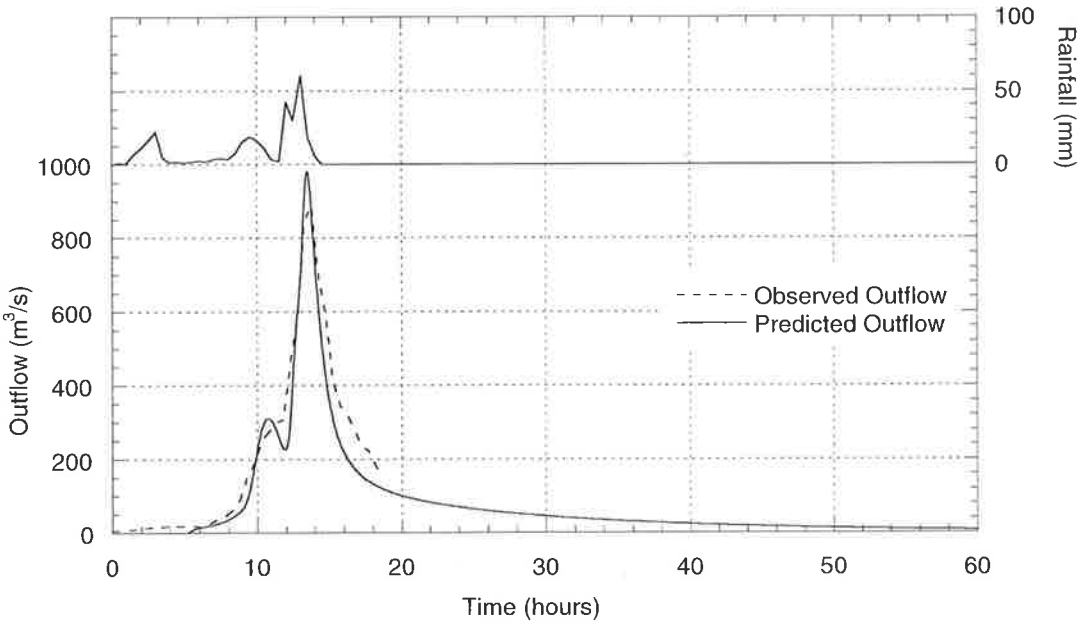

Figure 8.25 Alligator Creek: Calibration of event from 30/1/1978 to 31/1/1978.

Appendix O presents the calibration results for all events. The concurrent calibration of events at each site was very successful and in almost all cases the predicted hydrograph closely replicated the observed hydrograph. This suggests that the model provides a good description of the catchment processes and that the parameters chosen were indeed able to represent these processes for the given catchment. This latter point is related to the differences between determining parameters for each individual event compared to the concurrent calibration. When the events for a given site were calibrated independently, the replication of each observed hydrograph was slightly better than for the concurrent calibration but the parameters were very different. This suggests that the parameters obtained for each individual event may not actually be representative for a given catchment. Because the concurrent calibration of model parameters carried out was successful, it indicates that the method is more robust for determining actual parameters for the model and it allows better estimates of parameters to be used for the regionalisation of the model. More importantly for this study, the use of these common parameters with design rainfall input allow a reliable estimate of the outflow from the catchment to be obtained for design events.

8.3 Validation of the Proportional Loss-Frequency Curves

The proportional loss-frequency curves developed in Section 8.1 are intended to be used to transform design rainfall into design rainfall excess and associated infiltration loss. The use of the proportional loss-frequency curves in this way makes use of the existing design flood estimation framework but eliminates the need to estimate initial loss. To validate the use of the curves (and associated REFD proportions) the rainfall excess and infiltration resulting from the use of the curves was routed to a catchment outlet using the KinDog flood estimation model. The resulting flood frequency distribution was then compared with the observed distribution. As with the existing design method, the flood estimation model input parameters such as intensity, baseflow and the rainfall temporal and spatial distributions must be selected.

The choice of these flood estimation model input parameters is discussed in the following, along with the choice of REFD proportions (from the proportional loss-frequency curves) for each study catchment. Flood frequency distributions for each catchment are presented and the use of the proportional loss-frequency curves is validated by comparison with the observed distribution and that obtained using the recommended design event method and input parameter values from ARR (1987).

8.3.1 Design Input Parameters

In Chapter 1, the sensitivity of design flood estimation to the selected values for the input parameters were discussed. Rainfall loss, in particular initial loss, was established as having the second largest influence on the design flood, the first being rainfall intensity. The use of proportional-loss frequency curves eliminates the need to assume a value of initial loss. The effect and selection of the input values of rainfall intensity, baseflow and the spatial and temporal distributions of rainfall are discussed in the following.

Rainfall Intensity

Rainfall intensity is the most important design input parameter because it directly determines the maximum size of the flood event. In Australia, the design rainfall intensities presented in ARR (1987) are generally used. However, in Section 5.2 it was shown that these intensities are not always comparable to those obtained from long observed records, in part due to the very few long-term six-minute pluviograph records that are available in Australia. Because each of the pluviograph records used needed to have only a minimum of six years of data, the assumption that this period of observation was representative of long term conditions at that station may not have been reasonable. Walsh (1991) showed that the ARR (1987) design intensities may underestimate the observed intensities at a range of sites in New South Wales and that the adequacy of the current IFD data in regions with relatively short rainfall records needs to be addressed.

There is now up to 20 years more data available at many sites than that which was used in deriving the rainfall intensities in ARR (1987). As such, it is likely that analysis will show differences in estimates of intensity, particularly for higher ARIs. The continuous simulation of synthetic rainfall records offers an alternative to using design rainfall intensities and may provide a better estimate of the probabilities at higher ARI values. The intensities from ARR (1987) have been used here but improved estimates of rainfall intensities should be obtained from a combination of longer observed pluviograph records and continuous simulation for future work. This would provide more confidence for the use of rainfall intensities for high ARI values in applications including the derivation of flood frequency distributions for design.

Baseflow

Many runoff-routing models do not incorporate sub-surface event flow or baseflow and as

such it must be estimated and then added to the surface runoff hydrograph. It is difficult to know whether the value estimated will be ARI neutral and there is little guidance as to the probabilities associated with the choice of value. Because the runoff-routing model used in this study contains a sub-surface flow component, estimation of baseflow was not required.

Spatial Variability of Rainfall

The rainfall IFD values assumed from ARR (1987) are applicable only at a point, although they may be used to represent IFD values over small areas (ARR, 1987). For larger areas, it is not realistic to assume that the same intensity can be maintained over the entire area and some reduction has to be made. For design flood estimation the effects of areal variability are taken into account through the use of areal reduction factors (ARF). Rahman *et al.* (1998) suggested that the random nature of this variable may have a lesser effect on the results than the effect from the random nature of other variables. In addition, due to limited data, it is often difficult to derive its probability distribution.

ARR (1987) states that very little research has been done in the area of ARFs in Australia and recommends values derived from the United States National Weather Service. The values of the ARF are in the form of a depth to area ratio, which are related to catchment area and the duration of the rainfall burst. The ARF decreases (and hence the total depth of the rainfall burst decreases) with increased catchment area and decreased burst duration.

In this study, the catchments examined are small (less than 260 km^2) and the design rainfall IFD was estimated at a location on the mean rainfall isohyet within each catchment, allowing the spatial variability of rainfall to be taken into account. For the study catchments with areas less than 100 km^2 the ARR (1987) ARF values are close to one for all burst durations. For the larger of the study catchments examined, the maximum flood hydrograph peaks for a given ARI resulted from burst durations longer than 24 hours. Using ARR (1987), the ARF for these burst durations and catchment areas are also close to one. Therefore, an areal reduction factor of 1.0 was chosen for all catchments and burst durations.

Temporal Distribution of Rainfall

In Chapter 4 the influence of the temporal distribution of rainfall on design flood estimation was discussed and shown to be important. Current design flood estimation uses a series of temporal patterns described in ARR (1987), which are applied deterministically to the design rainfall. Australia has been divided into eight zones on the basis of climatology with the

boundaries generally following major drainage divides. It is assumed that rainfall patterns within these zones are similar and a series of patterns were determined from available data in each zone. However, these zones cover large areas, for example, Zone 1 ranges from the north of coastal New South Wales to the very south of Tasmania, and it is highly unlikely that such large regions could be classified as being climatically homogeneous (Walsh, 1991). In addition, the databases for a number of zones are often dominated by a small number of sites, namely the state capital cities. This may incorporate bias into the derivation of the patterns for a particular zone. Rahman *et al.* (2001) showed that the chosen ARR (1987) temporal pattern has considerable influence on the derived flood frequency distribution. The sensitivity of these patterns and whether they are representative of observed patterns requires more detailed investigation. An initial investigation was carried out in this study. The method used to derive the ARR (1987) temporal patterns was used to derive at-site patterns using the six-minute pluviograph data for each of the study sites.

The regional temporal patterns provided in ARR (1987) for design flood estimation were derived using the *average variability method* (Pilgrim *et al.*, 1969; Cordery *et al.*, 1984; Kennedy *et al.*, 1991). This procedure determines the most likely order of k periods of an event burst within a hyetograph and then determines the average magnitude of rainfall associated with this order.

For this study, a series of rainfall bursts for each site were selected using the following criteria (Kennedy *et al.*, 1991):

(a) each rainfall burst was one of the n highest in n observed years of record;

(b) bursts were independent in time such that there was no overlap;

(c) a burst was rejected if for a duration with m periods, at least $m/3$ periods had an equal rank. This occurred when a large portion of the burst had no rainfall; and

(d) the first period within the burst had rainfall.

The series of bursts for each site were then analysed using the average variability method procedure (Kennedy *et al.*, 1991), which involves:

(a) rainfall amounts in each period of each burst being expressed as a percentage of the total rainfall in the burst and these percentages ranked within each burst;

(b) each period number of the burst is assigned a rank using these percentages, for example, if period 3 of a particular burst has the highest rainfall then this has rank 1;

(c) the rank numbers for each period are averaged over the sample, for example, all the ranks in period 1 are averaged;

(d) the period with the lowest average rank are designated as rank 1, the second lowest as rank 2 and so on; and

(e) the average of the percentages for rank 1, rank 2 and so on calculated in part (a) are averaged and assigned to the designated ranked period from part (d), that is, rank1, rank 2 and so on to produce the temporal distribution.

The average variability method was applied to each of the six-minute pluviograph sites used for the study catchments, namely Whitfield, Williamstown, Townsville and Tottington. Of these sites, only the Townsville pluviograph has been used in the derivation of the ARR (1987) regional patterns.

Kennedy *et al.* (1991) stated that the top 15% of the sample for each zone could be used to estimate the temporal patterns for ARIs greater than 30 years, as suggested in ARR (1987). However, 100% of the sample was used to determine temporal patterns for ARIs less than 30 years, with adjustment ratios used to transform this to temporal patterns for ARIs greater than 30 years. This was done because of sample bias in that the small number of large ARI events in the records were not able to generate realistic high ranking intensities within extreme events (Walsh, 1991).

For durations of one hour or less, the ARR (1987) design patterns are identical for each zone. In addition, the differences between the patterns for ARIs greater than 30 years and for ARIs less than 30 years is small. A comparison of the one hour pattern for the study sites is shown in Figure 8.26. It can be seen that while Williamstown and Tottington follow the general shape of the design patterns, none overlap. The at-site patterns for Whitfield and Townsville are quite different. The large differences in the one hour patterns for the four sites highlights the inadequacy of a single pattern for all one hour durations across Australia.

At-site temporal patterns were derived from the available pluviograph for a range of durations. These were compared with the selected zonal design patterns indicated in Table 8.3 and are shown in Appendix P.

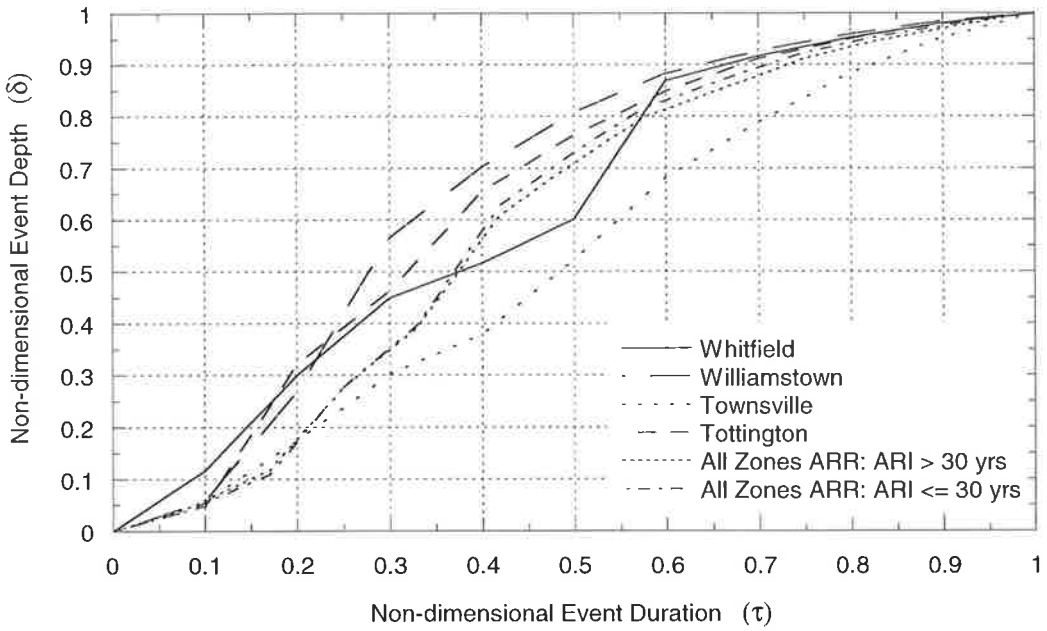

Figure 8.26 Comparison of 1 hour at-site and ARR (1987) temporal patterns for all sites.

Table 8.3 Regional design temporal patterns.

Site	Zone
Whitfield	1
Williamstown	6
Townsville	3
Tottington	2

These comparisons show that the ARR (1987) regional patterns do not adequately describe the observed patterns. For example, the design pattern for Whitfield should be selected from zone 2 in ARR (1987). However, because Whitfield is close to the boundary of zones 1 and 2, the observed patterns were compared with design patterns from both zones to determine which was the more appropriate pattern. The comparisons for four selected durations are shown in Figure 8.27 to Figure 8.30. The patterns for 2 and 12 hour durations show that neither zone 1 or 2 design patterns provide a satisfactory representation of the observed data. Similar poor fits between the at-site patterns and the design patterns were observed for most of the durations examined. The only exceptions were the 18 and 72 hour duration patterns, which were close to the zone 1 and zone 2 design patterns respectively. However, neither zonal pattern can satisfactorily reproduce the observed data across a range of durations. Because the zone 1 patterns were closer to the observed at-site patterns than those from zone 2, these were adopted. In addition, the zone 2 pattern underestimated the design flood

significantly. Rahman *et al.* (2001) has also showed that the zone 2 temporal pattern produced lower design floods than the zone 1 pattern when used for Boggy Creek.

Similar discrepancies were found between the at-site and zonal patterns for Scott Creek. For Avon River, a number of the at-site temporal patterns were similar to those for zone 2, namely for burst durations of 24 to 72 hours. The patterns for Townsville were similar to those for zone 3 for a number of burst durations. However, for other burst durations, both sites exhibited similar discrepancies to those at Scott Creek and Boggy Creek. The comparison of temporal patterns at all sites and for all burst durations are shown in Appendix P. Walsh (1991) showed that further investigation of the design temporal patterns is required, but that until such time as an alternative procedure is identified that can produce superior pattern estimation that makes full use of available data and are typical of observed rainfall, the patterns described in ARR (1987) should continue to be used for design flood estimation. Therefore, the ARR (1987) patterns have been used in this study.

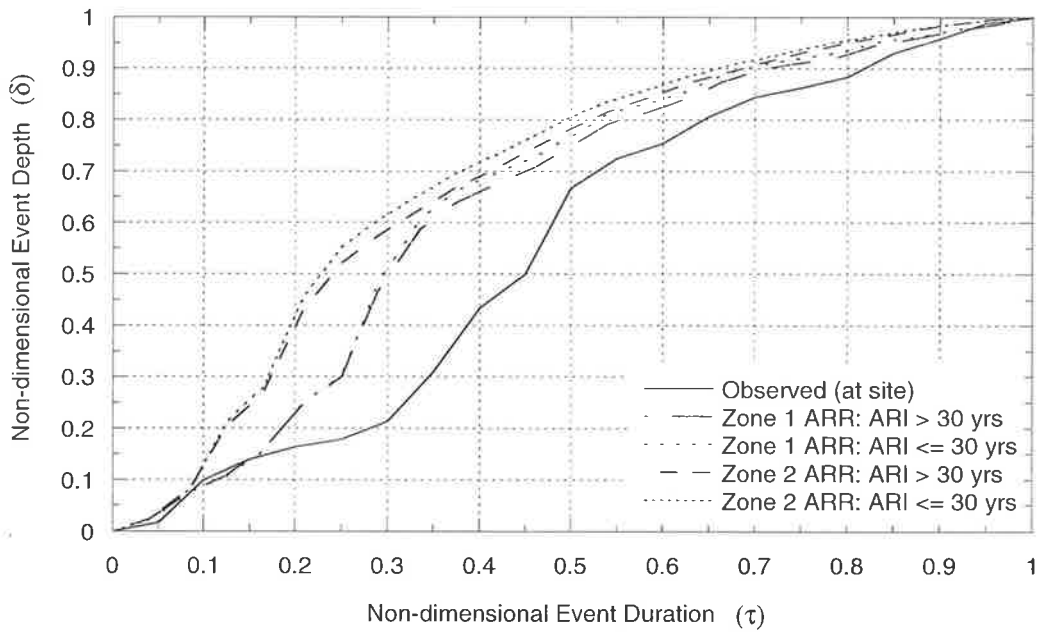

Figure 8.27 Comparison of 2 hour at-site and ARR (1987) temporal patterns for Whitfield.

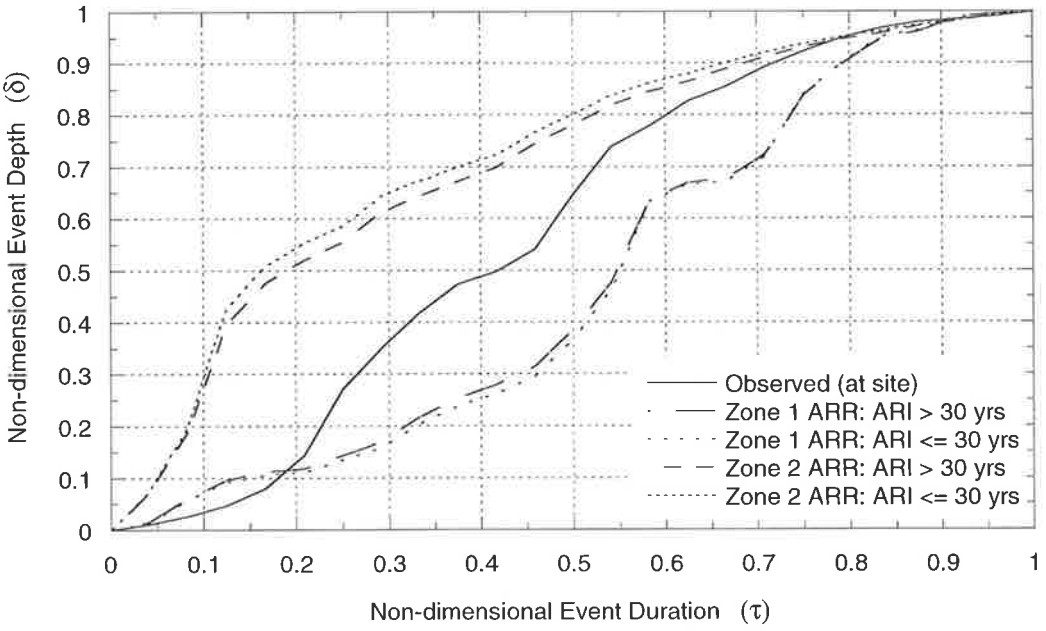

Figure 8.28 Comparison of 12 hour at-site and ARR (1987) temporal patterns for Whitfield.

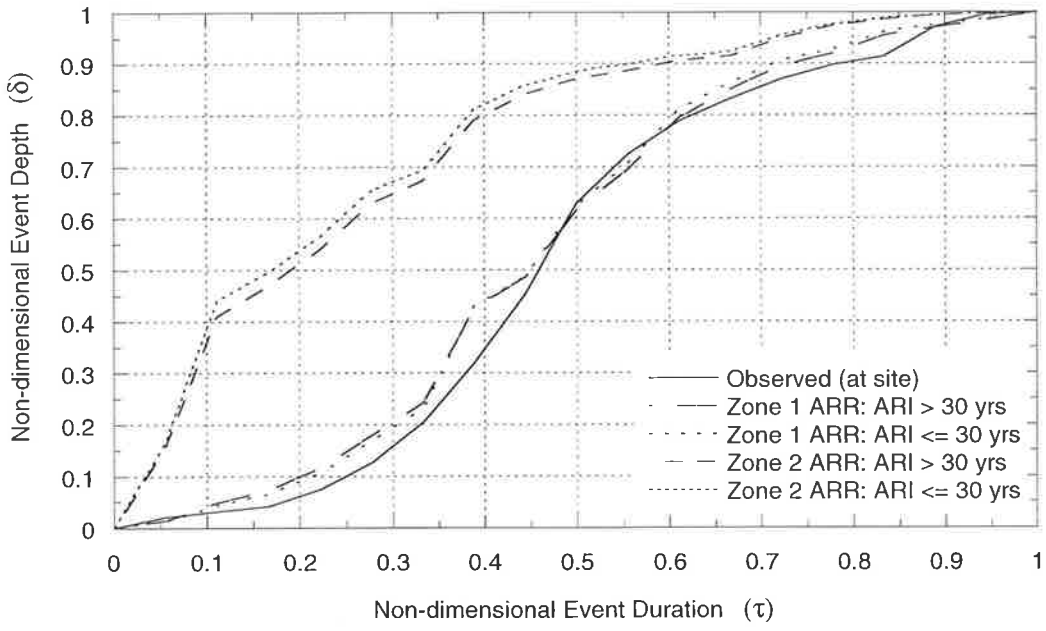

Figure 8.29 Comparison of 18 hour at-site and ARR (1987) temporal patterns for Whitfield.

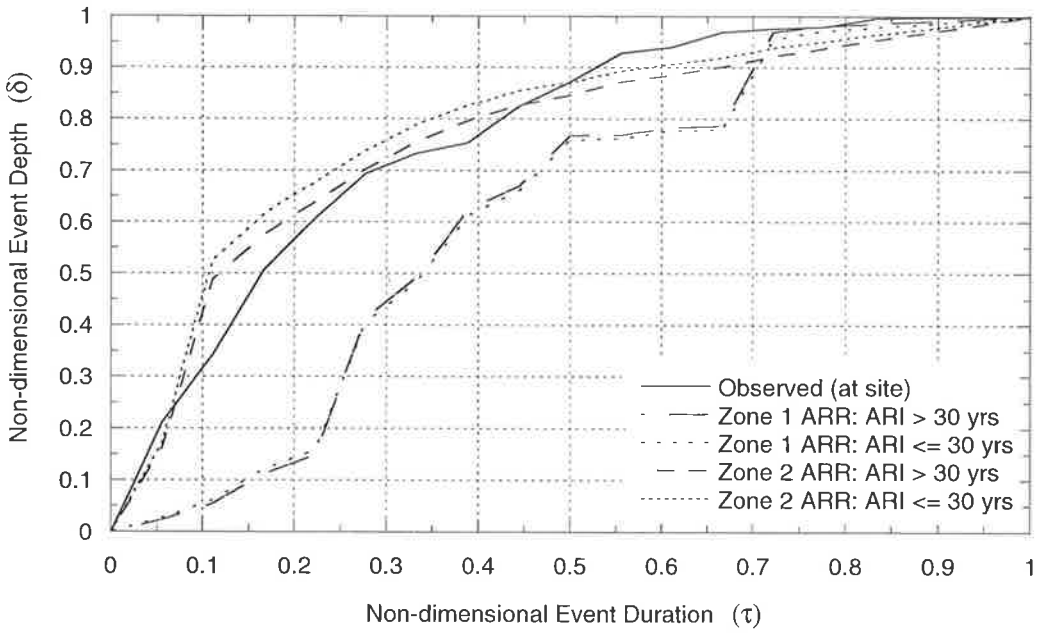

Figure 8.30 Comparison of 72 hour at-site and ARR (1987) temporal patterns for Whitfield.

8.3.2 Selection of Proportional Loss

The method for determining the REFD proportions and hence proportional loss in this study was discussed in Section 8.1. For increasing ARIs between 5 and 100 years the proportional loss-frequency curves appear to be approximately constant (Boggy Creek), have small increases over this frequency (Scott Creek) or increase steadily with ARI (Alligator Creek and Avon River), but provide a duration independent relationship. The REFD proportions used for this study were obtained directly from these curves and are shown in Table 8.4. Although not undertaken during this study, the similarities in the relationships between sites show the potential to either use constant values over the ARI range of 5/10 to 100 years or to fit a general function to the ratio of the REFD and the rainfall IFD.

Table 8.4 Proportional-loss values used for this study.

ARI	Alligator Creek	Avon River	Boggy Creek	Scott Creek
1	0.72	0.84	0.84	0.96
2	0.62	0.63	0.61	0.71
5	0.53	0.54	0.57	0.67
10	0.48	0.50	0.55	0.64
20	0.44	0.46	0.55	0.62
50	0.42	0.42	0.55	0.6
100	0.40	0.41	0.55	0.58

8.3.3 Comparison of Observed and Derived Flood Frequency Distributions

The ARR (1987) design rainfall burst for each site was converted into rainfall excess using the REFD proportions and then used as input into the KinDog runoff-routing model. In other words, an IL-PL model with an initial loss equal to zero and a proportional loss equal to one minus the REFD proportion was used as the loss model within the KinDog model. It is noted that the REFD proportions, the design rainfall and the ARR (1987) design temporal patterns were all obtained using rainfall burst data, which minimises any inconsistencies that may arise from using data obtained from full events.

Rainfall events over a range of burst durations and ARI values of 1, 2, 5, 10, 20, 50 and 100 years were evaluated using the model. The resulting maximum flows were compared with the observed data and the fitted distribution to this data. The fitted distribution was obtained from a frequency analysis of the observed annual maximum flows using either a GEV or LP3 distribution. The choice of distribution varied between sites and is shown in Table 8.5, together with the available data, maximum observed flow and minimum observed flow.

Table 8.5 Available data for observed flood frequency distribution.

Site	Number of Years	Distribution	Maximum Flow (m^3/s)	Minimum Flow (m^3/s)
Alligator Creek	25 (1975 - 1999)	LP3	888.84	18.01
Avon River	19 (1969 - 1995)[1]	GEV	147.06	0.78
Boggy Creek	34 (1967 - 2000)	LP3	90.12	0.49
Scott Creek	31 (1970 - 2000)	GEV	18.34	0.50

[1] Period missing: 6/1987-6/1993.

Design flood values were estimated using the current design event approach in order to compare the success of the methodology and whether it offers improvements. For each of these locations, the loss model recommended in ARR (1987) is an initial loss-continuing loss model (IL-CL). The events calibrated using KinDog with a proportional loss model were re-calibrated using the IL-CL model. The calibrated catchment parameters and reproduction of the observed hydrographs for each site are shown in Appendix O. To determine the design flood frequency distribution, values recommended in ARR (1987) for the initial loss and continuing loss parameters were used, as shown in Table 8.6.

Table 8.6 Initial Loss-Continuing Loss model parameters (Source: ARR, 1987).

Site	Initial Loss (mm)	Continuing Loss (mm/hr)
Alligator Creek	25	2.5
Avon River	20	2.5
Boggy Creek	20	2.5
Scott Creek	25[1]	4.0[1]

[1] Values recommended for Summer. Winter values are smaller and produced higher design flood values than those for Summer.

The flood frequency distribution derived from the REFD proportions is shown for Boggy Creek in Figure 8.31 and shows a good relationship to the fitted distribution between an ARI of 10 to 100 years. While it would be desirable to also reproduce the flood frequencies at ARIs lower than 5 years, the more important levels for flood estimation are in this higher range. The derived flood frequency values using the IL-CL model and the ARR (1987) parameters and method is slightly higher than that derived from the REFD proportions.

Figure 8.32 shows the flood frequency distribution derived for Scott Creek and Figure 8.33 for Avon River. In both cases the distributions lie within the confidence limits of the fitted distribution. More importantly, the derived flood frequency values using the IL-CL model and the ARR (1987) parameters and method are significantly higher for high ARI and generally outside the confidence limits of the observed flood frequency distribution. This suggests that the REFD proportion method provides an improved estimate of the flood frequency distribution over the current ARR (1987) recommended approach

Figure 8.34 shows the results for Alligator Creek. While the derived distribution is lower than the fitted distribution (observed) it is still within the confidence limits for this distribution. One of the common difficulties in validating derived distributions is the limited length of observed flood data. In the case of Alligator Creek there has only been one very large event in 25 years, which causes the fitted distribution to be significantly higher than it would otherwise be without this point being included. However, even though the derived distribution is lower than the observed data, the derived flood frequency values using the IL-CL model and the ARR (1987) parameters and method are significantly lower again. This again suggests improvement in design flood estimation by using the REFD approach.

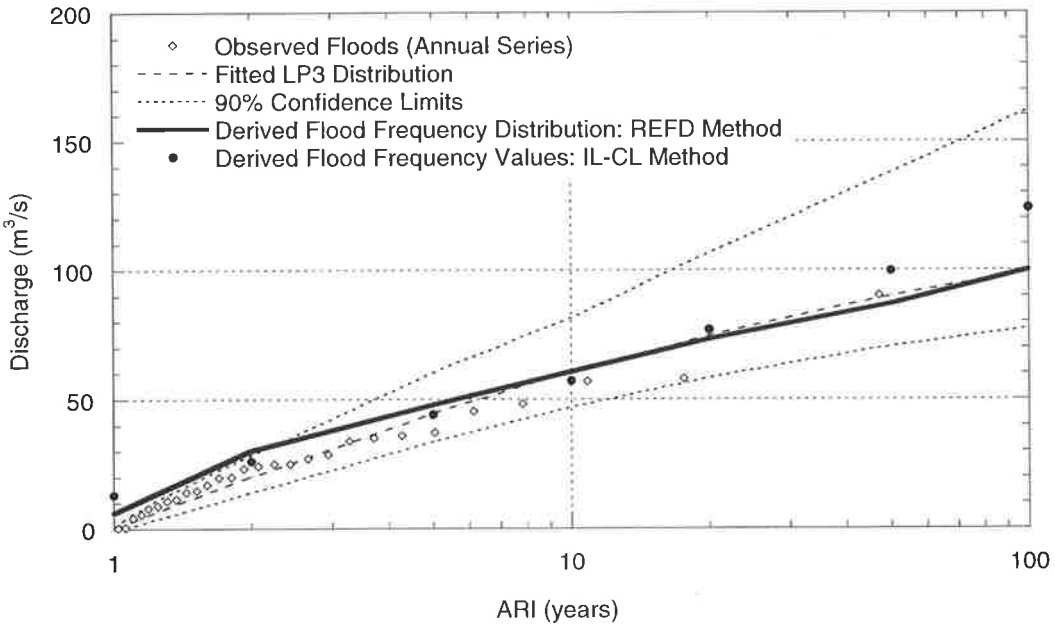

Figure 8.31 Boggy Creek: Comparison of derived flood frequency curve using REFD method with results from at-site flood frequency analysis and derived flood frequency values using IL-CL method.

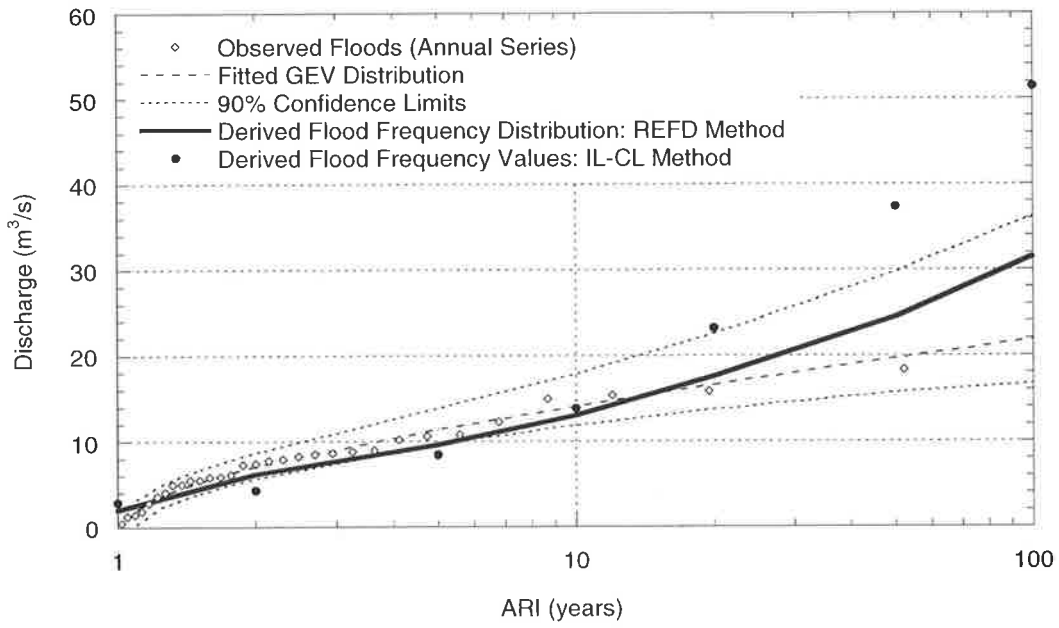

Figure 8.32 Scott Creek: Comparison of derived flood frequency curve using REFD method with results from at-site flood frequency analysis and derived flood frequency values using IL-CL method.

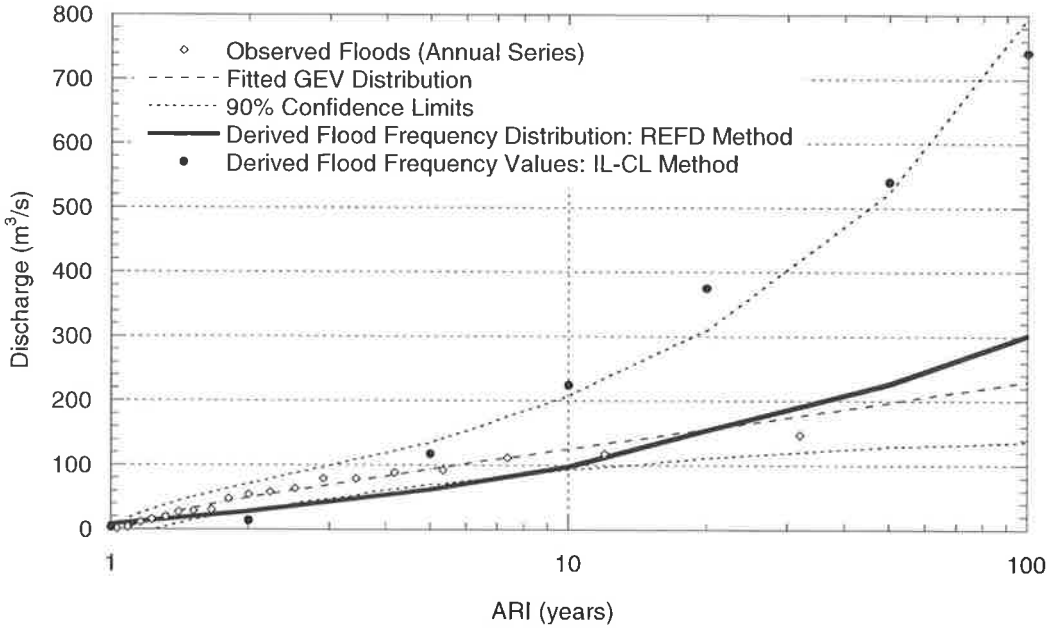

Figure 8.33 Avon River: Comparison of derived flood frequency curve using REFD method with results from at-site flood frequency analysis and derived flood frequency values using IL-CL method.

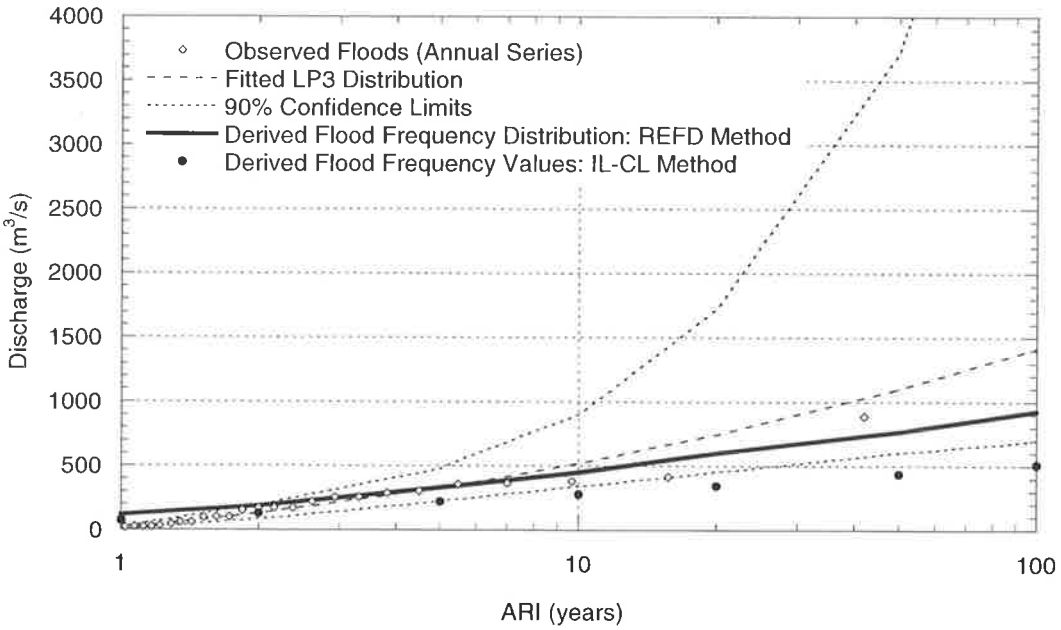

Figure 8.34 Alligator Creek: Comparison of derived flood frequency curve using REFD method with results from at-site flood frequency analysis and derived flood frequency values using IL-CL method.

8.4 CONCLUDING REMARKS

Rainfall loss, in particular initial loss, is an important and influential parameter in determining the magnitude of design floods. The technique developed in this study directly converts design rainfall into rainfall excess thereby eliminating the need to define initial loss. The ratio of the frequency distribution of rainfall excess (REFD), generated using a continuous catchment water balance simulation, to the frequency distribution of the rainfall input (IFD) for the four study sites, had a similar trend with increased ARI and generally the ratio was independent of duration. Two obvious patterns were observed. For Boggy Creek and Scott Creek the ratio appeared to be relatively constant, increasing only marginally between an ARI of 5 and 100 years, suggesting that the use of a constant value of the REFD proportion may be used for higher ARI considerations. For Alligator Creek and Avon River the ratios increased steadily with ARI, which is likely to require the ratio to be described using a mathematical function dependent on ARI. An option is a bi-linear function with fixed values for the REFD proportion at ARIs of 2, 10 and 100 years.

The ratio of the REFD to the rainfall IFD can be defined as a set of proportional loss-frequency curves, which define the separation of the design rainfall into rainfall excess and infiltration/loss that occurs after runoff has commenced. Using these curves as part of the KinDog runoff-routing model (Kuczera *et al.*, 2000) is effectively the equivalent of assuming a proportional loss model for the entire rainfall burst. This approach removes the need to assume a value of initial loss, as it has already been incorporated within the continuous catchment simulation. This was tested by calibrating the KinDog model using a number of events and determining a set of common catchment parameters, rather than calibrating the model to a single extreme event. The suitability of the common parameters were verified and found to be able to adequately reproduce the individual observed events.

The derived flood frequency distribution was then determined using the proportional loss-frequency curves in conjunction with the current ARR (1987) design rainfall IFD. Initial comparisons of the ARR (1987) temporal pattern data with at-site temporal patterns, derived using the same average variability method from observed pluviograph data, showed the regional patterns are a poor representation and that further investigation is required. For this study, given the current absence of further information, the ARR (1987) design patterns were used. The derived flood frequency distributions were then validated using observed flood frequency data. For each site examined, the derived flood frequency distribution fitted well

within the 90% confidence limits of the observed distribution for ARIs greater than 10 years, and inside or just outside the confidence limits for ARIs less than 10 years. This demonstrated the potential for the overall approach of this study. In addition, the derived flood frequency distribution using the REFD proportions provided an improved estimate of the flood frequency distribution over the current design event method recommended in ARR (1987).

If the approach for design flood estimation described in this section is to be used, it is important that it is easily regionalised. It may be possible to establish a relationship between catchment characteristics and the REFD proportions. If such a relationship could be established this would enable the definition of proportional loss-frequency curves for generic catchment types, which would further assist the design process. The availability of these curves for key catchment areas in Australia will greatly improve the accuracy of the current design methodology. At present, the major difficulty in some locations is a lack of available data. However, as the level of data increases, regionalisation of this approach should be straightforward.

9. CONCLUSIONS AND RECOMMENDATIONS

9.1 OVERVIEW

Determining the potential flood risk through design flood estimation is often required for the planning, design and construction stages of many engineering infrastructure projects. While a number of methods are available to determine a design flood, limited streamflow data throughout Australia has led to a probabilistic rainfall-based design event method being used for this purpose (ARR, 1987). Although this method is reasonably straightforward to use, there are difficulties associated with determining input parameter values for the key rainfall and runoff variables needed to successfully transform a rainfall event of a given Average Recurrence Interval (ARI) to a design flood of the same ARI. This study was initiated by the desire to address the selection difficulties for one of the key input parameters, initial loss, through the development of an alternative approach to engineering design flood estimation.

The selection of an initial loss value can have a significant effect on the determination of the design flood, with the current design method relying heavily on the judgement of the individual applying the method. This alternative approach used continuous simulation techniques to establish a relationship between design rainfall and rainfall excess, thereby eliminating the need to select a value of initial loss.

To undertake continuous simulation a suitable rainfall model was needed. Available research on stochastic rainfall models reported difficulties in obtaining a model that could effectively reproduce the statistical properties of observed rainfall, particularly the intense rainfall bursts, over a range of time scales (refer Chapter 2). To overcome these reported difficulties, a rainfall model was also developed as part of this study.

This chapter initially discusses the successful development of this rainfall model, together with associated evaporation and catchment water balance models used to undertake the continuous simulation. Current limitations in the new models are identified, and recommendations for further research are proposed. The chapter concludes with a discussion of the overall success of the proposed alternative design flood estimation methodology.

9.2 STOCHASTIC RAINFALL SIMULATION MODEL

9.2.1 Summary

The review of potential models for continuous simulation of rainfall focussed on previously reported and validated results, data requirements and effects of missing data, and parameter estimation and calibration techniques. This review did not identify a model suitable for the continuous simulation undertaken in this study and a new stochastic model was accordingly developed.

The model is based on an alternating renewal process with intra-event disaggregation through a conditional random walk on a dimensionless mass curve, with:

- the inter-event time and event duration distributions modelled using a generalised exponential distribution with the kernel defined using a combination of the generalised Pareto and power law distributions (refer Section 3.4);
- the average event intensity modelled by a generalised pareto distribution, with the parameters of this distribution related to the mean and standard deviation of the average event intensity conditioned on duration. A broken line function was developed to relate the mean and standard deviation of average event intensity to the event duration, to enable modelling of the observed conditional relationship; and
- the temporal distribution of intra-event rainfall modelled as a self-similar process with rainfall traces determined by the random combination of determined jumps and intra-event dry periods. A truncated log-normal distribution was used to represent the rainfall jumps, conditioned on the current position within the mass curve, with a combination of the uniform and beta distributions used to model the intra-event dry periods.

9.2.2 Conclusions & Recommendations

The synthetic rainfall generated by the stochastic model developed in this study provided a good representation of observed rainfall over a range of climatic regions. It also successfully reproduced Intensity-Frequency-Duration (IFD) statistics and aggregated statistics at a range of time scales, and importantly these measures were not used during model calibration. While the validation showed that for a few sites some of the aggregated statistics suggested that

improvements to the model could be pursued, the synthetic data produced for all sites was considered satisfactory. In particular:

- the selected distributions for the inter-event time and event duration were satisfactory, with monthly calibrated parameters producing better results than the application of harmonic variations to account for seasonal variability;

- the conditional nature of average event intensity and event duration, which is discussed in Section 3.5.2, was successfully modelled using parameters calibrated to monthly data. The simulated rainfall adequately replicated the observed marginal distribution and aggregated statistics over a range of time scales for a number of sites. The only exception was in the tail of some of the monthly marginal distributions. However, generally less than 0.1 percent of the total events for each month lie in the tail;

- the monthly model of average event intensity was generally successful although improvements to the method of calibrating the parameters defining this distribution is warranted. Calibration involved the need to manually determine breakpoints to describe the conditional relationship between average event intensity and event duration (Section 3.5). An added difficulty was introduced with the data from some of the locations having a small number of events over a series of months;

- A probabilistic approach to the disaggregation of total event rainfall was considered essential, as this allowed the joint probability of the intra-event rainfall distribution with other rainfall producing variables to be accounted for. The assumption of self-similarity was reasonable as a first approximation for the distribution of intra-event rainfall at the sites examined. However, if a stronger dependence upon duration is observed for a particular site, then a self-affine approach similar to Menabde and Sivapalan (2000) could be investigated;

- comparisons of simulated and observed average event profiles showed the self-similarity property to be well produced up to a dimensionless depth of 0.7. Between this point and the end of the event discrepancies were observed, which are possibly attributable to the parabolic functions used to represent the conditional jumps. The parabolic function for the standard deviation of the allowable jump range decreases significantly as the dimensionless depth approaches one, resulting in insufficient variability for the jumps in this range. This results in small jumps and a flatter trace than that observed in the

historical record. Also, the dimensionless depth remaining at a dimensionless time of 0.9 must fall before 1.0, causing this portion of the curve to be steeper than the observed record. However, the validated results of the overall model do not suggest this adversely affects the synthetic rainfall record. The jump model was therefore considered reasonable for this study;

- the random assignment of the dry periods within the wet periods for each event is thought to have led to the simulated one hour lag-one auto-correlation aggregated statistics not being representative of the observed values (although statistics at other time scales were reasonably reproduced). An option for improving the correlation between successive intervals within an event could be achieved through the use of an auto-correlation function similar to that used by Acreman (1990);

- the shorter and longer duration IFD were adequately reproduced, giving confidence in the appropriateness of the disaggregation procedure and the model of average event intensity, although at some sites the IFD curves for durations of 72 hours were underestimated compared to the historical record. The suggested improvements for the average event intensity model (below) should provide improved reproductions of the IFD curves for higher durations; and

- the mean, standard deviation and dry probability aggregated statistics were generally well produced at a range of time scales; nevertheless for some sites, the need to incorporate inter-annual variability into the model is suggested by an underestimation of the standard deviation of annual rainfall, and hence the ability to closely reproduce the observed rainfall variability.

Seasonal Variations

Strong seasonal variations in the inter-event time and event duration data was a characteristic of many of the study sites. Together with the monthly calibrated model, the use of harmonic variation of these parameters was also investigated. While the harmonic models produced statistically preferable models using criteria such as BIC and AIC, they were not able to adequately reproduce the observed distributions over a variety of time scales as well as the monthly models. As the main focus for model calibration and validation was goodness of fit and not parsimony, the monthly models were adopted.

The trade-off in selecting the monthly model is an increased number of parameters, which is not significant if they can be easily estimated. However, if there are strong seasonal variations within particular months, such as during changes in seasons, these will not be reproduced by a monthly model. For the study sites, the parameters for the monthly models were easily estimated, although calibration did become difficult for tropical locations where the observed record contained months with few recorded events during the dry seasons. Theoretically, an harmonic model should be able to overcome this. However, the extent of the seasonal variation over the year was so great, due to the vastly different rainfall patterns in the wet and dry seasons, that the harmonic model could not provide a superior representation. A more robust method of representing seasonal changes in tropical areas, where limited data is available or to reduce the number of parameters, may be investigated if a more rigorous analysis of tropical areas is required.

Strong seasonal variations in the average event intensity data were also observed at many sites. Harmonic variations were applied to the parameters of the straight line functions to overcome these variations, but they were then not able to reproduce the extreme differences in average event intensity between seasons at some sites. Using monthly values often led to difficulties in defining the function over a range of event durations, and on some occasions one or two observed events introduced a bias that was reflected through the simulation. This resulted in higher than expected average intensities. An investigation into a more general function to define the conditional relationship is recommended.

Dependency of Average Event Intensity and Event Duration

The incorporation of the dependence between event duration and average event intensity was crucial in reproducing the observed Intensity-Frequency-Duration (IFD) distributions. By their nature IFD distributions used for design purposes incorporate a dependence between rainfall intensity and duration. As such, the reproduction of these distributions is an important property for any synthetic rainfall series that is to be used for design flood estimation. When this dependency was not included, the model generated unrealistic combinations of average event intensity and duration and the IFD distributions were not able to be reproduced.

Disaggregation of Total Event Rainfall

It was observed that similarity in the model parameters for both the distribution of rainfall jumps and intra-event dry periods between varied climatic regions offers significant potential

for regionalisation and application of the approach to areas with limited or no data.

Comparison of ARR (1987) IFD Curves

Discrepancies were observed between IFD curves determined from actual pluviograph data and those from ARR (1987). Because of the importance and widespread use of the ARR (1987) IFD intensities for engineering design, further investigation into their accuracy is recommended.

9.3 Stochastic Evaporation Simulation Model

9.3.1 Summary

The combination of rainfall and evaporation models to generate concurrent data at a six-minute time scale has not been extensively undertaken by researchers. To achieve this in this study, a lag-one Markov model for generating synthetic daily evaporation was combined with a disaggregation model, with:

- daily evaporation parameters dependent on the evaporation on the previous day, the rainfall state (wet or dry) of the current and previous days and the time of year;
- a Wilson-Hilferty (1931) transformation to reproduce observed skewness in the daily values; and
- the disaggregation of the simulated daily evaporation to a six-minute times scale based on the method by Fleming (1972), which utilises two functions describing clear and cloudy days to distribute the total evaporation. A day with rainfall was classified as cloudy and one with no rainfall as clear.

9.3.2 Conclusions & Recommendations

The stochastic model of evaporation, in conjunction with the stochastic model of rainfall, was successful in simulating daily evaporation and disaggregating this over the year. In particular:

- the simulated evaporation statistics adequately replicated the observed statistics over a range of time scales, which indicated that the evaporation model was satisfactory and that the rainfall model was able to reproduce an appropriate number of wet and dry days;

- the Priestley-Taylor (1972) method provided an appropriate option for calculating potential evaporation at daily time scales in Australia, particularly in the absence of wind data;

- a comparison between observed pan and calculated potential evaporation showed them to be generally proportional, which means that each method can effectively be used interchangeably for a measure of evaporation in calibrating a water balance model; and

- while improvements to the observed underestimation of monthly and annual standard deviations could be further investigated, the results were consistent with those shown by Srikanthan and McMahon (1985) and were adequate for this study.

9.4 Catchment Water Balance Model

9.4.1 Summary

A number of water balance models currently used in Australia were reviewed in terms of published results, ease of parameter estimation and physical realism. It was noted that for most of these models, calibration and validation against observed runoff has been generally carried out at a monthly time scale. While this may be acceptable for studies solely involving yield, a smaller time scale is required for design flood applications. In fact, many of the published parameters are only suitable for use at monthly time scales as they do not produce the shape and peaks of observed hydrographs when comparisons to observed records are made at a daily scale. Rather than develop an entirely new model, the most flexible of those examined, the Australian Water Balance Model (AWBM) was chosen and modified to enhance its suitability for use at daily and sub-daily time scales. These enhancements included:

- incorporating an explicit calculation of the size of the soil stores and partial areas as opposed to using an average soil store capacity;

- using an alternative equation for the surface routing store;

- using daily estimates of evaporation instead of monthly averages;

- using an evaporation multiplier to transform pan evaporation to actual evaporation; and

- assigning a daily maximum infiltration volume.

9.4.2 Conclusions & Recommendations

The results of the calibration of the modified AWBM indicated its suitability for modelling the catchment water balance and generating the simulated rainfall excess for this study. In particular:

- the use of the alternative routing store allowed a better reproduction of the observed runoff, especially the representation of recessions immediately following peaks. This was particularly important for smaller catchments having a fast runoff response;

- the use of daily evaporation improved the representation of this important component of the water balance, as there are often large variations in daily values, particularly when seasons overlap;

- the evaporation multiplier allowed a better use of the pan or potential evaporation from a site that may not be on the catchment or if the spatial variability over the catchment was large;

- the incorporation of a daily maximum infiltration volume provided a reasonable first step to allow a better representation of higher runoff events. One of the common deficiencies with many catchment water balance models is an underestimation of peak flows, particularly at sites where there are few observed high level flows. While the use of a maximum infiltration volume did improve the representation, it did not fully fix the underestimation problem. This requires further investigation to ensure the peak flows are adequately reproduced, as this directly affects the resulting relationship between simulated rainfall and rainfall excess. Underestimation of the peak flows and hence overestimation of the amount of rainfall that becomes rainfall loss, may lead to an underestimation of the derived flood frequency curve;

- the values of the coefficient of determination (R^2) and the coefficient of efficiency (E) in the comparison of observed and predicted daily runoff indicates the predicted runoff adequately replicates the observed runoff. A comparison of observed and predicted runoff at a daily time scale showed a better representation in terms of R^2 and E than some of the published results achieved based on comparisons made at a monthly time scale, which

highlights the success of the alternative surface routing store;

- a comparison with the predicted monthly maximum daily runoff generally showed a good reproduction of the observed flows;

- the Box-Cox transformation applied to the residuals of both the daily runoff and monthly maximum daily runoff was generally successful in reducing the variance of the residuals and provides a better estimation of parameters. In some cases, a higher value of the Box-Cox λ_1 parameter was required to adequately reproduce the higher runoff events. This was identified as important for design flood estimation, particularly where runoff is highly seasonal and there are a small number of high-peaked events;

- the addition of Auto-Regressive (AR) parameters was able to successfully limit the correlation between residuals of the daily runoff sequence to within 95% confidence limits of white noise, which allowed an improved estimation of parameters and fit to the observed data;

- calibration using disaggregated daily rainfall to a six-minute time scale produced very similar parameters to those obtained using the daily rainfall. This indicated that the daily calibrated parameters could be used to adequately represent the catchment water balance at time scales less than a day. The assumption was made that the daily calibrated parameters were suitable for use at a six-minute time scale and hence could be used with the stochastic rainfall and evaporation models that were developed; and

- no seasonality in catchment response was taken into account when calibrating the lumped catchment water balance models; this was in part to limit the number of parameters required during calibration. However, if catchment conditions such as groundcover change dramatically over the year, which may affect the levels of runoff that occur during season changes, then a means of accounting for seasonality may be needed. By using a seasonal approach to some parameters an improvement in the fitting of the peak flows may be achievable. This requires investigation, although the resulting addition of further parameters is not recommended without confirming that the necessary data is available to calibrate these models.

9.5 ALTERNATIVE DESIGN FLOOD ESTIMATION METHODOLOGY

9.5.1 Summary

As outlined in Chapter 1, many researchers have discussed the limitations of the design event approach for flood estimation and have identified that the probabilistic behaviour of input parameters such as rainfall duration, temporal pattern, losses and baseflow are not well considered. As such, there is uncertainty surrounding the assumption of equality between the rainfall input and flood peak exceedance probabilities. The use of joint probability analysis or continuous simulation methods to determine flood frequency distributions has the potential to overcome many of the existing limitations. However, these methods are time and resource intensive and do not retain the simple approach of the current estimation techniques, which is an important aspect for routine design applications. The approach developed in this study utilises the potential of continuous simulation but at the same time fundamentally retains the design application advantage of using the simple design event approach.

Rainfall loss, in particular initial loss, is an important and influential parameter in determining the magnitude of design floods (refer Chapter 1). Little guidance is available for the selection of appropriate values to use. Continuous catchment water balance simulation models eliminate the need to estimate this loss because it is accounted for within the model structure, as rainfall is transformed into rainfall excess. The technique developed in this study utilises continuous simulation and its explicit accounting of loss to determine a relationship between rainfall and rainfall excess for design. The methodology of this study involved:

- the continuous simulation of rainfall and evaporation inputs into a model of the catchment water balance from which rainfall excess is generated;
- comparing the frequency analysis of the rainfall input (IFD) and the frequency analysis of the rainfall excess output (REFD) to obtain a ratio of these quantities (REFD proportions), which have similar trends with increased ARI and a ratio generally independent of duration;
- using the REFD proportions as a set of proportional loss-frequency curves to describe the separation of the design rainfall into rainfall excess and infiltration/loss that occurs after runoff has commenced for use in a flood estimation model;

- combining the flood estimation and proportional loss-frequency curves with current ARR (1987) design rainfall IFD and temporal pattern information to derive flood frequency distributions; and

- validating the design flood frequency distributions against observed flood frequency data.

9.5.2 Conclusions & Recommendations

From the examination of the results obtained by using the alternative design methodology for design flood estimation proposed in this study it was concluded that:

- the use of the proportional loss-frequency curves improves on the current techniques that require an estimation of initial loss by allowing the direct conversion of design rainfall, which is usually in the form of IFD curves, into design rainfall excess thereby eliminating the need to define initial loss;

- at the sites examined in this study, the derived flood frequency distribution was well within the 90% confidence limits of the observed distributions, which demonstrates the potential for the alternative design flood estimation approach;

- the similar trends in the relationship between the REFD proportions with ARI at the sites examined suggest a potential for easy and widespread application. For two sites the ratio appeared to be relatively constant, increasing only marginally between an ARI of 5 and 100 years, suggesting that the use of constant values of REFD proportions may be used for higher ARI considerations. For the other two sites the ratios increased steadily with ARI, suggesting a mathematical function could be used to describe the ratio. A possible option is a bi-linear function with fixed values for the REFD proportions at ARIs of 2, 10 and 100 years;

- the REFD proportions were generally independent of duration, in that the relative amount of rainfall loss during a two hour burst with an ARI of 50 years is the same as that lost during a 72 hour burst with the same ARI. This means that a single value or function for the REFD proportions for a particular ARI can be applied for each site, rather than a series of values to accommodate varying burst durations. This significantly improves the ease of application and suggests the possibility for regionalisation;

- the KinDog runoff-routing model proved to be an efficient tool for deriving flood

frequency distributions. Concurrently calibrating the model with multiple events prevented any single event significantly influencing the parameters and enabled the selection of parameters that were more representative of the catchment, rather than individual events. This gave confidence for use in simulating rainfall excess while still being able to adequately represent each individual observed event;

- the uncertainty as to the preservation of the ARI due to any joint probability between baseflow and other input parameters was reduced by using a flood estimation model that incorporates a sub-surface flow component. If a runoff-routing model that does not incorporate sub-surface flow is used, then an investigation into the probability distribution of baseflow needs to be undertaken to determine the effect on preserving the ARI; and

- while this study used the ARR (1987) temporal patterns, a comparison of these patterns with actual at-site temporal patterns, derived using the same average variability method used in ARR (1987), showed that the regional patterns are a poor representation and that further investigation is required to develop a more appropriate temporal distribution. Fundamentally, it is unrealistic to assume that patterns derived for a large region containing different climatic conditions will be representative of the temporal patterns for individual sites. Cordery *et al.* (1984) states that the average variability method is an effective tool that could be used to generate consistent and logical temporal patterns for design. However, from the initial investigation in this study it is recommended that it is best used where actual at-site data is available. Alternatively, the use of a probabilistic temporal pattern may be investigated as a robust alternative. ARR (1987) provides two temporal patterns for ARIs less than and greater than 30 years for a number of burst durations. However, the neutrality of these patterns during the transformation of rainfall to rainfall excess can not be assumed. Although deterministic temporal patterns are desirable for routine design, continuous simulation offers the potential to generate patterns for which the probability can be determined and should be investigated further.

The alternative design flood estimation methodology developed in this study has shown considerable promise in terms of providing a more reliable design flood estimation technique. Establishing a relationship between catchment characteristics and the REFD proportions has been considered but not examined. If such a relationship could be established this would enable the definition of REFD proportions or proportional loss-frequency curves for generic catchment types, which would further assist the design process. A sensitivity analysis of the

use of a constant value for the proportional loss needs to be undertaken. If, for sites where the relationship is relatively constant, using a fixed value across a range of ARIs has little effect on the derived flood frequency distribution, the potential for translation to catchments with limited data but similar hydrologic properties is increased. The availability of these curves for key catchment areas in Australia will greatly improve the accuracy of the current design methodology.

10. REFERENCES

Abbott, M. B., Bathurst, J. C., Cunge, J. A., O'Connell, P. E. and Rasmussen, J. (1986a), 'An introduction to the European Hydrological System - Systeme Hydrologique Europeen, "SHE". 1. Distributed modelling system'. *Journal of Hydrology*, 87, 45-59.

Abbott, M. B., Bathurst, J. C., Cunge, J. A., O'Connell, P. E. and Rasmussen, J. (1986b), 'An introduction to the European Hydrological System - Systeme Hydrologique Europeen, "SHE". 2. Structure of a physically-based, distributed modelling system'. *Journal of Hydrology*, 87, 61-77.

Acreman, M. C. (1987), 'Some investigations into rainfall profiles'. *Applied Hydrology Informal Note 102*. Institute of Hydrology, Wallingford, U.K.

Acreman, M. C. (1990), 'A simple stochastic model of hourly rainfall for Farnborough, England'. *Hydrological Sciences Journal*, 35(2), 119-148.

Ahern, P. A. and Weinmann, P. E. (1982), 'Considerations for design flood estimation using catchment modelling'. *Hydrology and Water Resources Symposium*, Melbourne, Victoria, 11-13 May, 1982.

Akaike, H. (1974), 'A new look at the statistical model identification'. *IEEE Transactions on Automatic Control*, AC19(6), 716-723.

Akan, A. O. (1992), 'Horton infiltration equation revisited'. *Journal of Irrigation and Drainage Engineering*, 118(5), 828-830.

Allen, R. G., Pereira, L. S., Raes, D. and Smith, M. (1998), 'Crop evapotranspiration. Guidelines for computing crop water requirements'. FAO Irrigation and Drainage Paper 56, Food and Agriculture Organization of the United Nations, Rome, Italy.

Ang, A. H.-S. and Tang, W. H. (1975), *Probability Concepts in Engineering Planning and Design*. John Wiley and Sons, New York.

Askew, A. J. (1975), 'Variations in estimates of design floods'. *Hydrology Symposium*, Armidale, New South Wales. The Institution of Engineers, Australia.

Bacchi, B., Burlando, P. and Rosso, R. (1989), 'Extreme value analysis of stochastic models of point rainfall'. *3rd Scientific Assembly of IAHS*, Baltimore, U.S.A., 10-19 May, 1989.

Bartlett, M. S. (1963), 'The spectral analysis of point processes'. *Journal of the Royal Statistical Society, Series B*, 25, 264-280.

Bates, B. C. (2000a), *Estimation of Potential Evapotranspiration for Australian Conditions.* Unpublished notes.

Bates, B. C. (2000b), *personal communication*, 30 March 2000.

Bates, B. C. (2000c), *personal communication*, 24 August 2000.

Bauer, S. W. (1974), 'A modified Horton equation for infiltration during intermittent rainfall'. *Hydrological Sciences Bulletin*, 19(2), 219-225.

Becciu, G., Brath, A. and Rosso, E. (1993), 'A physically based methodology for regional flood frequency analysis'. *ASCE Symposium on Engineering Hydrology*, San Francisco, California, 25-30 July, 1993. American Society of Civil Engineers, New York.

Benjamin, J. R. and Cornell, C. A. (1970), *Probability, Statistics, and Decision for Civil Engineers.* McGraw-Hill, New York.

Beran, M. A. (1973), 'Estimation of design floods and the problem of equating the probability of rainfall and runoff'. *Symposium on the Design of Water Resources Projects with Inadequate Data*, Madrid, Spain.

Betson, R. P. (1964), 'What is watershed runoff?'. *Journal of Geophysical Research*, 69(8), 1541-1552.

Beven, K. (1987), 'Towards the use of catchment geomorphology in flood frequency predictions'. *Earth Surface Processes and Landforms*' 12, 69-82.

Beven, K. J., Calver, A. and Morris, E. M. (1987), *The Institute of Hydrology Distributed Model.* Report No. 98, Institute of Hydrology, Wallingford, U.K.

Bickel, P. J. and Doksum, K. (1977), *Mathematical Statistics: Base Ideas and Selected Topics.* Holden-Day, Merrifield.

Biftu, G. F. and Gan, T. Y. (2000), 'Assessment of evapotranspiration models applied to a watershed of Canadian Prairies with mixed land-uses'. *Hydrological Processes*, 14, 1305-1325.

Bonta, J. V. and Rao, R. A. (1988), 'Factors affecting the identification of independent storm events'. *Journal of Hydrology*, 98, 275-293.

Boughton, W. C. (1980), 'A frequency distribution for annual floods'. *Water Resources Research*, 16(2), 347-354.

Boughton, W. C. (1984), 'A simple model for estimating the water yield of ungauged catchments'. *Civil Engineering Transactions, Institution of Engineers, Australia*, CE26(2), 83-88.

Boughton, W. C. and Carroll, D. G. (1993), 'A simple combined water balance/flood hydrograph model'. *Hydrology and Water Resources Symposium*, Newcastle, Australia, 30 June - 2 July, 1993.

Boughton, W. C. (1993), 'A hydrograph-based model for estimating the water yield of ungauged catchments'. *Hydrology and Water Resources Symposium*, Newcastle, Australia, 30 June - 2 July, 1993.

Boughton, W. C. and Hill, P. I. (1997), *A design flood estimation procedure using data generation and a daily water balance model*. Report 97/8, Cooperative Research Centre for Catchment Hydrology, Melbourne, Victoria.

Boughton, W. C., Muncaster, S. H., Srikanthan, R., Weinmann, P. E. and Mein, R. (1999), 'Continuous simulation for design flood estimation - a workable approach'. *Water '99 Joint Congress*, Brisbane, Queensland, 6-8 July, 1999.

Boughton, W., Srikanthan, S. and Weinmann, P. E. (2000), 'Benchmarking a new design flood estimation system'. *Hydro 2000, 3rd International Hydrology and Water Resources Symposium of The Institution of Engineers, Australia*, Perth, Western Australia, 20-23 November, 2000.

Boughton, W. (2000a), *A Continuous Simulation System for Design Flood Estimation - Operating Manual*. Unpublished Report (available as computer file with system software).

Boughton, W. C. (2000b), *A Model for Disaggregating Daily to Hourly Rainfall for Design Flood Estimation*. Technical Report 00/15, Cooperative Research Centre for Catchment Hydrology, Melbourne, Victoria.

Box, G. E. P. and Cox, O. R. (1964), 'The analysis of transformations'. *Journal of the Royal Statistical Society, Series B*, 26(2), 211-252.

Boyd, M. J., Pilgrim, D. H. and Cordery, I. (1979a), 'A storage routing model based on catchment geomorphology'. *Journal of Hydrology*, 42, 209-230.

Boyd, M. J., Pilgrim, D. H. and Cordery, I. (1979b), 'An improved runoff routing model based on geomorphological relations'. *Hydrology and Water Resources Symposium*, National Conference Publication No. 79/10, Institution of Engineers, Australia.

Boyd, M. J., Yau, Y. C. and Tedeschi, M. E. (1986), 'Application of the SFB rainfall-runoff model to a perennial catchment'. *Hydrology and Water Resources Symposium*, National Conference Publication No. 86/13, Institution of Engineers, Australia.

Boyd, M. J., Bates, B. C. and Pilgrim, D. H. (1987), 'WBNM: A general runoff routing model'. *4th National Local Government Engineering Conference*, National Conference Publication No. 87/9, Institution of Engineers, Australia.

Buishand, T. A. (1978), 'Some remarks on the use of daily rainfall models'. *Journal of Hydrology*, 36, 295-308.

Bureau of Meteorology (1983), *Climate of Australia*. Year Book of Australia No. 67, Australian Government Publishing Service, Canberra.

Bureau of Meteorology (2001), *Rainfall Variability in Australia*. Electronic reference, http://www.bom.gov.au/climate/averages/variability.shtml.

Bureau of Transport Economics (2001), *Economic Costs of Natural Disasters in Australia*. Report No. 103, Bureau of Transport Economics, Canberra.

Burlando, P. and Rosso, R. (1991), 'Comment on "Parameter estimation and sensitivity analysis for the modified Bartlett-Lewis rectangular pulses model of rainfall" by S. Islam, et al'. *Journal of Geophysical Research*, 96(D5), 9391-9395.

Burlando, P. and Rosso, R. (1993), 'Stochastic models of temporal rainfall: reproducibility, estimation and prediction of extreme events' in *Stochastic Hydrology and its Use in Water Resources Systems Simulation and Optimization*, eds J. B. Marco, R. Harboe and J. D. Salas. Kluwer Academic Publishers. pp 137-173.

Cadavid, L., Obeysekera, J. T. B. and Shen, H. W. (1991), 'Flood-frequency derivation from kinematic wave'. *Journal of Hydraulic Engineering*, 117(4), 489-510.

Cameron, D. S., Beven, K. J., Tawn, J., Blazkova, S. and Naden, P. (1999), 'Flood frequency estimation by continuous simulation for a gauged upland catchment (with uncertainty)'. *Journal of Hydrology*, 219, 169-187.

Carlson, R. F. and Fox, P. (1976), 'A northern snowmelt-flood frequency model'. *Water Resources Research*, 12(4), 786-794.

Caskey, J. E. J. (1963), 'A Markov chain model for the probability of precipitation occurrence in intervals of various length'. *Monthly Weather Review*, 91(6), 298-301.

Chang, T. J., Kavvas, M. L. and Delleur, J. W. (1984), 'Daily precipitation modeling by discrete autoregressive moving average processes'. *Water Resources Research*, 20(5), 565-580.

Chiew, F. H. S. and Jayasuriya, L. N. N. (1990), 'Applicability of Morton's complementary relationship method of estimating evapotranspiration in rainfall-runoff modelling'. *Conference on Agricultural Engineering*, Toowoomba, Queensland, 11-14 November, 1990. National Conference Publication 90/13, Institution of Engineers, Australia.

Chiew, F. H. S. and McMahon, T. A. (1991), 'The applicability of Morton's and Penman's evapotranspiration estimates in rainfall-runoff modeling'. *Water Resources Bulletin*, 27(4), 611-620.

Chiew, F. H. S., Stewardson, M. J. and McMahon, T. A. (1993), 'Comparison of six rainfall-runoff modelling approaches'. *Journal of Hydrology*, 147, 1-36.

Chiew, F. H. S. and McMahon, T. A. (1993a), *Complete Set of Daily Rainfall, Potential Evapotranspiration and Streamflow Data for Twenty Eight Unregulated Australian Catchments*. Centre for Environmental Applied Hydrology, University of Melbourne,

Melbourne, Victoria.

Chiew, F. H. S. and McMahon, T. A. (1993b), 'Data and rainfall-runoff modelling in Australia'. *Hydrology and Water Resources Symposium*, Newcastle, New South Wales, 30 June - 2 July, 1993.

Chiew, F. and McMahon, T. (1994), 'Application of the daily rainfall-runoff model MODHYDROLOG to 28 Australian catchments'. *Journal of Hydrology*, 153, 383-416.

Chiew, F. H. S., Pitman, A. J. and McMahon, T. A. (1996), 'Conceptual catchment scale rainfall-runoff models and AGCM land-surface parameterisation schemes'. *Journal of Hydrology*, 179, 137-157.

Cho, H.-R. (1985), 'Stochastic dynamics of precipitation: an example'. *Water Resources Research*, 21(8), 1225-1232.

Chow, V. T., Maidment, D. R. and Mays, L. W. (1988), *Applied Hydrology*. McGraw-Hill Book Company, New York.

Chu, S. T. (1978), 'Infiltration during an unsteady rain'. *Water Resources Research*, 14(3), 461-466.

Consuegra, D., Meylan, P. and Musy, A. (1993), 'A probabilistic approach to estimate design parameters for flood control projects'. *Proceedings of the ASCE Symposium on Engineering Hydrology*, San Francisco, California, 25-30 July, 1993. American Society of Civil Engineers, New York.

Cordery, I. (1970a), 'Antecedent wetness for design flood estimation'. *Civil Engineering Transactions, Institution of Engineers, Australia.* CE12(2), 181-184.

Cordery, I. (1970b), 'Initial loss for flood estimation and forecasting'. *Journal of the Hydraulics Division, ASCE*, 96(HY12), 2447-2466.

Cordery, I. (1971), 'Estimation of design hydrographs for small rural catchments'. *Journal of Hydrology*, 13, 263-277.

Cordery, I., Pilgrim, D. H. and Rowbottom, I. A. (1984), 'Time patterns of rainfall for estimating design floods on a frequency basis'. *Water, Science and Technology*, 16, 155-165.

Cowpertwait, P. S. P. (1991a), 'Further developments of the Neyman-Scott clustered point process for modeling rainfall'. *Water Resources Research*, 27(7), 1431-1438.

Cowpertwait, P. S. P. (1991b), *The Stochastic Generation of Rainfall Time Series*. PhD Thesis, University of Newcastle upon Tyne, Newcastle upon Tyne.

Cowpertwait, P. S. P. (1994), 'A generalized point process model for rainfall'. *Journal of the Royal Statistical Society, Series A*, 447, 23-37.

Cowpertwait, P. S. P. (1995), 'A generalized spatial-temporal model of rainfall based on a clustered point process'. *Journal of the Royal Statistical Society, Series A*, 450, 163-175.

Cowpertwait, P. S. P., O'Connell, P. E., Metcalfe, A. V. and Mawdsley, J. A. (1996a), 'Stochastic point process modelling of rainfall. I. Single-site fitting and validation'. *Journal of Hydrology*, 175, 17-46.

Cowpertwait, P. S. P., O'Connell, P. E., Metcalfe, A. V. and Mawdsley, J. A. (1996b), 'Stochastic point process modelling of rainfall. II. Regionalisation and disaggregation'. *Journal of Hydrology*, 175, 47-65.

Cowpertwait, P. S. P. (1998), 'A Poisson-cluster model of rainfall: high-order moments and extreme values'. *Journal of the Royal Statistical Society, Series A*, 454, 885-898.

Cox, D. R. and Isham, V. (1980), *Point Processes*. Chapman and Hall, London.

Crago, R. D. and Brutsaert, W. (1992), 'A comparison of several evaporation equations'. *Water Resources Research*, 28(3), 951-954.

Denmead, O. T. and Shaw, R. H. (1962), 'Availability of soil water to plants as affected by soil moisture content and meteorological conditions'. *Agronomy Journal*, 54(5), 385-389.

Dias, N. L. and Kan, A. (1999), 'A hydrometeorological model for basin-wide seasonal evapotranspiration'. *Water Resources Research*, 35(11), 3409-3418.

Diaz-Granados, M. A., Valdes, J. B. and Bras, R. L. (1984), 'A physically based flood frequency distribution'. *Water Resources Research*, 20(7), 995-1002.

Dingman, S. L. (1994), *Physical Hydrology*. Prentice Hall, Englewood Cliffs.

Duan, Q., Sorooshian, S. and Gupta, V. (1992), 'Effective and efficient global optimization for conceptual rainfall-runoff models'. *Water Resources Research*, 28(4), 1015-1031.

Dunne, T., Moore, T. R. and Taylor, C. H. (1975), 'Recognition and prediction of runoff-producing zones in humid regions'. *Hydrological Sciences Bulletin*, 20(305-327).

Durrans, S. R. (1995), 'Total probability methods for problems in flood frequency estimation'. *Statistical and Bayesian Methods in Hydrological Sciences, International Conference in Honour of Jacques Bernier*, UNESCO, Paris, 11-13 September, 1995.

Dyer, B. G., Nathan, R. J., McMahon, T. A. and O'Neill, I. C. (1994), *Development of regional prediction equations for the RORB runoff routing model.* Report 94/1, Cooperative Research Centre for Catchment Hydrology, Melbourne, Victoria.

Eagleson, P. S. (1970), *Dynamic Hydrology*. McGraw-Hill, New York.

Eagleson, P. S. (1972), 'Dynamics of flood frequency'. *Water Resources Research*, 8(4), 878-898.

Eagleson, P. S. (1978a), 'Climate, soil and vegetation. 1. Introduction to water balance dynamics'. *Water Resources Research*, 14(5), 705-712.

Eagleson, P. S. (1978b), 'Climate, soil and vegetation. 2. The distribution of annual precipitation derived from observed storm sequences'. *Water Resources Research*, 14(2), 713-721.

Eidsvik, K. J. (1980), 'Identification of models for some times series of atmospheric origin with Akaike's Information criterion'. *Journal of Applied Meteorology*, 19(4), 357-369

Eichinger, W. E., Parlange, M. B. and Stricker, H. (1996), 'On the concept of equilibrium evaporation and the value of the Priestley-Taylor coefficient'. *Water Resources Research*, 32(1), 161-164.

Entekhabi, D., Rodriguez-Iturbe, I. and Eagleson, P. S. (1989), 'Probabilistic representation of the temporal rainfall process by a modified Neyman-Scott rectangular pulses model: parameter estimation and validation'. *Water Resources Research*, 25(2), 295-302.

Federer, C. A., Vorosmarty, C. and Fekete, B. (1996), 'Intercomparison of methods for

calculating potential evaporation in regional and global water balance models'. *Water Resources Research*, 32(7), 2315-2321.

Feyerherm, A. M. and Bark, L. D. (1967), 'Goodness of fit of a Markov chain model for sequences of wet and dry days'. *Journal of Applied Meteorology*, 6, 770-773.

Field, W. G. and Williams, B. J. (1983), 'A generalised one-dimensional kinematic catchment model'. *Journal of Hydrology*, 60, 25-42.

Field, W. G. and Williams, B. J. (1987), 'A generalized kinematic catchment model'. *Water Resources Research*, 23(8), 1693-1696.

Flavell, D. J. and Belstead, B. S. (1986), 'Losses for design flood estimation in Western Australia'. *Hydrology and Water Resources Symposium*, National Conference Publication No. 86/13, Institution of Engineers, Australia.

Fleming, P. M. (1970), 'A diurnal distribution function for daily evaporation'. *Water Resources Research*, 6(3), 937-942.

Fontaine, T. A. and Potter, K. W. (1993), 'Estimating exceedance probabilities of extreme floods'. *ASCE Symposium on Engineering Hydrology*, San Francisco, California, 25-30 July, 1993. American Society of Civil Engineers, New York.

Foufoula-Georgiou, E. and Guttorp, P. (1986), 'Compatibility of continuous rainfall occurrence models with discrete rainfall observations'. *Water Resources Research*, 22(8), 1316-1322.

Foufoula-Georgiou, E. and Lettenmaier, D. P. (1986), 'Continuous-time versus discrete-time point process models for rainfall occurrence series'. *Water Resources Research*, 22(4), 531-542.

Foufoula-Georgiou, E. and Guttorp, P. (1987), 'Assessment of a class of Neyman-Scott models for temporal rainfall'. *Journal of Geophysical Research*, 92(D8), 9679-9682.

Foufoula-Georgiou, E. and Lettenmaier, D. P. (1987), 'A Markov renewal model for rainfall occurrences'. *Water Resources Research*, 23(5), 875-884.

Frost, A., Jennings, S., Thyer, M., Lambert, M. and Kuczera, G. (2000), 'Droughts, floods

and everything else in between'. *Hydro 2000, 3rd International Hydrology and Water Resources Symposium of The Institution of Engineers, Australia*, Perth, Western Australia, 20-23 November, 2000. The Institution of Engineers, Australia.

Gabriel, K. R. and Neumann, J. (1957), 'On a distribution of weather cycles by length'. *Quarterly Journal of the Royal Hydrological Society*, 83, 375-380.

Gabriel, K. R. and Neumann, J. (1962), 'A Markov chain model for daily rainfall occurrence at Tel Aviv'. *Quarterly Journal of the Royal Hydrological Society*, 88, 90-95.

Grace, R. A. and Eagleson, P. S. (1966), *The Synthesis of Short-Time-Increment Rainfall Sequences*. Hydrodynamics Laboratory Report No. 91, Department of Civil Engineering, Massachusetts Institute of Technology.

Grace, R. A. and Eagleson, P. S. (1967), 'A model for generating synthetic sequences of short-time-interval rainfall depths'. *The International Hydrology Symposium*, Colorado State University, Fort Collins, Colorado.

Grayman, W. M. and Eagleson, P. S. (1969), *Streamflow Record Length for Modelling Catchment Dynamics*. Hydrodynamics Laboratory Report No. 114, Department of Civil Engineering, Massachusetts Institute of Technology.

Grayson, R. B., Argent, R. M., Nathan, R. J., McMahon, T. A. and Mein, R. G. (1996), *Hydrological Recipes: Estimation Techniques in Australian Hydrology*. Cooperative Research Centre for Catchment Hydrology, Melbourne, Victoria.

Green, J. R. (1964), 'A model for rainfall occurrence'. *Journal of the Royal Statistical Society, Series B*, 26, 345-353.

Green, J. R. (1965), 'Two probability models for sequences of wet or dry days'. *Monthly Weather Review*, 93(3), 155-156.

Green, W. H. and Ampt, G. A. (1911), 'Studies on soil physics. Part I: the flow of air and water through soils'. *Journal of Agricultural Science*, 4(1), 1-24.

Gupta, V. K., Waymire, E. and Wang, C. T. (1980), 'A representation of an instantaneous unit hydrograph from geomorphology'. *Water Resources Research*, 16(5), 855-862.

Gyasi-Agyei, Y. and Willgoose, G. R. (1997), 'A hybrid model for point rainfall modeling'. *Water Resources Research*, 33(7), 1699-1706.

Gyasi-Agyei, Y. and Willgoose, G. R. (1999), 'Generalisation of a hybrid model for point rainfall'. *Journal of Hydrology*, 219, 218-224.

Gyasi-Agyei, Y. (1999), 'Identification of regional parameters of a stochastic model for rainfall disaggregation'. *Journal of Hydrology*, 223, 148-163.

Haan, C. T., Allen, D. M. and Street, J. O. (1976), 'A Markov chain model of daily rainfall'. *Water Resources Research*, 12(3), 443-449.

Haan, C. T. and Schulze, R. E. (1987), 'Return period flow prediction with uncertain parameters'. *Transactions of the ASCE*, 30(3), 665-669.

Haan, C. T. and Edwards, D. R. (1988), 'Joint probability estimates of return periods'. *Transactions of the ASCE*, 31(4), 1115-1119.

Harvey, R. A. (1982), 'Estimation of the probable maximum flood - Western Australia'. *Proceedings on the Workshop on Spillway Design*, Department of National Development and Energy, AWRC Conference Series No. 6.

Hashino, M. (1986), 'Stochastic formulation of storm pattern and rainfall intensity-duration curve for design flood'. *Hydrologic Frequency Modelling, International Symposium on Flood Frequency and Risk Analysis*, Louisiana State University, Baton Rouge, Louisiana., 14-17 May, 1986. D. Reidel Publishing Company.

Hebson, C. and Wood, E. F. (1982), 'A derived flood frequency distribution using Horton order ratios'. *Water Resources Research*, 18(5), 1509-1518.

Hill, P. I. (1994), *Catalogue of Hydrologic Data for Selected Victorian Catchments*. Working Document 94/1, Cooperative Research Centre for Catchment Hydrology, Melbourne, Victoria.

Hill, P. I., Maheepala, U.K., Mein, R. G. and Weinmann, P. E. (1996a), *Empirical Analysis of Data to Derive Losses for Design Flood Estimation in South-eastern Australia*. Report 96/5, Cooperative Research Centre for Catchment Hydrology, Melbourne, Victoria.

Hill, P. I., Maheepala, U. K. and Mein, R. G. (1996b), *Empirical Analysis of Data to Derive Losses: Methodology, Programs and Results*. Working Document 96/5, Cooperative Research Centre for Catchment Hydrology, Melbourne, Victoria.

Hill, P. I. and Mein, R. G. (1996c), 'Incompatibilities between storm temporal patterns and losses for design flood estimation'. *23rd Hydrology and Water Resources Symposium*, Hobart, Australia, 21-24 May, 1996. National Conference Publication No. 96/05, Institution of Engineers, Australia.

Hill, P. I. (1998), *How Much Rainfall Becomes Runoff? Loss Modelling for Flood Estimation.* Industry Report 98/5, Cooperative Research Centre for Catchment Hydrology, Melbourne, Victoria.

Hopkins, J. W. and Robillard, P. (1964), 'Some statistics of daily rainfall occurrence for the Canadian prairie provinces'. *Journal of Applied Meteorology*, 3, 600-602.

Horton, R. E. (1933), 'The role of infiltration in the hydrologic cycle'. *Transactions of the American Geophysical Union*, 14, 446-460.

Hounam, C. E. (1961), *Evaporation in Australia. A Critical Survey of the Network and Methods of Observation together with a Tabulation of the Results of Observations.* Bulletin No. 44, Bureau of Meteorology, Melbourne, Victoria.

Huber, W. C., Cunningham, B. A. and Cavender, K. A. (1986), 'Continuous SWMM modeling for selection of design events'. *UDM '86, International Symposium on the Comparison of Urban Drainage Models with Real Catchment Data*, Dubrovnik, Yugoslavia. Pergamon Press.

Huff, F. A. (1967), 'Time distribution of rainfall in heavy storms'. *Water Resources Research*, 3(4), 1007-1019.

Hutchinson, M. F. (1990), 'A point rainfall model based on a three-state continuous Markov occurrence process'. *Journal of Hydrology*, 114, 125-148.

Islam, S., Entekhabi, D., Bras, R. L. and Rodriguez-Iturbe, I. (1990), 'Parameter estimation and sensitivity analysis for the modified Bartlett-Lewis rectangular pulses model of rainfall'. *Journal of Geophysical Research*, 95(D3), 2093-2100.

Ison, N. T., Feyerherm, A., M. and Bark, L. D. (1971), 'Wet period precipitation and the gamma distribution'. *Journal of Applied Meteorology*, 10(4), 658-661.

Institution of Engineers, Australia (1987), *Australian Rainfall and Runoff, Volume One and Two*. Institution of Engineers, Australia.

Istok, J. D. and Boersma, L. (1989), 'A stochastic cluster model for hourly precipitation data'. *Journal of Hydrology*, 106, 257-285.

Jakeman, A. J. and Hornberger, G. M. (1993), 'How much complexity is warranted in a rainfall-runoff model?'. *Water Resources Research*, 29(8), 2637-2649.

James, W. and Robinson, M. (1986), 'Continuous deterministic urban runoff modelling'. *UDM '86, International Symposium on the Comparison of Urban Drainage Models with Real Catchment Data*, Dubrovnik, Yugoslavia. Pergamon Press.

James, W. P., Warinner, J. and Reedy, M. (1992), 'Application of the Green-Ampt infiltration equation to watershed modelling'. *Water Resources Bulletin*, 28(3), 623-634.

James, J., Dandy, G. and Teubner, M. (1999), 'Evaluation of potential for aquifer storage and recovery using streamflow'. *Water '99 Joint Congress*, Brisbane, Queensland, 6-8 July, 1999. The Institution of Engineers, Australia.

Jayasuriya, L. N. N., McMahon, T. A. and O'Neill, I. C. (1990), 'The selection of an optimization technique for rainfall-runoff modelling'. *Conference on Agricultural Engineering*, Toowoomba, Queensland, 11-14 November, 1990. The Institution of Engineers, Australia.

Jayatilaka, C. and Connell, L. D. (1995), *A review of catchment scale hydrologic modelling approaches*. Report 95/5, Cooperative Research Centre for Catchment Hydrology, Melbourne, Victoria.

Jayatilaka, C. J., Storm, B. and Mudgway, L. B. (1998), 'Simulation of water flow on irrigation bay scale with MIKE-SHE'. *Journal of Hydrology*, 208, 108-130.

Jensen, M. E. and Haise, H. R. (1963), 'Estimating evapotranspiration from solar radiation'. *Journal of Irrigation and Drainage Engineering, ASCE*, 89(IR4), 15-41.

Jimoh, O. D. and Webster, P. (1996), 'The optimum order of a Markov chain model for daily rainfall in Nigeria'. *Journal of Hydrology*, 185, 45-69.

Jones, J. W., Colwick, R. E. and Threadgill, E. D. (1972), 'A simulated environmental model of temperature, evaporation, rainfall and soil moisture'. *Transactions of the ASAE*, 15(2), 366-372.

Kass, R. E. and Raftery, A. E. (1994), *Bayes Factors*. Technical Report 254, University of Washington, Seattle, Washington.

Kass, R. E. and Raftery, A. E. (1995), 'Bayes factors'. *Journal of the American Statistical Association*, 90, 773-795.

Katz, R. W. and Parlange, M. B. (1995), 'Generalization of chain-dependent processes: Application to hourly precipitation'. *Water Resources Research*, 31(5), 1331-1341.

Kavvas, M. L., and Delleur, J. W. (1975), *The Stochastic and Chronologic Structure of Rainfall Sequence: Application to Indiana*. Technical Report No. 57, Water Resources Research Centre, Purdue University, West Layfayette, Indiana.

Kavvas, M. L. and Delleur, J. W. (1981), 'A stochastic cluster model of daily rainfall sequences'. *Water Resources Research*, 17(4), 1151-1160.

Keifer, C. J. and Chu, H. H. (1957), 'Synthetic storm pattern for drainage design'. *Journal of the Hydraulic Division, ASCE*, 83(HY4), 1-25.

Kennedy, M. R., Turner, L. H., Canterford, R. P. and Pearce, H. J. (1991), *Temporal Distributions within Rainfall Bursts*. HRS Report No. 1, Hydrometeorological Advisory Service, Bureau of Meteorology, Melbourne, Victoria.

Khaliq, M. N. and Cunnane, C. (1996), 'Modelling point rainfall occurrences with the modified Bartlett-Lewis rectangular pulses model'. *Journal of Hydrology*, 180, 109-138.

Koutsoyiannis, D. and Xanthopoulos, T. (1990), 'A dynamic model for short-scale rainfall disaggregation'. *Hydrological Sciences Journal*, 35(3), 303-322.

Koutsoyiannis, D. and Foufoula-Georgiou, E. (1993), 'A scaling model of a storm hyetograph'. *Water Resources Research*, 29(7), 2345-2361.

Koutsoyiannis, D. (1994), 'A stochastic disaggregation method for design storm and flood synthesis'. *Journal of Hydrology*, 156, 193-225.

Koutsoyiannis, D. and Pachakis, D. (1996), 'Deterministic chaos versus stochasticity in analysis and modeling of point rainfall series'. *Journal of Geophysical Research*, 101(D21), 26441-26451.

Kuczera, G. (1983a), 'Improved parameter inference in catchment models 1. Evaluating parameter uncertainty'. *Water Resources Research*, 19(5), 1151-1162.

Kuczera, G. (1983b), 'Improved parameter inference in catchment models 2. Combining different kinds of hydrologic data and testing their compatibility'. *Water Resources Research*, 19(5), 1163-1172.

Kuczera, G. (1994a), *NLFIT: A Bayesian Nonlinear Regression Program Suite*. Department of Civil, Surveying and Environmental Engineering, University of Newcastle, New South Wales.

Kuczera, G. (1994b), 'Comprehensive Bayesian at-site flood frequency inference'. *Water Down Under '94*, Adelaide, South Australia, 21-25 November, 1994.

Kuczera, G. (1997), 'Efficient subspace probabilistic parameter optimization for catchment models'. *Water Resources Research*, 33(1), 177-185.

Kuczera, G., Williams, B., Binning, P. and Lambert, M. (2000), 'An education web site for free water engineering software'. *Hydro 2000, 3rd International Hydrology and Water Resources Symposium of The Institution of Engineers, Australia*, Perth, Western Australia, 20-23 November, 2000. The Institution of Engineers, Australia.

Kuczera, G. (2001), *KinDog: A Kinematic Runoff-Routing Catchment Model (user manual).* Department of Civil, Surveying and Environmental Engineering, University of Newcastle, Newcastle, New South Wales.

Kuczera, G. (2002), *personal communication*, 18 July 2002.

Lambert, M. and Kuczera, G. (1996), 'A statistical model of rainfall'. *Stochastic Hydraulics '96*, Mackay, Queensland.

Lambert, M. and Kuczera, G. (1998), 'Seasonal generalised exponential probability models with application to interstorm and storm durations'. *Water Resources Research*, 34(1), 143-148.

Lambourne, J. J. and Stephenson, D. (1987), 'Model study of the effect of temporal storm distributions on peak discharges and volumes'. *Hydrological Sciences Journal*, 32(2), 215-226.

Laurenson, E. M. (1974), 'Modeling of stochastic-deterministic hydrologic systems'. *Water Resources Research*, 10(5), 955-961.

Laurenson, E. M. and Mein, R. G. (1985), *RORB - Version 3 Runoff Routing Program - User Manual*. Department of Civil Engineering, Monash University, Melbourne, Victoria.

Laurenson, E. M. and Mein, R. G. (1990), *RORB - Version 4 Runoff Routing Program: User Manual*. Department of Civil Engineering, Monash University, Melbourne, Victoria.

Le Cam, L. (1961), 'A stochastic description of precipitation'. *Fourth Berkeley Symposium on Mathematical Statistics and Probability*, University of California at Berkeley, California, 20 June - 30 July, 1960. University of California Press, Berkeley.

Legates, D. R. and McCabe, G. J. J. (1999), 'Evaluating the use of "goodness-of-fit" measures in hydrologic and hydroclimatic model validation'. *Water Resources Research*, 35(1), 233-241.

Lemeur, R. and Zhang, L. (1990), 'Evaluation of three evapotranspiration models in terms of their applicability for an arid region'. *Journal of Hydrology*, 114, 395-411.

Lewis, P. A. W. (1964), 'A branching Poisson process model for the analysis of computer failure patterns (with discussion)'. *Journal of the Royal Statistical Society, Series B*, 26, 398-456.

Lindsey, S. D. and Farnsworth, R. K. (1997), 'Sources of solar radiation estimates and their effect on daily potential evaporation for use in streamflow modeling'. *Journal of Hydrology*, 201, 348-366.

Linsley, R. and Crawford, N. (1974), 'Continuous simulation models in urban hydrology'. *Geophysical Research Letters*, 1(1), 59-62.

Liou, E. Y. (1970), *OPSET - Program for Computerized Selection of Watershed Parameter Values of the Stanford Watershed Model.* Research Report No. 34, Water Resources Institute, University of Kentucky, Lexington, Kentucky.

Lumb, A. M. and James, L. D. (1976), 'Runoff files for flood hydrograph simulation'. *Journal of the Hydraulics Division, ASCE*, 102(HY10), 1515-1531.

Marien, J. L. and Vandewiele, G. L. (1986), 'A point rainfall generator with internal storm structure'. *Water Resources Research*, 22(4), 475-482.

McCuen, R. H. (1998), *Hydrologic Analysis and Design.* Prentice Hall, Upper Saddle River.

McMahon, T. A. and Mein, R. G. (1986), *River and Reservoir Yield.* Water Resources Publications, Littleton, Colorado.

Mein, R. G. and Larson, C. L. (1973), 'Modeling infiltration during a steady rain'. *Water Resources Research*, 9(2), 384-394.

Mein, R. G. (1980), 'Recent developments in modelling of infiltration: Extension of the Green-Ampt model'. *Hydrology and Water Resources Symposium*, Adelaide, South Australia, 4-6 November, 1980.

Mein, R. G., Nandakumar, N. and Siriwardena, L. (1995), *Estimation of Initial Loss from Soil Moisture Indices (pilot study).* Working Document 95/1, Cooperative Research Centre for Catchment Hydrology, Melbourne, Victoria.

Menabde, M. and Sivapalan, M. (2000), 'Modeling of rainfall time series and extremes using bounded random cascades and Levy-stable distributions'. *Water Resources Research*, 36(11), 3293-3300.

Monteith, J. L. (1965), 'Evaporation and the environment'. *The State and Movement of Water in Living Organisms, 19th Symposium of the Society for Experimental Biology.* Cambridge University Press, New York.

Morrissey, M. L. and Krajewski, W. F. (1993), 'A point process model for tropical rainfall'. *Journal of Geophysical Research*, 98(D9), 16639-16652.

Morton, F. I. (1983), 'Operational estimates of areal evapotranspiration and their significance

to the science and practice of hydrology'. *Journal of Hydrology*, 66, 1-76.

Moughamian, M. S., McLaughlin, D. B. and Bras, R. L. (1987), 'Estimation of flood frequency: An evaluation of two derived distribution procedures'. *Water Resources Research*, 23(7), 1309-1319.

Muzik, I. (1993), 'Derived, physically based distribution of flood probabilities'. *Proceedings of the Yokohama Symposium, Extreme Hydrological Events: Precipitation, Flood and Droughts*, Yokohama, Japan, July, 1993. IAHS Publication No 213.

Nandakumar, N., Mein, R. G. and Siriwardena, L. (1994), *Loss Modelling for Flood Estimation - A Review*. Report 94/4, Cooperative Research Centre for Catchment Hydrology, Melbourne, Victoria.

Nathan, R. J. and McMahon, T. A. (1990a), 'The SFB model part 1 - Validation of fixed model parameters'. *Civil Engineering Transactions, Institution of Engineers Australia*, CE32(3), 157-161.

Nathan, R. J. and McMahon, T. A. (1990b), 'The SFB model part 2 - Operational considerations'. *Civil Engineering Transactions, Institution of Engineers Australia*, CE32(3), 162-166.

Natural Environment Research Council (NERC) (1975), *Flood Studies Report: Volume 1, Hydrological Studies*. London.

Nelder, J. A. and Mead, R. (1965), 'A simplex method for function minimisation'. *Journal of Computing*, 7(4), 308-313.

Newton, D. and Walton, R. (2000), 'Continuous simulation for design flood estimation in the Moore River catchment, Western Australia'. *Hydro 2000, 3rd International Hydrology and Water Resources Symposium of The Institution of Engineers, Australia*, Perth, Western Australia, 20-23 November, 2000. The Institution of Engineers, Australia.

Neyman, J. and Scott, E. L. (1958), 'Statistical approach to problems of cosmology'. *Journal of the Royal Statistical Society, Series B*, 20(1), 1-43.

Nicks, A. D. and Harp, J. F. (1980), 'Stochastic generation of temperature and solar radiation data'. *Journal of Hydrology*, 48, 1-17.

O'Loughlin, G. G. (1986), 'The ILSAX program for urban drainage design and analysis'. School of Engineering, New South Wales Institute of Technology.

Onof, C. and Wheater, H. S. (1993), 'Modelling of British rainfall using a random parameter Bartlett-Lewis Rectangular Pulse Model'. *Journal of Hydrology*, 149, 67-95.

Onof, C. and Wheater, H. S. (1994a), 'Improvements to the modelling of British rainfall using a modified Random Pulse Parameter Bartlett-Lewis Rectangular Pulse Model'. *Journal of Hydrology*, 157, 177-195.

Onof, C. and Wheater, H. S. (1994b), 'Improved fitting of the Bartlett-Lewis rectangular pulse model for hourly rainfall'. *Hydrological Sciences Journal*, 39(6), 663-680.

Onof, C. and Wheater, H. S. (1995), 'Modelling of rainfall time-series using the Bartlett-Lewis model'. *Water, Maritime and Energy*, 112, 362-374.

Ormsbee, L. E. (1989), 'Rainfall disaggregation model for continuous hydrologic modeling'. *Journal of Hydraulic Engineering*, 115(4), 507-525.

Pattison, A. (1965), 'Synthesis of hourly rainfall data'. *Water Resources Research*, 1(4), 489-498.

Penman, H. L. (1948), 'Natural evaporation from open water, bare soil and grass'. *Proceedings Royal Society London, Series A*, 193, 120-145.

Philip, J. R. (1957), 'The theory of infiltration: 1. The infiltration equation and its solution'. *Soil Science*, 83, 345-357.

Pilgrim, D. H., Cordery, I. and French, R. (1969), 'Temporal patterns of design rainfall for Sydney'. *Civil Engineering Transactions, Institute of Engineers, Australia*, CE11(1), 9-14.

Pilgrim, D. H. and Cordery, I. (1975), 'Rainfall temporal patterns for design floods'. *Journal of the Hydraulics Division, ASCE*. 101(HY1), 81-95.

Press, W. H., Teukolsky, S. A., Vetterling, W. T. and Flannery, B. P. (1992), *Numerical Recipes in FORTRAN*. Cambridge University Press, Cambridge.

Priestley, C. H. B. and Taylor, R. J. (1972), 'On the assessment of surface heat flux and evaporation using large-scale parameters'. *Monthly Weather Review*, 100(2), 81-92.

Raftery, A. E. (1995), 'Bayesian model selection in social research (with discussion)'. *Sociological Methodology 1995*, 111-195. P. Marsden. Oxford.

Raghuwanshi, N. S. and Wallender, W. W. (1998), 'Converting from pan evaporation to evapotranspiration'. *Journal of Irrigation and Drainage Engineering*, 124(5), 275-277.

Rahman, A., Hoang, T. M. T., Weinmann, P. E., and Laurenson, E. M. (1998), *Joint Probability Approaches to Design Flood Estimation: A Review*. Technical Report 98/8, Cooperative Research Centre for Catchment Hydrology, Melbourne, Victoria.

Rahman, A., Weinmann, P. E., Hoang, T. M. T., Laurenson, E. M., and Nathan, R. (2001), *Monte Carlo Simulation of Flood Frequency Curves from Rainfall*. Technical Report 01/4, Cooperative Research Centre for Catchment Hydrology, Melbourne, Victoria.

Raines, T. H. and Valdes, J. B. (1993), 'Estimation of flood frequencies for ungaged catchments'. *Journal of Hydraulic Engineering*, 119(10), 1138-1154.

Rajagopalan, B., Lall, U. and Tarboton, D. G. (1996), 'Nonhomogeneous Markov model for daily precipitation'. *Journal of Hydrologic Engineering*, 1(1), 33-40.

Rao, R. A. and Chenchayya, B. T. (1974), *Probabilistic Analysis and Simulation of the Short Time Increment Rainfall Process*. Technical Report 55, Water Resources Center, Purdue University, West Lafayette, Indiana.

Restrepo-Posada, P. J. and Eagleson, P. S. (1982), 'Identification of independent rainstorms'. *Journal of Hydrology*, 55, 303-319.

Richards, L. A. (1931), 'Capillary conduction of liquids through porous mediums'. *Physics*, 1, 318-333.

Rigby, E. H. and Bannigan, D. J. (1996), 'The embedded storm concept - A critical review'. *23rd Hydrology and Water Resources Symposium*, Hobart, Tasmania, 21-24 May, 1996. National Conference Publication No. 96/05, Institution of Engineers, Australia.

Robinson, J. S. and Sivapalan, M. (1997), 'Temporal scales and hydrological regimes: Implications for flood frequency scaling'. *Water Resources Research*, 33(12), 2981-2999.

Rodriguez-Iturbe, I. and Valdes, J. B. (1979), 'The geomorphologic structure of hydrologic

response'. *Water Resources Research*, 15(6), 1409-1420.

Rodriguez-Iturbe, I., Gonzalez-Sanabria, M. and Bras, R. L. (1982a), 'A geomorphoclimatic theory of the instantaneous unit hydrograph'. *Water Resources Research*, 18(4), 877-886.

Rodriguez-Iturbe, I., Gonzalez-Sanabria, M. and Caamano, G. (1982b), 'On the climatic dependence of the IUH: A rainfall-runoff analysis of the Nash model and the geomorphoclimatic theory'. *Water Resources Research*, 18(4), 887-903.

Rodriguez-Iturbe, I., Gupta, V. K. and Waymire, E. (1984), 'Scale considerations in the modeling of temporal rainfall'. *Water Resources Research*, 20(11), 1611-1619.

Rodriguez-Iturbe, I., Cox, D. R. and Isham, V. (1987a), 'Some models for rainfall based on stochastic point processes'. *Journal of the Royal Statistical Society, Series A*, 410, 269-288.

Rodriguez-Iturbe, I., Febres De Power, B. and Valdes, J. B. (1987b), 'Rectangular pulse point process models for rainfall: Analysis of empirical data'. *Journal of Geophysical Research*, 92(D8), 9645-9656.

Rodriguez-Iturbe, I., Cox, D. R. and Isham, V. (1988), 'A point process model of rainfall: further developments'. *Journal of the Royal Statistical Society, Series A*, 417, 283-298.

Roldan, J. and Woolhiser, D. A. (1982), 'Stochastic daily precipitation models. 1: A comparison of occurrence processes'. *Water Resources Research*, 18(5), 1451-1459.

Rosbjerg, D., Madsen, H. and Rasmussen, P. F. (1992), 'Prediction in partial duration series with generalized pareto-distributed exceedances'. *Water Resources Research*, 28(11), 3001-3010.

Russell, S. O., Kenning, B. F. I. and Sunnell, G. J. (1979), 'Estimating design flows for urban drainage'. *Journal of the Hydraulics Division, ASCE*, 105(HY1), 43-52.

Sariahmed, A. and Kisiel, C. C. (1968), 'Synthesis of sequences of summer thunderstorms volumes for the Atterbury watershed in the Tucson area'. *International Association of Hydrological Sciences Symposium on the Use of Analog and Digital Computers in Hydrology*.

Sharifi, R. and Boyd, M. J. (1994), 'A comparison of the SFB and AWBM rainfall-runoff

models'. *Water Down Under '94*, Adelaide, South Australia, 21-25 November, 1994.

Shuttleworth, W. J. (1993), 'Evaporation', in *Handbook of Hydrology*. McGraw-Hill, New York.

Siriwardena, L. and Mein, R. G. (1995), *Development and Testing of a Variable Proportional Loss Model Based on 'Saturation Curves' (A study on Eight Victorian Catchments)*. Working Document 95/2, Cooperative Research Centre for Catchment Hydrology, Melbourne, Victoria.

Siriwardena, L., Hill, P. I. and Mein, R. G. (1997), *Investigation of a Variable Proportional Loss Model for Use in Flood Estimation*. Report 97/3, Cooperative Research Centre for Catchment Hydrology, Melbourne, Victoria.

Sivapalan, M., Wood, E. F. and Beven, K. J. (1990), 'On hydrologic similarity 3. A dimensionless flood frequency model using a generalized geomorphologic unit hydrograph and partial area runoff generation'. *Water Resources Research*, 26(1), 43-58.

Small, M. J. and Morgan, D. J. (1986), 'The relationship between a continuous-time renewal model and a discrete Markov chain model of precipitation occurrence'. *Water Resources Research*, 22(10), 1422-1430.

Smith, E. R. and Schreiber, H. A. (1973), 'Point processes of seasonal thunderstorm rainfall, Part 1, Distribution of rainfall events'. *Water Resources Research*, 9(4), 871-884.

Smith, J. A. and Karr, A. F. (1983), 'A point process model of summer season rainfall occurrences'. *Water Resources Research*, 19(1), 95-103.

Smith, J. A. (1987), 'Statistical modeling of daily rainfall occurrences'. *Water Resources Research*, 23(5), 885-893.

Smith, M. (1991), *Report on the expert consultation on procedures for revision of FAO guidelines for prediction of crop water requirements*. Land and Water Development Division, Food and Agriculture Organization of the United Nations, Rome, Italy, 28-31 May, 1990.

Srikanthan, R. and McMahon, T. A. (1985), *Stochastic Generation of Rainfall and Evaporation Data*. Technical Paper No. 84, Australian Water Resources Council, Canberra.

Stannard, D. I. (1993), 'Comparison of Penman-Monteith, Shuttleworth-Wallace, and modified Priestly-Taylor evapotranspiration models for wildland vegetation in semiarid rangeland'. *Water Resources Research*, 29(5), 1379-1392.

Stern, R. D. and Coe, R. (1984), 'A model fitting analysis of daily rainfall data'. *Journal of the Royal Statistical Society, Series A*, 147(1), 1-34.

Sturman, A. P. and Tapper, N. J. (1996), 'Regional and Smaller Scale Climates', in *The Weather and Climate of Australia and New Zealand*. Oxford University Press Melbourne. pp 297-330.

Sumner, N. R., Fleming, P. M. and Bates, B. C. (1997), 'Calibration of a modified SFB model for twenty-five Australian catchments using simulated annealing'. *Journal of Hydrology*, 197, 166-188.

Thyer, M., Kuczera, G. and Bates, B. C. (1999), 'Probabilistic optimization for conceptual rainfall-runoff models: A comparison of the shuffled complex evolution simulated annealing algorithms'. *Water Resources Research*, 35(3), 767-773.

Thyer, M. and Kuczera, G. (2000), 'Modeling long-term persistence in hydroclimatic time series using a hidden state Markov model'. *Water Resources Research*, 36(11), 3301-3310.

Titmarsh, G. W., Pilgrim, D. H., Cordery, I. and Hoesein, A. A. (1989), 'An examination of design flood estimations using the US Soil Conservation Services Method'. *Hydrology and Water Resources Symposium*, Christchurch, New Zealand, 23-30 November, 1989. Institution of Engineers, Australia.

Todorovic, P. and Yevjevich, V. (1967), 'A particular stochastic process as applied to hydrology'. *The International Hydrology Symposium*, Colorado State University, Fort Collins, Colorado.

Todorovic, P. (1968), *A mathematical study of precipitation phenomena*. Report CER 67-68 PT65, Engineering Research Center, Colorado State University, Fort Collins, Colorado.

Todorovic, P. and Yevjevich, V. (1969), *Stochastic Processes of Precipitation*. Colorado State University Hydrological Report Paper 35, Colorado State University, Fort Collins, Colorado, pp 1-61.

Troch, P. A., Van De Velde, J. and De Troch, F. P. (1991), *A Stochastic Point Rainfall Generator Based on the Modified Neyman-Scott Rectangular Pulses Model. Application to two Italian raingauge stations at the Lago Maggiore: Pallanza and Ispra*. Laboratory of Hydrology and Water Management, State University of Gent, Gent, Belgium.

Troch, P. A., Smith, J. A., Wood, E. F. and de Troch, F. P. (1994), 'Hydrologic controls of large floods in a small basin: central Appalachian case study'. *Journal of Hydrology*, 156(285-309).

United States Department of Commerce (2000), *General Solar Position Calculations*. Surface Radiation Branch, National Oceanic and Atmospheric Administration, United States Department of Commerce. Electronic reference: http://www.srrb.noaa.gov.

United States Soil Conservation Service (1972), *National Engineering Handbook, Section 4: Hydrology*. Department of Agriculture, Washington D.C.

United States Soil Conservation Service (1985), *National Engineering Handbook, Section 4: Hydrology*. Department of Agriculture, Washington D.C.

Van Montfort, M. A. J. and Witter, J. V. (1986), 'The Generalized Pareto distribution applied to rainfall depths'. *Hydrological Sciences Journal*, 31(2), 151-162.

Veihmeyer, F. J. and Hendrickson, A. H. (1955), 'Does transpiration decrease as the soil moisture decreases?'. *Transactions, American Geophysical Union*, 36(3), 425-428.

Velghe, T., Troch, P. A., De Troch, F. P. and Van de Velde, J. (1994), 'Evaluation of cluster-based rectangular pulses point process models for rainfall'. *Water Resources Research*, 30(10), 2847-2857.

Vere-Jones, D. (1970), 'Stochastic models for earthquake occurrence'. *Journal of the Royal Statistical Society, Series A*, 32(1), 1-62.

Verhoest, N., Troch, P. A. and De Troch, F. P. (1997), 'On the applicability of Bartlett-Lewis rectangular pulses models in the modeling of design storms at a point'. *Journal of Hydrology*, 202, 108-120.

Vertessy, R. A., O'Loughlin, E. M., Beverly, C. R. and Butt, T. J. (1994), 'Australian experience with the CSIRO TOPOG model in land and water resources management'.

UNESCO International Symposium on Water Resources Planning in a Changing World, Karlsruhe, Germany.

Viessman, W. J., Lewis, G. L. and Knapp, J. W. (1989). *Introduction to Hydrology*. Harper Collins.

Volinsky, C. T. and Raftery, A. E. (2000), 'Bayesian Information Criterion for Censored Survival Models'. *Biometrics*, 56, 256-262.

Vorosmarty, C. J., Federer, C. A. and Schloss, A. L. (1998), 'Potential evaporation function compared on US watershed: Possible implications for global-scale water balance and terrestrial ecosystem modeling'. *Journal of Hydrology*, 207, 147-169.

Walsh, M. A., Pilgrim, D. H. and Cordery, I. (1991), 'Initial losses for design flood estimation in New South Wales'. *International Hydrology and Water Resources Symposium*, Perth, Western Australia, 2-4 October, 1991.

Walsh, M. A. (1991), *Initial Losses for Design Flood Estimation in New South Wales*. PhD Thesis, Department of Civil Engineering, University of New South Wales, Sydney, New South Wales.

Walsh, M. A. and Pilgrim, D. H. (1993), 'Re-assessment of some design parameters for flood estimation in New South Wales'. *International Hydrology and Water Resources Symposium*, Newcastle, New South Wales, 30 June - 2 July, 1993.

Watson, M.D. (1981), *Application of 'ILLUDAS' to stormwater drainage design in South Africa*. Urban Hydrology Series, Report No. 1/81, University of the Witwatersrand, Johannesburg, South Africa.

Waymire, E. and Gupta, V. K. (1981a), 'The mathematical structure of rainfall representations 1. A review of the stochastic rainfall models'. *Water Resources Research*, 17(5), 1261-1272.

Waymire, E. and Gupta, V. K. (1981b), 'The mathematical structure of rainfall representation 2. A review of the theory of point processes'. *Water Resources Research*, 17(5), 1273-1285.

Waymire, E. and Gupta, V. K. (1981c), 'The mathematical structure of rainfall representations 3. Some applications of the point process theory to rainfall processes'. *Water*

Resources Research, 17(5), 1287-1294.

Weinmann, P. E., Rahman, A., Hoang, T., Laurenson, E. M. and Nathan, R. J. (1998), 'A new modelling framework for design flood estimation'. *HydraStorm '98*, Adelaide, South Australia, 27-30 September, 1998.

Weiss, L. L. (1964), 'Sequences of wet or dry days described by a Markov chain probability model'. *Monthly Weather Review*, 92(4), 169-176.

Wilson, E. B. and Hilferty, M. M. (1931), 'The distribution of chi-square'. *Journal of the National Academy of Science*, 17, 684-688.

Wiser, E. H. (1965), 'Modified Markov probability models of sequences of precipitation events'. *Monthly Weather Review*, 93(8), 511-516.

Wong, T. H. F. (1996), 'Synthetic generation of storm sequence using a multi-module data generation technique'. *23rd Hydrology and Water Resources Symposium*, Hobart, Tasmania, 21-24 May, 1996. National Conference Publication No. 96/05, Institution of Engineers, Australia.

Wood, E. F. (1976), 'An analysis of the effects of parameter uncertainty in deterministic hydrologic models'. *Water Resources Research*, 12(5), 925-932.

Wood, E. F. and Hebson, C. S. (1986), 'On hydrologic similarity 1. Derivation of the dimensionless flood frequency curve'. *Water Resources Research*, 22(11), 1549-1554.

Woolhiser, D. A. and Pegram, G. G. S. (1979), 'Maximum likelihood estimation of Fourier coefficients to describe seasonal variations of parameters in stochastic daily precipitation models'. *Journal of Applied Meteorology*, 18(1), 34-42.

Woolhiser, D. A. and Roldan, J. (1982), 'Stochastic daily precipitation models: 2. A comparison of distributions of amounts'. *Water Resources Research*, 18(5), 1461-1468.

Woolhiser, D. A. and Osborn, H. B. (1985), 'A stochastic model of dimensionless thunderstorm rainfall'. *Water Resources Research*, 21(4), 511-522.

Woolhiser, D. A. and Roldan, J. (1986), 'Seasonal and regional variability of parameters for stochastic daily precipitation models: South Dakota, U.S.A'. *Water Resources Research*,

22(6), 965-978.

Ye, W., Bates, B. C., Viney, N. R., Sivapalan, M. and Jakeman, A. J. (1997), 'Performance of conceptual rainfall-runoff models in low-yielding ephemeral catchments'. *Water Resources Research*, 33(1), 153-166.

Yen, B. C. and Chow, V. T. (1980), 'Design hyetographs for small drainage structures'. *Journal of the Hydraulics Division, ASCE*, 106(HY6), 1055-1076.

Addendum

Abstract

- Page iii, second sentence
  The ratio of the IFD and REFD is more correctly stated as the ratio of the REFD and IFD.

Chapter 1

- Section 1.2.3, before last sentence
  Add 'Because the primary aim of the thesis was to eliminate the joint probability problem associated with initial loss estimates when using a rainfall-based flood estimation techniques, other specific techniques for estimating flood peaks at sites where there are no or limited streamflow records, such as, regional flood frequency methods were not evaluated. .'
- Section 1.3.3, end of paragraph 2
  Add 'Limited research in this area has been applied to Australian catchments. Blazkova and Beven (1997) and Cameron *et al.* (1999) showed the potential of the approach by using an hourly stochastic rainfall model and the TOPMODEL rainfall-runoff model to predict flood frequency distributions for a number of European catchments.'
- Page 20, end of paragraph 2
  Add 'Field and Williams (1983; 1987) also used the Phillip (1957) model.'
- Page 33, paragraph 3, second sentence
  Change to 'Due to numerous deficiencies in the current knowledge of atmospheric physics, attempts to deterministically model rainfall have met with limited success (Cho, 1985; Cowpertwait, 1991b).'

Chapter 2

- Section 2.6.3, page 59, end of paragraph 1
  Add 'A key criterion is whether the data contains sufficient information for the estimation of the parameters required.'

Chapter 3

- Page 65, at end of first sentence
  Add 'Standard checks for homogeneity were undertaken to ensure the data was of a good quality.'
- Page 96, after Equation (3.21), modify sentence 2 to read
  'A reasonable estimate was considered (Press *et al.*, 1992) to be ...'
- Page 96, to the end of the paragraph following Equation (3.21)
  Add 'A value of seven for *ofac* was chosen from recommendations in Press *et al.* (1992).'
- Page 97, end of paragraph 1
  Add 'The Nyquist frequency is the frequency at which a signal must be sampled so that it contains complete information about all spectral components (Press *et al.*, 1992).'
- Page 101, last paragraph, after second sentence
  Add 'These are model formulations in which the solution of a model with $f+1$ parameters also contains the solution of a model with f parameters, the latter referred to as the null hypothesis.'
- Page 103, after second sentence
  Add 'The AIC criterion is widely used and incorporates mean log-likelihood estimates as a measure of fit.'
- Section 3.4.10, page 105, after paragraph 2
  Add 'A monthly model has 48 parameters, which is equivalent to an harmonic model with 22 harmonics. Increasing the number of harmonics increases the difficulty in calibration (because they must be calibrated simultaneously) and as such calibration of a model with this many harmonics was not undertaken. Even though the monthly model has a significant number of parameters, they are easily estimated because four parameters only are being calibrated at any one time, to a subset of the total data.'
- Section 3.5.4, page 111, after paragraph 1
  Add 'It is also apparent that the variability of the average event intensity decreases with event duration, due in part because of the small number events at higher event durations. The nature of rainfall generation is also less likely to lead to long duration events with high intensities.'

Chapter 4

- On Figure 4.5, page 135,
  'Outliners' should be 'Outliers'.

Chapter 6

- Section 6.1.2, page 191, reword last sentence to read
  'An opposing view, put forward by Veihmeyer and Hendrickson (1955), is that …'
- Section 6.3.4, page 198, replace the first sentence with
  'The wet environment model of Morton (1983) is a better alternative to the Penman-Monteith model because its data requirements are less demanding.'
- Page 205, after paragraph 2
  Add 'The use of sunshine hours for the calculation of potential evaporation has also shown to be a reasonable alternative to the use of radiation data by a number of authors including Chiew and McMahon (1991).'
- Section 6.6.1,page 211, add this paragraph before the last paragraph
  'The WGEN stochastic daily weather model (Richardson and Wright, 1984) uses a first order Markov Chain model to generates rainfall, maximum and minimum temperature and solar radiation. Because of the limited solar radiation data available to calibrate this model, it was not considered further as a model to generate stochastic evaporation.'

Chapter 7

- Page 233, last two sentences of paragraph 1, change to
  'From this initial investigation, the AWBM was found to produce superior results. Although structural deficiencies in the AWBM have been shown (Bates and Campbell, 2001), with an identified potential for improvement to obtain a suitable relationship between observed and predicted streamflow hydrographs, this model was chosen.'
- Equation 7.3 on page 235
  RE should have the units mm/day.
  Change 't = time step in hours.' to 't = time step in days.'
- Page 235, paragraph 2, replace last sentence with
  'The use of E_m was considered satisfactory because it improved the calibration and required the addition of only one parameter.'

Chapter 8

- Page 296, after last paragraph
  Add 'The concurrent calibration was achieved by using all the available events to form a single objective function. This was then optimised to determine the best parameter values using the SCE method.'
- Section 8.2.4, page 302, after first sentence,
  Add 'Mass conservation checks were performed for each of the observed and predicted hydrographs shown in Figures 8.18 to 8.25 and were within the $0.95 < RC < 1.05$ range specified in Bates *et al.* (1991), where RC is the runoff coefficient.'

Chapter 10

Add references:

- Bates, B.C., Sumner, N.R. and Ganeshanandam, S. (1991), 'Calibration of nonlinear surface runoff models: Caution!'. *International Hydrology and Water Resources Symposium*, Perth, Western Australia, 2-4 October, 1991. The Institution of Engineers, Australia.
- Bates, B.C. and Campbell, E.P. (2001), 'A Markov chain Monte Carlo scheme for parameter estimation and inference in conceptual rainfall-runoff modelling. *Water Resources Research*, 37(4), 937-948.
- Blazkova, S. and Beven, K. (1997), 'Flood frequency prediction for data limited catchments in the Czech Republic using a stochastic rainfall model and TOPMODEL'. *Journal of Hydrology*, 195, 256-278.
- Cameron, D.S., Beven, K.J., Tawn, J., Blazkova, S. and Naden, P. (1999), 'Flood frequency estimation by continuous simulation for a gauged upland catchment (with uncertainty)'. *Journal of Hydrology*, 219, 169-187.
- Richardson, C.W and Wright, D.A. (1984), 'WGEN: A model for generating daily weather variables'. Report No. ARS-8, Agriculture Research Service, United States Department of Agriculture.